

**The P450 Biol Redox System**

**Thesis submitted for the degree of  
Doctor of Philosophy  
At the University of Leicester**

**By**

**Rachel Lawson  
Department of Biochemistry  
University of Leicester**

**May 2005**

UMI Number: U203810

All rights reserved

INFORMATION TO ALL USERS

The quality of this reproduction is dependent upon the quality of the copy submitted.

In the unlikely event that the author did not send a complete manuscript and there are missing pages, these will be noted. Also, if material had to be removed, a note will indicate the deletion.



UMI U203810

Published by ProQuest LLC 2013. Copyright in the Dissertation held by the Author.  
Microform Edition © ProQuest LLC.

All rights reserved. This work is protected against  
unauthorized copying under Title 17, United States Code.



ProQuest LLC  
789 East Eisenhower Parkway  
P.O. Box 1346  
Ann Arbor, MI 48106-1346



**The P450 BioI Redox System**

by

**Rachel Lawson**

Cytochrome P450 BioI is isolated from the soil bacterium *Bacillus subtilis*. It is located in an operon that encodes genes involved in the synthesis of the vitamin biotin. From knock-out studies it was concluded that BioI catalyses an early step in the biosynthetic pathway, forming a precursor to the isolatable intermediate pimelic acid. This thesis covers the characterisation of this P450 and its various endogenous redox partners. The data presented here reports upon the bio-physical properties of the P450 including information on the redox potentials, how its environment affects its properties and the factors that govern substrate binding. To produce a catalytically active BioI redox system, two flavodoxins were cloned from *B. subtilis* and their over-expression and preparation is described. These flavodoxins have been characterised according to their redox and structural properties. The ability of the two flavodoxins to reconstitute the oxidase activity of BioI was examined by kinetic and spectroscopic techniques culminating in the analysis of the monooxygenation of various fatty acids. To complete the redox chain two NADPH-oxidoreductase candidates and a di-flavin reductase from *B. subtilis* were assessed and their ability to complement the P450 BioI-flavodoxin system examined.

## Contents

<b>1.0</b>	<b>Introduction</b>	<b>1</b>
1.1	Cytochromes P450	2
1.2	Properties of Iron-oxygen systems	13
1.3	P450 Redox Partners	17
1.3.1	Flavodoxins	20
1.3.2	Ferredoxins	31
1.3.3	Reductases	44
1.4	Oxidation Reactions	57
1.4.1	Substrate binding and specificity	64
1.4.2	Commercial Interest in P450 monooxygenases	67
1.5	Biotin Biosynthesis genes in <i>B. subtilis</i>	71
1.6	Biotin: Functions and Biosynthesis	74
1.7	P450 BioI	86
<b>2.0</b>	<b>Materials and Methods</b>	<b>91</b>
2.1	Bacterial Strains	92
2.2	Common Reagents	93
2.2.1	Growth media for <i>E. coli</i>	93
2.2.2	Electrophoresis reagents	94
2.2.3	Protein purification reagents	96
2.3	General molecular biology techniques	98
2.3.1	Culture Growth	98
2.3.2	Maintenance and storage of cultures	98
2.3.3	Transformation of <i>E. coli</i> strains	99
2.3.4	Small-scale isolation of plasmid DNA	99
2.3.5	Diagnostic restriction enzyme digests	99
2.3.6	Agarose gel electrophoresis	100
2.4	Cloning of potential redox partners	100
2.4.1	Cloning of the flavodoxins <i>ykuN</i> and <i>ykuP</i>	100
2.4.2	Cloning the diflavin reductase domains from CYP102A2 and A3	103
2.4.3	Purification of the PCR product	104
2.4.4	Enzyme digest of the PCR product	104
2.4.5	Recovery of DNA from the agarose gel	105
2.4.6	Preparation of the vectors for cloning	105
2.4.7	DNA ligation	106
2.4.8	Transformation by electroporation	106
2.4.9	Transformation of chemically competent cells	107
2.4.10	PCR analysis of positive colonies	107
2.4.11	Cloning into a TOPO vector	107
2.4.12	Phenol/chloroform extraction of DNA fragments	108
2.5	Generation of the H75X mutants	108
2.5.1	Polymerase chain reaction	109
2.6	Protein preparation	110

2.6.1	Large-scale over-expression of proteins	110
2.6.2	Purification of proteins by column chromatography	111
2.6.3	Purification of P450 BioI (and its mutants)	113
2.6.4	Purification of YkuN/P	114
2.6.5	Reductase purification (YumC, YcgT and CYP102A3R)	115
2.6.6	<i>E. coli</i> flavodoxin (FldA) purification	116
2.6.7	<i>E. coli</i> Flavodoxin NADP <sup>+</sup> oxidoreductase (FldR) purification	117
2.6.8	<i>E. coli</i> GAPDH purification	117
2.7	Protein characterisation by SDS PAGE gel electrophoresis	118
2.7.1	Sample preparation	118
2.7.2	Gel preparation and assembly	119
2.7.3	Protein blotting	119
2.8	Protein characterisation; Biophysical techniques	119
2.8.1	Determination of extinction coefficients (flavoproteins)	119
2.8.2	Analysis of tertiary structure by fluorescence spectroscopy	120
2.8.3	P450 BioI UV-visible spectrometry	120
2.8.4	Effect of pH upon P450 BioI	121
2.8.5	Effect of temperature on P450 BioI	121
2.8.6	Disulphide Bond Assay (Chemical)	122
2.8.7	Ligand Binding Studies	122
2.8.8	Heme Reduction Studies	123
2.8.9	Stopped-flow studies of the rate of reduction of P450 BioI by <i>B. subtilis</i> flavodoxins	124
2.8.10	Rate of electron transfer; NAD(P)H reduction of the reductases	125
2.8.11	Rate of flavodoxin reduction by the NAD(P)-oxidoreductases	125
2.8.12	Steady-state kinetic analysis of <i>B. subtilis</i> reductase's interactions with artificial electron acceptors	126
2.8.13	Steady-state kinetic analysis with P450 BioI	127
2.8.14	Hydrogen peroxide determination	127
2.8.15	Electron Paramagnetic Resonance	128
2.8.16	Circular Dichroism	128
2.8.17	Resonance Raman Spectroscopy	128
2.8.18	Chemical Denaturation of P450 BioI (guanidine hydrochloride method)	129
2.8.19	Chemical denaturation of the <i>B. subtilis</i> flavodoxins (guanidine hydrochloride method)	130
2.8.20	Differential Scanning Calorimetry	131
2.8.21	Generation of the apoprotein of the two <i>B. subtilis</i> flavodoxins	131
2.8.22	FMN binding to apo-flavodoxins	132
2.8.23	ANS quenching of tryptophan fluorescence	132
2.8.24	Calculation of Stern-Volmer constants	133

2.8.25	P450 BioI: flavodoxin binding by UV-visible spectroscopy and tryptophan fluorescence	134
2.8.26	Redox titrations	134
2.8.27	Standardisation of the electrode	136
2.8.28	Catalytic turn-over studies	136
2.8.29	Identification of the ligand in <i>E. coli</i> purified P450 BioI	137
2.8.30	Homology modelling of P450 BioI	137
2.8.31	Protein Crystallography	138
<b>3.0</b>	<b>Biophysical characterisation of P450 BioI</b>	<b>140</b>
3.1	Expression Systems	142
3.2	Physical Properties of P450 BioI	145
3.3	Temperature and pH effects	146
3.4	Effect of solvents upon the spin state of P450 BioI	151
3.5	Analysis of the endogenously bound compound	153
3.6	Spectrophotometrically determined binding constants	156
3.6.1	Fatty Acids	156
3.6.2	The binding of steroids	161
3.6.3	Binding of polycyclic compounds	164
3.6.4	Imidazole inhibitors	165
3.6.5	Effect of the $\alpha$ carbon group upon binding	170
3.7	Modelling of P450 BioI	172
3.8	Redox Potentials of P450 BioI	175
3.9	Kinetic studies	181
3.10	Circular Dichroism of P450 BioI	184
3.11	EPR and Resonance Raman spectroscopy	186
3.12	Verification of the presence of a disulphide bond	190
3.13	Chemical denaturation of P450 BioI	193
3.13.1	Heme cofactor denaturation	193
3.13.2	Tertiary structure denaturation	195
3.13.3	Determination of the Stern-Volmer constant	198
3.13.4	Secondary structure loss (CD analysis)	202
3.14	Stability of P450 BioI: Thermal denaturation	204
3.15	Potential carboxylate binding site: Mutation of His75	206
3.16	Crystallisation trials	219
3.17	Conclusion	222
<b>4.0</b>	<b>Cloning, Expression and Characterisation of YkuN and YkuP</b>	<b>224</b>
4.1	Cloning of <i>ykuN</i> and <i>ykuP</i>	226
4.2	Over-expression and purification of YkuN and YkuP	231
4.3	UV-visible spectral characteristics of YkuN and YkuP	237
4.4	Secondary structure determination by CD	238
4.5	Midpoint reduction potentials	241
4.6	Midpoint reduction potentials of P450 BioI-Fld complexes	248
4.7	Kinetics of the single electron reduction of the flds	252

4.8	EPR spectroscopy of the semiquinone form	254
4.9	FMN cofactor binding	255
4.10	Chemical denaturation of YkuN and YkuP	257
4.11	The stability of the flavin cofactor	258
4.12	Gdn.HCl-induced loss of 3° structure	261
4.13	FMN fluorescence	264
4.14	Secondary structure denaturation	267
4.15	ANS fluorescence	274
4.16	Stern-Volmer constants	275
4.17	Flavodoxin binding to P450 BioI	278
4.18	Kinetics of electron transfer from YkuN/P to P450 BioI	280
4.19	Steady-state kinetics	285
4.20	Crystallisation trials	291
4.21	Conclusion	292
<b>5.0</b>	<b><i>B. subtilis</i> NADPH oxidoreductases</b>	<b>293</b>
5.1	Molecular Biology	295
5.2	Over-expression and purification	300
5.3	UV-visible absorbance, Fluorescence and CD profiles	306
5.4	Redox potentials	312
5.5	NADPH and NADH reduction kinetics	319
5.6	Steady-state rates of electron transfer from <i>B. subtilis</i> reductases to P450 BioI, cytochrome <i>c</i> and ferricyanide	325
5.7	Electron transfer to the flavodoxins and to P450 BioI	331
5.8	Reconstitution of the active catalytic P450 BioI system	335
5.9	Conclusion	346
<b>6.0</b>	<b>Conclusions</b>	<b>348</b>
6.1	Cytochrome P450 BioI	349
6.2	The flavodoxins; YkuN and YkuP	351
6.3	NAD(P)H oxidoreductases	353
6.4	Future Work	356
<b>7.0</b>	<b>References</b>	<b>359</b>

### Abbreviations

ACP	Acyl carrier protein
ADP	Adenosine diphosphate
Adx	Adrenodoxin
AdxR	Adrenodoxin Reductase
AMP	Adenosine monophosphate
<i>Anabaena sp.</i>	<i>Anabaena species</i>
<i>A. nidulans</i>	<i>Anacystis nidulans</i>
ANS	8-anilino-1-naphthalene sulphonate
ATP	Adenosine triphosphate
BCCP	Biotin carboxyl carrier protein
<i>B. megaterium</i>	<i>Bacillus megaterium</i>
BSA	Bovine serum albumin
<i>B. sphaericus</i>	<i>Bacillus sphaericus</i>
<i>B. subtilis</i>	<i>Bacillus subtilis</i>
cal	calorie
<i>C. beijerinckii</i>	<i>Clostridium beijerinckii</i>
<i>C. braakii</i>	<i>Citrobacter braakii</i>
CD	Circular dichroism
CHAPS	3-[(3-cholamidopropyl)dimethylammonio]-1-propanesulfonic acid
CO	Carbon monoxide
CoA	Acyl CoA ester
CPR	NADPH-cytochrome P450 oxidoreductase
CYP	Cytochrome P450 monooxygenase
Da	Dalton
DAPA	7,8-diaminopelargonic acid
<i>D. desulfuricans</i>	<i>Desulfovibrio desulfuricans</i>
DEAE	diethylaminoethyl
DEPC	diethylpyrocarbonate
DMSO	Dimethylsulphoxide
DNA	Deoxyribonucleic acid
DOEB	Deoxy-erythronolide B
DT	Sodium Dithionite
DTB	Dethiobiotin
DTNB	5,5'-dithiobis-(2-nitrobenzoic acid)
DTT	Dithiothreitol
<i>D. vulgaris</i>	<i>Desulfovibrio vulgaris</i>
E	Midpoint potential
<i>E. coli</i>	<i>Escherichia coli</i>
EDTA	Ethylenediaminetetra-acetate
EI	Electron ionisation
EPR	Electron paramagnetic spectroscopy
FAD	Flavin adenine dinucleotide
Fdx	Ferredoxin

Fld	Flavodoxin
FldR	Flavodoxin Reductase
FeS	Iron-sulphur
FMN	Flavin mononucleotide
FNR	Ferredoxin NADP <sup>+</sup> reductase
Fre	Flavin oxidoreductase
G	Gibbs free energy
GAPDH	Glyceraldehyde-3-phosphate dehydrogenase
GC-MS	Gas-chromatography coupled mass-spectrometry
Gdn.HCl	Guanidine hydrochloride
GTE	Glucose-Tris-EDTA buffer
HA	Hydroxyapatite
HEPES	N-2-hydroxyethylpiperazine-N'-2-ethane sulphonic acid
HTS	High throughput screening
HQ	Hydroquinone
<i>H. pylori</i>	<i>Helicobacter pylori</i>
Im	Imidazolyl
IPTG	Isopropyl-β-D-galactopyranoside
KAPA	7-keto-8-aminoperlagonic acid
LB	Luria-Bertani media
LUMO	Lowest unoccupied molecular orbital
MME	monomethyl ether
mol	mole
MOPS	3-(N-morpholino)-propane sulfonic acid
MS	Mass-spectroscopy
<i>M. smegmatis</i>	<i>Mycobacterium smegmatis</i>
MTNB	5-mercapto-2-nitro benzoate
<i>M. tuberculosis</i>	<i>Mycobacterium tuberculosis</i>
NADH	Nicotinamide adenine dinucleotide (reduced form)
NADPH	Nicotinamide adenine dinucleotide phosphate (reduced form)
NEB	New England Biolabs
NIST	National Institute of Science and Technology
NMR	Nuclear magnetic resonance
Ox	Oxidised
P450	Cytochrome P450 monooxygenase
PAGE	Polyacrylamide gel electrophoresis
PCR	Polymerase chain reaction
Pdx	Putidaredoxin
PEG	Polyethylene glycol
PhIO	iodosylbenzene
PIM	4-phenyl imidazole
PLP	Pyridoxal-L-phosphate
PNACL	Protein and Nucleic Acid Chemistry Laboratory
<i>P. putida</i>	<i>Pseudomonas putida</i>
PVDF	Polyvinyl difluoride
QEAE	Quaternary aminoethyl

RR	Resonance raman
SAM	S-adenosyl-L-methionine
SDS	Sodium dodecyl sulphate
<i>S. erythraea</i>	<i>Saccaropolyspora erythraea</i>
<i>S. griseus</i>	<i>Streptomyces griseus</i>
SHE	Standard hydrogen electrode
Sir-FP	<i>E. coli</i> sulphite reductase flavoprotein
SOC media	Glucose enriched transformation media
SQ	Semiquinone
TAE	Tris acetate-EDTA buffer
Tdx	Terpredoxin
TE	Tris-EDTA buffer
TOPO	Topoisomerase cloning
Tris	N-tris(hydroxymethyl)aminomethane
UV	Ultra-violet
WT	Wild-type
XRC	x-ray crystallography

#### Amino acids

Alanine	A	Ala
Arginine	R	Arg
Asparagine	N	Asn
Aspartate	D	Asp
Cysteine	C	Cys
Glutamine	Q	Gln
Glutamate	E	Glu
Glycine	G	Gly
Histidine	H	His
Isoleucine	I	Ile
Leucine	L	Leu
Lysine	K	Lys
Methionine	M	Met
Phenylalanine	F	Phe
Proline	P	Pro
Serine	S	Ser
Threonine	T	Thr
Tryptophan	W	Trp
Tyrosine	Y	Tyr
Valine	V	Val
Any	X	Xaa



# *Chapter 1*

## *Introduction*

## 1.1 Cytochromes P450

The cytochromes P450 are a family of heme-containing monooxygenases [Hayaishi, 1974] of around 46 to 57 kDa [Ortiz de Montellano, 1995]. Klingenberg and Garfinkel first detected them independently in rat liver in 1958 [Klingenberg, 1958, Garfinkel, 1958]. They have a characteristic visible absorption spectrum as a result of the non-covalently bound porphyrin IX heterocycle with a cysteine residue as the fifth co-ordinate ligand [Omura and Sato, 1964]. When reduced to their ferrous form and bound to exogenous carbon monoxide they exhibit the characteristic Soret  $\lambda_{\text{max}}$  at ~450 nm [Mason *et al.*, 1965]. The heme binding region, containing the conserved fifth co-ordinate cysteine, is the only strictly conserved region ~ 20 % from the C-terminus of the protein.

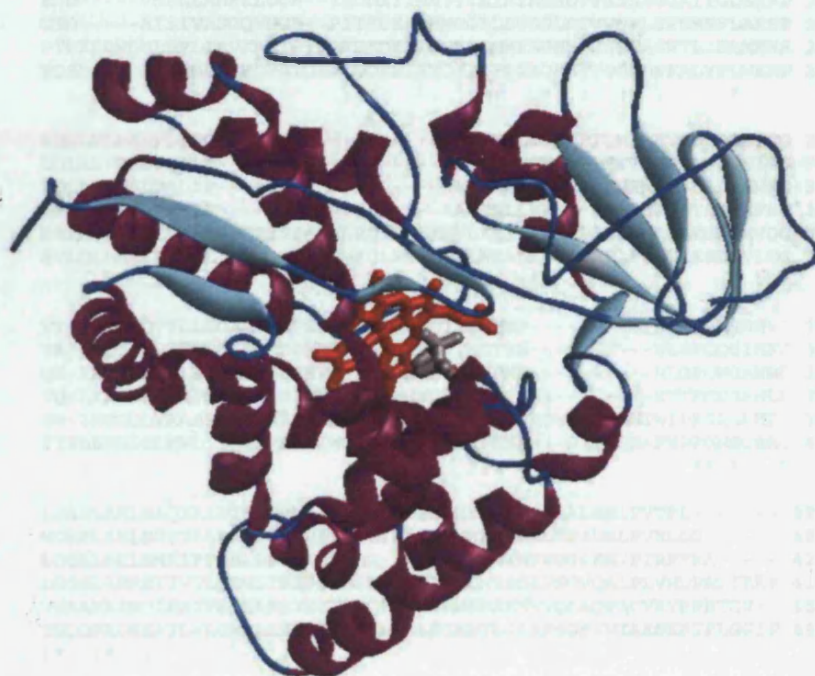


**Figure 1.1** The camphor (grey) bound structure of P450 CAM (CYP101) from *Pseudomonas putida* showing the heme (red) with its cysteine ligated iron. It exhibits the typical triangular shape of P450s with predominantly  $\alpha$ -helical structure (purple), a small amount of  $\beta$ -sheet (cyan) and the loops shown in blue. PDB code 1DZ4 [Schlichting *et al.*, 1997].

From the handful of structures solved to date the overall topology of cytochrome P450s is very similar, and those with a sequence identity of greater than 40 % are classed as being in the same family [Nelson *et al.*, 1993].

BioI	TLASGAFTPRTTESYQPYIIETVHLLDQVQGKK-KMEVISDFAPPLASFVIANIIGVPE	152
eryF	KLVSQEFTVRRVEAMRPRVEQITAEILLDEVGDSG-VVDIVDRFAHPLPIKVICELLGVD	161
P450terp	GLTLNWFQPASIRKLEENIRRIAQASVQRLDFFDGEDFMTDCALYYPHVVMTALGVPE	174
CAM	ALANQVVGMPVVDKLENRIQELACSLIESLRPQG-QCNFTEDYAEPPPIRIFMLLAGLPE	172
CYP51	GEQMKGHAATIEDQVRRMIADWGEAGEIDLLDFFAELTIYTSSACLIGKKFRDQLDGRFA	166
CYP102A1	HAMMVDIAVQLVQKWERLNADEHIEVPEDMTRLTLDTIGLCGFNYRNFNSFYRDQPHFIT	176
.		
BioI	EDREQKEWAASLIQTIDFT-----RSRKALTEGNIMAVQAMAYFKELIQKRKRHP	203
eryF	KYRGEGFRWSS-EILVMDPE-----RAE---QRQAAREVVNFILDLVERRRTEP	207
P450terp	DDEPLMLKLTDQDFGVHEPDEQAVAAPRQSADEAARFHEITATFYDYFNGFTVDRRSCP	234
CAM	EDIPHLKYLTDQMTDPDGSMT-----FAEAKALYDYLPIIEQRRQKP	216
CYP51	KLYHELERGTDPLAYVDPYLP-----IESFRRRDEARNGLVALVADIMNGRIANP	216
CYP102A1	SMVRALDEAMNKLQRANPDDP-----AYDENKRQFQEDIKVMNDLVDKIIADRKASG	228
. : . : *		
BioI	QQD-----MISMLLKGREKD---KLTEEEAASTCILLAIAGHETTVNLISNSVLCLLQHP	255
eryF	GDD-----LLSALIRVQDDDDG-RLSADELTSIALVLLLAGFEASVSLIGIGTYLLLTHP	261
P450terp	KDD-----VMSLLANSKLDGN--YIDDKYINAYYVAIATAGHDTSSSSGGAIIGLSRNP	287
CAM	GTD-----AISIVANGQVNGR--PITSDEAKRMCGLLLVGGGLDTVNLFSSMEFLAKSP	269
CYP51	PTDKSDRMLDVLIAVKAETGTTPRFSADEITGMFISMMFAGHHTSSGTASWTLIELMRHR	276
CYP102A1	EQSD---DLLTHMLNGKDPETGEPLDDENIRYQIITFLIAGHETTSGLLSFALYFLVKNP	285
. : : : : . : . * . . *		
BioI	EQLLKLRENPDIG-----TAVEECLRYESPTQMTARVASEDIDICG	297
eryF	DQLALVRDRPSALP-----NAVEEILRYIAPPETTRFAAEEVEIGG	303
P450terp	EQLALAKSDPALIP-----RLVDEAVRWTAAPVKSMRTALADTEVRG	329
CAM	EHRQELIERPERIP-----AACEELLRRFS-LVADGRILTSDYEFHG	310
CYP51	DAYAAVIDELDELVDGRSVSFHALRQIPQLENVLKETLRLHPPLIILMRVAKGEFEVQG	336
CYP102A1	HVLQKAAEEAARVLVDPVP-SYKQVQKLVGMVLNEALRLWPTAPAFSLYAKEDTVLGG	344
. : . : * : . *		
BioI	VT-IRQGEQVYLLLGAANRDPSIF-TNPDVFDITRSPNP-----HLSFGHGHVVC	345
eryF	VA-IPQYSTVLVANGAANRDPKQF-PDPHRFDVTRDTRG-----HLSFGQGIHFC	351
P450terp	QN-IKRGDRIMLSYPSANRDEEVF-SNPDEFDITRFPNR-----HLGFGWAHMC	377
CAM	VQ-LKKGDQILLPQMLSGLDEREN-ACPMHVDFSRQKVS-----HTTFGHGSHLC	358
CYP51	HR-IHEGDLVAASPAISNRIPEDF-PDPHDFVPARYEQPRQEDLLNRWTWIPFGAGRHR	394
CYP102A1	EYPLEKGBELMVLIPQLHRDKTIWGDVVEFRPERFENP---SAIPQHAFKPFNGQQRAC	401
: . . : . * ** * : *		
BioI	LGSSSLARLEAQIAINTLLQRMPSLNL--ADFEWRYRPLFGFRALEELPVTFE-----	395
eryF	MGRPLAKLEGEVALRALFGRFPALSLGIDADDVVWRRSLLLRGIDHLPVRLDG-----	404
P450terp	LGQHLAKLEMKIFFEELLPKLKSVELS---GPPRLVATNFVGGPKNVPIRFTKA-----	428
CAM	LGQHLARREIIVTLKEWLTRIPDFSIA--PGAQIQHKSGIVSGVQALPLVWDPATTKAV	415
CYP51	VGAAFAIMQIKAFISVLLREYEFEMAQPPESYRNDHSMVQVLAQAPACVRYRRRTGV--	451
CYP102A1	IGQQFALHEATLVLMMLKHFDHDTNYELDIKETLTLKPEGFVVKAKSKKIPLGGIP	460
:* : * : : .		

**Figure 1.2** A sequence alignment of cytochromes P450s from bacteria; *B.subtilis* P450 BioI (CYP107H1), *S.erythrae* P450 eryF (CYP107F), *Pseudomonas sp.* P450 terp (CYP108), *P. putida* P450 Cam (CYP101), *M. tuberculosis* CYP51 and *B. megaterium* P450 BM3 (CYP102A1). Performed using CLUSTAL W [Thompson *et al.*, 1984]. The cysteine that ligates the heme is shown in red, the heme binding motif residues in blue and the proton donor to dioxygen in green. Identical amino acids (\*), those of similar chemical nature (:), and those with some similarity (.) are marked.

P450s are known to be involved in a wide range of reactions involving the mono-oxidation of organic molecules by the reduction and insertion of an atom from molecular dioxygen [Guengerich *et al.*, 1991]. These reactions are found, for example, in steroid synthesis (14 $\alpha$ -demethylase), alkaloid biosynthesis (geraniol 10-hydroxylase [Collu *et al.*, 2001]), metabolism of xenobiotics (CYP3A family [Shou *et al.*, 1994]), activation of pro-carcinogens (human cytochrome P4501A2 [Yun *et al.*, 2001]) and catabolism of fatty acids (P450 BM1 [Munro and Lindsay 1996]) and cyclic hydrocarbons. In general their substrates are highly hydrophobic and oxygenation often leads to a more water-soluble product. Under anaerobic conditions P450s have also been shown to reductively dehalogenate halocarbons to the corresponding alkenes [Dawson, 1988].

There are approximately 55 different P450s found in humans of which around 30 exhibit polymorphism [Nelson *et al.*, 1999]. Some of these polymorphisms have an effect on an individual's ability to metabolise certain compounds e.g. in CYP2D6 [Wang *et al.*, 1999]. Mutations in several human P450s are known to cause disease (e.g. CYP1B1, CYP17, CYP19 and CYP2C9 [Hiratsuka *et al.*, 2000]).

Bacterial P450s are free from membranes and are therefore soluble, unlike their eukaryotic counterparts that are membrane bound, being associated either with the inner mitochondrial membrane or the endoplasmic reticulum. The first microbial P450 was identified in *S. cerevisiae* [Lindenmayer and Smith, 1964] and since then they have been found in many different yeasts, bacteria and fungi. Eukaryotic P450s have been well characterised, being frequently involved in the metabolism of xenobiotics. Notable exceptions are those of the adrenal mitochondria involved in the biosynthesis of steroids, e.g. aromatase [Akhtar *et al.*, 1982].

One of the most studied bacterial cytochrome P450s is P450 CAM from *P. putida* [Hedegaard and Gunsalus, 1965]. This P450 carries out the 5-*ex*hydroxylation of the monoterpene D-camphor that is the first step in the degradation of camphor to acetate and isobutyrate [Martinis *et al.*, 1991]. Camphor catabolism can provide enough carbon and energy for the organism to survive on camphor as its sole carbon source. P450 terp is another bacterial P450 known to be involved in a degradative pathway [Hasemann *et al.*, 1994]. It was isolated from a *Pseudomonad* species by culture enrichment techniques, which increased the proteins expression (1 % of all soluble cell protein) [Peterson *et al.*,

1992]. P450 terp was found to be specific for  $\alpha$ -terpineol. A member of an operon specific to the metabolism of terpineol, the other genes encoded its redox partners, and an alcohol and aldehyde dehydrogenase.

P450s that have a biosynthetic purpose are known in mammals, plants and bacteria. Several P450s have been identified and characterised that are involved in the synthesis of macrocyclic antibiotics [Shen and Hutchinson, 1993, Kelly and Townsend, 2002]. P450 eryF from *S. erythraea* catalyses the hydroxylation of 6-deoxyerythronolide B in the production of erythromycin A [Shafiee and Hutchinson, 1988, Cupp-Vickery *et al.*, 1995]. Other antibiotics produced by various soil inhabiting microbes include nikkomycin, in whose synthesis P450 NikQ is known to catalyse the  $\beta$ -hydroxylation of histidine; novobiocin, in whose synthesis P450 NovI also catalyses a  $\beta$ -hydroxylation (of tyrosine) [Chen *et al.*, 2002]; and vanomycin (*Amycolatopsis orientalis*) in whose biosynthesis P450 OxyB is believed to catalyse an oxidative phenol coupling [Zerbe *et al.*, 2002].

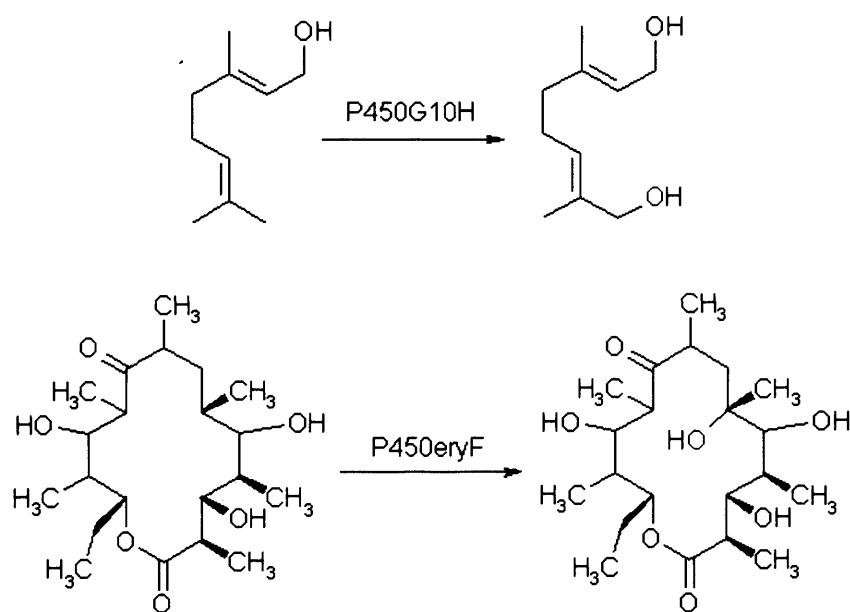


**Figure 1.3** The reactions catalysed by P450 G10H (top) and P450 eryF (bottom). P450 G10H oxidises geraniol to 10-hydroxygeraniol [Collu *et al.*, 2001], P450 eryF carries out a similar oxidation, but on the larger substrate 6-deoxyerythronolide B to give erythronolide B [Shafiee and Hutchinson, 1988]. Both P450s insert an atom of activated oxygen (red) into an inert C-H bond.

87 % of the plant P450 families and 97 % of the plant P450s identified to date have an *Arabidopsis* homolog [Nelson *et al.*, 1999]. The P450s found in plants are usually involved in functions to do with defence (synthesis of phytoalexins and toxic alkaloids [e.g. Burlat *et al.*, 2004]), the biosynthesis of hormones and growth regulators, metabolism of pollutants or pigmentation (particularly flowering plants [e.g. Maugard *et al.*, 2001]). Of the 273 P450 genes in *Arabidopsis* (including 26 pseudogenes) none bar the CYP51 genes (of which *Arabidopsis* contains two) bear clear homology to any animal or fungal P450s [Xu *et al.*, 2001].

CYP51 is probably the most commonly found P450 being identified in a large variety of species [Nelson *et al.*, 1996, Lamb *et al.*, 2002]. Being a sterol 14 $\alpha$ -demethylase, it or its homologue is found in mammals, plants, fungi, yeast and some bacteria (e.g. *M. tuberculosis* [Bellamine *et al.*, 1999]). Both photosynthetic and non-photosynthetic aerobic bacteria have been found to contain distinct sterol molecules. These and 'sterol-like' molecules are utilised within the structure of their cell walls e.g. the pentacyclic hopanoids are thought to increase membrane stability [Tippelt *et al.*, 1998]. These molecules are often synthesised directly from squalene (aerobic pathway), sterols are synthesised under anaerobic conditions (also from squalene).

P450 BM3 was for sometime unique as the only known bacterial P450 to be covalently attached to its flavin-containing redox partner [Li *et al.*, 1991]. From *B. megaterium* it is a fatty acid hydroxylase. It hydroxylates a variety of long chain fatty acids at the  $\omega$ -1,  $\omega$ -2 and  $\omega$ -3 positions [Boddupali *et al.*, 1992]. The 55 kDa heme-containing domain is linked by a hydrophilic peptide to the larger 66 kDa diflavin-containing domain [Nahri *et al.*, 1986]. The expression of P450 BM3 is inducible by barbiturates despite them not appearing to be substrates themselves [Wen *et al.*, 1987, Shaw and Fulco, 1993].

Several P450s with a variety of functions have been characterised from the actinomycetes. Actinomycete P450s do not seem to be involved in any essential metabolic function, often being xenobiotically induced [Nagy *et al.*, 1995]. Sulphonylurea-containing herbicides induce expression of P450 SU1 and P450 SU2 in the soil bacterium *S. griseolus* [O'Keefe *et al.*, 1991]. The streptomyces P450s have a relatively broad range of substrate specificity, being able to turn over a large variety of

compounds. They introduce their substrate compound into the primary metabolic pathway allowing their parent organism to utilise the compound as its sole carbon source (e.g. the demethylation of veratrole in *S. setonii* [Sutherland, 1986]).

Cytochrome P450s are typified by their optical absorption spectra. Their characteristic red colouration is due to the heme cofactor they contain. The strong colour arises from the ligand-to-metal charge transfer bands, which obscure the metal d - d transitions [Silver, 1993]. The Fe - S bond that occurs in P450s induces the  $\pi$  back donation to the bound oxygen, as the thiolate axial ligand is an extremely weak ligand, being both a soft base and a  $\sigma$  donor. It also has a significant effect on the visible spectrum [Mason *et al.*, 1965]. This is demonstrated by comparing the  $\lambda_{\text{max}}$  of haemoglobin (another heme *b*-containing macromolecule with histidine as the axial ligand) at 420 nm to the Soret band of the P450s (at 450 nm, thiolate ligand) when both are reduced and bound to exogenous CO. The water-associated low spin ferric form of the cytochrome P450s also gives rise to the characteristic  $\alpha$  and  $\beta$  bands (500 – 600 nm). The binding of substrate to the P450 can be observed by differences in the optical spectra generated. The binding of apolar substances, such as fatty acids, typically results in a blue shift in the Soret band as the hydrophobicity increases and the sixth axial water ligand is displaced. Inhibitory ligands such as imidazole-containing fungicides (e.g. fluconazole) cause a red shift to occur as they displace the water by ligating directly to the iron atom themselves [Ortiz de Montellano 1995]. The optical spectrum of the heme is therefore very characteristic of the state of the P450 and an effective tool in the study of these proteins.

The established catalytic cycle is mainly derived from studies on P450 CAM, but assumed common to all P450s [Mueller *et al.*, 1995]. In the resting state the heme iron exists in its ferric form with a molecule of water loosely associated in the sixth coordination position of the distorted octahedral form. Upon the substrate binding in the hydrophobic channel of the enzyme, its redox partner reduces the iron atom to the ferrous form. The ferrous iron then binds a molecule of dioxygen that it in turn reduces to result in a ferric-superoxo complex [Bangcharoenpaurpong *et al.*, 1986]. This relatively unstable complex receives a further electron that reduces the dioxygen to a peroxo form [Dawson, 1988]. The reactive dioxygen molecule undergoes bond scission to yield a



molecule of water and a high-energy ferryl-oxo species. It is this highly reactive form that is the attacking species in a variety of oxygenation reactions. Hydrogenation of the dioxygen molecule is achieved by the donation of protons from both solvent molecules and amino acid residues lining the active site (e.g. T268 in P450 BM3 [Ravichandran *et al.*, 1993] and T252 in P450 CAM [Gerber and Sligar, 1992]). The overall turnover rate is often dependent on the rate of dissociation of the product [Martinis *et al.*, 1991] and the concentration of both the product and substrate in solution [Brewer and Peterson, 1986]. Product release has been shown to be the rate-limiting step in CYP11B1-dependent aldosterone production [Imai *et al.*, 1998].

Figure 1.5 Plausible oxidative species of cytochromes P450 [Coon *et al.*, 1998]. The chemical nature of the species and the reactions they catalyze are shown.

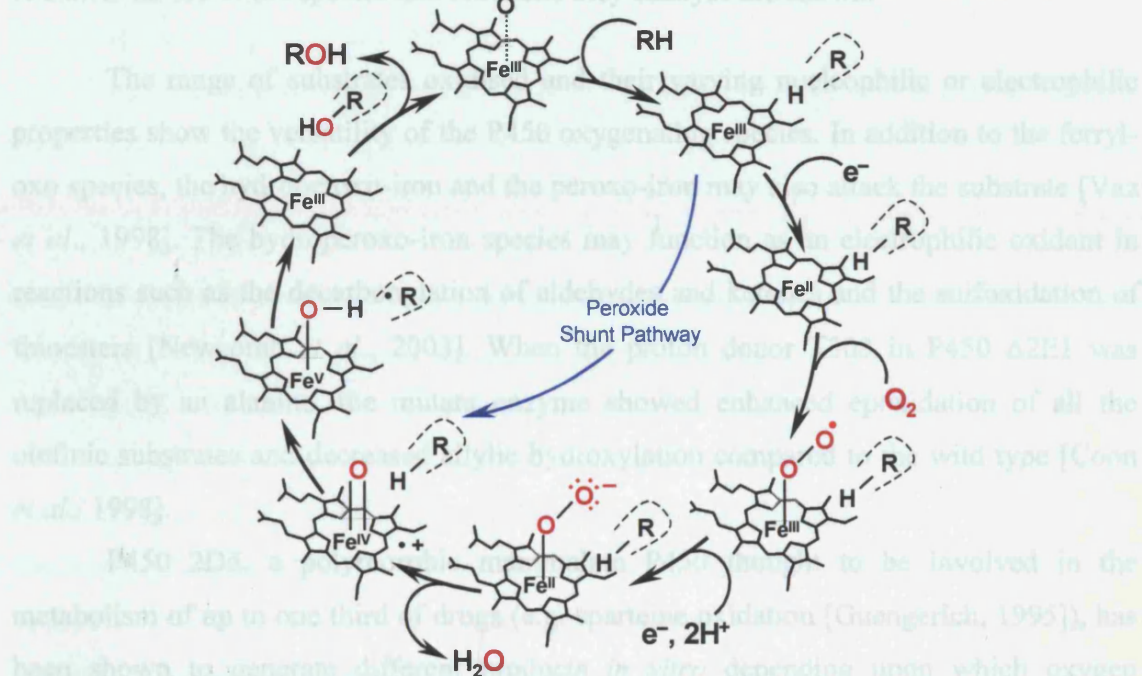


**Figure 1.4** The general catalytic cycle of cytochromes P450. A hydroxylation reaction is shown with atoms from the dioxygen molecule in red. The substrate is represented as R [Miles *et al.*, 2000].

Molecules that can act as oxygen donors (e.g. alkyl peroxides, peracids, sodium chlorite, sodium periodate and iodosobenzene) can short circuit the cycle, bypassing the dioxygen bond scission steps going direct from  $\text{RHF}e^{3+}$  to  $\text{RHF}e^{4+}\text{O}$  [Porter and Coon, 1991, White and Coon, 1980]. Hydrogen peroxide can also bind to the iron to form the



peroxo-ferric intermediate and will subsequently be reduced to give water and the active iron-oxo species [Coon *et al.*, 1998].

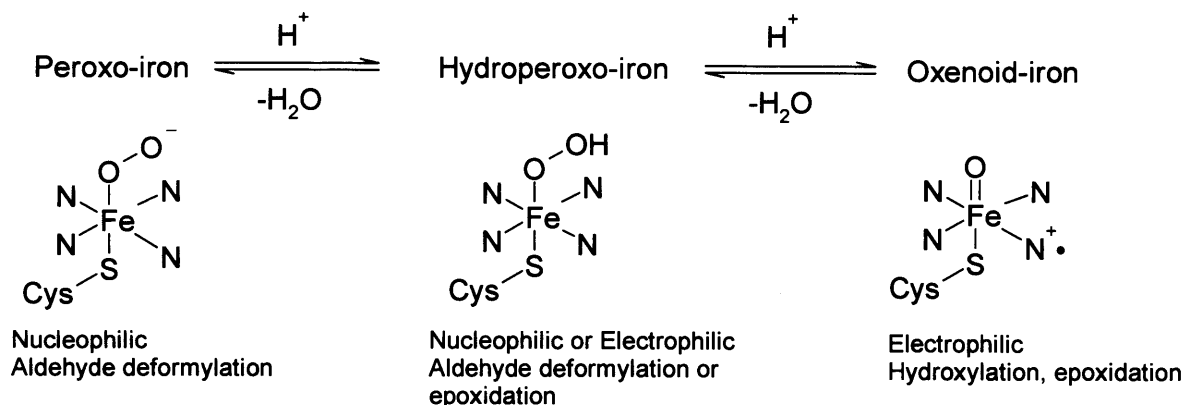


**Figure 1.5** Plausible oxidative species of cytochromes P450 [Coon *et al.*, 1998]. The chemical nature of the species and reactions they catalyse are shown.

The range of substrates oxidised and their varying nucleophilic or electrophilic properties show the versatility of the P450 oxygenating species. In addition to the ferryl-oxo species, the hydroperoxo-iron and the peroxo-iron may also attack the substrate [Vaz *et al.*, 1998]. The hydroperoxo-iron species may function as an electrophilic oxidant in reactions such as the decarbonylation of aldehydes and ketones and the sulfoxidation of thioesters [Newcomb *et al.*, 2003]. When the proton donor T303 in P450  $\Delta$ 2E1 was replaced by an alanine, the mutant enzyme showed enhanced epoxidation of all the olefinic substrates and decreased allylic hydroxylation compared to the wild type [Coon *et al.*, 1998].

P450 2D6, a polymorphic mammalian P450 thought to be involved in the metabolism of up to one third of drugs (e.g. sparteine oxidation [Guengerich, 1995]), has been shown to generate different products *in vitro* depending upon which oxygen donor/redox partners are used [Modi *et al.*, 1997]. The oxidation of metoprolol and bufuralol were supported either by a reduced oxygen donor (e.g. cumene hydroperoxide or iodosylbenzene (PhIO)) or by dioxygen with NADPH-P450 reductase donating the electrons (from NADPH). Different product profiles were observed when the different redox systems were used. This was thought due to the altered nature of the oxidising species rather than any effects from the docking of a redox partner protein. The putative  $FeO^{3+}$  species (as generated by the reductase) was involved in multiple oxidations whilst

the peroxo complexes (FeO(H)PhIOH) from iodosylbenzene had a more restricted scope [Hanna *et al.*, 2001]. P450 3A4, another xenobiotic metabolising human microsomal P450, has a very broad substrate specificity being thought to be involved in the oxidation of half the commercial drugs available [Guengerich, 1995]. Like 2D6, experiments *in vitro* showed that product profiles were affected by the redox system used. In the oxidation of aflatoxin B1 to give either the 8,9-epoxide or the 3 $\alpha$ -hydroxide, replacing the NADPH-P450 reductase with either flavodoxin or ferredoxin redox partners or an oxygen donor (iodosylbenzene [PhIO]), the pattern of products was altered [Ueng *et al.*, 1997]. With the reductase both the 8,9-epoxide and 3 $\alpha$ -hydroxide are seen in the ratio of approximately 6:1. When the flavodoxin or ferredoxin were used a lower overall rate was observed and no 3 $\alpha$ -hydroxylation seen. With PhIO only the 8,9-dihydrodiol is observed (the hydrolysis product of the epoxide).

A highly conserved residue in the heme-binding motif of P450s is a phenylalanine residue believed to have an important role in the electron transfer to the heme. This residue is thought, from mutagenesis of P450 BM3, to be involved in the control of the electronic properties of the heme through an interaction with the iron–cysteinyll sulphur bond. Its substitution with an alanine or histidine increased the redox potential of the iron [Ost *et al.*, 2001]. The mutants were observed to stabilise the oxyferrous form of the heme (half life of 30 s at 15 °C) relative to the superoxy-ferric form.

P450s have been sub-categorised according to the redox partners they use to transfer the electrons to them from reduced pyridine nucleotides [Miles *et al.*, 2000]. Traditionally class I P450s are defined as requiring a FAD-containing NAD(P)H ferredoxin reductase and an iron-sulphur protein (a ferredoxin) for the shuttling of electrons [Huang and Kimura, 1973]. These class I enzymes are usually found in bacterial and mitochondrial systems e.g. P450 CAM. Class II P450s are those described as having a FAD/FMN-containing NADPH P450 reductase partner [Vermillion and Coon, 1974]. This class of enzyme are found associated with the endoplasmic reticulum of eukaryotes e.g. CYP2B4, a drug metabolising microsomal P450. The class III P450s turn over substrates already containing reduced oxygen in the form of endoperoxides or hydroperoxides, so do not require an exogenous source of electrons e.g. CYP5A1, the mammalian thromboxane synthase [Leeder *et al.*, 1998].

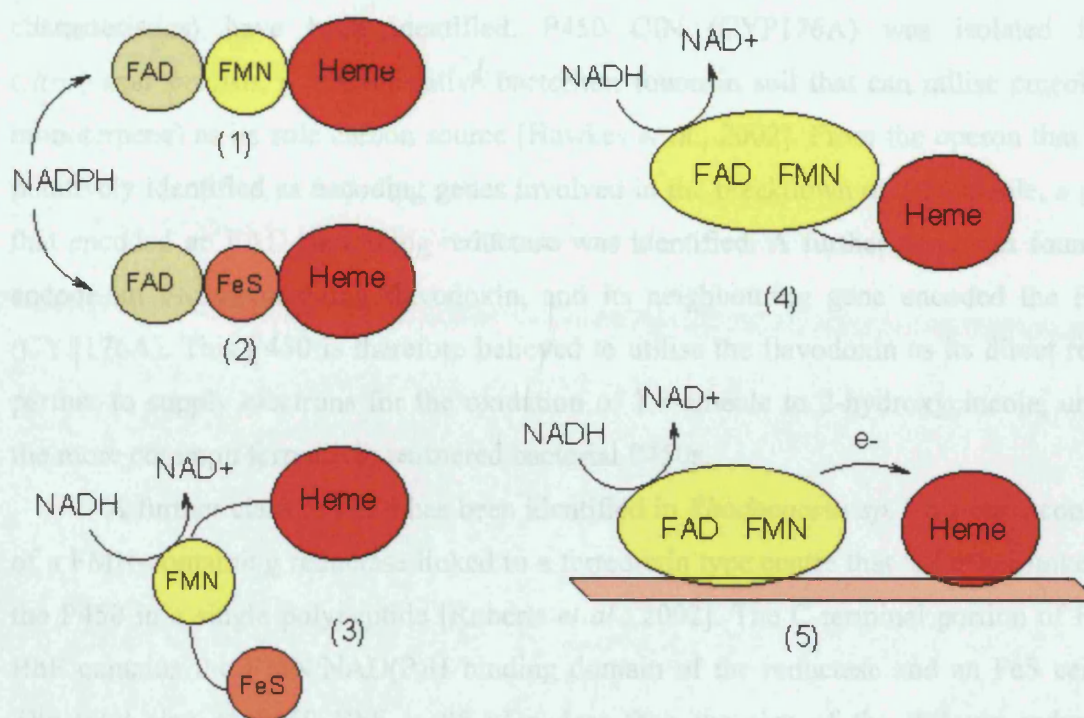


**Figure 1.6** Examples of some of the classes of P450 as determined by their redox partners. Shown are the heme containing P450, the FAD containing reductase and either an FMN or FeS (iron-sulphur) containing electron transport protein. The most common are the three-component systems found in bacteria (1) and (2). Several bacteria have evolved to fuse their redox partners to the P450 eg *Rhodococcus* sp. P450 RhF (3) and *B. megaterium* P450 BM3 (4). Mammalian systems (5) are typically two-component, with enzymes linked to the membrane by a hydrophobic peptide chain [Miles *et al.*, 2000].

CYP55A, from *Fusarium oxysporum*, is a P450 that receives its electrons directly from reduced pyridine nucleotides [Park *et al.*, 1997]. *Streptomyces carbophilus* contains a prokaryotic two-component system where the P450 is coupled with a single flavoprotein (FAD-FMN) P450 reductase [Serizawa and Matsuoka, 1993]. P450 BM3 is a single component system containing both the reductase and cytochrome functions on a single 119 kDa polypeptide [Nahri and Fulco, 1987]. The N-terminal portion of the reductase domain shows strong homology with flavodoxins whilst the C-terminal end is homologous to FAD containing reductases. The heme and reductase domain are linked by a single peptide chain of critical length to allow the correct orientation of the two domains for electron transfer to occur [Govindaraj *et al.*, 1997].

In the last few years several new classes of P450s (based upon their redox partner characteristics) have been identified. P450 CIN (CYP176A) was isolated from *Citrobacter braakii*, a gram-negative bacterium found in soil that can utilise cineole (a monoterpene) as its sole carbon source [Hawkes *et al.*, 2002]. From the operon that was putatively identified as encoding genes involved in the breakdown of 1,8-cineole, a gene that encoded an FAD-containing reductase was identified. A further gene was found to encode an FMN-containing flavodoxin, and its neighbouring gene encoded the P450 (CYP176A). This P450 is therefore believed to utilise the flavodoxin as its direct redox partner to supply electrons for the oxidation of 1,8-cineole to 2-hydroxycineole, unlike the more common ferredoxin partnered bacterial P450s.

A further class of P450 has been identified in *Rhodococcus sp.* This class consists of a FMN-containing reductase linked to a ferredoxin type centre that is further linked to the P450 in a single polypeptide [Roberts *et al.*, 2002]. The C-terminal portion of P450 RhF contains the FMN/NAD(P)H binding domain of the reductase and an FeS centre. The total size of P450 RhF is 85 kDa, less than the size of the diflavin reductase containing BM3. Although the exact physiological function and substrate of this P450 is unclear, it is known to catalyse the O-dealkylation of 7-ethoxycoumarin.

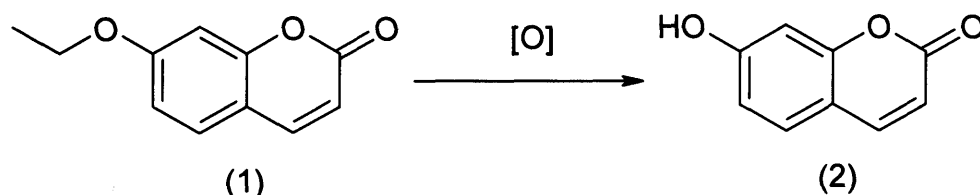


**Figure 1.7** Oxidation of 7-ethoxy coumarin (1) to give 7-hydroxy coumarin (2) by P450 RhF [Roberts *et al.*, 2002].

A cytochrome P450 from *Bacillus subtilis* (P450 Bs $\beta$ ) has been characterised that uses H<sub>2</sub>O<sub>2</sub> as an oxidant without the need for a redox partner. The fatty acid substrate's carboxylate group is proposed to aid cleavage of the peroxide O-O bond in a similar manner to the acid/base-catalysed cleavage seen with chloroperoxidases. The resulting intermediate hydroxylates the fatty acid at either the  $\alpha$ - or  $\beta$ -position [Lee *et al.*, 2003].

# **SPECIAL NOTE**

**THE FOLLOWING**  
**IMAGE IS OF POOR**  
**QUALITY DUE TO THE**  
**ORIGINAL DOCUMENT.**

**THE BEST AVAILABLE**  
**IMAGE HAS BEEN**  
**ACHIEVED.**



## 1.2 Properties of Iron - oxygen systems

The relationship between the iron atom at the centre of the heme cofactor and the dioxygen molecule is fundamental to the oxygenation reactions carried out by the cytochrome P450s. The dioxygen molecule naturally occurs as a paramagnetic molecule with two unpaired electrons occupying the anti-bonding  $2p\pi^*$  orbitals [Cotton *et al.*, 1999]. However, whilst dioxygen is thermodynamically very reactive it is kinetically inert and it is this property that can be overcome by complexation with the iron atom.

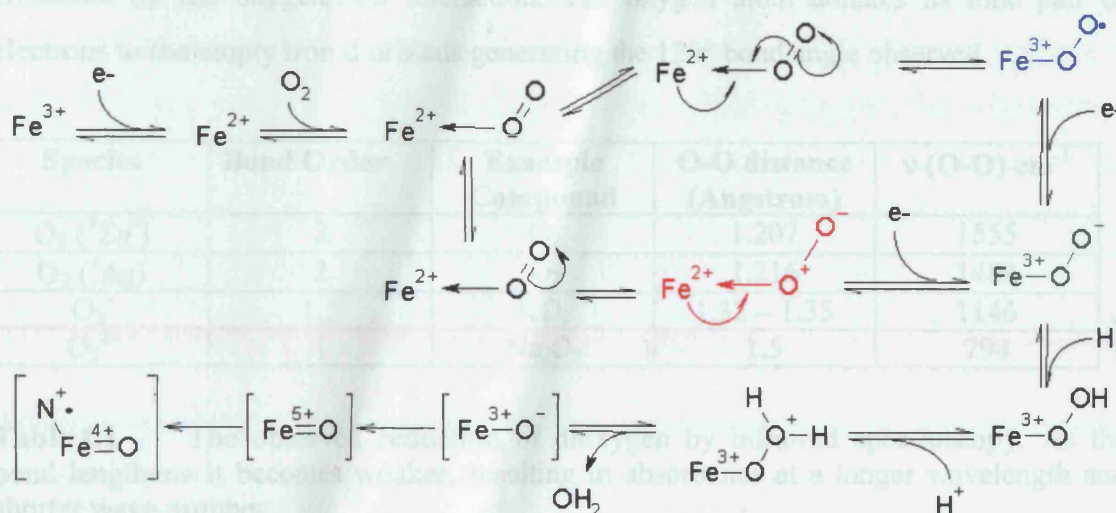


**Figure 1.8** Possible iron-oxygen species involved in the catalytic cycle of P450s. The formation of the ferric-superoxo is shown in blue, the alternative ferrous peroxo is shown in red and the ferric-peroxo in green.

Dioxygen's kinetic inertia is due to the high-energy barrier that has to be overcome for it to react. This high energy barrier is in part due to the strength of the double bond; the first step in the reduction of the double bond is endothermic ( $E^\theta = -0.131\text{V}$ ). The other factor is its paramagnetic property as in the ground state dioxygen exists in a triplet form ( $^3\text{O}_2$ ). In order for dioxygen to react it must become diamagnetic (i.e. singlet form  $^1\text{O}_2$ ) so that reactions are spin allowed [Ingraham and Meyer, 1985]. However, singlet dioxygen is of greater energy than the ground state triplet dioxygen. One way in which spin forbiddenness can be overcome is by complexation with certain

transition metals such as iron.  $\text{Fe}^{2+}$  will readily bind dioxygen due to its  $\pi$  donor ability [Hamilton, 1974]. Upon oxidation of the ferrous iron to ferric iron, the dioxygen molecule is reduced from paramagnetic  $^3\text{O}_2$  to a reactive superoxo species, which can then be further reduced to the peroxo ion.

As observed by infrared spectroscopy, the intra-molecular bond distance of the dioxygen molecule is affected by the reduction of triplet dioxygen. The increase in anti-bonding electron density results in a reduction in the bond order and a lengthening and weakening of the oxygen-oxygen bond. This reduction in bond strength is further enhanced by the oxygen/iron interaction. The oxygen atom donates its lone pair of electrons to the empty iron d orbitals generating the  $120^\circ$  bond angle observed.

Species	Bond Order	Example Compound	O-O distance (Angstrom)	$\nu$ (O-O) $\text{cm}^{-1}$
$\text{O}_2 (^3\Sigma_g^-)$	2	$\text{O}_2$	1.207	1555
$\text{O}_2 (^1\Delta_g)$	2	$\text{O}_2$	1.216	1484
$\text{O}_2^-$	1.5	$\text{KO}_2$	1.32 – 1.35	1146
$\text{O}_2^{2-}$	1	$\text{Na}_2\text{O}_2$	1.5	794

**Table 1.1** The observed reduction of dioxygen by infra-red spectroscopy. As the bond lengthens it becomes weaker, resulting in absorbance at a longer wavelength and shorter wave number.

In P450s, water is weakly associated with the iron in the absence of substrate. The iron exists in a distorted five co-ordinate state with the iron atom lying about 0.4 Angstrom out of the plane of the porphyrin ring [Ortiz de Montellano, 1995]. Oxygen, being a strong field ligand, causes an increase in the splitting energy of the iron atoms d orbitals so that the electrons are energetically favoured to pair up. Hence the low spin ferric super-oxo complex is observed, and as less orbitals are occupied the iron radius decreases.

Another attribute of the iron-dioxygen system that arises due to oxygen's electronegativity is the strong metal-oxygen back bonding that occurs. This is further enhanced by the electron rich ligands (the cysteinyl sulphur and the porphyrin ring) that all increase the electron density on the iron and encourage back bonding to occur. The excess metal electron density is donated into the vacant LUMO on the oxygen. This back

donation strengthens the oxygen/iron sigma bond and reduces the strength of (lengthens) the intramolecular dioxygen bond. By reducing the dioxygen molecule and weakening the intramolecular bond, the heme co-factor increases the reactivity of the dioxygen molecule. Several conserved amide protons moderate the negative charge of the thiolate sulphur ligand. Mutation of these residues (e.g. L358P in P450 CAM) results in an increase in the sulphur's negative charge and a greater 'push effect' as the amount of electron density on the iron increases [Yoshioka *et al.*, 2000]. This causes a decrease in the redox potential of the heme.

Whilst the activation of the dioxygen molecule may be essential for the oxygenation reaction to occur, it also poses further problems. One of these is that as a ferric-superoxo species it has formed an oxygen free radical that could, due to its reactive nature, be potentially very harmful to the cell (oxidant species such as the superoxide anion attack proteins and membranes [Halliwell, 1987]). The other is that metal-superoxo species are unstable and readily form bridging complexes [Hayaishi, 1974]. This is observed with free heme groups derived from haemoglobin where the bridging complex can form and eventually results in deactivation of the oxygen-carrying complex due to the formation of the stable adduct hematin [Nohl and Stolze, 1993]. The substrate binding cleft therefore plays an important function in protecting the reactive superoxo moiety from other cationic metals as well as its role in substrate specificity. The porphyrin ring and cysteine also contribute to the stabilisation of the end-on superoxo complex as, due to their considerable  $\pi$  acceptor properties, they promote the  $\pi$  back donation from iron to dioxygen and so help prevent the formation of end-on bridging peroxo complexes.

The binding and subsequent single electron reduction of dioxygen allows the acceptance of a second electron from the cytochrome's redox partner whereby the ferric-superoxo complex is further reduced to produce the ferric-peroxo species. This further reduction in the bond order causes scission of the dioxygen molecule to generate a molecule of water and an  $\text{Fe}^{5+}$ -oxo species. Water acts as the ultimate source of protons for the reduction of dioxygen. Various uncoupling reactions of dioxygen are promoted by the presence of protein associated as well as free water e.g. mutation of D251 in P450 CAM resulted in a more open active site containing a greater amount of solvent and the amount of uncoupling increased [Vidakovic *et al.*, 1998]. The active site-assisted proton



transfer from amino acid residues and/or water molecules facilitates this stepwise reduction of dioxygen [Gerber and Sligar, 1992, Harris, 2002]. The porphyrin ring is thought to donate an electron to the iron (unstable in such a high oxidation state) becoming a radical cation itself. The iron atom is therefore thought to exist as a highly reactive transient ferryl-oxo species.

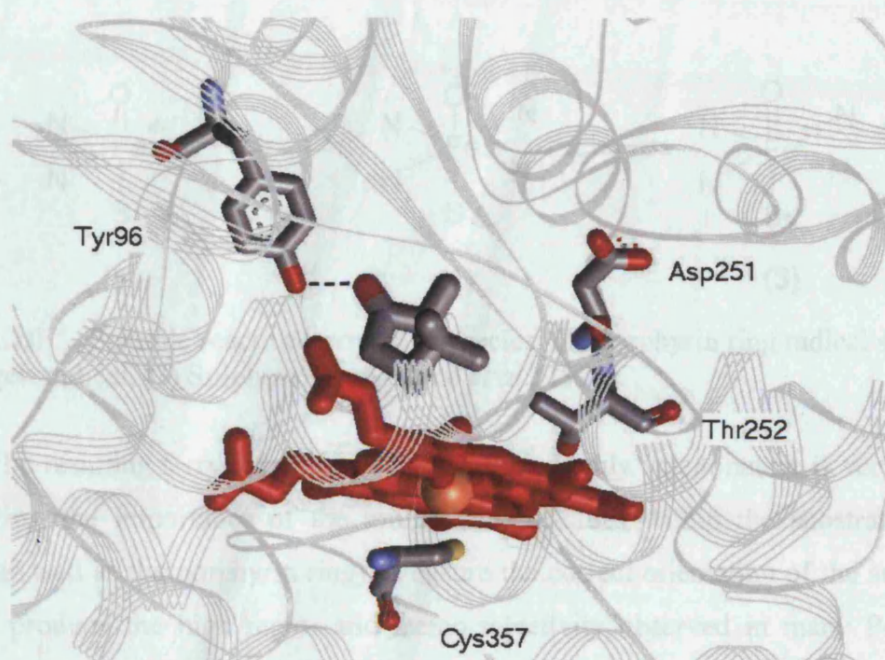


**Figure 1.9** In P450 CAM protons to reduce dioxygen are delivered from the external solvent pool to the bound oxygen via residues Asp251 and Thr252 both located in the distal I helix. Asp251 participates in a series of hydrogen-bond interactions near the molecule's surface [Vidakovic *et al.*, 1998] whilst Thr252 is known to interact with the oxygen intermediate [Hishiki *et al.*, 2000]. Mutation of either causes a reduction in the activity of P450 CAM too less than  $1/10^{\text{th}}$  of wild-type. The substrate, camphor, hydrogen bonded to Tyr96, is also shown.

The ferryl-oxo species is possible due to the stabilising steric bulk of the porphyrin ring and also the delocalisation of the positive charge and unpaired electron through the extensively conjugated  $\pi$  system. Porphyrin is a good  $\sigma$  donor and  $\pi$  acceptor tetradentate ligand for iron, thus aiding the reductive process [Dolphin *et al.*, 1997]. The thiolate ligand, due to its strong electron releasing nature, aids the cleavage of the oxygen-oxygen bond and helps stabilise the ferryl-oxo species.

The reactive iron-oxygen species is not fully characterised due to it being very short lived. Whilst the porphyrin ring is deemed to donate an electron to the iron atom, it is also feasible that an oxygen or sulphur radical could be part of the reactive species (see Figure 1.10). The cysteinyl sulphur would be more easily oxidised than the porphyrin macrocycle based upon thermodynamic data alone [Loew *et al.*, 1977, Ullrich, 1979, White and Coon, 1980].

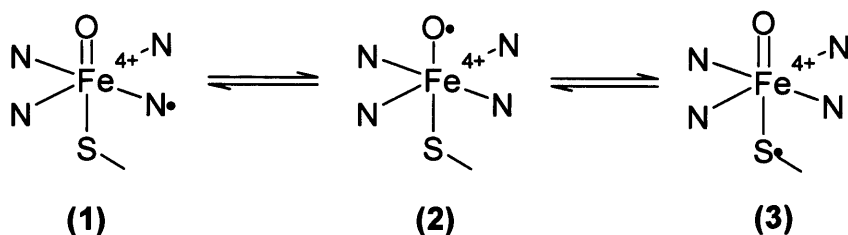


**Figure 1.10** Possible reactive Ferryl-oxo species; (1) Porphyrin ring radical species, (2) Oxygen radical, (3) Sulphur radical [Sono *et al.*, 1996].

The resulting ferryl-oxygen species having a highly valent nature is very reactive, highlighting the importance of the amino acid residues within the substrate binding pocket (as well as the porphyrin ring) to ensure the correct orientation of the substrate in order to produce the high regio- and stereo-selectivity observed in many P450s. The ferryl-oxo species, being very electrophilic, will preferentially attack the most electron rich carbon, i.e. a tertiary alkyl group if allowed (then 2°, then 1°). Mono-substituted aromatic compounds will be attacked mainly at the *ortho*- and *para*- positions.

### 1.3 P450 Redox Partners

The P450 being considered in this work is a class I cytochrome P450 defined as a prokaryotic P450 that, together with its redox partners, is soluble [Munro and Lindsay, 1996]. Electrons are delivered from a molecule of NAD(P)H via a FAD-containing ferredoxin reductase and a small iron-sulphur containing ferredoxin. The movement of electrons occurs down an electro-potential gradient [Ortiz de Montellano, 1995].

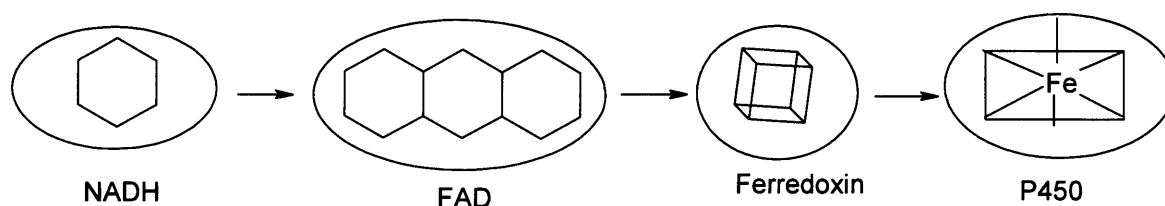


**Figure 1.11** Movement of electrons to reduce bacterial P450s. NAD(P)H is the ultimate electron donor supplying electrons to the *b*-type heme in the P450 via a FAD-containing ferredoxin reductase, and an iron-sulphur ferredoxin.

Where the redox system includes a flavodoxin (fld) or ferredoxin (fdx), the electron transfer to the P450 proceeds by two subsequent one-electron transfer steps. In class I bacterial systems the FAD containing reductase accepts electrons from NAD(P)H in a single two electron step. The fld or fdx is then reduced and transfers the electron to the P450 in two successive steps. For example, adrenodoxin (Adx) transfers a single electron from the reductase to the P450 via a shuttle type mechanism. Adx is known to complex with the P450 by both hydrophobic forces and electrostatic interactions between its carboxylic groups and positively charged groups on the P450's surface [Cao and Bernhardt, 1999]. Chemical cross linking between AdR and Adx has given weight to the shuttle model of electron transfer where Adx has to release, at least partially, AdR before binding and reducing CYP11A1 [Muller *et al.*, 2001].

In the absence of substrate, ferric P450 exists in a low-spin / high-spin equilibrium ( $K = 0.08$  favouring low-spin in the case of P450 CAM) characterised by a high entropy value ( $\sim 30 \text{ Jmol}^{-1}$ ). The redox potential of  $\text{Fe}^{2+} / \text{Fe}^{3+}$  in the P450 resting state is usually around -300 to -400 mV, the apo-protein affecting the exact value. The binding of a substrate causes a positive change in the negative redox potential of the heme (usually to between -250 and -150 mV). The change in redox potential is due to the displacement of the 6<sup>th</sup> coordinate water molecule and the participation of ionisable amino acids lining the substrate-binding pocket. This allows the transfer of an electron from the redox partner to the heme. In P450 CAM the heme iron redox potential rises from -300 mV to -173 mV upon camphor binding [Sligar and Gunsalus, 1976], and the binding of arachidonate to BM3 causes an increase in redox potential of 129mV (from -368 mV to -239 mV) [Daff *et al.*, 1997]. Upon the binding of  $\text{O}_2$ , the resulting

conversion of the ferrous high-spin complex to the ferric low-spin complex causes a further increase in the electro-potential of the heme [Sligar and Gunsalus, 1976].

The redox potential is related to the exposure of the heme to its aqueous surroundings [Lewis and Hlavica, 2000]. Upon removal of the distal aqua ligand due to substrate presence, the remaining axial ligand (thiolate), being a weak ligand, favours high-spin iron. Dehydration of the camphor-binding pocket in P450 CAM caused a 133 mV increase in reduction potential in part due to the decrease in the polarity of the heme [di Primo *et al.*, 1990]. A conformational change and shift of the iron's spin-state (and consequently its redox potential) induced by substrate binding triggers an interaction with the P450's redox partner. The binding of the substrate therefore acts as a control mechanism, promoting the transfer of electrons to the iron.

Usually the sources of electrons in redox reactions (via hydride ion donation) are pyridine nucleotide coenzymes such as NADH (reduced nicotinamide adenine dinucleotide). The phosphate group in NADPH often plays a role in the binding of the compound to the reductase via electrostatic interactions and the adenosine moiety may be bound in an extended or a bent conformation depending on the protein it interacts with. The nicotinamide (niacin) is the active part due to its strong reductive properties. The carbon atom *para*- to the  $sp^2$  hybridised nitrogen of the pyridine heterocycle is particularly reactive, its reactivity is enhanced by the presence of the amide group *ortho*- to it.

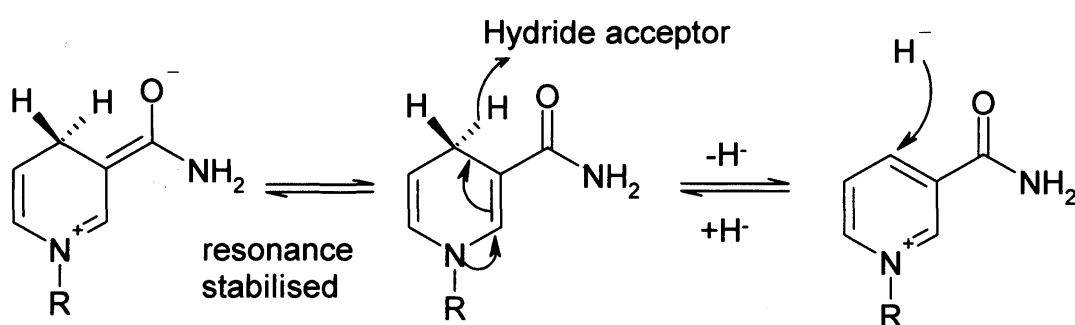


**Figure 1.12** Hydride donor/acceptor properties of the nicotinamide moiety of NAD(P)H [Silverman, 1999].

The flavin systems FAD (flavin adenine dinucleotide) and FMN (flavin mononucleotide) consist of highly conjugated isoalloxazine tricyclic ring systems. This results

in the observed redox properties, as they are strong electron acceptors/donators. Flavins are able to either accept one electron at a time, or two simultaneously. The conjugated ring system gives rise to a relatively strong UV absorbance with the oxidised form (OX) of the flavins appearing yellow and the neutral semiquinone (SQ) form blue [Silverman, 1999]. Anionic semiquinones have a reddish colouration.

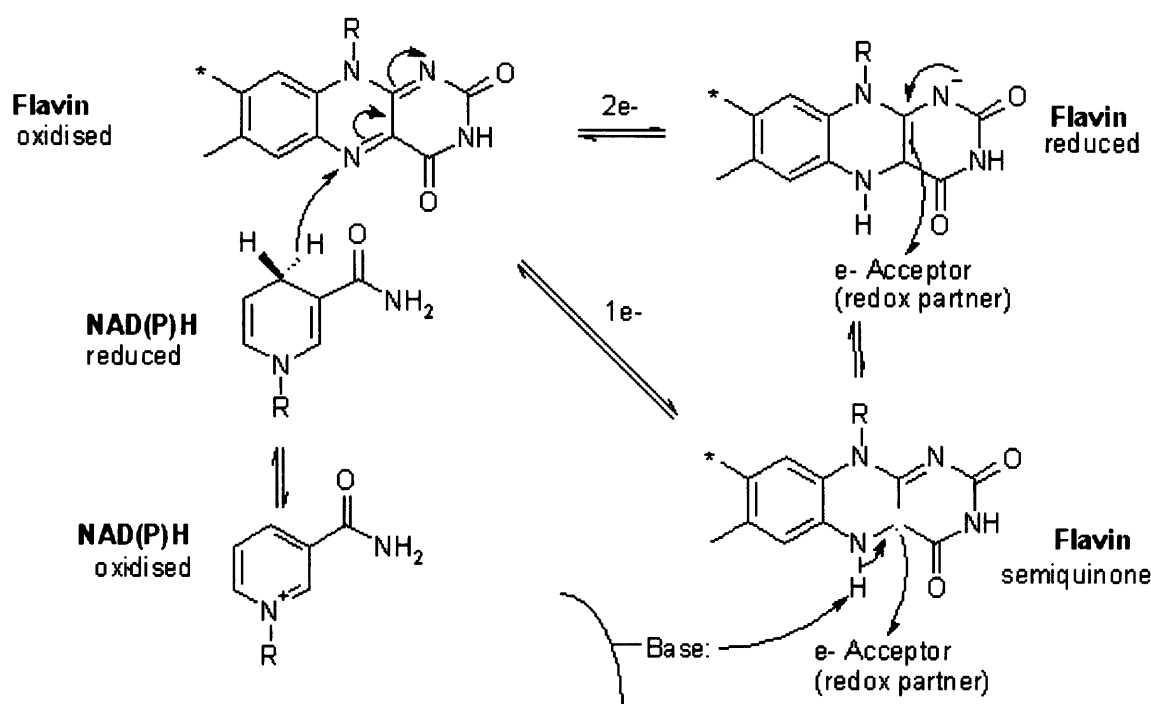


**Figure 1.13** Electron transfer processes from NAD(P)H to flavin cofactors, which can theoretically occur by either a two electron or two one electron steps [Silverman, 1995]. The reduced flavin is planar and the oxidised exhibits the isoalloxazine ring distorted by 30 degrees. With cytochrome P450s and their various reductases, the flavin coenzyme is non-covalently bound, but in some proteins it can be covalently bound to a cysteine or histidine residue at the 8α position (\*).

### 1.3.2 Flavodoxins

In this project two flavodoxins from *B. subtilis* were studied. Flavodoxins (flds) are a group of FMN-containing flavoproteins that function as electron transfer proteins [Mayhew and Tollin, 1992]. They are found in a variety of micro-organisms and eukaryotic algae and sometimes replace ferredoxins (fdxs) under conditions of iron shortage. For example, despite low sequence homology and a size difference of approximately 100 amino acids, the fdx and fld from *Anabaena PCC 7120* have been

shown to substitute for one another in many reactions [Rogers, 1987]. This is thought possible due to the small differences in redox potential (the fdx's  $\text{Fe}^{\text{II}} / \text{Fe}^{\text{III}}$  redox couple being -430 mV [Hurley *et al.*, 1993] and the fld's SQ/HQ couple being -436 mV [Pueyo *et al.*, 1991]) and the small negatively charged surface area they both have, containing residues involved in redox partner binding [Ullmann *et al.*, 2000]. Flds are categorised into two groups depending upon their size, the short-chain flds are typically 14 – 17 kDa in mass whilst the long-chain flds are usually 20 – 23 kDa [Mayhew and Ludwig, 1975]. The FMN cofactor is capable of one or two electron reduction/oxidation and, due to the stabilising effects of the apoprotein, the potential of the one electron reduction of the semiquinone (SQ) form to give the hydroquinone anion (HQ) is low, typically being in the range of -372 to -518 mV (*c.f.* -172 mV for free FMN [Anderson, 1983]). As a result flds typically operate in reactions of low redox potentials (e.g. nitrogen fixation, photosynthesis, sulphite and pyruvate reductases) [Ludwig and Luschinsky, 1992].

Type	Source	E <sub>ox/sq</sub>	E <sub>sq/hq</sub>
Short chain	<i>C. beijerinckii</i> <sup>a</sup>	-92	-399
	<i>D. vulgaris</i> <sup>b</sup>	-103	-438
	<i>D. desulfuricans</i> <sup>c</sup>	-40	-387
Long chain	<i>Anabaena sp.</i> <sup>d</sup>	-196	-425
	<i>Anacystis nidulans</i> <sup>e</sup>	-220	-415
	<i>Chondrus crispus</i> <sup>f</sup>	-222	-370
	<i>E. coli</i> <sup>g</sup>	-170	-410
	Free FMN <sup>h</sup>	-238	-172

**Table 1.2** Redox properties of long and short-chain flds from various organisms. E<sub>ox/sq</sub> is the midpoint potential for FMN oxidised/semiquinone transition (versus normal hydrogen electrode) and E<sub>sq/hq</sub> is the midpoint reduction potential for the semiquinone/hydroquinone transition. Values are taken from: a [Ludwig *et al.*, 1997] b [Curley *et al.*, 1991], c [Caldeira *et al.*, 1994], d [Pueyo *et al.*, 1991], e [Hoover *et al.*, 1999], f [Rogers *et al.*, 1995], g [McIver *et al.*, 1998], h [Anderson, 1983].

In most physiological systems flds function as single electron carriers that cycle only between the SQ and HQ forms without any direct involvement of the oxidised (OX) form. The structure of flds comprises of a central five-stranded parallel  $\beta$ -sheet sandwiched between the four surrounding  $\alpha$ -helices [Watt *et al.*, 1991, Watenpaugh *et al.*, 1976, Hoover and Ludwig, 1997]. At the C-terminus of the  $\beta$ -sheet the FMN cofactor is located and typically held between two aromatic residues, one sited in the 60 loop and the



other in the 90 loop. The loops are  $\beta$ -turns, a type I  $\beta$ -turn flanks the *si* face of the isoalloxazine (the 90 loop, residues 95 – 98 in *D. vulgaris* fld) and a type II  $\beta$ -turn flanks the *re* face (the 60 loop, residues 60 – 65 in *D. vulgaris* fld) [Watenpaugh *et al.*, 1976, Knauf *et al.*, 1996].

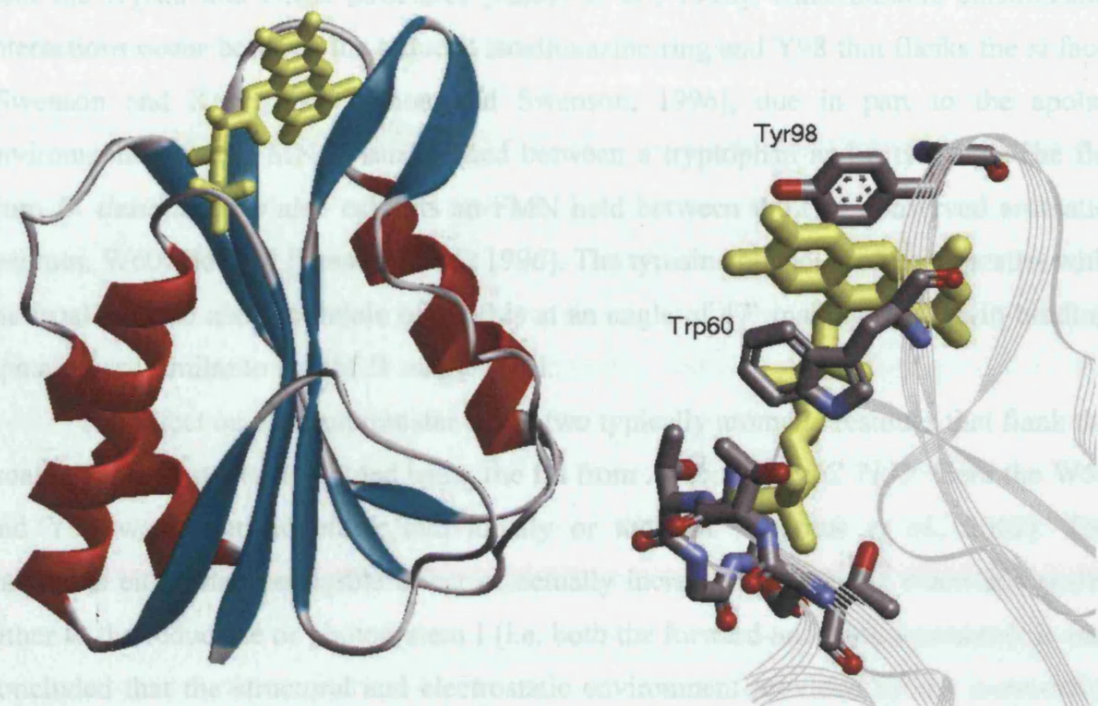


**Figure 1.14** The structure of the fld from *D. vulgaris* [Watenpaugh *et al.*, 1976]. A typical flavodoxin, it consists of a central  $\beta$ -sheet (cyan) surrounded by  $\alpha$ -helices (red). The FMN cofactor (yellow) is shown sandwiched between the two loops of the apoprotein. The detail of the FMN binding region (on right) shows the isoalloxazine moiety sandwiched between the aromatic residues (Trp60 and Tyr98) and the residues of the phosphate binding motif (Ser10 – Thr15).

The FMN is non-covalently bound but is strongly associated with the apoprotein ( $K_d$  values *ca.* 1 nM [Mayhew and Tollin, 1992]) via electrostatic, aromatic and hydrogen bonds. The FMN binding site in *D. vulgaris* fld (a 147 amino acid, 16.3 kDa protein) has the following structural components; S10 – T15 that provide hydrogen and electrostatic bonds to the negatively charged phosphate group (a dianion at pH 7), and also a second segment, S58 – D62 and D95 – G103 providing the residues that flank either face of the isoalloxazine ring [Watenpaugh *et al.*, 1976]. The pyrimidine moiety of the FMN forms hydrogen bonds to the peptide backbone of the residues D95, Y100 and C102 [Ruterjans *et al.*, 1996]. The dimethyl moiety of the FMN and part of its ribityl side chain are

located on the surface of the protein whilst the pyrimidine part is pointed towards the inner of the molecule and is less solvent exposed. The isoalloxazine is planar and, in this fld, sandwiched between the two aromatic molecules W60 and Y98. In the oxidised structure the aromatic side-chain of W60 diverges almost 45° from coplanarity as seen in both the crystal and NMR structures [Knauf *et al.*, 1996]. Unfavourable electrostatic interactions occur between the reduced isoalloxazine ring and Y98 that flanks the *si* face [Swenson and Krey, 1994, Zhou and Swenson, 1996], due in part to the apolar environment, as the FMN is sandwiched between a tryptophan and a tyrosine. The fld from *D. desulfuricans* also exhibits an FMN held between the two conserved aromatic residues, W60 and Y98 [Romero *et al.*, 1996]. The tyrosine phenol is almost parallel with the isoalloxazine and the indole of W60 is at an angle of 47° making this flavin-binding domain very similar to that of *D. vulgaris* fld.

The effect on electron transfer of the two typically aromatic residues that flank the isoalloxazine ring was examined using the fld from *Anabaena PCC 7119*. Here the W57 and Y94 were mutated either individually or together [Causaus *et al.*, 2002]. The mutations either had negligible effect or actually increased the rate of electron transfer either to the reductase or photosystem I (i.e. both the forward and back reactions). It was concluded that the structural and electrostatic environment provided by the aromaticity gave an efficient compromise between cofactor retention and the speed of electron transfer. The thermodynamic effect of the mutations with respect to the redox potential of the FMN cofactor was a significant factor in the alteration of the kinetics. In the fld from *C. beijerinckii*, a methionine flanks the *re* face of the isoalloxazine ring and an interaction between the methionine sulphur and the aromatic ring exists [Burnett *et al.*, 1974, Ludwig *et al.*, 1997]. Mutation of this methionine (M56) has shown it to be involved in modulation of the redox potential not only via its sulphur-flavin interaction, but also through steric, conformational and polarity effects [Druhan and Swenson, 1998]. As the protein is reduced the build-up of negative charge on the flavin renders the aromatic – sulphur interaction less favourable. Other principal interactions in this fld are the hydrogen bonds that exist between the N(5)H of the reduced flavin and the peptide of G57, the amide back-bone of E59 and the flavin C(4)O, and from N(3)H to E59 [Smith *et al.*, 1976, Kasim and Swenson, 2001].



In the HQ form of *D. vulgaris* fld the FMN is bound as an anion with the charge localised near N(1). This HQ complex is destabilised relative to the SQ form due to charge repulsions between the HQ FMN and the negatively charged residues in the flavin-binding site of the apoprotein [Vervoort *et al.*, 1986]. These charged acidic residues, in addition to the unfavourable interaction between the negatively charged 5'-phosphate group of the FMN and its N(1) atom, hinder the formation of the HQ anion [Moonen *et al.*, 1984]. Free energy calculations have shown the SQ form of the flavin cofactor to be bound strongly relative to the OX form and that the HQ form is bound the weakest (partly due to its negative charge) [Chang and Swenson, 1999]. The HQ is believed from NMR studies to remain unprotonated down to pH 4.6 [Yalloway *et al.*, 1999]. The bound HQ form of FMN is more planar than when free in solution [Moonen *et al.*, 1984] with greater destabilisation of the HQ complex seen when the pH of the solution is below that of the apparent pKa [Yalloway *et al.*, 1999].

The phosphate-binding site is a highly conserved area composed mainly of serine and threonine residues, where hydrogen bonding between their hydroxyl groups and the phosphate oxygen's predominates. A key fingerprint motif for the binding of the phosphate is T/S-X-T-G-X-T with a few exceptions such as the fld from *Helioacter pylori* where an alanine replaces a threonine, which cannot form the usual hydrogen bond with the phosphate oxygen. In this fld side chain atoms from N14 and D142 form hydrogen bonds to the ribityl chain [Freigang *et al.*, 2002].

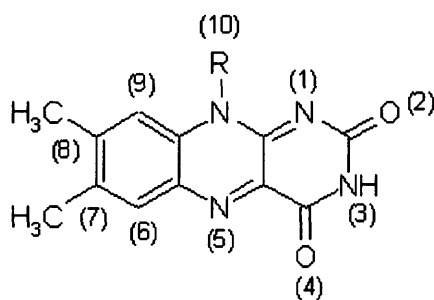


**Figure 1.15** The backbone structure of the flavin ring in its oxidised form showing the conventional numbering. R indicates the position of the ribityl chain.

NMR work combined with computer modelling of FMN and its derivatives have shown that the OX form is planar in all protonation states due to electron delocalisation and not because of its location within the protein. The SQ radical is also planar whilst the

HQ form is bent with a ring puckering of  $27.3^\circ$  along the N(5) and N(10) axis. This ring puckering relieves the electron repulsion and an equilibrium may exist between planar and puckered forms when free in solution, the protein environment forcing the planar state [Zhang and Ornstein, 1996]. Indeed, the neutral HQ form of FMN when free in solution has been calculated to be bent along the N(5) – N(10) axis by  $25 - 27^\circ$  with the energy barrier to inversion being less than  $6.5 \text{ kcalmol}^{-1}$  [Zhang and Ornstein, 1996, Rizzo, 2001].

In several flds the FMN is observed to form a new hydrogen bond between its N(5)H and the carbonyl oxygen of a residue (typically glycine or asparagine) upon its reduction. A change in the protein's conformation, known as the peptide flip, usually results (see Figure 1.16) [Watt *et al.*, 1991, Smith *et al.*, 1977, Luschinsky *et al.*, 1992]. The redox potential for the OX/SQ couple at pH 7.0 is affected by whether a glycine or an asparagine acts as the N(5)H proton acceptor. Flds that have an asparagine often have a redox potential of around  $-221 \text{ mV}$  (close to that of free FMN at  $-238 \text{ mV}$ ) whilst those with a glycine have a potential between  $-41$  and  $-143 \text{ mV}$  [Mayhew and Tollin, 1992].

Mutagenesis experiments have included altering the N(5)H proton-accepting glycine residue to see how the residue affects the functioning of the fld. In *D. vulgaris* mutation of this residue, G61, to an asparagine caused the SQ form to be less stable than the wild type [O'Farrell *et al.*, 1998]. Structural studies showed that in the OX form of the wild type, the carbonyl group of the glycine is directed away from the FMN cofactor. Upon reduction to the SQ the peptide flip occurs, resulting in the glycine moving to point towards the N(5), being just  $2.7 \text{ Angstrom}$  away. The residue remains in this conformation upon addition of the second electron to form the HQ, although the bond distance increases. Mutants where G61 was replaced by residues with longer side-chains all showed destabilisation of the SQ form. The reduction of the fld caused a large movement, a near doubling back of the loop containing the residues 60 – 65 (known as the 60 loop). In *D. vulgaris* the conformation of this loop is very constrained and in all the glycine mutants an unfavourable interaction between the additional  $\text{C}\beta$  atom and the carbonyl oxygen of W60 and S64 was observed. Reduction of the mutant crystals with dithionite caused them to bleach and crack indicating a structural change. In the wild type this conformational change is driven by the N(5) of the flavin being protonated upon

reduction and, as a result, an unfavourable H-H interaction with the NH of D62 is caused. In the mutants the distance from the N(5) of the flavin to the NH of D62 was reduced by around 0.6 Angstrom resulting in an increase in repulsion [O'Farrell *et al.*, 1998].

The fld from *D. desulfuricans* also exhibits a conformational change upon reduction due to a peptide flip of the G61 – M62 bond as the carbonyl of G61 moves to point towards the protonated N(5)H of the SQ form. The new orientation also provides a favourable hydrogen bonding interaction between the G61(NH) and the O(4) of the FMN group mediated by a water molecule.

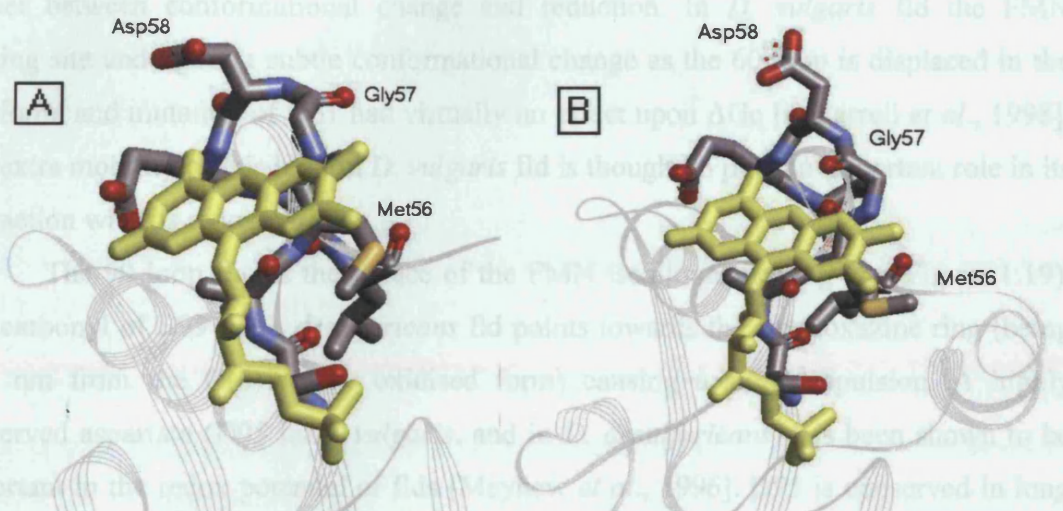


**Figure 1.16** Reduction of the fld from *C. beijerinckii* results in a peptide flip as Gly57 changes its conformation. In the oxidised protein the carbonyl oxygen of Gly57 points away from the FMN (1). Upon reduction it moves, pointing towards the protonated N(5) of the flavin (2). The residues Ser54 to Leu61 are shown, their conformation altered as a consequence of the hydrogen bond formation [Ludwig *et al.*, 1997].

In fld from *C. beijerinckii*, mutants of the equivalent glycine (G57) showed little or no change in structure upon reduction. The FMN binding loop in this fld is known to be capable of adopting three different conformations. One conformation (where the O(57) is stabilised by a hydrogen bond to N137) is unique to this fld, the other two (O(57) points either towards or away from the flavin) are equivalent to the SQ and OX forms of the *D. vulgaris* fld, respectively. All three of these conformations are seen as a mixture in the OX form of *C. beijerinckii* fld indicating that there is little of an energy barrier between them. In the reduced state the structure consists only of the type II' turn (O(57) *trans-up*). The fld from *C. beijerinckii* has an unusually high  $E_{OX/SQ}$  potential of  $-92$  mV.

This redox potential is modulated by conformational energies caused by the interaction of the G57 peptide and the flavin. Energy differences between the *cis*, *trans*-down and *trans*-up conformers ( $\Delta G_c$ ) and between the interactions of the FMN with each conformer ( $\Delta G_i$ ) all affect the potential. Mutation of G57 has a large effect on the  $E_{OX/SQ}$  potential with the free energies of the SQ form increasing by about 1.3 kcal/mol [Ludwig *et al.*, 1997]. Substitution of this glycine causes a steric clash to occur between the C $\beta$  atom and the NH of the adjacent residue when in the reduced conformation [Kasim and Swenson, 2000]. As a result, mutating this residue caused an increase in the energy barrier between conformational change and reduction. In *D. vulgaris* fld the FMN binding site undergoes a subtle conformational change as the 60 loop is displaced in the OX form, and mutation of G61 had virtually no effect upon  $\Delta G_c$  [O'Farrell *et al.*, 1998]. The extra mobility of this loop in *D. vulgaris* fld is thought to play an important role in its interaction with its redox partners.

The 90 loop flanks the *si* face of the FMN isoalloxazine ring (see Figure 1.19). The carbonyl of E99 in *D. desulfuricans* fld points towards the isoalloxazine ring (being 0.29 nm from the O(4) in the oxidised form) causing a slight repulsion. A highly conserved aspartate (D95 in *D. vulgaris*, and in *D. desulfuricans*) has been shown to be important in the redox potential of flds [Mayhew *et al.*, 1996]. D95 is conserved in long chain flds, its function being to modulate the redox potential via the interaction of its negative side chain with the N(1) of FMN and its electrostatic interaction with Y98, preventing the phenol group rotating to form a more favourable edge-to-face orientation with the isoalloxazine ring [McCarthy *et al.*, 2002].

Upon neutralising the side-chain of D95, a positive shift in the SQ/HQ couple was seen [Zhou and Swenson, 1995]. D95 provides the closest negative charge to the N(1) and O(2) of the FMN. All mutants of this residue showed a convergence of the two redox potentials indicating destabilisation of the SQ form. D95 is thought to contribute to the stability of the type I  $\beta$ -turn of the 90 loop. The carboxylate group forms a hydrogen bond to the amide and oxygen group of S97 [McCarthy *et al.*, 2002]. In *D. desulfuricans* fld the distance from the N(1) of the FMN to HN(D95) is too long for a favourable interaction to occur, which is thought to partly explain the differences in the redox potentials between this fld and that of *D. vulgaris*.



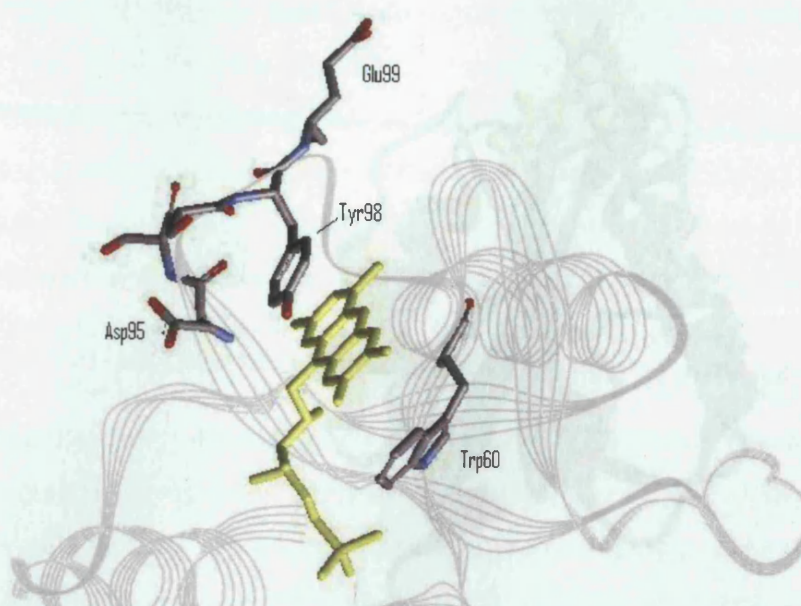


**Figure 1.17** Detail of the 90 loop in *D. vulgaris* fld [Watenpaugh *et al.*, 1976]. Glu99 causes a slight repulsion of the flavins O(4), whilst Asp95 is known to form a hydrogen bond to Tyr98 and the flavin's N(1).

The corresponding residue D90 in the long chain fld from *Anacystis nidulans* interacts with the N(1), O(2), and O(4) of the flavin, being six Angstrom or less away. Mutation to an asparagine caused little change to the  $E_{\text{OX/SQ}}$ , but a larger change (+ 41 mV) to the  $E_{\text{SQ/HQ}}$  due to the loss of the charge repulsion. There was no effect on the binding affinity of the cofactor in any redox state [Hoover *et al.*, 1999].

Long chain flds have a 20 residue segment inserted in the middle of the fifth strand of the central  $\beta$ -sheet. In all the structures of the long chain flds solved to date the N(5) of the oxidised FMN is hydrogen bonded to a main chain NH or side chain O $\gamma$ 1 group. *E. coli* fld is a 19.7 kDa protein with the FMN held between W57 and Y94 and other aromatic residues (Y59 and Y97) also present in its vicinity cause the cofactor to be buried within a hydrophobic environment [Hoover *et al.*, 1997, Osborne *et al.*, 1991]. The secondary structure of *E. coli* fld in solution is very similar to other long chain flds from *A. nidulans* and *Anabaena PCC 7120* with whom it shares approx. 44 % amino acid sequence identity [Ponstingl and Otting, 1997]. It has extra carboxy terminal residues though, which form a short helix of unknown function.

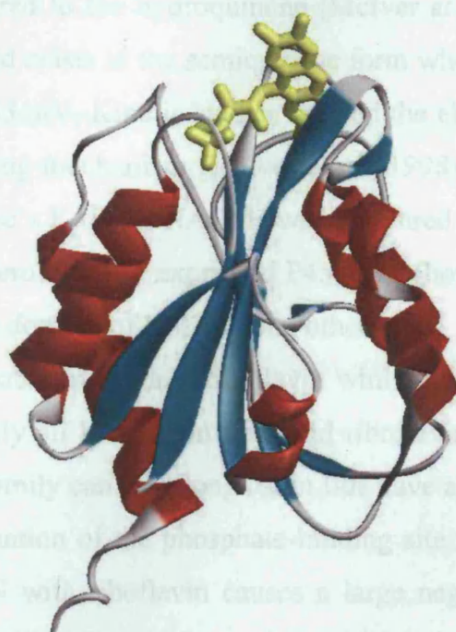


**Figure 1.18** The structure of *E. coli* flavodoxin [Hoover *et al.*, 1997]. As a long-chain flavodoxin it has an additional helix (helices shown in red) at the carboxy terminus and an insert in the fifth strand of the  $\beta$ -sheet (cyan). However, the environment around the FMN (yellow) is not so altered and the SQ/HQ redox potential is not very different from that of the short chain flds (see table 1.2).

The structure of the long chain fld from *A. nidulans* showed that this fld also exhibits a peptide flip and corresponding rearrangement of hydrogen bonds upon reduction. In this fld the N58-V59 peptide bond rotates to give the SQ conformation with O(58) pointing up to form a hydrogen bond with the N(5)H. This hydrogen bond is very strong, raising the pK<sub>a</sub> from 8.5 (free FMN) to around 13.1, and serves to counteract the repulsive dipole interactions between CO(N58) and C(4)-O(4) in the O-up conformer [Hoover *et al.*, 1999]. As in all long chain flds, the extra five residues inserted in the 90 region of *A. nidulans* fld create a more non-polar environment disfavoured the formation of the HQ anion and giving the low SQ/HQ potential.

Despite *E. coli* not containing any endogenous P450s, its reductase system (flavodoxin NADP<sup>+</sup> oxidoreductase (FldR) and flavodoxin (Fld)) is capable of supporting the function of heterologously expressed P450s [Ingleman *et al.*, 1997]. The *E. coli* fld acts as a single electron shuttle to the P450 alternating between its semiquinone form and oxidised form *in vitro*. Redox potentiometry showed strong stabilisation of the FMN



semiquinone form compared to the hydroquinone [McIver *et al.*, 1998]. Approximately 80 % of the FMN in the fld exists in the semiquinone form when coupled to the reductase with the  $E_{SQ/HQ}$  being  $-285$  mV. Kinetic studies showed the electron transfer through the fld to occur via a ping-pong mechanism [McIver *et al.*, 1998]. The rate of the reduction of the flavodoxin reductase's FAD by NADPH was measured as  $>20$  s<sup>-1</sup>. The system has been used to turnover heterologously expressed P450 c17 (bovine hydroxylase) [Jenkins *et al.*, 1994] and the heme domain of BM3 among others.

Some flds are capable of binding riboflavin whilst others are specific for the 5'-phosphate group. Generally all long chain flds bind riboflavin, but only the *D. vulgaris* fld from the short chain family can. The long chain flds have a more apolar FMN binding site although the conformation of the phosphate-binding site remains similar in all flds. The replacement of FMN with riboflavin causes a large negative change in the redox potential ( $E_{SQ/HQ}$  is  $-180$  mV) due to the loss of the phosphate-N(1) interaction described above and destabilisation of the semiquinone riboflavin complex. The binding of FMN to the apoprotein is slower than the binding of riboflavin, as the phosphorylated flavin is hindered in its access to the binding site, but the phosphate chain stabilises the resulting complex. The phosphate group of FMN aids the binding and retention of the cofactor in the correct orientation. The phosphate group induces a conformational change in the apoprotein and a phosphate or similar dianion (from buffer) is thought necessary for riboflavin binding. The 5'-phosphate group of FMN adds stability to the fld by reducing (via electrostatic and hydrogen bonds) the mobility of the ribityl chain of the cofactor. The binding of both riboflavin, FMN and riboflavin 3',5'-bisphosphate to the *D. vulgaris* apoprotein is very tight with the  $K_d$  values being of the order  $10^{-7}$ ,  $10^{-10}$  and  $10^{-9}$  M respectively [Pueyo *et al.*, 1996].

A dianion from the buffer is required for riboflavin binding to the *D. vulgaris* apoenzyme, stabilising the resulting complex. Compared to the native fld, the riboflavin-apoenzyme complex has a more positive SQ/HQ redox couple. Negative shifts of the SQ/HQ couple are as a result of an energetically disfavoured HQ anion. This may be due to unfavourable electrostatic interactions with the cofactor's phosphate groups [Vervoort *et al.*, 1986] and, as seen with *D. vulgaris* Y98 mutants, where the hydrophobic/aromatic nature of the binding site is lost [Zhou and Swenson, 1996]. The N(5) position was more

solvent exposed in the riboflavin complex in all redox states *c.f.* the native FMN complex [Chang *et al.*, 2001]. This gave a weakening or loss of the N(5) – backbone peptide hydrogen bond. The N(3)H hydrogen bond to Y100 was found to be stronger in the riboflavin complex and this interaction, relative to FMN, increased upon reduction to the HQ form.

The structures of the *D. vulgaris* apoflavodoxin with FMN or riboflavin bound differed at the isoalloxazine-binding region [Walsh *et al.*, 1998]. A change in the positioning of the 60 loop of the riboflavin complexes allowed greater solvent exposure of the cofactor and the loss of several hydrogen bonds. The greater solvent exposure aids moderation of unfavourable electrostatic interactions and hence an increase in the stability of the HQ riboflavin complex relative to the other redox states.

Structures of the apoprotein of flds show that the protein can fold to a conformation close to that of the native enzyme. The only significant differences have been found in the FMN binding region where, in the apoflavodoxin from *Anabaena PCC 7119*, the two aromatic residues W57 and Y94, that usually sandwich the isoalloxazine ring, pack together to reduce their solvent exposure, a sulphate or phosphate anion occupying the ribityl chain-binding site [Maldonado *et al.*, 1998].

### **1.3.2 Ferredoxins**

Iron- sulphur clusters in redox enzymes mediate the transfer of single electrons. They consist of one (rubredoxins) or more (ferredoxins) atoms of iron ligated by sulphur (sulphido- or thiolato-sulphur or both) [Silver, 1993]. Rubredoxins are found in bacteria, being low molecular weight proteins (<20 kDa) with redox potentials of around –50 mV [e.g. Eidsness *et al.*, 1999]. Ferredoxins often are comprised of the cubane type structures (Fe<sub>2</sub>S<sub>2</sub>)<sub>n</sub> showing strong structural similarity regardless of ligand type or oxidation level. In *P. putida* the ferredoxin (putidaredoxin [Pdx]) is a 106 residue globular protein containing a [2Fe-2S] cluster [Martinis *et al.*, 1996] Terpredoxin (Tdx) an 11.1 kDa, [2Fe-2S] cluster-containing protein shuttles electrons to P450 terp, in a system similar to that of Pdx and P450 CAM. The ferredoxins associated with P450 SU1 contain the more unusual [3Fe-4S] cluster [O’Keefe *et al.*, 1991] and a seven-iron fdx containing both a [4Fe-4S] plus a [3Fe-4S] cluster was found in *S. griseus* and supports P450 activity



[Trower *et al.*, 1990]. The fdx from the host of P450 BioI, *Bacillus subtilis*, contains a [4Fe-4S] cluster [Green *et al.*, 2003]. In the case of P450 CAM, the reductase, Pdx and the P450 are co-ordinately regulated and co-transcribed [Koga *et al.*, 1989]. This is also the case in *S. griseolus* where the two ferredoxins associated with P450 SU1 and SU2 are co-transcribed as they accumulate under the same conditions as their associated P450 [O'Keefe *et al.*, 1991].

The ferredoxins are a group of small electron transfer proteins of 80 to 130 residues in length. They tend to cycle between the Fe<sup>II</sup>/Fe<sup>III</sup> oxidation states at the metal cluster, their redox potentials being governed by a variety of factors such as hydrogen bonds between backbone and side chain groups to the metal cluster sulphur atoms, solvent accessibility and the presence of charged residues around the cluster. Plant-type ferredoxins consist of a common structural motif; a mixed four-stranded  $\beta$ -sheet and a long  $\alpha$ -helix packed across one face of the sheet [Muller *et al.*, 1999]. The structure of bovine adrenodoxin (truncated) displays a compact  $\alpha$  and  $\beta$  fold typical of a mammalian 2Fe-2S fdx, which is organised into two domains, a core (N-terminal lobe) and an interaction (C-terminal lobe) domain [Kostic *et al.*, 2002]. Plant type ferredoxins show high similarity amongst themselves (~ 79 %) and exhibit redox potentials in the range of -305 to -455 mV.

```

TERPREDOXIN    ---PRVVFIDEQSGEYAVDAQDGQSLMEVATQNGV-PGIVAECGGSCVCATCRIEIEDAW 56
PUTIDAREDOXIN  ---SKVVVYSHDGTRELDVADGVSLMQAAVSNGI-YDIVGDCGGSSACATCHVVYNEAF 56
ADRENODOXIN    EDKITVHFINRDGETLTTKGIGDSLDDVVQNNLDIDGFGACEGTLACSTCHLIFEQHI 60
SUBTILIS        -----MAKYTIVDK-----DTC---IACGACCGAAAPDIY 26
SPINACH         -AAYKVTLLVTPTG-NVEFQCPDDVYILDAAEEGI--DLPYSCRAG-SCSSCAGKLK--- 52
               * : . . . . . * . * : *

TERPREDOXIN    V---EIVGEANPDENDLLQSTGEPMTAGTR---LSCQVFIDPSMDGLIVRVPLPA- 105
PUTIDAREDOXIN  T---DKVPAANEREIGMLECVTAELKPNSR---LCCQIIMTPELDGIVVDVPDRQW 106
ADRENODOXIN    F---EKLEAITDEENDMLDLAYG-LTDRSR---LGCQICLTCKAMDNMTVRVP---- 105
SUBTILIS        DYDDEGIAFVTLDENKGVVEVPEVLEEDMIDAFEGCPTDSIKVADEPFEGDPLKFE 82
SPINACH         -----TGSLNQDDQSFLD--DDQIDEGWV---LTCAAYPVSDVTIETHKKEELTA 97
               . : : : : *
```

**Figure 1.19** A sequence alignment (performed using Clustal W [Thompson *et al.*, 1984]) of five ferredoxins from various bacteria and plants. The cysteines that ligate the iron-sulphur cluster are highlighted in red. The conserved sequence typical of FeS cluster containing proteins being CXX(XXX)CXXC. Amino acids of a similar chemical nature are marked with a semicolon and those of lesser similarity with a dot. The unusual 4Fe-4S cluster of the ferredoxin from *B. subtilis* is evidenced by the dissimilar N-terminus.



All plant-type fdxs are acidic proteins with overall negative charges of between -12 and -28. They contain several surface aspartate and glutamate residues, some of which are neutralised by salt bridges. In mammalian fdxs a solvent filled depression lies above the metal cluster lined by conserved residues (e.g. adrenodoxin [Muller *et al.*, 1999]). In the plant-type fdxs this depression extends into a channel leading from the surface to the core of the protein. The solvent molecules that fill it are involved in hydrogen bonding networks, some of which aid the attachment of the metal cluster to the apoprotein [Rypniewski *et al.*, 1991]. Plant-type fdxs contain a rudimentary, bipartite interaction domain that consists of the  $\alpha$ -helix f and the C-terminal helix k. These contain the residues F65 and E94 that are fundamental to reductase binding. Compared to plant-type fdxs, the metal binding loop in vertebrate fdxs is usually three residues longer. This is thought due to it interacting with a greater variety of redox partners [Muller *et al.*, 1999].

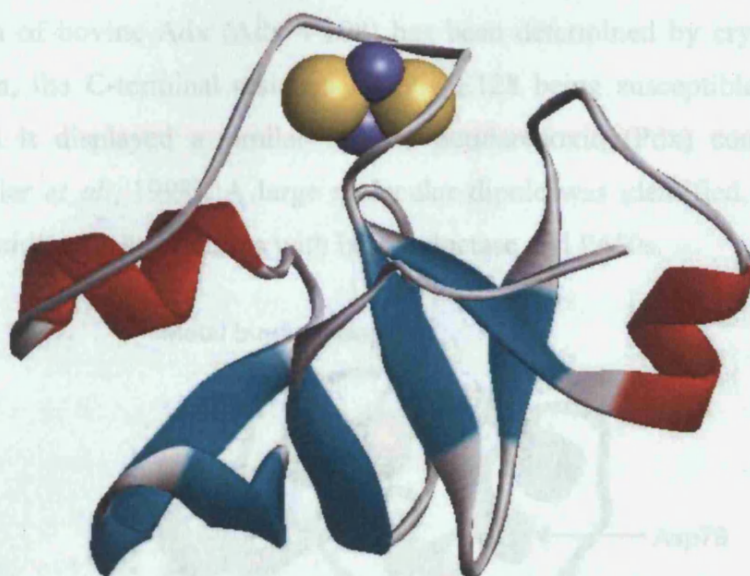


**Figure 1.20** The structure of a typical [2Fe-2S] ferredoxin, in this case that from spinach [Binda *et al.*, 1998]. The iron-sulphur cluster (purple and orange) is near the surface of the protein, ligated by four cysteine residues (Cys39, 44, 47 and 77). The protein's secondary structure consists of sheets (cyan), loops (grey) and helices (red).

Ferredoxin I from spinach has been used as a redox partner for P450 BioI in this work (see section 3.19). Spinach contains two fdxs involved in photosynthesis. Both are two iron, two sulphur [2Fe-2S] fdxs. Ferredoxin I has been studied on its own and fused



to its native reductase. The latter produced a chimeric protein that exhibited an ability to reduce cytochrome *c*, a property unique to the fusion protein [Aliverti and Zanetti, 1997].

Adrenodoxin (Adx) is a 14 kDa [2Fe-2S] fdx that is synthesised in the cytoplasm of cells in the adrenal cortex (as a precursor protein) and becomes localised in the matrix of mitochondria. As redox partner to CYP11A1, CYP11B1 and CYP11B2 it is instrumental in steroid biosynthesis [Bernhardt, 1996]. The recognition and interaction between Adx and its redox partners is mainly due to the presence of the negatively charged acidic surface residues (D72, E73, D76 and D79) that participate in electrostatic interactions with positively charged residues on the reductase or P450 [Lambeth and Kriensin, 1985]. A tyrosine residue (Y82) is necessary for its interaction with the P450s [Beckert *et al.*, 1994]. The reduction of the metal cluster of Adx is linked to conformational changes in the bulk of the protein via a hydrogen-bonding pathway that is mediated by H56 and includes Y82 [Miura and Ichikawa, 1991]. The structure of a truncated form of bovine Adx (Adx 4-108) has been determined by crystallography to 1.85 Angstrom, the C-terminal residues D109 - E128 being susceptible to proteolytic digestion, and it displayed a similar fold to putidaredoxin (Pdx) consisting of two domains [Muller *et al.*, 1998]. A large molecular dipole was identified, believed to be important in guiding its interactions with both reductase and P450s.

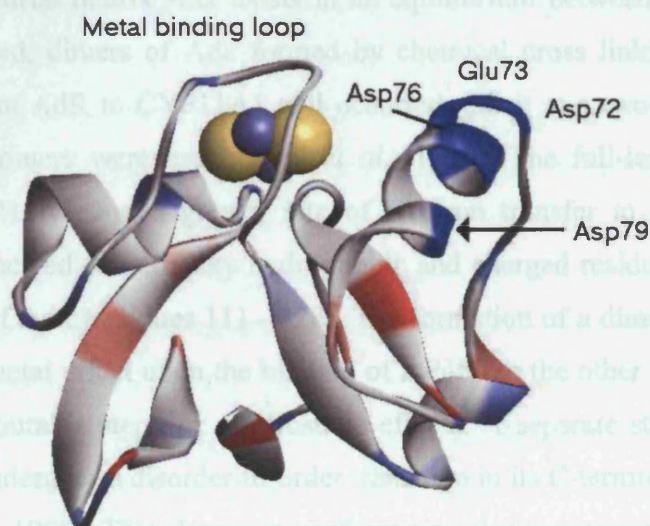


**Figure 1.21** The structure of bovine Adx with the residues involved in redox partner binding highlighted (Asp72, Glu73, Asp76 and Asp79) [Muller *et al.*, 1998] The proximity of the interaction domain to the iron-sulphur cluster (orange and purple) can be

seen, the metal binding loop containing three of the four conserved cysteine ligands is also labelled. Apoprotein coloured according to charge where red is positive and blue negative.

In Adx, Fe1 is thought to be the atom favoured for electron transfer due to its positioning and polar environment. In all fdxs there is a greater amount of hydrogen bonds between the ligands of Fe1 than those of Fe2, thus stabilising its reduced state [Holden *et al.*, 1994]. Adx is reported to have a potential of -273 mV (full length [Uhlmann *et al.*, 1997]). The structure of the truncated form of Adx (4-108) showed a greater similarity to the plant-type fdxs than predicted, as it shares less than 25 % amino acid identity [Holden *et al.*, 1994]. It retains the same overall fold as other [2Fe-2S] fdxs, the largest amount of deviation is in the interaction domain, probably reflecting the differences in the various redox partners [Grinberg *et al.*, 2000].

The structure of the full-length form of Adx was subsequently determined, although only a further three amino acids could be assigned by molecular replacement techniques [Pikuleva *et al.*, 2000]. This crystal structure showed extensive interactions between the two molecules in the asymmetric unit. The C-terminal part of each Adx monomer extends across the other molecule, being placed very close to the residues involved in interactions with the P450s. This, and hydrodynamic data, lead to the belief that in the mitochondrial matrix Adx exists in an equilibrium between monomeric and dimeric forms. Indeed, dimers of Adx formed by chemical cross linking, showed that electron transfer from AdR to CYP11A1 still occurred, albeit at a two fold slower rate than when the monomers were used [Hara *et al.*, 1989]. The full-length form has a weaker  $K_d$  for CYP11A1 and a greater rate of electron transfer to CYP11B1 when compared to the truncated form. Bulky hydrophobic and charged residues constitute the C-terminal portion of Adx (residues 111 - 128). The formation of a dimer via this region could have a detrimental effect upon the binding of a P450 to the other molecule of Adx as a result of unfavourable steric or electrostatic effects. A separate study showed that human ferredoxin undergoes a disorder-to-order transition in its C-terminal residues upon reduction [Xia *et al.*, 1998]. This change in conformation that accompanies the change in redox state is thought to have an effect on the association/dissociation with redox partners. Dimeric Adx molecules were observed to form spontaneously when Adx was



expressed on the surface of *E. coli* as a monomeric fusion protein with the translocation unit of the AIDA-I (adhesion involved in diffuse adhesion) autotransporter [Jose *et al.*, 2002]. Addition of AdR and CYP11A1 allowed synthesis of pregnenolone to be observed ( $0.21 \text{ h}^{-1}$ ).

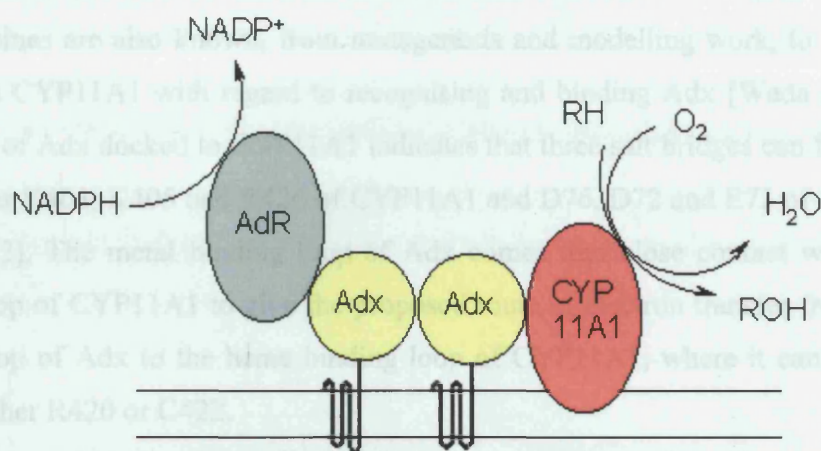


**Figure 1.22** Cartoon representation of the cell surface dimer of Adx when fused to AIDA-I in *E. coli*, used to support the function of exogenously expressed CYP11A1 [Jose *et al.*, 2002].

The structure of a chemically cross-linked Adx-AdR complex has been determined by crystallography, allowing the site of interaction to be identified [Muller *et al.*, 2001]. The interface between the two proteins is comprised of polar residues with Adx being in contact with both domains of AdR. Three regions of interaction were identified. The first is composed of polar contacts between the NADP<sup>+</sup> domain (in AdR) and the interaction domain of Adx. The second region also consisted of many polar interactions between the core domain of Adx and the FAD-binding domain of AdR (in this region the chemical crosslink exists between Adx D39 and AdR K27). The third region consists of the C-terminus of Adx lying in a cleft between the two globular domains of AdR. Some hydrogen bonding was found between the residues binding the metal cluster in Adx and those binding the isoalloxazine ring of the FAD in AdR. The two domains of AdR showed a small rotation of  $3.7^\circ$  when complexed with Adx, a movement that causes a reduction of 2.4 Angstrom in the distance between two residues (R240 and K27) known to be crucial to Adx binding.

Site directed mutagenesis has confirmed that the acidic residues D79, D76, E73 and D72 in Adx play an important role in charge driven interactions with AdR, where R240 and R244 have been identified as the key basic residues [Brandt and Vickery, 1993]. K243 is known to be a key residue in AdR as studies have shown that chemical modification of this residue inhibited the transfer of electrons to Adx [Hamamoto *et al.*, 1984]. Lysines are also known, from mutagenesis and modelling work, to be important residues in CYP11A1 with regard to recognising and binding Adx [Wada *et al.*, 1992]. Modelling of Adx docked to CYP11A1 indicates that three salt bridges can form between the residues K403, K405 and R426 of CYP11A1 and D76, D72 and E73 of Adx [Usanov *et al.*, 2002]. The metal binding loop of Adx comes into close contact with the heme binding loop of CYP11A1 to give the proposed route of electron transfer from the metal binding loop of Adx to the heme binding loop of CYP11A1, where it can travel to the iron via either R420 or C422.

The metal binding loop affects a fdx's ability to bind and receive/donate electrons to its redox partners. The loop surrounding the metal cluster in bovine Adx contains a threonine (T49) as its central residue [Muller *et al.*, 1998]. This residue is highly conserved amongst [2Fe-2S] ferredoxins. Deletion mutants of this and the other metal binding loop residues were made (E74Δ, G48Δ, T49Δ, L50Δ and A51Δ) [Zollner *et al.*, 2002]. By deletion of a single residue the loop becomes similar to a plant-type four-residue loop. In all the mutants conformational changes around the iron-sulphur cluster had occurred. The deletion of any residue reduced Adx's ability to interact efficiently with its redox partners, the effect being greater upon its interaction with CYP11A1 as opposed to the reductase. Despite the binding affinity of the Adx mutants to AdR being 3-fold higher than wild type, the rate of electron transfer was reduced by 6- to 20-fold. The mutants all showed a lowering of their redox potentials to be within the range typical of the plant-type ferredoxins. The redox potentials were thought altered mainly due to altered solvent accessibility of the FeS cluster and new hydrogen bonding networks.

The interaction between class one P450s and their redox partners is thought fairly specific, due to the individual redox potentials of the two proteins and also to the interactions required for the successful but brief docking of one protein to another [Schiffler *et al.*, 2001]. The best-known example of this specificity is that of the



interaction between P450 CAM and putidaredoxin (Pdx). Pdx (a 11.6 kDa, [2Fe-2S] fdx) is not replaceable by other electron donors e.g. Adx (who has almost 33 % amino acid sequence identity) and spinach fdx, despite them being low potential FeS proteins with high homology to Pdx [Stayton *et al.*, 1990]. Both of these proteins have shown themselves to be capable of passing a single electron to P450 CAM to generate the ferrous form, but are unable to donate a second electron thereby making functional turnover unobtainable. Alternatively, cytochrome *c* and rubredoxin are incapable of giving the first electron but can provide the second [Lipscomb *et al.*, 1976]. Several acidic residues in the metal binding loop of Pdx are known to be important in its interaction with P450 CAM and, likewise, certain arginines on the surface of CAM are required for the mediation of their association [Stayton *et al.*, 1989].

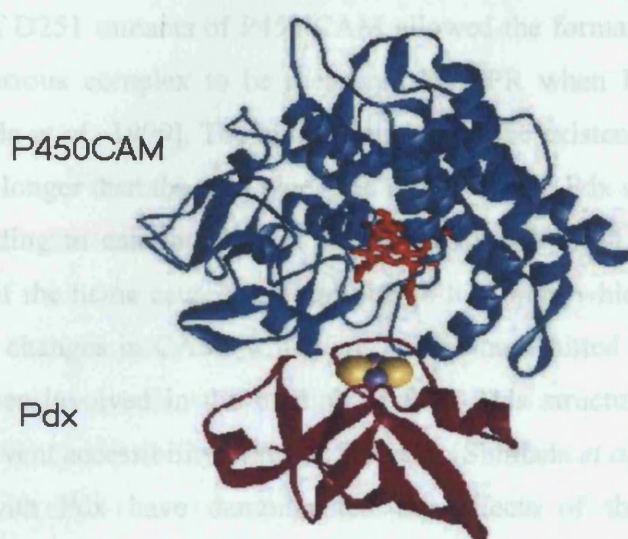


**Figure 1.23** The geometry of the Pdx-P450CAM complex (modelled) showing Pdx (maroon) docking to P450 CAM (blue) on the face of the protein under the cysteine-ligated heme (red) plane [Roitberg *et al.*, 1998]. The iron-sulphur cluster of Pdx is shown in space-fill (yellow and purple).

Pdx has two different binding sites for associating with the reductase and the P450 as it shuttles electrons between the two. Pdx binds to P450 CAM in a 1:1 complex with a  $K_d$  of 2.9  $\mu\text{M}$  at 298 K [Sligar and Gunsalus, 1976]. Upon the one electron reduction of Pdx the binding constant decreases to 0.49  $\mu\text{M}$  [Sligar and Gunsalus, 1976, Nakamura *et al.*, 1994]. Negatively charged residues on its  $\alpha$  helical segment as well as hydrophobic and steric effects are responsible for its interactions with the reductase



[Stayton and Sligar, 1990], whilst specific hydrogen bonds from the surface loop near the iron-sulphur cluster provide its interactions with the P450 [Aoki *et al.*, 1998].

Pdx has a redox potential of -240 mV and this has been shown to increase to -196 mV when it is bound to P450 CAM due to the FeS cluster becoming buried within the interface of the two proteins. This allows efficient transferral of the reducing equivalent to substrate-bound P450 CAM ( $E^0 = -173$  mV) at a rate of  $30\text{ s}^{-1}$  (under CO-saturated conditions, fully camphor bound). Raman spectroscopy has shown that camphor bound CAM becomes partially low spin upon the binding of oxidised Pdx [Unno *et al.*, 1997]. In the case of P450 BioI the opposite has been observed when its native ferredoxin (Fer) was bound, a high spin shift being measured [Green *et al.*, 2003]. This shift from low to high spin has also been observed upon the binding of Adx to substrate free CYP11A1. The generation of D251 mutants of P450 CAM allowed the formation of a catalytically competent oxy-ferrous complex to be measured by EPR when Pdx was used as the reductant [Shimada *et al.*, 1999]. The mutants supported the existence of the complex for around 500 times longer than the wild type. The FeS cluster in Pdx underwent a structural change upon binding to camphor bound oxy-ferrous P450 CAM. In this complex the oxygen ligation of the heme causes its transition to low spin, which is accompanied by several structural changes in CAM, which are in turn transmitted to Pdx via R112 and R109, two residues involved in the binding of Pdx. This structural change causes an increase in the solvent accessibility of the FeS cluster [Shimada *et al.*, 1999].

Studies with Pdx have demonstrated the effects of the protein's physical environment on its redox potential. The redox potential for Pdx has been shown to shift from -240 mV to -196 mV upon its binding to camphor-bound CAM. The dissociation constant between reduced Pdx and oxidised CAM increases by about 100 times when both are oxidised. NMR studies of Pdx [Popchapsky *et al.*, 2001] showed that a slowing of protein dynamics and a compaction of the metal binding region upon reduction contributed to its tighter interaction with CAM. Reaction entropies showed that Pdx is capable of undergoing conformational changes as thought necessary by its role as an electron transfer protein to different redox partners [Reipa *et al.*, 2000].

NMR studies of Pdx showed the greatest conformational changes upon reduction were in the C-terminal cluster [Popchapsky *et al.*, 2001]. W106 is the C-terminal residue

and has been shown to be important in Pdx-CAM interactions. This residue fits into a groove between A46 and V74 in oxidised Pdx, moving out of this groove upon reduction. Two glycine residues (G40 and G41) in the metal binding loop are crucial to the flexibility of this region. Upon reduction of the metal cluster the NH groups of G41, A43 and A46 move away from the cluster and the NH groups of S42, S44, and T47 closer. Their NH protons form H bonds to the cysteinyl sulphur atoms ligating Fe1 of the cluster (C39 and C45) with the strength of the H bonds increasing as the negativity of the cluster increases. These interactions cause a contraction of the loop, which has an effect upon the dynamics of adjacent regions. In a fdx from an *Anabaena sp.*, a single peptide bond in the metal cluster undergoes a reorientation when the protein is reduced [Morales *et al.*, 1999]. This movement allows the NH proton to form an additional hydrogen bond to the metal cluster.

The route of electron transfer from putidaredoxin to P450 CAM has been the subject of many theories and investigations [e.g. Baldwin *et al.*, 1991, Halliwell, 1991, Davies and Sligar, 1992, Pochapsky *et al.*, 1994]. Experiments carried out with the Pdx/P450 CAM system have shown that aromatic C-terminal residues in Pdx give tighter association between the reduced Pdx and the P450 than non-aromatic mutants. Upon the binding of Pdx to P450 CAM, Pdx's C-terminal tryptophan indole ring (W106) becomes hidden from solvent. The aromatic residue was not found to contribute to the actual electron transfer step itself [Davies and Sligar, 1992], but increases the affinity between the reduced Pdx and the P450. This resulted in 5-fold higher rate constants for reduction [Davies and Sligar, 1992]. This tighter association could be due to the energies of the redox states being changed (differential desolvation as the aromatic residues shielded the FeS from the aqueous media), the desolvation of the aromatic residues (transferral from the aqueous environment to the protein one), the smaller loss of conformational entropy required to immobilise an aromatic residue than a more flexible side chain, or a combination of all factors. When Pdx W106 was mutated or deleted, no great change in redox potential was observed [Davies *et al.*, 1990].

The W106 of Pdx is between 8 and 10 Angstrom away from the nearest iron in the FeS cluster [Pochapsky *et al.*, 1994] approaching the limit for direct electron transfer. The structure of reduced Pdx is little changed from its oxidised form. Mutants where

W106 was replaced with a variety of residues exhibit lowered activities despite structural analysis showing that the metal cluster had remained intact and the reduction potential was unchanged [Davies and Sligar, 1992].

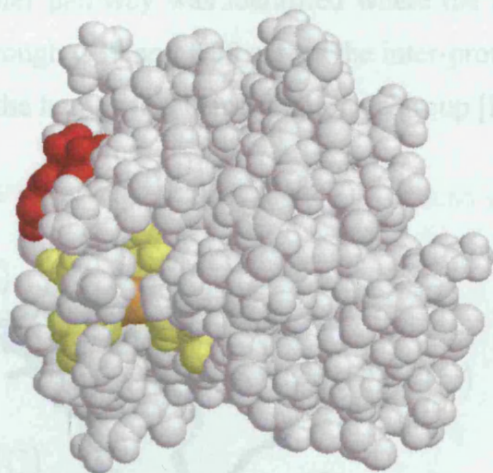


**Figure 1.24** NMR derived model of Pdx. The iron-sulphur cluster (orange) is ligated by four cysteines (yellow) with the W106 shown in red [Pochapsky *et al.*, 1999].

The binding site of Pdx to P450 CAM is believed to be on the proximal surface of the P450 near to the axial thiolate and heme prosthetic group [Tosha *et al.*, 2002, Stayton *et al.*, 1989]. In more recent modelling work it was found that Pdx and P450 CAM contain electrostatically complementary regions on their surfaces. These regions overlap strongly with regions in the proteins that contain likely electron transfer residues close to the redox centres [Roitberg *et al.*, 1998].

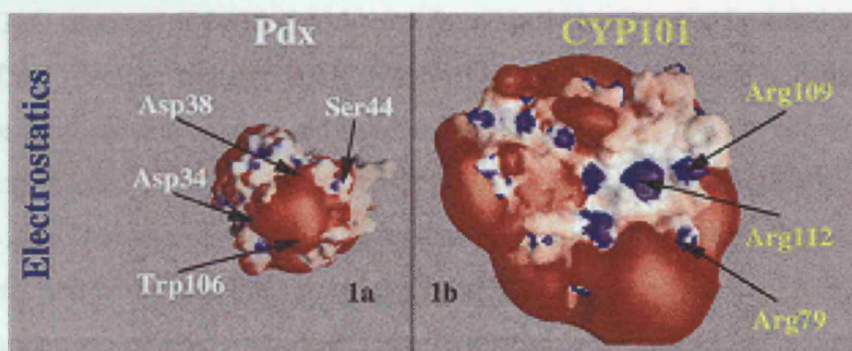


**Figure 1.25** Poisson-Boltzmann Electrostatic contour plots (red = -2 kcal/mol) for Pdx (a) and P450 CAM (b) (red = -2 kcal/mol, blue = +2 kcal/mol). The triangular region in



Pdx comprises negative potential residues Asp34, Asp38 and Trp106. There are patches of positive potential in the proximal face of P450 CAM [copied from Roitberg *et al.*, 1998].

An electron transfer pathway was identified where the electron moves from the 2Fe-2S cluster in Pdx through C39 and D38 across the inter-protein interface to R112 (in P450 CAM) and then to the heme via a heme propionate group [Roitberg *et al.*, 1998].

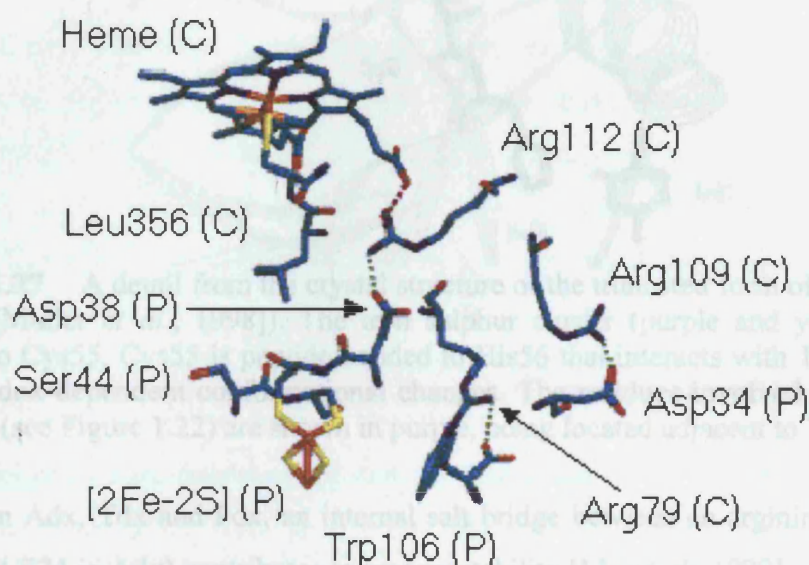


**Figure 1.26** Geometry of the Pdx-CYP101 complex showing the three ionic bridges thought responsible for binding. Adapted from [Roitberg *et al.*, 1998]. Residues belonging to CYP101 are labelled (C) and to Putidaredoxin (P).

R112C mutants of P450 CAM were found to have a poorer interaction with Pdx, the rate of the electron transfer being 1/400 of that of the wild-type and the  $K_d$  of the mutants for oxidised Pdx was raised several fold [Koga *et al.*, 1993, Unno *et al.*, 1996]. R112, being located on the surface of P450 CAM, is hydrogen bonded to one of the propionate side chains of its heme cofactor and plays a role in electron transfer from Pdx via its interaction with D38 (Pdx) [Aoki *et al.*, 1998].

Comparison of Pdx with other ferredoxins showed that Pdx has a high degree of homology with Terpredoxin (Tdx) and they share a similar overall topology [Mo *et al.*, 1999]. With Tdx and Pdx, the most notable structural differences between the two

proteins are in the regions involved in redox partner docking: the C-terminus. Tdx has greater similarity to Adx in this region, having a more random structure. The C-terminal, interaction, region of vertebrate ferredoxins are all very compact regions stabilised by intermolecular interactions such as hydrogen bonds and electrostatics.

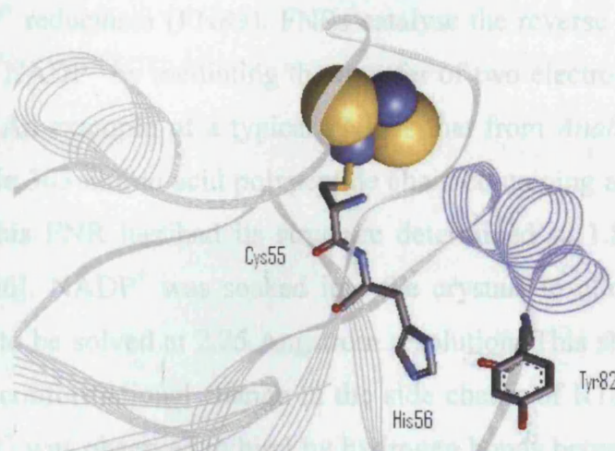


**Figure 1.27** A detail from the crystal structure of the truncated form of Adx (residues 5 – 108, [Muller *et al.*, 1998]). The iron sulphur cluster (purple and yellow) is shown ligated to Cys55. Cys55 is peptide bonded to His56 that interacts with Tyr82, thought to cause redox-dependent conformational changes. The residues involved in redox partner docking (see Figure 1.22) are shown in purple, being located adjacent to Tyr82.

In Adx, Tdx and Pdx, an internal salt bridge between an arginine and glutamate (R89 and E74 in Adx) contributes to protein stability [Mo *et al.*, 1999] and the conserved histidine in Adx and Pdx takes part in the important redox-modulated hydrogen-bonding network (H56 in Adx, H49 in Pdx). This histidine hydrogen bonds to Y82 (equivalent to position 49 in Tdx) in Adx and has been shown to be important in redox-regulated hydrogen bonding networks. Via hydrogen bonds with its imidazole group, H49 is thought to act as a mechanical linker between the metal binding loop and the C-terminal cluster [Miura and Ichikawa, 1991]. In Tdx the histidine is replaced by an arginine, a much stronger base. The decrease in conformational dynamics upon reduction is less for Tdx than either Pdx or Adx and it is believed that this is due the substitution of histidine for arginine [Kostic *et al.*, 2002]. The greater flexibility of the arginine side chain enables a dampening of the contraction of the metal binding loop, so its effect on the second domain is diminished.

### 1.3.3 Reductases

In typical class I P450 redox systems, the electrons are initially obtained via the oxidative dehydrogenation of NAD(P)H by a FAD-containing reductase. These reductases are evolutionarily related and, often as a result, structurally similar to plant ferredoxin NADP<sup>+</sup> reductases (FNRs). FNRs catalyse the reverse reaction, the reductive hydrogenation of NADP<sup>+</sup> by mediating the transfer of two electrons from photosystem I via a ferredoxin. An example of a typical FNR is that from *Anabaena* PC 7119, which consists of a single 303 amino acid polypeptide chain containing a non-covalently bound FAD cofactor. This FNR has had its structure determined to 1.8 Angstrom resolution [Serre *et al.*, 1996]. NADP<sup>+</sup> was soaked into the crystals to allow the structure of an 'active complex' to be solved at 2.25 Angstrom resolution. This showed NADP<sup>+</sup> binding to cause a slight conformational change in the side chains of R100, R224, R233, Y235 and Q237. NADP<sup>+</sup> was observed to bind by hydrogen bonds between the protein and the adenosine and 2'-phosphate moieties of NADP<sup>+</sup>. The nicotinamide and isoalloxazine are stacked against each other, the nicotinamide in turn being stacked against the side chain of F178. It was noted that hydride transfer from the isoalloxazine to the nicotinamide would necessitate movement of the flavin cofactor and/or the NADP<sup>+</sup> substrate towards one another causing the flavin- and NADP<sup>+</sup>-binding domains to actually move apart. This motion would result in the nicotinamide becoming sandwiched between the isoalloxazine and Y303 [Serre *et al.*, 1996].

In the *Anabaena* system the fdx binds in the cleft between the FAD and NADP<sup>+</sup>-binding domains of the reductase, making contact with both domains. Chemical cross-linking studies showed that residues K53, R77 and K294 are involved in fdx binding [Medina *et al.*, 1992]. Most of the residues required for fdx binding are invariant and both R77 and K294 are conserved in all known FNRs. A crystal structure of *Anabaena* fdx and FNR complexed together revealed a redox sensitive association, the fdx undergoing a redox-dependant conformational change [Morales *et al.*, 2000].

The overall structure of FNRs from photosynthetic organisms is highly conserved. The structures of FNRs from *Anabaena* PCC 7119 and spinach show high similarity in the FAD and NADP<sup>+</sup> binding sites and also in the large hydrophobic cavity in the C-terminus thought necessary for membrane interaction. The conformation and



environment of the FAD are very similar, with its C(7) and C(8) methyl groups being solvent exposed and the stacking of Y79 and Y303 (*Anabaena* numbering) with the isoalloxazine. The N(5) of the flavin interacts with a conserved serine known to be essential for productive FAD to NADP<sup>+</sup> interactions and a cysteine found in both FNRs (C261 in *Anabaena*) necessary for the correct positioning of the nicotinamide to allow hydride transfer [Aliverti *et al.*, 1993].

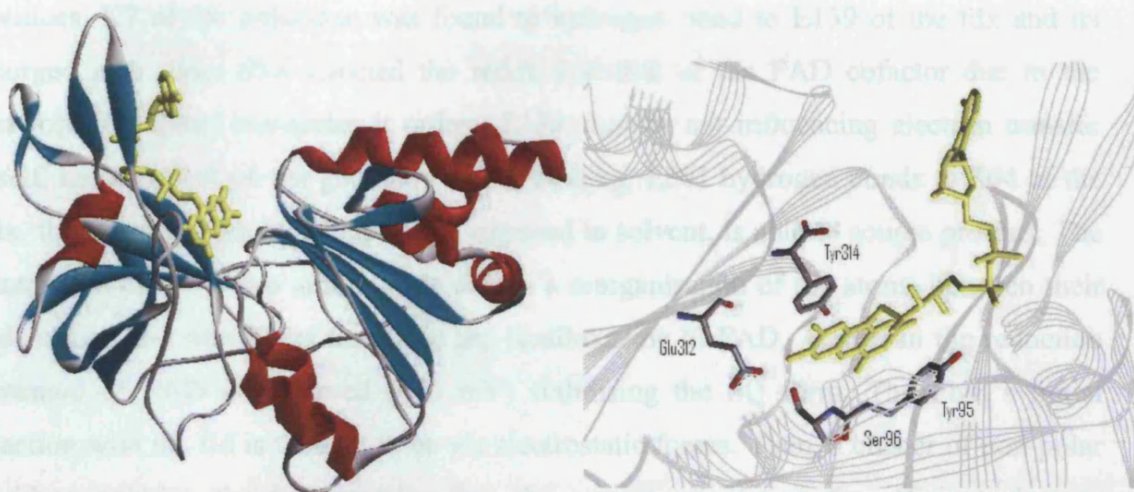


**Figure 1.28** The structure of spinach FNR as resolved by x-ray crystallography [Bruns and Karplus, 1995]. The protein is composed of  $\beta$ -sheets (cyan),  $\alpha$ -helices (red) and loops (grey) with the FAD cofactor (yellow) held in one domain. The FAD binds in an extended conformation as can be seen in the detail on the right. The O(4) of the FAD hydrogen bonds to Tyr95 and Ser96 interacts with the *si* face whilst Tyr314 covers the *re*-face. Glu312 interacts with the NADPH substrate.

Studies on the FNR from spinach have clarified the roles of several invariant residues. S96 is required for nicotinamide binding and charge transfer complex stabilisation. Y95 both interacts with the *si* face of the isoalloxazine and hydrogen bonds to the 4'-OH group. The C-terminal Y314 covers the *re*-face of the isoalloxazine and E312 is necessary for correct binding of NAD(P)H having a minor effect on the flavin's redox potential [Aliverti *et al.*, 1998, Mayoral *et al.*, 2000]. The tyrosine that typically stacks against the *re*-face of the isoalloxazine in FNRs is displaced upon the binding of NADP<sup>+</sup>. In the NADP<sup>+</sup> bound structure of pea FNR, the nicotinamide ring lies against the isoalloxazine's *re*-face at an angle of 30 degrees [Arakaki *et al.*, 2001]. The *si*-face of the isoalloxazine interacts with Y89 in this FNR via  $\pi$ - $\pi$  stacking, its 4'-ribityl hydroxy being



hydrogen bonded to the tyrosine's hydroxyl via K110, orientating the latter residue for interaction with NADP<sup>+</sup>. Y89 adopts the favoured edge-to-face interaction with the isoalloxazine, its aromatic nature necessary for FAD binding.

The interaction of FNR from *Anabaena PCC 7119* with its fdx was studied via mutagenesis of certain charged residues [Faro *et al.*, 2002]. The interface between the two proteins consists of mainly hydrophobic residues plus several conserved charged residues. K7 of the reductase was found to hydrogen bond to E139 of the fdx and its charged side chain also affected the redox potential of the FAD cofactor due to the network of solvent molecules it orders. E139, despite not influencing electron transfer itself, has an effect on the geometry of fdx binding. E301 hydrogen bonds to S64 of the fdx, the latter's hydroxyl group, being exposed to solvent, is able to source protons. The interaction of these two amino acids causes a reorganisation of the atoms between their side-chains and introduces torsion in the isoalloxazine of FAD. A shift in the reduction potential of FAD is observed (+25 mV) stabilising the SQ form. The FNR's initial reaction with the fld is thought to be via electrostatic forces. Then, a cluster of non-polar residues position the two proteins into the correct orientation for efficient electron transfer by establishing hydrophobic interactions, a secondary mechanism that is only possible once the ionic effects have brought the proteins close enough to one another [Nogues *et al.*, 2003]. In the FNR, the hydrophobic residues are L76, L78 and V136, which have all been shown necessary for this correct alignment with the fld.

The flavodoxin reductase (FldR) from *E. coli* shares little sequence similarity with the FNRs bar a sequence of four amino acids (R46 - S49) that are highly conserved within the FNR family. These residues are known to bind the isoalloxazine and influence the electron transfer process. S49 of FldR was found through mutagenesis to play a similar role to its homologue in the FNRs, interacting with the flavin's N(5) atom and affecting electron/hydride transfer. Its mutation to alanine caused a reduction in the  $k_{\text{cat}}$  for NADPH oxidation [Niviere *et al.*, 1996]. A second fingerprint motif observed in both FNRs and FldR is the C-terminal glycine rich region (G<sup>110</sup>-G-T-G<sup>113</sup> in FldR) known to interact with the pyrophosphate bridge of the nicotinamide.

The x-ray crystal structure of *E. coli* FldR showed the 27.6 kDa protein to consist of two domains (an FAD-binding and NADP<sup>+</sup>-binding domain), joined by a single

covalent linkage [Ingleman *et al.*, 1997]. It was noted that the two domains were orientated differently to one another and that the FAD was bound differently compared to that of the other FNRs. In FldR the O(2) of FAD hydrogen bonds to T116, and Y247 covers more of the isoalloxazine, being hydrogen bonded to S53. The FAD also adopts an unusual bent conformation as opposed to the typical extended one, the adenosine bent back to hydrogen bond to the N(1) of the isoalloxazine. *E. coli* FldR also has a shorter loop between the F $\beta$ 1 and F $\alpha$ 1 helices, a loop usually involved in binding the adenosine moiety. In FldR the C-terminal residue interacts with the adenosine instead.

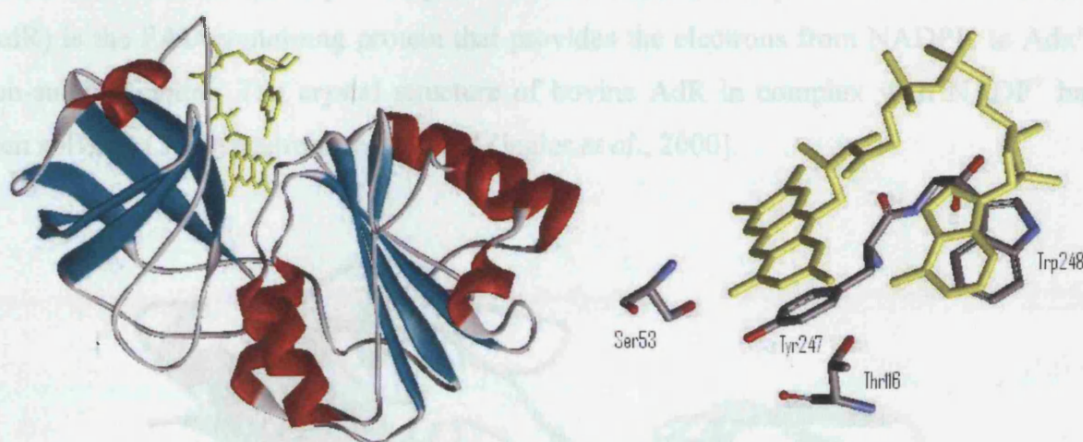


**Figure 1.29** The structure of *E. coli* FldR as solved by x-ray crystallography [Ingleman *et al.*, 1997]. On the left the whole protein is shown with the FAD cofactor (yellow) bound in the groove where the substrate NADPH will also bind. On the right a close-up of the binding of FAD showing the unusual bent conformation thought due to the adenosine bending back to hydrogen bond to the isoalloxazine.

The majority of the FAD in FldR exists in the hydroquinone form *in vivo*, being able to accept two reducing equivalents from the NAD(P)H hydride ion. The redox potential of the two-electron reduction of the FAD is  $-300$  mV, a little more positive than the  $\text{NADP}^+/\text{NADPH}$  couple ( $-317$  mV) [McIver *et al.*, 1998]. FldR's redox partner FldA is believed to bind in the depression between the two domains where its negatively charged glutamate and aspartate residues (E95, E127, D134) interact with the FldR's positive ones (R237, R238, R239). These residues in FldR are also thought to interact with  $\text{NADP}^+$  and the binding of the nicotinamide may regulate the redox properties of the flavin. Mutation of these charged residues caused a reduced ability to bind  $\text{NADP}^+$  and



reduce cytochrome *c* [Leadbeater *et al.*, 2000]. R174 is a highly conserved residue within the NADP<sup>+</sup>-dependent members of the FNR family, interacting with the 2'-phosphate group. The crystal structure of FldR showed the side-chain of the C-terminal tryptophan (W248) to block the NADP<sup>+</sup> binding site [Ingleman *et al.*, 1997]. In an R174A mutant the tryptophan fluorescence spectra and CD profile were altered and the NADPH dissociation constant lowered. This implied that W248 had undergone some degree of relocation suggesting the involvement of this terminal tryptophan in the regulation of the binding and subsequent release of NADP<sup>+</sup> [Leadbeater *et al.*, 2000].

Many steroid biosynthetic mitochondrial P450s utilise the iron-sulphur containing protein Adx as their redox partner [Lambeth and Kamin, 1979]. Adrenodoxin reductase (AdR) is the FAD containing protein that provides the electrons from NADPH to Adx's iron-sulphur centre. The crystal structure of bovine AdR in complex with NADP<sup>+</sup> has been solved to 1.7 Angstrom resolution [Ziegler *et al.*, 2000].



**Figure 1.30** Structure of an NAD(P)H reductase (bovine Adrenodoxin reductase), with the FAD cofactor (yellow) and NADP<sup>+</sup> (navy) bound. The NADPH binds in the characteristic Rossman fold of the enzyme [Ziegler and Schulz, 2000]. The protein is composed of  $\alpha$ -helices (red),  $\beta$ -sheets (cyan) and loops (grey).

As with *E. coli* FldR, the protein consists of two domains both containing a central  $\beta$ -sheet surrounded by  $\alpha$ -helices, and an FAD cofactor. However, AdR does not share the typical fold of the other members of the FNR family. In AdR the NADP<sup>+</sup> binds in an extended conformation with its adenine and nicotinamide rings in an anti-conformation as seen in glutathione reductase and its related proteins [Senda *et al.*, 2000]. The adenine moiety of NADP<sup>+</sup> was stacked between I329 and R197 with no hydrogen bonding interactions with the protein. The 2'-phosphate group formed ionic interactions with R197 and R198, and both the ribose groups were in the 2'-endo conformation, a formation more usually seen in disulfide oxidoreductases that bind NAD<sup>+</sup>.

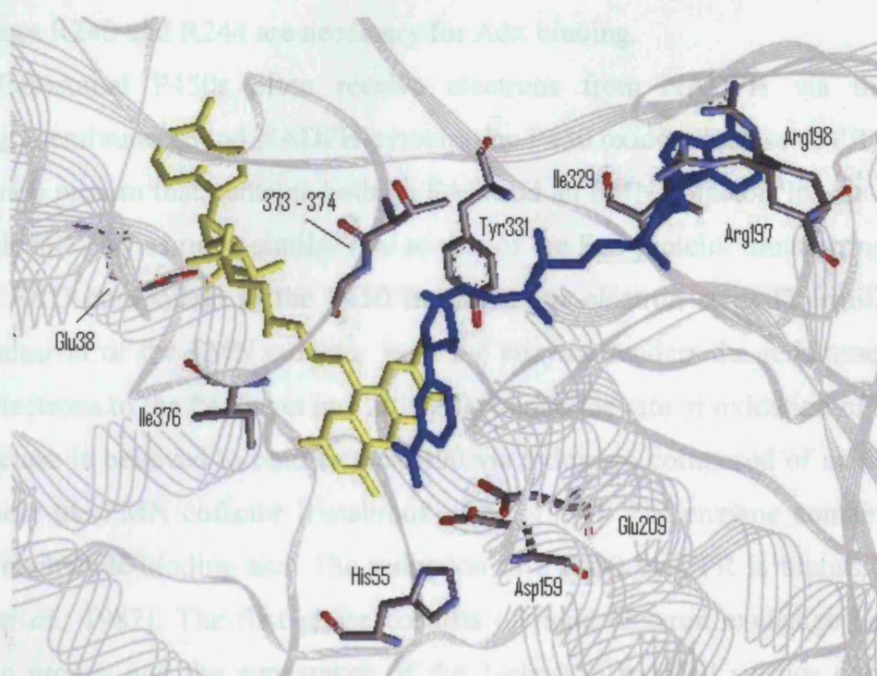


**Figure 1.31** The binding of NADP<sup>+</sup> (blue) and FAD (yellow) in bovine AdR. The various residues believed involved in the positioning of the cofactors are shown [Ziegler and Schulz, 2000].

The nicotinamide ring of NADP<sup>+</sup> is positioned at 20° to the isoalloxazine ring allowing hydride transfer from its C(4) atom to the N(5) of the flavin. Its positioning is aided by a hydrogen bond from its carboxamide to E209. Upon NADP<sup>+</sup> binding, AdR undergoes a conformational change with the peptide bond 373-374 flipping to bind the O(3) with the amide hydrogen. Several strictly conserved residues are involved in NADP<sup>+</sup> binding (Y331, R197, E209 and G374) and it contains the common



GXGXXG(A) motif for dinucleotide binding. AdR differs from the plant-type FNRs in that NADPH docks at the *re*-side of the isoalloxazine rather than the *si*. The FAD cofactor was bound in an extended conformation, the ribose group tightly bound to E38 and the isoalloxazine moiety pointing towards the NADP<sup>+</sup> binding domain, its *re*-face being solvent exposed. The O(2) of the isoalloxazine is stabilised by binding to I376(N) and the O(4) and N(5) are hydrogen bonded to fixed water molecules (held by H55 and D159). The cleft between the two domains is basic in character and the presence of an acidic cluster on AdR's opposite face brings about an asymmetric charge distribution. This aids the recognition and binding of the asymmetrically charged redox partner Adx [Lambeth *et al.*, 1979, Ziegler *et al.*, 1999]. Mutagenesis on bovine AdR revealed that the two residues R240 and R244 are necessary for Adx binding.

Microsomal P450s often receive electrons from NADPH via the diflavin containing membrane bound NADPH-cytochrome P450 oxidoreductase (CPR), a 78 kDa multidomain protein that contains both an FAD and an FMN cofactor. In this system the FMN molecule carries out a similar role to that of the FeS protein, transferring electrons from the FAD component to the P450 in single one-electron steps [Vermillion *et al.*, 1981]. Removal of the FMN cofactor from the enzyme renders the reductase unable to transfer electrons to the P450, yet has little effect upon the rate of oxidation of NAD(P)H. The reductase is believed to bind to the P450 via a domain composed of acidic residues located near the FMN cofactor [Estabrook *et al.*, 1996]. The enzyme contains a single pyridine nucleotide-binding site. The reduction of a P450 by CPR is biphasic in nature [Oprian *et al.*, 1982]. The first phase consists of rapid electron exchange between the two-flavin groups and the appearance of the 1-electron reduced species containing an FMN semiquinone. The second phase is slower and involves the formation of the 3-electron reduced species as shown in the scheme below (adapted from [Vermillion *et al.*, 1981]). The reductase exists as an air stable semiquinone, which is reduced by a single equivalent of NADPH to form FMNH<sub>2</sub>FADH<sup>•</sup>. The reductase is thought to cycle between the one electron reduced and the three electron reduced species. Reducing equivalents from NADPH enter the reductase only through the FAD moiety, the dissociation of NADP<sup>+</sup> from the two electron reduced enzyme being partially responsible for the slow rate constant associated with the second phase.

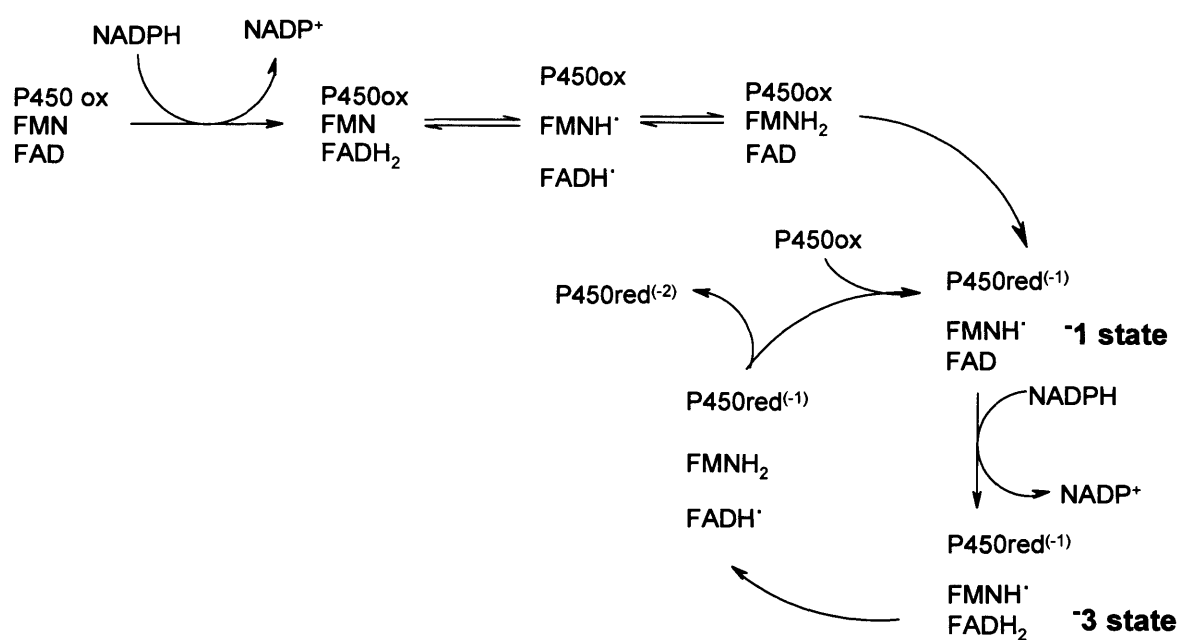


**Figure 1.32** The redox pathway of CPR. After initial reduction by NAD(P)H, the flavins cycle between their one and three electron reduced forms. The stability of the one electron reduced form means it is unlikely for them to return to their fully oxidised state.

Diflavin reductases are thought to have evolved from a gene fusion event between an FAD-containing reductase and an FMN-containing electron carrier [Porter *et al.*, 1991]. The amino terminal FMN binding domain of CPR has high sequence homology to the flds whilst its FAD/NADP<sup>+</sup> binding domain shows high similarity to the transhydrogenases, including the FNRs and NADH-cytochrome *b*<sub>5</sub> reductase. At the N-terminus of CPR there is a short membrane-binding domain of 6 kDa that is necessary for its electron transfer function to P450s when NADPH is the source of reducing equivalents [Estabrook *et al.*, 1996]. Membrane bound CPR can be solubilised by limited proteolysis to release the hydrophilic C-terminal domain (72 kDa). The reductase is believed to interact with the P450 via electrostatic interactions; CPR contains two clusters of acidic residues D207-D209 and E213-D215. Other members of the diflavin reductases are nitric oxide synthase [Griffith and Stuehr, 1995], the sulphite reductases [Zeghouf *et al.*, 1998] and P450 BM3 [Nahri and Fulco, 1987].

Like the FNRs, CPR abstracts the pro-R hydrogen of NADPH, which is bound in an anti-conformation. The three conserved residues S457, C630 and D675 are thought to

facilitate hydride transfer and/or stabilisation of the reduced FAD. S457, like its equivalent in a FNR, forms a hydrogen bond to the reduced flavin N(5). Substitution of this residue gave reduced rates of hydride transfer and lowered the redox potential [Shen *et al.*, 1996]. S457 is thought to stabilise a transition state or to control the orientation and positioning of the isoalloxazine relative to the nicotinamide ring. Removal of all three residues removed all catalytic activity, but had a negligible effect upon either the FAD or NADP<sup>+</sup> dissociation constants.

The reduction of oxidised CPR by NADPH occurs through the rapid formation of charge transfer complexes followed by the slower hydride transfer. NADPH reduction of CPR exhibits a biphasic absorbance change; the first phase corresponds to FAD reduction and inter-flavin electron transfer, and the second slower phase to the reduction by a second mole of NADPH to give the four electron reduced complex, the latter being limited by the rate of NADP<sup>+</sup> release. The hydride transfer process itself occurs as the reduced FAD is stabilised by S457 accepting a hydrogen bond from the FAD N(5). D675 then hydrogen bonds to S457, interactions that position the flavin and nicotinamide for optimal hydride transfer. C630 is postulated to aid hydride transfer by destabilising the C(4)-H bond and donating a proton to stabilise the reduced flavin [Shen *et al.*, 1996].

The structure of a proteolysed form of rat CPR was solved to 2.6 Angstrom resolution with the N-terminal residue being I57 (although the structure was disordered up to V64). The N-terminal FMN binding domain was of similar structure to bacterial flds (as sequence homology had suggested) and was connected via an  $\alpha$ -helical domain to the FAD-binding domain (similar in structure to FNRs [Wang *et al.*, 1997]). The two flavins lie end-on with the 7- and 8-methyl groups of the xylene moiety being nearest to one another (3.5 Angstrom apart), the isoalloxazines lying at an angle of 150° to each other. The FMN cofactor is held between two aromatic side-chains (Y140 and Y178) with the FAD bound in an extended conformation, its isoalloxazine between W677 and Y456 at the interface between the FAD- and NADPH-binding domains.

P450s are thought to interact with the negatively charged residues in the depression on the same side of the molecule as NADPH binds, away from the membrane-binding domain. Modelling, mutagenesis and chemical cross-linking studies have given



weight to this theory [Nisimoto *et al.*, 1992, Shen *et al.*, 1996] and the inhibition of P450 reduction by the presence of cytochrome *c* implied a communal binding site.

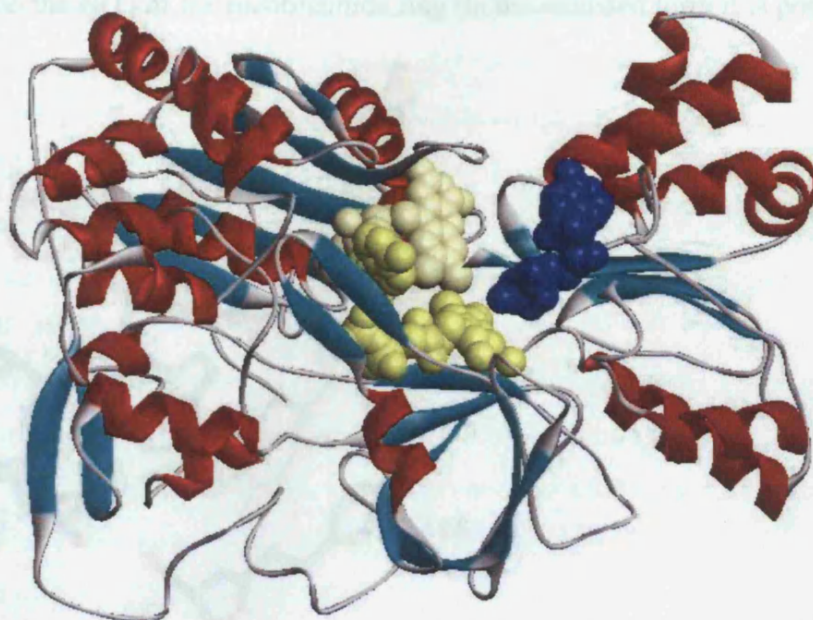


**Figure 1.33** The structure of rat CPR as solved by x-ray crystallography [Wang *et al.*, 1997]. The cofactors are FAD (yellow) and FMN (cream), with NADP<sup>+</sup> (blue) bound by soaking. The protein consists of  $\alpha$ -helices (red),  $\beta$ -sheets (cyan) and loops (grey).

The crystal structure of rat CPR showed the nicotinamide moiety of NADP<sup>+</sup> to be spatially separated from the FAD isoalloxazine by W677, i.e. movement of this side chain being necessary for electron transfer [Wang *et al.*, 1997]. The structure also showed that W677 partially shields the FAD cofactor from solvent and the equivalent residue in human CPR (W676) was found to be mobile during the catalytic process [Gutierrez *et al.*, 2000]. It is believed that, as the 2'-phosphate-AMP portion of NADPH binds strongly and the redox active portion less so, movement of the aromatic side chain is necessary for productive binding of NADPH. W676 is thought to be involved in the dissociation of NADP<sup>+</sup> (in contrast to NAD(P)H:Flavin oxidoreductase (Fre) from *E. coli* [Gassner *et al.*, 1995]), the release of this by-product having to be sufficiently quick to prevent it being trapped due to the binding of a second NADPH molecule in a non-catalytic site. By binding several analogues of NADPH to housefly CPR, it was found that the 2'-

phosphate group contributed about 50 - 60 % of the free energy of binding [Murataliev *et al.*, 2000]. The nicotinamide moiety of the oxidised form has little if any interaction with the enzyme whilst in the reduced state it does. This difference is believed mainly due to the charge on the N(1) of the nicotinamide ring (in the oxidised form it is positive).

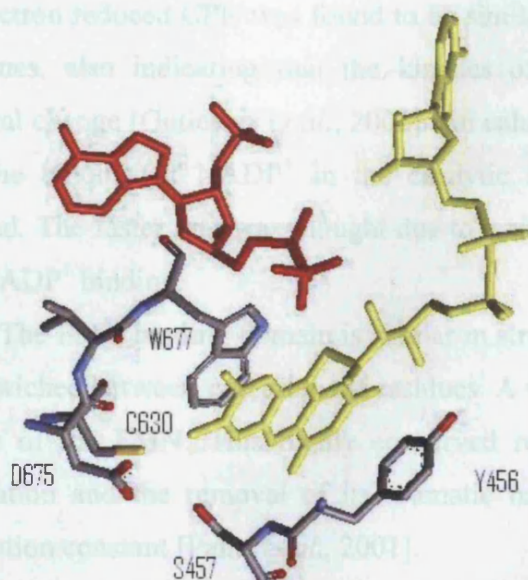


**Figure 1.34** Detail of the catalytic site of rat CPR. Shown is the FAD cofactor (yellow), the  $\text{NADP}^+$  bound by soaking (red) and the relevant residues are highlighted as discussed in the text [Wang *et al.*, 1997].

In a separate study, W677 in rat CPR was mutated and its removal or substitution allowed the nicotinamide ring of NADPH to bind through  $\pi$  -  $\pi$  interactions with the solvent exposed *re*-face of the isoalloxazine [Hubbard *et al.*, 2001]. From kinetic studies with these and other mutants the following theory was proposed for the interaction of CPR with NADPH; NADPH binds to CPR in a bipartite manner, the phospho-AMP region binds first causing displacement of W677's indole side chain. This allows the second interaction between the nicotinamide moiety and the protein. The carboxamide group of  $\text{NADP}^+$  hydrogen bonds to S457 and D675, and as a result the hydrogen bond between S457 and D675 is broken. This rearrangement results in C630 being positioned over the C(4) of the nicotinamide ring thereby promoting hydride transfer. The repositioning of W677 displaces oxidised  $\text{NADP}^+$ . The hydrogen bond network between S457, D675 and C630 can then reform, allowing the N(5) to be deprotonated.



The transfer of an electron from the reduced FAD to the FMN is thought accompanied by a movement of the respective domains to allow the close approach of the cofactors. In the crystal structure of rat CPR, disordered FAD and FMN domains implied movement [Hubbard *et al.*, 2001]. The rates of internal electron transfer for both one and two electron reduced CPR was found to be similar when measured by temperature jump techniques, also indicating that the kinetics of electron transfer were limited by a structural change [Gutierrez *et al.*, 2002]. An enhancement in the rate of electron transfer upon the binding of NADP<sup>+</sup> in the catalytic site (stoichiometric amount) was also observed. The faster rate was thought due to a subtle conformational change that occurs upon NADP<sup>+</sup> binding.

The FMN binding domain is similar in structure to flds. The FMN in human CPR is sandwiched between two aromatic residues. A third aromatic residue, F181, lies on the *si*- side of the FMN. This highly conserved residue was found necessary for FMN stabilisation and the removal of its aromatic nature caused a 50-fold increase in the dissociation constant [Paine *et al.*, 2001].

The 17  $\alpha$ -hydroxylation of pregnenolone by CYPc17 has been supported by the sulphite reductase from *E. coli* (SiR-FP) [Zeghouf *et al.*, 1998]. It is an octamer of 66 kDa that contains both FAD and FMN cofactors per polypeptide chain. SiR-FP is believed to interact with the P450 via its acidic cluster (D184-A-D186) homologous to the residues 207 - 209 in rat CPR. SiR-FP also contains an N-terminal fld like domain and a C-terminal FNR like domain. NMR has shown the environment of the flavin's phosphate groups to be different to that in CPR [Evard *et al.*, 1999] with the FMN not being in an extended conformation and the NADP<sup>+</sup> phosphate being more solvent exposed. The experiments indicated the close proximity of the cofactors predicting a compact functional domain. Bacterial sulphite reductases are never fully oxidised, cycling between a one electron and three electron-reduced state [Hishiki *et al.*, 2000].

P450BM3 (CYP102A1), and its *Bacillus subtilis* homologues CYP102A2/3, is one of the few known bacterial cytochrome P450s that is fused to its redox partner. In the case of BM3 the reductase domain is diflavin in nature, although some P450s that have iron-sulphur containing reductase domains are now known (e.g. P450 Rhf from *Ralstonia sp.* [Roberts *et al.*, 2002]). To date the crystal structure of full length BM3 has not been

solved. The heme domain [Ravichandran *et al.*, 1993] and an artificial complex between the heme and FMN binding domains (linker region proteolytically cleaved) have been solved [Sevrioukova *et al.*, 1999]. The latter complex revealed the FMN binding domain to be structurally similar to the flds. The methyl groups of the flavin (C7 and C8) were directed towards the heme, but 18.4 Angstrom away, the isoalloxazine forming a charge transfer complex with the indole of W574. Unlike flds and the FMN binding domain of CPR, the flavin binding site of BM3 is surrounded by mainly neutral and hydrophobic residues, despite the heme domain having the typical cluster of positively charged amino acids known to be critical for redox partner interactions [Hazzard *et al.*, 1997].

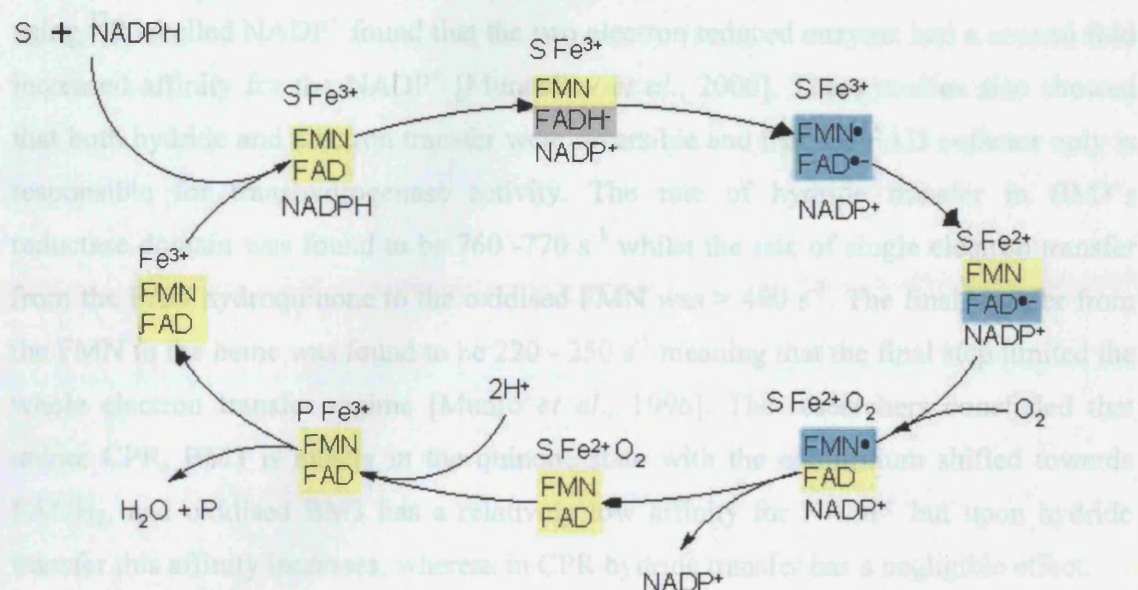


**Figure 1.35** Proposed catalytic cycle of P450 BM3 showing the redox state of the flavin cofactors. The enzyme is thought to cycle between the 0 and 2-electron reduced state, oxidised NADP<sup>+</sup> only being released after the transfer of the second electron to the FMN [Murataliev *et al.*, 1997].

Prolonged incubation of BM3 with NADPH is known to cause the enzyme to become inactive. This was thought due to the flavin domain becoming trapped in a three electron reduced state, as opposed to its two electron reduced active state (in contrast to CPR that cycles between a one and three electron reduced state). The active form of P450 BM3 is believed to consist of an FAD anionic semiquinone and an FMN neutral

semiquinone form, a complex that is partially stabilised by interactions with the charged nicotinamide of  $\text{NADP}^+$  [Murataliev *et al.*, 1997]. NADPH binding has an effect upon the electron transfer properties of BM3 by both its direct (on the FAD/FADH<sub>2</sub> redox couple) and indirect (induced conformational change) influence. In contrast to flds, the FMN binding domain of BM3 was found to destabilise the SQ form of FMN and stabilise the HQ form relative to one another [Sevrioukova *et al.*, 1996]. The partial neutralisation and stabilisation of the anionic HQ is due to the presence of the charged residues K572 and K580 within 10 Angstrom of the pyrimidine moiety.

In different studies it was found that NADPH binding was necessary for fast electron transfer from flavin to flavin. Measurement of the proteins affinity for  $\text{NADP}^+$  using <sup>32</sup>P labelled  $\text{NADP}^+$  found that the two electron reduced enzyme had a several fold increased affinity for the  $\text{NADP}^+$  [Murataliev *et al.*, 2000]. These studies also showed that both hydride and electron transfer were reversible and that the FAD cofactor only is responsible for transhydrogenase activity. The rate of hydride transfer in BM3's reductase domain was found to be 760 -770 s<sup>-1</sup> whilst the rate of single electron transfer from the FAD hydroquinone to the oxidised FMN was > 400 s<sup>-1</sup>. The final transfer from the FMN to the heme was found to be 220 - 250 s<sup>-1</sup> meaning that the final step limited the whole electron transfer regime [Munro *et al.*, 1996]. The researchers concluded that unlike CPR, BM3 is mostly in the quinone state with the equilibrium shifted towards FADH<sub>2</sub>, and oxidised BM3 has a relatively low affinity for  $\text{NADP}^+$  but upon hydride transfer this affinity increases, whereas in CPR hydride transfer has a negligible effect.

#### **1.4 Oxidation reactions**

Cytochrome P450s are known for their deactivation and primary metabolism of xenobiotics. They are also involved in the biosynthesis of steroids (e.g. 14 $\alpha$ -demethylase in lanosterol biosynthesis [Guengerich, 1991]) and have been known to catalyse the formation of potentially harmful compounds from seemingly stable and target-specific drugs (e.g. the oxidation of acetaminophen in the liver to produce the highly toxic N-acetyl-p-benzoquinone imine [Baum *et al.*, 2001]). In general cytochrome P450s catalyse mostly hydroxylations or epoxidation reactions that occur via free radical intermediates

[Halpert *et al.*, 1998]. Bacterial and biosynthetic mammalian P450s are usually very *stereo*- and *regio*-specific due to the rigid and *stereo*-specific binding of the substrate. The most common kind of oxidation reaction, hydroxylation, follows the general scheme:

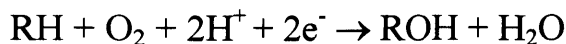


**Figure 1.36** Generalisation of the monooxygenations catalysed by P450s, showing insertion of an atom of oxygen from dioxygen (red) into the substrate (R).

Hydroxylation reactions can occur at unactivated carbons due to the high reactivity of the ferryl-oxo species and the properties of the substrate-binding pocket.  $\omega$ -oxidation at aliphatic and alicyclic carbon atoms is a chemically unfavourable process, the active site of the enzyme has to be favourably disposed for this *regio*-chemistry to occur. Hydroxylation of carbon atoms proceeds via a non-concerted process (a two step abstraction and recombination process) [White, 1991, Groves and Han, 1995]. The mechanism is shown below:

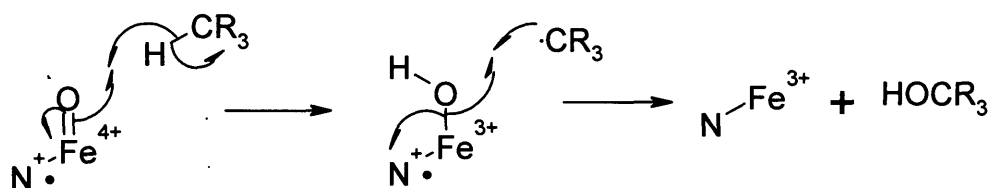


**Figure 1.37** Theoretical mechanism of P450-catalysed hydroxylation. Only one nitrogen atom of the porphyrin ring is shown for simplicity [Groves and Han, 1995].

Isotope studies with deuterium have given weight to this non-concerted pathway as, where the breaking of the C-H bond is rate limiting, a change in rate is observed [Vaz and Coon, 1994]. This process requires the abstraction of an unactivated H atom at the reaction centre to generate a carbon radical and a hydroxy radical [Groves *et al.*, 1978]. Recombination of the two radical species produces the alcohol. The rates of these radical reactions are very fast but they have been estimated by the use of radical clocks (substrates that contain a highly strained carbocyclic structure e.g. methylcyclopropane). A carbon radical located adjacent to the cyclopropane ring rearranges to the larger ring-opened carbon radical at a known rate (see below). This allows the rate of oxygen rebound ( $k_{\text{OH}} = 1.4 \times 10^{10} \text{ s}^{-1}$ ) to be estimated [Ortiz de Montellano and Stearns, 1987,



Newcomb *et al.*, 1995]. The oxygen rebound of the hydroxylation is estimated to be greater than  $10^{10} \text{ s}^{-1}$  in microsomal P450 [Atkinson and Ingold, 1993, Auclair *et al.*, 2002]. Hence the short-lived radical and hydroxy - Fe species have not been detected.

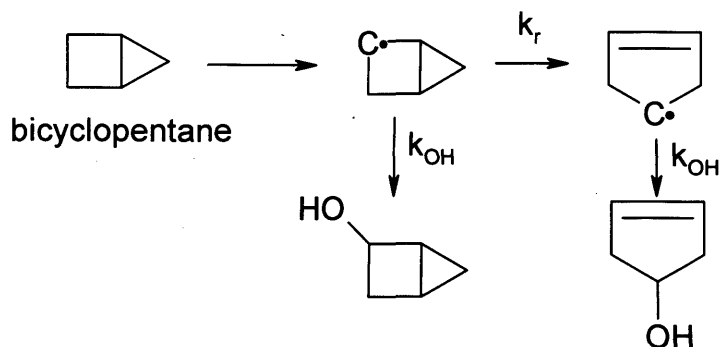


**Figure 1.38** Radical clock mechanism. The introduction of a carbon radical on a highly strained ring allows the estimation of the rate of oxygen rebound as the rate of formation of the two separate products can be measured [Sono *et al.*, 1996].  $k_{\text{OH}}$  = rate of oxygen rebound,  $k_r$  = the known rate of rearrangement.

Bacterial P450s often hydroxylate fatty acids during their metabolism. In *B. megaterium* P450 BM3 carries out a sub-terminal hydroxylation reaction on long chain-saturated fatty acids [Nahri and Fulco, 1986]. P450 BM3 is also capable of hydroxylating alcohols, alkanes and amides [Miura and Fulco, 1975]. The major product of palmitic monooxidation by P450 BM3 is the  $\omega$ -1(R) product (50 %, 0.97 ee). The mono-hydroxylated products of this reaction are able to undergo further oxidation reactions catalysed by BM3 under limiting substrate concentrations to form polyhydroxylates and ketones [Boddupalli *et al.*, 1990].

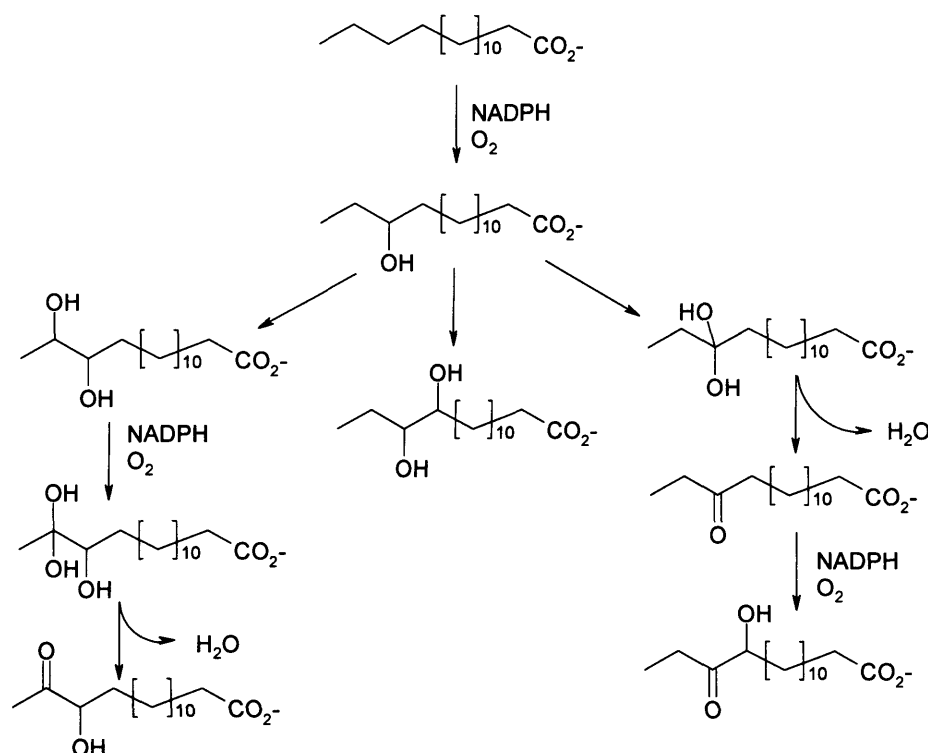


**Figure 1.39** Scheme showing an example of the oxidation of palmitic acid by P450 BM3 under conditions where the initial substrate is limiting [Boddupalli *et al.*, 1992]. The binding of the mono-hydroxylated compound is less favoured than the binding of the initial fatty acid (e.g.  $K_d$  of  $\omega$ -1 hydroxy palmitic acid being approx. 100-fold weaker [Truan *et al.*, 1999]). Under these conditions palmitic acid was oxidised to give a mixture of keto, hydroxy-keto and dihydroxy  $\omega$ -2 derivatives [Boddupalli *et al.*, 1992].

P450s also catalyse aromatic hydroxylation. Oxidation of polycyclic aromatic hydrocarbons produces highly carcinogenic products, but can be useful as the first step in biodegradation processes [England *et al.*, 1998]. Whilst epoxides have been observed (e.g. the microsomal P450-catalysed oxidation of naphthalene [Jerina *et al.*, 1968]), direct epoxidation of aromatic compounds is thought from isotope experiments to be unlikely. The mechanism is believed to involve the addition of a heme iron-oxo species to produce a tetrahedral intermediate that rearranges to form a ketone or epoxide [Korzekwa *et al.*, 1989, Silverman, 1999].

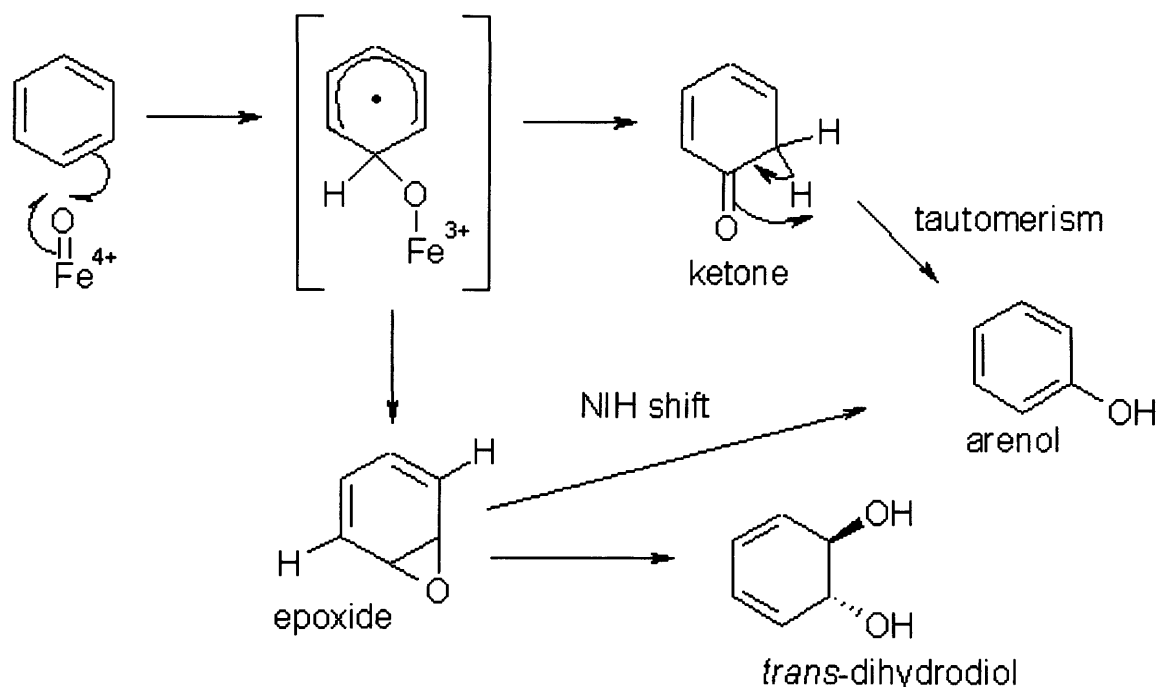


**Figure 1.40** Aromatic hydroxylation can follow two routes; the formation of the ketone or the epoxide from the tetrahedral intermediate [Korzekwa *et al.*, 1989]. This tetrahedral intermediate rearranges to form the product, tautomerism of the ketone to the corresponding arenol is observed, or, in the case of the epoxide a rearrangement to the arenol is seen (the NIH shift). Subsequent hydration to the *trans*-diol or reaction with a nucleophilic conjugate (e.g. glutathione) may occur [Silverman, 1999].

P450s can epoxidise alkenes, usually with the retention of stereochemistry [Komives and Ortiz de Montellano, 1987]. Further oxygenation of the epoxide group e.g. by epoxide hydrolases, can lead to the formation of diols. P450 BM3 is known to epoxidise unsaturated fatty acids [Buchanan and Fulco, 1978]. Terminal olefins are termed suicide substrates as they can give rise to heme modified products as well as the epoxide [Ortiz de Montellano, 1991]. Terminal olefins caused NADPH-dependent cytochrome P450 loss and the development of abnormal green hepatic pigments [Ortiz de Montellano and Mico, 1980]. The oxidation of 1-octene was observed to produce the 1,2-epoxide and N-alkylation of the heme concurrently [Ortiz de Montellano *et al.*, 1983].

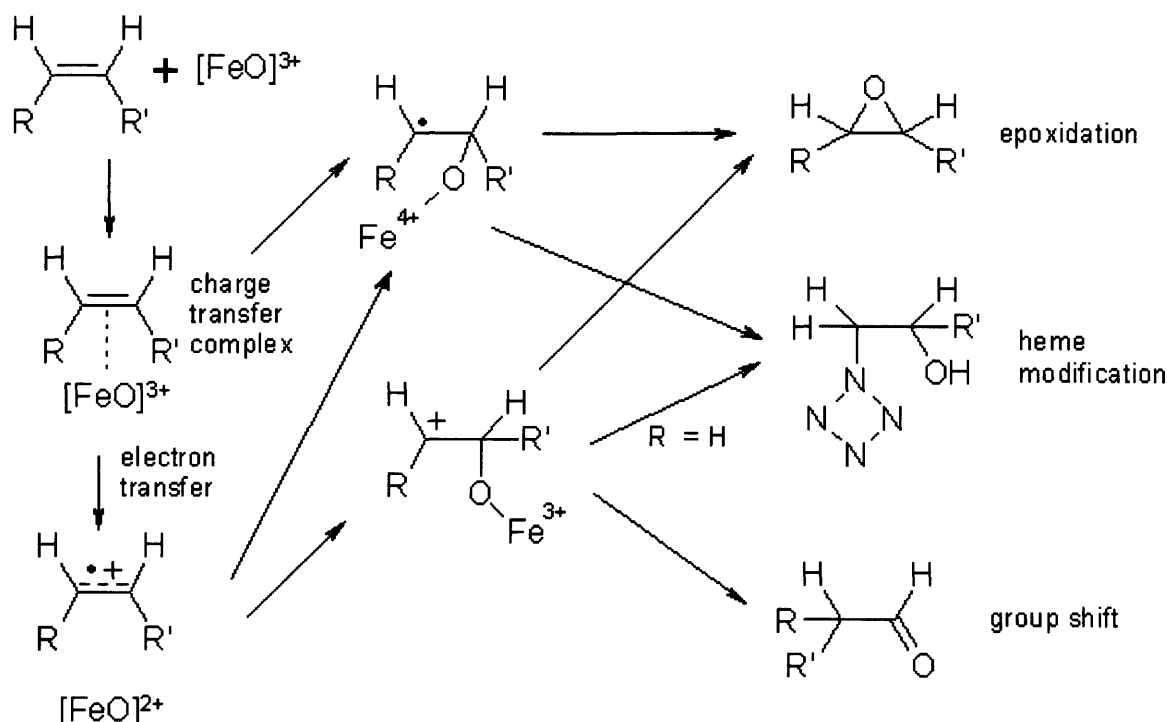


**Figure 1.41** Alkene epoxidation and the competing pathways. Terminal olefins can lead to covalently modified heme products as shown [Ortiz de Montellano 1991]. Unusually, the stereochemistry for the N-alkylation requires the addition of the oxygen and nitrogen to the same side of the double bond. Whilst both the S and R enantiomers are formed in similar amounts upon oxidation of the epoxide, the heme-alkylation only occurs during oxidation of the *re* face as this orientation allows close proximity between the terminal carbon and pyrrole nitrogen of the D ring.

The oxidation of carbon-heteroatom systems is also catalysed by P450s, e.g. P450 2D6 carries out the N- and O-demethylation of amphetamines [Miller *et al.*, 2001]. Carbon - nitrogen systems undergo oxidation by cytochrome P450s to result in C-N bond cleavage or, where there are no  $\alpha$  hydrogens available for abstraction, N-oxidation reactions that do not lead to C-N cleavage [Bondon *et al.*, 1989]. Usually only non-basic or aromatic amines of intermediate basicity are oxidised by P450s [Bhakta and Wimalasena, 2002]. Carbon-oxygen systems undergo oxidative O-dealkylation reactions via hydroxylation of the  $\alpha$  carbon followed by C-O bond cleavage to produce an alcohol and carbonyl. O-dealkylation is rapid, but the dealkylation of longer chain n-alkyl substituents is slow and often competes with  $\omega$ -1 hydroxylations. Carbon - sulphur systems can be oxidised in one of three ways: oxidative S-dealkylation, desulphation or S-oxidation [Mitchell *et al.*, 1986].

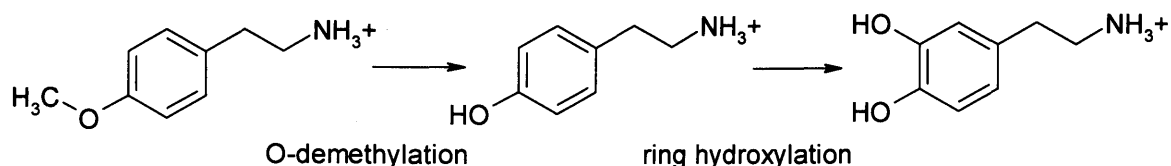


**Figure 1.42** The oxidation of phenylethylamines by P450 2D6. The protonated amine is usually 5 – 7 Angstrom from the site of oxidation. The 3- and 4- hydroxy derivatives are further oxidised to dopamine (a neurotransmitter) [Miller *et al.*, 2001].

P450-mediated oxidative cleavage of carbon-carbon bonds in biosynthetic pathways is known e.g. bile acid and steroid production. These reactions are very *regio*- and *stereo*-specific. Several P450s involved in steroid biosynthesis carry out consecutive hydroxylations ending in a C-C bond-breaking step e.g. cholesterol side chain cleavage [Pikuleva *et al.*, 1995]. The formation of  $\beta$ -estradiol from testosterone is catalysed by aromatase [Akhtar *et al.*, 1982]. Here the methyl group is hydroxylated twice to give an aldehyde that is oxidatively removed as an acid via C-C bond cleavage to give a double bond (see below) [Townsend and Brodie, 1968]. The ferryl-oxo species may be involved as studies have shown the ferryl-oxo cation exclusively oxidises aldehydes to carboxylic acids [Cole and Robinson, 1988, Vaz *et al.*, 1991].

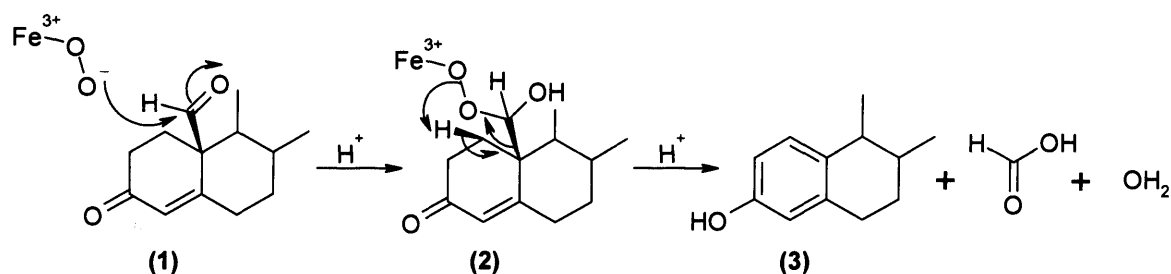


**Figure 1.43** Aromatase-catalysed formation of  $\beta$ -estradiol (3) from testosterone (1) via the peroxyhemiacetal intermediate (2) [Akhtar *et al.*, 1982]. For simplicity only the A and B rings of the steroid are shown (for steroid structure see Figure 3.9).

Sterol 14 $\alpha$ -demethylase is a P450 involved in the biosynthesis of steroids that catalyses C-C bond cleavage [Ramm and Caspi, 1969]. It performs two sequential hydroxylation steps to produce the 14 $\alpha$ -formyl steroid derivative (see below). The ferric-peroxide intermediate then attacks to produce a peroxyhemiacetal type intermediate (2)



which then undergoes a Bayer-Villiger type rearrangement to yield the 14 $\alpha$ -formyloxy derivative (4) [Fischer *et al.*, 1991, Shyadehi *et al.*, 1996].

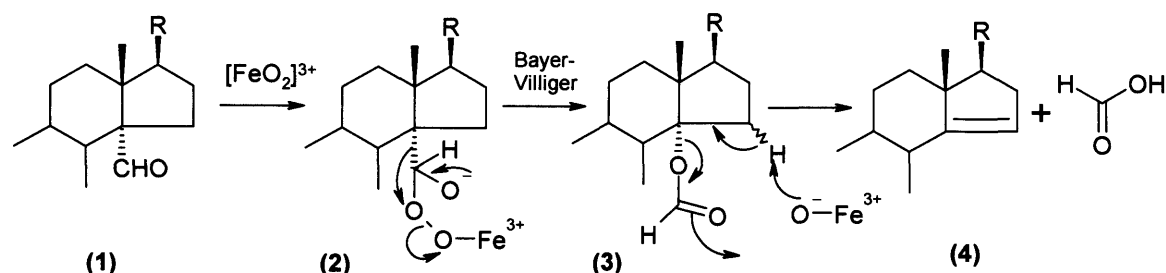


**Figure 1.44** Catalytic pathway of 14 $\alpha$ -demethylase (CYP51). For simplicity only the steroid C and D rings are shown. Adapted from [Shyadehi *et al.*, 1996].

### 1.4.1 Substrate Binding and Specificity

Whilst xenobiotically-induced P450s are often non-specific in their action, many microbial, plant and biosynthetic mammalian P450s are highly selective of substrate and perform *regio*- and *stereo*-specific reactions. Substrate- or ligand-binding involves several different interactions such as Van der Waals forces, hydrogen bonding, and desolvation energies of both the protein and the ligand [di Primo *et al.*, 1990]. High mobility of a substrate in the binding cavity and loss of specificity are highly correlated. In P450 BM3 fairly large conformational changes are seen to occur when the crystal structures of the substrate-free and fatty acid-bound protein are compared [Ravichandran *et al.*, 1993, Li and Poulos, 1997]. Catalytic turnover of a fatty acid by BM3 may involve a 6 Angstrom movement of the substrate within the active site from the initial binding position to the catalytically relevant position [Modi *et al.*, 1996].

The optimal length of fatty acids for BM3 is thought to be between 16 and 20 carbons in length from binding and kinetic data. The crystal structure of the heme domain of BM3 shows a long binding cavity connecting the surrounding solvent to the heme [Li and Poulos, 1997]. An arginine residue (R47) at the mouth of the binding channel binds the polar carboxylate group of the fatty acid [Oliver *et al.*, 1997] and Y51 is also involved to a lesser extent in this interaction [Noble *et al.*, 1999]. F87 is involved in the regioselectivity of the hydroxylation and is shown to undergo a large degree of

movement upon substrate binding [Li and Poulos, 1997]. A second aromatic residue, F42, is located at the access to the binding site to act as a hydrophobic lid. This residue repositions upon substrate binding increasing the nonpolar contacts with the ligand and repelling solvent molecules. The channel is lined by hydrophobic residues (that include L75, L181, I263, L437), which upon mutation to residues capable of ionic or protic interactions caused a 100 fold increase in the  $K_d$  for palmitic acid [Ost *et al.*, 2000]. Structures of substrate free and camphor-bound P450 CAM are almost identical with the active site not being directly accessible to the solvent [Poulos *et al.*, 1987].

Generally, polar substances bind either on the surface or at sites that are directly solvent accessible: whilst non-polar ligands bind in buried cavities. Introducing cavities by mutating aromatic hydrophobic residues to ones with smaller side-chains has been shown to have a destabilising effect on the protein [Eriksson *et al.*, 1992]. A cavity that then binds a small hydrophobic compound (e.g. benzene) can cause a net increase in the protein's stability [Eriksson *et al.*, 1992]. Substrate binding can increase the stability of the protein as interactions between the enzyme and substrate can reduce the mobility and increase the occupancy of ionic sites to make the protein more inert. Solvent molecules are often present in the active site and can be involved in hydrogen bonding networks between ligand and protein [Yoshioka *et al.*, 2002]. Highly mobile, loosely binding compounds give rise to disordered solvent molecules in the binding cavity. The iron spin state is used to indicate the water accessibility of the heme [Fisher and Sligar, 1987] and the degree of solvation of the active site. Usually low spin indicates water held as the sixth ligand and high spin indicates when it is removed. With the camphane bound form of P450 CAM the water ligand is present and the iron spin has intermediate value [Atkins *et al.*, 1988]. In the crystal structure of adamantane bound P450 CAM, the iron remains hexa-coordinate with the distal aqua ligand bound despite it being fully high spin spectroscopically. The water ligand was very mobile and distanced further from the heme *c.f.* the unbound state resulting in the high spin form. The closeness of the water molecule to the adamantane implied an electrostatic interaction [Raag and Poulos, 1991].

Crystallographic data from P450 CAM showed that compounds binding with less affinity were smaller (less Van der Waals interactions) or able to form fewer hydrogen bonds. When camphor is bound to P450 CAM, Y96 hydrogen bonds to the carbonyl

group [Poulos *et al.*, 1987]. Upon its mutation, loss of *regio*-specificity was observed [Sligar *et al.*, 1991]. Compounds that lacked the proton accepting carbonyl of camphor exhibited weaker binding and reduced *regio*-selectivity [Schlichting *et al.*, 2000]. The carbonyl group also had a steric role interacting with bulky non-polar groups (e.g. F87) [Loida and Sligar, 1993]. Camphor binding is favoured due to large enthalpy-entropy compensation as water molecules are lost from the active site and non-polar hydrocarbons enter. Analysis of the binding of various substrate analogues showed that the hydrophobicity and size/shape had the greatest effect on binding affinity [Helms *et al.*, 1996]. Protein engineering has allowed P450 CAM to oxidise substrates such as alkanes [Stevenson *et al.*, 1996] and naphthalene [England *et al.*, 1998].

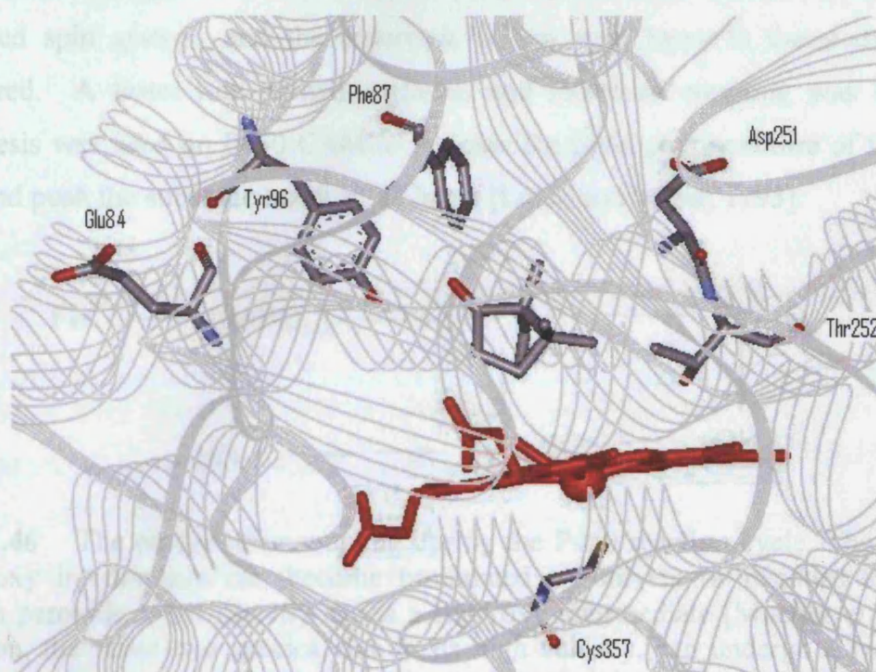


**Figure 1.45** X-ray crystal structure of P450 CAM (PDB code 1DZ4) bound to (1S)-camphor (CPK colouring). The sulphur (yellow) of Cys357 ligates the iron atom of the heme (red) [Schlichting *et al.*, 2000]. Residues that comprise the heme-binding motif are shown in cyan (Phe350 – Gly359) and those that are involved in substrate binding are labelled. Thr252 is the proton donor in the reduction of dioxygen. The hydrogen bond from Tyr96 to camphor is shown (dashed line).

Maximal productivity requires 100 % coupling between the acceptance of reducing equivalents and the oxidation of product. Correct orientation of the substrate molecule within the active site shields the heme iron from solvent and obtains the maximal overlap between the vacant  $sp^2$  oxygen orbital (of the putative Fe=O species)

and the substrate hydrogen orbitals [Raag and Poulos, 1991]. In the absence of the 'correct' substrate the reaction may become uncoupled resulting in the generation of either a superoxo or peroxo species [Mueller *et al.*, 1995], generation of  $\text{H}_2\text{O}_2$  ( $[\text{FeO}]^{3+}$  intermediate), or at a point further downstream the 4 electron reduction of dioxygen to generate water [Loida and Sligar, 1993, Kadkhodayan *et al.*, 1995]. In camphene oxidation by P450 CAM, only a 46 % conversion to high spin is seen and only 8 % of the NADPH consumed was coupled to hydroxylation. However, there is no direct relation between the degree of high spin and peroxide generation. The access of water to the heme as measured spectroscopically is thought to differ from the water involved in uncoupling. The ligation of dioxygen to the iron would displace the weaker water-iron interaction in any mixed spin system, and the reduction of low spin heme is thermodynamically disfavoured. A faster rate of hydroxylation and increased coupling was seen when mutagenesis was used on P450 CAM to increase the hydrophobic nature of the binding pocket and push the substrate towards the heme [Loida and Sligar, 1993].

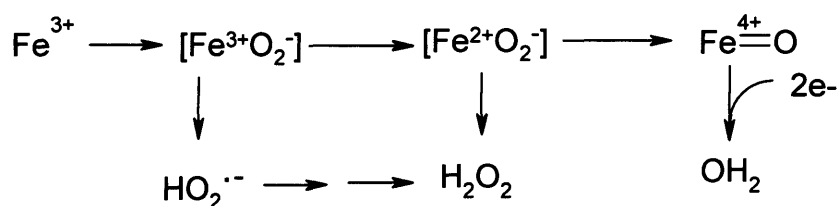


**Figure 1.46** The modes of uncoupling during the P450 reaction cycle. The ferric and ferrous oxy intermediate can become protonated by solvent or residues to generate hydrogen peroxide either directly or via a superoxy intermediate [Mueller *et al.*, 1995]. Further on, the ferryl-oxo species, due to its high valency, can undergo a two-electron reduction to generate water [Loida and Sligar, 1993, Kadkhodayan *et al.*, 1995].

#### 1.4.2 Commercial Interest in P450 monooxygenases

P450s such as CYP19 and CYP51 have been identified as drug targets and are of interest in the pharmaceutical industry [Brodie *et al.*, 1994, Vanden Bossche *et al.*, 1995]. Various microsomal P450s that occur in the liver play a role in the metabolism of drugs [Bailey *et al.*, 1991]. High throughput screens (HTS) using fluorescent probes are used to allow many candidate compounds to be assessed for interactions with microsomal P450s at one time [Dunn *et al.*, 2002]. As many toxic metabolites of xenobiotics are derived



either directly or indirectly from P450-catalysed reactions [Guengerich, 1991], potential problems are looked for early on in the drug discovery process.

P450s are involved in the production and manufacture of pharmaceutical agents [Falck *et al.*, 2001, Morant *et al.*, 2003, Guengerich, 2002]. Natural products are commonly used in the pharma- and nutraceutical industries as products themselves or as a template for the development of new active compounds. Taxol (an antimitotic agent in cancer therapy) is isolated from Yew. It is now known that oxygenation of the taxane ring is mediated by one or more cytochrome P450s [Jennewein *et al.*, 2001] (see Figure 1.47).

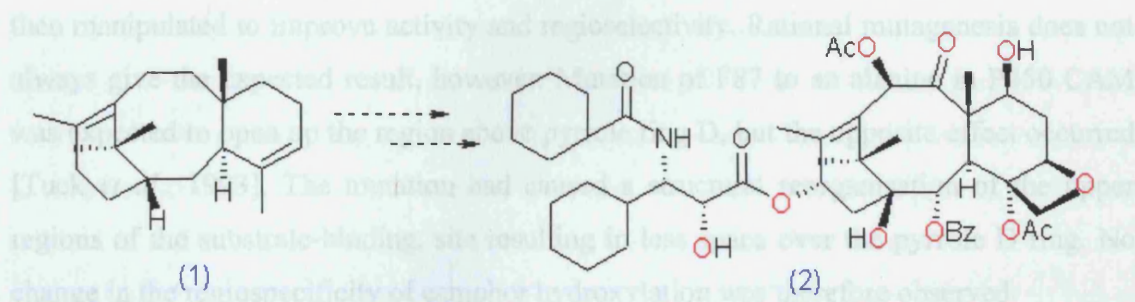


**Figure 1.47** Formation of Taxol (2) from Taxa-4(5),11(12)-diene (1). Oxygen atoms known or thought to be inserted by the actions of P450s are shown in red [Jennewein *et al.*, 2001].

P450s have been examined in terms of engineering them to carry out specific oxidations on alternative substances. Techniques such as rational protein design, directed evolution [Arnold, 1998] and (for the generation of more random mutants) alternate DNA shuffling methods (e.g. random chimeragenesis on transient templates [Coco *et al.*, 2001]) are used to develop novel function [Sieber *et al.*, 2001, Zhao *et al.*, 2002]. Directed evolution by error prone PCR has been used to convert P450 BM3 from a long chain fatty acid  $\omega$ -2 hydroxylase to an efficient octane hydroxylase [Farinas *et al.*, 2001]. A mutant of P450 CAM that could utilise  $\text{H}_2\text{O}_2$  as the source of reduced oxygen for a rapid and highly coupled reaction was also developed [Joo *et al.*, 1999].

Mutation of binding site residues has allowed the development of P450s with novel functions or the refinement of their native catalytic role [Ramarao *et al.*, 1995, Ost *et al.*, 2000]. In P450 BM3 R47 was replaced with a glutamate to increase activity towards C12 – C16 alkyltrimethyl ammonium compounds [Oliver *et al.*, 1997]. A triple mutant of BM3 was generated that was capable of efficiently hydroxylating indole to

indigo and indirubin [Li *et al.*, 2000], and subsequently, of hydroxylating several alkanes, arenes, cycloalkanes and heteroarenes [Appel *et al.*, 2001].

P450 CAM has been engineered via rational site directed mutagenesis to turn it into an alkane hydroxylase [Stevenson *et al.*, 2000, Bell *et al.*, 2003] and also, separately, to oxidise chlorinated benzenes and (+)- $\alpha$ -phapinene [Bell *et al.*, 2003]. The preparation of an alkane-hydroxylating mutant was achieved by targeting specific residues placed further from the heme (e.g. F87, Y96, V247 and V396) to allow improved binding of small alkanes such as butane ( $C_4H_{10}$ ). Residues nearer to the heme/ $O_2$  binding site were then manipulated to improve activity and regioselectivity. Rational mutagenesis does not always give the expected result, however. Mutation of F87 to an alanine in P450 CAM was expected to open up the region above pyrrole ring D, but the opposite effect occurred [Tuck *et al.*, 1993]. The mutation had caused a structural reorganisation of the upper regions of the substrate-binding, site resulting in less space over the pyrrole D ring. No change in the regiospecificity of camphor hydroxylation was therefore observed.

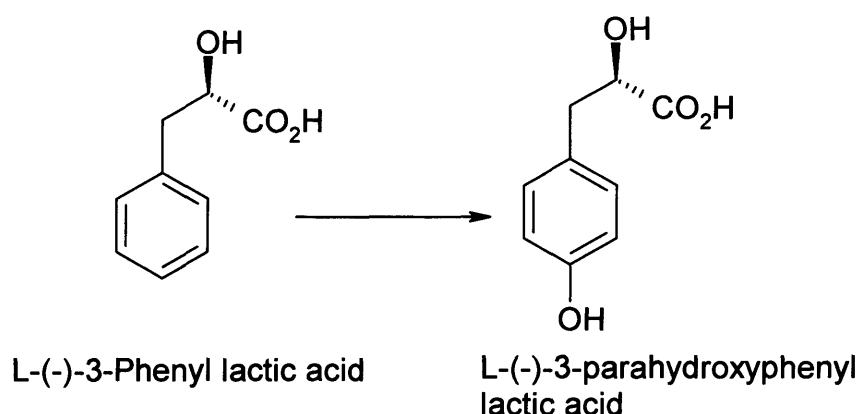


**Figure 1.48** The commercially P450-catalysed hydroxylation of phenyl lactic acid carried out by fungal fermentation [Urlacher and Schmid, 2002]. The use of a biocatalyst allows the retention of the *stereo*-centre and eliminating the need for protecting groups.

The possibilities afforded by mutagenesis to alter binding affinities and product profiles of cytochrome P450s are huge. Given their ability to catalyse chemically unfavourable oxidations (e.g. see Figure 1.48); the P450s lend themselves to exploitation as biocatalysts in the biotechnology industry. Whilst P450s are currently utilised in the manufacture of steroids and antibiotics [Anderson *et al.*, 1993, Shen and Hutchinson, 1993, Demain, 2000], other synthetic processes that require high quality *regio*- and

*stereo*-specific oxidations remain probable targets for P450 catalysis. With an increasing demand on industrial processes to be economic and “green,” the use of biocatalysts is attractive. Bioremediation is another area where P450s feature, the oxidation of many substances often being the first step in the breakdown of pollutants [Bumpus *et al.*, 1985]. For example, P450 PipA from *M. smegmatis* is a piperidine inducible P450 that can degrade a variety of 2° amines including piperidine, pyrrolidine and morpholine [Poupin *et al.*, 1999].

P450s are generally not the most active enzymes and not particularly stable – the loss of their heme cofactor and intolerance to many substances being a problem. Many microbial P450s require additional redox partners to source reducing equivalents from NAD(P)H – an expensive reagent itself. Artificial fusion proteins have been synthesised in an effort to make class I P450s more commercially viable. A fusion protein consisting of the heme domain of CYP102 and the flavodoxin from *D. vulgaris* has been made [Gilardi *et al.*, 2002]. Electrodes have been used to supply electrons to the P450 rather than using NAD(P)H and other proteins to transfer electrons. However, due to the heme cofactor being buried and P450’s lack of stability, direct reduction of the heme by mounting on electrodes is inefficient. Instead semiconductor electrodes have been used to reduce putidaredoxin that then passed the electron to the P450. This technique allowed electron transfer to P450 CAM and a near stoichiometric conversion of camphor to 5-exo-hydroxycamphor [Reipa *et al.*, 1997]. An electrode has also been used to reduce spinach ferredoxin that transferred electrons to P450 CAM via a second order reaction. The reductive dehalogenation of haloalkanes to produce haloalkenes was observed [Wirtz *et al.*, 2000].

An alternate approach is the use of artificial electron donors to reduce dioxygen e.g. NADPH was replaced by zinc dust with cobalt (III) sepulchrates acting as a mediator to successfully reduce a mutant of P450 BM3 [Faulkner *et al.*, 1995]. P450 BM3 F87A was able to carry out multiple turnovers of *p*-nitrophenoxydodecanoic acid with this artificial source of electrons, although the activity dropped to 20 % of that seen with NADPH [Schwanenberg *et al.*, 2000].

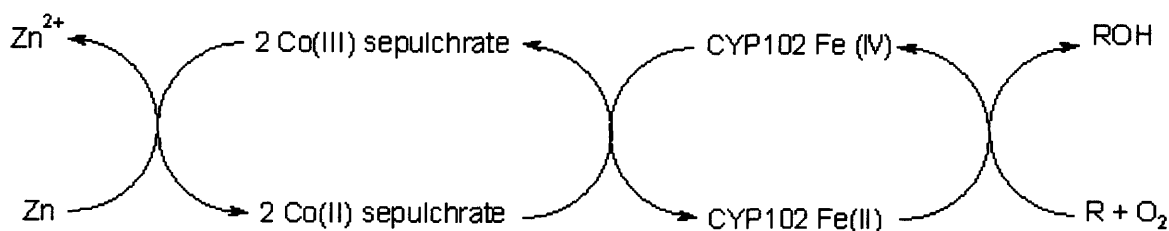


**Figure 1.49** Illustration of an artificial electron transfer pathway utilising the oxidation of zinc dust to donate electrons for the reduction of CYP102 (P450 BM3) mediated by cobalt sepulchrate [Schwanenberg *et al.*, 2000].

A further factor restricting the use of P450s on an industrial scale is the nature of the reaction they catalyse. In general P450s oxidise hydrophobic compounds to introduce one or more polar groups, thus increasing the compound's water solubility [Raadt *et al.*, 2002]. P450s are typically water soluble in character and have their maximal activity in aqueous systems. The solubility of their substrate is therefore a limiting factor both in whole cell fermentations and isolated enzyme systems. Approaches to overcome this problem include the use of biphasic reaction mixtures where the reaction occurs at the interface (e.g. the hydroxynitrile lyase catalysed reaction in diisopropyl ether/water [Hickel *et al.*, 1999]), the use of ionic liquids (typically consisting of 1-alkyl-3-methylimidazolium salts with PF<sub>6</sub> or BF<sub>4</sub> salts [Panke *et al.*, 2002]) and microencapsulation (entrapment of enzymes and whole cells within permeable polymeric micro-capsules containing an aqueous phase [Khan *et al.*, 2002]).

### 1.5 Biotin biosynthesis genes in *B. subtilis*

The complete genome of *B. subtilis* was sequenced in the 1990's [Kunst *et al.*, 1997] and this showed that the organism contained eight putative P450s. One of these P450 encoding genes was *bioI*, a member of the biotin biosynthesis operon (the *bio* operon). This operon was already the subject of investigation and analysis [Bower *et al.*, 1995, Perkins *et al.*, 1996] due to the potential to produce biotin by fermentation. The *bio* operon was recognised by a promoter sequence ( $\sigma^A$ ) upstream of the *bioW* gene [Bower *et al.*, 1996]. A 33 bp segment followed this, that had strong sequence homology to the regulatory sites of the *B. sphaericus* *bio* operons [Gloeckler *et al.*, 1990, Bower *et al.*, 1995]. The *bioI* and *ythQ* genes (395 and 253 amino acids respectively) are located at the



3' end of the *bio* operon in *B. subtilis*, separated from their preceding genes by intercistronic regions of 68- and 67-bp respectively. These genes showed no similarity to any of the known *bio* genes, but *bioI* encoded a protein similar to cytochrome P450s from *B. megaterium*, *S. erythraea* and other organisms. The *ytbQ* gene showed significant similarity to putative NAD/NADH binding sites of short chain alcohol dehydrogenases, dehydratases and the  $\beta$ -ketoreductase enzyme of *S. erythraea* (GXGXXG nucleotide binding motif). A ribosome-binding site precedes each of the genes within the *bio* operon, translational coupling possibly regulating their expression [Bower *et al.*, 1996].

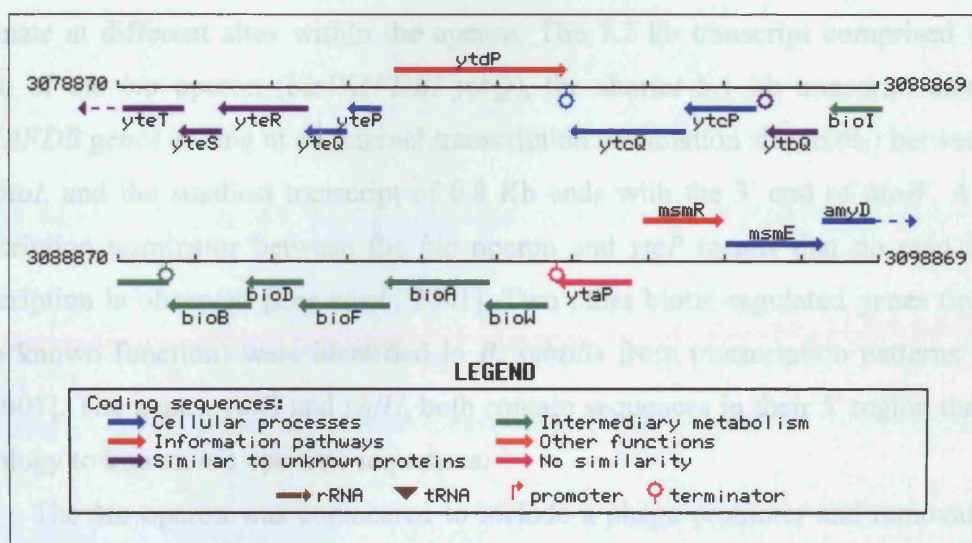


**Figure 1.50** The region of the genome that includes the genes responsible for biotin biosynthesis in *B. subtilis* (genes *bioW*, *bioA*, *bioF*, *bioD*, *bioB* and *bioI*). Data are from the *B. subtilis* genome sequence [http://genolist.pasteur.fr/SubtiList/, Pasteur Institute].

The *bioI* gene was found to be involved in an early step in biotin biosynthesis (see Figure 1.53). It could complement both *E. coli* *bioC* and *bioH* mutants [Bower *et al.*, 1996] and, when insertions were made into the *bioI* gene, colonies were produced that were partially deficient in biotin (they grew well in the presence of the vitamin but poorly in its absence). As a result, *bioI* was thought not essential; derivatives with a *bioI* knockout grew as well as the wild type on biotin free media that contained pimelic acid. Both *B. subtilis* and *B. sphaericus* readily utilise exogenous pimelic acid, which is converted to pimeloyl-CoA by the product of the *bioW* gene (pimeloyl-CoA synthase) [Gloeckler *et al.*, 1990].

Three steady state transcripts were detected in the RNA in cells grown in the absence of biotin (7.2, 5.1 and 0.8kb in the ratio 1:8:3) none of which were detected in the RNA from cells grown in the vitamin's presence [Perkins *et al.*, 1996]. Therefore it appeared that biotin tightly regulates its own synthesis in *B. subtilis*. The *bio* operon is negatively regulated by the action of *birA*, a repressor that binds to the translational control region of the *bio* operon. In *B. subtilis*, the BirA protein has been identified as a 36.2 kDa bifunctional protein acting as both an enzyme (ligase activity) and a regulator. It has a similar amino acid sequence to that of *E. coli* BirA (27 % identity) [Bower *et al.*, 1995]. The transcripts all appeared to be initiated from the putative P<sub>bio</sub> promoter and terminate at different sites within the operon. The 7.2 kb transcript comprised the full length of the *bio* operon (*bioWAFDBI ytbQ*), the shorter 5.1 kb transcript covers the *bioWAFDB* genes ending at an internal transcription termination site (biot<sub>1</sub>) between *bioB* and *bioI*, and the smallest transcript of 0.8 Kb ends with the 3' end of *bioW*. A strong transcription terminator between the *bio* operon and *ytcP* means that no read through transcription is observed [Lee *et al.*, 2001]. Two other biotin-regulated genes (currently of no known function) were identified in *B. subtilis* from transcription patterns [Lee *et al.*, 2001]. The genes, *yuiG* and *yhfU*, both contain sequences in their 5' region that show homology to known *bio* operator sequences.

The *bio* operon was engineered to include a phage promoter and removal of the *bio* regulatory region. The steady state transcription levels of the mRNA were found to increase ten-fold. This increased gene transcription gave increased biotin production; around thirty times more biotin and intermediates than the wild type [Perkins *et al.*, 1996]. Upon deletion of the active terminator sequence biot<sub>1</sub> the 7.2 kb transcript was observed to accumulate. This increased transcription of *bioI* and *ytbQ* coincided with a further two fold increase in production of intermediates. This finding related the expression of *bioI/ytbQ* with biotin production and was further enhanced when higher expression of *bioI* (by inserting a phage promoter upstream of *bioI*) was shown to cause a four-fold increase in production of intermediates. The biot<sub>1</sub> terminator seemed independent of the BirA regulatory mechanism. By the omission of the biot<sub>1</sub> region, higher levels of intermediates result, indicating that *bioI* expression could be rate-limiting for intermediate synthesis and for biotin synthesis itself.

## 1.6 Biotin; Functions and Biosynthesis

Biotin is a member of the water-soluble vitamins (vitamin H) belonging to the B complex. It was first reported in 1935 and its chemical structure elucidated in 1942 [Roche Vitamins]. Biotin can exist in eight isomeric forms of which only one, the D(+) form, is biologically active [Livaniou *et al.*, 2000].

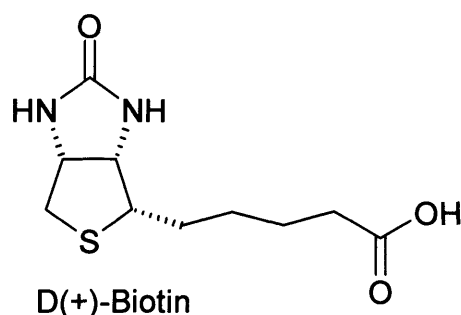


**Figure 1.51** The structure of the physiologically relevant D(+)-isomer of Biotin.

Various bacteria, higher plants and some fungi produce biotin, whilst animals and several micro-organisms have to meet their need for this vitamin by dietary intake. Biotin is known to be an essential vitamin being required as a co-factor (co-enzyme R) in enzymatic carboxylation reactions, e.g. in humans there are five biotin dependent carboxylases; in the glucogenesis pathway pyruvate carboxylase is a biotin-dependent enzyme that catalyses the conversion of pyruvate to oxaloacetate [Stryer, 1999].

In fatty acid synthesis, biotin is involved in the control of the carboxylation of acetyl-coenzyme A to malonyl-coenzyme A [Chapman-Smith *et al.*, 1999]. Biotin deficiency is known to impair lipogenesis, a deficiency reducing the fatty acid content of skin [Proud *et al.*, 1990]. Biotin is involved in fatty acid elongation and desaturation. In biotin deficient animals, two fatty acids (20:3 $\omega$ 6 and 20:4 $\omega$ 6) are reduced causing a reduction in precursors for prostaglandins, thromboxanes and prostacyclin, a possible contributory factor to cardiovascular disease in humans [Ho *et al.*, 2000]. Biotin is involved in amino acid catabolism [Pacheco-Alvarez *et al.*, 2002] and it affects protein synthesis through its influence on the nature and rate of formation of ribonucleic acid. This is important in controlling the rate of production and deposition of scleroproteins (structural proteins such as keratin). Some conditions that result from biotin deficiency

have pointed to this vitamin's role in the transcriptional regulation of certain proteins, probably via biotinylation of histones and hence the triggering of signal cascades [Hymes *et al.*, 1996, Chauhan and Dakshinamurti, 1991].

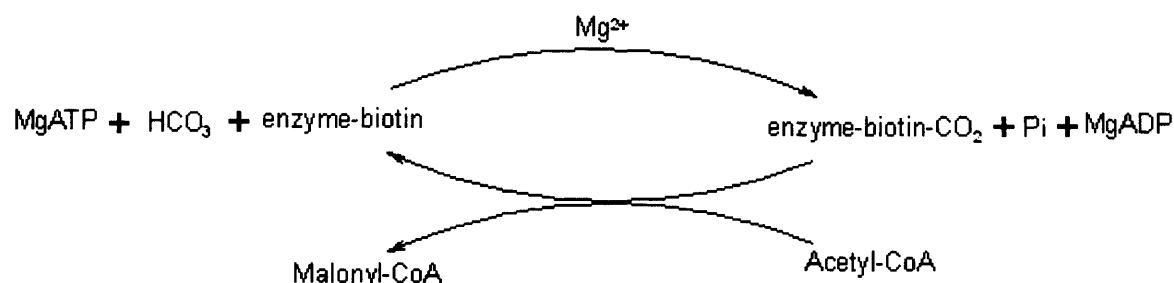


**Figure 1.52** Reaction scheme for conversion of acetyl-CoA to malonyl-CoA. Step one involves the formation of the carboxylated enzyme, step two the transfer of the carboxy group to acetyl-CoA [Blanchard *et al.*, 1999].

Commercial production of biotin is traditionally by chemical synthesis. The method developed by Goldberg and Sternbach in the 1940s is still used today [Goldberg and Sternbach, 1947]. The method uses fumaric acid as the starting material to produce the D(+) isomer. All chemical syntheses suffer from the disadvantage that stereoisomeric mixtures of intermediates are formed. As the biotin molecule contains three stereocentres (of which 50 % of each stereocentre will be the wrong compound) the amount of waste from the synthesis is huge. This results in either the lengthy and costly separation of isomers, a highly impure product, or the use of expensive asymmetric reagents and catalysts.

The genes involved in the biosynthesis of biotin (the *bio* genes) have been identified in several different micro-organisms and recombinant strains produced [Bower *et al.*, 1995, Gloeckler *et al.*, 1990, Birch *et al.*, 1994]. This has allowed extensive characterisation of the last four steps in the pathway and the structures of the enzymes have been elucidated. The last four steps in the biosynthesis of biotin appear to be common to most bacteria, from the reaction of pimeloyl-CoA with L-alanine to the formation of biotin itself [Schneider *et al.*, 2001]. The earlier steps differ between species and even between gram-positive and gram-negative bacteria.

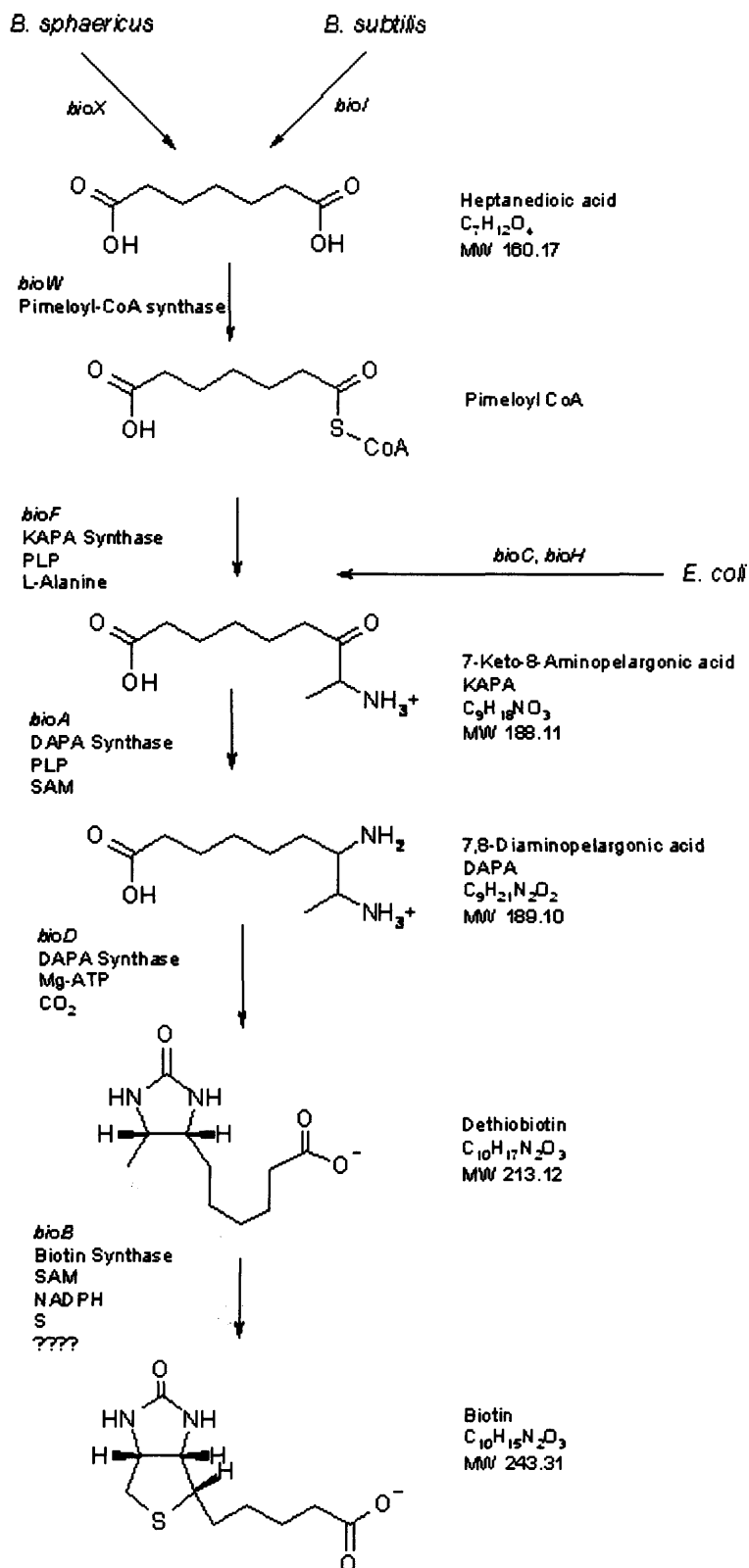


**Figure 1.53** Biotin biosynthesis in micro-organisms. Relevant genes, their protein products, required cofactors and the intermediates are shown where known.



The genes responsible for biotin biosynthesis were first identified in *E. coli* where they are located in a five genes cluster, *bioABFCD* [Otsuka *et al.*, 1988]. Another gene, *bioH*, exists outside the operon. In *B. sphaericus* the genes are arranged as two clusters, *bioXWF* and *bioDAYB*. The genes *bioF*, *D*, *A* and *B* have the same function as their equivalents in *E. coli*, and *bioW* encodes the pimeloyl synthase [Ploux *et al.*, 1992, Gloeckler *et al.*, 1990]. In *B. subtilis*, the single operon consists of *bioWAFDBI* [Bower *et al.*, 1996].

The earlier steps in the pathway are less well characterised. In *Bacillus*, pimeloyl-CoA synthase catalyses the earliest known step, the formation of a thioester of pimelic acid. It is an ATP- and  $Mg^{2+}$ -dependent reaction [Binieda *et al.*, 1999]. The addition of pimelic acid to the culture media of several different microbes has been shown to enhance the biosynthesis of biotin and its intermediates [Izumi *et al.*, 1981]. Studies in *B. sphaericus* and *E. coli* indicate that pimelate passively diffuses into the cell without any involvement of an acyl-carrier protein [Ploux *et al.*, 1992]. *E. coli* arrives at pimeloyl-CoA by a different and so far unclear pathway. Two genes (*bioC* and *bioH*) are thought to be involved in these early steps [Ifuku *et al.*, 1994]. BioH is a Coenzyme A donor to pimeloyl-ACP to release the pimeloyl-CoA intermediate [Tomoczyk *et al.*, 2002].

Regulation of biotin biosynthesis occurs through the presence of biotin itself within the cell via the difunctional protein BirA. BirA acts as the biotin operon repressor, the regulation occurring at the transcriptional level [Xu *et al.*, 1996]. In *E. coli*, BirA plays an essential role in both the regulation and retention of biotin within the cell. The synthesis of biotinyl-5'-AMP from biotin and ATP is catalysed by BirA. The adenylate is the active moiety in both of BirA's functions. The affinity of the enzyme for adenylate is greater than for biotin and the binding of either causes a large conformational change in the protein [Xu *et al.*, 1995]. BirA binds site-specifically to *bioO* (the biotin operator consisting of a 40 b.p. sequence) to repress transcription initiation in a biotin-dependent mechanism. BirA has a second function catalysing the covalent linking of biotin to lysine residues of the biotin carboxyl carrier protein (BCCP) of acetyl-CoA carboxylase. The reaction consists of two separate stages as shown in Figure 1.54.

BirA is a monomer of 35.3 kDa in mass with three distinct domains: the N-terminal domain contacts the DNA in the holoBirA-bioI complex; the central domain is

responsible for the adenylyate synthesis and biotin transfer to BCCP and also in the high affinity DNA binding; and the C terminal domain is instrumental in small ligand (i.e. biotin) and site-specific DNA binding [Streaker *et al.*, 1999]. Two holoBirA monomers bind co-operatively to the two operator half-sites. The binding of a monomer of one BirA causes a subtle structural change in the section of DNA prior to the binding of the second [Streaker *et al.*, 1998]. The adenylyate-bound BirA is observed to assemble into a dimer, the adenylyate promoting the binding of BirA to *bioO* [Eisenstein *et al.*, 1999].

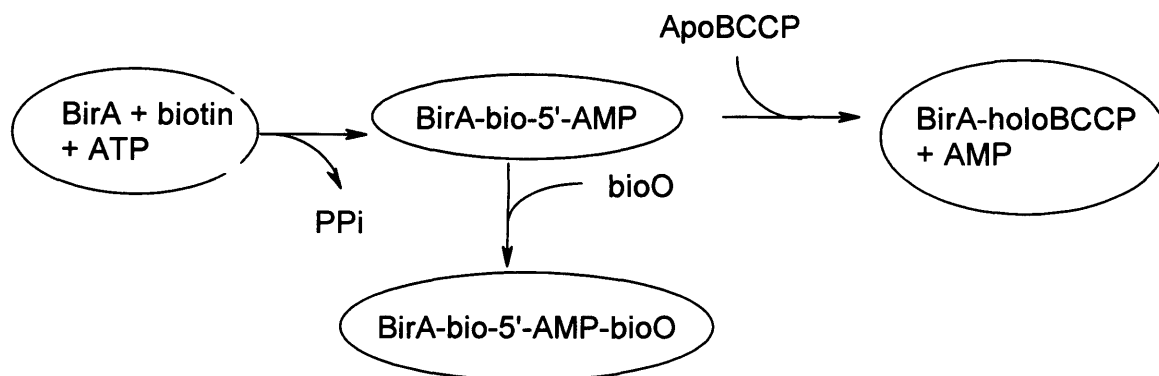


**Figure 1.54** Functions of BirA; BirA activates biotin by converting it to biotinyl-5'-AMP via the addition of biotin to lysines of certain biotin accepting proteins and the reaction of ATP. When all the apoprotein has been biotinylated, the non-covalent complex BirA-biotinyl-5'-AMP accumulates and binds to the *bio* operator *bioO*, repressing transcription of the *bio* genes [Xu *et al.*, 1995].

Of the steps common to most biotin forming organisms, the first is the inclusion of L-alanine *stereo*-specifically to give the intermediate 7-keto-8-aminopelargonic acid (KAPA). The reaction is catalysed by the aminotransferase KAPA synthase. A 42 kDa homodimer it is a vitamin B6 dependent enzyme, with each subunit consisting of three domains. KAPA synthase contains a pyridoxal-L-phosphate (PLP) cofactor that binds (via bonds with lysine residues from both monomers) to a crevice between the two subunits of the dimer [Alexeev *et al.*, 1998]. KAPA synthase catalyses the reaction by the formation of an external aldamine between its PLP group and L-alanine. A quinoid intermediate then forms by abstraction of the aldamine C2 proton by K236. This quinoid intermediate attacks the thioester carbonyl of pimeloyl-CoA producing  $\beta$ -ketoacid aldamine that decarboxylates to form the product, KAPA (see Figure 1.56).

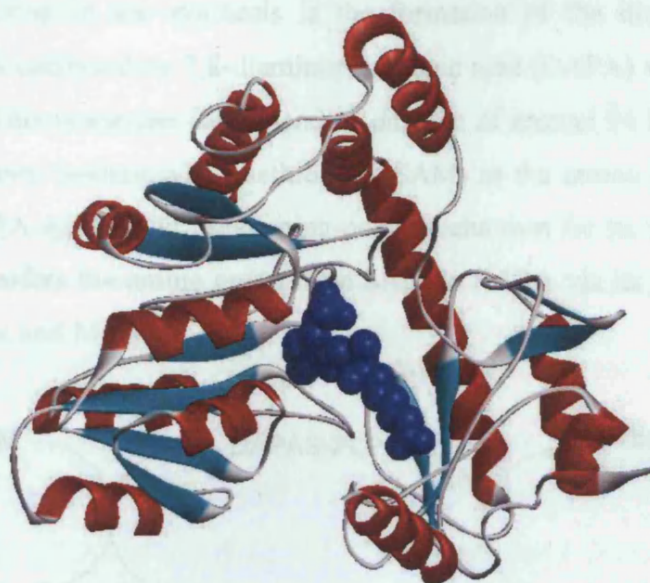


**Figure 1.55** Crystal structure of the PLP-bound form of 8-amino-7-oxonanoate synthase (KAPA synthase) [Webster *et al.*, 2000]. The PLP cofactor is shown in navy, helices in red, loops in grey and sheets in cyan.

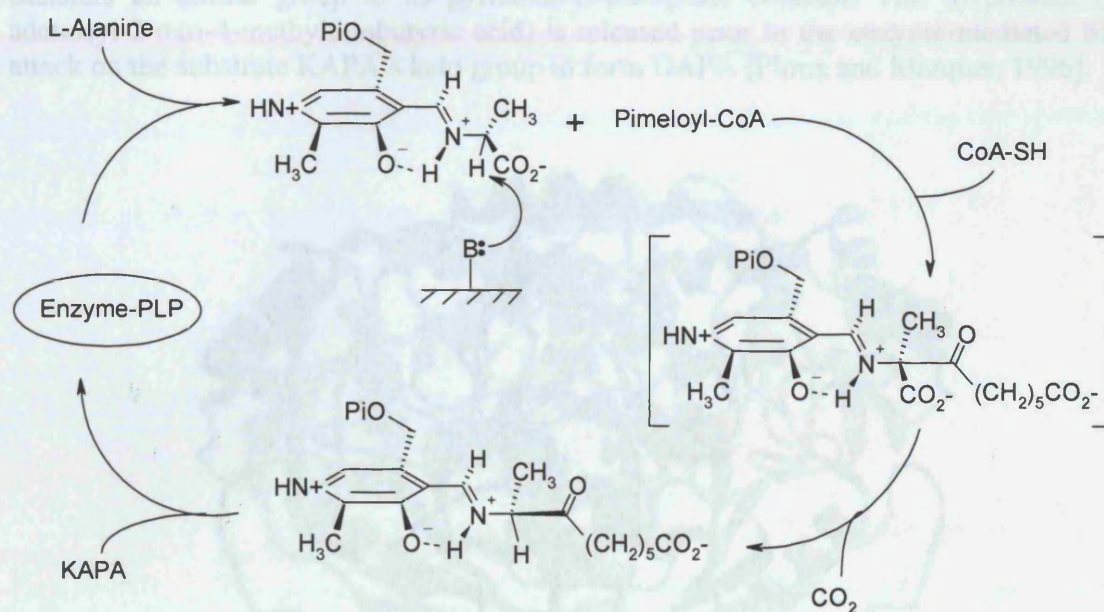


**Figure 1.56** The formation of 7-keto-8-aminopelargonic acid as catalysed by KAPA synthase. Adapted from [Ploux *et al.*, 1999]. L-alanine is bound to pyridoxal-5'-phosphate before reacting with pimeloyl-CoA to form a  $\beta$ -oxo- $\alpha$ -amino acid intermediate (shown in brackets) whose exact configuration is not known, and release the thioester. The intermediate then undergoes a decarboxylation reaction to produce the PLP-bound product.



The next step in the synthesis is the formation of the diamine from the  $\beta$ -ketoamine. This is catalysed by 7,8-diaminopelargonic acid (DAPA) synthase [Eisenberg and Star, 1968]. This is another B6-dependent enzyme of around 94 kDa in mass. It is a homodimer that uses S-adenosyl-L-methionine (SAM) as the amino group donor [Kack *et al.*, 1999]. DAPA synthase utilises a ping-pong mechanism for its transamination. The PLP co-factor transfers the amine group from SAM to KAPA via its pyridoxamine form (see below) [Ploux and Marquet, 1996].

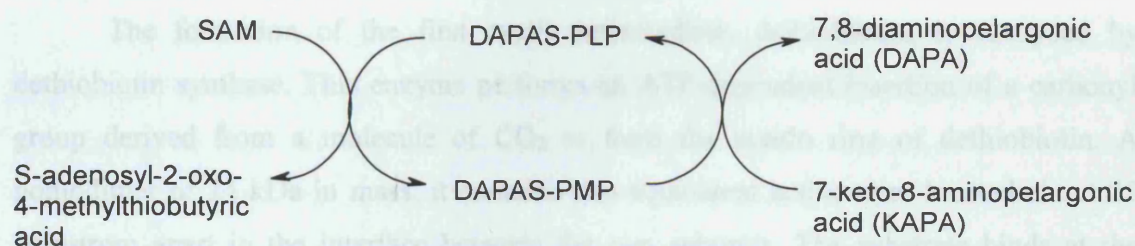


**Figure 1.57** Ping-pong mechanism of DAPA synthase. The protein binds SAM and transfers an amino group to its pyridoxal-L-phosphate cofactor. The by-product (S-adenosyl-2-oxo-4-methylthiobutyric acid) is released prior to the enzyme-mediated  $\text{S}_\text{N}^2$  attack on the substrate KAPA's keto group to form DAPA [Ploux and Marquet, 1996].

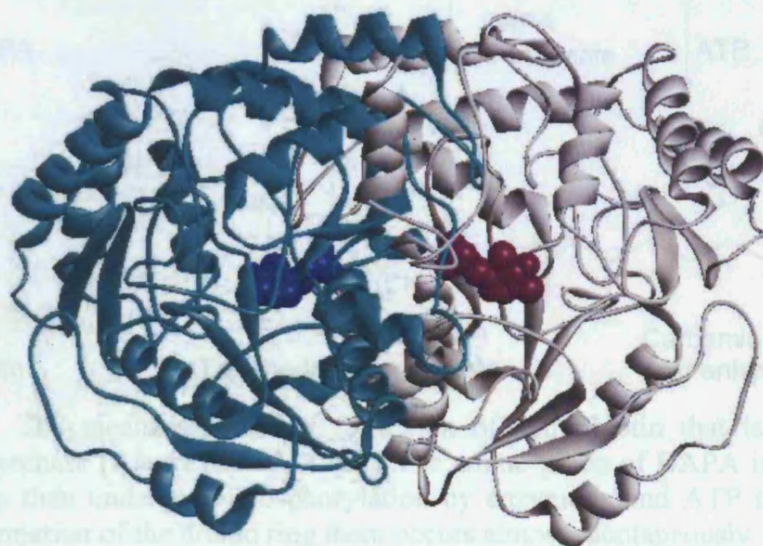


**Figure 1.58** Crystal structure of 7,8-diaminopelargonic acid (DAPA) synthase [Alexeev *et al.*, 2000]. The individual monomers of the dimeric protein are shown in different colours. The PLP cofactors are shown in spacefill, the purple PLP molecule being bound to the grey apoprotein monomer and the navy PLP to the cyan monomer.

The structure of DAPA synthase plays an important role in allowing the substrate (KAPA) to act as an amine group acceptor and not as the donor. The residue R391 forms hydrogen bonds to the terminal carboxyl of KAPA [Elliot *et al.*, 2002]. The dimer contains two equal active sites and each monomer contains two domains. Its cofactor, PLP, binds to a cleft that is formed by both the domains of one subunit and the large domain of the second subunit. PLP is held covalently to the highly conserved K274 and interacts with the main chain nitrogen atoms and a serine side-chain [Ploux and Marquet, 1992, Alexeev *et al.*, 2000].

The formation of the first cyclic intermediate, dethiobiotin, is catalysed by dethiobiotin synthase. This enzyme performs an ATP-dependent insertion of a carbonyl group derived from a molecule of CO<sub>2</sub> to form the ureido ring of dethiobiotin. A homodimer of 24 kDa in mass, it contains two equivalent active sites located about 25 Angstrom apart in the interface between the two subunits. The substrate binds at the interface and interacts with residues from both subunits [Sandalova *et al.*, 1999].

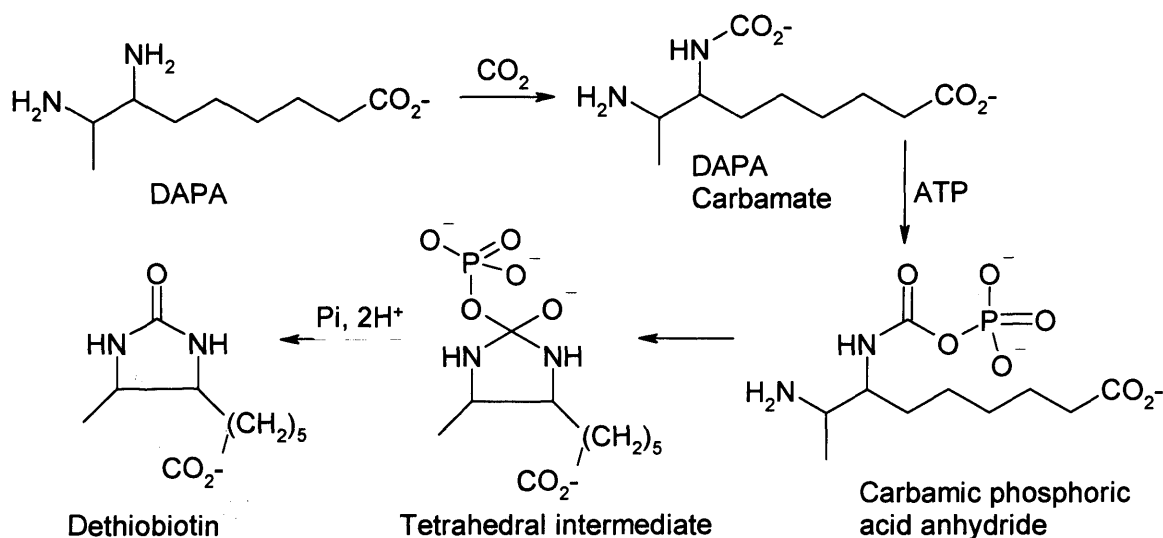


**Figure 1.59** The mechanism of the formation of dethiobiotin that is catalysed by dethiobiotin synthase [Alexeev *et al.*, 1998]. The amine group of DAPA is carboxylated and this group then undergoes phosphorylation by enzyme-bound ATP to produce the anhydride. Formation of the ureido ring then occurs almost spontaneously.

The reaction involves the *regio*-specific formation of the N<sup>7</sup> carbamate [Gibson *et al.*, 1995]. The second reactive intermediate, the carbamic phosphoric acid anhydride, is



formed via donation of the  $\gamma$ -phosphoryl group from ATP [Alexeev *et al.*, 1998]. The negative charges at both phosphate groups after phosphoryl transfer are stabilised by  $\text{Mg}^{2+}$  ions. K51 also helps stabilise the intermediate by formation of a salt bridge [Kack *et al.*, 1998]. The final step involves the nucleophilic attack of the  $\text{N}^8$  onto the carbonyl group with subsequent release of the phosphate group. This allows the formation of the ureido group of dethiobiotin. This ring closure step requires the rotation of the ureido ring by almost  $180^\circ$ , suggesting considerable displacement of the substrate atoms. For the enzyme itself only minor conformational changes are observed.

The insertion of an atom of sulphur to form the second fused heterocycle is catalysed by biotin synthase [Yang *et al.*, 1997]. The exact structure and mechanism of this enzyme is not yet known. Encoded by *bioB*, it is a homodimer of 38.5 kDa monomers each containing a [2Fe-2S] cluster which reduces to an oxygen sensitive [4Fe-4S] cluster [Ugulava *et al.*, 2000 and 2002]. A sequence motif of 3 cysteine residues (known as the cysteine box, C53, 57, and 60) is contained within the enzyme, a sequence found in other SAM-dependent enzymes. These residues are essential ligands to the iron atoms of the cluster. Biotin synthase shares this characteristic motif (CXXXCXXC), believed necessary for iron binding, with enzymes such as lipoate synthase and pyruvate formate lyase [Marquet *et al.*, 2001]. The reaction requires the presence of NADPH, a flavodoxin, flavodoxin  $\text{NADP}^+$  reductase and SAM [Sanyal *et al.*, 1996]. In *E. coli*, MioC (an FMN binding protein of 15.7 kDa) is believed to form part of the redox chain, passing electrons to the FeS cluster of BioB [Birch *et al.*, 2000]. The reduced form of the cluster,  $[\text{4Fe-4S}]^+$ , is able to carry out the single electron reduction of SAM [Cosper *et al.*, 2002]. Biotin synthase is analogous to pyruvate formate lyase, anaerobic ribonucleotide reductase, lysine-2,3-aminotransferase and lipoic acid synthase. The first three of these enzymes all require SAM to function, the cleavage of which generates a methionine and a radical species, the latter being required to cleave a C-H bond. Studies with biotin synthase have also shown that SAM acts not as the sulphur donor, but cleaves to methionine and a 5'-deoxyadenosyl radical [Ugulava *et al.*, 2003]. This radical reacts with the dethiobiotin, abstracting a hydrogen atom from the unreactive methyl group, and a second equivalent abstracts a hydrogen from the methylene group.

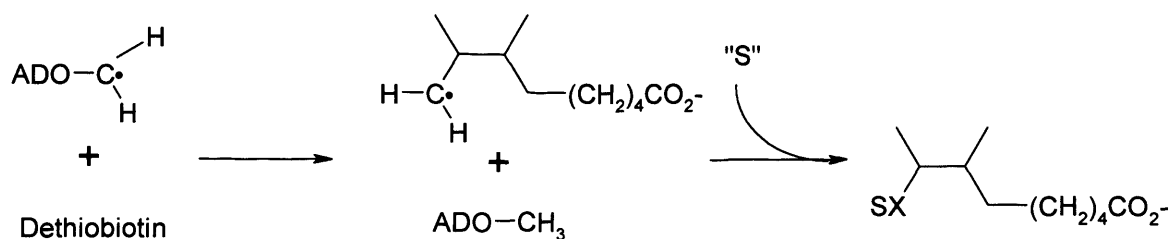


**Figure 1.60** Cleavage of the inert C-H bond by activated S-adenosylmethionine (SAM), represented here as ADO-CH<sub>2</sub> [Ugulava *et al.*, 2000]. The source of the sulphur atom (“S”) is still disputed.

Biotin synthase's FeS cluster may act as the source of the sulphur atom itself. Investigations using reaction analogues have shown that [4Fe-4S] clusters are capable of cleaving sulfonium cations in a two-electron reduction process [Daley and Holm, 2001]. The bond cleaved results in the formation of a radical. Attack of a FeS cluster cysteine ligand by SAM appears unlikely from Mossbauer and resonance Raman data. The 5'-deoxyadenosyl radical generated is sufficiently stabilised so as to abstract a hydrogen from dethiobiotin without it undergoing reduction itself.

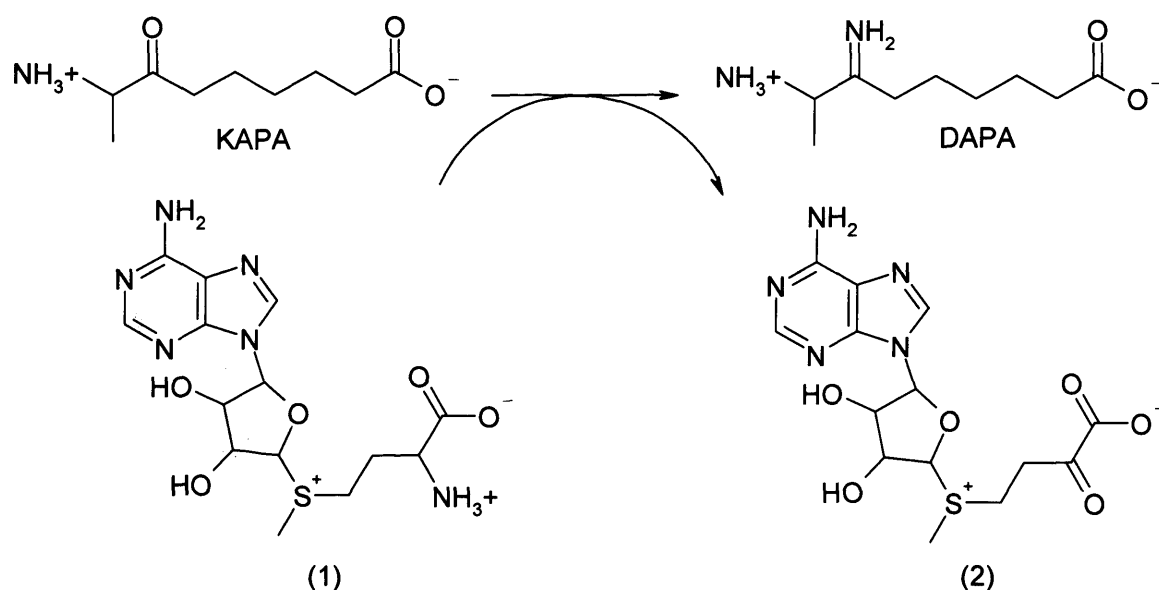


**Figure 1.61** DAPA-catalysed aminotransferase reaction with SAM (1) as the source of the amine group. This reagent and its postulated side-product (2) are not believed plausible sulphur donors for biotin synthase [Daley and Holm, 2001].

Work by Sanyal in the mid 1990's used anaerobic assays of purified proteins in addition to anaerobic ones using crude extracts. From these results it was thought that the FeS cluster donated the sulphur atom. Three successive turnovers were observed meaning replenishment of the FeS cluster would be necessary [Sanyal *et al.*, 1996]. From their data the authors concluded that neither SAM nor the products from the previous transamination reaction (see below) were the sulphur donors. These results disagreed with some earlier work [Birch *et al.*, 2000] but in Birch's work crude extracts were used and the  $^{35}\text{S}$  from labelled cysteines that Birch saw incorporated into biotin could have been via an intermediate.

The source of the sulphur atom is still disputed; Marquet and co-workers believe the sulphur to be donated from the FeS cluster of BioB itself [Bui *et al.*, 1998]. By use of labelled sulphur in the BioB FeS cluster,  $^{34}\text{S}$  was found to be incorporated into 67 % of the biotin produced. They observed some exchange of the cluster sulphides with external sulphides, but concluded that as free  $\text{S}^{2-}$  is unable to trap the radical species thought to be involved, free sulphides are not a plausible intermediate. Other work suggested that two FeS clusters are present in biotin synthase, the [4Fe-4S] cluster used to reduce SAM and a [2Fe-2S] one thought to be involved in the donation of sulphur [Ulgava *et al.*, 2000]. Donation by BioB itself, which is then regenerated by another enzyme catalysed reaction to insert a sulphur into the apoenzyme, would mean that BioB acts as both a substrate as well as aiding the mechanism of biotin formation. BioB has been shown to display a PLP-dependent cysteine desulfurase activity in the presence of DTT, in which the residues C97 and C128 are involved [Ollagnier de Choudens *et al.*, 2002]. Free L-cysteine is converted into alanine in this process and a protein bound persulfide is observed to form. The PLP is believed to bind via K49 near the cysteine box. Reported activities of BioB assay mixtures are rarely in excess of 1 nmol of biotin per nmol of monomer (typically  $\sim 0.08/\text{hr}$ ). Only single turnovers are observed *in vitro* with purified proteins, either due to some irreversible inactivation occurring or since some as yet unidentified, factor is missing, such as an FeS cluster-forming protein.

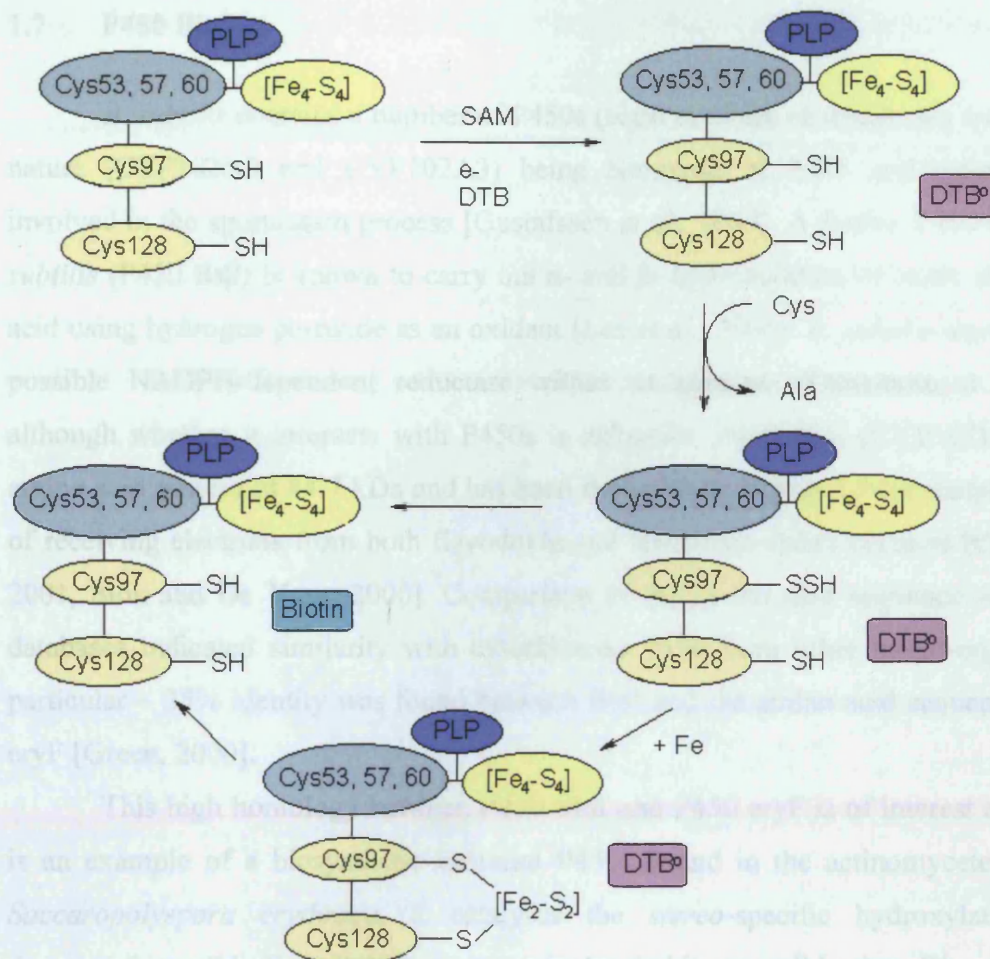


**Figure 1.62** Postulated mechanism by which biotin synthase utilises cysteinyl sulphur. In the first step the FeS cluster catalyses the one electron reduction of SAM via reduced flavodoxin. The 5'-deoxyadenosyl radical then abstracts a hydrogen from dethiobiotin (DTB). In the second step there is a sulphur transfer from cysteine to the substrate radical via the formation of a protein bound persulfide at either cysteine 97 or 128 [Bui *et al.*, 1998].

Mossbauer studies of <sup>57</sup>Fe-reconstituted biotin synthase showed that the anaerobically prepared enzyme contained two [4Fe-4S] clusters per dimer, contrary to earlier reports where a single [4Fe-4S] cluster bridged the two subunits [Ollagnier de Choudens *et al.*, 2000]. It was noted that, if prepared strictly anaerobically, the related enzyme lipoyl synthase also contained a [4Fe-4S] cluster per subunit. The FeS clusters of both enzymes were highly air-sensitive and readily decomposed to [2Fe-2S] centres upon exposure to oxygen.

## 1.7 P450 BioI

*B. subtilis* contains a number of P450s (eight in total), of which two are class II in nature (CYP102A2 and CYP102A3) being homologs of BM3 and believed to be involved in the sporulation process [Gustafsson *et al.*, 2004]. A further P450 found in *B. subtilis* (P450 Bs $\beta$ ) is known to carry out  $\alpha$ - and  $\beta$ - hydroxylation of lauric and myristic acid using hydrogen peroxide as an oxidant [Lee *et al.*, 2003]. *B. subtilis* also contains a possible NADPH-dependent reductase within its genome [Yamamoto *et al.*, 1997] although whether it interacts with P450s is unknown. P450 BioI (CYP107H) is a 395 amino acid protein of 44.7 kDa and has been shown to be a class 1 P450 enzyme capable of receiving electrons from both flavodoxin and ferredoxin redox partners [Green *et al.*, 2001, Stok and De Voss, 2000]. Comparison of the amino acid sequence with protein databases indicated similarity with cytochromes P450 from other micro-organisms. In particular  $\sim 35\%$  identity was found between BioI and the amino acid sequence of P450 eryF [Green, 2000].

This high homology between P450 BioI and P450 eryF is of interest as the latter is an example of a biosynthetic bacterial P450. Found in the actinomycete bacterium *Saccaropolyspora erythraea*, it catalyses the *stereo*-specific hydroxylation of 6-deoxyerythronolide B (6-DOEB), a large hydrophobic macrolide ring. The structure of P450 eryF is characterised by its large active site that accommodates the bulky substrate. The B helix is in an altered position and, in contrast to the B helix of P450 CAM, its side-chains do not make contact with the bound substrate [Poulos *et al.*, 1986]. This causes the F helix to be shifted away from the substrate-binding site, and the side chains of I174 and L175 make contact with the C15 and C16 of 6-DOEB.

Unusually, P450 eryF does not contain the conserved threonine residue (T252 in P450 CAM) in the distal I helix that is critical in dioxygen binding and cleavage. P450 eryF has an alanine instead, but its I helix still has a similar distortion partially stabilised by a hydrogen bonding network. This hydrogen bonding pattern involves, unusually, the substrate. A water molecule is positioned so that it replaces the hydroxy group of the missing threonine and a second water molecule (Wat519) is positioned very close (3.8 Angstrom) to the iron atom acting as a proton donor [Cupp-Vickery *et al.*, 1996]. It is



thought that in P450 eryF the substrate plays a critical role itself as a hydrogen bond donor (via its C5 hydroxyl group) and that the correct hydrogen bond network is paramount for efficient catalysis [Cupp-Vickery *et al.*, 1997]. P450 eryF is, as a result, a highly specific hydroxylase requiring precise positioning of its substrate within the active site, which is in keeping with its role as a biosynthetic enzyme.

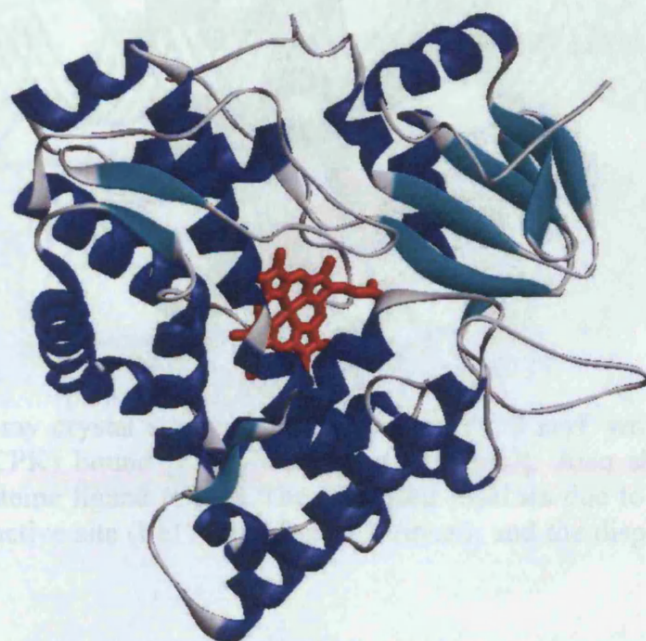


**Figure 1.63** Structure of P450 eryF, a biosynthetic P450 from the actinomycete bacterium *Saccaropolyspora erythraea*. [Cupp-Vickery *et al.*, 2001] The heme (red) is embedded in the protein core. The apo-protein is composed mainly of helices (navy) and some  $\beta$ -sheet (cyan) with the interconnecting loops in grey.

P450 eryF can bind certain steroids shifting from a low to high spin upon binding. P450 BioI exhibits several similarities with P450 eryF such as the ability to bind steroids and bulky polycyclic molecules as reported in chapter 3. P450 eryF bound androstenedione co-operatively ( $K_d$  of 365  $\mu$ M) and the crystal structure showed this to be due to two steroid molecules being simultaneously bound in the active site without any major conformational changes in the protein [Cupp-Vickery *et al.*, 2000]. Hong's group showed that by mutating A245 to the more usual threonine residue, oxidation of testosterone could be catalysed [Xiang *et al.*, 2000].



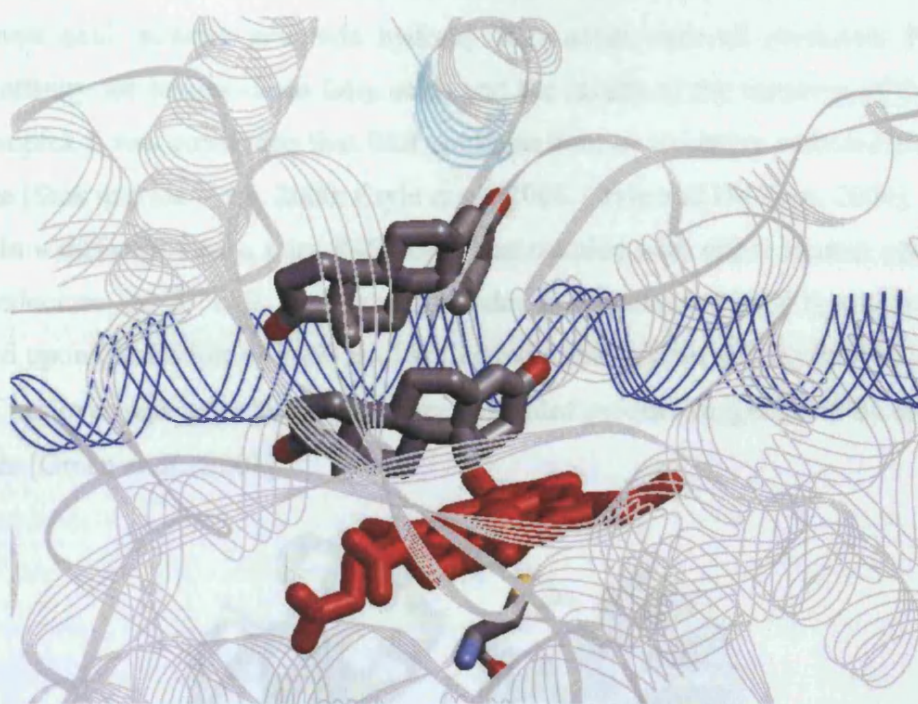


**Figure 1.64** X-ray crystal structure of cytochrome P450 eryF with two molecules of androstendione (CPK) bound [Cupp-Vickery *et al.*, 2000]. Also shown are the heme (red), and the cysteine ligand (CPK). The displaced residues due to the binding of two molecules in the active site (Ile174 and Leu175) (cyan), and the displaced I-helix (navy) are also shown.

P450 BioI has a UV-visible spectrum characteristic of a P450, with the Soret band at 448 nm when reduced and bound to exogenous CO [Green *et al.*, 2001]. Key amino acids were identified from the sequence; C345 is the proximal sulphur ligand to the heme iron, T238 a possible proton donor/acceptor to the heme and F338 is thought involved in control of heme iron electronegativity. All the spectroscopic studies done to date (EPR, MCD and Resonance Raman) indicated the presence of some high spin heme as well as the expected low spin in the preparations of P450 BioI. This is unusual for bacterial P450s, as these tend to only show high spin on the binding of substrate to the heme [Lewis and Taylor 1996]. P450 BioI was reported to be co-purified with an acyl-carrier protein (ACP) [Stok and De Voss, 2000]. Electrospray mass spectrometry analysis showed the ACP to be bound to a range of fatty acids. Incubation of P450 BioI, ACP with *E. coli* flavodoxin reductase, cindoxin and NADPH in the presence of various fatty acids showed the formation of ACP-bound pimelic acid (5 %). The turnover of palmitic



acid showed that the products varied with the ratio of BioI to redox partners, and that undecanoic acid, pimelic acid and hydroxy fatty acids were all produced. From the ACP's affinity for longer chain fatty acids and the results of the turnover of the ACP - BioI complex it was concluded that BioI could perform an oxidative carbon-carbon bond cleavage [Stok and De Voss, 2000, Cryle *et al.*, 2003, Cryle and De Voss, 2004].

In a different study, pure P450 BioI was coupled with either human cytochrome P450 reductase or *E. coli* flavodoxin/flavodoxin reductase. NADPH oxidation was observed upon incubation of P450 BioI with a reductase system and myristic acid. A low level of turnover was recorded to give a hydroxylated product suggested to be  $\omega$ -hydroxy myristate [Green *et al.*, 2001].

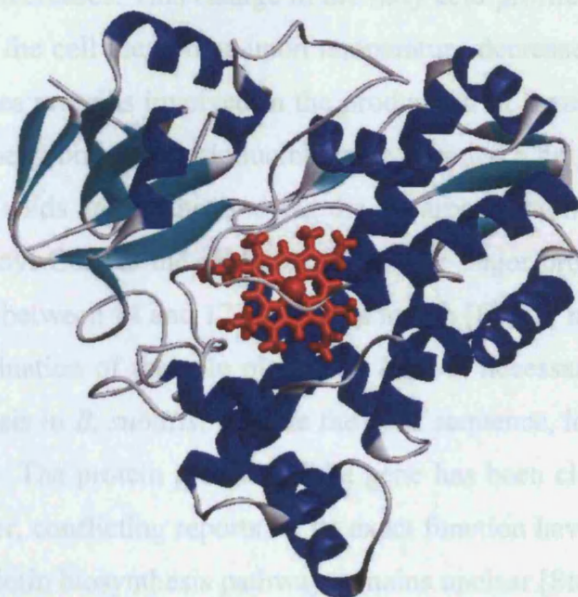


**Figure 1.65** Homology model of P450 BioI [produced by Prof. M.J. Sutcliffe, University of Leicester] showing the possible structure of the P450. For details on how the model was built see section 3.7. The heme co-factor is shown in red, the loops in grey,  $\alpha$ -helices in navy and  $\beta$ -sheets in cyan.

On the basis of BioI being a P450, it is believed that *B. subtilis* synthesises pimelic acid by an oxidative route such as the oxidation of an unsaturated fatty acid, carbon-carbon bond cleavage or terminal hydroxylation [Cryle *et al.*, 2003]. BioI is thought to use either a free fatty acid or its CoA thioester as a substrate to produce pimelic acid or pimeloyl CoA respectively.

Several types of fatty acids are known in *B. subtilis*, all being potential substrates for BioI. Being a soil microbe it has adapted to live in a variety of conditions. In low temperatures the bacteria are known to produce a number of branched chain and unsaturated fatty acids in addition to the straight chain saturated ones normally found (palmitic acid typically constitutes 5 – 10 % of the cellular lipids [Kaan *et al.*, 2002]). Transcriptional profiling of *B. subtilis* has shown that the operons encoding biotin and thiamin biosynthesis show the strongest decrease in their mRNA levels when the organism undergoes a cold-shock response [Kaan *et al.*, 2002]. This reduced expression is thought due to the lower growth rate after cold-shock (18 °C). Under these conditions the content of *anteiso*-branched chain fatty acids increases whilst the levels of *iso*-branched fatty acids decreases. This change in the fatty acid profile is in accordance with the reorganisation of the cell membrane upon temperature decrease. The transcription of an operon that encodes proteins involved in the production of branched chain carboxylic acids increases and the strongest cold-inducible gene encoded a fatty acid desaturase. The branched chain fatty acids are synthesised via the decarboxylation of branched chain  $\alpha$ -keto acids with malonyl-CoA as the chain extender. The major products are the *iso*- and *anteiso* fatty acids of between 14 and 17 carbons in length [Oku *et al.*, 1988].

Further examination of the role played by BioI is necessary to clarify the early steps in biotin synthesis in *B. subtilis*. To date the gene sequence, location and regulation have been elucidated. The protein product of the gene has been cloned, over-expressed, and purified. However, conflicting reports on its exact function have arisen and therefore its exact role in the biotin biosynthesis pathway remains unclear [Stok and DeVoss, 2000, Green *et al.*, 2001]. As a result, this project had two main goals; a greater understanding of the biochemical and biophysical properties of P450 BioI and the clarification of its function and interactions. Further characterisation of the P450 in regards to its binding, redox and electron transfer properties was undertaken including investigations into the protein's stability and interactions with various heterologous redox partners. The cloning, over-expression and characterisation of *B. subtilis* flavodoxins and NAD(P)H-oxidoreductases was also performed, their interaction with BioI analysed and the ability of this native *B. subtilis* redox system to oxidise various compounds was assessed.

## *Chapter 2*

### *Materials and Methods*



## 2 Materials and Methods

All reagents were purchased from Sigma and were of the highest grade available, unless specified otherwise. UV-visible absorption spectra were recorded between 250-750 nm using a Varian Cary 50 spectrophotometer and a quartz cuvette of 1 cm path length. Fluorescence measurements were made using a Varian Cary 50 Fluorimeter. Unless stated otherwise sterilised, de-ionised water was used to make all reagents/dilutions (UV irradiation and 0.22 µm filtration, Gilson).

### 2.1 Bacterial Strains

*E. coli* strains used in cloning work and for recombinant protein expression are shown in the table below. Unless stated otherwise all strains came from Novagen.

Strain	Genotype	Reference
<i>E. coli</i> TG-1	<i>supE hsdΔ5 thi Δ(lac-proAB) F<sup>-</sup> [traD36 proAB<sup>+</sup> lacI<sup>q</sup> lacZΔM15]</i>	Gibson, 1984
<i>E. coli</i> JM109 (DE3)	<i>recA1 supE44 endA1 hsdR17 gyrA96 relA1 thi Δ(lac-proAB)</i>	Yannisch-Peron <i>et al.</i> , 1985
<i>E. coli</i> BL21 (DE3)	<i>F<sup>-</sup>ompT hsdS<sub>B</sub>(r<sub>B</sub><sup>-</sup>m<sub>B</sub><sup>-</sup>) gal dcm (λDE3)</i>	Studier and Moffat, 1986
<i>E. coli</i> BL21 (DE3) pLysS	<i>F<sup>-</sup>ompT hsdS<sub>B</sub>(r<sub>B</sub><sup>-</sup>m<sub>B</sub><sup>-</sup>) gal dcm (λDE3) pLysS(Cm<sup>R</sup>)</i>	Studier and Moffat, 1986; Studier, 1991
<i>E. coli</i> Origami (DE3)	<i>Δara-leu7697 ΔlacX74 ΔphoAPvuII phoR araD139 ahpC gale galK rpsL F<sup>0</sup>[lac<sup>-</sup>(lacI<sup>f</sup>)pro] gor522 ::Tn10(Tc<sup>R</sup>) trxB::kan (DE3)</i>	Bessette <i>et al.</i> , 1999; Ritz <i>et al.</i> , 2001
<i>E. coli</i> HMS174 (DE3)	<i>recA1 hsdR rif<sup>r</sup> (λDE3)</i>	Studier and Moffat, 1986
<i>E. coli</i> BL21 codon plus (DE3) RP	<i>B F- ompT hsdS(r<sub>B</sub>-m<sub>B</sub>-) dcm<sup>+</sup> Tet<sup>R</sup> gal λ (DE3) endA Hte [argU proL Cam<sup>R</sup>]</i>	Jerspeth <i>et al.</i> , 1998; Greener <i>et al.</i> , 1997
<i>E. coli</i> XL-1 Blue	<i>recA1 endA1 gyrA96 thi-1 hsdR17 supE44 relA1 lac [F<sup>'</sup>proAB lacI<sup>q</sup>ZΔM15 Tn10 (Tet<sup>f</sup>)]</i>	Jerspeth <i>et al.</i> , 1992
<i>E. coli</i> XL-10 Gold	<i>Tet<sup>r</sup> Δ(mcrA)183 Δ(mcrCB-hsdSMR-mrr)173 endA1 supE44 thi-1 recA1 gyrA96 relA1 lac Hte [F<sup>'</sup> proAB lacI<sup>q</sup>ZΔM15 Tn10 (Tet<sup>f</sup>) Amy Cam<sup>r</sup>]</i>	Jerspeth <i>et al.</i> 1998; Aslanidis and de Jong 1990

## 2.2 Common Reagents

### 2.2.1 Growth media for *E. coli*

All media was prepared as detailed below [Sambrook *et al.*, 1989] and sterilised by autoclaving (124 °C for 20 minutes).

#### Luria-Bertani Medium

	per litre (dH <sub>2</sub> O)
Bacto-tryptone	10 g
Bacto-yeast extract	5 g
NaCl	10 g

#### SOC Medium

	per litre
Bacto-tryptone	20 g
Bacto-yeast extract	5 g
NaCl	0.5 g
dH <sub>2</sub> O	950 ml
250 mM KCl	10 ml

Media was cooled (60 °C) and sterile glucose solution was added (20 ml, 1.0 M). Prior to use, a sterile solution of magnesium chloride was added (5 ml, 2.0 M).

#### Agar Plates

	per litre (dH <sub>2</sub> O)
Bacto-tryptone	10 g
Bacto-yeast extract	5 g
NaCl	10 g
Agar	15 g

The agar solution was cooled (50 °C), the appropriate antibiotic added (see table below) and the agar poured into plates. Plates were stored (4 °C) for up to four weeks.

## Antibiotics

	Stock solution	Working concentration
Ampicillin	50 mgml <sup>-1</sup>	50 µgml <sup>-1</sup> in liquid media 100 µgml <sup>-1</sup> in solid media
Chloramphenicol	34 mgml <sup>-1</sup> (in ethanol)	50 µgml <sup>-1</sup> in liquid media 50 µgml <sup>-1</sup> in solid media
Kanamycin	50 mgml <sup>-1</sup>	15 µgml <sup>-1</sup> in solid media 15 µgml <sup>-1</sup> in liquid media
Tetracycline	30 mgml <sup>-1</sup>	12.5 µgml <sup>-1</sup> in liquid media
Rifampicin	10 mgml <sup>-1</sup> in 67% methanol, 0.17 NaOH	200 µgml <sup>-1</sup> in liquid and solid media

Solutions of antibiotics were sterilised (0.22 µm filter, Amicon) immediately prior to use.

### 2.2.2 Electrophoresis Reagents

#### 50 × TAE buffer

	Per litre (dH <sub>2</sub> O)
Trizma base	242g
Glacial acetic acid	57.1 ml
0.5 M EDTA (pH 8.0)	100 ml

#### Resolving Gel (per 10 ml)

	10 % (ml)	15 % (ml)
dH <sub>2</sub> O	4.0	2.3
30 % Acrylamide	3.3	5.0
1.5 M Tris.HCl (pH 8.8)	2.5	2.5
10 % SDS	0.1	0.1
10 % APS	0.1	0.1
TEMED	0.004	0.004

#### 4 % Stacking Gel

	per 2 ml (ml)
dH <sub>2</sub> O	1.4
30 % Acrylamide	0.33
1.0 M Tris.HCl (pH 6.8)	0.25
10 % SDS	0.02
10 % APS	0.02
TEMED	0.002

#### 5 × Running Buffer

	per litre (dH <sub>2</sub> O) (g)
Tris base	15
Glycine	72
SDS	5

#### WET Blotting 10 x Transfer Buffer

	per litre (dH <sub>2</sub> O)
dH <sub>2</sub> O	900 ml
39 mM Glycine	
48 mM Tris.HCl	5.82 g
SDS	0.3 g
Methanol	100 ml

#### WET blotting Stain (Coomassie Blue)

	per litre (dH <sub>2</sub> O)
dH <sub>2</sub> O	500 ml
Coomassie Blue R-250	10 g
Acetic Acid (glacial)	100 ml
Methanol	400 ml

#### WET Blotting Destain

	per litre (dH <sub>2</sub> O)
dH <sub>2</sub> O	500 ml
Acetic Acid (glacial)	100 ml
Methanol	400 ml



### 2.2.3 Protein Purification Reagents

All column chromatography was performed at 4 °C. All buffers used during purification contained the protease inhibitor benzamidine hydrochloride (0.1 mM) and all were filtered (0.22 µm filter, Gilson) prior to use.

#### 50 mM Tris.HCl (pH 7.2) (Buffer A)

	per litre
Trizma base	6.06 g
EDTA	0.38 g
dH <sub>2</sub> O	900 ml

The pH of the solution was adjusted (pH 7.2) by the addition of HCl (1.0 M, *ca* 2.0 ml). A high salt version of this buffer was made for eluting ion-exchange columns by adding KCl (0.50 or 1.0 M) to Buffer A to give **Buffer B**.

#### 25 mM Potassium phosphate buffer (Buffer C)

Solutions of KH<sub>2</sub>PO<sub>4</sub> and K<sub>2</sub>HPO<sub>4</sub> (25mM) were prepared and mixed together to achieve the final pH of 6.5. **Buffer D** was prepared in an identical manner to Buffer C but was of higher molarity (500 mM).

#### DEAE Anion-exchange Column

The DEAE column (15 cm × 3 cm wet volume of diethylaminoethane covalently cross-linked to cellulose (Pharmacia)) was pre-equilibrated with Buffer A (2 column volumes, pH 7.2). The protein was loaded (0.2 ml/min) and washed (Buffer A, 4 column volumes, 0.2 – 0.3 ml/min). After use the column was regenerated (1.0 M KCl, 1 column volume followed by NaOH, 1 column volume, 1.0 M) and washed (water, 2 column volumes). The cleaned material was then re-equilibrated (Buffer A, 2 column volumes).

### **Hydroxyapatite Column**

Hydroxyapatite (BioRad) is crystalline calcium phosphate  $[\text{Ca}_5(\text{PO}_4)_3\text{OH}]_2$ . The column material was suspended ( $10 \times$  volume of Buffer C), the slurry left to settle and the finings removed. A 15 cm  $\times$  2 cm column was poured and washed with buffer. Regeneration of the hydroxyapatite material was achieved by washing (500 mM KPi, pH 6.5), before re-equilibrating with Buffer C.

### **Quaternary Ammonium (Q-) Sepharose Column**

Q-Sepharose ( $\text{CH}_2\text{N}^+(\text{CH}_3)_3$ ) is a strong anion exchanger (Pharmacia). The column was equilibrated by extensively washing with Buffer A (2 column volumes). After use, the column was washed (2.0 M KCl, 1 column volume), regenerated (1.0 M NaOH, 1 column volume), washed (water, 2 column volumes) and then re-equilibrated (Buffer A).

### **Sephadex G-200 column**

A Sephadex G-200 (Pharmacia) gel filtration column was used to separate proteins between 3,000 and 50,000 Da. Sephacryl-G50 (Pharmacia) gel filtration columns were used for low molecular weight proteins (1,000 – 50,000 Da). The material was suspended in buffer (10 mM Tris.HCl, pH 7.5) and a column (25 cm  $\times$  2 cm) was poured and washed with several volumes of the buffer. After use, the column was cleaned/re-equilibrated by washing extensively with Buffer A.

### **Phenyl Sepharose column**

Phenyl Sepharose fast flow (Pharmacia) separates proteins according to the varying strength of their hydrophobic interactions with the hydrophobic groups on the uncharged gel matrix. Bound proteins are eluted by reducing the hydrophobic interaction, in this case by reducing the concentration of the salt ions in the buffer. The column was equilibrated prior to use by extensively washing with a solution of ammonium sulphate

(1.5 M) in Buffer A. Proteins were eluted via a decreasing salt gradient (1.5 to 0 M ammonium sulphate). After use, the column was washed (1.0 M NaOH 2 column volumes, water 2 column volumes) and then re-equilibrated (1.5 M ammonium sulphate in Buffer A).

### **2',5'-ADP Sepharose column**

For purification of the flavodoxin reductase from *E. coli*, a 2',5'-ADP Sepharose affinity column (Sigma) (1 x 20 cm) was used. This column ligand mimics the nicotinamide cofactor of the reductase, thereby binding the protein. The column is pre-equilibrated with the loading buffer (KPi 25 mM, pH 7.0) and the protein bound. The bound protein was washed (loading buffer, 3 column volumes) and eluted by increasing the ionic strength of the buffer (addition of 500 mM KCl).

## **2.3 General Molecular Biology Techniques**

### **2.3.1 Culture Growth**

*E. coli* cells were grown by inoculating a single colony in the appropriate broth. These cultures were then incubated (37 °C, 220 rpm) until the appropriate cell density was achieved.

### **2.3.2 Maintenance and storage of cultures**

Bacterial colonies were maintained on agar plates (up to 4 weeks at 4 °C). For long-term storage, a fresh overnight culture (0.90 ml) was mixed with sterile glycerol (80 % v/v, 0.10 ml) then snap-frozen using a dry ice/ethanol bath and stored (– 80 °C). Prior to use these stocks were thawed and streaked onto fresh agar plates.

### **2.3.3 Transformation of *E. coli* cell strains**

*E. coli* cells were grown overnight (16 hrs, 37 °C, 220 rpm) in LB (5.0 ml) in the presence of the appropriate antibiotic (see section 2.2.1). The cells were pelleted (6000 rpm, 1 minute) and re-suspended (0.5 ml, 50 mM calcium chloride). The suspension was cooled (4 °C, 1 hour) and plasmid DNA added (1 - 3 µg). After cooling (4 °C, 1 hour) the suspensions were heat shocked (42 °C, 1 minute) and returned to ice (2 minutes). SOC media (0.8 ml) was added and the suspensions incubated (37 °C, 1 hour, 220 rpm) prior to pelleting the cells (6000 rpm, 1 minute). The cells were re-suspended (100 µL LB) and spread onto agar plates (LB agar, appropriate antibiotic). The colonies were allowed to grow (37 °C, 10 - 14 hours) before being picked out and re-plated.

### **2.3.4 Small-scale isolation of plasmid DNA**

Qiagen Kits were used for the extraction of plasmid DNA from transformed *E. coli* cultures. LB (5.0 ml), containing the appropriate antibiotic was inoculated with a single colony of the plasmid-carrying strain and incubated overnight (37 °C, 220 rpm). The culture was transferred to microcentrifuge tubes and pelleted (6000 rpm, 1 minute). The resulting pellet was resuspended in the manufacturer's lysis buffer (TE containing RNaseA, 250 µL) and treated as in accordance with the manufacturer's protocol (for a microfuge scale preparation).

Larger scale preparations were carried out using a Qiagen maxi-prep kit. An overnight culture (500 ml) was grown up as described above. The cells were collected (5000 rpm, 10 minutes) re-suspended in lysis buffer (TE containing RNaseA, 5.0 ml) and treated in accordance with the manufacturer's protocol.

### **2.3.5 Diagnostic restriction enzyme digests**

Restriction digests were performed using the applicable DNA (0.2 - 1 µg), 10 x Bovine Serum Albumin (BSA) (1.5 µl) if required, 10 x enzyme buffer (1.5 µl), ~ 10

units of the enzyme and sterile dH<sub>2</sub>O (to 15 µl total volume). The digest mixture was incubated (37 °C, 1 hour).

### **2.3.6 Agarose gel electrophoresis**

DNA fragments were separated by agarose gel electrophoresis. Agarose gel (1 % w/v, electrophoresis grade) was made up in 1 × TAE buffer (see section 2.2.2). Ethidium bromide (0.5 µgml<sup>-1</sup>) was added for visualisation of the DNA. DNA samples (10 µl) were mixed with loading buffer (2 µl). The loading buffer consisted of Bromophenol blue (0.25 % w/v), Xylene cyanol FF (0.25 % w/v) and Ficoll Type 400 (Pharmacia) (15 % w/v) in water. A 1 kb ladder (4 µl) (NEB) was used as a marker. Gels were run (60 mA for *ca* 30 minutes) and the DNA was visualised by UV illumination.

## **2.4 Cloning of potential redox partners**

### **2.4.1 Cloning of the flavodoxins *ykuN* and *ykuP* (with Dr Claes von Wachenfeldt, Lund University, Sweden)**

#### **2.4.1.1 Isolation of *B. subtilis* chromosomal DNA (Caesium chloride density method)**

LB (2 x 400 ml) was inoculated with an overnight culture (25 ml) of *B. subtilis* and grown (37 °C, 200 rpm, 10 hours). Cells were harvested by centrifugation (9000 rpm, 20 minutes, 4 °C). The cell pellet was resuspended (10 ml, GTE) and re-pelleted (as before). After resuspending (4 ml, GTE), lysozyme (0.5 ml, 5 mg/ml stock) and RNaseA (0.2 ml, 2 mg/ml stock) were added and the mixture incubated (37 °C, 30 minutes). Triton X-100 (0.7 ml, 8 % v/v in GTE) and Pronase (0.3 ml, 5 mg/ml stock) were added and the suspension incubated (37 °C, 1 hour). Caesium chloride (5.92 g, *ca* 1w/v) was added and swirled to dissolve. Ethidium bromide (0.3 ml, 10 mg/ml) was added and the resulting pink solution poured into Beckman Optiseal tubes (4.9 ml) and centrifuged (55000 rpm, 20 °C, 16 hours).



The DNA was visualised (UV light) and extracted via a syringe. After transfer to a siliconised glass tube, the ethidium bromide was removed (isopropyl alcohol/10 mM TE, pH 7.5, 5.0 M sodium chloride). Sterile, distilled water (2 vol) was added to the colourless aqueous layer and ethanol (2 vol, 95% v/v, -20 °C) was added that precipitated the DNA. The DNA was recovered by centrifugation (15000 rpm, 15 minutes, 4 °C), washed (75 % v/v ethanol, -20 °C) and stored (4 °C, 16 hours). The pellet was resuspended (sterile water, 1.0 ml) and phenol (pH 8.0, 1.0 ml) was added. The aqueous layer was retained and extracted (water saturated phenol:chloroform, 1:1, 1 ml), and the DNA precipitated by the addition of ethanol (95 % v/v, 2.5 vol, -20 °C). The DNA was pelleted by centrifugation (4000 rpm, 10 minutes) and the pellet washed (75 % v/v ethanol, -20 °C) and dried under vacuum (-25 mBar). The dry pellet was resuspended in TE (1 ml) and stored (4 °C).

The purity of the chromosomal DNA prepared from both methods was analysed by 1 % w/v agarose gel.

#### **GTE Buffer**

	per litre
Tris pH 8.0 (1M)	25 ml
Glucose (1M)	50 ml
dH <sub>2</sub> O	885 ml
EDTA pH 8.0 (250mM)	40 ml

#### **2.4.1.2 Polymerase Chain Reaction**

The PCR reactions were carried out using the Roche High Fidelity PCR kit and a Perkin Elmer PCR machine. Eppendorfs (0.5 ml) were used with a 100 µl reaction volume. Template DNA (1 µl, 50-100 ng), the primers (1 µl, 50 pmol) and the dNTP mix (2 µl) were mixed in one tube (made up to 50µl with sterile, distilled water) and, just before the reaction, added to a second tube which contained the High Fidelity enzyme mix (*Taq* and *Pwo* polymerase, 0.75 µl) and the manufacturer's buffer (10 µl, 1.5 mM magnesium chloride) made up with sterile, distilled water (50 µl).

2.4.2 The PCR machine was programmed according to the temperature profile shown on the next page. After the first ten cycles had been completed, each subsequent cycle was the same but with an extra 5 seconds added to the elongation step per cycle. A total of 30 cycles were run. The PCR product was analysed by running a sample (2  $\mu$ l) on an agarose gel (0.8 % w/v).

The PCR reaction used the following method;

Initial denaturation	94°C, 120 secs
	First 10 cycles
Denaturation	94°C, 30 secs
Annealing	50°C, 30 secs
Elongation	72°C, 120 secs
Final elongation	72°C, 15 min
Final cooling	5°C, infinite

#### PCR primers designed for cloning of *ykuN*

Oligo	Sequence	Restriction site engineered
YkuN-N-term	ATA <u>ACC</u> <u>ATG</u> GCT AAA GCC TTG ATT ACA TAT G	<i>NcoI</i> site at 5' end
YkuN-C-term	<u>CCG</u> <u>GAT</u> <u>CCT</u> TTA TGA AAC ATG GAT TTT TTC C	<i>BamHI</i> site at 3' end

#### PCR Primers designed for cloning of *ykuP*

Oligo	Sequence	Restriction site engineered
ykuP-N-term	GAA <u>TCC</u> <u>ATG</u> GCG AAG ATT TTG CTC GTT TAT G	<i>NcoI</i> site at 5' end
ykuP-C-term	<u>CCG</u> <u>GAT</u> <u>CCT</u> GAT TTT CTA CCT CAT TAC TGT	<i>BamHI</i> sites at 3' end

The bases underlined differ from the sequence of the template DNA, while the bases not underlined are a match. The red bases indicate the restriction sites introduced.

### 2.4.2 Cloning of the diflavin reductase domains from CYP102A2 and CYP102A3

The two diflavin-reductase domains of the class II cytochrome P450s CYP102A2 and CYP102A3 were amplified from chromosomal DNA extracted from strain PY79, which is a prototrophic derivative of *B. subtilis* 168 'Marburg' [Youngman *et al.*, 1984].

#### PCR primers designed for cloning of CYP102A2 (*yetO*) and CYP102A3 (*yrhJ*) reductase domain

Primer Name	Sequence (5' - 3')	Restriction site engineered
yetO N-term	<u>ACG</u> <u>TGC TAG CAT</u> <u>GGA</u> GAA AAC GGA AGC AAA GGG	<i>NheI</i> at 5' end
yetO C-term	<u>ACG</u> <u>TGG ATC</u> <u>CTA</u> TCT ATA TCC CTG CCC AGA CAT CCT TAG C	<i>BamHI</i> at 3' end
yrhJ N-term	<u>ACG</u> <u>TGC TAG CAT</u> <u>GAA</u> AGA AAC CAA ACC TAA ACA C	<i>NheI</i> at 5' end
yrhJ C-term	<u>ACG</u> <u>TGG ATC</u> <u>CAT</u> TTT ACA TTC CTG TCC AAA CGT CTT TCA C	<i>BamHI</i> at 3' end

The bases underlined differ from the sequence of the template DNA, while those bases not underlined are a match. The red bases indicate the restriction sites introduced.

The PCR reactions were carried out using Herculase polymerase (Stratagene, 5 units) and a Perkin Elmer PCR machine. Eppendorfs (0.5 ml) were used with a 50  $\mu$ l reaction volume. Template DNA (*B. subtilis* PY79 chromosomal DNA, 1  $\mu$ l, 150 ng), the primers (5  $\mu$ l of each, 100  $\mu$ M), the dNTP mix (BioRad, 1  $\mu$ l, 10 mM) and the manufacturer's 10x buffer (10  $\mu$ l, 1.5 mM magnesium chloride) were mixed in one tube and made up with sterile, distilled water (to give a final volume of 50  $\mu$ l) and, just before the reaction, the polymerase was added (2 units, 0.75  $\mu$ l).

The PCR reaction used the method shown on the next page;



Initial denaturation	94°C, 2 min
	Repeat of 30 cycles
Denaturation	94°C, 30 secs
Annealing	52°C, 30 secs
Elongation	72°C, 60 secs
Final elongation	72°C, 15 min
Final cooling	5°C, infinite

The PCR product was analysed by running a sample (5 µl) on an agarose gel (1.0 %).

### 2.4.3 Purification of the PCR product

Two methods were used. For the flavodoxins, the product from the PCR (98 µl) was purified using the Qiagen Mini Elute Column purification kit. Recovery of the product eluted from the column (20 µl, 10 mM Tris.HCl, pH 7.5) was checked by running an agarose gel (0.8 % w/v). For the diflavin reductases, the PCR product (45 µl) was purified using Wizard Mini Elute Column purification kit (Promega) following manufacturer's guidelines. Recovery of the product eluted from the column (20 µl, nuclease free water) was checked and the DNA quantified by UV spectroscopy ( $A_{260} = 1$  µg/ml).

### 2.4.4 Enzyme Digest of the PCR product

The purified PCR product of the flavodoxins was added to a solution of restriction enzyme (2 units, 2 µl each of *NcoI* and *BamHI* (NEB)), the buffer (10 µl buffer 2, NEB) and this mixture was diluted with sterile, distilled water (100 µl total volume). The solution was incubated (37 °C, 5 – 6 hours). The digests had loading buffer (25 µl) added and were resolved by running on an agarose gel (0.8 % w/v). The PCR product of the diflavin reductases was treated similarly, the restriction enzymes being slightly different (2 units, 2.0 µl each of *NheI* and *BamHI* (NEB)). These digests were resolved by running on a denser agarose gel (1.0 % w/v).

#### **2.4.5 Recovery of DNA from the agarose gel**

DNA bands were visualised (under UV light) and the appropriate band was excised (using a scalpel) and purified from the agarose using the Qiagen Gel Extraction Kit™ following the manufacturer's protocol. To the gel fragment sodium iodide (3 vol) and absorbent beads were added and the agarose was heated (55 °C, 10 minutes). The beads were pelleted by centrifugation (13000 rpm, 1 minute) and washed (2 x buffer:ethanol, 1:1). The beads were air-dried (37 °C, 20 minutes) to remove any final traces of ethanol. Sterile water (20 µl) was added to the beads and this was centrifuged (13000 rpm, 1 minute) and the supernatant retained. The concentration and purity of the recovered DNA was checked on an agarose gel (0.8 % w/v), prior to subsequent use.

Alternatively, after the addition of sodium iodide, as already described, the solution was added to an absorbent column (Qiagen) and centrifuged (13000 rpm, 1 minute). The column was washed (2 x Tris buffer:ethanol, 1:1). Remaining solvent was removed by an additional spin (as before) to remove any traces of ethanol. Water (20 µl) was added to the column and this was centrifuged (13000 rpm, 1 minute) and the eluent retained. The concentration and purity of the recovered DNA was checked on an agarose gel (1.0 % w/v), prior to subsequent use.

#### **2.4.6 Preparation of the vectors for cloning**

##### **2.4.6.1 Vector pET16b for the flavodoxins**

pET16b was recovered from an overnight culture of *E. coli* TG1 (50 ml LB, 37 °C, 200 rpm) via the Qiagen Kit (manufacturer's protocol followed, 5-50 ml preparation). The vector (10 µg, 20 µl) was mixed with restriction enzymes (2 µl each of *Nco*I and *Bam*HI (2 units, NEB)), the buffer (10 µl buffer 2, NEB), shrimp phosphatase (2 units, 2 µl) and this mixture was diluted with sterile, distilled water (100 µl total volume). The solution was incubated (37 °C, 5 hours). The digests had loading buffer (25 µl) added and



were resolved by running on an agarose gel (0.8 % w/v). The vector was extracted from the gel as described above.

#### **2.4.6.2 Vector pET21a for the reductases**

pET21a was recovered from an overnight culture of *E. coli* XL-10 (500 ml LB, 37 °C, 220 rpm) via the Qiagen HiSpeed Plasmid Purification® maxi-prep Kit (manufacturer's protocol followed, 500 ml preparation, yielded typically 250 – 350 µg/ml plasmid DNA, 100 µl). The vector (20 µl) was mixed with restriction enzymes (2.0 µl each of *Nhe*I and *Bam*HI (2 units, NEB), buffer, etc as described above) and treated as described in 2.4.6.1. The completed digests were purified by running on an agarose gel (1.0 % w/v). The vector was extracted from the gel as previously described.

#### **2.4.7 DNA ligation**

Vector DNA (50-100 ng, 2 µl), buffer (1 µl, 10 mM Tris.HCl pH 7.2, 1 mM EDTA, 10 mM MgCl<sub>2</sub>, 10 mM DTT and 1 mM ATP) and T4 DNA ligase (2 units, 2 µl, Roche) plus a varying amount of the PCR product (0, 100, or 200 ng) and sterile, distilled water (total volume 10 µl) were mixed, and the reaction mixture was incubated (16 °C, 16 hours).

#### **2.4.8 Transformation by electroporation**

*E. coli* XL1-Blue competent cells (50 µl) were transformed with the ligation mixtures (2 µl) by electroporation (200 Ω, 1.8 V). Transformed cells had SOC media (2 ml) added to them and were incubated (37 °C, 45 minutes) before being spread onto agar plates (LB, 50 µg ml<sup>-1</sup> ampicillin) and left to grow (37 °C, 16 hours).

#### **2.4.9 Transformation of chemically competent cells**

*E. coli* XL-10 competent cells (Stratagene) were transformed with the ligation mixtures (2  $\mu$ l) using the following method; Aliquots of competent cells (50  $\mu$ l) were thawed on ice and 1  $\mu$ l of 1 in 10 diluted  $\beta$ -mercaptoethanol added. The mixture was swirled gently and held on ice for 10 minutes. Plasmid DNA (1 – 50 ng) was added and after incubating on ice for a further 30 minutes the cells were heat shocked (42 °C, 20 seconds). The cells were returned to ice (2 minutes) before SOC medium was added (0.9 ml, pre-heated to 42 °C). The cells were incubated at 37 °C (1 hour, 220 rpm agitation) before aliquots (ca 200  $\mu$ l) were plated out (LB agar plates, 100  $\mu$ g/ml ampicillin). Colonies appeared after 14 hours at 37 °C. Single colonies were picked, re-plated and analysed via PCR for the clone.

#### **2.4.10 PCR analysis of positive colonies**

Copies of the positive colonies were made by imprinting a fresh agar plate (LB agar, 100  $\mu$ g/ml ampicillin). The colony was suspended in a solution of Triton X-100 (25  $\mu$ l, 0.5 % v/v) and heated (95 °C, 15 minutes). Part of this solution (10  $\mu$ l) was then added to a PCR tube containing the primers (1  $\mu$ l, 100  $\mu$ M), the dNTP mix (1  $\mu$ l, 10 mM (BioRad)) and the manufacturer's 10 x buffer (10  $\mu$ l, 1.5 mM magnesium chloride) made up with water (to a final volume of 50  $\mu$ l) and the polymerase was added (Roche High Fidelity Mix®, *Taq* and *Pwo* polymerase, 2 units, 1.0  $\mu$ l). The product of the PCR reaction (5  $\mu$ l) was run on an agarose gel (1.0 % w/v) and a band of ca 1.7 kb sought for proof of reaction success.

#### **2.4.11 Cloning into a TOPO vector**

To enable quick and easy screening of PCR products ( $\beta$ -galactosidase blue/white screening) and preparation of a large amount of plasmid for sequencing, the amplified gene was initially ligated into a high copy number TOPO 2.1 vector (Invitrogen). A

Qiagen A-addition kit was used to provide modification of the blunt-ended PCR products for UA- and TA- cloning. Purified PCR DNA product (6  $\mu$ l) was added to the Qiagen A-addition master mix (2  $\mu$ l) and the solution incubated at 37 °C for 30 minutes. Part of this mixture was then taken and added to the manufacturer's sodium chloride solution (1  $\mu$ l) and the TOPO2.1 vector (1  $\mu$ l). The resulting solution was mixed gently and incubated at 22 °C for 5 minutes. The solution was chilled on ice and used directly to transform competent cells as detailed in 2.3.1. The transformed cells were plated onto LB agar plates containing X-gal (50  $\mu$ g/ml) and ampicillin (100  $\mu$ g/ml). This enabled blue/white screening as the insert disrupted the *galE* promoter and white colonies were picked for checking by PCR.

#### **2.4.12 Phenol/chloroform extraction of DNA fragments**

As an alternative means of purification, the DNA from digest mixtures was purified by phenol/chloroform extraction. The digest mixture (30  $\mu$ l) was added to water (70  $\mu$ l) and sodium acetate (10  $\mu$ l, 3.0 M) added. To this solution water saturated phenol/chloroform (1:1 v:v, 100  $\mu$ l) was added and the mixture was vortexed (1 minute) then centrifuged (13000 rpm, 2 minutes). The upper phase was removed and had ethanol added to precipitate the DNA (2.5 vol, -20 °C). The mixture was centrifuged (13000 rpm, 30 minutes) and any liquid removed by pipette. The DNA pellet was dried under vacuum to remove any residual ethanol and resuspended in sterile, distilled water (25  $\mu$ l). A sample of the digested DNA (4  $\mu$ l) was run on an agarose gel (1.0 % w/v).

### **2.5 Generation of the H75X mutants (with Dr K Marshall, University of Leicester)**

Site-directed PCR was used to mutate the BioI His75 codon to ones encoding an arginine and an alanine. Primers designed to introduce the mutation are shown below. A restriction site was engineered in both cases via the incorporation of additional silent

mutations so that the appropriate enzyme digest could be used to confirm the introduction of the mutation.

#### PCR primers designed for H75A mutation

Oligo	Sequence	Restriction site engineered
H75A-forward	GAC CTT TCA <u>GCT</u> GTG CAA AAT C	<i>Pvu</i> II site
H75A-reverse	GAT TTT GCA <u>CAG</u> CTG AAA GGT C	<i>Pvu</i> II site

#### PCR primers designed for H75R mutation

Oligo	Sequence	Restriction site engineered
H75R-forward	GAC CTT TCA <u>CGT</u> GTG CAA AAT C	<i>Pml</i> I site
H75R-reverse	GAT TTT GCA <u>CAC</u> GTG AAA GGT C	<i>Pml</i> I site

Underlined bases indicate the restriction site, those in red are different to those in the wild-type sequence, and the triangles indicate where the restriction enzyme would cut the DNA.

### 2.5.1 Polymerase Chain Reaction

The PCR reactions were carried out using a Techne Genius PCR thermocycler. Eppendorfs (0.5 ml) were used with a 100  $\mu$ l reaction volume. Template DNA (1  $\mu$ l, 50 ng), the primers (1  $\mu$ l, 125 ng of each), the dNTP mix (1.0  $\mu$ l, 200  $\mu$ M (Clontech)), *Pfu* Turbo DNA polymerase (Stratagene), 2.5 units, 1.0  $\mu$ l) and the manufacturers buffer (5.0  $\mu$ l, 1.5 mM magnesium chloride) were made up with nuclease free water (total volume 50  $\mu$ l).

The PCR reaction used the method detailed on the following page;

Initial denaturation	95°C, 120 secs
	First 16 cycles
Denaturation	95°C, 30 secs
Annealing	55°C, 60 secs
Elongation	68°C, 90 secs
Final elongation	68°C, 8 mins
Final cooling	5°C, infinite

A total of 16 cycles were run. *DpnI* restriction enzyme (5 units, 1 µl, NEB) was added to the reaction mixtures after cooling on ice. After incubating (37 °C, 1 hour) the PCR product was analysed by running a sample (5 µl) on an agarose gel (1.0 % w/v). The product of the PCR reaction was gel purified (1.0 % w/v agarose gel) and recovered from the gel in accordance with the procedure described in 2.4.5. Plasmid (10 ng) was transformed into *E. coli* JM109 cells (see 2.4.9 for method). Cells were cultured via incubation of the transformation mixture (LB, 50 µM ampicillin plates, 37 °C, 14 hours) and for each mutant six colonies picked out. The colonies were grown (8 hours, 37 °C, 5 ml LB, 50 µg/ml ampicillin) and the plasmid recovered (Qiagen mini-prep kit, method detailed in section 2.3.4).

The introduction of the mutation was checked by digestion (for method see section 2.3.5) with the appropriate restriction enzyme (5 units, 1.5 µL (NEB enzymes) on 100 ng of plasmid DNA). The H75A mutant introduces an additional *Pvu* II site resulting in two fragments being observed upon restriction digest compared to just one for the wild-type clone (gene cloned in the vector pET11a). In the case of the H75R mutant a unique *Pml* I site was introduced, that resulted in linearization of the mutant clone (6.8 kb).

## 2.6 Protein Preparation

### 2.6.1 Large-scale over-expression (> 6.0 l) of proteins

The following generic method was used for the preparation of all proteins. Conditions specific for each protein can be found in Table 2.1 below. LB media (12 x 0.5 L) containing the appropriate antibiotic was inoculated with an overnight culture (100 ml)



of the required transformant. The flasks were incubated (37 °C, 250 rpm, 24 hours) and at the specified OD<sub>600</sub> IPTG (0.5 mM) was added if required. The cells were harvested by centrifugation (5000 rpm, 10 minutes) and the cell pellet frozen (-20 °C) until required.

Protein	Plasmid	<i>E. coli</i> host strain	Antibiotic (µgml <sup>-1</sup> )	IPTG	OD <sub>600</sub> when induced	Growth time (total/post induction) (hours)
<b>P450 BioI (+ mutants)</b>	pET11a	Origami (DE3)	Amp (50) Kan (15) Tet (12.5)	No	N/A	24
<b>YkuN</b>	pET16b	HMS 174 (DE3) pLysS	Amp (50) Rif (200)	Yes	1.0	19 / 16
<b>YkuP</b>	pET16b	HMS 174 (DE3) pLysS	Amp (50) Rif (200)	Yes	1.0	19 / 16
<b>YumC</b>	pBlue-script KS II <sup>+</sup>	TG1	Amp (50)	No	N/A	12
<b>YcgT</b>	pUC18	TG1	Amp (50)	No	N/A	12
<b>CYP102A3</b>	pET21a	BL21 (DE3) codon plus RP	Amp (50) Cm (50)	Yes	0.8	19 / 16
<b><i>E. coli</i> FldA</b>	pET11a	BL21 (DE3)	Amp (50)	Yes	1.0	24 / 21
<b><i>E. coli</i> FldR</b>	pET11a	BL21 (DE3)	Amp (50)	No	N/A	16
<b><i>E. coli</i> GAPDH</b>	pSKgap A	TG-1	Amp (50)	No	N/A	24

**Table 2.1** Summary of *E. coli* host strains and plasmids used for recombinant protein expression. Detailed are the antibiotics required for selection of both plasmids and strains (Amp = ampicillin, Kan = kanamycin, Cm = chloramphenicol, Tet = tetracycline, Rif = rifampicin), and if IPTG addition was required to induce protein expression (via the T7 *lac* promoter).

## 2.6.2 Purification of proteins by column chromatography

The following generic method was used to extract and purify all proteins. Details specific to each protein can be found in Table 2.2.

Cells were thawed in the presence of benzamidine (1 mg/ml) and resuspended in Buffer A (typically 100 ml) (see section 2.2) and sonicated (5 x 15 seconds bursts, interspaced by 2 minutes, 50 % power, on ice). The cell suspension was passed through a

Protein	NH <sub>4</sub> SO <sub>4</sub>	Column 1	Eluted	Column 2	Eluted	Column 3	Eluted
<b>P450 BioI</b> Section 2.63	No	DEAE	0 – 500 mM KCl gradient. Elutes at 100 mM	Hydroxy-Apatite	0 – 500 mM KPi gradient. Elutes at 150 mM	Q-Sephadex	0 – 500 mM KCl gradient. Elutes at 100 mM
<b>YkuP</b> Section 2.64	70 % cut	Phenyl Sephadex	2.0 – 0 M NH <sub>4</sub> SO <sub>4</sub> linear gradient	DEAE	0 – 1.0 M KCl gradient. Elutes at 500 mM	Q-Sephadex	0 – 1.0 M KCl gradient. Elutes at 500 mM
<b>YkuN</b> Section 2.64	50 % cut	Phenyl Sephadex	1.5 – 0 M NH <sub>4</sub> SO <sub>4</sub> linear gradient	DEAE	0 – 1.0 M KCl gradient. Elutes at 450 mM	Q-Sephadex	0 – 1.0 M KCl gradient. Elutes at 450 mM
<b>YumC</b> Section 2.65	35 % cut	DEAE	0 – 0.5 M KCl gradient. Elutes at 150 mM	Phenyl-sephadex	1.5 – 0 M NH <sub>4</sub> SO <sub>4</sub> linear gradient	Q-sephadex	0 – 0.5 M KCl gradient. Elutes at 150 mM
<b>YcgT</b> Section 2.65	45 % cut	DEAE	0 – 0.5 M KCl gradient. Elutes at 150 mM	Phenyl-sephadex	1.5 – 0 M NH <sub>4</sub> SO <sub>4</sub> linear gradient	Hydroxy Apatite	0-500 mM KPi Elutes at 100 mM
<b>CYP102A3</b> Section 2.65	35 % cut	DEAE	0 – 0.5 M KCl gradient. Elutes at 150 mM	Phenyl-sephadex	1.5 – 0 M NH <sub>4</sub> SO <sub>4</sub> linear gradient	Q-sephadex	0 – 0.5 M KCl gradient. Elutes at 150 mM
<b>FldR</b> Section 2.67	N/A	DEAE	0 – 1.0 M KCl. Elutes at 450 mM	Q-sephadex	0 – 1.0 M KCl. Elutes at 350 mM	ADP sephadex	500 mM KCl
<b>FldA</b> Section 2.66	N/A	DEAE	0 – 1.0 M NaCl. Elutes at 400 mM	QEAE	0 – 1.0 M NaCl. Elutes at 350 mM	N/A	N/A
<b>GAPDH</b> Section 2.68	66 %	Phenyl-sephadex	2.0 – 0 M ammonium sulphate in buffer A	DEAE	0 – 0.5 M KCl. Elutes at 100 mM	N/A	N/A

**Table 2.2** Summary details of columns and conditions for the purification of the various redox proteins reported in this thesis. Full particulars can be found in the text below.

French press (2 x 10000 psi) to give a viscous suspension. Further sonication (as before) was followed by centrifugation (15000 rpm, 45 minutes 4°C) to yield a clear coloured supernatant. The soluble cell extract (*ca* 100 ml) was then either dialysed against Buffer A (2.0 L, 4 °C, 3 - 16 hours) prior to loading onto a DEAE column (see section 2.2) or underwent ammonium sulphate precipitation.

### **2.6.3 Purification of P450 BioI (and its mutants)**

The protein solution was loaded onto a DEAE column and washed with buffer A (4 column volumes, 0.3 ml/min) prior to eluting with a linear salt gradient (0 – 500 mM potassium chloride (Buffer B), 2 column volumes). P450 BioI was observed to elute at *ca* 100 mM KCl. The fractions were analysed (UV-visible spectroscopy) and those containing heme were kept and concentrated (Centricons (Amicon) 30 kDa cut-off, 1000 rpm, *ca* 15mg/ml). The protein solution (*ca* 70 ml) was dialysed against Buffer C (16 hours, 4 °C) prior to loading onto a pre-equilibrated hydroxyapatite column (*ca* 0.15 ml/min flow rate).

After washing (3 column volumes, Buffer C) the protein was eluted with a linear salt gradient (25 – 500 mM KPi (Buffer D), 2 column volumes). The red protein was observed to elute at *ca* 150mM KPi. The fractions were analysed by UV-visible spectroscopy and those containing the P450 with a 280 : 418 nm ratio of < 4: 1 were retained. After concentrating (as before, *ca* 15 mg/ml) the red solution (*ca* 30 ml) was dialysed against buffer A (2.0 L, 6 hours, 4 °C) and loaded on a pre-equilibrated Q-Sepharose column (0.15 ml/min).

The bound protein was washed (3 column volumes, 0.15 ml/min) and eluted with a linear salt gradient (0 – 500 mM KCl (buffer B), 2 column volumes). P450 BioI was observed to elute at *ca* 100 mM KCl. The fractions were analysed as before and those containing the P450 with a 280 : 418 nm absorption ratio of < 1 : 1 were retained and concentrated (conditions as before).

Small aliquots of the concentrate (1 ml, 20 mg/ml) were run through a Sephadex-200 gel filtration column in buffer A (0.10 ml/min). Fractions were collected and analysed as above, those with a 280 : 418 nm absorption ratio of 0.65 were regarded as

pure and retained. The protein solution was concentrated (as before, 15 mg/ml), dialysed against glycerol (50 % v/v in buffer A, 1.0 L, 6 hr, 4°C) and stored in small aliquots at -20°C.

#### **2.6.4 Purification of YkuN/P**

The soluble blue cell extract (*ca* 100ml) had ammonium sulphate added to give a final concentration of 1.5 M (YkuN) or 2.0 M (YkuP). The suspension became yellow upon addition of the precipitant. Insoluble impurities were removed via centrifugation (15 000 rpm, 20 minutes, 4 °C) and the yellow solution containing the flavodoxin loaded directly onto a phenyl Sepharose column pre-equilibrated with an ammonium sulphate solution of the same molarity.

The phenyl Sepharose column was washed with ammonium sulphate in buffer A (3 column volumes, 0.5 ml/min) prior to eluting the flavodoxin with a linear gradient (1.5 or 2.0 M ammonium sulphate to 0 M in buffer A, 2 column volumes). Fractions were analysed by UV-visible spectroscopy and those containing flavodoxin with a 280 : 460 nm absorption ratio of 10:1 or less were retained. The fractions were pooled and concentrated to *ca* 50 ml (Centricons (Millipore) 10 kDa cut-off, 2500 rpm). The concentrate was dialysed against buffer A (2.0 L, 4 °C, 6 hours) prior to loading onto a DEAE column. After washing with buffer A (4 column volumes, 0.2 ml/min) the protein was eluted with a linear salt gradient (0 – 1.0 M KCl (buffer B), 2 column volumes). YkuN was observed to elute at *ca* 400 mM KCl and YkuP at *ca* 450 mM. The fractions were analysed (as before) and those containing flavin (280 : 461 nm absorption ratio < 8) were kept and concentrated (as before, final volume *ca* 20 mg/ml).

The resulting concentrate was dialysed against buffer A (2.0 L, 4 °C, 16 hours) prior to loading onto a Q-Sepharose column. After washing with buffer A (4 column volumes, 0.15 ml/min) the protein was eluted with a linear salt gradient (0 – 1.0 M KCl in buffer A, 2 column volumes). YkuN was observed to elute at *ca* 450 mM KCl and YkuP at *ca* 500 mM. The fractions were analysed (UV-visible spectroscopy) and those containing flavodoxin (yellow in colour) were kept and concentrated (as before, to a final volume of *ca* 20 mg/ml).

A final step was included if necessary to purify the flavodoxins further. Small aliquots of the concentrate (1 ml, 20 mg/ml) were run through a Sephadex-200 gel filtration column in buffer A (0.10 ml/min). Fractions were collected and analysed; YkuN with a 280 : 461 nm absorption ratio of 5.8 : 1 was regarded as pure (as confirmed by SDS PAGE) and pure YkuP had an absorption ratio of 3.2 : 1. The protein solutions were concentrated (as before, 15 mg/ml), dialysed against glycerol (50 % v/v in buffer A, 1.0 l, 6 hr, 4 °C) and stored in small aliquots at -80°C.

### **2.6.5 Reductase Purification (YumC, YcgT and CYP102A3R)**

The first step for the three *B. subtilis* reductases was the same; all the lysate solutions were loaded onto a DEAE column and washed with buffer A (3 column volumes, 0.3 ml/min) prior to eluting with a linear salt gradient (0 – 500 mM potassium chloride (Buffer B), 2 column volumes). YumC and CYP102A3 were observed to elute at *ca* 100 mM KCl, and YcgT at 150 mM. The fractions were analysed (UV-visible spectroscopy) and those containing flavin were kept and concentrated (Centricons (Millipore) 30 kDa cut-off, 1000 rpm, to a final concentration of *ca* 10 mg/ml). The protein solutions (*ca* 100 ml) were treated with ammonium sulphate to give the following cuts; YumC 35 % w/v, YcgT 45 % w/v and CYP102A3R 35 % w/v. Precipitated protein was removed via centrifugation (15000 rpm, 15 minutes, 4 °C). The reductase-containing supernatants (yellow) were loaded onto a pre-equilibrated phenyl Sepharose column (buffer A plus 1.5 M ammonium sulphate, 2 column volumes). The proteins were washed (2 column volumes) and eluted via a salt gradient (1.5 – 0 M ammonium sulphate in buffer A, 2 column volumes). All yellow fractions were analysed by UV-visible spectroscopy and those containing the reductase retained (280 : 460 nm absorption ratio of < 10 : 1) and concentrated as before. The final column chromatography step differed between proteins.

Both YumC and CYP102A3R were dialysed against Buffer A (16 hours, 4 °C) prior to loading onto a pre-equilibrated Q-Sepharose column (1.0 ml/min). The bound proteins were washed (2 column volumes, buffer A) and eluted with an increasing salt gradient (0 – 500 mM KCl (buffer B)). Fractions (3.0 ml in size) were analysed (as



before) and those with a 280 : 460 nm absorption ratio of < 6:1 were pooled and concentrated (20 mg/ml), dialysed against glycerol (50 % v/v in buffer A, 1.0 l, 6 hr, 4 °C) and stored in small aliquots at -80°C.

YcgT was dialysed against buffer C (16 hours, 4 °C) and loaded onto a hydroxyapatite column (*ca* 0.5 ml/min flow rate). After washing (buffer C, 4 column volumes) the protein was eluted by increasing the buffer molarity (0 – 500 mM KPi) and the yellow fractions retained and analysed as before. Those with a 280 : 460 nm absorption ratio of < 4.5 : 1 were collated and concentrated (conditions as before). The protein was dialysed against glycerol (50 % v/v in buffer C, 1.0 L, 6 hr, 4 °C) and stored in small aliquots at -80°C.

#### **2.6.6 *E. coli* Flavodoxin (FldA) Purification**

This protein was produced and purified in accordance with the documented method [McIver *et al.*, 1998]. The cell extract (*ca* 100 ml) was dialysed (sodium acetate buffer, 100 mM, pH 5.0, 2.0 l, 4 °C, 6 hours) and re-centrifuged (15000 rpm, 40 minutes) prior to loading onto a DEAE column. After washing (3 column volumes, 0.2 ml/min) the protein was eluted with a linear salt gradient (0 – 1 M NaCl in sodium acetate, 2 column volumes). The flavodoxin was observed to elute at *ca* 400 mM sodium chloride (NaCl). The fractions were analysed (UV-visible spectroscopy) and those containing flavin (orange in colour) were kept and concentrated (Centricons) 30 kDa cut-off, 1000 rpm, *ca* 30mg/ml).

The concentrate was dialysed (buffer A, 2.0 l, 4 °C, 16 hours) to raise the pH and loaded onto a QAE column. After washing with buffer A (4 column volumes, 0.2 ml/min) the protein was eluted (linear salt gradient, 0 – 1 M NaCl in buffer A, 2 column volumes). FldA was observed to elute at *ca* 350 mM sodium chloride (NaCl). The fractions were analysed (UV-visible spectroscopy) and those containing flavin (orange in colour, 280 : 366 nm absorption ratio of 5 : 1) were kept and concentrated (as before, *ca* 30 mg/ml). The concentrate was dialysed against glycerol (50 % v/v glycerol in buffer A) to give an orange protein stock (*ca* 6.5 mM) that was stored (- 80 °C).

### **2.6.7 *E. coli* Flavodoxin NADP<sup>+</sup> oxidoreductase (FldR) purification**

FldR was purified in accordance with the method published in the literature [McIver *et al.*, 1998]. Cell extract (*ca* 100 ml) was dialysed (buffer A, 3.0 l, 4 °C, 6 hours) and re-centrifuged (15000 rpm, 40 minutes) prior to loading onto a DEAE column. After washing (3 column volumes, buffer A, 0.2 ml/min) the protein was eluted with a linear salt gradient (0 – 1 M KCl in buffer A, 2 column volumes). The reductase was observed to elute at *ca* 450 mM KCl. The fractions were analysed (UV-visible spectroscopy) and those containing flavin (yellow in colour) were pooled and concentrated (Centricons, 30 kDa cut-off, 1000 rpm, *ca* 30 mg/ml).

The concentrate was dialysed against buffer A (2.0 l, 4 °C, 16 hours) and loaded onto a Q-sepharose column. After washing with buffer A (4 column volumes, 0.2 ml/min) the protein was eluted (linear salt gradient, 0 – 1 M NaCl in buffer A, 2 column volumes). The reductase was observed to elute at *ca* 350 mM KCl and the fractions were analysed (as before) and those containing flavin (yellow in colour, 280 : 456 nm absorption ratio of < 10 : 1) were kept and concentrated (as before, *ca* 30 mg/ml). The concentrate was dialysed (KPi buffer, 25 mM, pH 7.0) and loaded onto a 2',5'-ADP Sepharose column (1 x 20 cm) pre-equilibrated with the loading buffer. The bound protein was washed (loading buffer, 3 column volumes) and eluted (KPi 25 mM, 500 mM KCl, pH 7.0). Fractions were checked for purity and those with a 280 : 456 nm absorption ratio of < 6 : 1 were pooled and concentrated (as before to 15 mg/ml). The concentrate was dialysed into buffer A (3.0 l, 4 °C, 6 hours) and subsequently into glycerol (50 % v/v glycerol in buffer A) to give a yellow protein stock (*ca* 0.5 mM) that was stored (-80 °C).

### **2.6.8 *E. coli* GAPDH purification**

The soluble cell extract (*ca* 100ml) had ammonium sulphate added to give a final concentration of 66 % w/v. Insoluble impurities were removed via centrifugation (15 000 rpm, 20 minutes, 4 °C) and the clear solution containing the GAPDH was loaded onto a

phenyl Sepharose column pre-equilibrated with an ammonium sulphate solution of the same concentration.

The phenyl Sepharose column was washed with ammonium sulphate in buffer A (3 column volumes, 0.5 ml/min) prior to eluting the GAPDH with a linear gradient (2.0 M ammonium sulphate to 0 M in buffer A, 2 column volumes). Fractions were analysed by SDS-PAGE and those containing GAPDH with no significant contaminants were retained (typically the first 20 3.0 ml fractions). The fractions were collated and concentrated to *ca* 30 ml (Centricons, 30 kDa cut-off, 1000 rpm). The concentrate was dialysed against buffer A (2.0 l, 4 °C, 6 hours) to remove any salt prior to loading onto a DEAE column. After washing with buffer A (2 column volumes, 0.2 ml/min) the protein was eluted with a linear salt gradient (0 – 0.5 M KCl (buffer B), 2 column volumes). GAPDH was observed to elute at *ca* 100 mM KCl, the fractions were analysed (as before) and those containing GAPDH only were kept and concentrated (as before, final volume *ca* 20 mg/ml). Protein was stored at 4 °C or dialysed against 50 % glycerol in buffer A and frozen (-20 °C) in 1.5 ml aliquots.

## **2.7 Protein characterisation by SDS PAGE gel electrophoresis**

### **2.7.1 Sample preparation**

Protein samples were prepared (approximately 50 µg of protein) by the addition of 3 × SDS-PAGE loading buffer (10 µl, New England BioLabs (NEB)), and water (total volume 30 µl). Pre-stained broad-range markers (8 µl, NEB) were mixed with loading buffer (10 µl). Prior to loading onto the gel, the samples were heated (5 minutes, 95 °C). Whole cell samples were prepared by resuspending cell pellets (150 µl TE) and heating with loading buffer (20 µl resuspended material, 10 µl buffer (1 part DTT (1 M), 9 parts loading buffer), 95 °C, 5 minutes).

### **2.7.2 Gel preparation and assembly**

SDS polyacrylamide gel electrophoresis was used to identify proteins according to their molecular weight. A two-phase gel (resolving gel, 10 %, and a stacking gel, 4 %) was prepared (see section 2.2.1). The resolving gel was poured between 2 glass plates, overlaid (ethanol) and left to polymerise. After the gel had set, the ethanol was removed and the stacking gel was poured on top. The set gel was placed into the electrophoresis tank (BioRad) filled with running buffer and the samples (typically 0.1 µg total protein) loaded into the wells. The gel was run (200 mV) until completion and stained (5 minutes, 0.1 % Coomassie blue R-250, 40 % methanol, 10 % acetic acid). The gel was then destained (40 % methanol, 10 % acetic acid, 1 hour).

### **2.7.3 Protein Blotting**

Following protein separation by SDS PAGE (see 2.7.2), the protein was transferred to a polyvinylidene difluoride (PVDF) membrane. The SDS PAGE gel was placed onto the PVDF membrane, which was sandwiched between two Scotch pads™ and held in place in a cassette (BioRad). The cassette was placed into a tank filled with transfer buffer (see 2.2.1) with the PVDF membrane on the positive side of the SDS PAGE gel. The transfer was carried out (125 mA, 2 hours) and the PVDF membrane stained (1 hour, for stain see 2.2.1) and de-stained (1 hour, for destain see 2.2.1). The band corresponding to the protein of interest was cut out and submitted for N-terminal sequencing at the PNACL facility (University of Leicester).

## **2.8 Protein Characterisation; Biophysical techniques**

### **2.8.1 Determination of extinction coefficients (flavoproteins)**

To determine the extinction coefficient ( $\epsilon$ ) of the various flavoproteins studied and the cofactor they contained, the following procedure was followed [Macheroux 1999]. A sample of protein (5 µl, *ca* 1.0 mM) was added to Tris buffer (10 mM, pH 7.5, 995 µl) and its UV-visible absorbance spectrum measured (reading 1). The cofactor was

then liberated from the apoprotein by the addition of SDS (20  $\mu$ l of a 10 % w/v solution). After incubating the denatured protein solution on ice (5 minutes), any resulting precipitate was removed by centrifugation (13000 rpm, 1 minute) and the UV-visible spectrum re-measured (reading 2). The absorbance was corrected for dilution and the following equation used to calculate the coefficient:

$$\epsilon = \epsilon_{\text{FMN/FAD}} \times (\text{reading 1} / \text{reading 2})$$

$$\epsilon_{450} = 11300 \text{ M}^{-1}\text{cm}^{-1} \text{ for FAD}$$

$$\epsilon_{446} = 12200 \text{ M}^{-1}\text{cm}^{-1} \text{ for FMN}$$

$$\epsilon_{473} = 9200 \text{ M}^{-1}\text{cm}^{-1} \text{ for a mixture of FMN and FAD}$$

### **2.8.2 Analysis of tertiary structure by fluorescence spectroscopy**

The aromatic residue content of all proteins was studied using fluorescence spectroscopy (Varian CARY 50 fluorimeter) [Uversky and Fink, 2002]. Proteins (typically 3 nmol) were added to KPi buffer (50 mM, pH 7.0, 3.0 ml) in a quartz cell (1 cm path-length) and their fluorescence spectrum measured (excitation at 290 nm, recorded emission between 300 and 400 nm, 5 nm slit widths, at 25 °C). The fluorescence of the various flavin cofactors was also analysed under the same conditions but with the excitation at 450 nm (emission from 500 to 600 nm recorded).

### **2.8.3 P450 BioI UV-visible spectrometry**

The binding of carbon monoxide to P450 BioI (4  $\mu$ l, 1.9  $\mu$ M) was studied using enzyme in buffer A (1 ml). Carbon monoxide (CO) binding was performed by first reducing the P450 BioI protein with sodium dithionite (few grains). CO was bubbled slowly through the solution (1 minute). These additions were performed inside a fume hood. To minimise the formation of denatured P420 an alternate approach was used.

Buffer A (20 ml) was de-oxygenated (Argon sparging, 20 minutes) and fully saturated with CO (sparged 20 minutes). This buffer was loaded anaerobically into the



cuvette (0.95 ml), sealed and P450 BioI (7.5  $\mu$ l, 0.5mM) injected through the septum. A solution of sodium dithionite (*ca* 10 mM, 50  $\mu$ l) was then injected into the protein solution.

#### 2.8.4 Effect of pH upon P450 BioI

P450 BioI (5  $\mu$ l, 0.75 mM) was mixed with the applicable buffer (1.0 ml, see below) and the UV-visible spectrum (250 – 750 nm) measured. Each buffer was examined in the range of pH 6.0 to 10.5 at 0.5 pH unit intervals.

Buffer	Concentration (mM)	Buffer type
HEPES.HCl	50	organic
Tris.HCl	50	organic
KPi	50	inorganic
NaPi	50	inorganic

Data from these experiments ( $\Delta_{\text{abs}}$  versus the pH) were fitted to a sigmoidal (Hill) function (Equation 1) to find the midpoint values ( $K^{\text{H}}$ ).

$$A_{\text{obs}} = A_{\text{max}} S^{\text{H}} / (K^{\text{H}} + S^{\text{H}}) \quad \text{Equation 1}$$

$A_{\text{obs}}$  = observed absorption at a given pH

$A_{\text{max}}$  = maximal absorption

$K^{\text{H}}$  = midpoint value

$S^{\text{H}}$  = the pH of the solution

#### 2.8.5 Effect of temperature on P450 BioI

P450 BioI (13  $\mu$ l, 0.5 mM) in Buffer A (1 ml) was cooled (12 °C) in the temperature-regulated cuvette holder (Peltier) in the spectrophotometer (Varian Cary 50). The UV-visible spectra (250 – 750nm) were recorded. The temperature was increased in 2 °C steps [Sligar 1976, Sligar and Gunsalus, 1979]. The protein solution was held (2

minutes) at each new temperature prior to the spectrum being measured. The difference spectra (by subtracting the initial spectrum from each spectrum) were subsequently generated and used to calculate the spin-state change at each point.

### **2.8.6 Disulphide Bond Assay (Chemical)**

To determine the presence and number of disulphide bonds in P450 BioI, a colorimetric assay was used [Ellman 1959]. All operations were carried out anaerobically (Belle Technology glove-box) unless otherwise stated. Buffer (100 mM KPi, pH 7.0) was de-oxygenated (argon sparged) and used to prepare solutions of dithiothreitol (DTT) (50 mM) and Ellman's reagent (5,5'-dithiobis-(2-nitrobenzoic acid), DTNB) (10 mM). The production of 5-mercapto-2-nitro benzoate (MTNB) gives rise to a yellow colouring ( $\lambda_{\max}$  412 nm,  $\epsilon = 14150 \text{ M}^{-1}\text{cm}^{-1}$ ) and the formation of this colouring was followed over time (60 minutes, Cary 50 spectrophotometer) [Bulaj *et al.*, 1998]. Initially a sample of DTNB in assay buffer was run as a blank. A sample of P450 BioI (20  $\mu\text{l}$ , 0.5 mM) was added to the buffer (970  $\mu\text{l}$ ) and the cuvette sealed. DTNB (40  $\mu\text{l}$ , 10 mM) was injected into the cuvette and the absorbance at 412 nm followed. A second sample of P450 BioI (20  $\mu\text{l}$ , 0.5 mM) was incubated (25°C, 1 hour) with DTT (10  $\mu\text{l}$ , 50 mM) in the buffer (890  $\mu\text{l}$ ). DTT was removed from the solution by gel filtration (G-25) and the protein solution transferred to the cuvette. DTNB (40  $\mu\text{l}$ , 10 mM) was added and the absorbance collected as before.

### **2.8.7 Ligand Binding Studies**

The concentration of P450 BioI used in the titrations was typically 1-5  $\mu\text{M}$  in assay buffer (1 ml, 50 mM Tris.HCl, pH 7.2). All spectral titrations with fatty acids (saturated fatty acids ranging from C<sub>8</sub>-C<sub>20</sub>), steroids and imidazoles (imidazole, 4-phenyl imidazole (4-PIM), and  $\omega$ -imidazolyl acid derivatives) were performed at 30 °C due to the limited solubility of many of the compounds in aqueous buffer. Small aliquots (0.1-2  $\mu\text{l}$ , less than 5  $\mu\text{l}$  total) of the ligand stock solution were added to the enzyme. Spectra were recorded after each addition of ligand. Difference spectra were generated by

subtraction of each spectrum recorded from the original ligand-free spectrum. Apparent  $K_d$  values were determined by plotting the absorbance changes calculated from each difference spectrum against the concentration of ligand, and by fitting the data to the relevant equation using Origin software (Microcal). For substrates with  $K_d$  values less than five times the amount of enzyme used in the assay, data was fitted to a quadratic function (Equation 2) as previously described [Murataliev *et al.*, 2000].

$$A_{\text{obs}} = (A_{\text{max}}/(2E_t)(S + E_t + K_d) - (((S + E_t + K_d)^2 - 4SE_t)^{0.5}) \quad \text{Equation 2}$$

$A_{\text{obs}}$  = the observed absorption at a given substrate concentration

$A_{\text{max}}$  = the maximal absorption at the wavelength

$E_t$  = total enzyme concentration

$S$  = substrate or ligand concentration

$K_d$  = apparent dissociation constant

Substrates that had an apparent  $K_d$  greater than five times the amount of enzyme used in the assay were fitted to a hyperbolic function (Equation 3, parameters as in Equation 2).

$$A_{\text{obs}} = (A_{\text{max}}[S])/(K_d + [S]) \quad \text{Equation 3}$$

### 2.8.8 Heme Reduction Studies

De-oxygenated (argon sparged) buffer A (100 ml) was saturated with CO (CO sparged, 30 minutes). Under anaerobic conditions (Belle Technology glove-box) a quartz cuvette had buffer (0.98 ml), P450 BioI (5  $\mu$ l, 1.5 mM), *E. coli* FLDR (25  $\mu$ l, 200  $\mu$ M) and either *E. coli* FLD (2  $\mu$ l, 6.5 mM) or spinach ferredoxin (13  $\mu$ l, 0.1 mM) added. The cuvette was sealed and transferred to the spectrophotometer (Varian Cary 50). A solution of NADPH (15  $\mu$ l, 20 mM) was added and spectra recorded (250 – 750 nm, 1 minute intervals, 30 cycles). Substrates if required (myristic acid or testosterone, 1  $\mu$ l, 50 mM) were added prior to the addition of NADPH.

### 2.8.9 Stopped-flow studies of the rate of reduction of P450 BioI by *B. subtilis* flavodoxins

The rate of the single electron transfer from the *B. subtilis* flavodoxins to P450 BioI was measured via stopped-flow mixing (Applied Photophysics SX18MV) coupled to a photodiode array UV-visible detector. The experiment was carried out under anaerobic conditions (Belle Technology glove box). The proteins were added to KPi buffer (pH 7.0, 50 mM) that had been degassed (argon-sparged) and saturated with carbon monoxide to give a solution of the flavodoxin YkuN or P (80 µM) and a solution of P450 BioI (4.0 µM). P450 BioI was converted to either its high- or low-spin form by the addition of palmitoleic acid (10 µmol) or testosterone (30 µmol) respectively. The flavodoxin was reduced by titration of sodium dithionite until the hydroquinone form was generated (some residual semiquinone). Excess dithionite was removed via gel filtration (BioRad 10DG column) and the two solutions were mixed in the stopped-flow. The spectrum was recorded (250 – 750 nm) at 30 °C, the slit widths set at 1.0 mm. A sample of P450 was also mixed with a buffer blank and the spectrum recorded over 8 minutes to account for photo-bleaching. This rate was subtracted from all rates with the flavodoxins present. The concentration of the flavodoxins was altered and the corresponding formation of the 1-electron reduced ferrous form of P450 BioI trapped with CO (448 nm) was observed. Rates were determined by analysing spectra with global analysis software (Applied photophysics ProKin software). These rates were plotted against flavodoxin concentration and fitted to a rectangular hyperbola function (Equation 4) in Origin (Microcal) to obtain the apparent binding constants ( $K_d$ ) and apparent limiting rate for electron transfer ( $k_{red}$ ).

$$k_{obs} = (k_{red}/2E_t)(S + E_t + K_d) - (((S + E_t + K_d)^2 - 4SE_t)^{0.5}) \quad \text{Equation 4}$$

$k_{obs}$  = the observed rate

$k_{red}$  = the apparent limiting rate

$E_t$  = total enzyme concentration

$S$  = substrate or ligand concentration

$K_d$  = apparent dissociation constant

### 2.8.10 Rate of electron transfer; NAD(P)H reduction of the reductases

The rate of the single electron transfer from both NADH and NADPH to the *B. subtilis* flavodoxin reductases (YumC, YcgT and A3R) was measured via stopped-flow mixing (Applied Photophysics SX18MV) coupled to a UV-visible detector. The experiment was carried out under anaerobic conditions in a Belle Technology glove box (< 4 ppm O<sub>2</sub>). The proteins were diluted in KPi buffer (pH 7.0, 50 mM) that had been degassed (argon sparged) to give separate stock solutions of the reductases (30 µM) and the nicotinamide cofactors (0.004 – 40 mM). The two solutions were mixed in the stopped-flow and the flavin absorbance recorded (460 nm). The experiment was carried out at 30 °C, the slit widths set at 1.0 mm. A sample of reductase was also mixed with a buffer blank and the spectrum recorded over 5 minutes. The oxidised FMN signal is observed to decrease due to photo-bleaching. This rate was subtracted from all rates with the nicotinamide cofactor present. The concentration of the reductant was altered and the corresponding rate of reduction of the reductase flavin was calculated by fitting to a double exponential process (Spectrakinetics software). These rates were plotted versus NAD(P)H concentration and fitted to a rectangular hyperbola (Equation 5, parameters as defined in Equation 4) using Origin (Microcal) to find the  $k_{red}$  and apparent  $K_d$ .

$$k_{obs} = (k_{red}[S])/(K_d + [S]) \quad \text{Equation 5}$$

### 2.8.11 Rate of flavodoxin reduction by the NAD(P)-oxidoreductases

The rate of the single electron transfer from both the *E. coli* flavodoxin reductase and the *B. subtilis* flavodoxin reductases to the *B. subtilis* flavodoxins (YkuN and YkuP) was measured via stopped-flow mixing (Applied Photophysics SX18MV) coupled to a photodiode array UV-visible detector. The experiment was carried out under anaerobic conditions in a Belle Technology glove box (< 4 ppm O<sub>2</sub>). The proteins were diluted in degassed (argon-sparged) KPi buffer (pH 7.0, 50 mM) to give separate solutions of the



flavodoxin (30  $\mu\text{M}$ ) and the reductase (225  $\mu\text{M}$ ). The reductase was reduced by the addition of excess NADPH (48 mM) to generate the hydroquinone form. The two solutions were mixed with each other and the spectrum recorded (250 – 750 nm). The experiment was carried out at 30 °C, the slit widths set at 1.0 mm. A sample of flavodoxin was also mixed with a buffer blank and the spectrum recorded over 8 minutes. The oxidised FMN signal (*ca* 460 nm) is observed to decay due to photo-bleaching. This photo-bleaching rate was subtracted from all rates with the reductase present. The concentration of the flavodoxin reductase was altered and the corresponding rate of formation of the 1-electron reduced neutral semiquinone (*ca* 595 nm) calculated by fitting to a single exponential process (Spectrakinetics software), in addition to global analysis (Applied photophysics ProKin software). These rates were plotted versus reductase concentration and fitted to a rectangular hyperbola function (Equation 5) in Origin.

#### 2.8.12 Steady-state kinetic analysis of *B. subtilis* reductase's interactions with artificial electron acceptors

To determine kinetic parameters for the three *B. subtilis* reductases, steady-state analysis with the two-hydride donors (NADH and NADPH) coupled with two different electron acceptors (potassium ferricyanide and cytochrome *c* from horse heart (Sigma)) were carried out. The reductase (1.0  $\mu\text{M}$ ) was added to a solution of the electron acceptor (varying concentration, typically 0 – 0.1 mM) in KPi buffer (50 mM, pH 7.0, to a total volume of 1.0 ml). The hydride donor (varying concentration, typically 0 – 0.1 mM) was added, the solution rapidly mixed and the formation of reduced species ( $\Delta\epsilon_{420\text{ nm}} = 1.02\text{ mM}^{-1}\text{ cm}^{-1}$  ferricyanide,  $\Delta\epsilon_{550\text{ nm}} = 22.64\text{ mM}^{-1}\text{ cm}^{-1}$  cytochrome *c*) followed over time (1 minute). The absorbance change per minute was calculated and converted to a specific rate, and a plot of the rate ( $\text{min}^{-1}$ ) versus concentration of either acceptor or donor made using Origin software (Microcal) and fitted to a rectangular hyperbola function to derive the  $K_m$  and  $k_{cat}$  values.

$$k_{obs} = (k_{cat}[S])/(K_m + [S])$$

Equation 6

$k_{\text{obs}}$  = the observed rate

$k_{\text{cat}}$  = the apparent limiting rate

$S$  = substrate or ligand concentration

$K_{\text{m}}$  = apparent rate constant

### 2.8.13 Steady-state kinetic analysis with P450 BioI

To assess the ability of the two *B. subtilis* flavodoxins to act as catalytically functional electron donors to P450 BioI, steady state analysis was carried out. A solution of P450 BioI (typically 2.0 nmol) and *E. coli* flavodoxin reductase (30.0 nmol) or either YumC or YcgT (*B. subtilis* reductases) (18.0  $\mu\text{mol}$ ) in aerobic KPi buffer (50 mM, pH 7.0, to give a total volume of 1.0 ml) was prepared and the flavodoxin (typically 2.0 to 20  $\mu\text{mol}$ ) added. The substrate was added (palmitoleic acid (20.0  $\mu\text{M}$ ), lauric, myristic or palmitic acid (25.0  $\mu\text{M}$ ), or the steroid testosterone (50  $\mu\text{M}$ )) and the solution allowed to equilibrate for 2 minutes at 30 °C. NADPH (0.2 mmol) was injected, the protein solution rapidly mixed (by shaking), and the decay of the NADPH absorbance ( $\Delta\epsilon_{340\text{ nm}} = 6.21\text{ mM}^{-1}\text{ cm}^{-1}$ ) measured over a period of 3 minutes. Reaction rates were determined in duplicate at each concentration of flavodoxin (ranged from 0 to 30  $\mu\text{mol}$ ). The initial linear decay rate was taken and converted to  $\mu\text{mol NADP}^+$  formed/minute/ $\mu\text{mol P450}$ . This rate was plotted versus the concentration of flavodoxin in Origin and data fitted to Equation 6 to derive the  $K_{\text{m}}$  and  $k_{\text{cat}}$  values.

### 2.8.14 Hydrogen peroxide determination

To determine the degree of uncoupling (leading to peroxide formation) that occurs during the steady-state turnover of myristic acid by P450 BioI, a colorimetric assay was used [Macheroux *et al.*, 1991]. Following steady state analysis (see above), the sample was incubated (1 hour, 23 °C) to ensure total depletion of NADPH. A solution of *o*-dianisidine (8 mM, 20 % v/v Triton X-100) [Noble *et al.*, 1999] was prepared and added (50  $\mu\text{l}$ ) to the reaction mixture. Horseradish peroxidase (50 mg/ml, 13.5 units/ $\mu\text{l}$ ) was added (2  $\mu\text{l}$ ), the solution mixed by inversion and incubated (2 minutes, 30 °C), and

the increase in absorbance measured ( $\Delta\epsilon_{440\text{ nm}} = 11600\text{ M}^{-1}\text{ cm}^{-1}$ ) and converted into a specific rate of peroxide production.

#### **2.8.15 Electron Paramagnetic Resonance (performed with Dr Myles Cheesman, University of East Anglia, Norwich)**

EPR spectra were recorded on an X-band ER-200D spectrometer (Bruker Spectrospin) fitted with a liquid helium flow-cryostat (ESR-9, Oxford Instruments). The samples were prepared in buffer A (pH 7.0 and 9.5). The protein concentrations were *ca* 0.50 to 1.0 mM (P450 BioI) and 1.0 mM (YkuN/P). The spectra recorded at 10 K with microwave power = 2.01 mW and modulation amplitude = 10.0 G

#### **2.8.16 Circular Dichroism (carried out with Dr Sharon Kelly, University of Glasgow)**

Far UV Circular Dichroism (CD) spectra (190-260 nm) and near UV-Visible CD spectra (260-600 nm) were recorded at 20 °C in a JASCO J600 spectropolarimeter purged with nitrogen. The concentration of P450 BioI used for near UV-visible spectra was 6  $\mu\text{M}$ , and 0.5 mM for the far UV spectra. All samples were in 50 mM Tris.HCl, pH 7.2.

CD spectra of the flavodoxins (YkuN and YkuP) and reductases (YumC, YcgT and CYP102A3) were carried out in house on a JASCO J-750 spectropolarimeter. The concentration of the proteins was 1 mg/ml in KPi buffer (50 mM, pH 7.0) with a path-length of 10 mm (near UV/visible) and 0.1 mg/ml, path-length 1.0 mm (far UV).

#### **2.8.17 Resonance Raman Spectroscopy (aided by Dr John Clarkson, University of Strathclyde, Glasgow)**

Resonance Raman spectra of P450 BioI were recorded using a Coherent Innova 100 Krypton ion laser as the source of 413.1 nm radiation. Power at the sample was 30 mW. Scattered radiation was collected at 180°, analysed by a Spex 1877 triple

monochromator and measured by a Princeton Instruments 1152E LN/CCD detector. The concentration of the P450 BioI was 0.1  $\mu$ M in 0.1 M KPi buffer at pH 7.0.

### 2.8.18 Chemical Denaturation of P450 BioI (guanidine hydrochloride method)

The stability of P450 BioI was analysed by the use of the chemical chaotropic reagent guanidine hydrochloride (Gdn.HCl) that disrupts hydrophobic interactions [Arakawa *et al* 1984]. P450 BioI (for concentration see below) was added to buffer A (varying volume) and the ligand, if any (*ca* 5  $\mu$ M to fully saturate P450 BioI, as monitored by UV-visible spectra) added. A stock solution of Gdn.HCl (8 M) was prepared and the appropriate volume added to the protein solution to give the required concentration (0 – 8 M). After the addition of Gdn.HCl, the solution was incubated at room temperature (*ca* 23 °C, 15 minutes) and then analysed either by UV-visible spectrophotometry (300 – 750 nm, 1 cm path-length, Cary Varian 50 spectrometer), fluorescence (excitation at 290 nm, emission measured at 300 – 400 nm, slit widths 5 nm, 1 cm path-length, CARY 50 fluorimeter), or Far UV CD (190 – 260 nm, 0.1 cm path-length, JASCO J750 spectropolarimeter).

Technique	P450BioI ( $\mu$ L of 1.5mM stock)	Total sample volume (ml)
UV-Visible	3	1.0
Fluorescence	1	3.0
CD	0.5	0.4

The percentage change in CD, absorption or fluorescence was plotted versus the concentration of denaturant and fitted to Equation 7 to find the concentration of Gdn.HCl at which 50% of the protein's secondary or tertiary structure is lost, or at which 50% of the heme is dissociated from its native binding site ( $K^H$ ):

$$F_{\text{obs}} = F_{\text{max}} D^H / (K^H + D^H) \quad \text{Equation 7}$$

$F_{\text{obs}}$  = observed emission/absorption/dichroism at a wavelength

$F_{\text{max}}$  = maximal emission/absorption/dichroism at a wavelength

$D^H$  = concentration of denaturant

$K^H$  = midpoint value

For the percentage unfolded:

$$\% \text{ structural change} = ((F_{\text{obs}} - F_{\text{min}})/(F_{\text{max}} - F_{\text{min}})) \times 100 \quad \text{Equation 8}$$

$F_{\text{min}}$  = the fluorescence emission at 0 M Gdn.HCl

$F_{\text{max}}$  = the fluorescence emission at 8 M Gdn.HCl

### 2.8.19 Chemical denaturation of the *B. subtilis* flavodoxins (guanidine hydrochloride method)

The flavodoxin YkuN or YkuP (for concentration see below) was added to KPi buffer (50 mM, pH 7.0, varying volume) and the appropriate volume of Gdn.HCl (8 M) added to give the required concentration (0 – 7 M). After the addition of Gdn.HCl, the solution was incubated at room temperature (23 °C, 15 minutes) and then analysed either by UV-visible spectrophotometry of the FMN cofactor (300 – 750 nm, 1cm path-length, CARY 50 spectrophotometer), tryptophan fluorescence (excitation at 290 nm, emission measured at 300 – 400 nm, slit widths 10 nm, Cary 50 fluorimeter), FMN fluorescence (excitation at 450 nm, emission measured at 500 – 600 nm, slit widths 5 nm, Cary 50 fluorimeter) or far UV CD (190 – 260 nm, 0.1 cm path-length, JASCO J750 spectropolarimeter). Data were analysed as described above for P450 BioI in order to determine protein and cofactor-binding stability.

Technique	Flavodoxin (nmol)	Total sample volume (ml)
UV-Visible	12.0	1.0
Fluorescence	3.0	3.0
CD	570	0.4



### **2.8.20 Differential Scanning Calorimetry**

Differential scanning calorimetry experiments were performed to analyse the heat-induced conformational transition of P450 BioI. DSC allowed the unfolding transition midpoint temperature ( $T_m$ ) to be determined. DSC scans were performed using a MicroCal VP-DSC (MicroCal LLC, Norhampton MA, USA) at a heating scan rate of 1 °C per minute. The DSC was interfaced to a Gateway PIII computer, data acquisition was achieved using Origin 5.0 (MicroCal LLC, Northampton MA, USA). The reference cell was filled with buffer containing any ligand (as appropriate) and instrumental baselines were measured by placing buffer in both cells. These baselines were subtracted from scans of the protein prior to data analysis. A solution of P450 BioI (0.137 mM) in potassium phosphate (pH 7.5, 50 mM), was aliquoted. One fraction was treated with DTT, the excess DTT removed from the enzyme (BioRad 10DG column) in the anaerobic glove box (Belle Technology, < 4 ppm O<sub>2</sub>), and the sample sealed anaerobically prior to analysis. Another 1 ml fraction of the protein was scanned in the DSC without adding any DTT or ligands. The remainder of the protein was used to investigate the effects on P450 BioI stability of adding various substrates or ligands. Substrates and ligands were added in sufficient amounts to facilitate near-complete saturation of the P450 BioI active site, as previously established by optical titration experiments. Stoichiometric concentrations of substrates/ligands were mixed with BioI: econazole, testosterone and palmitoleic acid. DMSO solvent for these ligands/substrates was present at a constant 1 % v/v in each of these samples. In control DSC experiments 1 % v/v DMSO was added to P450 BioI in isolation and the effect on enzyme stability was found to be negligible.

### **2.8.21 Generation of the apoprotein of the two *B. subtilis* flavodoxins**

To generate the apoproteins of the two *B. subtilis* flavodoxins, the following method was used: A sample of flavodoxin (2.0 µmol) was dialysed into KPi buffer (pH 7.0, 50 mM) for 4 hours at 4 °C. Trichloroacetic acid (5 % w/v) was added to the protein solution and the resulting yellow suspension incubated on ice (30 minutes). The protein

was recovered by centrifugation to yield a small off-white pellet. The apoprotein pellet was resuspended in KPi buffer (pH 7.0, 50 mM) and dialysed against the same buffer (2 l, 16 hours, 4 °C) to yield an off-white, clear solution. The apoprotein solution was then dialysed into KPi buffer (pH 7.0, 50 mM) containing 50 % v/v glycerol (1 l, 6 hours, 4 °C), divided into small aliquots (200 µl) and frozen (-20 °C) [Wassink *et al* 1975, and Pueyo *et al* 1996].

### 2.8.22 FMN binding to apo-flavodoxins

A solution of FMN (0.1 µM) was prepared in KPi buffer (50 mM, pH 7.0). Aliquots of the apoprotein solutions (1 µl of an approximately 10 µM solution) were added to the FMN solution. The fluorescence emission of the FMN cofactor was measured (Cary 50 fluorescence spectrometer, excitation at 450 nm, emission read from 500 – 600 nm, slit widths both 5 nm). The quenching of the fluorescence was corrected for dilution and the addition of apoprotein in the absence of FMN. Riboflavin binding was also assessed using the same procedure [Pueyo *et al* 1996 and Curley *et al.*, 1991]. Data were fitted to a modified version of equation 2 (Equation 9) to find the apparent  $K_d$  values for FMN binding.

$$F_{\text{obs}} = (F_{\text{max}}/(2C_t))([Apo] + C_t + K_d) - ((([Apo] + C_t + K_d)^2 - 4[Apo]C_t)^{0.5}) \quad \text{Equation 9}$$

$F_{\text{obs}}$  = observed fluorescence emission change at a concentration of apoprotein added

$F_{\text{max}}$  = maximal fluorescence emission observed at saturation

[Apo] = concentration of apoprotein

$C_t$  = total amount of FMN cofactor

$K_d$  = dissociation constant for the binding of FMN to the apoprotein

### 2.8.23 ANS quenching of tryptophan fluorescence

To see if a molten globule is formed during the Gdn.HCl-induced unfolding of the *B. subtilis* flavodoxins, the reagent 8-anilino-1-naphthalene sulphonate (ANS) was used

[Apiyo 2000, John *et al.*, 2001 and Ali *et al.*, 1999]. A solution of ANS was prepared (0.3 mM) and added (1.0 ml) to the protein solution (4  $\mu$ M) in KPi (1.0 ml, pH 7.0, 50 mM). The protein/ANS solution was incubated (25 °C, 5 minutes) before KPi (50 mM, pH 7.0, varying volume) and Gdn.HCl (8 M stock, varying volume) was added to give a solution of the required molarity (total volume 3.0 ml). The solution was incubated (25 °C, 15 minutes) before the ANS fluorescence was measured (excitation at 395 nm, emission 450 – 600 nm, slit widths were both 5 nm).

#### **2.8.24 Calculation of Stern-Volmer constants**

To a solution of either flavodoxin (4 nmol) in KPi (3.0 ml, pH 7.0, 50 mM) aliquots (10  $\mu$ l of a 2 M stock solution) of succinimide (2,5-pyrrolidinedione) were added [Eftink *et al.*, 1976, Lehrer *et al.*, 1971, Moore *et al.*, 1993, Eftink *et al.*, 1984, Radford *et al.*, 1992]. The tryptophan emission was measured (excitation at 290 nm, emission 300 – 400 nm, slit widths at 5 nm). The emission spectra were corrected for dilution and the emission maximum ( $F_0/F_x$ ) plotted against the succinimide concentration (where  $F_0$  is the fluorescence emission with no succinimide and  $F_x$  is the fluorescence at x molarity of succinimide). The quenching constant ( $K_q$ ) can then be found from the linear fit.

$$F_0/F_x = 1 + K_q\tau[Q]$$

**Equation 10**

Q = quencher

$F_0$  = the intensity in the absence of Q

$F_x$  = the intensity in the presence of Q at concentration x

$\tau$  = the lifetime in the absence of Q

$K_q$  = the quenching constant

### **2.8.25 P450 BioI: flavodoxin binding by UV-visible spectroscopy and tryptophan fluorescence**

The binding of the flavodoxins induced a small shift in the Soret band of unbound P450 BioI to high-spin (maximum at 394 nm). To a solution of P450 BioI (1.6  $\mu$ mol) in buffer A (0.78 ml), aliquots of the flavodoxin (1.0  $\mu$ l, 40  $\mu$ M) were added and the resulting UV-visible spectra recorded (250 – 750 nm, 1 cm path length) at 25 °C. The shift in the Soret band was plotted against the concentration of flavodoxin and fitted to a rectangular hyperbola function (Equation 3) in Origin.

The interaction of the flavodoxins with P450 BioI was also analysed by the quenching of tryptophan fluorescence due to both flavodoxins containing a tryptophan in close proximity to their FMN cofactor. P450 BioI (2.1 nmol) was added to buffer A (total volume 3.0 ml) and aliquots of flavodoxin added (0.5  $\mu$ l, 0.15 mM stock solution) and the emission spectra of the tryptophans measured (excitation at 290 nm, emission 300 – 400 nm, slit widths were both 5 nm) at 25 °C. The assay was repeated in the absence of P450 BioI and the spectra with P450 BioI absent were subtracted from those with P450 BioI present to compensate for the increase in tryptophan emission due to the total level of protein increasing. The quenching of tryptophan emission was plotted against the concentration of flavodoxin and data fitted to a sigmoidal function (Equation 1) in Origin.

### **2.8.26 Redox titrations**

Redox titrations were carried out anaerobically (Belle Technology glove-box) using the method of Dutton (1978). All solutions were degassed (argon sparged). During experiments oxygen levels were maintained at less than 4 ppm. The protein was loaded onto a 10DG gel filtration column (BioRad) pre-equilibrated with the relevant degassed buffer. P450 BioI was diluted to 5.0 ml (100  $\mu$ M), the flavodoxins YkuN/P also to 5.0 ml (0.15 mM), and the reductases to 6.0 ml (0.6 to 0.8 mM). Soluble mediators (2  $\mu$ l of 2 mg/ml each) were added. Ligands (~5  $\mu$ l, 50 mM stocks) were added, the exact volume depending upon their affinity for P450 BioI, and a spectrum recorded to check for full spin-state conversion. The solution was titrated electrochemically with successive small

volumes of the reductant (sodium dithionite, 10 mM) and an oxidant (potassium ferricyanide, 10 mM). Time was allowed for stabilisation of the electrode between each addition. The spectra at each point were recorded on a Varian Cary 50 UV-Visible spectrophotometer (300 - 750 nm). The electrochemical potential of the solution was measured using a pH 211 microprocessor (Hanna Instruments) coupled to a Pt/Calomel electrode (ThermoRussell Ltd). The experiment was carried out at 25 °C. Data for the heme ferrous/ferric transition was fitted to a single-electron Nernst equation (Equation 11) and that of the flavodoxins FMN transitions between oxidised, semiquinone and hydroquinone to a two-electron redox process (Equation 12) as previously described [Munro *et al.*, 2001].

$$A = \frac{a + b10^{(E_1' - E)/59}}{1 + 10^{(E_1' - E)/59}} \quad \text{Equation 11}$$

$$A = \frac{a + 10^{(E - E_1')/59} + b + c10^{(E_2' - E)/59}}{1 + 10^{(E - E_1')/59} + 10^{(E_2' - E)/59}} \quad \text{Equation 12}$$

$A$  = the total absorbance

$a$ ,  $b$  and  $c$  = absorbance due to the heme or flavin cofactor in different oxidation states

$E$  = the observed potential

$E_1'$  and  $E_2'$  = the midpoint potentials for the 0/-1 state and -1/-2 state respectively

The mediators described above had the following midpoint potentials;

Mediator	Midpoint potential (mV vs SHE)
Phenazine methosulfate (PMS)	+ 80
Methyl Viologen (MV)	-430
Benzyl Viologen (BV)	-311
2-hydroxy-1,4-naphthoquinone (HNQ)	-145



### **2.8.27 Standardisation of the electrode (Dr. O. Roitel, University of Leicester)**

The calomel electrode was calibrated using a de-oxygenated solution of 0.5 mM potassium ferricyanide to generate the ferric ions (10 ml, 10 mM EDTA and 0.1 M acetate buffer, pH 5.0). Ferrous iron sulphate (10  $\mu$ l) was titrated into the ferric solution and the potential recorded. The corrected potentials (relative to the standard hydrogen electrode) were plotted against  $\log_{10}([\text{ox}]/[\text{red}])$  to produce a straight line with a gradient of 59  $\pm$  2 mV and an intercept of 240 mV.

### **2.8.28 Catalytic turn-over studies**

The catalytic hydroxylation of myristic acid by P450 BioI was carried out in 25 ml sterilin reaction vials in MOPS buffer (20 mM, 100 mM KCl, pH 7.0, 12.0 ml) at room temperature (23 °C) with continuous stirring. Myristic acid (4.0  $\mu$ mol) was suspended in the buffer and the following proteins added; P450 BioI (80.0 nmol), YkuN or YkuP (20.0 nmol), and a flavodoxin reductase (20.0 nmol). The resulting orange coloured mixture was stirred (5 minutes, 23 °C) prior to the addition of NADPH (12.0  $\mu$ mol). The reaction was allowed to proceed for 16 hours before being terminated by acidification (pH 2.0, 0.5 ml 1.0 M HCl). The fatty acids were extracted into chloroform (2 x 3.0 ml), the organic layers combined, back extracted with brine (1 x 3.0 ml), dried ( $\text{MgSO}_4$ ) and evaporated to dryness. The off-white residue was resuspended in methanol and analysed by electrospray mass-spectrometry (mass spectra were obtained in negative mode EI (70 eV ionisation) using a Micromass Quattro triple quadrupole mass spectrometer).

Further fractionation of the reaction mixture was achieved by silica gel column chromatography. The fatty acid solution was refluxed (68 °C, 10 minutes) in acidic methanol (5.0 ml, pH 2.0, conc. HCl) to generate methyl esters. The methanolic solution was cooled (20 °C) and neutralised (addition of 1.0 M  $\text{NaHCO}_3$ , pH 7.0) prior to extraction with dichloromethane (2 x 3.0 ml). The organic layers were combined and extracted with brine (1 x 3.0 ml) before being dried ( $\text{MgSO}_4$ ) and evaporated to dryness. The pale-yellow residue was re-dissolved in hexane and loaded onto a pre-equilibrated

silica column (3 cm bed depth). The column was washed with hexane (3 x column volumes) and the fatty acid methyl esters were eluted with hexane:diethyl ether (97:3, 1 vol). The hydroxylated fatty acid methyl esters were eluted with hexane:diethyl ether (50:50, 1 vol). The fractions were evaporated to dryness, re-dissolved in hexane (1.5 ml) and analysed by gas-chromatography-mass-spectrometry (Perkin-Elmer Turbomass GC-MS, Zebron ZB-5 column 30 m x 0.25 mm x 0.25  $\mu$ m, He mobile phase).

#### **2.8.29 Identification of the ligand in *E. coli* purified P450 BioI**

Determination of the lipid bound to *E. coli*-purified P450 BioI (indicated by a partial conversion to high-spin) was done by acidifying (1.0 M HCl, 0.5 ml) a sample of purified P450 BioI (1.0  $\mu$ mol) prior to extraction (dichloromethane, 3.0 ml). The organic layer was dried (magnesium sulphate) and the solvent removed under vacuum. The residue was resuspended (methanol, 1.5 ml) and analysed by electrospray mass-spectrometry, the mass spectra were obtained in EI (70 eV ionisation, negative ionisation) mode using a Micromass Quattro triple quadrupole mass spectrometer. To confirm identification of the sample, it was converted to a methyl ester by refluxing (65 °C, 5 minutes) in acidic methanol (5.0 ml, pH 2.0, conc. HCl), and then analysed by GC-MS (GC-MS analysis was performed with an RSL-150 column (25m  $\times$  0.25 mm) on a Perkin Elmer gas chromatograph coupled to a Micromass Quattro triple quadrupole mass spectrometer, 20  $\mu$ l injection volume, ionisation voltage 70 eV. The retention time, m/z and fragmentation pattern were compared to known standards and a library search was carried out (Micromass (Waters) NIST library).

#### **2.8.30 Homology modelling of P450 BioI (with Prof. M.J. Sutcliffe, University of Leicester)**

A molecular model of P450 BioI was built to obtain further information regarding the overall structure and active site architecture, and also to help explain our binding data that indicated unusual molecular binding characteristics. The model was based on known 3D structures of other P450s. Proteins of known three-dimensional structure homologous

to P450 BioI were identified by scanning the amino acid sequence of P450 BioI against the sequences of P450s in the Protein Data Bank [Berman *et al.*, 2000] using PSI-BLAST [Altschul *et al.*, 1997]. This resulted in the P450s CAM [Poulos *et al.*, 1986], terp [Hasemann *et al.*, 1994], BM3 [Ravichandran *et al.*, 1993], 2C5 [Williams *et al.*, 2000] and eryF [Cupp-Vickery *et al.*, 1995] being identified as templates. These templates were used to generate comparative models by aligning them structurally to produce a profile using Malign3D within Modeller [Sali *et al.*, 1993]. This was then aligned against the sequence of P450 BioI using CLUSTALX [Thompson *et al.*, 1994]. The resulting alignment was checked to ensure that all of the secondary structural elements have a minimum number of insertions/deletions in them and any residues crucial to catalytic activity, such as the proximal cysteinate in the fifth co-ordination site of the heme [Lewis *et al.*, 1986], were conserved. Correlation between the secondary structural elements observed in a template (obtained from the Database of Secondary Structure in Proteins [Kabsch *et al.*, 1983] [DSSP]) and the secondary structure predicted for P450 BioI (using PSIPRED [Jones *et al.*, 1999]) was used to modify the sequence alignment. Once an acceptable alignment had been produced, an ensemble of fifteen models of P450 BioI was generated using Modeller [Sali *et al.*, 1993], and the “most representative” model selected (Kelley *et al.*, 1996). P450 BioI-myristate and P450 BioI-testosterone complexes were then modelled by docking the respective ligand into the active site using the program GOLD [Jones *et al.*, 1997].

### **2.8.31 Protein Crystallography**

Crystals of P450 BioI were grown using both the sitting- and hanging-drop method. Initial attempts at crystallisation involved the use of a commercial screen (Molecular Dimensions Ltd Clear Strategy Screens I and II) each containing 24 precipitant solutions across a wide range of crystallising conditions. Each of these solutions (0.5 µl) was placed in a 24 well tray. A drop of protein solution (2 µl, 10 or 14 mg/ml in 10 mM Tris.HCl pH 7.5) was placed either in a well or on a silanised glass cover slip, and the precipitant solution (2 µl) added. The wells were sealed (paraffin wax), and the tray stored (20 °C or 4 °C). This allowed the vapour pressure of the protein

drop and the well to equilibrate, permitting any crystallisation to occur. From these screens, promising conditions were expanded upon. The buffer system, pH, nature of the precipitant, and the presence of salts were all altered to determine the optimal crystallisation conditions. The crystals were frozen in the presence of glycerol (cryoprotectant) in a stream of liquid nitrogen to protect the crystal from high-energy radiation. Diffraction data were collected at the synchrotron source at Daresbury.

Subsequent screens were set-up using a complex of GAPDH (16 mg/ml, 0.45 mM) and P450 BioI (10 mg/ml, 0.22 mM). Stock solutions of both proteins were prepared at double the concentration required in Tris.HCl buffer (10 mM, pH 7.5) and a ligand (4-phenyl imidazole, ketoconazole or econazole) added to the stock solution of P450 BioI to try and aid stabilisation of the protein. The two stock solutions were then mixed 1:1 and drops of the mixture (2  $\mu$ l) were added to a drop of the mother liquor (2  $\mu$ l) in the sitting drop wells. Various manufacturers screens were used e.g. Hamilton crystallisation screens and Molecular Dimensions Ltd Clear Strategy Screens I and II.

The two *B. subtilis* flavodoxins were screened via the sitting drop method (2  $\mu$ l drops, 20 mg/ml) using an in house salt screen comprised of a total of 160 different conditions (four different precipitants versus 40 salts), an ammonium sulphate screen (ammonium sulphate concentration versus pH and buffer) and a commercial screen (Molecular Dimensions Ltd Clear Strategy Screens I and II) the latter containing 24 solutions of a wide range of crystallising conditions. Each of these solutions (0.5 ml) was placed in the reservoir of a 24 well tray, the protein drop added to a drop of the solution (1.0  $\mu$ l) and the tray stored (20 °C or 4 °C). Trays were examined by light microscopy for the formation of any crystals.

*Chapter 3*  
*Biophysical characterisation*  
*of P450 Biol*



The cloning and basic spectral characterisation of P450 BioI has already been described [Green *et al.*, 2001, Stok and DeVoss, 2000]. However, this early work produced some discrepancies and failed to clearly resolve the function and physical properties of the protein. For example, P450 BioI has been isolated from an *E. coli* expression host bound to an acyl carrier protein loaded with a range of long-chain fatty acids [Stok and DeVoss, 2000] whilst in parallel studies no such association with an acyl carrier protein was seen [Green *et al.*, 2001]. Whilst P450 BioI is thought to be involved in an early step in biotin synthesis from data gained through gene knock-out studies in *B. subtilis* [Bower *et al.*, 1996], its exact role is unclear. Evidence that it may function as a carbon-carbon bond cleaving enzyme was obtained [Stok and DeVoss, 2000] when the P450 was coupled to exogenous redox partners from *C. braackii*. In studies where the P450 was coupled to redox systems from *E. coli* or the di-flavin reductase human CPR, no carbon-carbon bond breakage was observed. Of the little activity that was observed only a hydroxylated product was found [Green *et al.*, 2001].

In this chapter further, more thorough, analysis of the P450's properties is described, encompassing both biophysical and biochemical attributes. The expression of the recombinant protein was evaluated and the expression system improved to gain greater yield of soluble protein. The isolated protein was analysed to gain data on its physical state and stability and the findings were compared to those of other well characterised bacterial P450s such as that from *B. megaterium*.

With a view to catalytic function, the reduction potentials of the P450 were measured both in a substrate-bound and substrate-free state. These measurements aid an understanding of the electron transfer pathways and are useful in looking to see what potential redox partners are available in the host organism. Binding constants for various compounds were measured with the aim of predicting possible substrates and inhibitors of the P450. Modelling studies were also used to gain a greater understanding of how the various types of compounds that bound to the protein did so, what interactions occur and so forth. An attempt was made to crystallise the protein with the aim of obtaining a structure of this P450 both in bound and un-bound forms. Chemical agents were also used to modify particular amino-acid residues to identify what effect certain residues had on the structure and binding capability of the protein.

### 3.1 Expression Systems

P450 BioI had been previously cloned into a pET11a vector (Promega) [Green *et al.*, 2001]. This plasmid was transformed into several different *E. coli* cell strains (Novagen and Stratagene) as detailed in Chapter 2.1. Small-scale induction studies (5.0 ml LB cultures) were carried out and SDS PAGE analysis of the cell extracts was performed to evaluate the amount of P450 BioI over-expressed. Three of the cell strains assessed for their ability to express P450 BioI had the *trxB* mutation, which allows the formation of a disulphide bond in the cytoplasm. These were included as the early homology model of P450 BioI (see Section 1.5) showed the possible existence of a disulphide bond in the protein between Cys250 and Cys275.

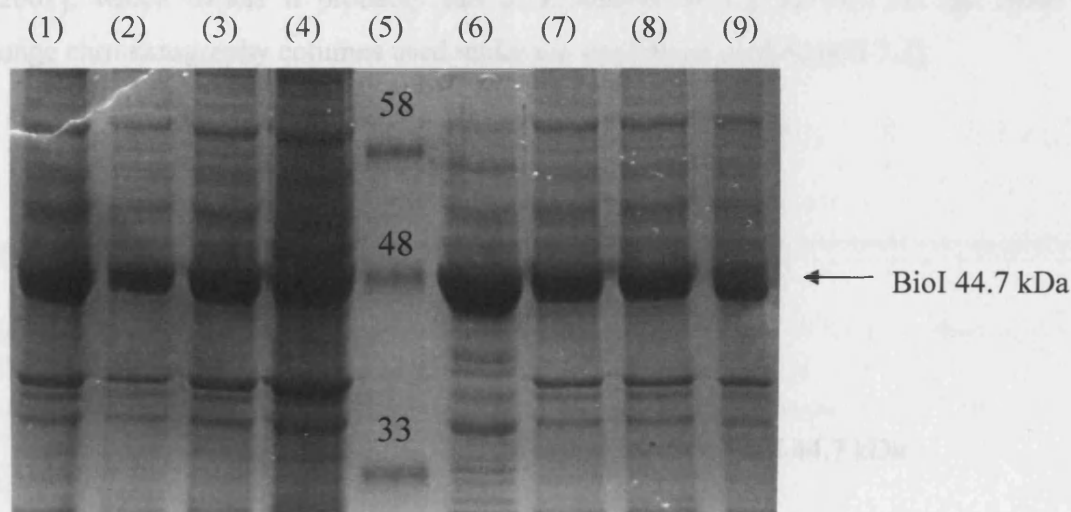


**Figure 3.1** SDS PAGE showing over-expression of P450 BioI in Origami (DE3). Note there is no discernible difference in the level of expression between the induced (shown in lanes 1 – 4, samples taken at 0, 1, 3 and 14 hours respectively) and un-induced cells (shown in lanes 6 to 9, time-points as before). A molecular weight marker is shown in lane 5 (NEB pre-stained broad-range). The bands shown are equal to 58, 48 and 33 kDa, respectively (as indicated above the bands).

The Origami (DE3) strain of *E. coli* (for genotype see Section 2.1) was found to be by far the best expression host for the preparation of P450 BioI, a finding that supports the possibility of a disulphide bond being contained in the protein. This strain was therefore used in all subsequent preparations of the protein. As P450 BioI was cloned into a pET11a expression vector, its expression is under a T7 promoter system with induction

by the addition of isopropyl- $\beta$ -D-galactopyranoside (IPTG) once the cells reach optimal density ( $OD_{600} = 1.0$ ) [Rosenburg *et al.*, 1987, Sambrook *et al.*, 1989]. However, with some strains of *E. coli* tested the addition of IPTG had little effect, indicating a leaky expression system. This was the case with Origami (DE3), the strain that was ultimately used in all further work.

The Origami DE3 pET11a/P450 BioI strain was grown on a 6.0 L scale (12 x 0.5 L LB cultures in 2 l shake-flasks). Successful over-expression of P450 BioI could be seen by the reddish colouring of the *E. coli* cells and, upon lysing, the red/brown colouring of the cell extract. P450 BioI was purified by anion exchange and gel filtration column chromatography (see Section 2.6). The theoretical pI of P450 BioI is *ca* 6.20 [Green *et al.*, 2001], which means it probably has a reasonably strong affinity for the anion exchange chromatography columns used under the conditions applied (pH 7.2).

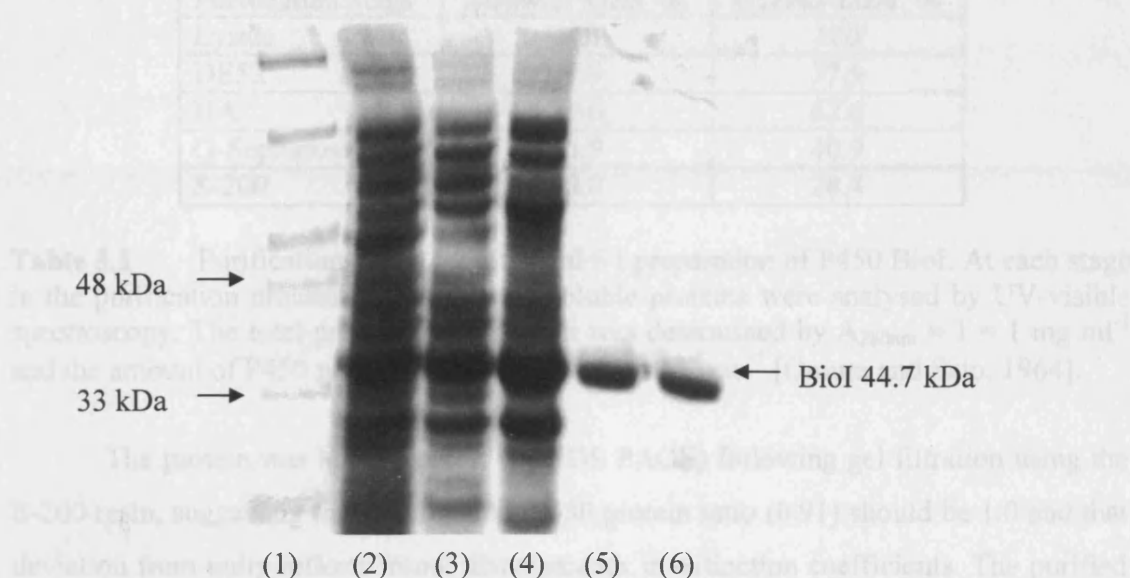


**Figure 3.2** SDS PAGE gel of P450 BioI (*ca* 10 ng) at various stages through the purification procedure; the pre-stained marker (NEB) is in lane 1, Origami DE3 pET11a P450 BioI cell extract (lane 2), post DEAE column (lane 3), post hydroxyapatite column (lane 4), post Q-sepharose column (lane 5), post sephacryl-200 gel filtration column (lane 6). Arrows indicate the positions of relevant molecular weight markers.

The purity at each stage of the purification protocol was determined by measuring the ratio of the peak heights at  $A_{280 \text{ nm}}$  (total protein) and  $A_{448 \text{ nm}}$  (carbon-monooxy bound P450 BioI Soret peak  $\Delta\epsilon_{448 - 490} = 91 \text{ mM}^{-1}\text{cm}^{-1}$  [Omura and Sato, 1964]). The absorbance

of the CO complex at 448 nm was measured rather than the value at 418 nm because of the mixed-spin nature of the isolated protein (i.e. the high spin form absorbs at 394 nm and so the absorbance at 418 nm underestimates the concentration of P450 BioI). A 280 : 448 ratio of 0.8:1 in the reduced CO-bound form was indicative of pure P450 BioI.

Purification Stage	Total protein (mg)	Total P450 (mg)	P450/ Protein	Stepwise purification fold	Overall purification fold
Cell Lysate	6042	208	0.03	1	1
DEAE	1164	162	0.14	4.7	4.7
HA	694	129	0.19	1.4	6.3
Q-Sepharose	119	85	0.71	3.7	23.7
S-200	65	59	0.91	1.3	30.3

Purification Stage	Stepwise Yield %	Overall Yield %
Lysate	100	100
DE52	77.9	77.9
HA	79.6	62.0
Q-Sepharose	65.9	40.9
S-200	78.0	28.4

**Table 3.1** Purification tables for a typical 6 l preparation of P450 BioI. At each stage in the purification process samples of the soluble proteins were analysed by UV-visible spectroscopy. The total protein concentration was determined by  $A_{280\text{nm}} = 1 = 1 \text{ mg ml}^{-1}$  and the amount of P450 present by  $\Delta\epsilon_{448-490} = 91 \text{ mM}^{-1} \text{ cm}^{-1}$  [Omura and Sato, 1964].

The protein was homogeneous (by SDS PAGE) following gel filtration using the S-200 resin, suggesting that the apparent P450/protein ratio (0.91) should be 1.0 and that deviation from unity reflects minor discrepancies in extinction coefficients. The purified protein was blotted onto a polyvinyl difluoride membrane and submitted for N-terminal sequencing at the in-house facility (PNACL) to confirm its identity (see Section 2.7). N-terminal sequencing showed that P450 BioI was intact with the N-terminal methionine removed. The response for the serine residues was slightly lower than the other residues, but this is an artefact of the method as serines undergo a disproportionately high amount of degradation through the cycling. The N-terminal methionine has been removed as is often the case for *E. coli* expressed proteins [Hirel *et al.*, 1989]. The sequence of the first six residues was determined to be as follows:

Cycle No.	Residue	Amount (pmol)
1	Thr	70.50
2	Ile	120.67
3	Ala	104.72
4	Ser	22.72
5	Ser	20.79
6	Thr	40.15

### 3.2 Physical Properties of P450 BioI

It was found that P450 BioI was isolated in a mixed-spin form, as was previously observed [Green *et al.*, 2001], and other studies had found P450 BioI to be co-purified with an acyl-carrier protein [Stok and DeVoss, 2000]. Usually P450s are isolated in their low-spin form e.g. P450 BM3 with a  $\lambda_{\text{max}}$  at 419 nm [Munro *et al.*, 1994], although mutants of P450s (where the mutated residue is situated near to the heme's sixth axial ligand) are often mixed-spin [Imai and Nakamura, 1989, Iwasaki *et al.*, 1991].

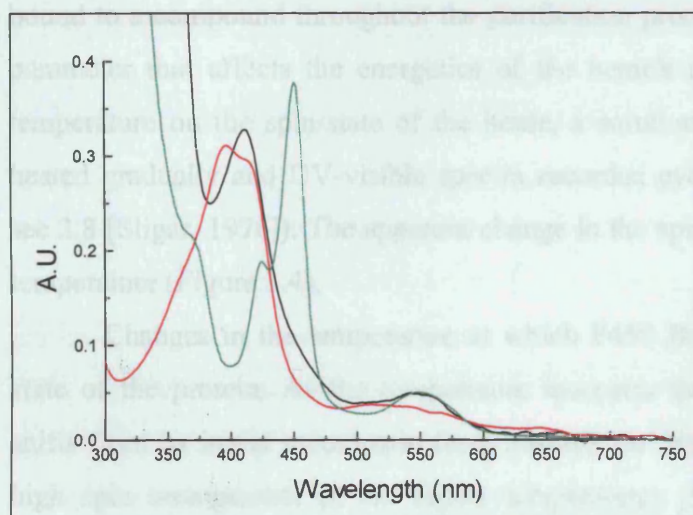


**Figure 3.3** UV-visible spectra of a typical preparation of P450 BioI (4.0  $\mu\text{M}$ ) in the following states; oxidised as isolated in mixed-spin form (red) maximum at 394 nm; reduced to ferrous (black) maximum 408 nm; and ferrous-CO form (green). When reduced and bound to CO the Soret band shifts to 448 nm, typical of a P450. The  $\alpha$  and  $\beta$  bands alter position and intensity to form a single band with its maximum at 550 nm.

Carbon monoxide (CO) binding to 1-electron reduced P450s gives rise to the characteristic Soret maximum close to 450 nm [Ortiz de Montellano, 1995]. P450 BioI



was added to a deoxygenated (Argon sparged) and carbon monoxide-saturated Tris.HCl buffer (50 mM, pH 7.2). After measurement of the spectrum a concentrated solution of sodium dithionite was added (*ca* 10 mM) and a spectrum of the CO-bound form of P450 BioI obtained with the Soret maximum at 448 nm.

A small shoulder at 420 nm was observed. This absorbance is believed to be due to denatured P450 where the cysteine ligation is lost or the cysteine thiolate has become protonated. From electron paramagnetic resonance (EPR) experiments (see Section 3.8) it is known that there is a little 'dead' iron (an EPR signal distinct from the water/cys-ligated heme). Potentially, this could be responsible for the P420 content in the samples of P450 BioI. However, it is also possible that the small amount detected could be as a result of freezing the protein sample in liquid nitrogen for the EPR analysis.

### **3.3 Temperature and pH effects**

The isolation of mixed-spin P450 BioI was believed due to it either being partially bound to a compound throughout the purification process, or due to some other physical parameter that affects the energetics of the heme's iron core. To assess the effect of temperature on the spin-state of the heme, a solution of P450 BioI in KPi buffer was heated gradually and UV-visible spectra recorded every two degrees (for methodology see 2.8 [Sligar, 1976]). The apparent change in the spin-state was then plotted versus the temperature (Figure 3.4).

Changes in the temperature at which P450 BioI is incubated affected the spin-state of the protein. As the temperature increases the protein's spin-state equilibrium shifts from its initial mixed-spin form towards the high-spin form. The iron favours its high spin arrangement at the higher temperatures [Sligar, 1976] with an absorption maximum around 392 nm. The increase in the amount of energy in the system means that electron transfer between the iron's split 3d orbitals is favoured over electron pairing (see Section 1.2). The mobility of the solvent molecules lining the binding channel increases with the rise in temperature and this may also favour the formation of the high-spin form as the interaction with the aqua ligand is weakened [Sligar and Gunsalus, 1979].



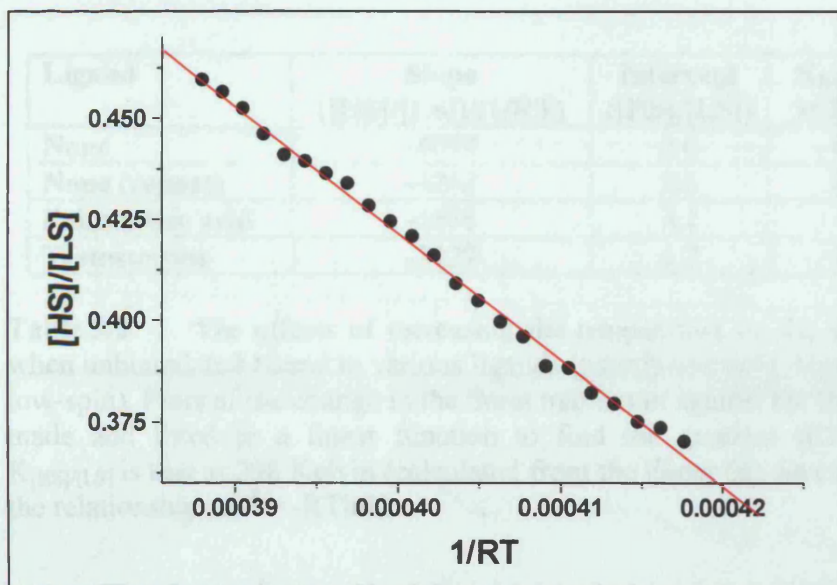


**Figure 3.4** The effect of the temperature on testosterone (30  $\mu\text{M}$ )-bound P450 BioI (0.3  $\mu\text{M}$ ) in KPi (100 mM, pH 7.0). Increasing the temperature results in an increasing proportion of the heme converted to its high-spin (absorbance maximum at 392 nm) form. The concentration at each spin state (approximated by using  $\epsilon_{448} = 91 \text{ mM}^{-1}\text{cm}^{-1}$ ) is plotted versus the inverse of the temperature multiplied by the molar gas constant ( $R = 8.314 \text{ Jmol}^{-1}\text{K}^{-1}$ ) and fitted to a linear function (Origin software, Microcal).

The effect of heme ligation (fatty acid-bound and steroid-bound) upon the equilibrium between high- and low-spin was investigated. The temperature was ramped up at one-degree intervals, with the sample being held at the new temperature for two minutes to equilibrate prior to measurement of the spectrum.

From the data tabulated below it can be seen that the binding of the fatty acid thermodynamically favours the formation of the high-spin form of the heme (negative  $\Delta G^\theta$ ) and that the steroid bound form energetically favours the low-spin iron. The free energy values under standard conditions are in agreement, with the steroid ligation having a large positive  $\Delta G^\theta$  ( $2.2 \text{ kJmol}^{-1}$ ) disfavouring the formation of the high-spin form. This is consistent with the presence of an electronegative group such as oxygen is interacting with the heme.

Ligand	Slope ([HS]/[LS])/(1/RT)	Intercept ([HS]/[LS])	$K_{[HS]/[LS]}$ at 298 K	$\Delta G^\theta$ (Jmol <sup>-1</sup> )
None	-4094	2.6	0.9	185
None (repeat)	-4242	2.6	0.8	438
Palmitoleic acid	-6856	4.1	1.3	-686
Testosterone	-3127	1.7	0.4	2210

**Table 3.2** The effects of increasing the temperature on the spin-state of P450 BioI when unbound and bound to various ligands (palmitoleic acid, high-spin and testosterone, low-spin). Plots of the change in the Soret maximum against the temperature change were made and fitted to a linear function to find the gradient ( $([HS]/[LS])/(1/RT)$ ). The  $K_{[HS]/[LS]}$  is that at 298 Kelvin (calculated from the linear fit), and the  $\Delta G^\theta$  calculated from the relationship  $\Delta G^\theta = -RT \ln K$ .

The change in the pH of the protein solution was examined by adding P450 BioI to various solutions of Tris.HCl and HEPES buffers (organic buffers), and the inorganic potassium and sodium phosphate buffers of differing pH values. The protein was stable in the range tested from pH 10.0 to pH 6.0, although at lower pH values protein degradation/aggregation was observed through an increase in turbidity. This was believed to be due to precipitation as various side-chains in the protein become protonated and/or lose hydrogen-bonding interactions that are crucial to tertiary structure formation. Structural disruption leads to non-specific intermolecular interactions and aggregation between proteins to form larger insoluble complexes that scatter light.

In the two organic buffers examined, a shift from predominantly low-spin (Soret maximum at 418 nm) in the alkaline pH solutions to high-spin (Soret maximum at 394) as the pH dropped was observed (as shown in Figure 3.5). This pH effect was less evident in the inorganic potassium and sodium phosphate buffers. In these buffers the change in pH gave a relatively smaller change in the iron's spin-state. Therefore, the spin-state change observed in the organic buffers could be due to active site protonation and altered hydrogen bonding pathways which in turn have an effect upon the energetics of the heme cofactor and/or the distance from the iron atom to the water ligand (unbound state). The organic anions, being weaker bases than their inorganic counterparts, allow a greater likelihood of amino acid protonation as the buffer and protein compete for the free protons.

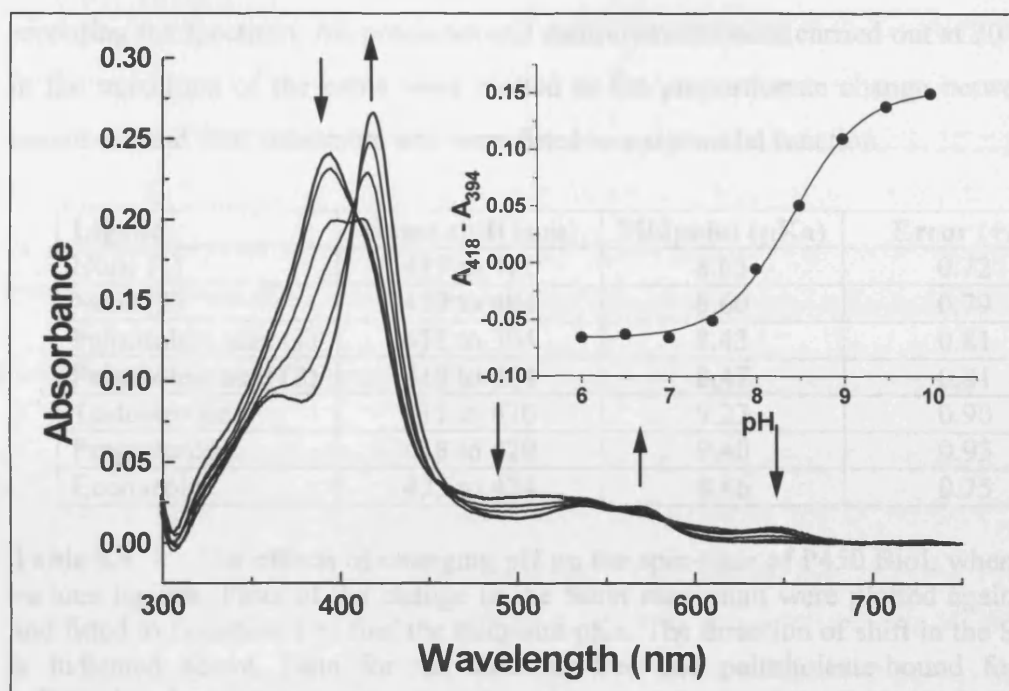


**Figure 3.5** The effect of changing the pH of Tris.HCl buffer (50 mM) on the spin state of fatty acid-bound P450 BioI (2.7  $\mu$ M). Arrows indicate the direction of change in the absorbance as the pH is increased from 6.5 (the protein is high-spin (maximum at 394 nm)) to 10.5 (protein goes low-spin (maximum at 418 nm)). Inset shows the pH change versus the change in the Soret absorbance maximum fitted to Equation 1 (Origin software, Microcal). The change to the low-spin form suggests that a single residue may be involved in substrate binding, acting as a proton donor.

This pH effect upon spin-state is observed with other heme containing proteins. For example cytochrome *c* peroxidase (a monomeric protein which contains a non-covalently bound protoheme) shows a spin-state affected by the pH of its environment. In the range of pH from 4.0 to 10.0, the EPR spectra of this protein showed that the heme exists as pure high-spin at pH 4.0 and became mixtures of high- and low-spin as the pH increased. It is totally low-spin at pH 10.0 (all measured by EPR at 77 K). The transition was believed due to proton dissociation – association of the distal ligand (His52) or the water ligand [Hori *et al.*, 1985].

The experiment was repeated with P450 BioI fully bound to either a high-spin (fatty acid) or low-spin (steroid) ligand under standard conditions (Tris.HCl buffer, 50 mM, pH 7.5). Aliquots of the protein (2.7  $\mu$ M) were saturated with the ligand (10.0  $\mu$ M) and diluted with Tris.HCl buffer (50 mM, 100 vol) to give solutions of varying pH values (pH 6.0 to 10.5). The solutions were allowed to equilibrate for 2 minutes prior to

recording the spectrum. All processes and measurements were carried out at 20 °C. Shifts in the maximum of the heme were plotted as the proportionate change between initial maximum and final maximum and were fitted to a sigmoidal function.

Ligand	Heme shift (nm)	Midpoint (pKa)	Error (+/-)
None (1)	419 to 411	8.65	0.72
None (2)	419 to 404	8.60	0.79
Palmitoleic acid (1)	418 to 394	8.43	0.81
Palmitoleic acid (2)	418 to 404	8.47	0.81
Testosterone	417 to 420	9.27	0.90
Progesterone	418 to 420	9.40	0.93
Econazole	423 to 424	8.46	0.75

**Table 3.3** The effects of changing pH on the spin-state of P450 BioI, when bound to various ligands. Plots of the change in the Soret maximum were plotted against the pH and fitted to Equation 1 to find the midpoint pKa. The direction of shift in the Soret band is indicated above. Data for the substrate-free and palmitoleate-bound forms were collected in duplicate.

The high-spin palmitoleic acid-bound form of P450 BioI shows the most dramatic shift in Soret maximum from high-spin (394 nm) at pH 6.0 to low-spin (418 nm) at pH 10.5. This is consistent with an ionisable amino acid group that interacts with the fatty acid carboxylate (e.g. R47 interacting with palmitoleate in P450 BM3 [Li and Poulos, 1997]) becoming stripped of its proton at the higher pH values and is, as a result, unable to act as proton donor to the fatty acid leading to loss of binding of the substrate. The midpoint of 8.4 suggests that, if the event is due to a single ionisable group, that the side chain must have a pKa value in the same region.

The steroid-bound protein exhibited a higher pH midpoint value (9.3). This sample shows high turbidity at the low pH values, which could be due to the presence of the steroid destabilising the protein and causing aggregation, or reduced solubility of the steroid under these conditions. This destabilisation at the low pH values may underline the higher apparent midpoint value. However, the shift to a longer wavelength as the pH decreases suggests that the main binding mode of the steroid is via co-ordination of the heme iron by the carbonyl group directly. Due to its very low pKa value (~2.0) the carbonyl group will not be protonated in these experiments. The shift to a longer wavelength as the pH increases suggests that the steroid becomes closer to the iron

strengthening the carbonyl-iron interaction as the proposed hydrogen bond between the C17 hydroxyl and Glu65 is lost (see Section 3.7). Alternatively, at the higher pH values the environment of the heme may change (due to the protonation states of surrounding residues and its propionate groups) to give increased electron density on the iron. This could strengthen the back-bond to the ligated heteroatom. Changes in the fine structure of the steroids caused a slight change in the midpoint pKa (progesterone versus testosterone), indicating that there may be some ionic interaction of the substituent groups with a proton donor residue (see Section 3.7).

The binding of econazole is unaffected by pH. It remains fully bound at all values, its main mode of binding being co-ordination of the iron by the  $sp^2$  nitrogen [Bartoli *et al.*, 1998]. A small shift to a longer wavelength is seen as the pH increases, possibly due to the strength of the Fe – N bond increasing, as either protonation of the imidazole group no longer competes with ligation at the higher pH or as the electron density on the iron increases, as discussed above.

The calculated pKa of the various bound forms of P450 BioI seems to be related to a single amino acid residue from the simple sigmoidal relationship observed. Whilst the pKa value of cysteine (pKa 8.25) is near to those observed above the only cysteine near the bound compounds is the one ligating the heme iron (Cys345). Protonation of this cysteine could conceivably alter the heme spectrum, but it is unlikely to affect the binding of fatty acids that do not co-ordinate to the iron. It is more likely that, in the case of fatty acid-binding, a histidine residue (pKa 6) interacts either directly or indirectly with the ligand, unlike the serine (pKa 16) and tyrosine (pKa 10) implicated by our model (see Section 3.7). However, the pKa values of amino acid side chains can vary greatly depending upon their environment and so it is hard to pinpoint an individual residue.

### **3.4 Effect of solvents upon the spin state of P450 BioI**

P450 BioI has always been isolated from *E. coli* in a mixed-spin form, raising the question of whether a proportion of the protein has a compound bound in the active site or whether the heme is mixed-spin under the conditions used to study it (which may differ somewhat from its intracellular environment). The effects of altering the proportion

of organic to aqueous solvent in the protein's environment were examined to assess whether raising the proportion of the organic component (0 – 20 % v/v) to allow higher concentrations of the protein's lipophilic substrates to be dissolved in reaction solutions. However, it was found that, whilst the protein was able to tolerate quite high levels of the organic phase without denaturing, a low-spin form resulted. This result appeared to be consistent with P450 BioI binding to an endogenous compound in *E. coli* that then dissociates at higher concentrations of organic solvent.

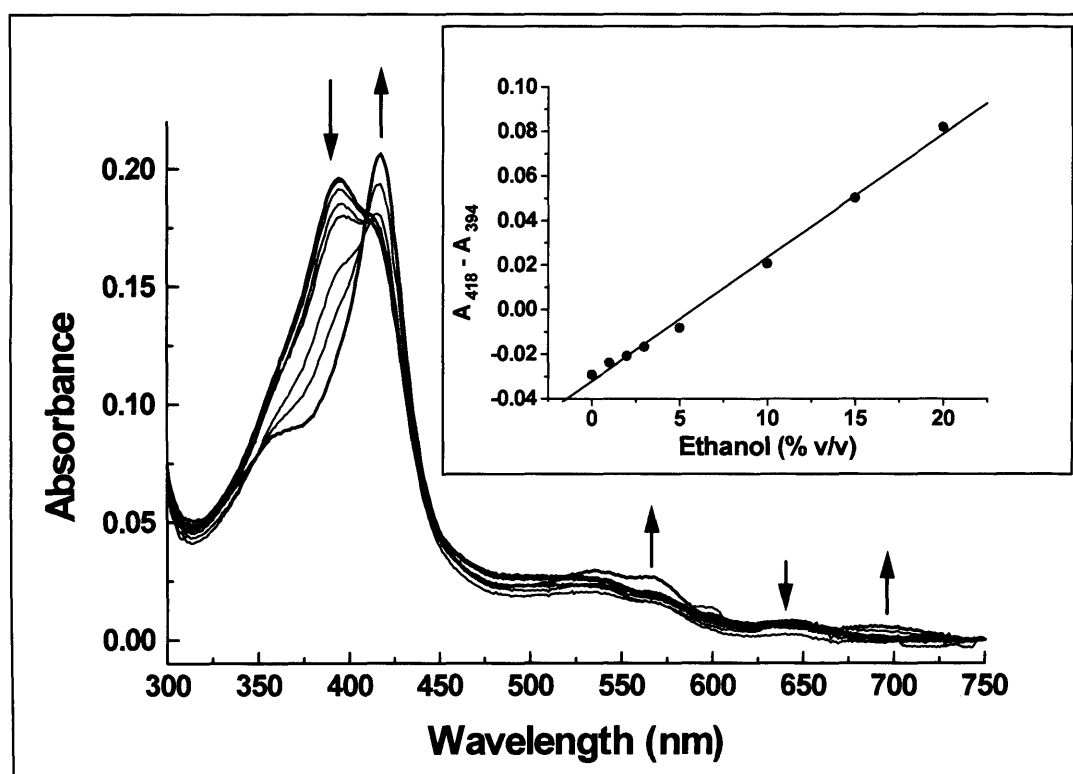


**Figure 3.6** The effect of increasing the proportion of organic solvent upon the spin state of P450 BioI (2.0  $\mu$ M) in Tris.HCl buffer (50 mM, pH 7.2). Shown in the spectra above is the effect of the addition of ethanol from 0 where the absorption is characteristic of the mixed spin form (maximum at 394 nm) to 20 % v/v where the absorbance is characteristic of the low spin form (maximum at 418 nm). The shift in wavelength of the Soret band is plotted against the ethanol concentration (inset) and fitted to a linear function (Origin software, Microcal).

This effect was seen with all four solvent systems tested (acetonitrile, ethanol, methanol, DMSO/methanol mix [1 vol:1 vol]) to different degrees. These results point towards the isolation of a partially bound form of P450 BioI. Increasing the organic proportion of the environment causes a decrease in the thermodynamic driving force for



the substrate to bind and therefore an increase in the theoretical  $K_d$ . This results in the true, unbound low-spin form being obtained.

Tabulated below are values from fitting a linear function to the solvent-induced spin-state change. The acetonitrile content induced a sigmoidal change in the range studied (0 to 25 % v/v) giving a value of 50 % spin-state change at 8.37 % v/v, the linear function tabulated below being calculated for the range 5 to 20 % v/v. At the higher concentrations (>15 %), acetonitrile was found to co-ordinate directly to the iron through its cyanide group (as shown by the endpoint maximum at 421 nm). This interaction with the heme itself may explain the sigmoidal nature of the fit as the solvent competes with the endogenous ligand for the binding site.

Solvent system	Soret shift (nm)	$\Delta\text{Abs} / \% \text{ v/v}$
Acetonitrile	394 to 421	$1.2 \times 10^{-2}$
Ethanol	394 to 418	$0.6 \times 10^{-2}$
Methanol	394 to 419	$0.6 \times 10^{-2}$
DMSO/methanol	394 to 418	$0.7 \times 10^{-2}$

**Table 3.4** The effects of adding organic solvents on the spin-state of P450 BioI. Plots of the change in the Soret maximum against the concentration of solvent were fitted to a linear function to find the gradient ( $\Delta\text{Abs}$  (e.g.  $A_{421}$  minus  $A_{394}$ ) against the solvent content (% v/v)). The concentration of P450 BioI used was 2.0  $\mu\text{M}$ .

These data indicate that P450 BioI is recovered from *E. coli* in a partially substrate-bound form. From its behaviour in the pH studies (Section 3.3) it is most likely to be binding a fatty acid type substrate. The studies here showed that organic solvents can displace this substrate and so it was decided to attempt to extract and identify the compound(s).

### 3.5 Analysis of the endogenously bound compound

P450 BioI has always been isolated in a mixed-spin form due, as evidenced by pH titrations (Section 3.3), solvent effects (Section 3.4) and the fact that NADPH-induced turnover produces a low-spin form (data not shown). This is consistent with a compound being bound in a large proportion of the isolated enzyme's active site. To identify this substance, a sample of predominantly high-spin P450 BioI that had been purified in the

typical manner (described in Chapter 2.8) was extracted by acidifying to pH 1.0 with 1 M HCl and partitioning against chloroform. The organic layer was taken and dried (using  $\text{MgSO}_4$ ) before being evaporated under vacuum to dryness. The pale cream residue was re-dissolved in methanol and analysed by electrospray mass-spectrometry (Micromass Quattro electro-spray mass-spectrometer, ionisation voltage -70 eV). The compound present was found to have an  $m/z$  of 255 (ES<sup>-</sup>). This mass corresponded to palmitic acid that is known to be highly abundant in *E. coli* and to bind strongly to P450 BioI ( $K_d$  of 5 – 7  $\mu\text{M}$ ). This fatty acid has also been found to co-purify in the active site of another *B. subtilis* P450 over-expressed in *E. coli*, P450  $\beta\text{SB}$ , as identified by x-ray crystallography of the ‘unbound’ protein [Lee *et al.*, 2003]. To further confirm or disprove that the compound was indeed palmitic acid, the sample was methylated (refluxed for 20 minutes in acidic methanol, neutralised and extracted into dichloromethane) and analysed on the GC-MS (Perkin Elmer Turbomass GC-MS, Zebron ZB-5 column, 30 m x 0.25 mm x 0.25  $\mu\text{M}$ ). Comparison of the retention time (r.t. = 15.67 mins), mass spectrum and fragmentation pattern (see Figure 3.7) with that of a known standard prepared in an identical manner (r.t. = 15.64 mins), and the Micro-mass library search facility (National institute of standards and technology library) confirmed the compound’s identity as palmitic acid.

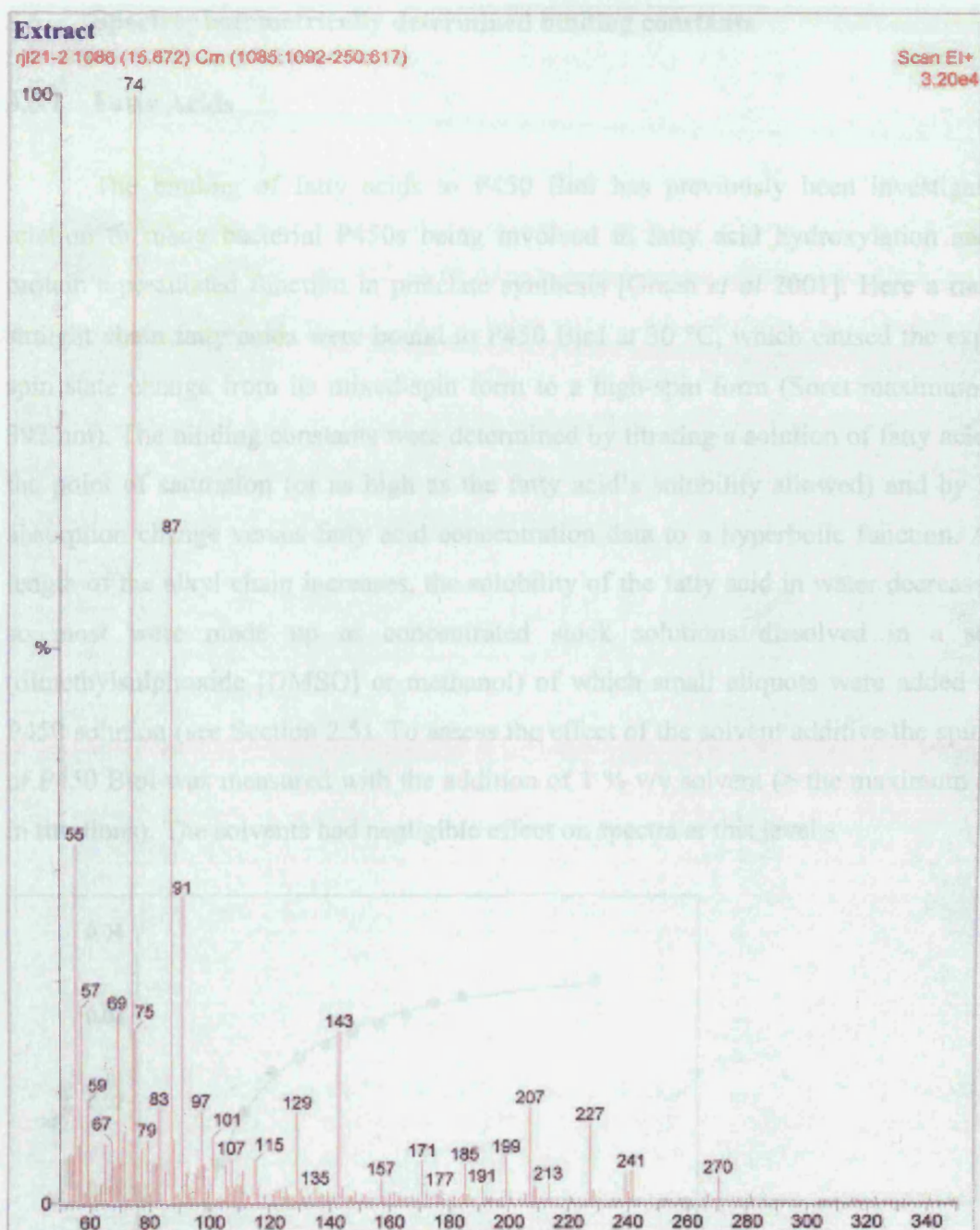


**Figure 3.7** Fragmentation pattern of the extracted fatty acid (retention time 15.67 minutes). The characteristic McLafferty rearrangement peak of methyl esters can be seen with an  $m/z$  of 74. Samples were analysed on a GC-MS (Perkin Elmer Turbomass GC-MS, Zebron ZB-5 column, 30 m x 0.25 mm x 0.25  $\mu$ M). P450 BioI (25  $\mu$ M) was extracted with chloroform (2 x 1.0 ml) to isolate the substrate. The compound was then methylated (refluxed in 5.0 ml methanol, pH 1.0, 20 minutes) and analysed.

### 3.6 Spectrophotometrically determined binding constants

#### 3.6.1 Fatty Acids

The binding of fatty acids to P450 BioI has previously been investigated in relation to many bacterial P450s being involved in fatty acid hydroxylation and this protein's postulated function in pimelate synthesis [Green *et al* 2001]. Here a range of straight chain fatty acids were bound to P450 BioI at 30 °C, which caused the expected spin state change from its mixed-spin form to a high-spin form (Soret maximum at *ca* 392 nm). The binding constants were determined by titrating a solution of fatty acid until the point of saturation (or as high as the fatty acid's solubility allowed) and by fitting absorption change versus fatty acid concentration data to a hyperbolic function. As the length of the alkyl chain increases, the solubility of the fatty acid in water decreases and so most were made up as concentrated stock solutions dissolved in a solvent (dimethylsulphoxide [DMSO] or methanol) of which small aliquots were added to the P450 solution (see Section 2.5). To assess the effect of the solvent additive the spin state of P450 BioI was measured with the addition of 1 % v/v solvent (> the maximum added in titrations). The solvents had negligible effect on spectra at this level.

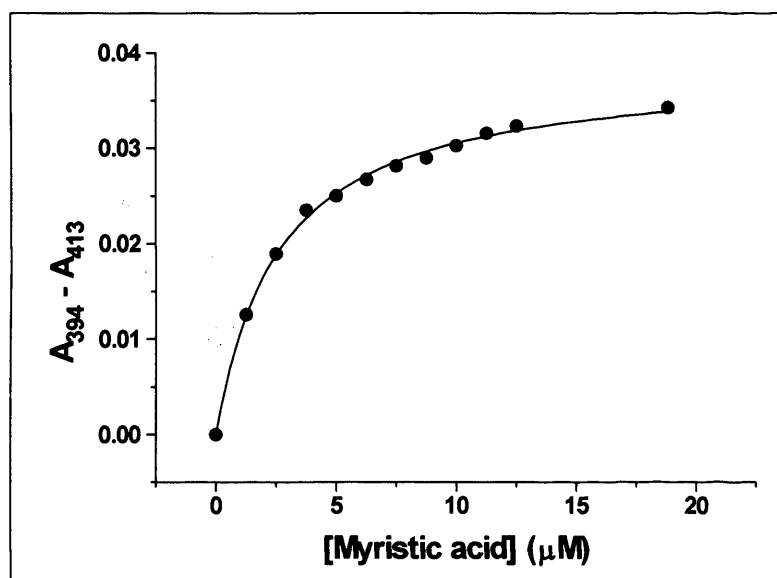


**Figure 3.8** Titration of myristic acid (a C14 straight chain saturated fatty acid) against a constant concentration of P450 BioI (2 μM). The change in absorbance due to the

formation of the high spin species (maximum 394 nm) is recorded. Points are fitted to a rectangular hyperbola (Equation 3) to give an apparent  $K_d$  value of  $2.6 \pm 0.2 \mu\text{M}$ .

A series of straight chain saturated fatty acids from C8 to C18 were assayed for their affinity to P450 BioI. The effect of decreasing the saturation of the fatty acids by the introduction of a double bond ( $\Delta 9$ ) was also examined. The three unsaturated fatty acids (myristoleic, palmitoleic and oleic acid) all bound more tightly than their saturated counterparts. Whilst increasing the hydrophobicity of a substrate may be expected to increase its affinity for the protein, unsaturated fatty acids all contain a *cis* double bond, which introduces a kink in the molecule and reduces its flexibility. In P450 BioI this modification has no detrimental effect thereby indicating no unfavourable steric interactions or a large and relatively flexible active site.

Fatty Acid	Molecular formula	$K_d$ ( $\mu\text{M}$ ) at 30°C	Error (+/-)	Shift (nm)
Decanoic	$\text{C}_{10}\text{H}_{22}\text{O}_2$	21.5	2.6	413 - 393
Dodecanoic	$\text{C}_{12}\text{H}_{24}\text{O}_2$	11.0	1.0	414 - 394
Tridecanoic	$\text{C}_{13}\text{H}_{26}\text{O}_2$	7.69	0.55	414 - 394
Tetradecanoic	$\text{C}_{14}\text{H}_{28}\text{O}_2$	2.63	0.21	414 - 394
Pentadecanoic	$\text{C}_{15}\text{H}_{30}\text{O}_2$	5.23	0.74	414 - 393
Hexadecanoic	$\text{C}_{16}\text{H}_{32}\text{O}_2$	7.19	0.55	414 - 393
Octadecanoic	$\text{C}_{18}\text{H}_{34}\text{O}_2$	33.02	5.58	413 - 394
Myristoleic ( $\Delta 9$ )	$\text{C}_{14}\text{H}_{26}\text{O}_2$	1.46	0.09	414 - 394
Palmitoleic ( $\Delta 9$ )	$\text{C}_{16}\text{H}_{28}\text{O}_2$	0.87	0.06	413 - 394
Oleic ( $\Delta 9$ )	$\text{C}_{16}\text{H}_{30}\text{O}_2$	0.92	0.09	413 - 394
Myristoyl-CoA	$\text{C}_{35}\text{H}_{62}\text{N}_7\text{O}_{17}\text{P}_3\text{S}$	12.41	0.88	414 - 394

**Table 3.5** Binding constants for the range of fatty acids evaluated in this study. The final column indicates the maximal absorbance shift induced in each case (peak to trough from difference spectra); and these difference values were plotted against substrate concentration to derive the  $K_d$  values.

All the long chain, saturated, unbranched fatty acids showed tight binding. The rather high value for octadecanoic acid was possibly due to solubility problems. The addition of the CoA group reduced binding affinity, possibly due to the large bulk of the CoA group being disfavoured due to either steric clashes with active site residues, or its increased aqueous solubility.

From the  $K_d$  values, P450 BioI appears to favour the binding of longer chain fatty acids, which given the physiological environment of *B. subtilis*, implies that its substrate could be a C12 to C16 saturated straight chain fatty acid [Oku and Kaneda, 1988]. This supports its function as an oxidative cleavage enzyme if it is to produce the C7 diacid (pimelic acid) as proposed by Stok and De Voss [Stok and De Voss, 2000]. Recent modelling studies (Section 3.6) have shown this to be unlikely as the fatty acids are positioned with the carboxylate head hydrogen bonded near the opening of the access channel (Figure 3.17). This means that, unless there is a dramatic conformational change upon reduction, any oxygenation reaction occurring near the heme plane would be at the  $\omega$ -methyl end of the ligand. However, the modelling work may be biased towards the conformation adopted by the fatty acid substrate in the P450 BM3 enzyme [Li and Poulos, 1997].

As *B. subtilis* is known to contain a high proportion of branched chain fatty acids, particularly when growing at low temperatures [Klein *et al.*, 1999, Choi *et al.*, 2000], the binding of three *iso*- fatty acids was examined to see if they bound as tightly as their straight chain saturated and unsaturated counterparts (Figure 3.9).

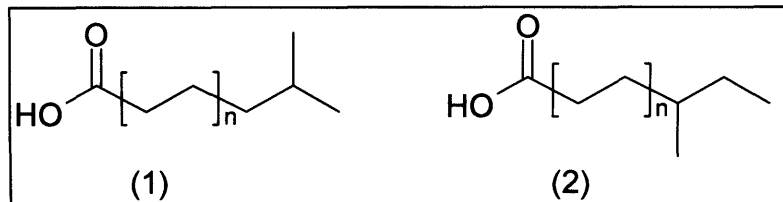


**Figure 3.9** *B. subtilis* is known to contain *iso*- (1) and *anteiso*- (2) branched chain fatty acids, particularly for inclusion in the cell membrane when growing at low temperatures [Klein *et al.*, 1999].

An unusual result was observed. With the two longer *iso*-methyl fatty acids (14-methyl pentadecanoic and 15-methyl palmitic acid) a shift in the heme's spin-state to a low-spin form (maximum *ca* 421 nm) was seen after an initial shift to the high-spin maximum (394 nm) characteristic of substrate binding. With the smaller 13-methyl myristic acid the typical shift to high-spin was observed. This shift to low-spin at high concentrations of the two larger *iso*-methyl fatty acids could be due to their size and hence slightly different positioning of the methyl group at the heme site. Being bigger



and bulkier, the C14 and C15 branched chain fatty acids could (at high concentrations) conceivably cause the water molecule (usually loosely associated with the iron) to be forced closer to the iron atom causing an interaction and therefore shifting the Soret band to a longer wavelength (421 nm) than the resting state (418 nm). Since these fatty acids initially induce some conversion to high-spin, a dual binding site model for these fatty acids would be consistent with the data.

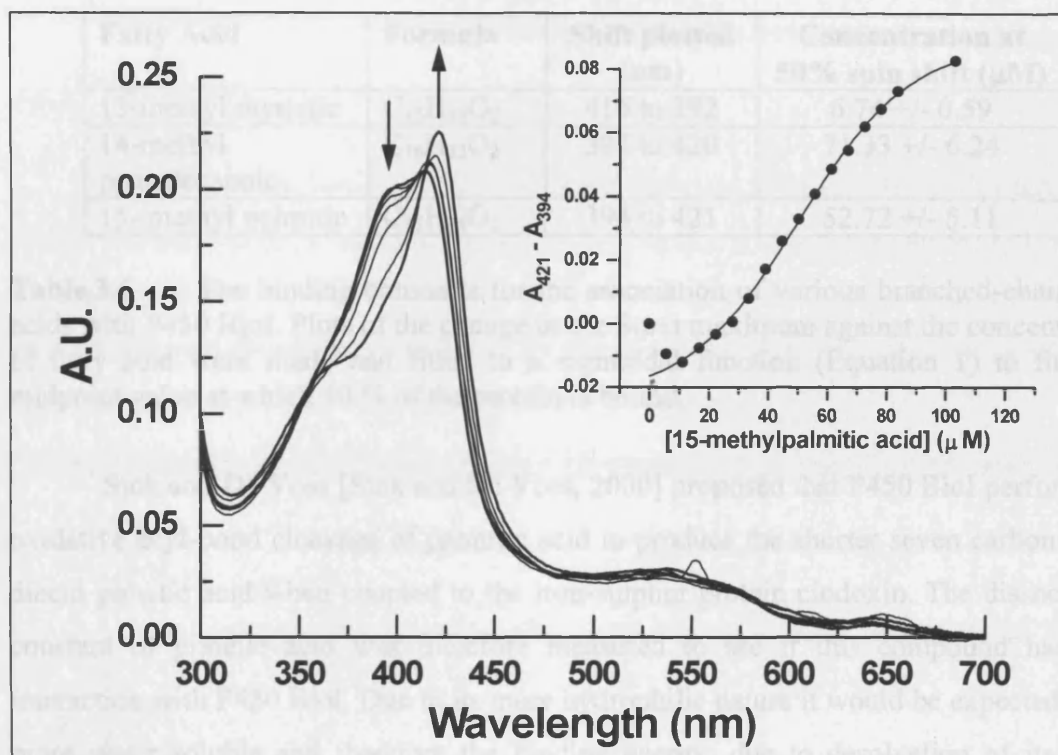


**Figure 3.10** Spectra recorded during the binding of 15-methyl palmitic acid to P450 BioI (2.3  $\mu\text{M}$ ). After the initial spin state shift from 418 nm to high-spin (11.21  $\mu\text{M}$  fatty acid) maximum at 395 nm, the heme then goes to a different low-spin form with the maximum at 421 nm. By fitting the spin state shift (A.U.) to a sigmoidal function (Equation 1) (inset) the 50 % change in spin state towards low-spin occurs at a concentration of 52.7  $\pm$  1.9  $\mu\text{M}$  fatty acid.

The sigmoidicity implies a cooperative process. The first molecule may bind in a substrate-like fashion whilst a second molecule binds in a different orientation that presumably causes structural reorientation of the first. The smaller fatty acid (13-methyl myristate) may cause less steric hindrance in the active site, allowing the water molecule to be displaced from its proximity to the heme surface in the typical rearrangement of

solvent molecules in the binding cavity upon substrate binding. However, even for this fatty acid plots of absorption change versus substrate concentration were sigmoidal suggesting dual binding sites. The values tabulated below show the concentration of fatty acid added to achieve a 50 % change in heme spin state. These were all calculated from sigmoidal fits including the initial change from the ‘unbound’ form of P450 BioI to the final low- or high-spin form.

Fatty Acid	Formula	Shift plotted (nm)	Concentration at 50% spin shift ( $\mu\text{M}$ )
13-methyl myristic	$\text{C}_{15}\text{H}_{30}\text{O}_2$	416 to 392	6.74 $\pm$ 0.59
14-methyl pentadecanoic	$\text{C}_{16}\text{H}_{32}\text{O}_2$	394 to 420	71.33 $\pm$ 6.24
15- methyl palmitic	$\text{C}_{17}\text{H}_{34}\text{O}_2$	394 to 421	52.72 $\pm$ 5.11

**Table 3.6** The binding constants for the association of various branched-chain fatty acids with P450 BioI. Plots of the change in the Soret maximum against the concentration of fatty acid were made and fitted to a sigmoidal function (Equation 1) to find the midpoint value at which 50 % of the protein is bound.

Stok and De Voss [Stok and De Voss, 2000] proposed that P450 BioI performs an oxidative acyl-bond cleavage of palmitic acid to produce the shorter seven carbon chain diacid pimelic acid when coupled to the iron-sulphur protein cindoxin. The dissociation constant of pimelic acid was therefore measured to see if this compound had any interaction with P450 BioI. Due to its more hydrophilic nature it would be expected to be more water soluble and therefore the binding energy, due to desolvation of its alkyl moiety, would be less than that of the mono-carboxylic fatty acids. As expected this fatty acid bound fairly weakly with a  $K_d$  value of 670  $\pm$  21  $\mu\text{M}$ , several fold less than that of mono-carboxylic fatty acids such as myristic ( $K_d$  of 3 - 5  $\mu\text{M}$ ), and showed only a partial conversion to high-spin upon saturation. A further probable function of P450 BioI is that of a typical fatty-acid hydroxylase. A binding titration was performed with the commercially available  $\beta$ -hydroxymyristic acid. P450 BioI was postulated to be a  $\omega$ -hydroxylase [Green, 2000] and  $\beta$ -hydroxymyristate would mimic the solubility and increased lipophobicity of a  $\omega$ -hydroxymyristic acid. This fatty acid was found to bind weakly to P450 BioI, but after the typical initial shift to high-spin (maximum moved to 394 nm with  $\beta$ -hydroxymyristic acid in the range of 0 to 50  $\mu\text{M}$ ) the heme was then

observed to undergo a shift back to low-spin (maximum at 422 nm) with a  $K_d$  for this reverse type I shift of  $174 \pm 5.4 \mu\text{M}$ . This inhibitory shift at high concentrations could indicate that this type of compound could act as an end product inhibitor of P450 BioI when its intracellular concentration is high enough. The much reduced binding affinity *c.f.* myristic acid ( $K_d < 5.0 \mu\text{M}$ ) means that it is unlikely that P450 BioI would carry out more than one hydroxylation reaction whilst there is still reasonable abundance of saturated fatty acids present, unless the mono-oxidation product remains bound.

### 3.6.2 The binding of steroids

P450 BioI is believed to be involved in pimelate synthesis due to its postulated role in the early steps of biotin biosynthesis. In random screening of compounds known to bind to microbial P450s (various fatty acids, steroids, and polyketides etc) an unpredicted interaction was observed. In the presence of certain steroids P450 BioI exhibits a Soret band shift to its low-spin form (418 nm).

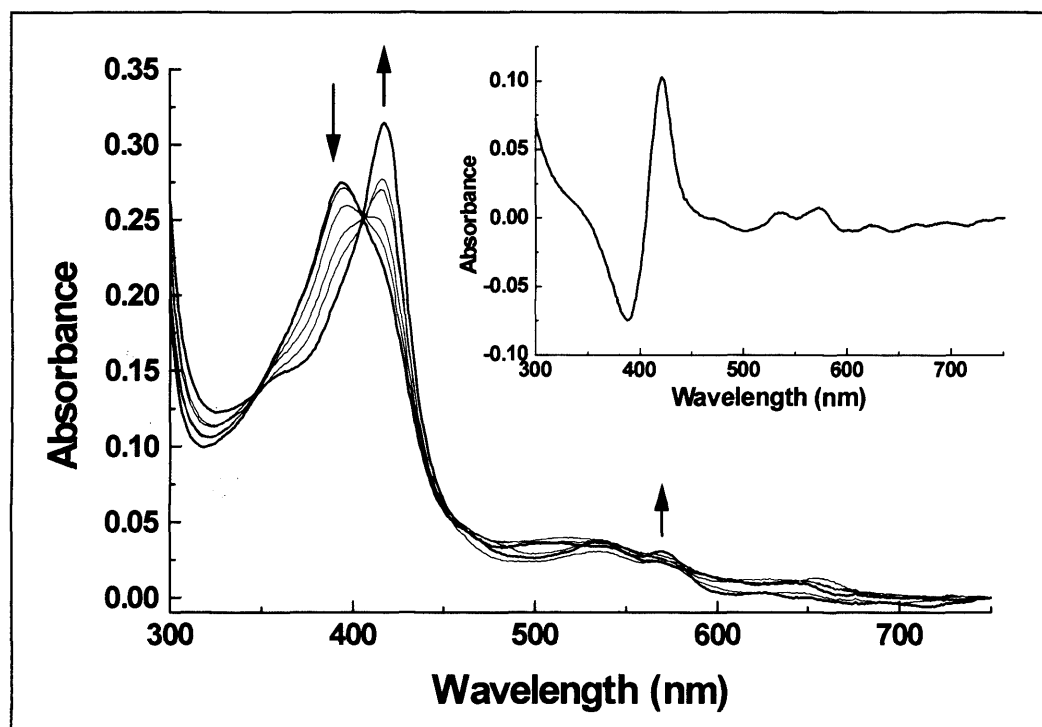


**Figure 3.11** A typical binding titration of a steroid (6 $\alpha$ -Methyl-17 $\alpha$ -Hydroxy-Progesterone) to P450 BioI. The predominantly high-spin sample of isolated P450 BioI ( $0.35 \mu\text{M}$ ,  $A_{\text{max}} = 390 \text{ nm}$ ) shifts to the low-spin form at longer wavelength ( $A_{\text{max}} = 419$

nm). The  $\alpha$  and  $\beta$  bands separate to form two clear signals. The inset shows the difference spectrum (formed by subtracting the unbound spectrum from the fully saturated spectrum) that shows clearly the formation of the low-spin peak and separation and increasing intensity of the heme's  $\alpha$  and  $\beta$  bands.

A variety of commercially available steroids were screened for their ability to bind to P450 BioI. The binding constants were determined for those that gave a spin state shift to low-spin (see Table 3.7).

Compound name	$K_d$ ( $\mu$ M) at 30°C	Error (+/-)	Shift (nm)
Androstenedione	133.1	5.4	393 - 419
CHAPS	DNB		
Cholesterol	DNB		
Estrone	DNB		
$\beta$ -estradiol	DNB		
Hydrocortisone	62.8	6.1	393 - 419
Progesterone	11.6	0.8	394 - 419
Testosterone	6.6	0.3	394 - 419
Corticosterone	156.6	13.9	393 - 419
Testosterone Enanthate	ND		394 - 419
Prednisolone	DNB		
6 $\alpha$ -Methyl-17 $\alpha$ -Hydroxy- Progesterone	139.2	20.6	394 - 419
5-Pregnen-3 $\beta$ -ol-20-one	DNB		

**Table 3.7** The binding constants derived from fitting the maximal absorption shift (calculated from the difference spectra of bound minus unbound) versus ligand concentration to a rectangular hyperbola (Equation 3). DNB = did not induce a spectral shift, ND = not determined.

A typical steroid backbone is shown in Figure 3.12. From the binding data gathered it was immediately apparent that steroids containing the conjugated carbonyl type A ring (1) appeared to bind tightly to P450 BioI, whilst no binding at all was observed with those containing the phenol A ring (2).

The binding of the type I steroids could be due to carbonyl ligation of the heme or due to the relative planarity of these steroids. Those containing the aromatic A ring contain a kink of almost 90 degrees. Substituents on the C ring reduced the affinity of the steroid to P450 BioI (possibly due to a steric clash) whilst substituents on the D ring (R) appeared to have a lesser effect. Steroid binding to P450 BioI was characterised by the heme shift to its low-spin form (Soret maximum approx. 418 nm). The low-spin heme

could arise from direct ligation of the carbonyl group of the steroid to the iron itself as indicated in the pH work (see Section 3.3). Whilst iron carbonyl complexes are usually ligated to the iron via the carbon atom (e.g.  $\text{Fe}(\text{CO})_6$  complexes), complexes in which the oxygen atom of the carbonyl group interacts directly with the iron are known, particularly in biological systems [for examples see Que, 1993, Sanders-Loehr, 1989]. In methane monooxygenase (MMO), a mixed function oxygenase that contains a dinuclear iron centre, the ferrous irons are co-ordinated by histidine residues and two carboxylate groups (through the oxygen atoms) [Lippard, 1993, Krebs and Strater, 1994].

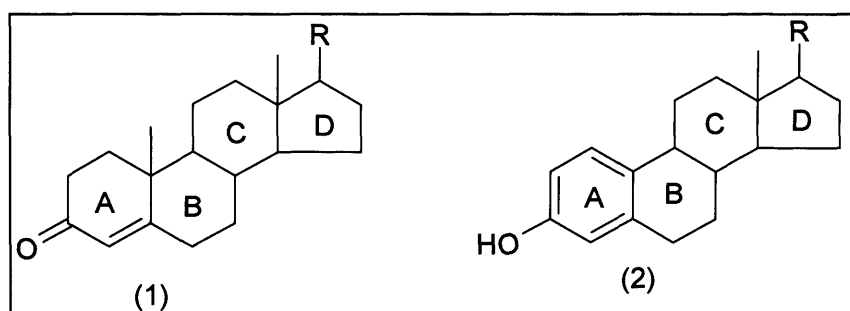


**Figure 3.12** Models of the steroids assayed for their ability to bind to P450 BioI. Functionality on the A-ring appears to be of most importance with the carbonyl containing steroids (1) binding to give clear P450 optical shifts, whilst those with the phenolic group (2) did not.

Recent modelling work docked the steroid testosterone into the active site of a homology model of P450 BioI (see Section 3.6). The steroids containing the carbonyl A ring appear to ligate directly to the iron with the carbonyl oxygen (2.8 – 4.1 Angstrom Fe to O distance). The modelling work also found that the steroids containing the phenol type A ring (see Figure 3.12) could be docked into the active site of P450 BioI despite the aromaticity of the A ring inducing an almost 90° bend in the molecule (the carbonyl-containing ones are near planar). However, these molecules are not predicted to co-ordinate to the iron via the hydroxy group, the distance from the iron to the steroid is increased due to the steric constraints predominantly due to the two phenylalanines (Phe83 and Phe384) that line the active site, not allowing the “bent” steroids near to the heme. Therefore, whilst no spectral shift is observed for these steroids, they may be binding in the active site. Modification of the substrate-binding channel may allow closer approach of “bent” compounds to the iron and as a result allow them to be oxidised.

As the modelling predicted that steroids containing the phenol A ring (2) could be docked in the active site of P450 BioI, but too far away from the heme to cause a spectral change, the titrations of both estrone and  $\beta$ -estradiol against the low-spin testosterone bound and high-spin palmitate bound protein were carried out. Testosterone was titrated in (1.5  $\mu$ l of a 12.5 mM stock in DMSO) or palmitic acid (1.0  $\mu$ l of a 15 mM stock in ethanol) to give fully saturated P450 BioI (10  $\mu$ l of a 1 mM stock) in Tris.HCl buffer (50 mM, pH 7.2, 0.985 ml). Aliquots of the hydroxy-steroid were then added (1.0  $\mu$ l additions of 25 mM stocks in DMSO). As in previous studies with the mixed-spin form of P450 BioI, no spin shift was seen to either the low- or the high-spin form by displacement of either the testosterone ligand (i.e. a decrease in the 418 nm Soret band and an increase in the 394 nm absorbance), or the palmitate (increase at 418 nm). Therefore these steroids are thought either to bind so weakly they are unable to displace the palmitate or testosterone, or not to bind to P450 BioI at all, contrary to the modelling predictions.

### **3.6.3 Binding of polycyclic compounds**

P450 eryF is known to be able to bind certain polycyclic compounds due to the nature of its binding site being formed to accommodate the large macrocycle erythromycin [Cupp-Vickery *et al.*, 1996]. As one of the P450s with high sequence homology to P450 BioI, together with the fact that P450 BioI can bind certain steroids, the capability of P450 BioI to bind polycyclic compounds was investigated. The two ‘un-functionalised’ polycyclics, fluorene and phenanthrene were examined in addition to the amine-containing 9-aminophenanthrene.

The binding of fluorine and phenanthrene to P450 BioI was observed via a reverse type I shift in the Soret peak (increase in the absorbance at 417 nm) as they displaced the endogenous palmitic acid bound in the active site. Whilst these compounds bind tightly enough to displace the substrate ( $K_d$  of 45.6  $\mu$ M and 0.24  $\mu$ M, respectively) they do not behave in a substrate-like manner, probably being bound too far away from the heme iron (sixth axial water ligand not displaced) to be oxidised. Indeed their binding might promote a greater rate of uncoupling. Fluorene bound in a co-operative manner,



possibly reflecting the accommodation of two molecules within the active site. 9-aminophenanthrene produced an inhibitory shift with the Soret band moving to a longer wavelength of 420 nm. A further shift to  $\sim 424$  nm might be expected if coordination to the heme iron occurs, but this compound bound relatively weakly ( $K_d$  of  $30.2 \mu\text{M}$ ) and its presence had a detrimental effect upon the enzyme, possibly due to its basic character, causing great turbidity at low concentrations ( $0.05 \text{ mM}$ ).

### 3.6.4 Imidazole Inhibitors

Many P450 inhibitors work by exploiting the strong ligation properties of nitrogen to iron [Bartoli *et al.*, 1998]. Most of the currently marketed anti-fungals that target P450s (such as sterol  $14\alpha$ -demethylase) include a nitrogen heterocycle such as a pyridine or imidazole ring [Tafi *et al.*, 1996 and Szklarz *et al.*, 1998]. The binding of these  $\text{sp}^2$  nitrogen-containing compounds produces a characteristic shift of the Soret band to around 423 nm, due to the strong electron withdrawing effects of the nitrogen [Ortiz de Montellano, 1995].

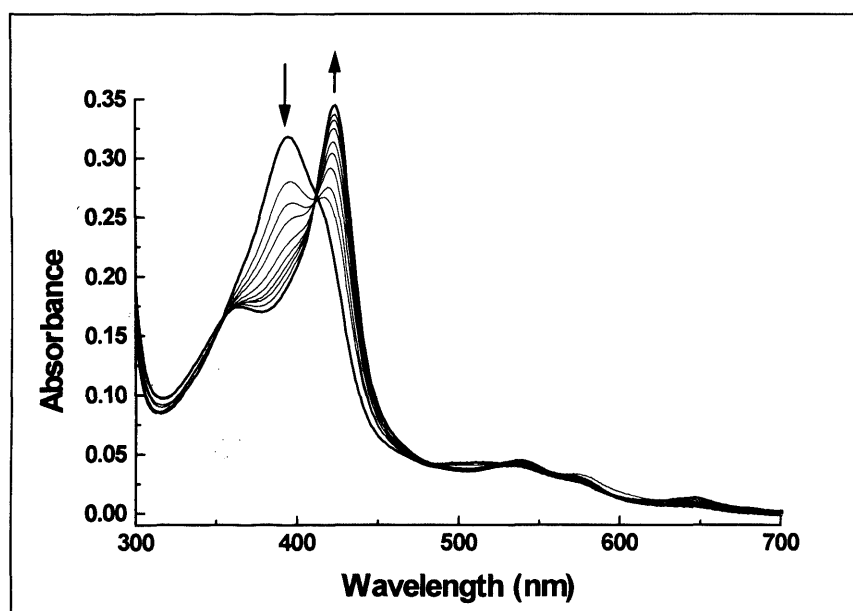


**Figure 3.13** The binding of 4-phenyl imidazole to P450 BioI ( $3 \mu\text{M}$ ) produces the characteristic shift from the predominantly high-spin form ( $A_{\text{max}} = 394 \text{ nm}$ ) to the nitrogen-ligated heme form at  $422 \text{ nm}$ . A lesser change is observed in the  $\alpha$  and  $\beta$  bands, compared to that seen in sterol binding.

The distinct shift seen means that the binding constants of many nitrogen-containing heterocyclic compounds can be determined by spectrophotometric titrations. The shift of the Soret absorption to the longer wavelength is due to the donation of the nitrogen lone pair to the iron. As nitrogen is a strong field ligand, it causes an increase in the splitting of the iron d orbitals (see Section 1.2), which therefore causes any electron transitions to be of greater energy. This results in low-spin iron (hence the shift to a longer wavelength), but as can be seen the relationship ( $E = hf$  where  $E$  = energy,  $h$  = Planck's constant and  $f$  = frequency) is masked by the re-distribution of electron density as the electrons are withdrawn from the porphyrin ring through the iron to the N-ligated atom. Despite nitrogen being a better electron acceptor than oxygen, there is only a 4 – 5 nm difference between the Soret band for N-ligated ( $\sim 423$  nm) and O-ligated (low spin,  $\sim 418$  nm) compounds. Oxygen is better at back-bonding to the iron than nitrogen (due to complementation of the energy levels of the relevant orbitals), which will affect the spectrum as the electron distribution differs.

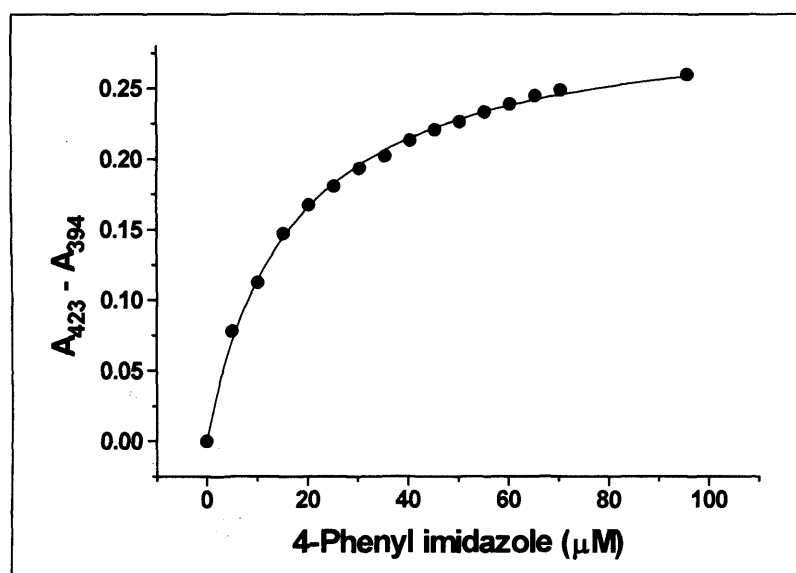


**Figure 3.14** Binding profile for 4-phenyl imidazole to P450 BioI. The absorption difference from the bound form ( $A_{\text{max}} = 423$  nm) to the unbound ( $A_{\text{max}} = 394$  nm) is plotted against the concentration of inhibitor added. Data are fitted to a rectangular hyperbola (Equation 3). Conditions as previously described. The  $K_d$  value was determined to be  $16.5 \pm 0.6$   $\mu\text{M}$ .

The affinity of imidazole, and its various derivatives, for P450 BioI were measured. The addition of a carboxylic acid side-chain increased the affinity of the

inhibitors to P450 BioI by a substantial margin. This implies the presence of a carboxylic acid binding site in the P450 (i.e. hydrogen donor residues positioned in the active site at a distance from the iron core). It is known that, in P450 BM3, R47 tethers the fatty acid carboxylate group [Li and Poulos, 1997].  $\omega$ -imidazolyl carboxylic acids have been shown to be potent inhibitors of P450 BM3 ( $K_{ic}$  = 0.9 to 7.5  $\mu$ M) [Noble *et al.*, 1998].

Compound name	Formula	$K_d$ ( $\mu$ M) at 30°C	Error (+/-)	Shift
Imidazole	C <sub>3</sub> H <sub>4</sub> N <sub>2</sub>	208.1	12.3	392 – 421
Im-C10	C <sub>13</sub> H <sub>23</sub> N <sub>2</sub> O <sub>2</sub>	2.6	0.2	389 – 421
Im-C11	C <sub>14</sub> H <sub>25</sub> N <sub>2</sub> O <sub>2</sub>	1.5	0.2	389 – 421
Im-C12	C <sub>15</sub> H <sub>27</sub> N <sub>2</sub> O <sub>2</sub>	1.0	0.1	389 – 421
4-phenylimidazole	C <sub>9</sub> H <sub>9</sub> N <sub>2</sub>	16.5	0.6	394 – 423
4-bromo-1H-imidazole	C <sub>3</sub> H <sub>4</sub> N <sub>2</sub> Br	348.2	20.1	392 – 421

**Table 3.8** Binding constants for a range of imidazole inhibitors to P450 BioI (3  $\mu$ M) as determined by titrations at 30°C, in Tris.HCl buffer (50 mM, pH 7.2). Im = imidazole, C10 etc = alkyl chain length of alkanoic acid group attached to the imidazole at the  $\omega$ -position. Shift indicates the movement of the Soret peak from unbound (392 nm) to bound (~ 422 nm). Apparent  $K_d$  values were obtained by plotting the absorbance difference (peak minus trough) data for bound minus unbound forms against the concentration of inhibitor at each point, and fitting data to a rectangular hyperbola (Equation 3) (Origin, Microcal).

The presence of the hydrophobic phenyl group also increased the affinity for the ligand. This, along with the knowledge that P450 BioI binds long alkyl chains including the electron rich unsaturated fatty acids, implies a region of hydrophobic residues with little functionality/hydrogen bonding activity in the active site at not too great a distance from the heme. In the recent model this has been shown to be the case, with two phenyl groups of phenylalanine residues lining the binding cavity (see Figure 3.17). The poor binding of 4-bromo-1H-imidazole is possibly due to the large bulky bromine atom causing steric clashes or (as bromine is electronegative) removal of some of the electron density from the  $sp^2$  nitrogen, thereby causing a weaker ligation to the iron.

Three commercial azole antifungals were also bound to P450 BioI. These are all relatively large molecules and therefore acted as good probes for evaluating the size and flexibility of the active site. Binding of these azole antifungals at pH 7.2 was characterised by a sigmoidal shaped curve at low concentrations. These were fitted with

the Hill function. The co-operative binding observed is most likely due to the antifungals competing with the endogenous fatty acid ligand. However, it may also be due to the binding of two molecules in the active site (implying a large binding cavity, see Section 1.6) or that P450 BioI is dimeric and the binding of one molecule to one monomer affects the binding of a second molecule to the other monomer.

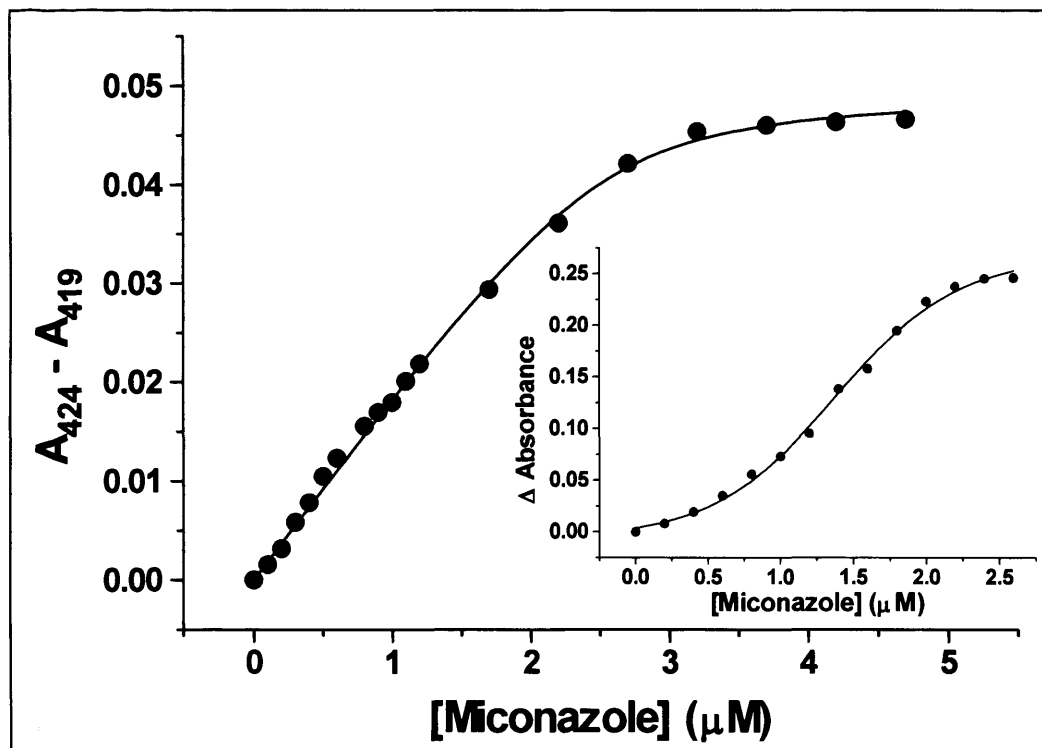


**Figure 3.15** Binding constant determination for miconazole to P450 BioI (3  $\mu$ M) in Tris.HCl buffer (50 mM, pH 9.5) at 30°C. This example of a commercial imidazole-based antifungal binds very tightly to P450 BioI with the apparent  $K_d = 0.10 \pm 0.03 \mu$ M (data fitted to Equation 2). The inset shows the same binding titration at pH 7.2. The Hill plot (Equation 1) implies that there may be a competitive interaction with the endogenous fatty acid occurring at this pH.

The tight binding is not surprising, as these molecules have been selected from huge libraries of compounds for their ability to inhibit P450s. The heme iron interaction is strong in these molecules, enhanced by their design with electron withdrawing groups adjacent to the nitrogen donating imidazole ring, and due to the presence of the bulky hydrophobic chlorinated phenol groups, which can bury themselves within the hydrophobic core.

Compound name	Formula	$K_d$ ( $\mu$ M) at 30°C	Error (+/-)
Econazole	$C_{18}H_{15}Cl_3N_2O$	0.37	0.01
Miconazole	$C_{18}H_{14}Cl_4N_2O$	2.01	0.35
Ketoconazole	$C_{26}H_{28}Cl_2N_4O_4$	2.31	0.35

**Table 3.9** Binding constants for commercially available azole antifungals to P450 BioI (3  $\mu$ M) in Tris.HCl buffer (50 mM, pH 7.2) at 30 °C. Data were determined from a binding titration where aliquots of the azole (0.5  $\mu$ l) in DMSO were added to a solution of P450 BioI. The change in the Soret maximum was plotted versus concentration of azole and fitted to a sigmoidal function (Equation 2) (Origin, Microcal).

Low-spin P450 BioI was obtained by suspending the protein in pH 9.5 Tris.HCl buffer (see Section 3.3). Due to the azole-containing compounds binding by ligating the heme iron via their nitrogen atom, their binding seems less affected by the pH *c.f.* fatty acids. Upon titration of these compounds, the main Soret peak of P450 BioI is observed to shift from 419 nm to 424 nm, and from this shift the  $K_d$  values were determined. It was found that, upon removal of the endogenous substrate to convert all the protein to its unbound form, the relationship between the concentration of azole added and the change in spin-state altered from a sigmoidal one to that of a hyperbolic.

Antifungal	$K_d$ ( $\mu$ M)	Error (+/-)
Econazole	0.02	0.001
Ketoconazole	0.03	0.01
Miconazole	0.10	0.03

**Table 3.10** The binding constants for the ligation of various imidazole-containing antifungals with P450 BioI. Plots of the change in the Soret maximum against the concentration of ligand were made and data fitted to Equation 2 to find the value at which 50 % of the protein is bound ( $K_d$ ).

The binding of azole antifungals is known to occur through both coordination to the iron atom via the lone pair of the  $sp^2$  hybridised nitrogen of the heterocyclic ring and the hydrophobic interactions with the active site [Tafi *et al.*, 1996]. The halogenated phenyl groups bind tightly into deep hydrophobic clefts, which would usually be occupied by the alkyl chains of substrate molecules. A  $\pi$  -  $\pi$  stacking interaction between the phenyl rings of the inhibitors and those of the aromatic residues is also thought to strengthen binding. Ketoconazole, being a very large molecule, is believed to exceed the

size of the active site when bound to CYP51 and interact with residues in the substrate access channel [Raag *et al.*, 1993, Ji *et al.*, 2000].

The binding of certain inhibitors is known to induce conformational changes in P450s. For example the binding of both enantiomers of the nitrogen co-ordinating 1-imidazolyl-2-hydroxy-2-(2,4-dichlorophenyl)-octane to P450 CAM was observed to displace the aromatic amino acid residues (Trp96 and Phe193) ‘opening’ up the solvent access channel that is normally ‘closed’ in the camphor-bound form [Raag *et al.*, 1993]. Modelling of P450 BioI indicates that, for the strong nitrogen ligation of the iron to occur, phenylalanine residues (Phe83 and Phe384) are displaced to allow accommodation of, and interaction with, the large di-chlorophenol groups (see Section 3.7).

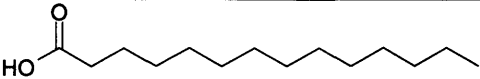
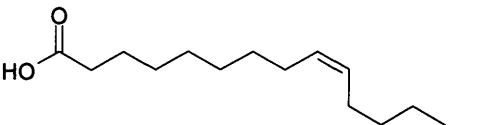
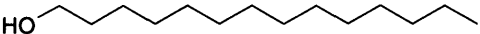
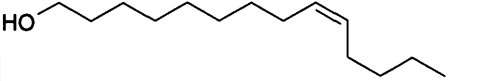
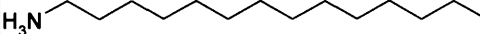
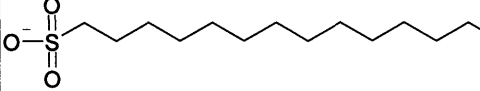
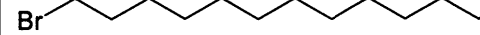
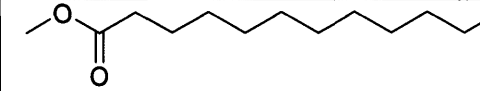
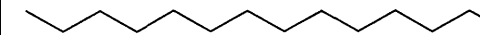
### **3.6.5 Effect of the $\alpha$ -carbon group upon binding**

Various derivatives/similar compounds to myristic acid were analysed for their ability to bind to P450 BioI. Given that, from modelling studies (Section 3.7), the carboxylate group is thought to hydrogen bond to a tyrosine and a serine residue, the effect of changing this carboxylate group to other proton acceptors was evaluated. As the optimal carbon chain length for binding to P450 BioI is 14 to 15 carbons, this was kept constant at 14.

With both the alcohols, a further shift back to the low-spin unbound form was seen. This is thought due to excess compound acting as a solvent increasing the organic component of the protein’s environment and, as a result, pushing the equilibrium back towards the unbound form. The  $K_d$  values are calculated from a rectangular hyperbolic fit for the initial shift to high-spin as the enzyme reaches saturation. All compounds containing an electro-negative group on their  $\alpha$ -carbon bound tightly to give a type I shift. The exception was tetradecylamine that, because of its primary amine group, gave an inhibitory type II shift as the nitrogen donates its lone pair to the heme iron.

Tetradecane gave a high-spin shift despite not containing an electronegative group on its alpha carbon. However, full saturation of the protein was not reached despite the difference spectra reaching a plateau, as a slight shoulder with absorbance around 412 nm could still be seen. The presence of this absorbance indicates that some axial water ligand



Compound name	Structure	Shift (nm)	K <sub>d</sub> (μM)	Error (+/-)
Myristic acid		394	2.62	0.12
Δ <sup>9</sup> -myristoleic acid		394	1.46	0.09
Tetradecanol		394	0.94	0.10
Δ <sup>9</sup> -tetradecanol		394	1.16	0.19
Tetradecyl amine		423	5.41	0.54
Tetradecyl sulphate		393	0.97	0.08
1-bromotetradecane		394	1.69	0.64
methylmyristate		394	3.00	0.21
tetradecane		394	0.023	0.003

**Table 3.11** The binding constants for the association of various 14-carbon chain-containing compounds with P450 BioI. Plots of the change in the Soret maximum against the concentration of the compound were made and data fitted to a quadratic function to determine the dissociation constant ( $K_d$ ). The direction of change in the Soret band is shown. Most compounds gave a typical type I shift (to 394 nm) although full conversion of the heme to high-spin was not seen at saturating concentrations of any of the ligands.

is still retained. This may be due to tetradecane binding further from the heme or being more mobile in the active site. As a result, oxidation of tetradecane by P450 BioI may cause a larger proportion of uncoupling to occur [Sligar *et al.*, 1991, Loida and Sligar, 1993]. Therefore the presence of an  $\alpha$ -carboxylate group would seem necessary for the correct positioning of a substrate within the active site. The tight binding of tetradecane

shows that the balance between compound solubility and complementation of the binding site cavity (maximum hydrophobic contacts) is as of as much importance as the presence of an electronegative  $\alpha$ -carbon group as regards dissociation constants.

### **3.7 Modelling of P450 BioI**

In the absence of a crystal structure of P450 BioI, a homology model was built to obtain structural information. By using the PSI-BLAST search tool [Altschul *et al.*, 1997] to screen the Protein Data Bank [Berman *et al.*, 2000] several proteins were identified as templates with which to generate comparative models (see 2.6). From these, fifteen models of P450 BioI were generated (using Malign 3D within Modeller [Sali and Blundell 1993]) that were then aligned against the amino acid sequence of P450 BioI using CLUSTALX [Thompson *et al.*, 1994] to select the most representative model [Kelley *et al.*, 1996]. Complexes were created by docking either myristate or testosterone into the active site using the programme GOLD [Jones *et al.*, 1997].

The model of P450 BioI predicts a hydrophobic binding site lined with residues that include Phe83, Leu84, Ala235 (methyl side-chain), Thr239 and Phe384. From the ligand docking studies, myristate is predicted to bind with its  $\omega$ -terminus closest to the heme and its carboxylate group hydrogen bonded to the hydroxyl-groups of Ser67 and Thr179. This positioning would seem to favour  $\omega$ -terminal oxidation as previously suggested [Green *et al* 2001] as opposed to the oxidative attack at the  $\omega$ -9 (palmitate) and  $\omega$ -7 (myristate) observed more recently [Cryle *et al.*, 2003]. The docking of testosterone predicts the steroid to bind with its C3 carbonyl close to, and possibly co-ordinating to, the heme and Glu65 acting as a hydrogen acceptor from the C17 hydroxyl.

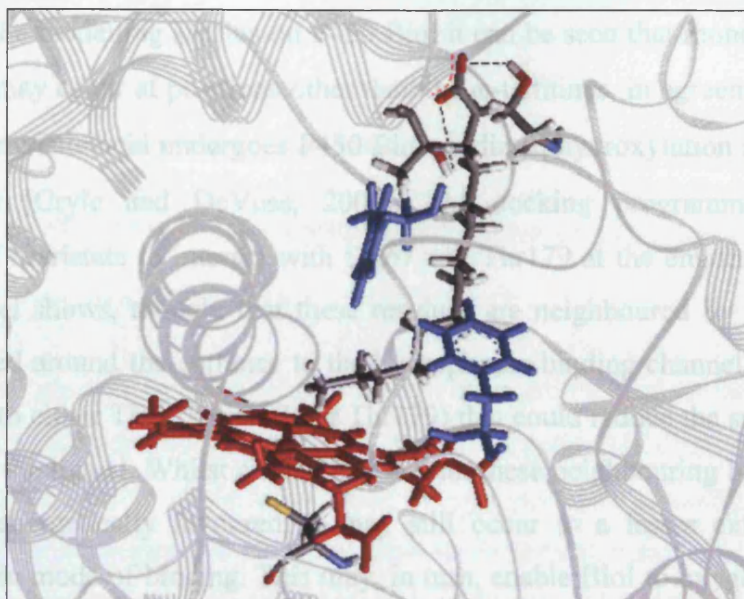


**Figure 3.16** A homology model showing myristic acid (CPK colouring) docked in the active site of P450 BioI. The carboxylate group of the fatty acid hydrogen bonds (black-line) to the hydroxyl of Ser67 and Thr179. Phe83 and Phe384 (purple) position the fatty acid causing a slight bending of the fatty acid. The terminal methyl group is positioned above the iron atom of the sulphur (yellow) ligated heme (red).

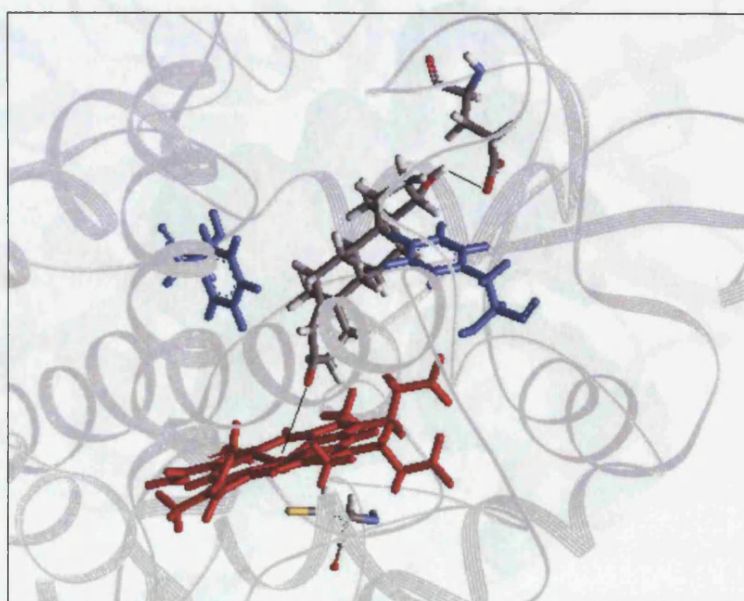


**Figure 3.17** P450 BioI homology model with testosterone (CPK) docked into the active site. The carbonyl group points towards the heme iron and the C17 hydroxyl hydrogen bonds to Glu65. Two phenylalanine residues (Phe83 and Phe384, blue) help position the steroid in the active site. Hydrogen bonds are shown in black, the protein chain in grey, the heme red, and its cysteinyl ligand also in CPK.



From the modelling studies on P450 BioI it can be seen that mono-hydroxylation of fatty acids may occur at positions other than the  $\omega$ -terminus, in agreement with recent findings that myristic acid undergoes P450 BioI-mediated hydroxylation at  $\omega$ -1,  $\omega$ -2 and  $\omega$ -3 positions [Cryle and DeVoss, 2004]. The docking programme predicts the carboxylate of myristate to interact with Ser67 and Thr179 at the entrance to the active site. The model shows, though, that these residues are neighboured by other hydrogen donors arranged around the entrance to the hydrophobic binding channel (Ser66 – Ser – Thr68, paired to either Thr172, Ser174 or Thr179) that could reduce the specificity of the positioning of the ligand. Whilst an interaction with these neighbouring hydrogen donors may be less energetically favoured, it may still occur to a lesser extent, producing heterogeneity in mode of binding. This may, in turn, enable BioI to oxygenate substrates at different positions. Heterogeneity predicted in binding mode may be consistent with previous data suggesting cooperative binding of lipid substrates.

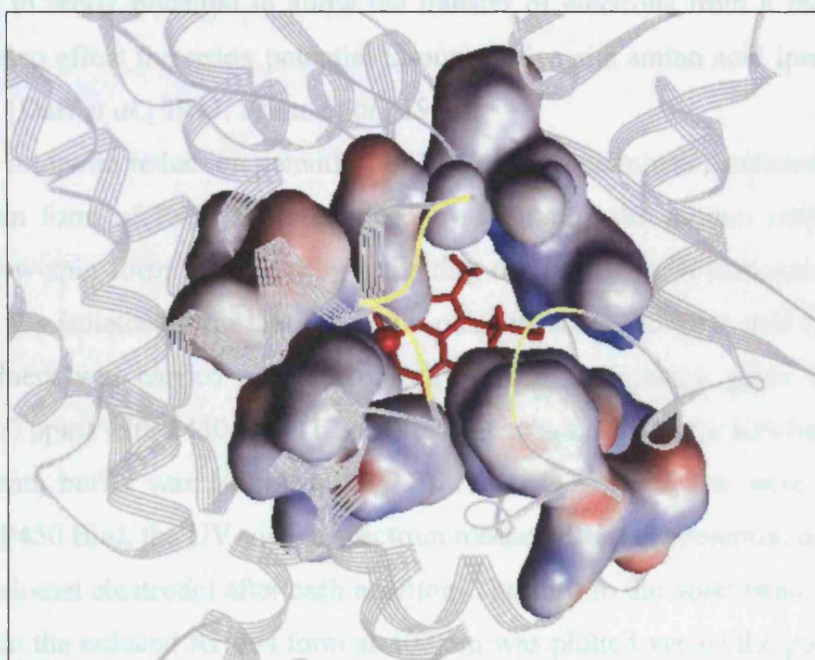


**Figure 3.18** A topological view of the entrance to the putative active site of P450 BioI. This region contains many potential proton donors to the fatty acid carboxylate group arranged along the loops shown in yellow. The heme is shown in red and the surfaces of the residues lining the active site coloured according to their electronegativity (blue = +ve, red = -ve). Model compiled as described in the text.

In this unrestrained model it was observed that, as in previous models, the side-chains of Cys250 and Cys275 are located in close proximity to each other (4.1 Angstrom apart) suggesting a disulphide bond may exist on the surface of the protein approximately 11 Angstrom away from the edge of the heme macrocycle (see Figure 3.22).

### **3.8 Redox Potentials of P450 BioI**

The one electron reduction of the ferric iron in P450 BioI was followed by anaerobic redox titration and the midpoint reduction potentials derived from plots of absorption change versus applied potential data. A solution of sodium dithionite is titrated in and the movement of the Soret band to its ferrous maximum at ~ 407 nm is observed, regardless of whether BioI is substrate-free or substrate-bound. It has been shown that the reduction potential of the heme is affected by its spin-state. This is usually due to the binding of ligands (i.e. the binding of substrate causes a shift to high-spin and an increase in redox potential to allow the transfer of electrons from a redox partner), which can also affect the redox potential through active site amino acid interactions and desolvation [Daff *et al.*, 1997, Primo *et al.*, 1990].

The midpoint reduction potentials of P450 BioI determined consisted of those for the high-spin form of P450 BioI (obtained by saturating the protein with palmitoleic acid), the low-spin form (achieved by saturating the protein with testosterone) and the mixed-spin (as isolated) form that we know contains some palmitic acid (Section 3.4). The experiment was carried out anaerobically (Belle Technology glove box, residual oxygen < 1.0 ppm) with P450 BioI (12  $\mu$ M) being exchanged into the KPi buffer (BioRad 10DG column, buffer was 100 mM, pH 7.0). Aliquots of dithionite were added to the solution of P450 BioI, the UV-visible spectrum measured and the potential of the solution recorded (calomel electrode) after each addition. The shift in the Soret band from 394 nm or 417 nm to the reduced ferrous form at 407 nm was plotted versus the potential of the solution and data fitted to a single electron Nernst equation to find the midpoint potential for the ferric/ferrous transition (Equation 11, Origin software, Microcal). A typical set of redox spectra is displayed in Figure 3.19 showing the movement of the Soret band from the palmitate-ligated form (maximum 393 nm) through to the reduced form (maximum

407 nm). Redox potentials for the ferric/ferrous couple were calculated by fitting a one electron Nernst Equation to the absorbance shift from the high- or low-spin starting form to the reduced (407 nm) form (an example is shown in Figure 3.20).

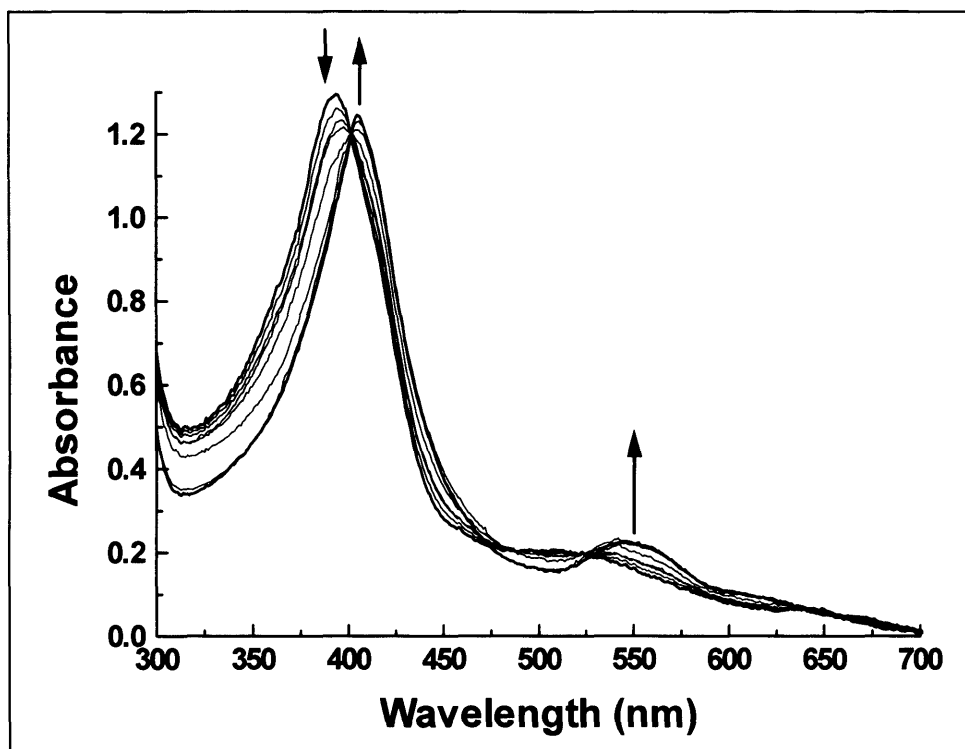


**Figure 3.19** Redox dependent changes, from oxidised palmitate-bound P450 BioI (13  $\mu$ M) (maximum at 393 nm) to the fully reduced protein (maximum at 407 nm). The spectrum for the reduced form of the enzyme is essentially the same regardless of the presence or absence of lipid or steroid. The  $\alpha$  and  $\beta$  bands are also observed to merge during reduction. The arrows show the direction of change in the absorbance from the oxidised to reduced form at key wavelengths. The experiment was carried out anaerobically in KPi buffer (100 mM, pH 7.0, 5 % v/v glycerol) with ligand (*ca* 30  $\mu$ M) added.

To measure the redox potential of low-spin P450 BioI with no compound present in the active site, a solution of mixed-spin P450 BioI (as isolated, some palmitic acid bound) was added to KPi buffer (100 mM, pH 7.0, 10 % v/v glycerol) that contained 15 % v/v ethanol. The ethanol causes the loss of the fatty acid ligand from the active site, probably by enhancing its solubility in the media and reducing the strength of any electrostatic bonds.



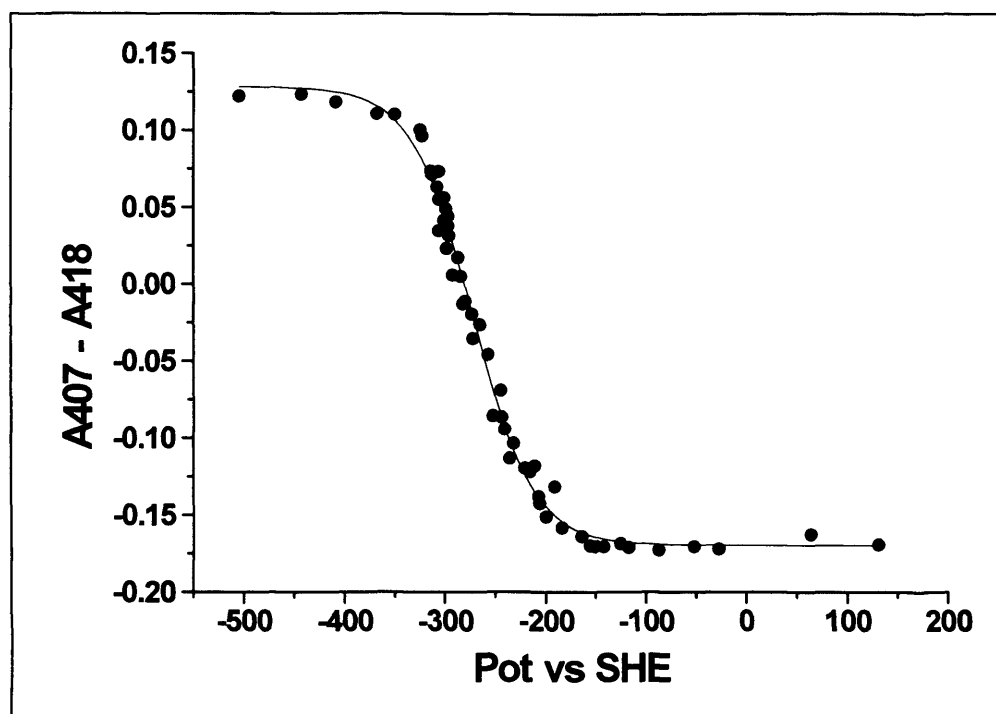


**Figure 3.20** Calculation of the midpoint potential (Potential versus standard hydrogen electrode [SHE]) of low-spin testosterone-bound P450 BioI (12  $\mu$ M) by plotting the shift in the Soret band from 418 nm (A418, oxidised form) to 407 nm (A407, reduced form) against the solution potential. Data were fitted to a single electron Nernst function (Equation 11) to give the midpoint as  $-273 \pm 3$  mV. The experiment was carried out anaerobically in KPi buffer (100 mM, pH 7.0, 5 % v/v glycerol) with testosterone (*ca* 30  $\mu$ M) added.

Tabulated below (Table 3.12) are the measured redox potentials of the various forms of P450 BioI (for the half reaction  $\text{Fe}^{3+} + \text{e}^- \rightarrow \text{Fe}^{2+}$ ) and their  $\Delta G^\theta$  values relative to the standard hydrogen electrode. As can be seen, the binding of a substrate molecule (palmitoleic acid) and resultant shift of the heme to high-spin causes an increase in the redox potential by *ca* 80mV from that of the low-spin steroid bound form (in KPi buffer).

Ligand	pH	Buffer	E (mV)	$\Delta G^\theta$ (kJmol <sup>-1</sup> )
None (partial palmitate)	7.0	KPi	-228	22.0
Palmitoleic acid	7.0	KPi	-199	19.2
Testosterone	7.0	KPi	-273	26.3
None (EtOH)	7.0	KPi	-330	31.8

**Table 3.12** Midpoint reduction potentials for P450 BioI either unbound or bound to saturating amounts of palmitoleic acid or the steroid testosterone. Buffer was 100mM KPi with 5 % v/v glycerol and the protein concentration was typically 12  $\mu$ M. Midpoints

are calculated from fitting a single electron Nernst equation to plots of the shift in the Soret maximum against the solution potential (normalised to the standard hydrogen electrode).  $\Delta G^\theta$  values are obtained from  $\Delta G^\theta = -nFE^\theta$  (where  $n$  = number of electrons,  $F$  = Faraday's constant (96500 coulombs per mole) and  $E^\theta$  is relative to a  $H^+/H_2$  half cell (-0.00 mV)). For worked example see below:

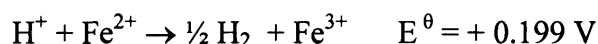
The difference between the values for the unbound low- and fatty acid-bound high-spin form of P450 BioI is similar to that expected (difference of *ca* 127 mV for P450 CAM [Sligar and Gunsalus, 1976]). The removal of a substrate-like molecule from the active site causes the redox potential to become more negative (-330 mV) compared to the low-spin form with testosterone bound measured under the same conditions (-273 mV). This is probably due in part to the desolvation of the binding site by the presence of the steroid. However, the effect of the steroid's carbonyl on the electronic arrangement of the heme will also contribute. The value for the fully high-spin form obtained by saturating P450 BioI with palmitoleic acid under the same conditions (-199 mV) shows how the change in the spin state of the heme causes an increase in the heme's potential by + 131 mV thus thermodynamically favouring its reduction.

For example, in the case of the palmitoleic acid-bound form of P450 BioI;

The two half reactions are;



Which are combined to give the following redox reaction:



The calculation of the standard oxidation potential ( $E^\theta$ ) allows the different forms of the P450 to be ranked from that of the EtOH-treated low spin form, which is the strongest reducing agent ( $E^\theta = 330 \text{ mV}$ ), to that of the weakest reducing agent, the palmitoleic acid-bound form ( $E^\theta = 199 \text{ mV}$ ). For comparison, the reduction of dioxygen to water under standard conditions has a standard oxidation potential of -1.23 V (i.e. the reduction by the palmitoleic bound form of P450 BioI is thermodynamically favourable).

From using  $\Delta G^\theta = -nFE^\theta$  the free energy for the reduction can be found;

$$\Delta G^\theta = -1 \times 96500 \times 0.199$$

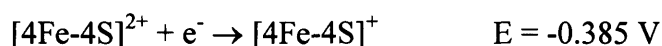
$$\Delta G^\theta = -19203.5 \text{ Jmol}^{-1}$$

$$\Delta G^\theta = -19.2 \text{ kJmol}^{-1}$$

The calculation of the  $\Delta G^\theta$  values allows comparison of the different redox forms of P450 BioI. It can be seen from the large negative  $\Delta G^\theta$  that it is easier to oxidise the low-spin form of P450 BioI ( $-31.8 \text{ kJmol}^{-1}$ ), and therefore the high-spin fatty acid bound form is easiest to reduce with the smallest positive free energy ( $\text{Fe}^{3+} + \text{e}^- \rightarrow \text{Fe}^{2+}$  transition gives  $\Delta G^\theta = +19.2 \text{ kJmol}^{-1}$  relative to the  $\text{H}_2$  electrode, i.e. thermodynamically disfavoured).

The difference between the redox partners potential (in this case *B. subtilis* Fer [Green *et al.*, 2003]) and P450 BioI indicates which form of P450 BioI is easiest to reduce in a catalytically relevant redox system.

The half reactions are:



they are combined to give the following redox reaction:



The positive potential implies that the reaction is feasible. The free energy of the reaction is then calculated:

$$\Delta G^\theta = -1 \times 96500 \times 0.186$$

$$\Delta G^\theta = -17949 \text{ Jmol}^{-1}$$

$$\Delta G^\theta = -17.9 \text{ kJmol}^{-1}$$

The negative value shows that reduction of P450 BioI by *B. subtilis* Fer is thermodynamically favoured. The  $\Delta G^\theta$  for the low-spin unbound form of P450 BioI ( $E = +0.055\text{V}$ ,  $\Delta G^\theta = -5.3 \text{ kJmol}^{-1}$ ) shows that whilst reduction is still possible, it is less favourable as there is less net energy gain. The effect of the heme's state on the ability of Fer to reduce P450 BioI can thus be summarised (Figure 3.21);

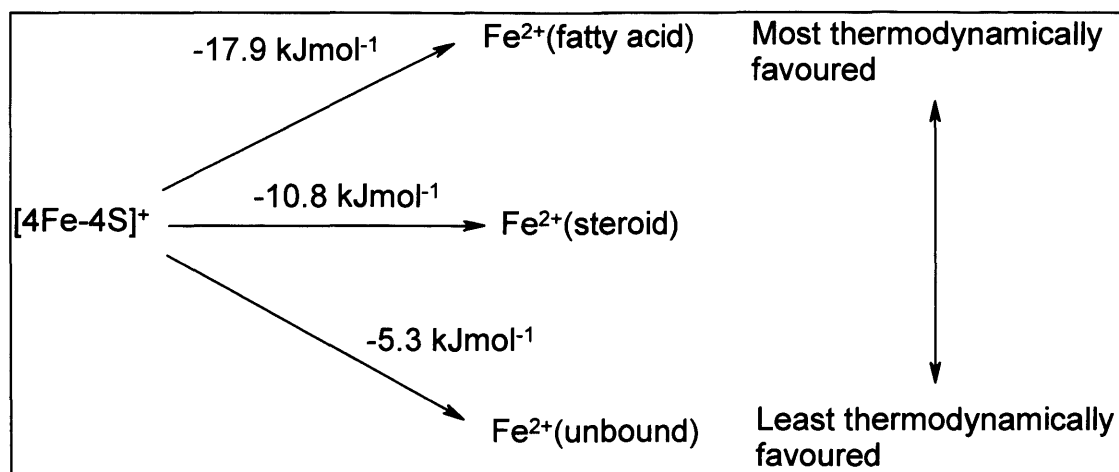
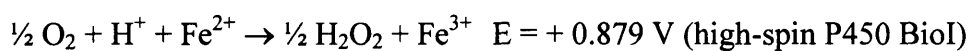


**Figure 3.21** A schematic showing the transfer of an electron from the Fer iron-sulphur cluster to the heme iron. The free energy values for the reduction of P450 BioI by *B. subtilis* Fer are shown next to the transition they refer to.

The midpoint potentials show that the low-spin unbound form of P450 BioI may be the strongest reducing agent and so more capable of reducing dioxygen, as the  $E$  for the reaction is more positive;



However, its own reduction by the redox partner is much less favourable and so the use of a redox partner with a midpoint potential much closer to that of the P450 prevents the reduction of dioxygen in the absence of substrate to produce radical species. For example, reduction of camphor bound P450 CAM ( $E = -0.173 \text{ V}$ ) by putidaredoxin ( $E = -0.196 \text{ V}$ ) is favoured ( $\Delta G^\theta = -2.2 \text{ kJmol}^{-1}$ ) compared to the unbound form ( $\Delta G^\theta = + 10.0 \text{ kJmol}^{-1}$ ), which is disfavoured [Lewis *et al.*, 2000]. The values for P450 CAM being directly reduced by NADH ( $E = -0.317 \text{ V}$ ) are  $\Delta G^\theta = -1.6 \text{ kJmol}^{-1}$  for the unbound form and  $\Delta G^\theta = -13.9 \text{ kJmol}^{-1}$  for the camphor-bound protein, i.e. if P450 CAM received its electrons directly from NADH, reduction would be more thermodynamically favourable and direct reduction of the substrate-free form might lead to a reduction of molecular oxygen. Therefore whilst the smaller difference in the redox potentials of the P450 and the ferredoxin may seem to favour electron transfer to a lesser extent *c.f.* direct reduction by NADH, they act as a control mechanism fine-tuning the reactivity of the

monooxygenase and gating electron transfer. Specifically, the potential of the ferredoxin is poised to favour reduction of substrate-bound P450.

### 3.9 Kinetic Studies

The rate of formation of the one electron reduced form of P450 BioI can be followed by trapping the  $\text{Fe}^{2+}$  ion with carbon monoxide, which forms a virtually irreversible complex (i.e. the  $K_d$  for the complex is low and the rate constant for CO association is considerably faster than for its dissociation). This CO-bound form gives a Soret maximum at 448 nm, as can be seen in Figure 3.22.

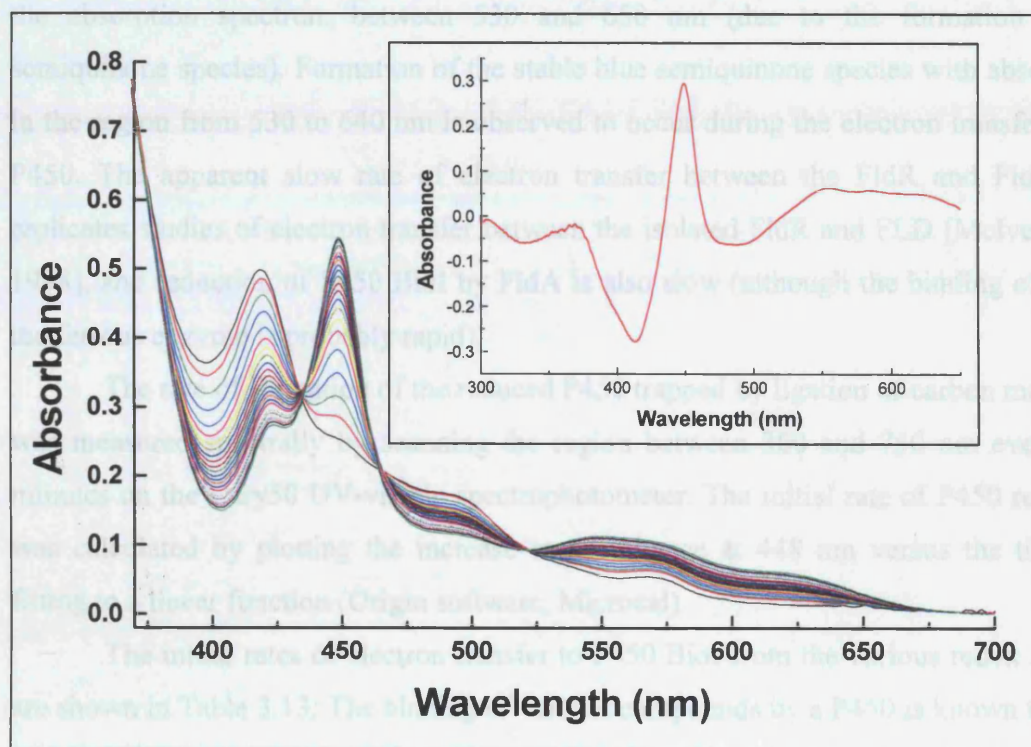


**Figure 3.22** Conversion of testosterone-bound P450 BioI (5.8  $\mu\text{M}$ ) (Soret maximum at 417 nm) to its one electron reduced CO-bound form (Soret maximum at 448 nm). These spectra were recorded with the *E. coli* FldR/FldA system being used to shuttle electrons from NADPH (20  $\mu\text{M}$ ) to P450 BioI. Spectra were recorded at 1 minute intervals for 30 minutes. The inset shows the difference spectrum obtained by subtracting the initial spectrum from that of the fully CO-complexed form.

The enzyme was added to an anaerobic (argon-sparged) carbon monoxide saturated buffer (KPi, 50 mM, pH 7.0) and a variety of exogenous redox partners were

used to shuttle electrons to the P450 from NADPH. The redox systems from *E. coli* (FldA and FldR), and either the spinach ferredoxin (Fdx), or the *M. tuberculosis* ferredoxin (coupled with *E. coli* FldR) were all assessed for their ability to reduce P450 BioI. The ferredoxin from *M. tuberculosis* is a  $\text{Fe}_3\text{S}_4$  cluster-containing ferredoxin that has been used to support the catalytic activity of isolated *M. tuberculosis* P450 14DM [Bellamine *et al.*, 1999]. P450 BioI was also bound to either a steroid (low-spin form) or a fatty acid (high-spin form) to assess the effect of ligation (and as a result redox potential) upon reduction rate.

As well as the increase in the absorbance at 448 nm, the reduction of the FMN and FAD cofactors of the flavin containing redox system can be observed by changes in the absorption spectrum between 530 and 650 nm (due to the formation of the semiquinone species). Formation of the stable blue semiquinone species with absorbance in the region from 530 to 640 nm is observed to occur during the electron transfer to the P450. The apparent slow rate of electron transfer between the FldR and FldA here replicates studies of electron transfer between the isolated FldR and FLD [McIver *et al.*, 1998], and reduction of P450 BioI by FldA is also slow (although the binding of CO to the ferrous enzyme is probably rapid).

The rate of formation of the reduced P450 trapped by ligation of carbon monoxide was measured spectrally by scanning the region between 300 and 750 nm every 0.15 minutes on the Cary50 UV-visible spectrophotometer. The initial rate of P450 reduction was calculated by plotting the increase in absorbance at 448 nm versus the time and fitting to a linear function (Origin software, Microcal).

The initial rates of electron transfer to P450 BioI from the various redox systems are shown in Table 3.13. The binding of various compounds by a P450 is known to affect the rate of reduction due mainly to thermodynamic reasons [Jung *et al.*, 2002]. It can be seen that the binding of a fatty acid caused an increase in the rate of electron transfer to P450 BioI, whilst the binding of the steroid (causing a shift to low-spin and a more negative potential) slows down the rate of electron transfer. As a result of this slowing of electron transfer by steroid binding, it can be seen that the redox potential of the heme (Section 3.8) is likely to have a greater effect upon reduction rate than any desolvation (of the active site) energetics. The rate of reduction of the heme by the spinach ferredoxin



was much faster *c.f.* the flavodoxin system. The faster rate could be due to either more complementary redox values or better binding *c.f.* the *E. coli* flavodoxin.

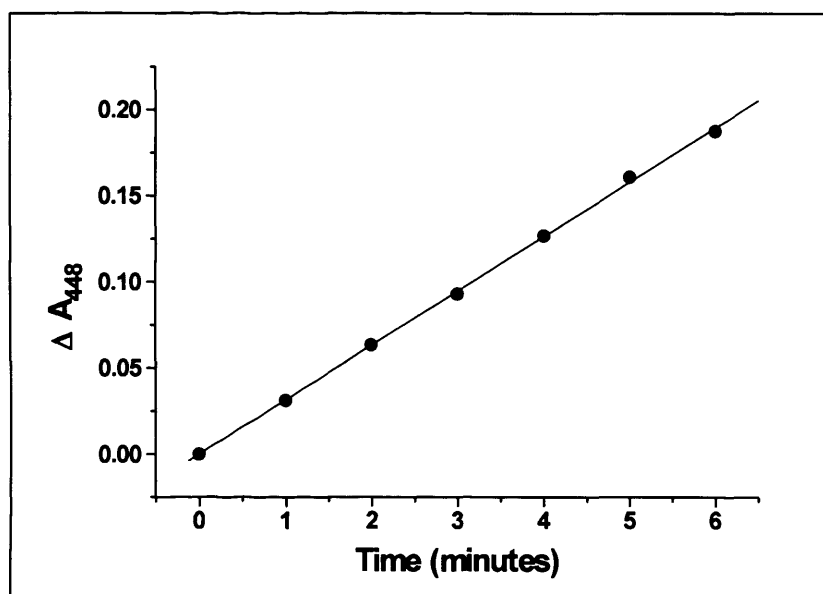


**Figure 3.23** Initial rate of the formation of the CO bound form of steroid-bound P450 BioI (5.8  $\mu\text{M}$ ) in Tris.HCl buffer (50 mM, pH 7.2) with FLD (12.1  $\mu\text{M}$ ), FLDR (50  $\mu\text{M}$ ) and excess NADPH. Data were plotted and fitted to a linear function, the second order rate constant determined under these conditions was 0.06  $\mu\text{M min}^{-1}$ .

Redox System	Ligand	Initial Rate ( $\mu\text{M min}^{-1}$ )
<i>E. coli</i> FLD/FLDR	Unbound	0.111
	Myristic acid	0.177
	Testosterone	0.060
Spinach Fdx	Unbound	0.155
	Testosterone	0.092
	Myristic acid	0.194
Mtb Fdx	Unbound	0.028
	Myristic acid	0.038

**Table 3.13** The rate of electron transfer from NADPH to P450 BioI via various redox partners when P450 BioI (5.8  $\mu\text{M}$ ) was either unbound or bound to myristic acid or testosterone, conditions as described previously. Plots of the formation of the carbon-monoxo bound heme (maximum at 448 nm) against time (seconds) were made and fitted to a linear function to find the initial rate of P450 ( $\mu\text{M}$ ) reduced per minute ( $\text{min}^{-1}$ ).

The conversion of the heme to high-spin upon fatty acid binding accelerates the electron transfer compared to that of the low-spin steroid-bound form regardless of the

redox partner involved. The rates of the reduction of the fatty acid-bound form of P450 BioI were sufficiently fast to require analysis using stopped-flow techniques. The P450 (4  $\mu\text{M}$ ) was bound to palmitoleic acid (16  $\mu\text{M}$ ) to give the high-spin complex in anaerobic CO-saturated buffer (KPi, 50 mM, pH 7.0). The rates of the single electron reduction were calculated from the spectral changes (300 nm – 700 nm, measured using a photodiode array device (Applied Photophysics)) that resulted upon the rapid mixing of pre-reduced (dithionite) spinach ferredoxin or *E. coli* flavodoxin (various concentrations) with P450 BioI in a stopped-flow apparatus. The reduction of the P450 was obvious due to the formation of the 448 nm  $\text{Fe}^{2+}$ -CO adduct, the oxidation of the redox partner could also be observed spectrally to a smaller extent. The rates from the global analysis (Applied Photophysics ProKin software) of the data were as follows:

Redox partner	$k_{\text{red}}$ ( $\text{s}^{-1}$ )	Error (+/-)	$K_d$ ( $\mu\text{M}$ )	Error (+/-)
Spinach Fdx	1.04	0.03	2.18	0.29
<i>E. coli</i> FldA	0.19	0.01	2.10	0.25

**Table 3.14** The rate of electron transfer from NADPH to P450 BioI via various redox partners when P450 BioI (5.8  $\mu\text{M}$ ) was bound to myristic acid. Measured using stopped-flow equipment under anaerobic conditions. Plots of the formation of the carbon-monooxy bound heme (maximum at 448 nm) against time (seconds) were fitted to a quadratic equation (Equation 4) to find the limiting reduction rate ( $k_{\text{red}}$ ) ( $\text{s}^{-1}$ ).

The rate of reduction of P450 BioI is approximately 10-fold faster with the spinach ferredoxin as its redox partner, although both flavodoxin and ferredoxin have similar  $K_d$  values. The rates of single electron reduction of P450 BioI when bound to either steroid or fatty acid have been measured with the *B. subtilis* electron donors (two flavodoxins, YkuN and YkuP and the [4Fe-4S] ferredoxin, Fer) and are reported in Section 4.18.

### 3.10 Circular Dichroism (CD) of P450 BioI

Far UV and near UV-visible CD spectra of P450 BioI were recorded with the protein in its partially bound (as isolated from *E. coli*) form. The far UV CD spectrum is dominated by a negative sign, of a shape indicative of an  $\alpha$ -helical protein, as would be

expected from the known structures of other P450s [Cupp-Vickery and Poulos, 1995, Poulos *et al.*, 1986, Ravichandran *et al.*, 1993]. The spectrum shows two minima, one at 221 and the other at 207 nm with the trace dissecting the x axis at 202 nm.

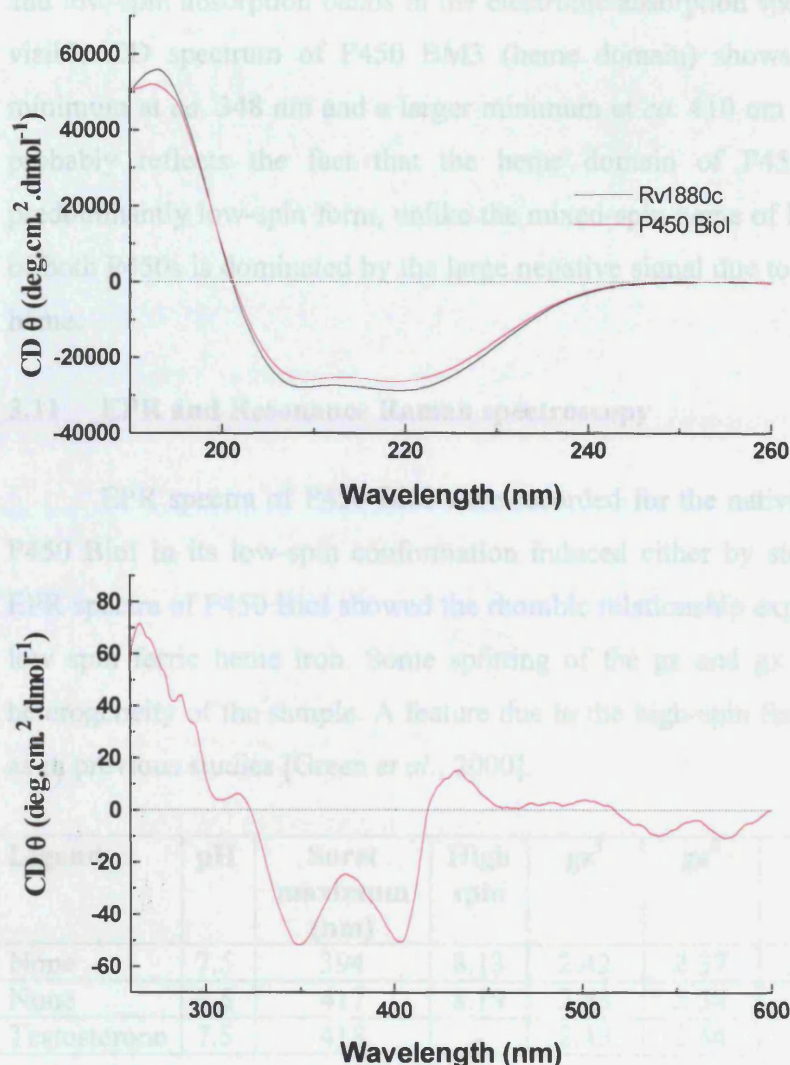


**Figure 3.24** The CD spectra of P450 BioI in the far UV (top) and near UV-visible (bottom) region. The top spectrum shows comparison with another P450 (CYP140 from *M. tuberculosis* encoded by the Rv1880c gene), both have the characteristic predominantly  $\alpha$ -helical trace of a P450. The spectrum shows two minima at 221 and 207 nm respectively, the trace crosses the x axis at 202 nm. The bottom spectrum shows the presence of mixed-spin heme, from the split Soret band features (with negative CD) with the minima at 348 and 404 nm close to the respective high- and low-spin absorption bands in the electronic absorption spectrum.

The near UV-visible CD spectra shows the mixed-spin state of the heme in isolated P450 BioI and reports on the environment of aromatic amino acids and cysteines in the 260 – 320 nm region. The spectrum shows the presence of mixed-spin heme, the heme signal being split with two minima at 348 and 404 nm close to the respective high- and low-spin absorption bands in the electronic absorption spectrum. In comparison, the visible CD spectrum of P450 BM3 (heme domain) shows a proportionally smaller minimum at *ca.* 348 nm and a larger minimum at *ca.* 410 nm [Munro *et al.*, 1996]. This probably reflects the fact that the heme domain of P450 BM3 is isolated in a predominantly low-spin form, unlike the mixed-spin heme of P450 BioI. The visible CD of both P450s is dominated by the large negative signal due to the asymmetrically bound heme.

### 3.11 EPR and Resonance Raman spectroscopy

EPR spectra of P450 BioI were recorded for the native unbound protein and for P450 BioI in its low-spin conformation induced either by steroid binding or high pH. EPR spectra of P450 BioI showed the rhombic relationship expected for a six co-ordinate low spin ferric heme iron. Some splitting of the  $g_z$  and  $g_x$  peaks is observed due to heterogeneity of the sample. A feature due to the high-spin ferric heme iron is also seen, as in previous studies [Green *et al.*, 2000].

Ligand	pH	Soret maximum (nm)	High spin	$g_z^1$	$g_z^2$	$g_y$	$g_x^1$	$g_x^2$
None	7.5	394	8.13	2.42	2.37	2.24	1.98	1.92
None	9.5	417	8.19	2.43	2.38	2.25	1.98	1.92
Testosterone	7.5	418	-	2.43	2.54	2.24	1.89	1.92

**Table 3.15** The g-values of the heme in the EPR spectra of unbound P450 BioI and low-spin P450 BioI, induced by either pH or ligand binding. Conditions as in Figure 3.24 legend.

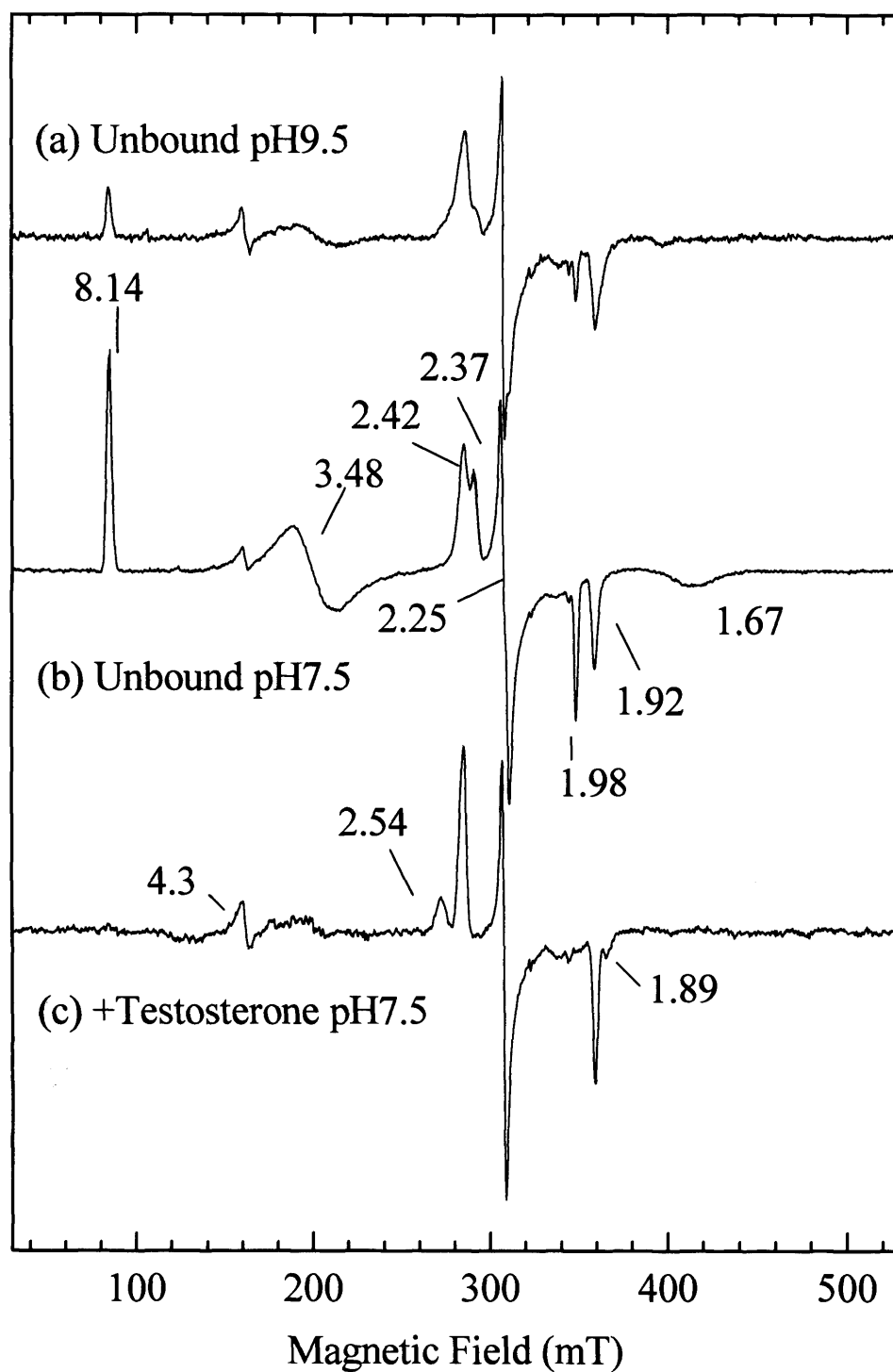


**Figure 3.25** EPR spectra of P450 BioI (1mM) that demonstrates the g-value features of the low-spin form at pH 9.5 (panel A), the mixed-spin unbound form at pH 7.5 (panel B), and the low-spin steroid bound form (panel C). Spectra collected at 10K, 2mW, 9.66GHz, protein was in Tris.HCl buffer (50 mM).

For comparison with the g-values for P450 BioI (see Table 3.15), the EPR spectra for substrate-free P450 BM3 heme domain has g values of  $g_z = 2.42$ ,  $g_y = 2.26$ ,  $g_x = 1.92$  with no high-spin iron observed [Miles *et al.*, 1992]. The environment of the heme axial ligands and their orientation is known to affect the g-values of the heme iron. Therefore, the heme ligation in P450 BioI is likely to be subtly different to P450 BM3 as, while the g-values are similar, the splitting of the  $g_x$  and  $g_z$  peaks is not usually observed. This shows a second minor conformation is present (possibly due to a small proportion being bound to palmitate – Section 3.5). This could be related to the differences in the association of the water ligand or protonation and weakening of the cysteine ligand.

The EPR spectra for the low-spin forms of P450 BioI differ slightly depending upon whether the spin state shift is induced through the binding of a ligand (testosterone) or the protein's ionisation (pH 9.5). The splitting of the  $g_x$  and  $g_z$  is always present, but the ratio between the two resulting peaks and their exact position changes. It is therefore possible that the exact position of these peaks is as a result of the binding site conformation affecting the orientation of the heme, or that some hydrogen bonding interactions in the active site near the heme affect the iron's electron distribution through the delocalised porphyrin ring. P450 CAM, when oxygen ligated through binding to cyclohexanone, gave g values of  $g_z = 2.46$ ,  $g_y = 2.27$ ,  $g_x = 1.91$ , which were not greatly different to the values for that of the unbound water-ligated resting state species ( $g_z = 2.45$ ,  $g_y = 2.26$ ,  $g_x = 1.91$ ) [Dawson *et al.*, 1982]. The larger shifts in g-values with the steroid-bound P450 BioI could be due to purely the bulk of the steroid causing greater desolvation and conformational distortion of the binding channel.

Resonance Raman spectra of native P450 BioI and both its high spin and low spin bound forms were recorded and are shown below in Figure 3.26. The cysteine ligated ferric high-spin iron gives rise to the dominant signal at  $1371\text{ cm}^{-1}$  ( $\nu_4$ ) [Macdonald *et al.*, 1996]. The  $\nu_2$  and  $\nu_3$  bands gives an indication of the spin state of the heme ( $1585\text{ cm}^{-1}$  and  $1501\text{ cm}^{-1}$  for low-spin) and the signal intensity at  $1635\text{ cm}^{-1}$  ( $\nu_{10}$ ) shows the iron is in a six co-ordinate state (present in the low-spin spectra) [Green *et al.*, 2001]. The iron to sulphur bond produces a band at  $350\text{ cm}^{-1}$  and the iron-oxygen stretching interaction gives other low frequency bands ( $400 - 500\text{ cm}^{-1}$ ). Bands at *ca*  $678\text{ cm}^{-1}$  and  $756\text{ cm}^{-1}$  ( $\nu_7$  and  $\nu_{15}$ ) are thought to result from the Jahn-Teller active vibration seen for



metalloporphyrins [Bovill *et al.*, 1992]. For comparison, the resonance Raman spectra of substrate-free P450 BM3 (heme domain) showed predominantly low-spin ferric iron ( $\nu_4$  at  $1371\text{ cm}^{-1}$ ) and the spin-state sensitive bands ( $\nu_2$  and  $\nu_3$ ) at  $1585$  and  $1500\text{ cm}^{-1}$ , respectively [Miles *et al.*, 1992]. A similar spectrum is also seen for low-spin P450 CAM [Champion *et al.*, 1978].

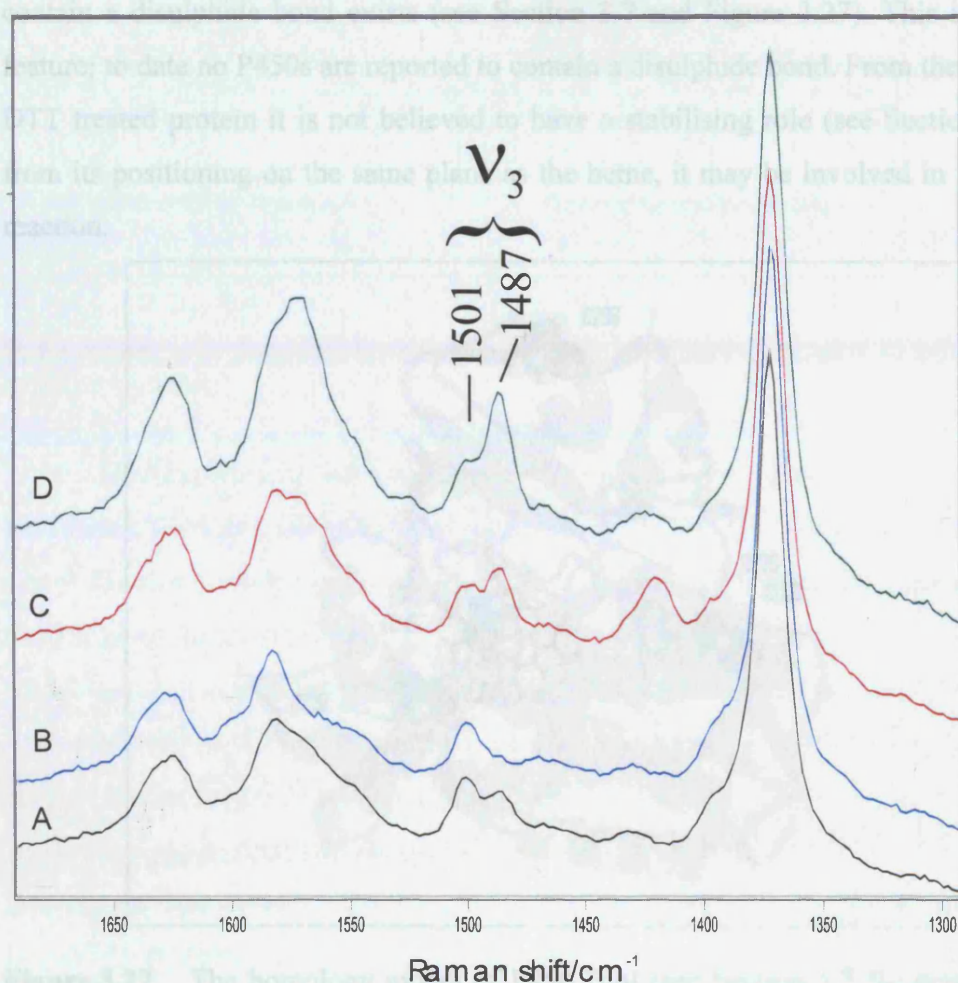


**Figure 3.26** Resonance Raman spectra of P450 BioI in its unbound and bound forms.  $\nu_3$  is a key heme iron spin-state marker band. The distinct peak due to the sulphur-ligated ferric iron stretch can be seen at *ca*  $1350\text{ cm}^{-1}$ . The peak at  $1425\text{ cm}^{-1}$  is believed to be due to varying amounts of DMSO from the ligand stock solutions. Shown are P450 BioI as isolated from *E. coli* (A), testosterone-bound (B), palmitoleic acid-bound (C), and myristoleic acid-bound (D).

When myristoleic or palmitoleic acid was added to the samples of P450 BioI, a broader band at  $1487\text{ cm}^{-1}$  ( $\nu_3$ ) was seen, typical of the high-spin form of P450 BioI. This

lower frequency is indicative of a five co-ordinate heme, as is the intensity seen at  $1625\text{ cm}^{-1}$  ( $\nu_{10}$ ), a pattern similar to that of palmitate-bound P450 BM3 [Miles *et al.*, 1992].

### 3.12 Verification of the presence of a disulphide bond

From the early homology model of P450 BioI, the possibility that the protein may contain a disulphide bond exists (see Section 3.7 and Figure 3.27). This is an unusual feature; to date no P450s are reported to contain a disulphide bond. From the DSC data of DTT treated protein it is not believed to have a stabilising role (see Section 3.14), but, from its positioning on the same plane as the heme, it may be involved in the oxidative reaction.

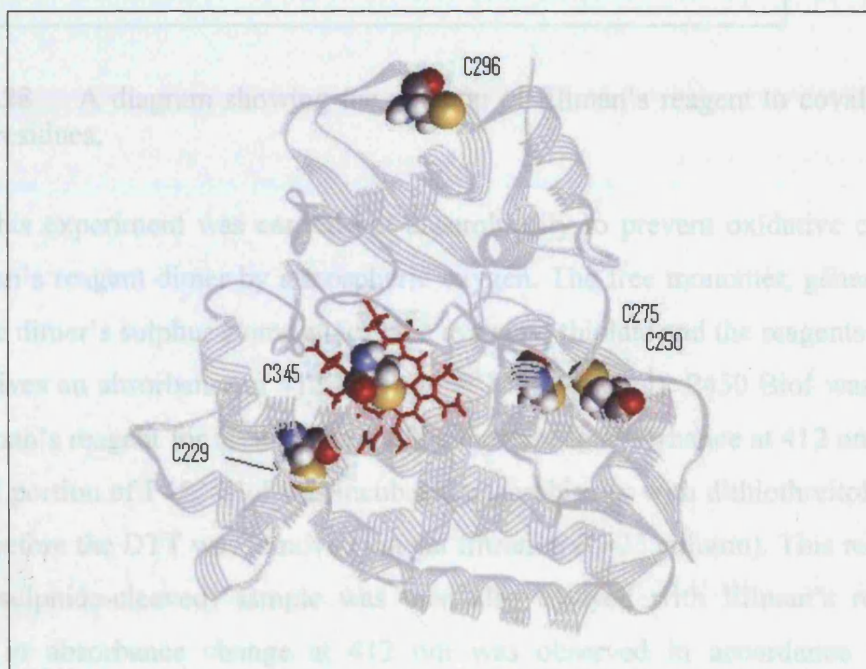


**Figure 3.27** The homology model of P450 BioI (see Section 3.7 for details) showing all five of the protein's cysteine residues (CPK) and the heme (red). Cys250 and Cys275 are believed to form the disulphide, and Cys375 to ligate the heme. Cys229 is buried and Cys296 appears, partially, on the surface.

To look for evidence of the disulphide's existence, P450 BioI was reacted with Ellman's reagent (5,5'-dithiobis(2-nitrobenzoic acid), also known as DNTB), which forms a covalent thio-ester bond to a cysteine residue and concurrently releases one molecule of yellow dye (MTNB, see Figure 3.28).



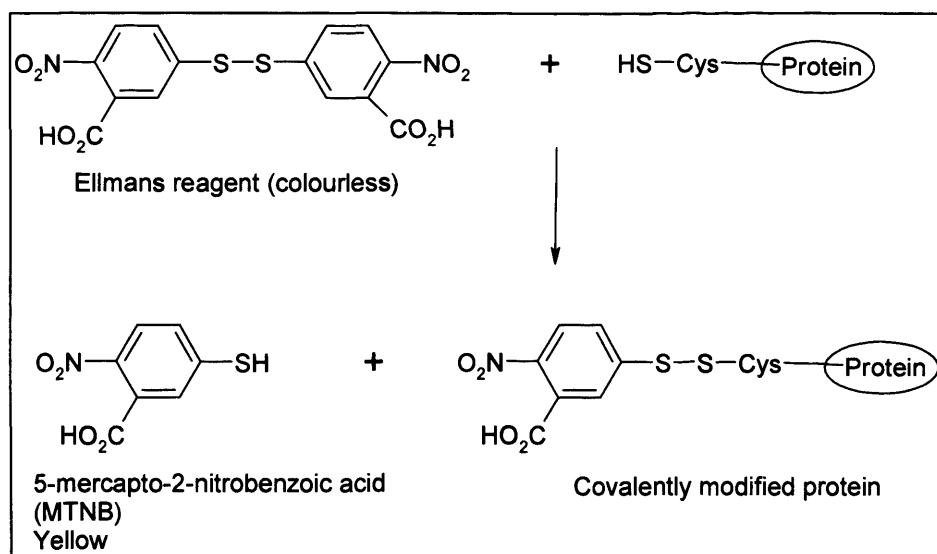


**Figure 3.28** A diagram showing the reaction of Ellman's reagent to covalently label cysteine residues.

This experiment was carried out anaerobically to prevent oxidative cleavage of the Ellman's reagent dimer by atmospheric oxygen. The free monomer, generated when one of the dimer's sulphur atoms attacks the cysteinyl thiolate and the reagents disulphide breaks, gives an absorbance at 412 nm ( $\epsilon_{412} = 1450 \text{ M}^{-1}\text{cm}^{-1}$ ). P450 BioI was incubated with Ellman's reagent for 60 minutes and the increase in absorbance at 412 nm followed. A second portion of P450 BioI was incubated anaerobically with dithiothreitol (DTT) for an hour before the DTT was removed via gel filtration (G-25 column). This reduced (and hence disulphide-cleaved) sample was then also assayed with Ellman's reagent. An increase in absorbance change at 412 nm was observed in accordance with more accessible cysteines being present and able to react. However, the results were not stoichiometric (see Table 3.16).

P450 BioI is known to contain 5 cysteines from its sequence, one of which is predicted to be partially on the surface (Cys296) and two of which are predicted to be in the putative disulphide bond (Cys250 and Cys275), with another ligated to the heme (Cys375) (see Figure 3.27). Whilst Ellman's reagent is unlikely to react with the cysteine ligated to the heme, a possible explanation of the lack of stoichiometry is that i) not all the cysteines are solvent and hence reagent accessible, and ii) the disulphide could

compete with Ellman's reagent for cysteine ligation (as one monomer binds the other cysteinyl thiolate attacks its disulphide partner to reform the disulphide bond and release a second molecule of dye, Figure 3.29).

Experiment	DTT	P450 BioI ( $\mu\text{M}$ )	MTNB ( $\mu\text{M}$ )	No of Cysteines
1	No	10.0	5.65	>0.5
2	No	20.0	10.6	>0.5
3	Yes	10.0	14.1	1.4
4	Yes	20.0	40.0	2.0

**Table 3.16** The results of the DTNB incubation with P450 BioI. An increase in the amount of MTNB generated is observed after incubation of P450 BioI with the reducing agent DTT.

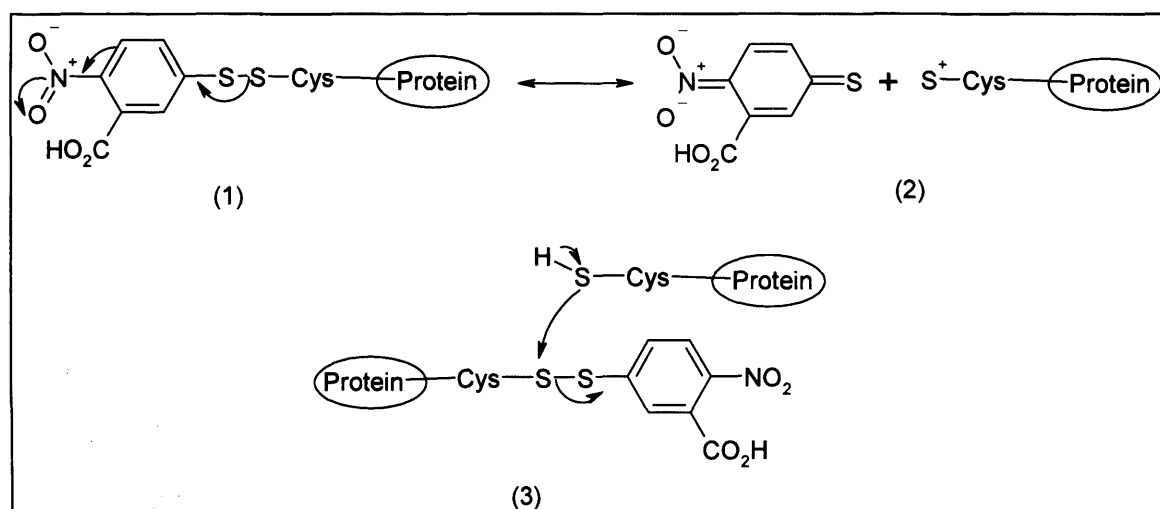


**Figure 3.29** The proposed competitive reaction between Ellman's reagent and the cysteine of a disulphide bond. Being in close enough proximity to react, the second cysteine can displace the reagent to generate a second molecule of dye (3). The resonance-stabilised form of Ellman's reagent (2) could enhance the reaction.

Overall, it is likely that P450 BioI does indeed contain a disulphide bond given the data from reactivity with Ellman's reagent and the finding that there is increased expression of the protein in *trxB* deleted *E. coli* strains (Section 3.1).

### 3.13 Chemical denaturation of P450 BioI

Guanidine hydrochloride (Gdn.HCl) has been used as a chemical denaturant in many studies examining the folding and stability of various proteins [e.g. Munro *et al.*, 1996]. By monitoring the spectral properties of the protein and its cofactor, information on the protein's overall stability and the cofactor's role in maintaining structure can be obtained. The stability of P450 BioI as regards chemical denaturation was examined via three spectroscopic techniques; the loss of ligation and protein association of the heme cofactor was assayed by UV-visible spectroscopy, the loss of secondary structure was monitored by CD and the loss of tertiary structure by fluorescence methods. The native form of P450 BioI was assayed for stability with increasing concentrations of Gdn.HCl, the various ligand-bound forms of the protein were also examined in a similar fashion. It is known that, in general, ligands can help to stabilise a protein (see Section 1.2) thus affects of ligand binding to P450 BioI were of interest.

#### 3.13.1 Heme cofactor denaturation

Gdn.HCl-induced loss of the heme cofactor was monitored by UV-visible spectroscopy. With the chemical denaturation, no increase in the turbidity of the sample is observed (as seen with temperature denaturation) as the Gdn.HCl ion acts by disrupting hydrophobic interactions, preventing protein aggregation.

Loss of ligation of the heme and its subsequent dissociation from the protein matrix was observed by a decrease in the Soret band at a wavelength between 394 and 419 nm (depending upon ligation type) followed by an increase in the absorbance at 370 nm from the heme in a different state. The diminished absorption likely reflects loss of heme ligation, followed by heme dissociation from the enzyme. The samples examined all exhibited a sigmoidal relationship between the concentration of Gdn.HCl and the proportion of denatured enzyme (calculated via Equation 8). The resulting curve (residual native heme absorption against Gdn.HCl concentration) was fitted using a sigmoidal function (Equation 7).

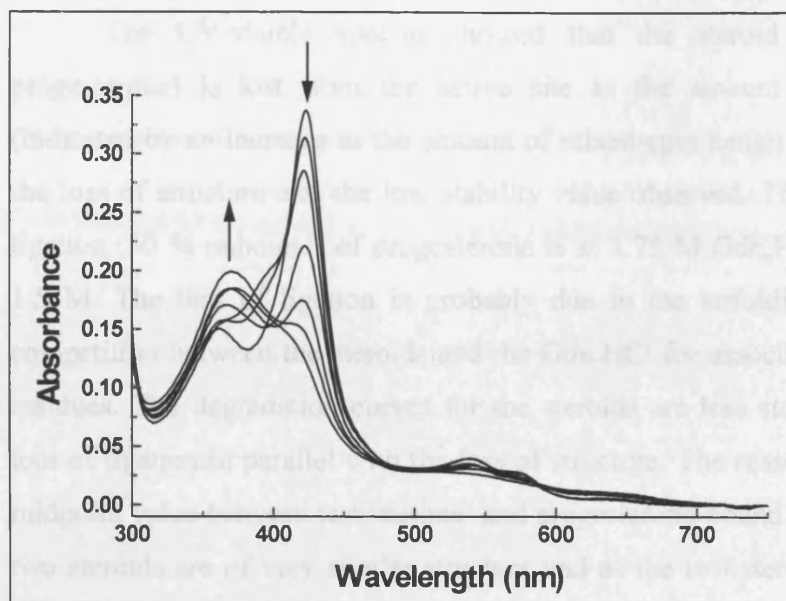


**Figure 3.30** Gdn.HCl-induced degradation of 4-phenylimidazole-bound P450 BioI (3.4  $\mu$ M) as followed by UV-visible spectroscopy. The heme cofactor appears stable to 3.0 M Gdn.HCl, then unfolding of the enzyme produces a loss in the ligated Soret peak at 424 nm and an increase in the species at 370 nm (probably heme dissociated from the protein matrix).

Ligand	50% heme denatured [Gdn.HCl] Molar	Error (+/-)
None	2.38	0.07
None	2.46	0.13
None (DTT treated)	2.34	0.13
None (pH 9.5)	1.47	0.15
Palmitoleic Acid	2.67	0.05
Myristic Acid	2.50	0.09
Testosterone	1.76	0.22
Progesterone	2.40	0.07
DMSO	2.59	0.10
Econazole	3.67	0.16
Nitric oxide (NO)	3.10	0.18
4-phenylimidazole	3.54	0.11

**Table 3.17** The effect of substrate binding and ligation upon stability of native heme association. The concentration of Gdn.HCl at which 50 % of the native heme signal is lost is shown. Data reported are for absorption loss at the Soret maximum with a plot of absorption loss versus [Gdn.HCl] fitted to a sigmoidal function. Ligands were at saturating concentrations, as determined from spectral titration data.



The UV-visible spectra showed that the steroid ligand (testosterone and progesterone) is lost from the active site as the amount of Gdn.HCl is increased (indicated by an increase in the amount of mixed-spin heme) and this may contribute to the loss of structure and the low stability value observed. The loss of native-like heme ligation (50 % unbound) of progesterone is at 1.75 M Gdn.HCl, and for testosterone at 1.5 M. The loss of ligation is probably due to the unfolding of the protein and the competition between the steroids and the Gdn.HCl for association with the hydrophobic residues. The degradation curves for the steroids are less steep, possibly reflecting the loss of ligation in parallel with the loss of structure. The reason for the difference in the midpoint value between testosterone- and progesterone-bound P450 BioI is not clear. The two steroids are of very similar structure and as the two steroids have very similar and tight  $K_d$  values ( $< 12 \mu\text{M}$ ), it is unlikely that there is a great amount of free steroid in solution to undergo an interaction with Gdn.HCl.

The nitrogen-containing heme-ligating compounds remain fully bound during the degradation process; the shift is fully to the denatured heme with no peak at 394 nm or 416 nm forming. Nitrogen ligation of the heme appears to stabilise the prosthetic group, the larger, tight binding molecules increasing this effect via active site interactions (*c.f.* econazole and NO). There is apparently some loss of fatty acid ligation, shown by an increase in the low-spin content, as the concentration of Gdn.HCl increases. This is possibly due to the Gdn.HCl competing with the fatty acid's alkyl chain for the hydrophobic residues that line the substrate-binding cavity. The solvent DMSO is known to produce a very weak low-spin shift ( $> 5 \%$  v/v), yet in this experiment the mixed-spin heme exhibits a slight shift to low-spin as the Gdn.HCl is added (*i.e.* if the DMSO is binding to the heme, it is not being displaced by the denaturant). DMSO appears to have little effect on the stability of the heme, despite its solvating properties.

### **3.13.2 Tertiary Structure Denaturation**

Fluorescence was used to monitor the disruption of tertiary structure. Excitation of tryptophan residues was at 290 nm, with the emission from 300 to 400 nm being recorded. A decrease in the fluorescence emission maximum at 340 nm was followed by

an increase in the emission at 358 nm as the protein unfolds. The intensity of the initial emission at 340 nm is very similar to that of the final unfolded form at 358 nm for all of the unbound and bound forms tested. The data are fitted as percent tertiary structure lost (i.e. fluorescence change) versus [Gdn.HCl] to a sigmoidal function.

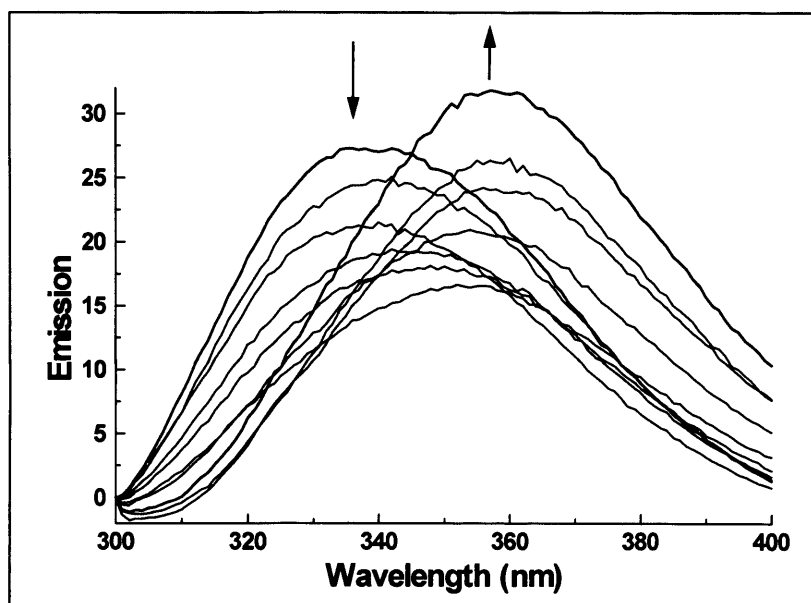


**Figure 3.31** The fluorescence emission spectra of econazole-bound P450 BioI (0.75  $\mu$ M) mixed with varying concentrations of Gdn.HCl. As the protein unfolds a decrease in the emission at 340 nm is observed prior to a shift of the emission spectrum to a longer wavelength (358 nm) and an increase in intensity back to surpass original levels. The lack of change in overall emission intensity implies that none of the tryptophan residues are strongly quenched in the folded protein.

From the early model of P450 BioI, the three tryptophan residues (Trp37, Trp161 and Trp376) are all on the surface of the protein being solvent accessible. The change in emission maximum as the protein unfolds is probably due to their environment changing from being partially embedded by neighbouring residues to being free in solution, but without notable effect on apparent quantum yield. As the wavelength of emission increases it follows that the energy of emission is decreasing. As in the folded state some of the neighbouring residues are aromatic in nature, a contribution or resonance effect with nearby residues on neighbouring chains could explain the initial maximum at a shorter wavelength (e.g. Trp40 is neighboured by Tyr30 and Tyr37 in the folded model). In a similar study with P450 BM3 heme domain, the Gdn.HCl-induced loss of tertiary

structure caused a red-shift of approximately 20 nm in tryptophan emission (336 to 355 nm) with an increase in the intensity (*ca.* 3.5-fold increase) bigger than that seen here [Munro *et al.*, 1996]. A buried tryptophan (W97) was thought to be quenched by the heme in the folded protein, due to its close proximity to the cofactor [Ravichandran *et al.*, 1993].

Ligand	[Gdn.HCl]Molar at 50% deg.	Error (+/-)
None	1.58	0.14
None	1.51	0.13
None (DTT treated)	1.62	0.15
None (pH9.5)	1.29	0.22
Palmitolate	2.12	0.08
Myristate	2.42	0.07
Testosterone	1.76	0.15
Progesterone	2.63	0.10
DMSO	2.84	0.11
Econazole	2.35	0.13
NO	2.30	0.11

**Table 3.18** The values of [Gdn.HCl] at which 50 % of P450 BioI's tertiary structure is degraded (deg), as measured by tryptophan fluorescence changes. P450 BioI (0.75  $\mu$ M) was in Tris.HCl buffer (50 mM, pH 7.2) containing a saturating concentration of the relevant ligand (typically 10 x the  $K_d$  value as determined in Section 3.6).

The emission spectrum of the buffer and ligand solution were deducted from the protein spectra. All ligands (except testosterone) appear to stabilise the protein via active site interactions, but the high value observed for DMSO could indicate the impediment of Gdn.HCl – protein interactions possibly via organic solvation of hydrophobic regions, such as those containing a number of aromatic residues (including tryptophan). The presence of an organic solvent can strengthen the hydrophobic interactions between protein chains by acting as a ‘mediator’. This means that the presence of DMSO could be strengthening the forces that the guanidinium ion is trying to disrupt. The high pH would increase the nucleophilicity of Gdn.HCl in addition to destabilising the protein structure by disrupting hydrogen bonds. Overall, P450 BioI appears to have a less stable tertiary structure than that of the ligand-free heme domain of P450 BM3 that is reported as losing 50 % of its tertiary structure at 2.6 M Gdn.HCl [Munro *et al.*, 1996].

### 3.12.3 Determination of the Stern-Volmer constant for P450 BioI

Quenching agents such as succinimide can be used to determine the location and degree of solvent exposure of tryptophan and tyrosine residues [Etfind *et al.*, 1976]. Working via a collision process, the quencher makes contact with the fluorophore and reduces the fluorescence intensity in a manner proportional to the concentration of the quencher. This is described by the Stern-Volmer equation ( $F_{0M}/F_{XM} = 1 + K_{SV}[Q]$ ) (see Section 2.8 for details).

The Stern-Volmer constant ( $K_{SV}$ ) was determined for both P450 BioI and the heme domain of P450 BM3. P450 BioI contains three tryptophan residues, which from early homology modelling work are predicted to be at least partially in contact with solvent and to be near the surface of the molecule. From the crystal structure of the heme domain of P450 BM3, it is known that four of its five tryptophan residues are at least partially solvent exposed [Ravichandran *et al.*, 1993].

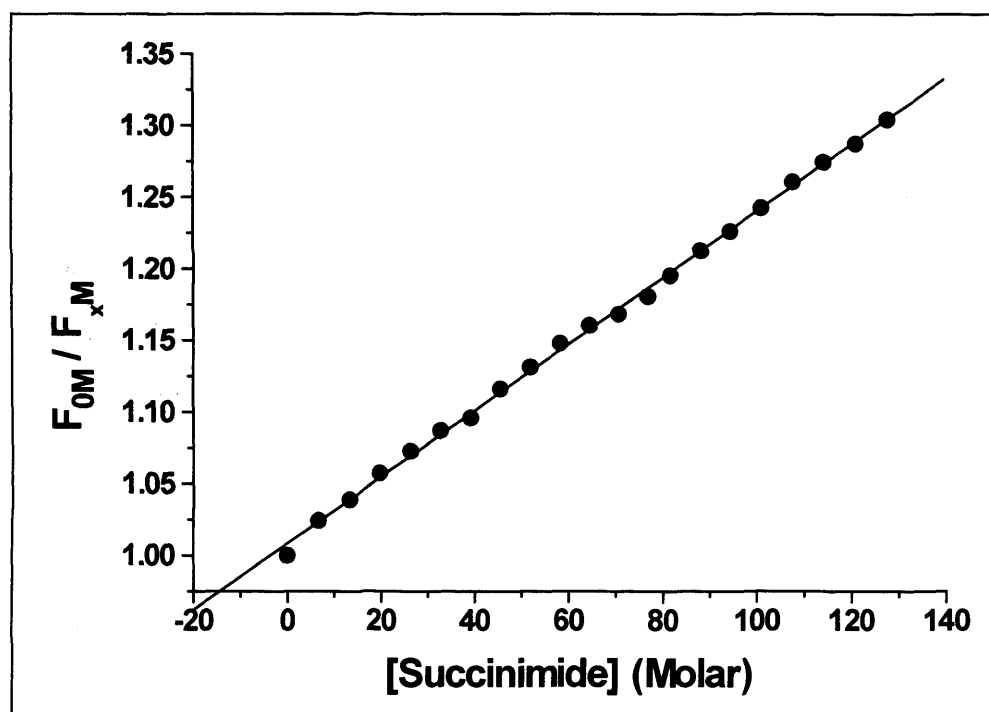


**Figure 3.32** Plot of the change in the fluorescence of the tryptophan residues in P450 BioI (1.0  $\mu$ M) caused by the addition of aliquots (10.0  $\mu$ l) of the quencher succinimide (2.0 M). Data shown are calculated from the reduction in the intensity of the tryptophan fluorescence emission of P450 BioI at the maximum of 341 nm. The Stern-Volmer constant is calculated from the linear fit to be  $(2.31 \pm 0.02) \times 10^{-3}$ . Data were collected at 25 °C in KPi buffer (50 mM, pH 7.0). Slit widths were 5 nm (Varian Eclipse

fluorimeter), the excitation wavelength was 290 nm, a 1 cm pathlength cell was used, and the emission was measured between 300 and 400 nm.  $F_{0M}$  and  $F_{XM}$  indicate the fluorescence values at 0 M and X M succinimide, respectively.

The progressive addition of aliquots of succinimide (10  $\mu$ l aliquots of a 2 M stock) causes a reduction in the tryptophan fluorescence (measured by excitation at 290 nm, emission at 341 nm recorded). Succinimide (2,5-pyrrolidinedione), being an uncharged hydrophilic molecule, quenches fluorescence via colliding with fluorophores, hence the Stern-Volmer value obtained represents the degree of solvent exposure and hence likelihood of collision each tryptophan residue has with the quencher [Moore *et al.*, 1993]. The change in fluorescence  $F_{0M}/F_{XM}$  versus the concentration of the quencher was plotted and fitted to a linear function to calculate the Stern-Volmer constants that are tabulated below:

Protein	Stern-Volmer constant ( $K_{SV}$ ) $((F_{0M}/F_{XM})/[Q])$
BioI (1)	$(2.31^{+/- 0.02}) \times 10^{-3}$
BioI (2)	$(2.55^{+/- 0.03}) \times 10^{-3}$
BM3 Heme domain	$(2.65^{+/- 0.03}) \times 10^{-3}$

**Table 3.19** Stern-Volmer constants for the P450s BioI and BM3. Calculated by fitting a linear function to a plot of the change in fluorescence ( $F_{0M}/F_{XM}$ ) against the concentration of the quencher ([Q], succinimide) using Origin software (Microcal). The data for P450 BioI were from duplicate titrations under identical conditions.

From the results tabulated above it can be seen that P450 BM3 heme domain and P450 BioI have very similar values for the Stern-Volmer constants, despite P450 BM3 containing two more tryptophans than P450 BioI. All of P450 BioI's three tryptophans appear to be solvent exposed from the model, and four of P450 BM3's tryptophans appear to be at least partially solvent exposed from its solved structure [Ravichandran *et al.*, 1993]. Therefore the Stern-Volmer constant is surprisingly low (being 0.08 for the smaller flavodoxin YkuN, see Section 4.18) for both these P450s, indicating either impediment of the succinimide by neighbouring residues, quenching of the tryptophan's fluorescence by neighbouring residues (e.g. tyrosines) or poor correlation between crystal and solution structures.

### 3.13.3 Effect of unfolding upon the Stern-Volmer constant

By unfolding P450 BioI using the chaotropic agent Gdn.HCl, the tryptophan residues should become more exposed to solvent and, as a result, the Stern-Volmer constant ( $K_{SV}$ ) should increase [Lehrer *et al.*, 1971]. This was the case, although after 4M Gdn.HCl the guanidinium ion (or impurities in the Gdn.HCl) also starts to quench the fluorescence and the  $K_{SV}$  decreases again.

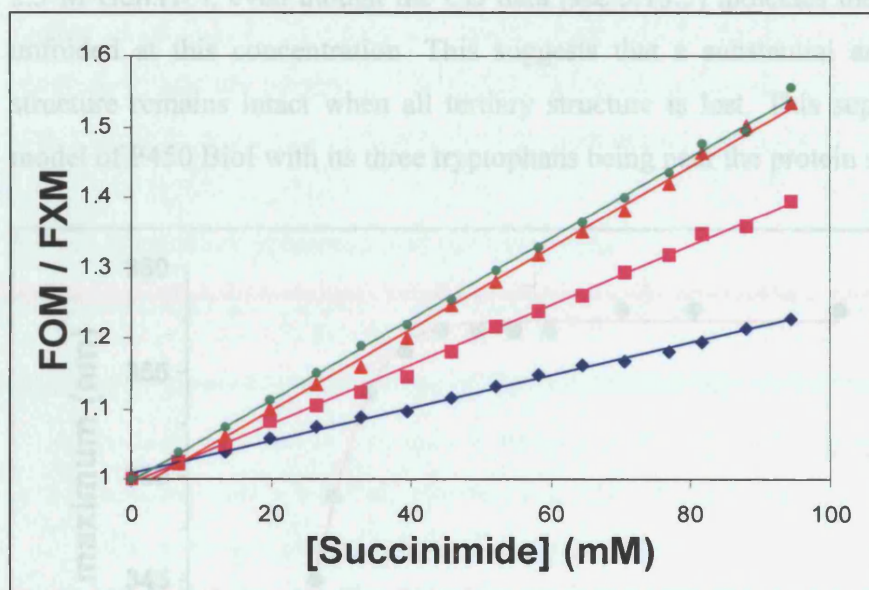


**Figure 3.33** The effect of protein unfolding on the  $K_{SV}$ . P450 BioI (2  $\mu$ l of 1.0 mM stock) was incubated in Gdn.HCl of varying concentration (navy = 0M, magenta = 1M, red = 2M, green = 4M) for 15 minutes at 20 °C prior to measurement of the  $K_{SV}$  by succinimide quenching (addition of 10  $\mu$ l aliquots of a 2 M stock solution). The concentration of succinimide is plotted versus the fluorescence at 0 M succinimide divided by the fluorescence at X M succinimide ( $F_{0M}/F_{XM}$ ).

[Gdn.HCl] (Molar)	$K_{SV}$
0	$(2.31 \pm 0.002) \times 10^{-3}$
1	$(4.21 \pm 0.005) \times 10^{-3}$
2	$(5.74 \pm 0.007) \times 10^{-3}$
4	$(6.42 \pm 0.006) \times 10^{-3}$
6	$(4.59 \pm 0.006) \times 10^{-3}$
8	$(5.13 \pm 0.009) \times 10^{-3}$

**Table 3.20** Stern-Volmer constants ( $K_{SV}$ ) for P450 BioI when incubated with various [Gdn.HCl] for 15 minutes at 20 °C. Values were calculated by fitting a linear function to



a plot of the change in fluorescence ( $F_{0M}/F_{XM}$ ) against the concentration of the quencher ([Q], succinimide) using Origin software (Microcal).

As the protein unfolds and the tryptophan residues are exposed to a more polar environment, the emission maximum undergoes a shift to a longer wavelength. This shift in emission maximum versus the concentration of Gdn.HCl is plotted below in Figure 3.34. The shift indicates that the tryptophans in P450 BioI are fully solvent accessible at 2.5 M Gdn.HCl, even though the CD data (see 3.13.5) indicates the protein is not fully unfolded at this concentration. This suggests that a substantial amount of secondary structure remains intact when all tertiary structure is lost. This supports the homology model of P450 BioI with its three tryptophans being near the protein surface.

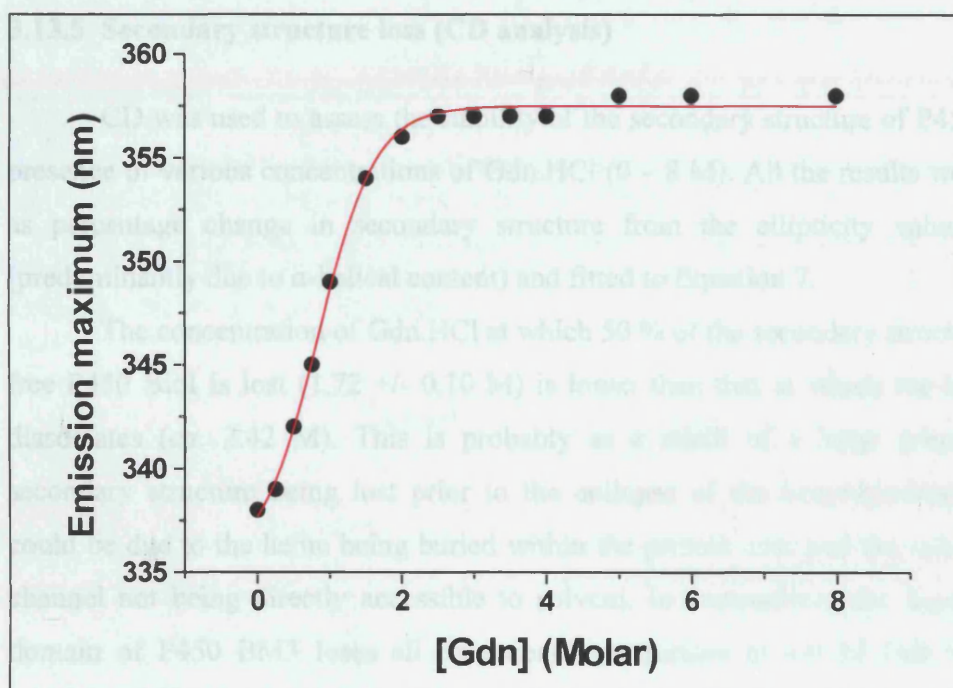


**Figure 3.34** The effect of Gdn.HCl-induced unfolding upon the emission maximum ( $\lambda_{max}$ , nm) of the three tryptophan residues in P450 BioI (3  $\mu$ M). The sigmoidal fit indicates a single phase co-operative unfolding of the protein. The shift to a longer wavelength indicates the transfer of the tryptophans to a more polar environment. The emission maximum is shifted by 50 % at  $0.84 \pm 0.2$  M Gdn.HCl. The experiment was carried out using various [Gdn.HCl] in KPi buffer (3 ml, 50 mM, pH 7.0) with slit widths at 5 nm (Varian Eclipse Fluorimeter). The excitation wavelength was 290 nm, a 1 cm path-length cell was used, and the emission was measured between 300 and 400 nm.

The Stern-Volmer constants calculated in the presence of various [Gdn.HCl] show that the aromatic residue's fluorescence continues to increase up to 4 M Gdn.HCl whilst the change in the tryptophan's emission maximum (above) plateaus at 2.5 M Gdn.HCl. This discrepancy can be explained on the basis of the quenching agent (succinimide) working via a collision mechanism. Whilst the emission maximum may indicate that the tryptophans are fully solvent exposed at 2.5 M Gdn.HCl, they may still not be fully accessible to the succinimide molecule until the protein has unravelled further (4 M Gdn.HCl). From CD studies (see 3.10.5) we know that there is still some secondary structure present at 4 M Gdn.HCl (*ca* 15 % folded). The neighbouring residues may therefore impede the interaction of the succinimide with the aromatic side-chain.

### **3.13.5 Secondary structure loss (CD analysis)**

CD was used to assess the stability of the secondary structure of P450 BioI in the presence of various concentrations of Gdn.HCl (0 – 8 M). All the results were calculated as percentage change in secondary structure from the ellipticity value at 219 nm (predominantly due to  $\alpha$ -helical content) and fitted to Equation 7.

The concentration of Gdn.HCl at which 50 % of the secondary structure of ligand-free P450 BioI is lost (1.72 +/- 0.10 M) is lower than that at which the heme cofactor dissociates (*ca.* 2.42 M). This is probably as a result of a large proportion of the secondary structure being lost prior to the collapse of the heme-binding region. This could be due to the heme being buried within the protein core and the substrate-binding channel not being directly accessible to solvent. In comparison, the ligand free heme domain of P450 BM3 loses all its secondary structure at 4.0 M Gdn.HCl, with the midpoint value being *ca.* 1.5 M Gdn.HCl [Munro *et al.*, 1996], similar to that observed here with P450 BioI.

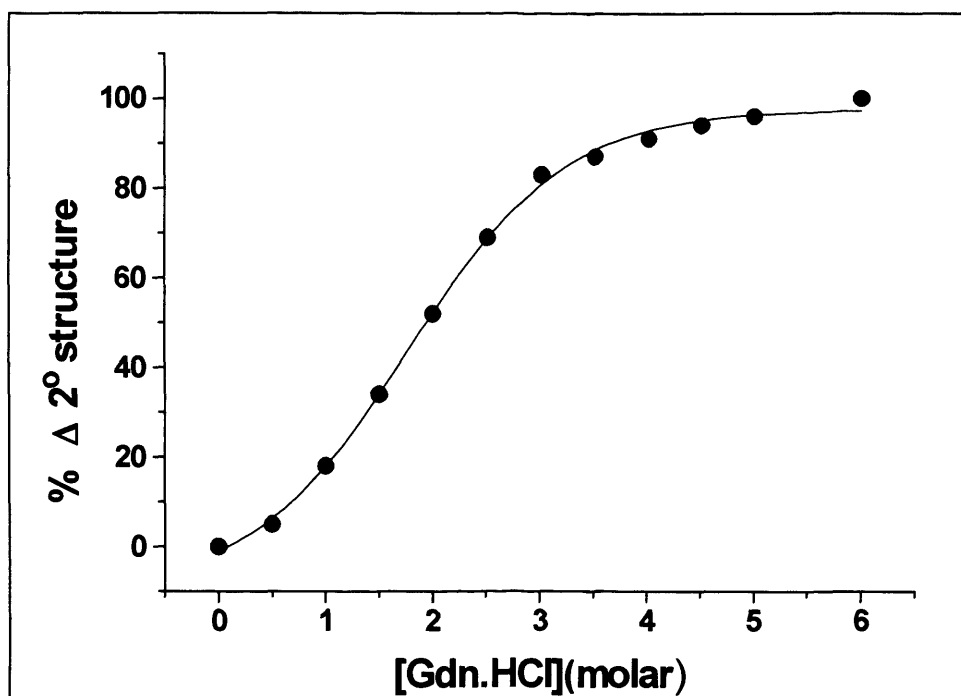


**Figure 3.35** CD monitoring of the Gdn.HCl-induced degradation of palmitoleate-bound P450 BioI (3  $\mu$ M). The ellipticity values (219 nm) of solutions of P450 BioI incubated in various concentrations of Gdn.HCl (in KPi buffer, pH 7.0) were measured at 25 °C in a 1 mm path-length cell. The % change in ellipticity was then calculated and plotted versus [Gdn.HCl]. Data are fitted to a sigmoidal function yielding a midpoint value of 1.80  $\pm$  0.18 M Gdn.HCl.

Ligand	[Gdn.HCl] 50% structure lost (M)
None	1.72 $\pm$ 0.10
Palmitoleic acid	1.80 $\pm$ 0.18
Myristic acid	0.92 $\pm$ 0.13
Testosterone	1.62 $\pm$ 0.08
Progesterone	1.52 $\pm$ 0.13
Econazole	1.97 $\pm$ 0.10
4-Phenylimidazole	1.30 $\pm$ 0.05
DMSO	1.88 $\pm$ 0.08

**Table 3.21** The concentration of Gdn.HCl at which 50 % of the secondary structure of P450 BioI is lost. The % change in ellipticity (at 219 nm) was calculated and plotted versus [Gdn.HCl]. Data are fitted to a sigmoidal function to determine the midpoint values (Origin, Microcal).

The general increase in stability observed by all the techniques when P450 BioI is bound to econazole could reflect expulsion of solvent from the active site in the ligated

form, thereby not allowing Gdn.HCl molecules to attack the protein's hydrophobic core. The effect of the DMSO is unclear. Low concentrations (1 – 5 % v/v) of organic solvents are known to stabilise proteins as they interact with hydrophobic moieties. As a solvent known for its properties of solvating cationic species, it is possible that when DMSO is not loosely associated with a ligand (large excess of ligands were added) it has some interaction with either the heme or the Gdn.HCl itself, which perhaps impedes the Gdn.HCl's chaotropic properties.

### **3.14 Stability of P450 BioI: Thermal denaturation**

The stability of P450 BioI against chemical (Gdn.HCl-induced) denaturation has previously been assessed in this study and it has been found that ligation of the heme and occupation of the active site can affect the stability of the protein. To see if these effects are purely due to ligand-protein interactions, or whether there is some Gdn.HCl-ligand interaction, the stability of four forms of P450 BioI (unbound, palmitoleate bound, testosterone bound and econazole bound) were assessed by thermal denaturation. It has been found that the binding of 1R-camphor increased the thermal stability of P450 CAM via active site interactions [Murugan and Mazumdar, 2004].

Differential scanning calorimetry (DSC) was used to follow the heat-induced unfolding of the protein structure. All DSC scans were performed using a MicroCal VP-DSC (MicroCal LLC, Northampton MA, USA) at a heating scan rate of 1 °C per minute. The DSC was interfaced to a Gateway PIII computer and used Origin 5.0 (MicroCal LLC, Northampton MA, USA) for data acquisition. The reference cell was filled with buffer (KPi, 50 mM, pH 7.5) in addition to any ligand (as appropriate) and instrumental baselines were measured by placing buffer in both cells. Buffer baselines were subtracted from scans of the protein prior to data analysis using Origin 5.0 (Microcal). A stock solution of protein, (0.137 mM), was divided into aliquots for the DSC experiments. One aliquot was treated with DTT (5 equivalents) under anaerobic conditions (Belle Technology glove box, <4 ppm O<sub>2</sub>), any excess DTT being removed from the protein by filtration (BioRad 10DG column), and the sample was sealed anaerobically immediately



prior to DSC experiments. Another aliquot of the protein was scanned in the DSC without adding any DTT or ligands.

The thermal denaturation of P450 BioI was not reversible as all samples after DSC scans were turbid. The starting solutions were not turbid. The DSC traces show a large exotherm due to the collapse of the protein's structure and the aggregation of the unfolded protein. A large difference in the baseline is observed particularly with the soapy compounds (steroid and fatty acid) that can adhere to the walls of the glass sample holder. Unbound P450 BioI has a  $T_M$  of 69.1 °C and this is unaffected by the pre-incubation with DTT. The scans show that the unfolding of P450 BioI in the presence of DTT may be more complex than in the absence of the reducing agent. A small shoulder in the DSC endotherm in the temperature range 50 – 60 °C is observed, implying that the transition is clearly non-two-state in the DTT-reduced form.

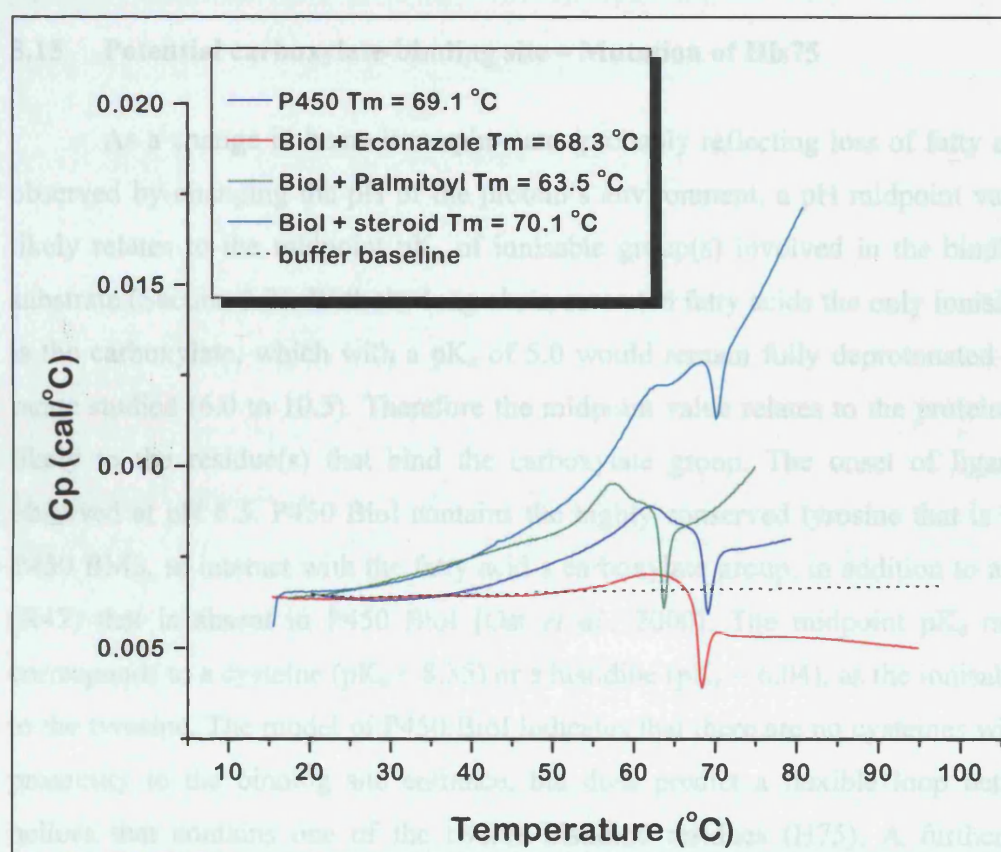


**Figure 3.36** DSC traces of various forms of P450 BioI (0.137 mM). All buffer solutions (50 mM KPi, pH 7.5) contained 1% v/v DMSO. DSC scans were conducted at 60 K/h. P450 BioI was denatured in the unbound form (blue) and in several bound forms

(saturating concentrations of ligands). The ligands were econazole (red), palmitoyl (green) and testosterone (cyan).  $T_M$  is the transition midpoint temperature and  $C_p$  is the heat capacity.

Thermal denaturation of P450 BioI showed that, whilst the heme-ligating compounds (steroid, Fe-O ligation and econazole Fe-N ligation) have negligible effect on the  $T_M$ , the fatty acid (five coordinate high-spin heme) destabilises the protein by *ca* 4 °C. This could be due to the fatty acid acting as a soap disrupting hydrophobic interactions. Thermal denaturation of the heme domain of P450 BM3 showed two distinct transitions with a  $T_M$  at 58.7 and 64.9 °C respectively, the lower temperature reading being a shoulder on the higher temperature peak [Munro *et al.*, 1996]. The value for the higher temperature peak is in the region of the values seen here and it was also a non-reversible transition.

### **3.15 Potential carboxylate-binding site – Mutation of His75**

As a change in heme iron spin-state (probably reflecting loss of fatty acids) was observed by changing the pH of the protein's environment, a pH midpoint value of 8.5 likely relates to the midpoint  $pK_a$  of ionisable group(s) involved in the binding of the substrate (Section 3.3). With the long chain saturated fatty acids the only ionisable group is the carboxylate, which with a  $pK_a$  of 5.0 would remain fully deprotonated in the pH range studied (6.0 to 10.5). Therefore the midpoint value relates to the protein and most likely to the residue(s) that bind the carboxylate group. The onset of ligand loss is observed at pH 6.5. P450 BioI contains the highly conserved tyrosine that is known, in P450 BM3, to interact with the fatty acid's carboxylate group, in addition to an arginine (R47) that is absent in P450 BioI [Ost *et al.*, 2000]. The midpoint  $pK_a$  most likely corresponds to a cysteine ( $pK_a = 8.35$ ) or a histidine ( $pK_a = 6.04$ ), as the ionisable partner to the tyrosine. The model of P450 BioI indicates that there are no cysteines within close proximity to the binding site entrance, but does predict a flexible loop between two helices that contains one of the twelve histidine residues (H75). A further histidine residue (H236) is located further within the binding channel near to the conserved threonine (T238). In P450 CAM the relevant threonine residue (T252) is known to be



involved in proton transfer to the reduced dioxygen [Vidakovic *et al.*, 1998, Hishiki *et al.*, 2000]. It is therefore possible that the histidine on the flexible loop could act as a 'hook' to pick up on any acidic groups in the vicinity using an initial ionic interaction to bring the substrate near enough to the active site to allow the secondary hydrophobic interactions with the long alkyl-chain.

Histidine residues can be selectively chemically modified by the reagent diethylpyrocarbonate (DEPC), which is attacked by the imidazole nitrogen to form an irreversible alkylated product, as shown in Figure 3.37 [Fersht, 1985].

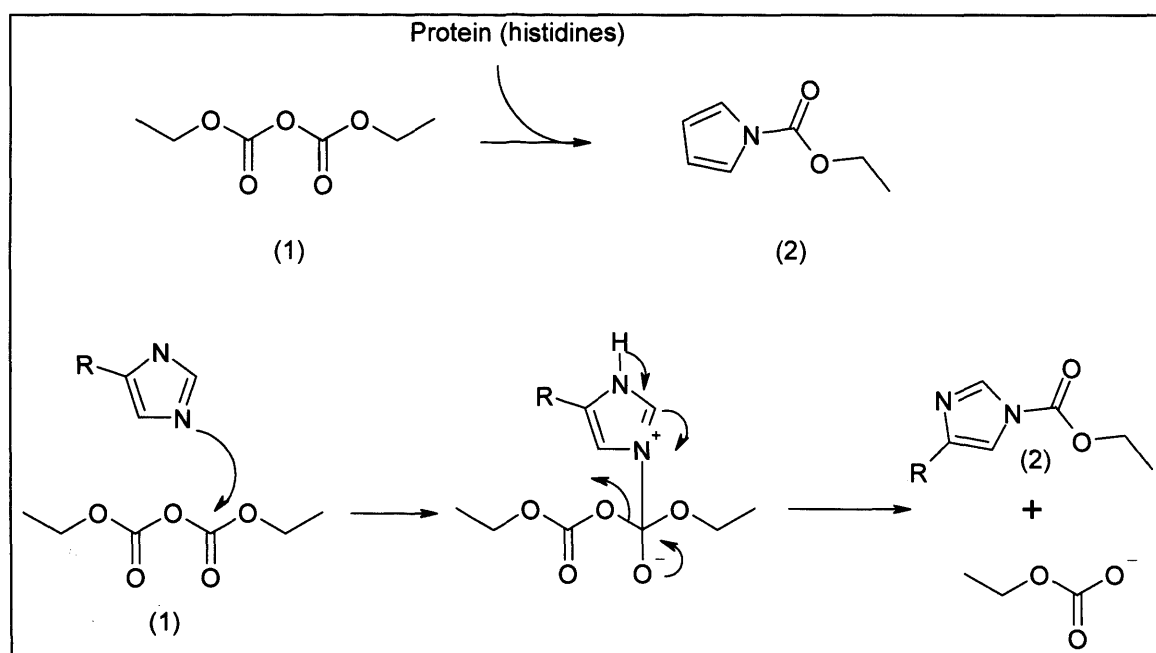


**Figure 3.37** DEPC (1) covalently modifies histidines, as shown in the scheme above, to give the product (2) plus the by-product ethoxyformate. The figure shows the overall reaction (top) and a more detailed mechanistic scheme (bottom). The modification of the histidine by this reagent therefore removes the ionic character of the histidine's usually protonated\* nitrogen (\* at physiological pH).

DEPC was titrated (aliquots of 12 x 0.5  $\mu$ l, 1.31 mM stock DEPC solution) into a solution of myristate (0.05 mM)-bound P450 BioI (2.6  $\mu$ M) in Tris.HCl buffer (50 mM, pH 7.5) at 20 °C. The loss of ligation was monitored by the decrease in high-spin content of P450 BioI (absorption maximum at 393 nm) and apparent increase in content of the substrate-free protein (absorption maximum at 417 nm). DEPC was also added to a

solution of econazole (0.05 mM)-bound P450 BioI, as this molecule binds through ligation of the heme iron and therefore should not be displaced by DEPC. The addition of DEPC caused no change in the pH of the solution, but its poor solubility meant that an increase in the turbidity of the solution is seen in excess of 20  $\mu\text{M}$ .

The amount of DEPC that caused the loss of 50 % of the bound fatty acid was  $5.08 \pm 0.49 \mu\text{M}$ . As there are two equivalents of the reactive ester per mole of DEPC (see Figure 3.37), this equates to 10.16 nmoles of the active ester species causing 1.3 nmol P450 BioI to lose ligation (at the 50 % point). As P450 BioI contains twelve histidine residues, the smaller amount of DEPC required indicates the residue(s) involved in fatty acid binding are likely to be reasonably solvent exposed. With the econazole bound form of P450 BioI the addition of DEPC did not cause ligand loss; the Soret band remained at 423 nm. This indicates that DEPC addition does not affect the overall fold of the protein, its ability to retain the heme and capacity to bind azoles.

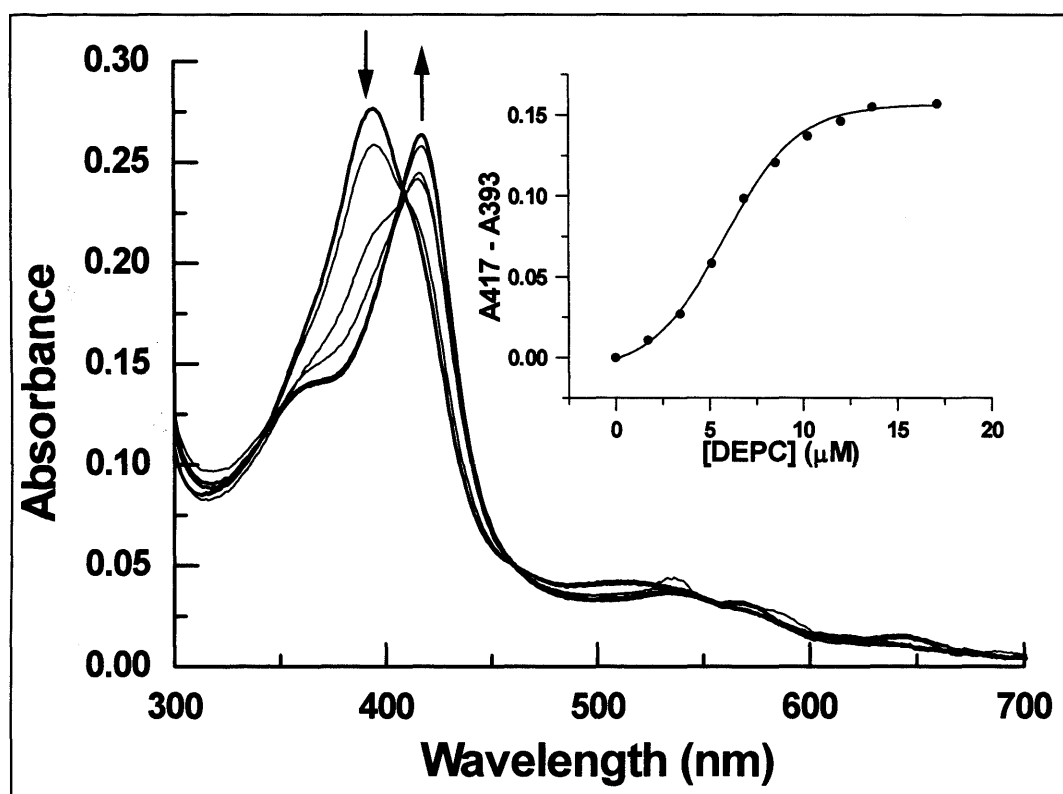


**Figure 3.38** The addition of aliquots of DEPC (1.31 mM stock solution) causes spectral changes due to the loss of bound myristic acid from P450 BioI (2.6  $\mu\text{M}$ ). A decrease in the high-spin form can be seen at 393 nm and a corresponding increase in the low-spin protein at 417 nm. The shift in the Soret band (from 393 nm to 417 nm) is

plotted against the concentration of DEPC and fitted to a sigmoidal function (inset) to calculate the amount of DEPC that causes a 50 % shift in the heme's spin-state ( $5.08 \pm 0.49 \mu\text{M}$ ).

From these data, the model and the pH profiles, it is proposed that His75 could be the residue that forms an ionic interaction with the carboxylate of fatty acids, possibly complementing the tyrosine group (Y49) in binding fatty acids. To seek further proof H75 was mutated to an alanine and an arginine, residues that should weaken or strengthen the interaction with the carboxylate, respectively.

### **3.15.1 Generation of the H75A and H75R mutants**

His75 was mutated to an arginine and an alanine by PCR-mediated oligonucleotide directed mutagenesis. Restriction sites were introduced by additional silent mutations in the PCR primers, so that an enzyme digest could be used to confirm the introduction of the mutation (Section 2.5). With the H75A mutant an additional *PvuII* site was introduced, which would result in two fragments being observed upon restriction digest of the mutant plasmid compared to one for the wild-type (cloned in the vector pET11a). In the H75R mutant a unique restriction site was introduced (a *PmlI* site) that would result in linearization of the DNA.

The product of the PCR reaction was incubated (1 hour,  $37^\circ\text{C}$ ) with the restriction enzyme *DpnI* (selective for non-mutant methylated DNA) gel purified (1% agarose gel) and transformed into *E. coli* JM109 cells. Following overnight incubation of the transformation mixture on LB ampicillin plates ( $37^\circ\text{C}$ ), six colonies were picked and grown up (5 ml LB ampicillin-containing cultures) to allow recovery of the plasmid. The successful introduction of the mutation into the vector was checked by digestion with the appropriate restriction enzyme (1.0 Unit, 100 ng of plasmid DNA) (Section 2.5). A gel of the *PmlI* digest of the H75R plasmid is shown below. Unfortunately, the other enzyme, *PvuII* showed some nonspecific activity, so the digest was not useful in characterisation of H75A clones. Samples of those plasmids believed (from the diagnostic digests) to contain the correct mutation were submitted for sequencing by the in house facility (PNACL).

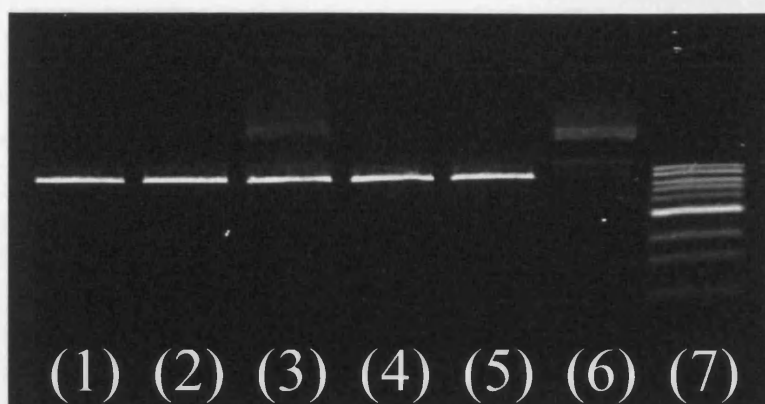


**Figure 3.39** Agarose gel (1%) of H75R containing plasmid DNA following digestion with *PmlI*. The enzyme linearises the DNA to give a single band in correctly mutated H75R clones. DNA was visualised by UV light following staining with ethidium bromide. The marker (NEB 1 kb ladder) is shown in lane (7), an incomplete digest can be seen in lane (3) and a negative result in lane (6). Other lanes show successful digests of H75R DNA with a single band at 6.2 kb.

*E. coli* Origami DE3 cells were transformed with the relevant mutant plasmids and a small scale expression study (5 ml LB containing 50  $\mu\text{g ml}^{-1}$  ampicillin) was performed to see if their expression differed from that of wild-type. Cells were grown at 37 °C and one sample of each culture was induced with IPTG (1 mM) when the  $\text{OD}_{600} = 1.0$ . The cells were allowed to grow, samples were taken at 1 and 3 hours post induction and the protein expression analysed by running samples of the cells on SDS PAGE (see 2.2.4). From the SDS PAGE analysis it was apparent that induction with IPTG was not necessary for the protein's expression. Therefore over-expression of the mutants was carried out using the same protocol as used to prepare large quantities of the wild type protein (see 2.5). A total of three large-scale (7 litre) preparations were performed. Isolation and purification of the protein from the cells again followed the protocol used with WT P450 BioI (four column chromatography steps as described in Section 2.6).

The proteins behaved in a similar fashion to the wild-type, although a greater affinity of H75A for the DEAE column was noted, it eluting at nearly 100 mM higher KCl compared to the wild-type protein. The yields following the purification of the mutants from the total of 21 litres of culture grown were 135 mg of H75A and only 41 mg of H75R. This lower yield was due to a lower level of over-expression of the arginine mutant within the cell.

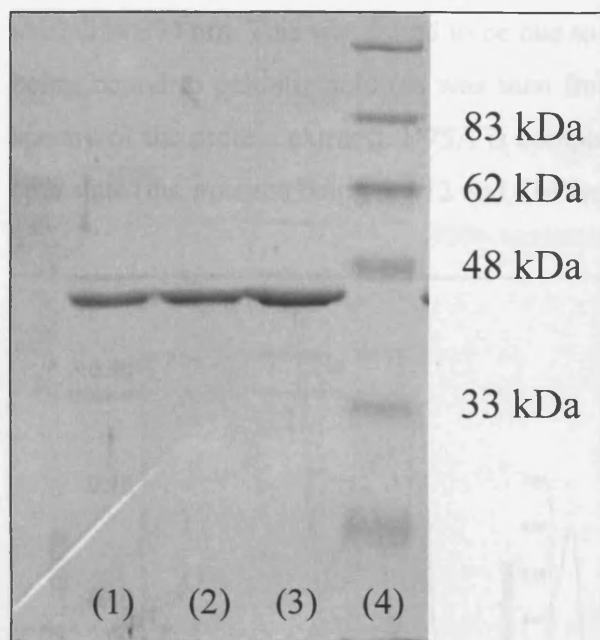


**Figure 3.40** SDS PAGE analysis of the two mutants of P450 BioI. Samples (10 ng) of the purified proteins were run, H75A in lane (1), H75R in lane (2), wild-type P450 BioI in lane (3) and BioRad broad-range pre-stained protein marker in lane (4). The mass of the relevant marker bands is shown on the right. Wild-type and mutant P450 BioI forms migrate with an apparent molecular mass of 45 kDa.

### 3.15.2 Physical properties of the H75 mutants

To see if the mutation had had any unforeseen effect upon the P450, a fingerprint UV-visible spectrum was taken of each of the mutants and compared to the wild type protein. Spectra were taken of the proteins in their oxidised, reduced (dithionite) and CO-bound states. All the proteins were prepared in the same buffer (Tris.HCl 50 mM, pH 7.5) and spectra were recorded at 20 °C.

The absorption maxima of the proteins all fall at the same wavelength depending upon the state of the protein, i.e. the reduced P450 has a maximum at 409 nm regardless of mutation and the CO-bound adduct has its Soret maximum at 448 nm. These data show that, as expected, the mutation of the surface histidine has had no effect on the immediate surrounding of the heme. However, a notable difference is seen in the wavelength of the oxidised Soret peak's maximum, due to the proportion of high-spin protein isolated. As can be seen from the UV-visible spectrum shown below, the protein H75R is isolated from *E. coli* in an almost totally high-spin state, with the maximum



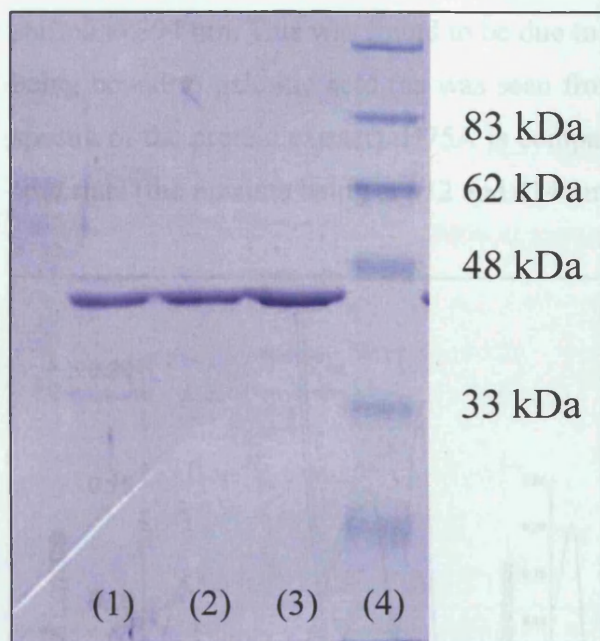


**Figure 3.40** SDS PAGE analysis of the two mutants of P450 BioI. Samples (10 ng) of the purified proteins were run, H75A in lane (1), H75R in lane (2), wild-type P450 BioI in lane (3) and BioRad broad-range pre-stained protein marker in lane (4). The mass of the relevant marker bands is shown on the right. Wild-type and mutant P450 BioI forms migrate with an apparent molecular mass of 45 kDa.

### 3.15.2 Physical properties of the H75 mutants

To see if the mutation had had any unforeseen effect upon the P450, a fingerprint UV-visible spectrum was taken of each of the mutants and compared to the wild type protein. Spectra were taken of the proteins in their oxidised, reduced (dithionite) and CO-bound states. All the proteins were prepared in the same buffer (Tris.HCl 50 mM, pH 7.5) and spectra were recorded at 20 °C.

The absorption maxima of the proteins all fall at the same wavelength depending upon the state of the protein, i.e. the reduced P450 has a maximum at 409 nm regardless of mutation and the CO-bound adduct has its Soret maximum at 448 nm. These data show that, as expected, the mutation of the surface histidine has had no effect on the immediate surrounding of the heme. However, a notable difference is seen in the wavelength of the oxidised Soret peak's maximum, due to the proportion of high-spin protein isolated. As can be seen from the UV-visible spectrum shown below, the protein H75R is isolated from *E. coli* in an almost totally high-spin state, with the maximum



shifted to 394 nm. This was found to be due to a greater proportion of the isolated protein being bound to palmitic acid (as was seen from the  $m/z$  255<sup>+</sup> peak in electrospray mass spectra of the protein extract). H75A is comparable to the WT protein being in a mixed-spin state (the maxima being at 412 and 414 nm, respectively).

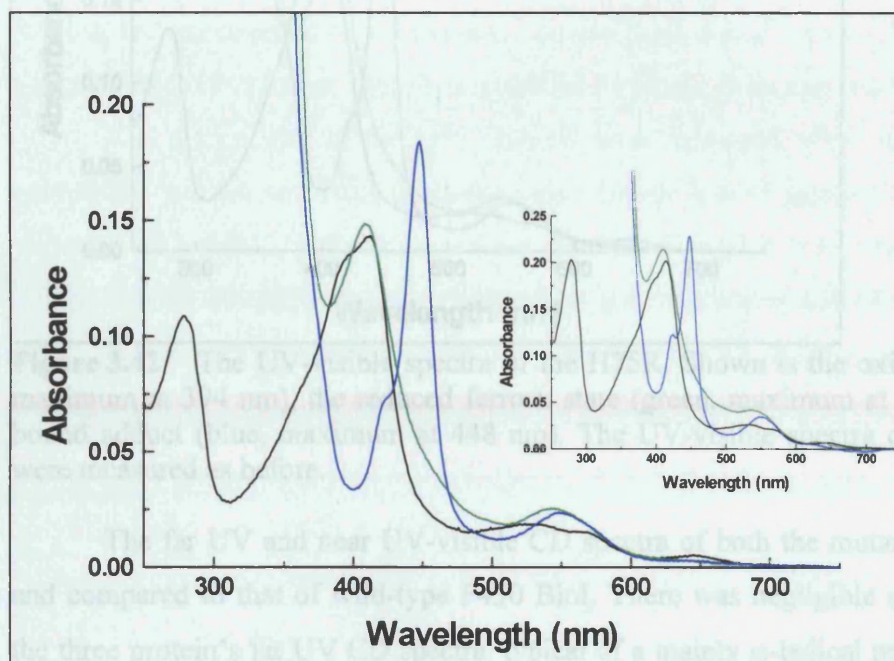


**Figure 3.41** The UV-visible spectra of the H75A and wild type (inset) forms of P450 Biol. Shown is the oxidised state (black, maximum at 418 nm), the reduced ferrous state (green, maximum at 409 nm) and CO bound adduct (blue, maximum at 448 nm). The UV-visible spectra of H75A (1.9  $\mu$ M) and wild-type (2.5  $\mu$ M) were measured in Tris.HCl buffer (50 mM, pH 7.5).

The isolation of H75R in an extensively high spin form suggests the mutation has increased the affinity of fatty acids for the protein. This feature is further investigated via binding titrations with a variety of compounds (see Section 3.15.4).

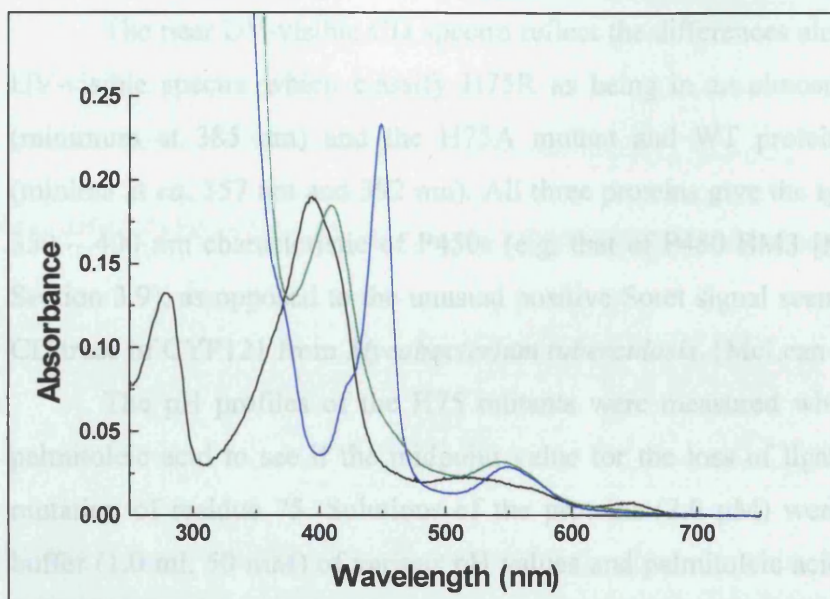


**Figure 3.42** The UV-visible spectra of the H75R. Shown is the oxidised state (black, maximum at 394 nm), the reduced ferrous state (green, maximum at 409 nm) and CO-bound adduct (blue, maximum at 448 nm). The UV-visible spectra of H75R (2.3  $\mu$ M) were measured as before.

The far UV and near UV-visible CD spectra of both the mutants were measured and compared to that of wild-type P450 Biol. There was negligible difference between the three protein's far UV CD spectra, typical of a mainly  $\alpha$ -helical protein with minima at 221 and 207 nm (Figure 3.43) [Kabsch and Sander, 1983].

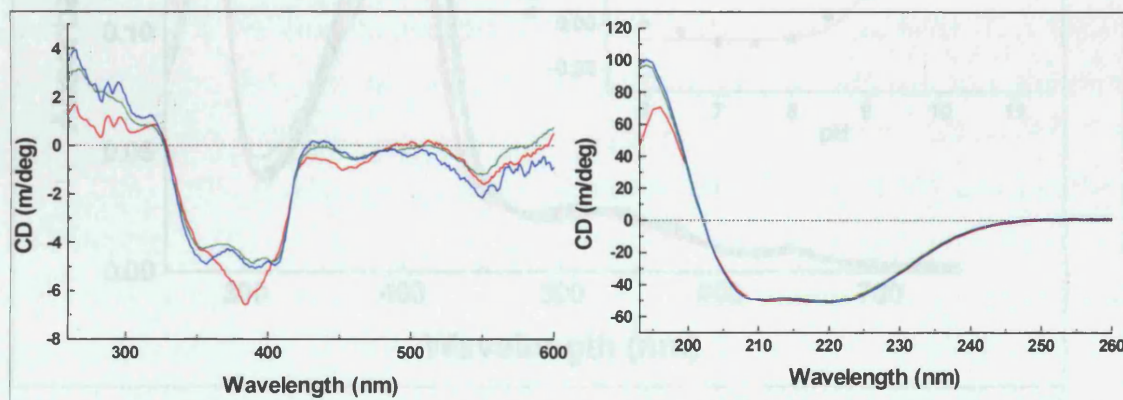


**Figure 3.43** Near UV-visible (left) and far UV CD spectra (right) of the wild-type and H75 mutants of P450 Biol. Wild-type (red), H75R (green), H75A (blue). Spectra were recorded on a JASCO 750 spectropolarimeter at 25 °C with a pathlength of 1.0 and 0.1 cm, respectively for the near UV-visible and far UV regions. Proteins were at 1.0 and 0.1 mg/ml (near UV-visible and far UV respectively) in KPi buffer (50 mM, pH 7.0).



The near UV-visible CD spectra reflect the differences already seen in the optical UV-visible spectra which classify H75R as being in an almost totally high-spin state (minimum at 385 nm) and the H75A mutant and WT protein as being mixed-spin (minima at *ca.* 357 nm and 392 nm). All three proteins give the typical negative peaks at 350 – 400 nm characteristic of P450s (e.g. that of P450 BM3 [Munro *et al.*, 1996] see Section 3.9), as opposed to the unusual positive Soret signal seen in the near UV-visible CD trace of CYP121 from *Mycobacterium tuberculosis*. [McLean *et al.*, 2002].

The pH profiles of the H75 mutants were measured when fully saturated with palmitoleic acid to see if the midpoint value for the loss of ligation was altered by the mutation of residue 75. Solutions of the proteins (2.0  $\mu$ M) were prepared in Tris.HCl buffer (1.0 ml, 50 mM) of various pH values and palmitoleic acid (3.0 mM) was added. After incubating at 25 °C for 5 minutes the UV-visible spectra were measured. An example of the change in P450 absorbance at different pH values is shown below.

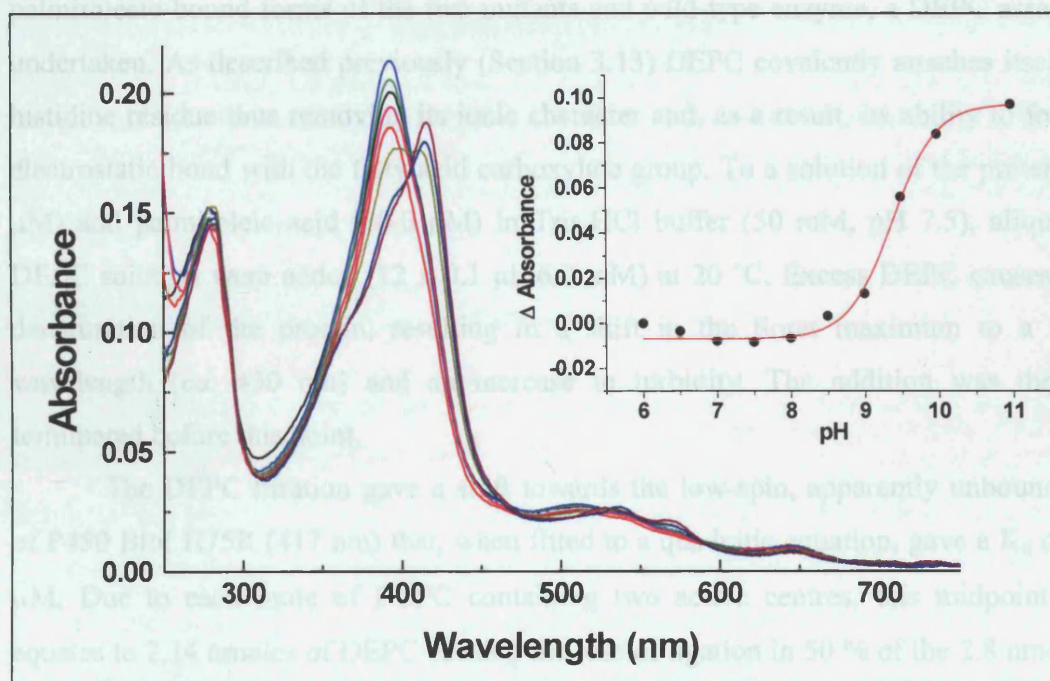


**Figure 3.44** Change in the spin-state of H75R (2.0  $\mu$ M) when fully saturated with palmitoleic acid (0.3 mM) and incubated in Tris.HCl buffer (50 mM, 1.0 ml) at various pH values. The absorbance maximum shifts from 392 nm (blue) at pH 6.0 to 417 nm at pH 10.0 (purple). When the shift in the Soret maximum ( $A_{392} - A_{417}$ ) is plotted against pH and fitted to a sigmoidal function, the midpoint  $pK_a$  is at  $9.39 \pm 0.90$  (inset).

The midpoint  $pK_a$  values for the fatty acid-bound mutants were higher than that of the WT protein. The mutation of the histidine ( $pK_a$  6.04) has altered the apparent pH value at which 50 % of the fatty acid ligand is lost, increasing it by  $> 0.6$  pH units. It is possible that His75 is therefore involved in fatty acid binding, if not directly then perhaps by modulating the ionic environment around the entrance to the binding site.

Protein	$pK_a$
Wild-type	8.45 $\pm$ 0.78
H75A	9.15 $\pm$ 0.81
H75R	9.39 $\pm$ 0.90

**Table 3.22** The midpoint  $pK_a$  values for the three proteins when bound with a near saturating amount of palmitoleic acid. Conditions were as described in Figure 3.44.

In view of the small differences seen between the various pH midpoint for the palmitoleate-bound forms of the two mutants and wild-type enzyme, a DEPC assay was undertaken. As described previously (Section 3.13) DEPC covalently attaches itself to a histidine residue thus removing its ionic character and, as a result, its ability to form an electrostatic bond with the fatty acid carboxylate group. To a solution of the protein (2.8  $\mu$ M) and palmitoleic acid (30.0  $\mu$ M) in Tris.HCl buffer (50 mM, pH 7.5), aliquots of DEPC solution were added (12 x 0.1  $\mu$ l, 6.9 mM) at 20 °C. Excess DEPC causes some denaturation of the protein, resulting in a shift in the Soret maximum to a longer wavelength (*ca.* 430 nm) and an increase in turbidity. The addition was therefore terminated before this point.

The DEPC titration gave a shift towards the low-spin, apparently unbound form of P450 BioI H75R (417 nm) that, when fitted to a quadratic equation, gave a  $K_d$  of 1.07  $\mu$ M. Due to each mole of DEPC containing two active centres, this midpoint value equates to 2.14 nmoles of DEPC causing the loss of ligation in 50 % of the 2.8 nmoles of P450 BioI present. This decreased  $K_d$  (compared to that obtained with the wild-type enzyme) indicates that either another histidine residue modified that is related to the spin-state shift is modified, or else an unexpected alternate interaction is occurring.



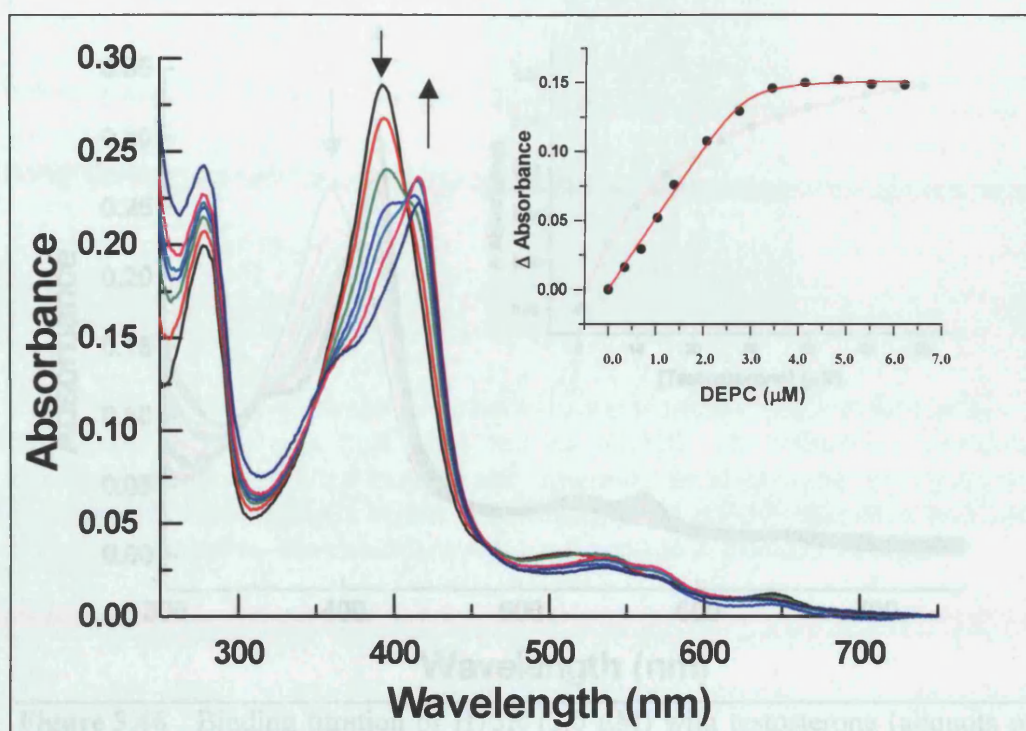


**Figure 3.45** Effect of the addition of aliquots of DEPC upon the spin-state of palmitoleic acid-bound H75R P450 BioI (2.8  $\mu\text{M}$ ). The Soret maximum shifts from 392 to 417 nm as DEPC is added. Arrows show the direction of change. Fitting the shift in the Soret maximum ( $A_{392} - A_{417}$ ) versus the concentration of DEPC to a quadratic equation gave a  $K_d$  of  $1.07 \pm 0.03 \mu\text{M}$  (inset).

#### 3.15.4 Binding constants of the H75 mutants

The binding constants for a selection of compounds (fatty acids, steroids and azoles) to the mutants was measured by spectral titration and compared to that of freshly prepared WT protein. Two or three examples of compounds from each of the classes of substances that P450 BioI is known to bind were assessed; i.e. three fatty acids (myristic, palmitic and lauric acid), two steroids (progesterone and testosterone) and two nitrogen containing inhibitors ( $\omega$ -imidazolyl-decanoic acid and 4-phenyl imidazole). In view of the observation that H75R is purified in a high-spin form, it was postulated that the arginine might result in tighter dissociation constants for the fatty acids evaluated.

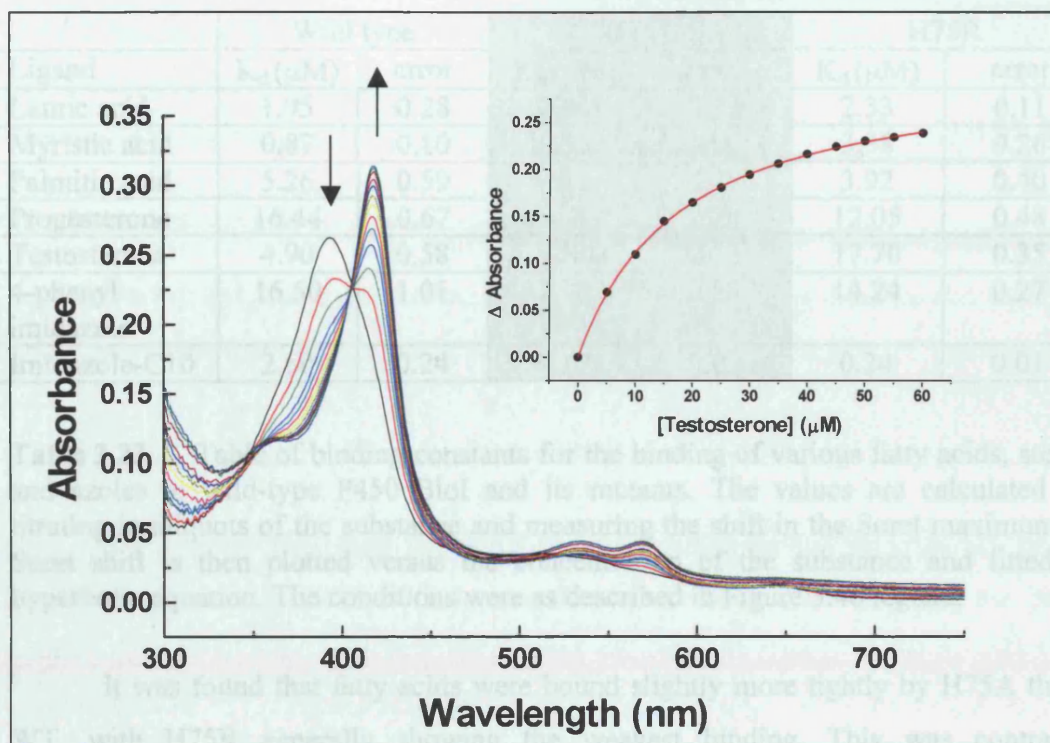


**Figure 3.46** Binding titration of H75R (3.0  $\mu\text{M}$ ) with testosterone (aliquots of a 12.5 mM stock solution) carried out in KPi buffer (50 mM, pH 7.0) at 30  $^{\circ}\text{C}$ . Shift in the Soret maximum from 392 nm to 417 nm can be seen, the arrows show the direction of change. Inset shows the plot of the change in Soret absorbance ( $A_{417} - A_{392}$ ) plotted against concentration of ligand, fitted to a rectangular hyperbola to give a  $K_d$  of 17.70  $\pm$  0.35  $\mu\text{M}$ .

The binding of fatty acids to the mutants caused the expected shift towards the high-spin form. As H75R is isolated in a high-spin form and H75A is mixed-spin (see Figures 3.40 and 3.41), all the proteins (8.0 nmol) were incubated with *E. coli* flavodoxin reductase (1.0 nmol) and YkuN (2.0 nmol) in the presence of a limiting amount of NADPH (8.0 nmol) to generate their low-spin forms prior to titration. The samples were incubated (30 minutes, 25  $^{\circ}\text{C}$ ) to allow full oxidation of any NADPH present prior to the addition of aliquots of fatty acid ligand. This procedure was not undertaken for the other reverse type I and type II shift ligands as the partial high-spin character of the protein aids their measurement. However, it should be noted that this means that the binding of these ligands (steroids and imidazolyl compounds) competes with varying amounts of the endogenous fatty acid.



Ligand	Wild type		H75A		H75R	
	$K_d$ ( $\mu$ M)	error	$K_d$ ( $\mu$ M)	error	$K_d$ ( $\mu$ M)	error
Lauric acid	1.95	0.28	0.90	0.13	2.33	0.11
Myristic acid	0.87	0.10	0.55	0.06	3.38	0.26
Palmitic acid	5.26	0.59	3.12	0.27	3.92	0.40
Progesterone	16.44	0.67	21.73	1.70	12.05	0.48
Testosterone	4.90	0.58	14.11	0.13	17.70	0.35
4-phenyl imidazole	16.50	1.01	7.93	0.83	14.24	0.27
Imidazole-C10	2.60	0.24	0.17	0.03	0.24	0.01

**Table 3.23** Table of binding constants for the binding of various fatty acids, steroids, and azoles to wild-type P450 BioI and its mutants. The values are calculated from titrating in aliquots of the substance and measuring the shift in the Soret maximum. The Soret shift is then plotted versus the concentration of the substance and fitted to a hyperbolic equation. The conditions were as described in Figure 3.46 legend.

It was found that fatty acids were bound slightly more tightly by H75A than by WT, with H75R generally showing the weakest binding. This was contrary to expectations, with the increasing charge of the side-chain being postulated to increase the strength of the ion-pairing with the substrate's carboxylate. The change in the D ring substituent of the steroid (hydroxyl for testosterone and a methyl-ketone for progesterone) caused an alteration in the order of binding affinity, with the WT binding testosterone tightest and H75R binding progesterone tightest. This may reflect the change in the substituent from the H-donor hydroxy group to the H-acceptor ketone. Mutation to the neutral alanine aided binding of 4-phenylimidazole, whilst replacement of the histidine with either alanine or arginine caused a lowering of the  $K_d$  value for Imidazole-C10. The size, flexibility and hydrophobicity of the side-chain may also play a role in these binding constants, as whilst arginine is the stronger base it has a larger more flexible side-chain.

Turnover of the mutants was carried out to confirm that the mutations were benign with respect to the capacity of P450 BioI to oxygenate fatty acids (see Section 2.8 for turnover experimental details). *E. coli* flavodoxin reductase (20 nmol), YkuN (20 nmol) and either mutant (50 nmol) were incubated in MOPS buffer (20 mM, pH 7.0, 100 mM KCl, 12 ml) for 16 hours at 23 °C, containing a suspension of myristic acid (1.0 mg, 4.0  $\mu$ mol) and NADPH (16  $\mu$ mol). Fatty acids were collected by acidification (1 M HCl,

pH 2.0) and extraction with chloroform (2 x 2.0 ml). The organic layer was evaporated to dryness, resuspended in methanol (1.5 ml) and analysed by electrospray ionisation mass-spectrometry (as previously described). Signals with an  $m/z$  of 243 corresponding to mono-hydroxylated myristic acid were observed for both mutants. H75A had converted 58.5 % of the starting material whilst H75R had converted 49.7 % compared to 60 % conversion for WT, i.e. the mutation had negligible effect upon the catalytic function of P450 BioI in hydroxylating myristic acid.

### **3.15.6 Conclusions**

The residue H75 does not seem to be the main residue involved in the ionic binding of ligands to P450 BioI. Its mutation had differing effects upon the binding properties of P450 BioI, and little effect upon catalysis. Its change to the neutral alanine residue caused an increasing affinity for fatty acids, the opposite result to that expected. From this, the influence of solvents and the binding of other C14 compounds, it is believed that P450 BioI binds substrates through mainly hydrophobic interactions.

### **3.16 Crystallisation Trials**

P450 BioI has been crystallised in earlier work (see Section 1.6.3) but attempts to solve the structure by molecular replacement methods proved unsuccessful. Samples of P450 BioI were screened in a variety of conditions using the Molecular Dimensions Ltd Clear Strategy Screen kits I and II at 4 and 20 °C. In most of the conditions a brown precipitate was observed to form. The stability of P450 BioI is enhanced by the binding of nitrogen donor ligands (see Section 3.10) and so the protein was mixed with 4-phenylimidazole and re-screened. Small brown rhombic crystals were observed to form under the following conditions;

Sodium formate (0.8 M), polyethylene glycol (PEG) 2K MME (25 %) at pH 6.5 (sodium cacodylate) and pH 8.5 (Tris.HCl).

Further hanging drop trays were set up with these conditions. Crystallisation of P450 BioI proved not very reproducible, with approximately one in four trays giving a crystalline product and all showing varying amounts of brown precipitate.

The crystals diffracted to 2.0 Angstrom resolution. Heavy atom soaking (mercury) was used to resolve the structure. The structure showed a tetrameric protein, which was found to be not P450 BioI, but glyceraldehyde-3-phosphate dehydrogenase (GAPDH) from *E. coli* [Duce *et al.*, 1996, Mougin *et al.*, 1998]. N-terminal sequencing of an early sample of P450 BioI revealed the presence of a small but significant amount of a second protein in the sample following purification using a Q-Sepharose column. From a search of the *E. coli* database, four proteins were identified that complied with the sequence and this confirmed the co-purified protein to be GAPDH from the *E. coli* host. The sequence of *E. coli* GAPDH is shown below, with the four sequenced residues shown in blue.

```
METKDLIVIGGGINGAGIAADAAGRGLSVLMLEAQDLACATSSASSKLIHGGLRYLEHYEFLVSE
ALAEREVLLKMAPHIAFPMPFRPLPHRPHLRPAWMIRIGLFMYDHLGKRTSLPGSTGLRFGANSVL
KPEIKRGFEYSDCWVDDARLVLANAQMVVRKGGEVLTRTRATSARRENGLWIVEAEDIDTGKKY
SWQARGLVNATGPWVKQFFDDGMHLPSPYGIRLIKGSHIVVPRVHTQKQAYILQNEDEKRVFVIP
WMDEFSIIGTTDVEYKGDPAVKIEESEINYLNVYNTHFKKQLSRDDIVWTYSGVRPLCDDSDS
PQAITRDYTLDIHDENGKAPLLSVFGGKLTTRYKLAHALEKLTPTYQYGIGPAWTKESVLPGGAIE
GDRDDYAARLRRYPFLTESLARHYARTYGSNSELLGNAGTVSDLGEDFGHEFYEAELKYLVD
HEWVRRADDALWRRTKQGMWLNADQQSRVSQWLVEYTQQRSLAS
```

**Figure 3.46** The amino-acid sequence of *E. coli* GAPDH that was found to co-purify with P450 BioI, as taken from the SWISS-PROT database. The first four residues that were sequenced are shown in blue.

This protein, due to its tetrameric nature [Duce *et al.*, 1996], formed a large lattice with P450 BioI occupying the gaps in the structure to give the red/brown colouring of the crystals. It was found that P450 BioI interacted with one monomer of GAPDH per every dimer of the tetrameric arrangement. However, it was seen that P450 BioI could bind in two places or in two different orientations to a monomer of GAPDH, with neither one being favoured over the other. As a result of this randomised placement of P450 BioI within the lattice its structure cannot be solved. Only the large iron atom can be accurately positioned. This association of P450 BioI with GAPDH does not appear to have any physiological relevance. No interaction of P450 BioI with GAPDH was observed by visible spectroscopy, the addition of GAPDH did not perturb the Soret absorbance. GAPDH is known to interact with proteins such as glycerol-3-phosphate dehydrogenase (GPDH) [Sullivan *et al.*, 2003], and specifically to proteins implicated in the pathogenesis of a variety of neurodegenerative disorders including the p-amyloid precursor protein [Schulze *et al.*, 1993] and the huntingtin protein [Mazzola and Sirover,

2001]. The subunit, GapB, is thought to mediate any protein-protein interactions [Baalmann *et al.*, 1996]. The presence of GAPDH was not resolved from P450 BioI by SDS-PAGE analysis of the protein prior to crystallisation, i.e. there are only trace amounts of GAPDH; but these impurities are sufficient to form the crystal lattice occupied by P450 BioI. The remaining P450 BioI sample used for crystallography was purified further by gel filtration (Sephacryl-200, see Section 2.6), which separated the proteins according to their bulk (the larger and heavier being quicker to elute). GAPDH, forming a tetramer of *ca* 224 kDa in mass [Yun *et al.*, 2000], is over three times larger than P450 BioI. The effectiveness of this purification step was assessed by carrying out an assay for GAPDH activity in accordance with the scheme below [Harris and Waters, 1976]:



The reaction can therefore be followed spectrophotometrically by the formation of NADH, which has an absorbance maximum at 342 nm. Analysis of purified P450 BioI revealed that the rate of NADH production had fallen by over 22-fold to virtually zero. This sample was therefore deemed pure.

Further screens were set-up with this purified sample of P450 BioI. However, so far no crystals have been obtained. It is likely that the previous crystals generated also contained this GAPDH lattice, as they were of similar shape and colour [Green, 2000]. This probably explains why molecular replacement methods failed to solve the structure. Further screens were prepared with a mixture of P450 BioI (either unbound, or bound to ketoconazole or 4-phenyl imidazole) and recombinantly expressed *E. coli* GAPDH (2 molar equivalents). The purified proteins were mixed together and sitting drop trays were prepared. A wide variety of conditions were screened using commercial screens (as before) but the only crystals generated were in identical conditions to those described above. This reflected formation of co-crystals in the same spacegroup as previously found and therefore they were also unsolvable. The crystallogenesis of P450 BioI was therefore abandoned. Future attempts to crystallise P450 BioI will probably focus on co-crystallising it. For example, it could be fused to a large maltose binding protein that is

relatively easy to crystallise by cloning into a vector such as pMAL c2G [NewEnglandBiolabs], e.g. a purine nucleoside phosphorylase from *S. mansoni* was crystallised by fusing to a maltose-binding protein [Pereira *et al.*, 2003], as was porcine heart mitochondrial NADP<sup>+</sup>-dependent isocitrate dehydrogenase [Ceccarelli *et al.*, 2002]. Alternatively, the GAPDH monomer could be mutated so that there is only one site of interaction per monomer resulting in a symmetrical arrangement. However, it would be difficult to predict the position of an appropriate mutation.

### 3.17 Conclusions

P450 BioI was over-expressed and isolated from a variety of *E. coli* hosts. Expression of the P450 was optimised in a strain of *E. coli* called Origami DE3, a strain that has been developed to aid formation of disulphide bonds in exogenous proteins. From this and unrestrained modelling of the protein it was thought that a disulphide bond may be present. Cysteine counting with Ellman's reagent indicated that upon reductive treatment with DTT more cysteines do indeed become available.

The thermal degradation of P450 BioI showed that the putative di-sulphide bond has negligible effect on the  $T_M$  of the protein (65.5 °C), as the value was consistent irrespective of pre-incubation of the protein with the reducing agent DTT. The saturation of the P450 with the fatty acid ligand palmitoleate did produce a destabilisation of the protein, reducing the  $T_M$  by *ca.* 4 °C. The binding of substrates such as fatty acids made little impact on the stability of the protein with regard to chemical degradation by the chaotrope Gdn.HCl. The loss of the heme cofactor from the apoprotein appeared unaffected by the addition of various ligands to the protein, the exception being the binding of nitrogen containing compounds such as azoles. These compounds are able to co-ordinate to the heme iron through the nitrogen's lone pair and hence have very tight binding constants. This may have resulted in these ligands remaining bound in the active site of the protein for longer and thereby aiding stabilisation of the protein.

The UV-visible absorption spectrum and both the far UV and visible-near UV CD spectra of P450 BioI in its native form as isolated from *E. coli*, were typical of a microbial P450 in an oxidised state. Various spectroscopic techniques such as EPR and

resonance Raman showed P450 BioI to have spectral characteristics typical of a P450 in a mixture of low- and high-spin states. Typically, bacterial P450s are isolated in the low-spin, unbound state, a shift to the high-spin form being induced by the addition of an exogenous lipophilic ligand.

Previous studies on *B. subtilis* P450 BioI had always isolated the protein in a high-spin form and whilst one group of researchers found this to be due to the presence of a fatty acid bound acyl-carrier protein [Stok and De Voss, 2000] a different group had found no trace of such a protein [Green *et al.*, 2001]. In this study P450 BioI was again isolated in a predominantly high-spin form and this was found to be due to palmitic acid being bound to a large proportion of the isolated protein. The high abundance of this fatty acid in *E. coli* and the tight binding of such a substrate by P450 BioI enabled this interaction. It was found that the flavodoxin native to *E. coli* was unable to drive the catalytic cycle of P450 BioI efficiently, meaning that any fatty acid bound to the protein in the expression host was unlikely to be oxidised and so would be retained.

P450 BioI was found to be capable of binding a variety of compounds including fatty acids native to *B. subtilis* and more exotic polycyclic substances. An ability to bind non-polar alkanes and arenes indicate that the P450 binds compounds mainly through hydrophobic interactions although the single ionic interaction of the fatty acid's carboxylate may aid correct positioning of the substrate and reduce any side reactions. The protein's ability to bind steroids was interesting given its high sequence similarity with another biosynthetic bacterial P450 – P450 eryF, but in BioI's case steroids bound through an iron-oxygen interaction resulting in a low-spin complex that disfavours product formation on thermodynamic grounds. Redox potentiometry showed that whilst the presence of a fatty acid in the active site raised the heme's potential by over 130 mV, encouraging electron transfer, the low-spin steroid form could only cause an increase of *ca.* 74 mV. From these studies it is proposed that P450 BioI's native substrate is a long-chain fatty acid such as palmitate.



***Chapter 4***  
***Cloning, Expression and***  
***Characterisation of YkuN and YkuP***

P450 BioI is typical of a class I cytochrome P450 in that it requires the presence of redox partners for it to carry out its catalytic role. Typically bacterial P450s are partnered by flavodoxins or ferredoxins, small proteins that contain either a flavin or iron-sulphur cofactor, respectively. These proteins shuttle the electrons from various NAD(P)H-oxidoreductases to their various redox partners such as P450s [Hawkes *et al.*, 2002], methionine and biotin synthase [Hall *et al.*, 2001, Wan and Jarrett, 2002] and photosystems [Nogues *et al.*, 2003]. The genome of *B. subtilis* contained two putative flavodoxin genes, *ykuN* and *ykuP*, with high sequence similarity to the well characterised flavodoxin from *D. vulgaris* (Hildenborough), the structure of which is shown below [Watenpaugh *et al.*, 1976]. These two genes were cloned, over-expressed and characterised in the context of their ability to act as functional redox partners to P450 BioI.

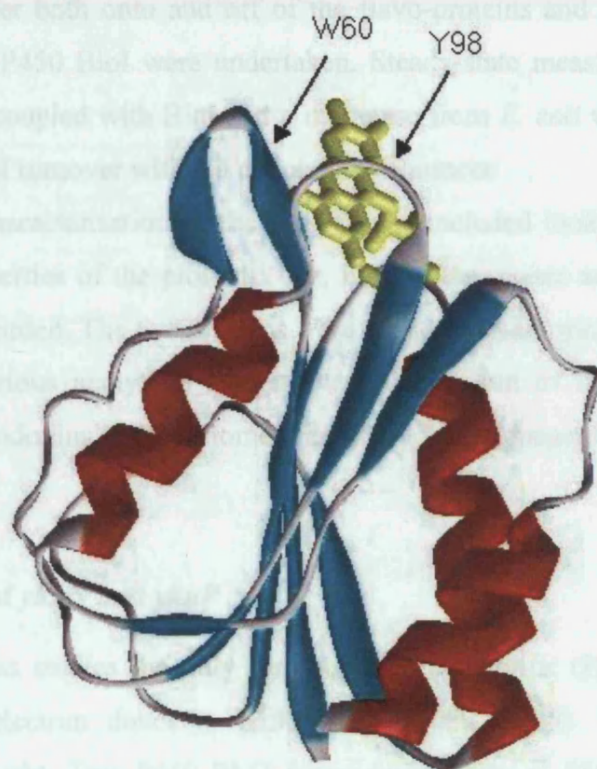


**Figure 4.1** Structure of the flavodoxin from *D. vulgaris* (Hildenborough) in its oxidised state [Watenpaugh *et al.*, 1976]. The FMN cofactor (yellow) is held between a highly conserved tryptophan in the 60 loop (W60) and tyrosine of the 90 loop (Y98). This flavodoxin has the typical fold of a central  $\beta$ -sheet (cyan) surrounded by  $\alpha$ -helices (red).

The following studies on the two *B. subtilis* flavodoxins YkuN and YkuP can be subdivided into several stages. Initially the genes were identified via BLAST searches of the *B. subtilis* genome using short-chain flavodoxins from species such as *D. vulgaris* and *D. desulfuricans* as templates. The flavodoxins are typically identifiable from the flavin binding region. The putative flavodoxin genes were then cloned into expression vectors to enable high expression of soluble protein in an *E. coli* expression host. Subsequent expression trials were carried out to maximise the yield of target protein. Basic characterisation such as N-terminal sequencing was then undertaken before the isolated proteins were examined for their electron transfer capabilities.

The overall aim being to build an *in vitro* catalytic system for P450 BioI, the flavodoxins from *B. subtilis* were examined for their ability to take-up and pass-on electrons. Studies such as measuring the reduction potentials of their cofactors, kinetics of electron transfer both onto and off of the flavo-proteins and more importantly their ability to reduce P450 BioI were undertaken. Steady-state measurements involving the two flavodoxins coupled with BioI and a reductase from *E. coli* were also carried out to gauge the speed of turnover within a cellular environment.

Further characterisation of the flavodoxins included looking at the stability and bio-physical properties of the proteins. CD, EPR, fluorescence and visual spectra of the proteins were recorded. The two proteins were found to be surprisingly similar kinetically and therefore various analytical studies were undertaken to find out why *B. subtilis* encodes two flavodoxins in its genome when they both appeared to function in a highly similar manner.

#### **4.1 Cloning of *ykuN* and *ykuP***

In previous studies the only ferredoxin in *B. subtilis* (Fer) had proved to be a relatively poor electron donor to P450 BioI [Green, 2000]. Thus alternative redox partners were sought. Two P450 BM3 homologues (class II P450s) exist in *B. subtilis* (CYP102A2 and CYP102A3) that could theoretically reduce P450 BioI, due to the flexible nature of the covalent link between their heme and flavin (reductase) domains. However, a more likely system is that of P450 BioI receiving electrons from one of the two flavodoxins in the *B. subtilis* genome, YkuN (158 amino acids) and YkuP (178



amino acids). These genes both show characteristic flavin binding domains and so the cloning, over-expression and purification of both proteins was carried out to assess their abilities as redox partners. Both genes are located in an operon consisting of four genes, *ykuN*, *ykuO*, *ykuP* and *ykuQ*. From alignments *ykuO* is believed to be a homologue of *E. coli* MioC, a flavin-containing protein [Birch *et al.*, 2000] and *ykuQ* to be involved in tetrahydropicolinate synthesis.

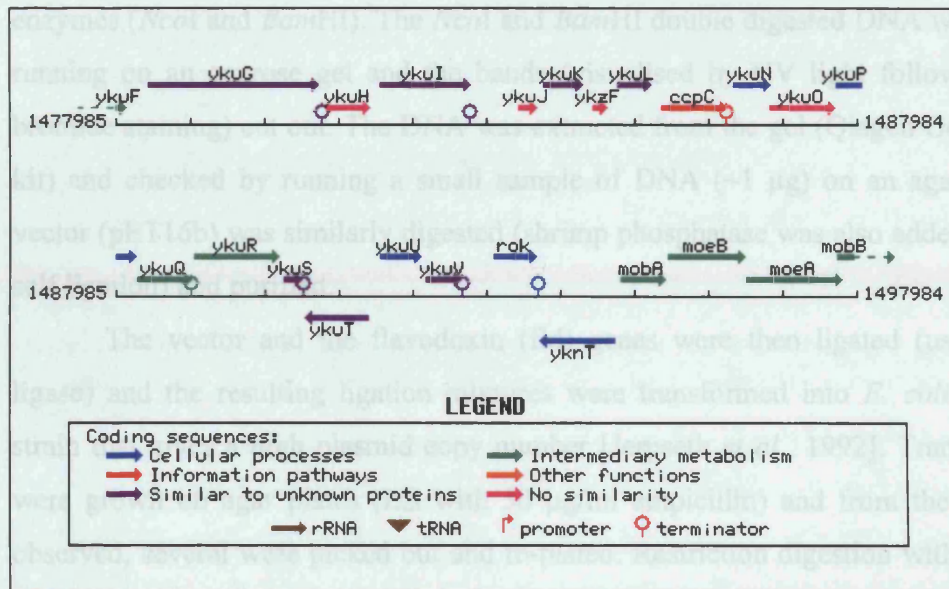


**Figure 4.2** Location of the only two flavodoxins in *B. subtilis*, *ykuN* and *ykuP*. The two genes are thought to be transcribed together with *ykuO* from a  $\sigma^A$ -type promoter with a further  $\sigma^A$ -type promoter downstream of *ykuP*, to control the transcription of *ykuQ*. The figure is taken from the *B. subtilis* genomic database (Pasteur Institute) [<http://genolist.pasteur.fr/Subtilist/>].

Chromosomal DNA from *B. subtilis* was prepared so that both the *ykuN* and *ykuP* genes could be amplified by PCR (polymerase chain reaction) in order for their subsequent cloning into expression vectors. An extensive method involving caesium chloride density centrifugation was used to isolate pure chromosomal DNA. An overnight culture of *B. subtilis* was inoculated into fresh LB and grown (37 °C) for ten hours to restrict sporulation. Cells were harvested by centrifugation and the DNA extracted and purified as described in Section 2.4.

Both the *ykuN* and *ykuP* genes were amplified via hot-start PCR techniques. Suitable primers (see 2.4.1) were designed to selectively amplify the region of DNA

encoding the *ykuN* or *ykuP* genes. The Roche Expand High Fidelity™ cloning kit was used to carry out the PCR work using a Perkin Elmer PCR cycler (for methodology see Section 2.4). The products of the PCR reaction were run on an agarose gel (1 %) to reveal bands of the correct size (*ykuN* was 0.59 kb, *ykuP* was 0.63 kb). The vector (pET16b) had been previously prepared by extraction of the vector (Qiagen kit) from an overnight culture of *E. coli* TG1. The PCR products were purified using a Qiagen Mini-elute column kit. The purified products were then double digested using the appropriate enzymes (*NcoI* and *BamHI*). The *NcoI* and *BamHI* double digested DNA was purified by running on an agarose gel and the bands (visualised by UV light following ethidium bromide staining) cut out. The DNA was extracted from the gel (Qiagen Gel Purification kit) and checked by running a small sample of DNA (~1 µg) on an agarose gel. The vector (pET16b) was similarly digested (shrimp phosphatase was also added to minimise self ligation) and purified.

The vector and the flavodoxin (*fld*) genes were then ligated (using T4 DNA ligase) and the resulting ligation mixtures were transformed into *E. coli* XL1-Blue, a strain that gives a high plasmid copy number [Jerpseth *et al.*, 1992]. Transformed cells were grown on agar plates (LB with 50 µg/ml ampicillin) and from the few colonies observed, several were picked out and re-plated. Restriction digestion with *NcoI/BamHI* was diagnostic for clones containing the appropriate inserts – producing bands of appropriate size for both vector and insert (*ykuN* was 0.59 kb, *ykuP* was 0.63 kb, vector 5.8 kb). Several clones were selected and submitted for sequencing.

The sequences of YkuN clones were identical to that reported in the database. Sequencing of the multiple YkuP clones revealed the absence of a single adenosine nucleotide compared to the *B. subtilis* genome sequence data. As a result, the protein product from the *ykuP* gene would be shorter than previously thought, the altered gene sequence having a stop codon (TGA) earlier than that of the original sequence (Figure 4.3). This would make the protein product of the *ykuP* gene 152 amino acids in length and not 178 as recorded in the data bank. This would mean that YkuP is a short chain fld (similar to YkuN) and not a long chain fld like that from *E. coli*. The shorter YkuP peptide has a predicted molecular weight of 16.77 kDa and a theoretical pI of 4.04 [NCBI SwisProt].

```

1 - ttg gcg aag att ttg ctc gtt tat gca aca
31 - atg tca ggc aac act gaa gct atg gca gat
61 - ttg att gaa aag ggg ctt cag gag gcg tta
91 - gca gaa gta gac cgt ttc gaa gca atg gat
121 - att gat gat gcc cag ctg ttt acc gat tat
151 - gac cat gtc ata atg gga acc tac acg tgg
181 - gga gac gga gat ctg cct gat gaa ttt tta
211 - gat ctt gtt gaa gac atg gag gag att gat
241 - ttt tcc ggc aaa aca tgc gct gta ttc ggt
271 - tcc ggt gat aca gca tat gaa ttt ttc tgc
301 - gga gcg gtt gat acg cta gag gca aaa ata
331 - aaa gaa cgc ggt gga gac att gtg ctg cct
361 - tcg gta aaa atc gaa aat aat cca gaa ggt
391 - gaa gaa gag gaa gaa tta ata aac ttc ggg
421 - aga caa ttc gca aag aaa aag cgg gtg cgc
451 - tgt ctg atc act cac tgg gaa ctg cta aaa
481 - cgg ctg ttc ctt ttt ttc ttg tct ttg tat
511 - ctt tcc ttt gat aca gta atg agg

```

**Figure 4.3** The documented DNA sequence of *ykuP* [Pasteur Institute (<http://genolist.Pasteur.fr/Subtilist/>)]. Shown in red is the additional base on the database sequence which DNA sequencing showed my clone did not have, and shown in blue is the termination site of my clone, the lack of a single adenosine residue resulting in a frame shift.

A sequence alignment of the two *B. subtilis* flavodoxins was performed with the well-studied short-chain flds from *C. beijerinckii* [Watt *et al.*, 1991] and *D. vulgaris* [Watenpaugh *et al.*, 1976], and the long chain flds from *E. coli* [Osborne *et al.*, 1991] and *Anacystis nidulans* [Hoover *et al.*, 1999] (Figure 4.4). The two aromatic residues that flank either side of the FMN cofactor are shown in red (tryptophan and tyrosine, except in the fld from *C. beijerinckii* where Met56 flanks the *re*-face) and the key region for binding the phosphate chain is highlighted in blue. This phosphate-binding motif can be represented as T/S-X-T-G-X-T with few exceptions [Mayhew and Tollin, 1992], so the substitution of a serine (Ser12) for a threonine in both *B. subtilis* flds is of note, although both residues can act as proton donors to the flavin.



YkuP long	MAKILLVYATMSGNTEAMADLIEKGLQEALAEVDRFEAMDIDDAQLFTDYYDHVIMGTYTW	60
YkuP short	MAKILLVYATMSGNTEAMADLIEKGLQEALAEVDRFEAMDIDDAQLFTDYYDHVIMGTYTW	60
YkuN	MAKALITYASMSGNTEDIAFI IKDTLQEYELDIDCVEINDMD-ASCLTSYDYVLIGTYTW	59
A. variabilis	SKKIGLFYGTQTGKTESVAEII RDEFG--NDVVTLHDVVSQA EVDTLNDYQYLIIGCPTW	57
Synechococcus	-SKIGLFFGTQTGNTTEELAQA IQAAFGG--SDIVELFVAEVDIEALRDFDQLIIGCPTW	57
E. coli FldB	-MNMGLFYGSSTCYTEMAAEKIRDIIG--PELVTLHNLKDDSPKLMEQYDVLIIGIPTW	56
E. coli FldA	-AITGIFFGSDTGNTENIAKMIQKQLG--KDVADVHDI AKSSKEDLEAYDILLGIPTW	56
C. crispus	--KIGIFSTSTGNTTEVADF IGKTLGA--KADAPIDVDDVTPQALKDYDLLFLGAPTW	56
D. vulgaris	MPKALIVYGSTTGNT EYTAETIARELADAGYEVDSDRAASVEAGGLFEGFDLVLLGCSTW	60
C. beijerinckii	---MKIVVWSGTGNT EKMAELIAGGIIESGKDVNTINVSVDNIDELLN-EDILILGCSAM	56
	: : : : * * * :	: : : : *
YkuP long	GDG---DLPDEFELD-LVEDMEEIDFSGKTC AVFGSGDTA--YEFFCGAVDTLEAKIKER	113
YkuP short	GDG---DLPDEFELD-LVEDMEEIDFSGKTC AVFGSGDTA--YEFFCGAVDTLEAKIKER	113
YkuN	GDG---DLPYEAED-FFEEVKQIQNLGLKTACFGSGDYS--YPKFCEAVNLFNVMLQEA	112
A. variabilis	NIG---ELQSDWEG-LYSELDDVDFNGKLVAYFGTGDQIGYADNFQDAIGILEEKISQR	112
Synechococcus	NVG---ELQSDWEA-LYDDLDDVDFSGKTITAYFGAGDQVGYADNFQDAMGVLEEKITSL	112
E. coli FldB	DFG---EIQEDWEA-VWDQLDDLNLGKIVALYGLGDQLGYGEWFLDALGMLHDKLSTK	111
E. coli FldA	YYG---EAQCDWDD-FFPTLEEIDFNGKLVALFGCGDQEDYAEYFCDALGTIRDIIEPR	111
C. crispus	NTGADTERSGT SWDEFLYDKLPEVDMKDL PVAIFGLGDAEGYPDNFCDAIEEIHDCFAKQ	116
D. vulgaris	GDD--SIELQDDFIP-LFDSLEETGAQGRKVACFGCGDSS--YEFYFCGAVDAIEEKLKNL	115
C. beijerinckii	GDEV---LEESEFEP--FIEEISTKISGKKVALFGSYGWGD----GKWMRDFEERMNGY	106
	. . . * : *	: : :
YkuP long	GGDIVLP-----SVKIENNPEGEEEE--LINFGRQFAKKKRV	150
YkuP short	GGDIVLP-----SVKIENNPEGEEEE--LINFGRQFAKKS--G	148
YkuN	GAAVYQE-----TLKIELAPETDEDVESCR AFARGFLAWADY	150
A. variabilis	GGKTGVYWS TDGYDFNDSK-ALRNGK-FVGLALDEDNQSDLTDDRIKSWVAQLKSEFGL	169
Synechococcus	GGKTGVGQWPTAGYDHSESK-AERD GK-FVGLAIDEDNQPELTAERIQAWVAQLKPAFGL	169
E. coli FldB	GVKFVG YWPTEGYEFTSPKPVIADQGLFVGLALDET NQYDLSERIQSCEQILNEMA EH	171
E. coli FldA	GATIVGHWP TAGYHFEASK-GLADDDHFVGLAIDEDRQPELTAERVEK VVKQISEELHLD	170
C. crispus	GAKPVGFSNPDDYDYEEKS-SVRD GK-FLGLPLDMVNDQIPMEKR VAGVWEAVVSETGV	173
D. vulgaris	GAEIVQD-----GLRID--GDPRAARD D IGVWAHDVRGAI---	148
C. beijerinckii	GCVV VET-----PLIVQNEPDEAEQDCIEFGKKIANI---	138
	* : : . :	.
YkuP long	CLITHWELLKRLFLFFLSLYLSFDTVMR	178
YkuP short	CAV-----	151
YkuN	NKE-----KIHVS	158
A. variabilis	-----	
Synechococcus	-----	
E. coli FldB	YA-----	173
E. coli FldA	EILNA-----	175
C. crispus	-----	
D. vulgaris	-----	
C. beijerinckii	-----	

**Figure 4.4** An amino acid sequence alignment of the *B. subtilis* flavodoxins YkuN and YkuP with flavodoxins from other species. The alignment uses the YkuP sequence determined from our clones (YkuP short) and the sequence predicted from genome sequencing (YkuP long). These sequences are aligned with the short chain flavodoxins from *Desulfovibrio vulgaris* (D. vulgaris) and *Clostridium beijerinckii* (C. beijerinckii), and the long chain flavodoxins from *E. coli* (E. coli FldA and E. coli FldB), *Anabaena variabilis* 7120 (A. variabilis), *Synechococcus* sp. PCC 7002 (Synechococcus) and *Chondrus crispus* (C. crispus). Performed using the CLUSTAL W programme [Thompson *et al.*, 1994]. Asterisks indicate identical residues in each protein. Double and single dots indicate conservation of highly similar and similar amino acids, respectively, according to criteria set in the program. Interestingly, the additional residues of YkuP long appear at the end of the alignment and not in the insertion region seen in the typical long chain flds, a further indication that my short chain clone is correct.

## 4.2 Over-expression and purification of YkuN and YkuP

The plasmids containing the putative flavodoxins YkuN and YkuP were transformed into four *E. coli* cell strains and the expression of the flds assessed by SDS PAGE. Transformants were grown (37 °C, 230 rpm) on a small scale (10 ml LB) and at an OD<sub>600</sub> of 1.0 split into two and one half induced with IPTG (0.1 mM). Samples were taken after 1, 5 and 14 hours to look for over-expression of the proteins. From the results of the SDS PAGE analysis it was clear that YkuN, the 17.8 kDa protein, was expressed in all four cell strains when induced with IPTG (0.1 mM). YkuP was also expressed in all cell lines tested, again under the induction of IPTG.

<i>E. coli</i> strain	Description	Genotype	Expression of YkuN	Expression of YkuP
BL21(DE3)	General purpose expression host	F <sup>-</sup> ompT hsdS <sub>B</sub> (r <sub>B</sub> <sup>-</sup> m <sub>B</sub> <sup>-</sup> ) gal dcm (DE3)	Very Good	Very Good
HMS174 (DE3)	General expression host	F <sup>-</sup> recA1 hsdR(r <sub>12</sub> <sup>-</sup> m <sub>12</sub> <sup>-</sup> ) rif <sup>r</sup> (λDE3)	Good	Good
HMS174 (DE3) pLysS	High-stringency expression host	F <sup>-</sup> recA1 hsdR(r <sub>12</sub> <sup>-</sup> m <sub>12</sub> <sup>-</sup> ) Rif <sup>R</sup> (λDE3) pLysS(Cm <sup>R</sup> )	Very Good	Very Good
Rosetta (DE3)	Enhances expression of codons rare in <i>E. coli</i>	F <sup>-</sup> ompT hsdS <sub>B</sub> (r <sub>B</sub> <sup>-</sup> m <sub>B</sub> <sup>-</sup> ) gal dcm lacYI (DE3)pRARE (Cm <sup>R</sup> )	Poor	Good

**Table 4.1** Expression of the flavodoxins YkuN and YkuP in various *E. coli* strains, as assessed by growth of cultures on a small (5 ml) scale and analysis of whole cell samples by SDS PAGE. Expression was judged by eye according to the intensity of the flavodoxin protein bands following gel staining. All cultures were grown to stationary phase and their OD<sub>600</sub> measured. The isolated samples were diluted (with sterile LB) to achieve an OD<sub>600</sub> of 1.0 to enable identical aliquots to be added to the gel for consistency.

Large scale (6 l) cultures of the YkuN transformant were carried out using the HMS174 (DE3) pLysS cell strain, as this gave good over-expression of the protein and the pLysS T7 lysozyme function would aid protein recovery (it cuts a specific bond in the peptidoglycan layer of the *E. coli* cell wall [Inouye *et al.*, 1973]). The large scale preparation (6.0 l LB) yielded a small cell pellet, but it was dark blue in colour indicating high expression of YkuN in its semiquinone form. Reduction of a sample of the cell

extract with sodium dithionite gave a bleaching of the absorbance between 500 and 600 nm indicative of the reduction of a semiquinone flavodoxin to its hydroquinone form. Unlike the *E. coli* flavodoxin, which had been prepared previously for use in turnover studies (see Section 2.6), the YkuN flavodoxin remained in its semiquinone blue state upon the lysing of the cells and during dialysis of the cell extract. Only after binding to and washing of the Q-Sepharose anion exchange column was YkuN observed to fully oxidise to its yellow form. It is likely that YkuN has a more stable semiquinone in the presence of atmospheric O<sub>2</sub> compared to that of *E. coli* flavodoxin (FldA) that is isolated in its oxidised form [McIver *et al.*, 1998].

Two 3.0 l preparations of the *ykuP*-containing construct transformed into the expression cells BL21 (DE3) pLysS and HMS174 (DE3) pLysS were undertaken to evaluate which produced the most protein. As with YkuN, the HMS174 (DE3) pLysS transformant produced a small dark blue pellet indicative of high protein expression. The BL21 (DE3) pLysS transformant (a strain deficient in the *lon* and *ompT* proteases [Grodberg and Dunn, 1988]) produced a slightly larger pellet of green colouration. As the lighter colour could be due to equal expression but more flavodoxin in the oxidised form, the cell extracts were analysed for flavin content. After dialysing the cell extract overnight (in Tris.HCl buffer, 50 mM, pH 7.0) most of the flavin content had oxidised. To ensure full oxidation, air was gently bubbled into the samples until the absorbance at 466 nm did not change. The absorbance of the FMN peak at 466 nm was used to calculate the amount of flavoprotein present ( $A_{466} = 1 = 8250 \text{ M}^{-1}\text{cm}^{-1}$  [Macheroux 1999]) as shown in Table 4.2.

Cell line	Cell extract (ml)	A <sub>466</sub> nm (A.U.) (corrected for dilution)	Flavin (mg/ml)	Total flavoprotein (mg)
BL21 (DE3) pLysS	75	1.615	3.97	298
HMS174 (DE3) pLysS	76	1.590	3.91	297

**Table 4.2** Comparison of the expression level of YkuP in two *E. coli* cell strains. Spectra were measured (spectrum from 250 to 750 nm recorded) with a Varian Cary50 UV-visible spectrophotometer using a 1 cm pathlength cell. Cell extract was diluted (20 fold) in Tris.HCl buffer (50 mM, pH 7.5) prior to measurements. A.U. refers to the relative absorption of the undiluted sample. This assay measured total cellular flavin, the

assumption is made that the expression levels of flavin-containing proteins native to *E. coli* are the same in both strains.

As both of the cell strains expressed YkuP in similar amounts, HMS174 (DE3) plysS was chosen for all future work as this gave direct comparison with YkuN and the dense blue colour of the cells made assessment of expression easy. It was notable that YkuP appeared to be more easily oxidised than YkuN, converting to the oxidised yellow flavin form upon dialysis.

#### 4.2.1 Purification of YkuN and YkuP

The purity at each stage of the purification protocol was determined by measuring the ratio of the peak heights at  $A_{280}$  nm (total protein) and  $A_{460}$  nm (FMN cofactor peak). A 280 nm : 462 nm ratio of 6:1 was indicative of pure YkuN and a ratio of 280 nm : 456 nm of 3.5:1 was indicative of pure YkuP. These values were calculated from the absorption features of the electrophoretically homogeneous flavodoxins. YkuN, containing two tryptophans compared to YkuP's one, would be expected to have a higher protein : flavin absorbance ratio.

Purification Stage	Total protein (mg)	Total Fld (mg)	Fld/ Protein	Stepwise purification fold	Overall purification fold
Cell Lysate	6658	531	0.08	1	1
Ammonium sulphate	2365	449	0.19	2.4	2.4
Phenyl-Sephadex	861	353	0.41	2.2	5.1
Q-Sephadex	265	191	0.72	1.8	9.0
S-200	118	112	0.95	1.3	11.9

Purification Stage	Stepwise Yield %	Overall Yield %
Lysate	100	100
Ammonium sulphate	84.6	84.6
Phenyl Sephadex	78.6	66.5
Q-Sephadex	54.1	36.0
S-200	58.6	21.1

**Table 4.4** Purification data from a typical 6.0 litre preparation of YkuP (16.8 kDa). YkuP concentration was determined from the FMN oxidised flavodoxin spectra using  $\epsilon$

$_{446} = 10.62 \text{ mM}^{-1}\text{cm}^{-1}$  (see method 2.8 for determination of coefficient). Total protein concentration was determined spectrophotometrically by  $A_{280} = 1 = 1 \text{ mg ml}^{-1}$ . Ammonium sulphate refers to protein left in solution after addition of 70 % w/v ammonium sulphate. Phenyl Sepharose and Q-Sepharose are hydrophobic interaction and anion exchange column chromatography matrices; the values refer to the composition of the protein collated post elution. S-200 is a Sephacryl S-200 gel filtration step.

The protein was analysed by SDS PAGE (15 %) to gauge the purity after each step in the purification procedure. A gel of the pure protein is shown in Figure 4.5. As *E. coli* expresses several flavin-containing proteins itself, the amount of YkuP in the cell extract determined from flavin absorbance alone will be over-estimated. Indeed, *E. coli* is known to contain both FAD-containing reductase and FMN-containing flds, both of which have been purified in this work (see Section 2.6).

The analysis of the purity of YkuP by SDS PAGE revealed that the protein migrates with a mass corresponding to 20 kDa (see Figure 4.5). Whilst this mass is in agreement with that published in the *B. subtilis* sequence database, it does not agree with our sequence data (see Section 4.1). Further characterisation of the protein's mass was undertaken to ascertain whether the protein ran anomalously on the SDS PAGE or if the sequencing data are incorrect. Due to the acidity of the protein (theoretical pI = 4.1 [Subtilist web server, Pasteur Institute]) electro-spray mass-spectrometry was not possible as removal of buffer ions (necessary for mass determination by this technique) causes precipitation of the protein to occur. MALDI mass-spectrometry was therefore used, a technique that, although less accurate, uses a matrix to fix the protein for ionisation. This gave the mass of YkuP to be 16.53 kDa and the mass of YkuN to be 17.68 kDa. Both these measured values were within 1.3 % of the theoretical values.

For YkuN, as before, the values for the protein-to-flavin ratio as determined spectroscopically do not take into account *E. coli*'s endogenous flavin-containing proteins in the cell lysate. Following column chromatography using the matrices shown below (for techniques see 2.6) the flavoproteins were deemed to be pure by SDS PAGE analysis. An apparent difference in the mass between the two proteins can be clearly seen in the gel shown below. The SDS PAGE indicates that YkuP's migration rate is slower than might be expected for a protein of its size. From the MALDI mass-spectrometry and

the DNA sequencing we know that *B. subtilis* contains two short chain flds. Thus, YkuP's migration on SDS-PAGE leads to an overestimation of its true molecular mass.

Purification Stage	Total protein (mg)	Total Fld (mg)	Fld/ Protein	Stepwise purification fold	Overall purification fold
Cell Lysate	3608	492	0.14	1	1
Ammonium sulphate	2304	481	0.21	1.5	1.5
Phenyl-Sephadex	1191	381	0.32	1.5	2.3
Q-Sephadex	231	157	0.68	2.1	4.9
S-200	114	103	0.90	1.3	6.4

Purification Stage	Stepwise Yield %	Overall Yield %
Lysate	100	100
Ammonium sulphate	97.8	97.8
Phenyl sephadex	79.2	77.4
Q-Sephadex	41.2	31.9
S-200	65.6	20.9

**Table 4.5** Purification data from a typical 6.0 litre preparation of YkuN (17.8 kDa). YkuN concentration was determined from the FMN oxidised flavodoxin spectra using  $\epsilon_{446} = 10.94 \text{ mM}^{-1}\text{cm}^{-1}$  (for coefficient calculation see Section 2.8). Total protein concentration was determined spectrophotometrically by  $A_{280\text{nm}} = 1 = 1 \text{ mg ml}^{-1}$ . Ammonium sulphate refers to protein left in solution after addition of 60 % w/v ammonium sulphate. Phenyl Sephadex and Q-Sephadex are the column chromatography matrices; the values refer to the composition of the protein collated post elution. S-200 is a Sephadex S-200 gel filtration step.



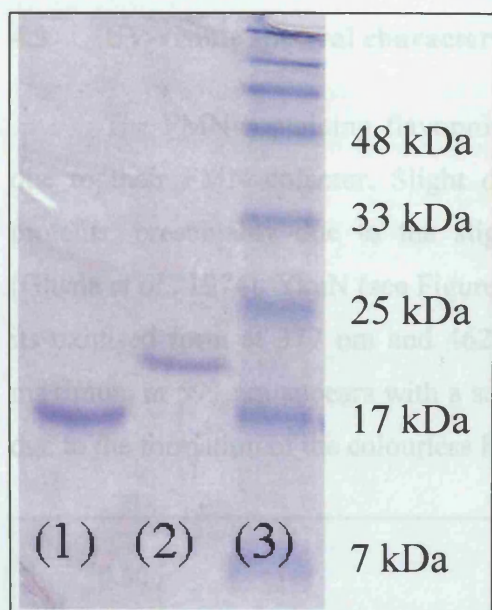


**Figure 4.5** SDS PAGE of the purified samples of YkuN (lane 1, predicted mass 17.8 kDa) and YkuP (lane 2, predicted mass 16.8 kDa) showing the difference in the apparent molecular weight of the two flds. The molecular weight marker (lane 3) is pre-stained broad-range marker from NEB, the mass of relevant bands is indicated alongside. YkuP shows low electrophoretic mobility, with an apparent mass of *ca.* 20 kDa on the gel.

The isolated and purified protein was WET blotted (see Section 2.7) and submitted for N-terminal amino acid sequencing at the in-house PNACL facility.

Cycle No	YkuN		YkuP	
	Residue	Amount (pmol)	Residue	Amount (pmol)
1	Alanine	810.87	Alanine	580.90
2	Lysine	564.30	Lysine	405.94
3	Alanine	781.55	Isoleucine	627.37
4	Leucine	625.91	Leucine	504.08
5	Isoleucine	781.30	Leucine	549.27
6	Threonine	351.05	Valine	508.75
7	Tyrosine	608.87		

**Table 4.4** The results of N-terminal sequencing of the two flavodoxins. Comparison with the *B. subtilis* genome database showed that the sequences are correct for both proteins, with the N-terminal methionine having been lost.

### 4.3 UV-visible spectral characteristics of YkuN and YkuP

The FMN-containing flavoproteins YkuN and YkuP have characteristic spectra due to their FMN cofactor. Slight differences exist between the spectra of the two proteins, presumably due to the slightly differing environment of the chromophore [Ghisla *et al.*, 1974]. YkuN (see Figure 4.6) exhibits two peaks due to the FMN moiety in its oxidised form at 377 nm and 462 nm. When reduced to its semiquinone form the maximum at 593 nm appears with a second peak at 351 nm. These peaks then disappear due to the formation of the colourless hydroquinone as the second electron is added.

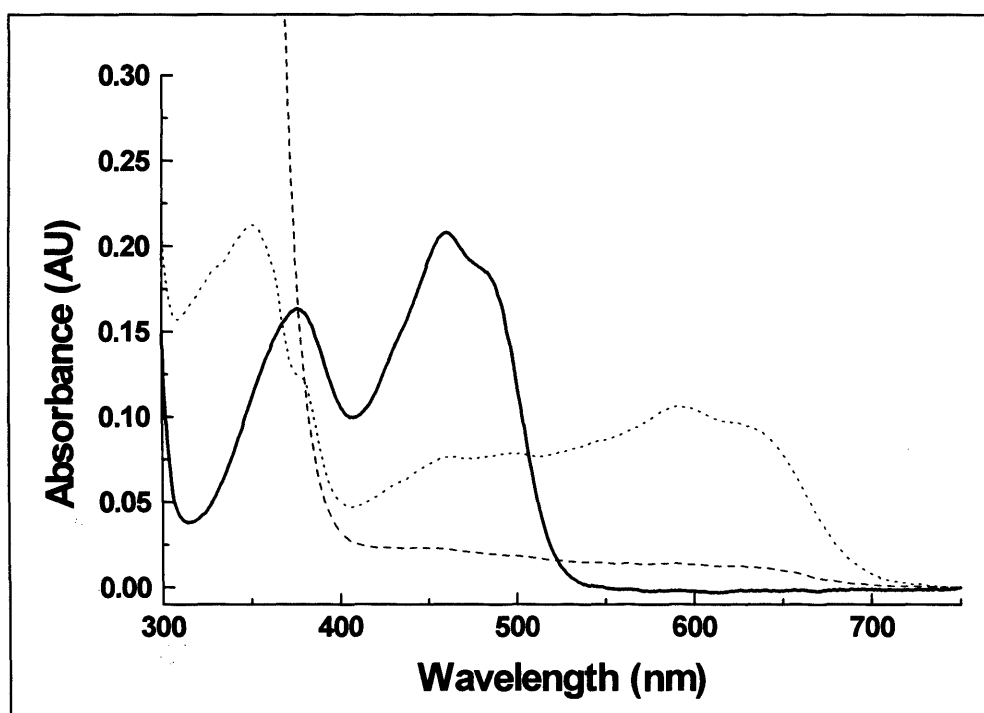


**Figure 4.6** Spectra of pure YkuN (24  $\mu$ M) showing the oxidised (solid line) form with spectral maxima at 377 and 462 nm, semiquinone (dotted line) form with maxima at 593 nm and 351 nm, and the reduced form (dashed line) of the fld. Spectra were obtained at 20°C in KPi buffer (50 mM, pH 7.0), in a 1 cm path-length cell using a Varian Cary50 spectrometer.

The UV-visible spectrum of YkuP (see Figure 4.7) also shows the typical flavin features, although the maximum for the longer wavelength oxidised peak is blue shifted by five nanometres (457 nm) compared to YkuN (462 nm). This shift in the maximum suggests that the FMN cofactor is more buried in YkuN, being shielded from solvent [Losato *et al.*, 1997, Maldonado *et al.*, 1998]. The fully reduced hydroquinone form of

YkuP is very difficult to isolate. This is possibly as a result of the semiquinone/hydroquinone redox potential being very negative. For comparison, the *E. coli* flavodoxin exhibits an oxidised form with FMN maxima at 372 and 466 nm, and the semiquinone maximum at 583 nm [McIver *et al.*, 1998]. The different values suggest a less solvent exposed cofactor in the oxidised state in the *E. coli* FLD, but in the semiquinone state the FMN maximum at 583 nm implies slightly greater solvent exposure than the *B. subtilis* fld's FMN at approx. 590 nm. Therefore less of a conformational change may be expected in the FMN-binding region upon reduction of YkuN/P *c.f.* *E. coli* FLD [Hoover *et al.*, 1997].

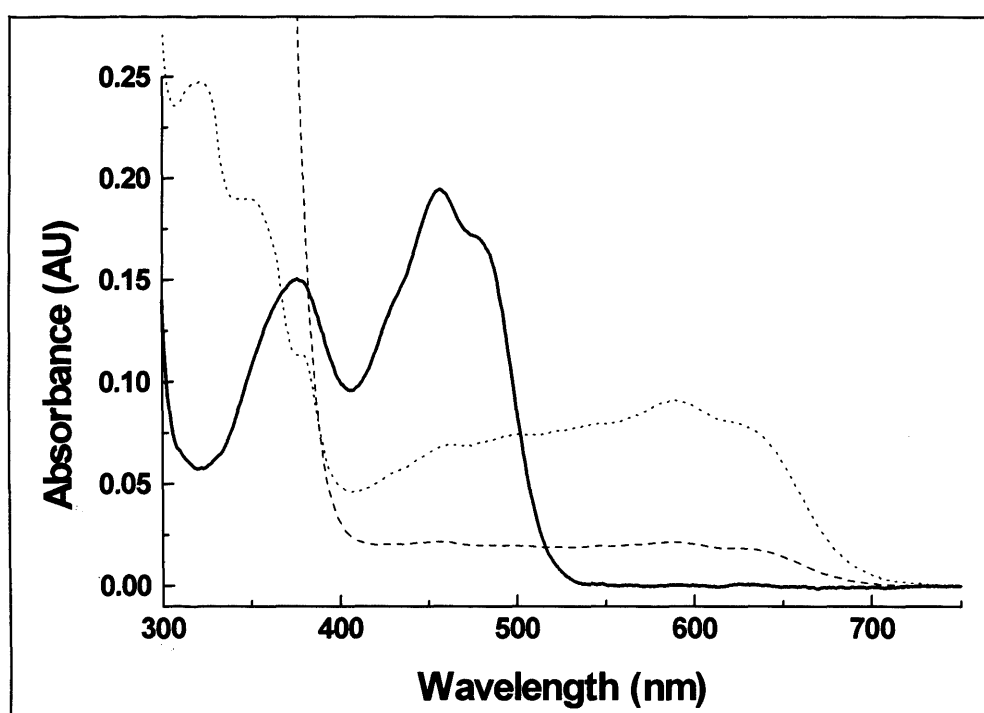


**Figure 4.7** UV-visible spectra of YkuP (22  $\mu$ M) showing the oxidised (solid line) form with spectral maxima at 377 and 457 nm, the semiquinone (dotted line) form with maxima at 590 nm and 351 nm, and the reduced form (dashed line) of the fld. Residual semiquinone can be seen in the sample treated with excess dithionite. Conditions as described in Figure 4.6.

#### 4.4 Secondary structure determination by CD

Fingerprint far UV and near UV-visible CD spectra of the two holoflavodoxins are shown below in Figure 4.8. Of the flds characterised to date, all exhibit a similar fold

(see Figure 4.1) consisting of a five-stranded central parallel  $\beta$ -sheet sandwiched between four  $\alpha$ -helices, the FMN cofactor held non-covalently between two loops [Watt *et al.*, 1991, Romero *et al.*, 1996, Hoover *et al.*, 1997, Freigang *et al.*, 2002]. The far UV CD spectra of the two *B. subtilis* flds is in agreement with this general topology, with a large amount of  $\alpha$ -helix structure predicted. There is a notable difference in the overall profile of the fld far UV CD spectra implying that YkuN has a lower amount of  $\alpha$ -helix in its secondary structure compared to YkuP.

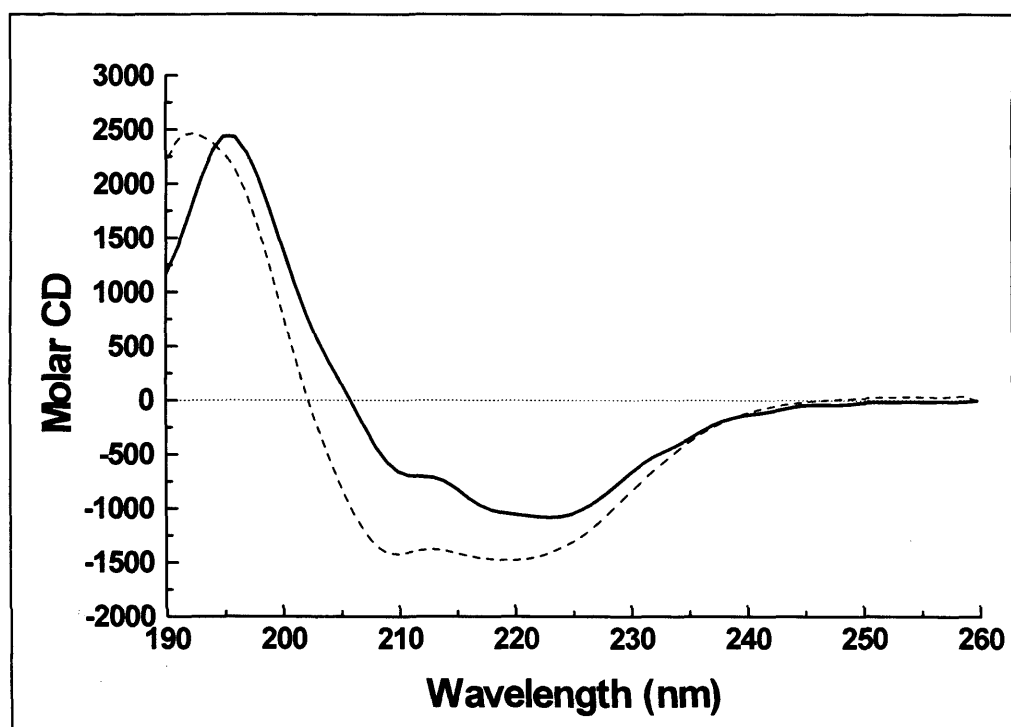


**Figure 4.8** CD spectra of YkuN (solid line) and YkuP (dashed line) at 0.2 mg/ml in KPi (50 mM, pH 7.0). The spectra show YkuP to be mostly  $\alpha$ -helical in nature whilst YkuN apparently contains a lesser amount of helix. Spectra were recorded using a JASCO spectropolarimeter, 0.1 cm pathlength, at 25 °C.

The far UV CD of the fld apoproteins was also measured (Figure 4.9). The apoflavodoxins were generated by acid precipitation with trichloroacetic acid (for methodology see Section 2.8 [Wassink and Mayhew, 1975]). There is little difference between the profiles of the holo- and apo-enzyme in the case of YkuN, but a notable difference can be seen upon removal of the FMN for the structure of YkuP.

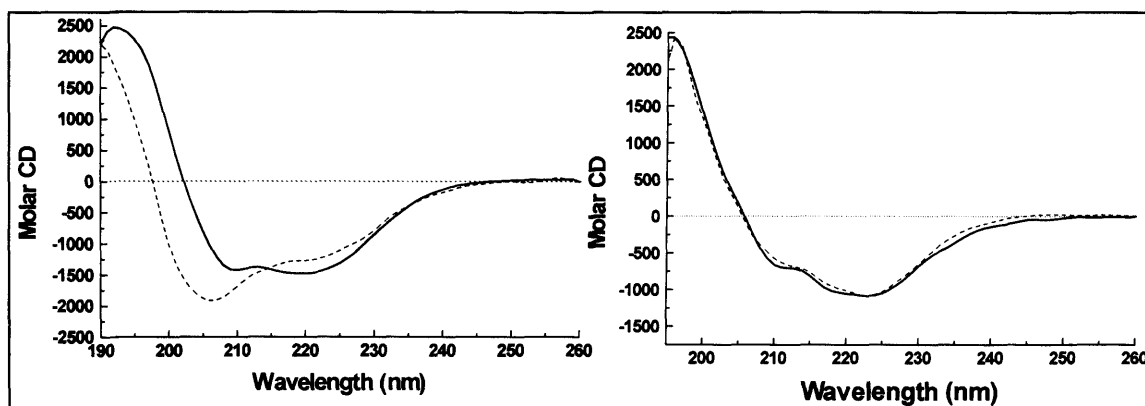


**Figure 4.9** Far UV CD profiles of the holo- (solid line) and apoproteins (dashed) of YkuP (on left) and YkuN (on right) are compared. Both proteins are at a concentration of 0.25 mg/ml, conditions as described in Figure 4.8.

The generation of the apoprotein of YkuP has either caused a loss in the degree of  $\alpha$ -helical content or an increase in the amount of random coil. Both possibilities seem quite extreme as the FMN is held between two loops on the surface of the protein, but it is possible that the treatment to remove the cofactor has caused partial unfolding or restructuring of the apoprotein. For example, it has been seen that removal of the FMN can cause subtle rearrangement of the flavin-binding loops in the *D. vulgaris* flavodoxin [D'Anna and Tollin, 1972] and that the close stacking of the two loops in *Anabaena* PCC 7119 apoflavodoxin give rise to a new compact fold [Genzor *et al.*, 1996].

Near UV-visible CD spectra for both the flavoproteins were carried out on the holoprotein forms (Figure 4.10). There is little difference in the visible spectrum between the two flds, they both show negative ellipticity between 300 and 425 nm typical of flavodoxins mainly due to the chiral signal from the FMN cofactor [Edmondson and Tollin, 1971], with a minima in the visible CD signal at approximately 303 and 375 nm. They show a slight difference in the wavelength of the minimum between 350 and 400 nm (YkuN minimum at 375 and YkuP at 370 nm), which is reflected also in the differences observed in the UV-visible spectra of the two flds. For comparison, the long-chain flavodoxin from *E. coli* (FldA) also shows negative ellipticity (310 – 450 nm), but has a single maximum at 365 nm [Munro *et al.*, 1999]. In the near-UV region, 260 – 300 nm, the spectrum has a band of negative ellipticity at 270 nm (the minimum ellipticity for YkuN is at 275 nm, and at 272 nm for YkuP) followed by a strong positive signal at around 285 nm (maximum for YkuN at 287 nm, and for YkuP at 285 nm).



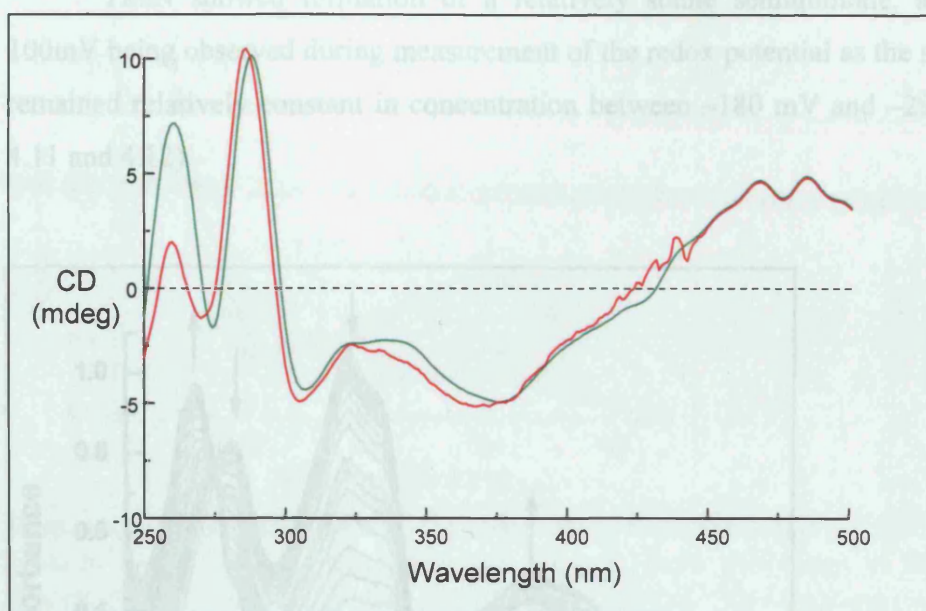


**Figure 4.10** The near UV-visible CD of YkuN (green) and YkuP (red) at approx. 2.5 mg/ml in a 1 cm path-length cell in KPi (pH 7.0, 50 mM) at 22 °C.

#### 4.5 Midpoint reduction potentials

The midpoint reduction potentials for the oxidised/semiquinone and semiquinone/hydroquinone couples of both the *B. subtilis* flavodoxins were measured to understand their thermodynamic properties and to rationalise their relative abilities in passing electrons from an FAD-containing reductase onto the ferric form of P450 BioI.

Midpoint reduction potentials were measured by potentiometric titration [Dutton 1978]. The redox potentials of both flavodoxins were measured anaerobically (Belle technology glove box, < 4 ppm O<sub>2</sub>) with a calomel electrode by addition of small aliquots of sodium dithionite to reduce the FMN, and potassium ferricyanide to oxidise the cofactor. After each addition of either oxidising or reducing agent, the UV-visible spectrum was recorded and the potential of the solution noted (see Section 2.8) [Munro *et al.*, 2001]. A plot of the potential versus either the formation and decay of the semiquinone (maximum at *ca* 590 nm) or the decrease of the yellow oxidised FMN peak (*ca* 460 nm) allows the determination of both the oxidised/semiquinone (OX/SQ) and the semiquinone/hydroquinone (SQ/HQ) couples from fitting to a two electron Nernst equation (Equation 12).



YkuN showed formation of a relatively stable semiquinone, a plateau of *ca* 100mV being observed during measurement of the redox potential as the stable blue form remained relatively constant in concentration between -180 mV and -290 mV (Figures 4.11 and 4.12).

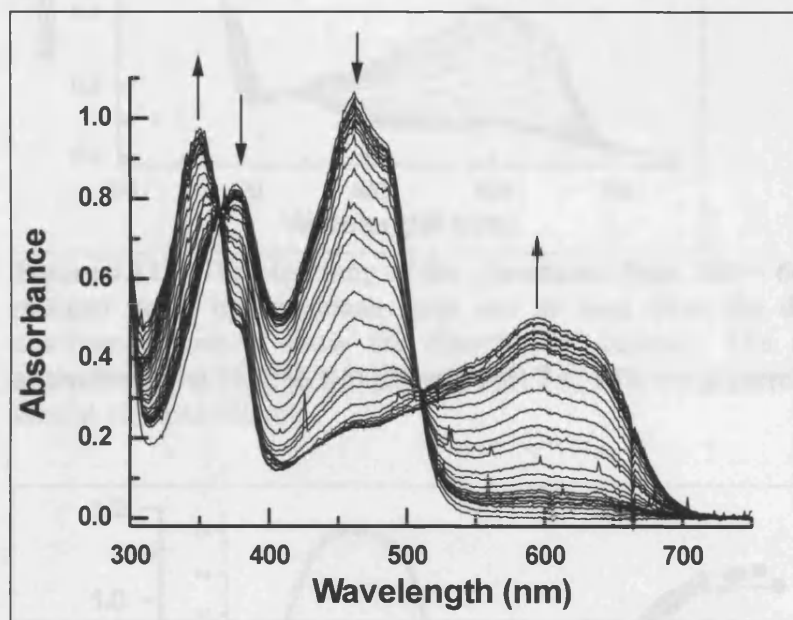


**Figure 4.11** Spectral changes observed as the flavodoxin (YkuN [0.12 mM]) is reduced from the oxidised (yellow) to the neutral semiquinone (blue) form. Arrows indicate the direction of absorption change during the reduction process between +100 mV and -190 mV. The titration was carried out anaerobically at 25°C in KPi (50 mM, pH 7.0, 10% v/v glycerol). Two isosbestic points can be seen at 365 nm and 510 nm during the transition from oxidised to semiquinone form

The spectra of YkuN show two isosbestic points at 365 nm and 510 nm upon the reduction of the oxidised FMN cofactor to its semiquinone form. Further reduction to the hydroquinone form yielded isosbestic points at 331 nm, 368 nm and 431 nm. As expected the FMN of YkuN forms the blue neutral semiquinone upon single electron reduction indicative of the protonation of the flavin N(5) atom. The semiquinone is stable over a range of approximately 150 mV, this stabilisation of the semiquinone is typical of flavodoxins [Mayhew and Tollin, 1992, Jenkins and Waterman, 1998] resulting in a very negative potential for the addition of the second electron to form the hydroquinone.

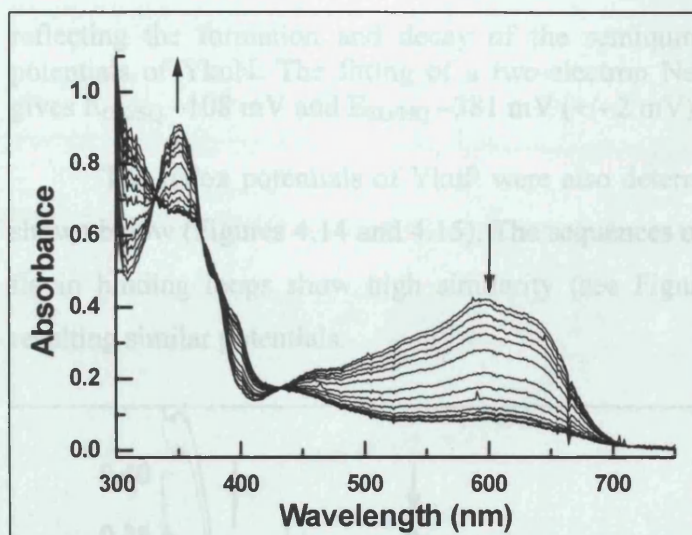


**Figure 4.12** The bleaching of the absorbance from 500 – 600 nm as YkuN is further reduced to its hydroquinone form can be seen from the decay of the semiquinone absorbance (arrows show the direction of change). The titration was carried out anaerobically at 25°C in KPi (50 mM, pH 7.0, 10% v/v glycerol). Isosbestic points can be seen at 429 and 370 nm.

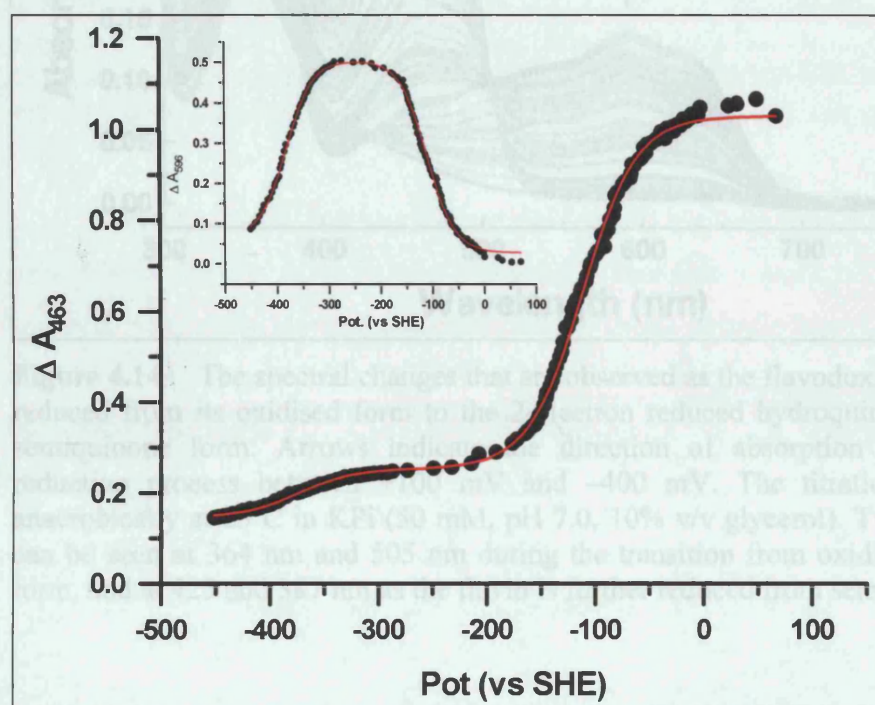


**Figure 4.13** The redox potential (Pot) of YkuN as determined from plotting the absorption change at the oxidised flavin maximum (463 nm) against the potential of the solution corrected to the standard hydrogen electrode (SHE) and by fitting to a two-electron Nernst equation, producing values of  $E_{OX/SQ}$  -110 mV and  $E_{SQ/HQ}$  -374 mV ( $\pm 3$  mV). The inset shows a two electron Nernst equation fitted to the absorption at 596 nm,

reflecting the formation and decay of the semiquinone form to calculate the redox potentials of YkuN. The fitting of a two-electron Nernst equation to the 596 nm data gives  $E_{\text{OX/SQ}} -108$  mV and  $E_{\text{SQ/HQ}} -381$  mV ( $\pm 2$  mV).

The redox potentials of YkuP were also determined in the same manner and are shown below (Figures 4.14 and 4.15). The sequences of the two *B. subtilis* flavoproteins' flavin binding loops show high similarity (see Figure 4.1) and this may explain the resulting similar potentials.

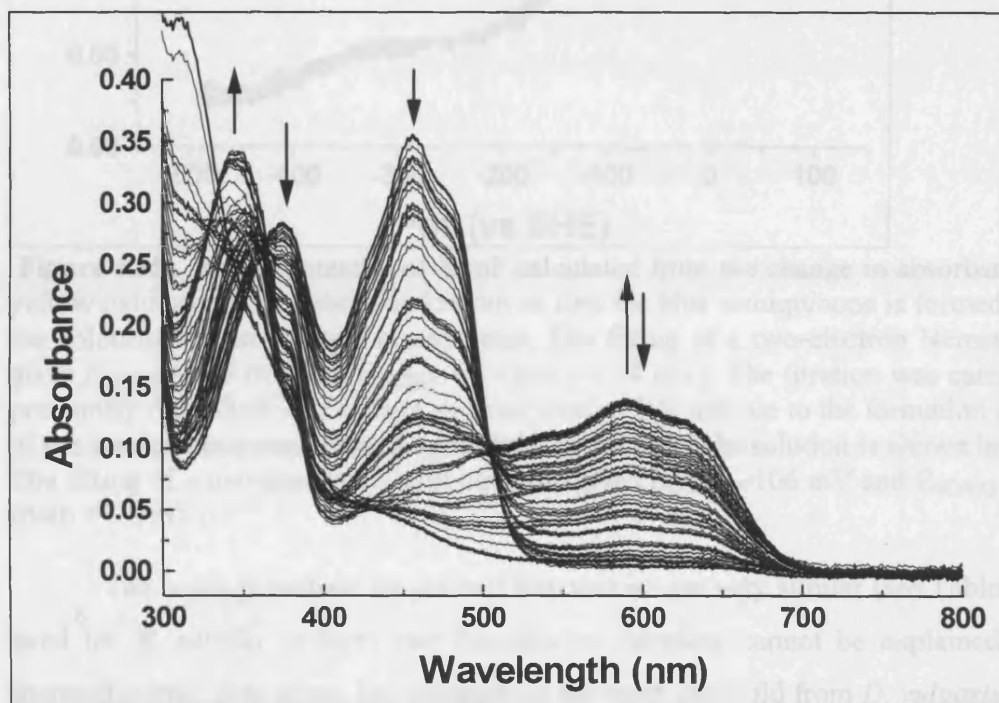


**Figure 4.14** The spectral changes that are observed as the flavodoxin (YkuP, 36  $\mu\text{M}$ ) is reduced from its oxidised form to the 2-electron reduced hydroquinone via the neutral semiquinone form. Arrows indicate the direction of absorption change during the reduction process between +100 mV and -400 mV. The titration was carried out anaerobically at 25°C in KPi (50 mM, pH 7.0, 10% v/v glycerol). Two isosbestic points can be seen at 364 nm and 505 nm during the transition from oxidised to semiquinone form, and at 425 and 387 nm as the flavin is further reduced from semi- to hydroquinone.



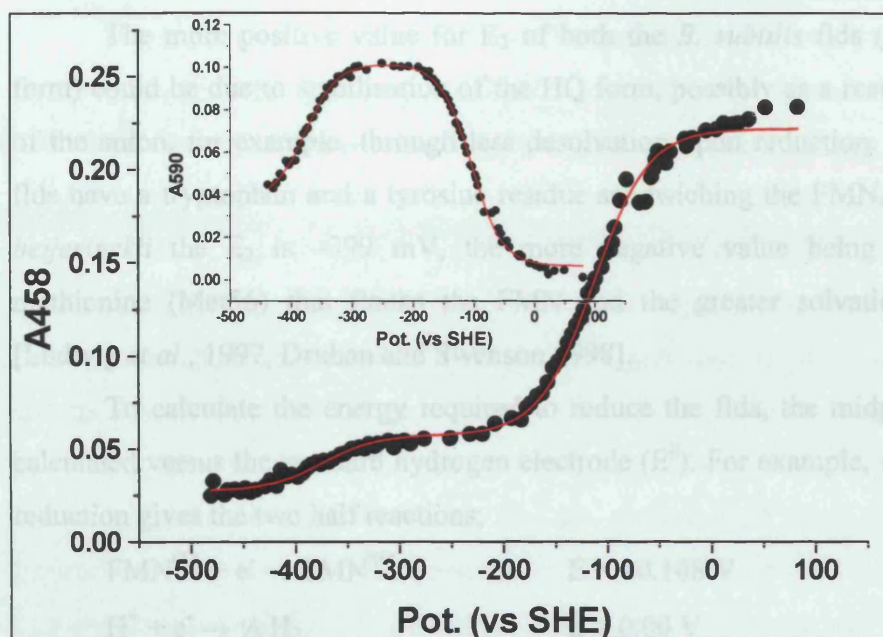


**Figure 4.15** Redox potential of YkuP calculated from the change in absorbance of the yellow oxidised chromophore at 458 nm as first the blue semiquinone is formed and then the colourless hydroquinone accumulates. The fitting of a two-electron Nernst equation gives  $E_{OX/SQ}$   $-115$  mV and  $E_{SQ/HQ}$   $-374$  mV ( $\pm 4$  mV). The titration was carried out as previously described. The change in absorption at 590 nm due to the formation and decay of the semiquinone peak plotted against the potential of the solution is shown in the inset. The fitting of a two-electron Nernst equation gives  $E_{OX/SQ}$   $-106$  mV and  $E_{SQ/HQ}$   $-376$  mV (both  $\pm 3$  mV).

The redox potentials for the two flavodoxins are very similar (see Table 4.5). The need for *B. subtilis* to carry two flavodoxins therefore cannot be explained by these thermodynamic data alone. For comparison the short-chain fld from *D. vulgaris* has an  $E_1$  (OX/SQ) of  $-103$  mV and an  $E_2$  (SQ/HQ) of  $-440$  mV [Curley *et al.*, 1991, O'Farrell *et al.*, 1998] (see Table 1.2). The latter, physiologically relevant, potential differs markedly between the flds from the different species.

Flavodoxin	$E_1$ (mV) Semiquinone formed ( <i>ca</i> $A_{590}$ )	$E_2$ (mV) Semiquinone loss ( <i>ca</i> $A_{590}$ )	$E_1$ (mV) loss of oxidised peak ( <i>ca</i> $A_{455}$ )	$E_2$ (mV) loss of oxidised peak ( <i>ca</i> $A_{455}$ )
YkuN	-108	-381	-110	-374
YkuP	-106	-376	-115	-374

**Table 4.5** Redox potentials for YkuN and YkuP as calculated from the fitting of the absorption versus applied potential data to a two electron Nernst equation.  $E_1$  is the OX/SQ potential and  $E_2$  the SQ/HQ.

The more positive value for  $E_2$  of both the *B. subtilis* flds (*c.f.* the *D. vulgaris* form) could be due to stabilisation of the HQ form, possibly as a result of less repulsion of the anion, for example, through less desolvation upon reduction. However, all three flds have a tryptophan and a tyrosine residue sandwiching the FMN. In the fld from *C. beijerinckii* the  $E_2$  is  $-399$  mV, the more negative value being partly due to the methionine (Met56) that flanks the FMN and the greater solvation of the cofactor [Ludwig *et al.*, 1997, Druhan and Swenson 1998].

To calculate the energy required to reduce the flds, the midpoint potentials are calculated versus the standard hydrogen electrode ( $E^0$ ). For example, with YkuN the first reduction gives the two half reactions;



Which are combined to give the following redox reaction;



From using  $\Delta G^0 = -nFE^0$  the free energy for the reduction of the various forms of the flds can be calculated (see Section 2.8). For example, the free energy for the reduction of oxidised YkuN to its semiquinone ( $E^0 = +0.108$  V);

$$\Delta G^0 = -1 \times 96500 \times 0.108$$

$$\Delta G^0 = -10422 \text{ Jmol}^{-1}$$

$$\Delta G^0 = -10.4 \text{ kJmol}^{-1}$$

The free energy values for each of the one-electron reductions calculated for the *B. subtilis* flds are shown below;

	YkuN $E^1$	YkuN $E^2$	YkuP $E^1$	YkuP $E^2$
$\Delta G^0$ (kJmol <sup>-1</sup> ) versus $\text{H}^+/\text{H}_2$	-10.4	-36.8	-10.2	-36.3
$\Delta G^0$ (kJmol <sup>-1</sup> ) versus $\text{Fe}^{3+}/\text{Fe}^{2+}$	8.8	-17.6	9.0	-17.1

It can be seen from the values above that the reduction of the fatty acid-bound heme couple ( $\text{Fe}^{3+}/\text{Fe}^{2+}$ ) is energetically favoured when the flds are in their 2e<sup>-</sup> reduced hydroquinone form. However, the HQ/SQ couple of *E. coli* FldR has been reported to be -268 +/- 4 mV [McIver *et al.*, 1998], a value that would make the reduction of the flds SQ difficult ( $\Delta G^{\circ} \sim + 10.8 \text{ kJmol}^{-1}$ ). As NADPH has a more negative potential than fatty acid-bound P450 BioI (-0.317 V *c.f.* -0.199 V respectively) the transfer of the first electron from NADPH is therefore energetically favoured overall ( $\Delta G^{\circ} = -11.4 \text{ kJmol}^{-1}$ ) and the energy liberated by the whole reaction (dioxygen bond scission etc) may make the energy expended in electron transfer itself seem rather small.

It should be noted, however, that the potentials of these two flavodoxins are measured whilst they are free in solution. Desolvation of the relevant cofactor is known to have an effect on the redox potential, making its value more positive [Hoover *et al.*, 1999, McCarthy *et al.*, 2002] and, in addition, conformational changes in the FMN-binding loop are thought to occur upon reduction [Ludwig *et al.*, 1997, Kasim and Swenson, 2000]. From fluorescence data it is shown that for both YkuN and YkuP the flavin cofactor is at least partially solvent exposed (see Section 4.9). For efficient electron transfer to occur it can be hypothesised that the FMN of the flavoproteins will dock into a binding cavity or groove of the relevant redox partner. This interaction would involve the transfer of the FMN from the aqueous environment to a more hydrophobic one, and hence would be expected to cause an increase in its redox potential [Causaus *et al.*, 2002]. Therefore, whilst the redox potentials measured above are useful benchmarks, they do not report upon the exact potential of the flavodoxin in its physiologically relevant state. As the degree of exposure, and therefore desolvation, of the FMN cofactor may differ between the two flavoproteins, their actual functional potentials may be quite different. Mutagenesis work with flds from *D. vulgaris* [Zhou and Swenson, 1996 and O'Farrell *et al.*, 1998], *C. beijerinckii* [Druhan and Swenson, 1998] and *A. nidulans* [Hoover *et al.*, 1999] has shown that exposure of the cofactor to solvent by replacement of bulky hydrophobic aromatic residues with amino acids such as alanine had little effect on the oxidised/semiquinone potential (around a 30 mV deviation *c.f.* wild-type) but, a slightly larger effect (around a 100 mV difference) on the physiologically relevant semiquinone/hydroquinone potential. This greater difference was found to be mainly due



(70 – 80 %) to a combination of factors, such as steric, electrostatic, unfavourable coplanar aromatic stacking interactions and the polarity of the flavin-binding site [Druhan and Swenson, 1998].

One difference that was noted in this and other experiments is that whilst the thermodynamic values for the reduction of the flavodoxins are similar, the kinetics of reduction and oxidation may differ. YkuP is notably more ‘difficult’ (slower) to reduce from its semiquinone to hydroquinone form using dithionite. This may be due to slight conformational differences between the two proteins in regard to the binding and positioning of the cofactor and possibly poorer interactions between flavin and dithionite/mediators in YkuP.

#### **4.6 Midpoint reduction potentials of P450 BioI-Fld complexes**

The redox potential of both P450 BioI and the two flds was measured when each of the flds was complexed with P450 BioI in solution. The  $K_d$  for the interaction between the flds and P450 BioI is known to be very tight ( $< 5 \mu\text{M}$ ) when both are in their oxidised forms (Section 4.17), and studies with P450 CAM and Pdx indicate that upon reduction of the ferredoxin the interaction becomes tighter [Sligar *et al.*, 1976]. A 1:1 molar ratio of proteins was prepared in solution, P450 BioI (12  $\mu\text{M}$ ) being saturated with myristic acid (0.2 mM) to make its heme potential more positive and imitate a physiological scenario. The visible spectrum of the protein complex was measured as aliquots of dithionite or ferricyanide were added. The potential of the solution was measured upon the addition of each aliquot, and data were analysed to define reduction potentials for the flavodoxin and P450 in the complex.

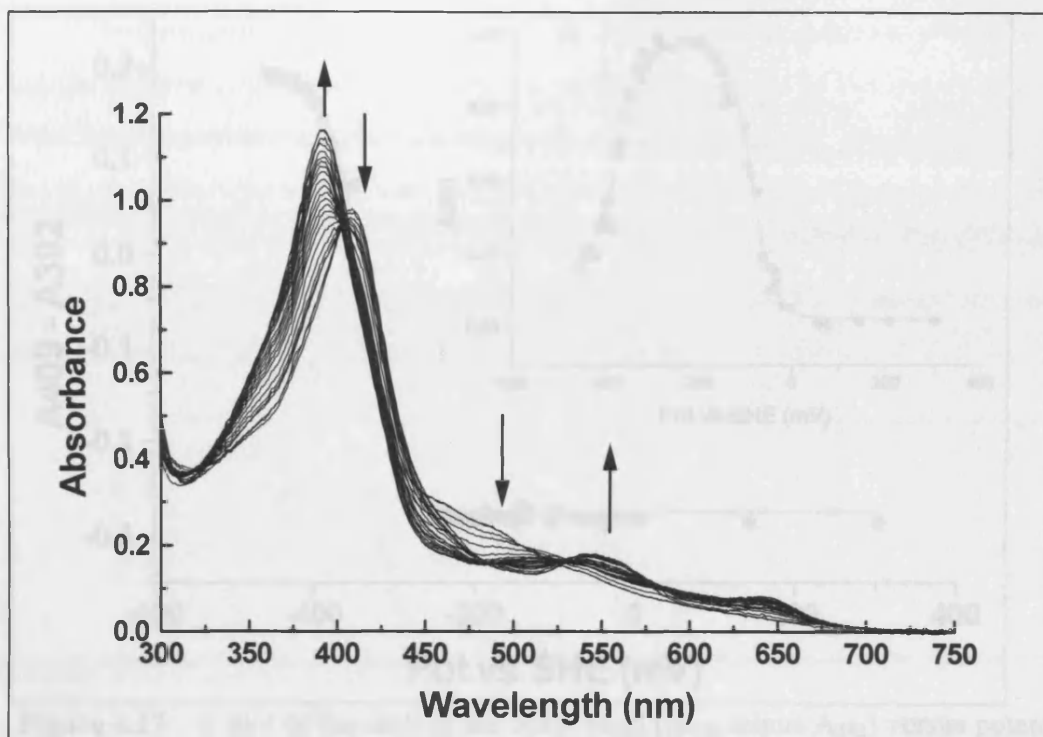


**Figure 4.16** Selected absorbance spectra from the anaerobic redox titration of a complex of myristic acid (0.2 mM) bound P450 BioI (12  $\mu$ M) with YkuP (12  $\mu$ M). Arrows show the direction of absorbance change during addition of dithionite. The Soret band shifts from high-spin (max 393 nm) to reduced (max 409 nm). The titration was carried out anaerobically at 28°C in KPi (50 mM, pH 7.0, 10% v/v glycerol).

The reduction of the heme caused the typical shift in the Soret band to *ca* 409 nm from its initial high-spin positioning (*ca* 392 nm). The difference in its absorbance maximum from the oxidised to the reduced forms was plotted against the solution's potential. A single electron Nernst equation (Equation 11) was then fitted to find the redox potential of the heme (Figure 4.17). As the flavin absorbance coefficient for the flds are much lower than that of the P450's heme, the rise and fall of the semiquinone is hard to observe. However, it is sufficiently removed from the increase in the absorbance due to the merging of the heme's  $\alpha$ - and  $\beta$ -bands to allow the oxidation state of the fld to be determined. The amount of semiquinone formed was therefore determined by plotting  $A_{590}$  and  $A_{596}$  (for YkuP and YkuN, respectively) against the potential of the solution, allowing calculation of the fld's redox potentials.

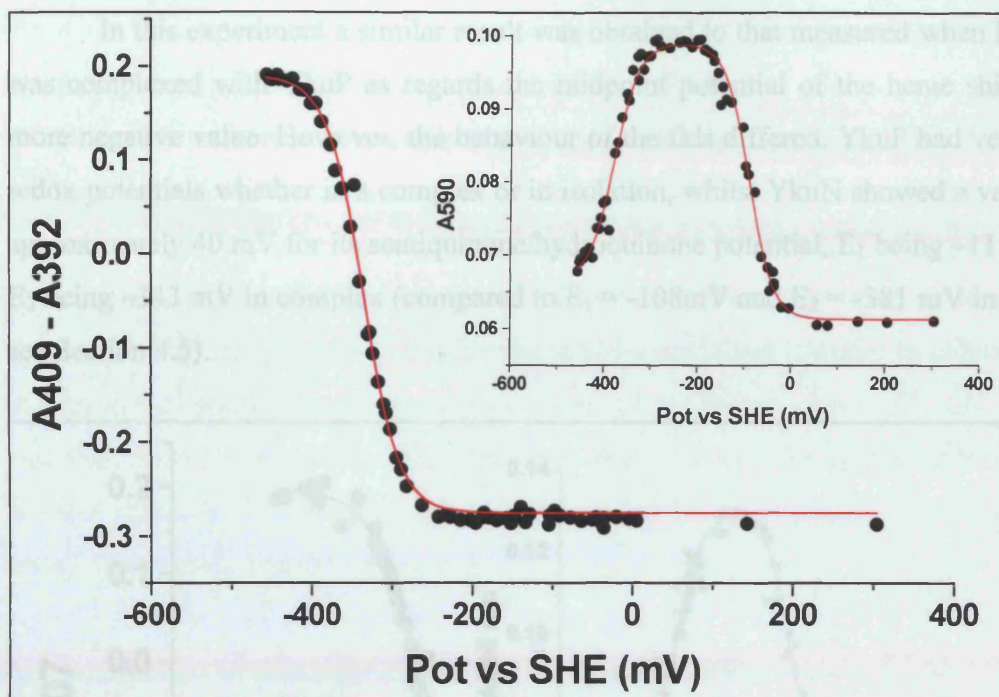


**Figure 4.17** A plot of the shift in the Soret band ( $A_{409}$  minus  $A_{392}$ ) versus potential of the solution fitted to a single electron Nernst equation (Equation 11) to allow the calculation of heme redox potential ( $-337 \pm 4$  mV) from the anaerobic redox titration of a complex of myristic acid (0.2 mM) bound P450 BioI (12  $\mu$ M) with YkuP (12  $\mu$ M) in KPi buffer (50 mM, pH 7.0). The inset shows the calculation of the redox potential of YkuP in complex with P450 BioI by fitting a two electron Nernst equation (Equation 12) to a plot of  $A_{590}$ , reflecting the formation and decay of the semiquinone, versus the solution potential standardised to the hydrogen electrode (Pot vs SHE) giving the values  $-105 \pm 5$  mV ( $E_{\text{Ox/SQ}}$ ) and  $-378 \pm 3$  mV ( $E_{\text{SQ/HQ}}$ ).

Work with systems such as that of P450 CAM and Putidaredoxin has shown that the binding of redox partners and resulting desolvation of their redox cofactors produces an increase in the redox potential [Lewis and Hlavica, 2000] thus enhancing electron transfer via increasing the thermodynamic driving force. However, in this experiment there is little change to either redox potential of the fld, with values being similar to the values measured in isolation. In addition, the heme potential becomes more negative despite starting as high-spin and fully fatty acid bound. When measured in isolation, palmitoleate-saturated P450 BioI (almost full conversion to high-spin) was found to have a midpoint potential of  $-199$  mV (see Section 3.7). The experiment was repeated with a complex of myristate-saturated P450 BioI and YkuN.

In this experiment a similar result was obtained to that measured when P450 BioI was complexed with YkuP as regards the midpoint potential of the heme shifting to a more negative value. However, the behaviour of the flds differed. YkuP had very similar redox potentials whether in a complex or in isolation, whilst YkuN showed a variation of approximately 40 mV for its semiquinone/hydroquinone potential,  $E_1$  being  $-111$  mV and  $E_2$  being  $-343$  mV in complex (compared to  $E_1 = -108$  mV and  $E_2 = -381$  mV in isolation, see Section 4.5).

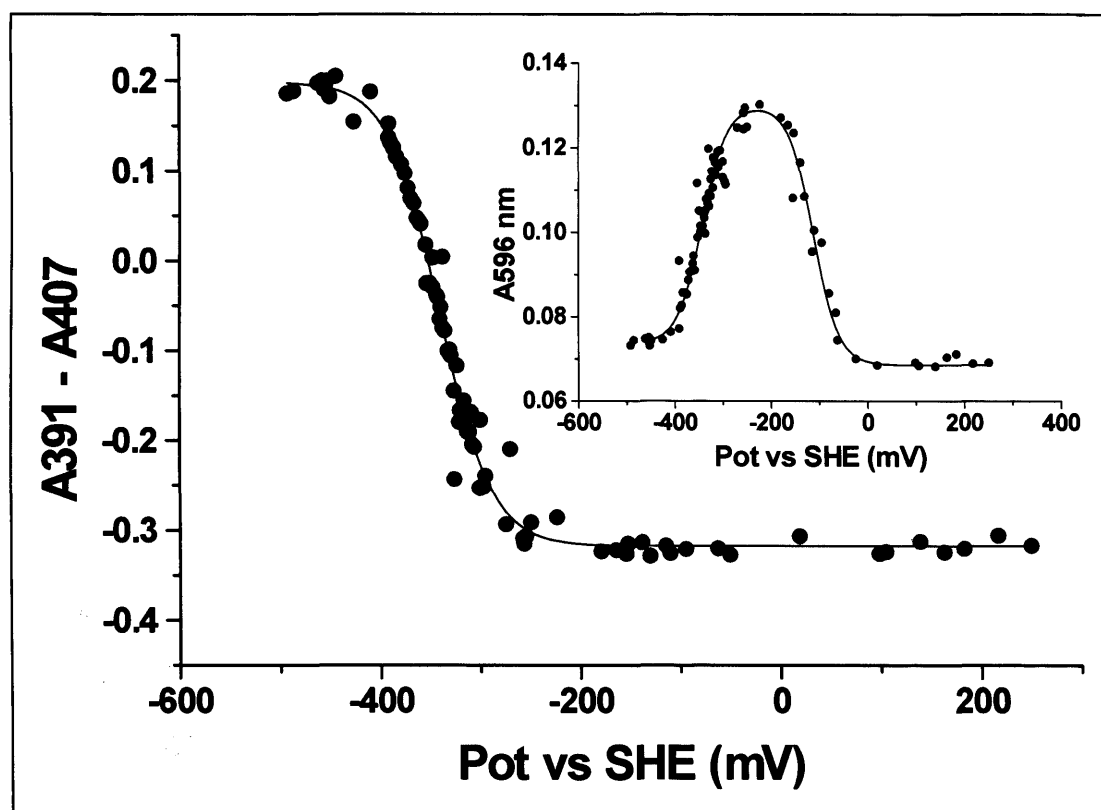


**Figure 4.18** A plot showing the shift in the Soret band absorption ( $A_{408}$  minus  $A_{391}$ ) versus potential of the solution from an anaerobic redox titration of a complex of myristic acid (0.2 mM) bound P450 BioI (12  $\mu$ M) with YkuN (12  $\mu$ M). The P450 data were fitted to a single electron Nernst equation to allow the calculation of redox potential ( $-339 \pm 3$  mV). The inset shows the calculation of the redox potential of YkuN by fitting a two electron Nernst equation to a plot of  $A_{596}$ , reflecting the formation and decay of the semiquinone, versus the solution potential standardised to the hydrogen electrode (Pot vs SHE). The fit produced values  $-111 \pm 3$  mV ( $E_{\text{OX/SQ}}$ ) and  $-343 \pm 4$  mV ( $E_{\text{SQ/HQ}}$ ).

The change in the value of YkuN's semiquinone/hydroquinone midpoint potential (around 40 mV more positive in complex) could reflect a conformational change in the

fld upon binding to the P450. It is possible that the FMN cofactor of YkuN is more solvent exposed *c.f.* YkuP and therefore docking to P450 BioI causes a greater shielding of the cofactor from solvent. This desolvation would favour the formation of the uncharged protonated hydroquinone form. However, UV-visible spectra of YkuN indicate that its cofactor is less solvent exposed than that of YkuP, YkuN's oxidised peak having a maximum at 462 nm compared to YkuP's at 457 nm. The more positive value of the redox potential indicates that either the semiquinone form is easier to reduce, i.e. less stable, or the hydroquinone form is more stable *c.f.* the isolated form of YkuN. As the  $E_1$  midpoint potential is virtually unchanged it is likely that it is the hydroquinone form that is most affected, not the semiquinone form, or that the fully reduced form of YkuN is much more tightly bound to P450 BioI.

#### **4.7 Kinetics of the single electron reduction of the flds**

Flds can be reduced by electrons derived ultimately from NAD(P)H and shuttled to the FMN via an FAD containing reductase (see Section 1.3) [Jenkins and Waterman, 1994]. This type of system has been shown to support P450 function *in vitro*. The ability of *E. coli* Fld reductase (FldR) to pass reducing equivalents to the *B. subtilis* flds was examined. FldR was pre-reduced with NADPH and mixed with the oxidised *B. subtilis* flds under anaerobic conditions in a stopped-flow instrument, to determine the rate of reduction of the FMN cofactor. The formation of the semiquinone (maximum at approx. 600 nm) and the decrease in the oxidised flavodoxin absorbance (maximum at 457 or 462 nm depending on which fld was under investigation) were observed using photodiode array (PDA) UV-visible scanning spectrophotometry. The rates of the reductive reaction were determined from the whole PDA spectra, using global analysis with data fitted to a single exponential function.



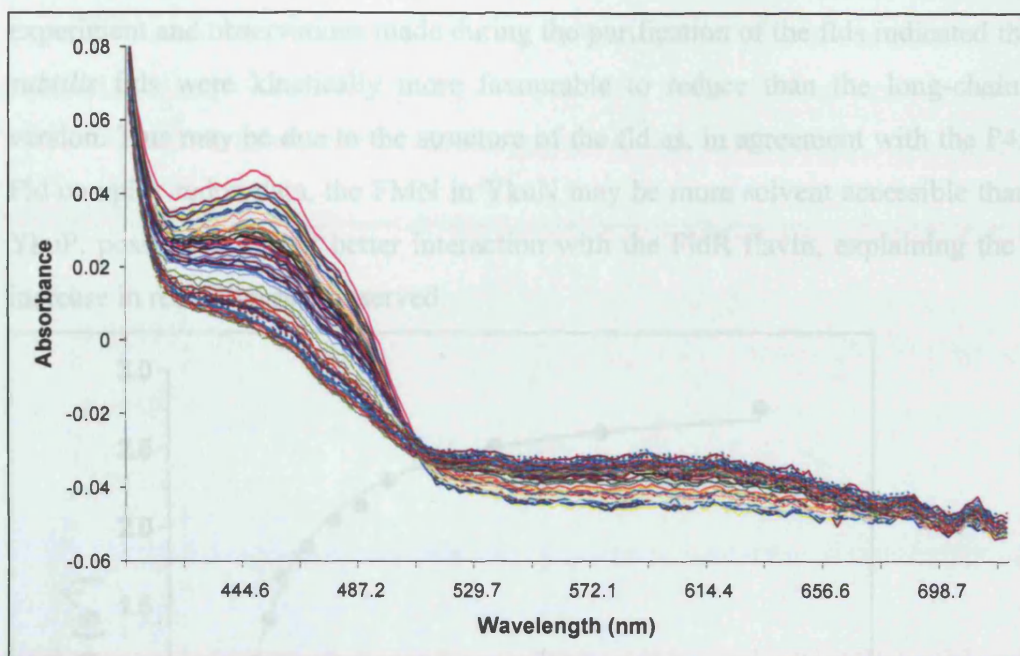


**Figure 4.19** The absorbance spectra for the reduction of YkuP (15  $\mu\text{M}$ ) by *E. coli* FldR (22.5  $\mu\text{M}$ ) in KPi (50 mM, pH 7.0) at 30 °C under anaerobic conditions in the presence of excess NADPH (45  $\mu\text{M}$ ). The formation of the semiquinone can be seen at  $\sim 600$  nm and the decay of the oxidised peak at  $\sim 457$  nm is also observed as the first electron is delivered to the FMN.

The rates were corrected for the photo-bleaching of the FMN cofactor that was observed upon prolonged illumination. The rate of the decrease in the oxidised FMN peak was followed over 8 minutes and this value was used as the basal rate.

Protein	$k_{\text{red}}$ ( $\text{s}^{-1}$ )	Error ( $\pm$ )	$K_d$ ( $\mu\text{M}$ )	Error ( $\pm$ )
YkuN	3.23	0.12	16.24	1.72
YkuP	2.89	0.04	6.84	0.38

**Table 4.7** Kinetic data from the stopped-flow analysis of the reduction of the *B. subtilis* flds by *E. coli* FldR (pre-reduced with excess NADPH). Rates were found by analysing PDA data with the simplest model ( $A + B \rightarrow C + D$ ) that gave a good fit ( $R^2 = 0.98$ ).

In agreement with earlier observations, YkuP was slower to reduce than YkuN when coupled to the *E. coli* reductase. For comparison, the *E. coli* NADPH reductase to *E. coli* flavodoxin electron transfer proceeds at  $0.034 \text{ s}^{-1}$  under similar conditions, i.e. about 100 times slower than the rates observed here [McIver *et al.*, 1998]. Both this



experiment and observations made during the purification of the flds indicated that the *B. subtilis* flds were kinetically more favourable to reduce than the long-chain *E. coli* version. This may be due to the structure of the fld as, in agreement with the P450 BioI-Fld complex redox data, the FMN in YkuN may be more solvent accessible than that of YkuP, possibly giving it better interaction with the FldR flavin, explaining the ~ 20 % increase in reduction rate observed.

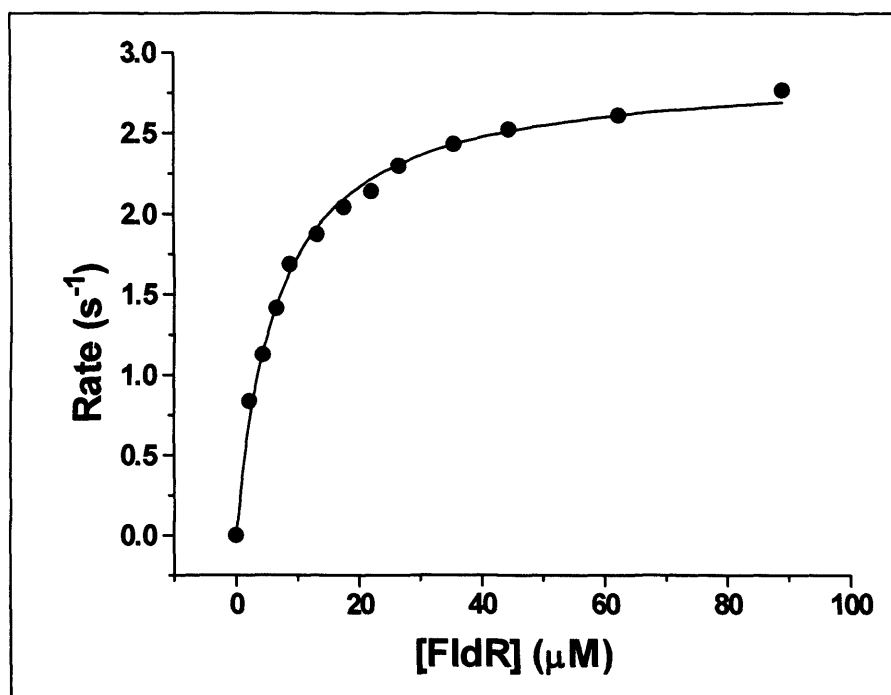


**Figure 4.20** The rate of the single electron reduction of YkuP (15  $\mu\text{M}$ ) by pre-reduced *E. coli* flavodoxin reductase (FldR, varying concentration between 0.5 and 90  $\mu\text{M}$ ). The experiment was performed in a stopped-flow spectrophotometer by mixing a solution of NADPH reduced reductase with oxidised fld. Experiment was carried out at 30°C in KPi (50 mM, pH 7.0). The apparent maximal rate of reduction of the fld ( $k_{\text{red}}$ ) is  $2.9 \pm 0.1 \text{ s}^{-1}$  with the apparent binding constant ( $K_d$ ) being  $6.84 \pm 0.38 \mu\text{M}$ .

#### 4.8 EPR spectroscopy of the semiquinone form

EPR data for the SQ forms of the two flds were collected. YkuN and YkuP were both reduced using dithionite to the one electron neutral blue semiquinone form. EPR spectra were recorded at apparent flavo-semiquinone concentrations of 0.1 mM (YkuN and YkuP). For both proteins, an EPR spectrum typical of the blue neutral semiquinone form of flavin was recorded – centred at a Gauss value of 2.007. This is typical of a neutral flavin radical species [Muller *et al.*, 1970] such as that seen in the reductase

domain of P450 BM3 [Murataliev *et al.*, 1997] and the flavodoxin from *A. vinelandii* [Steensma *et al.*, 1996]. The spectrum of the YkuP neutral semiquinone is shown below (Figure 4.21), YkuN exhibited a similar spectrum.

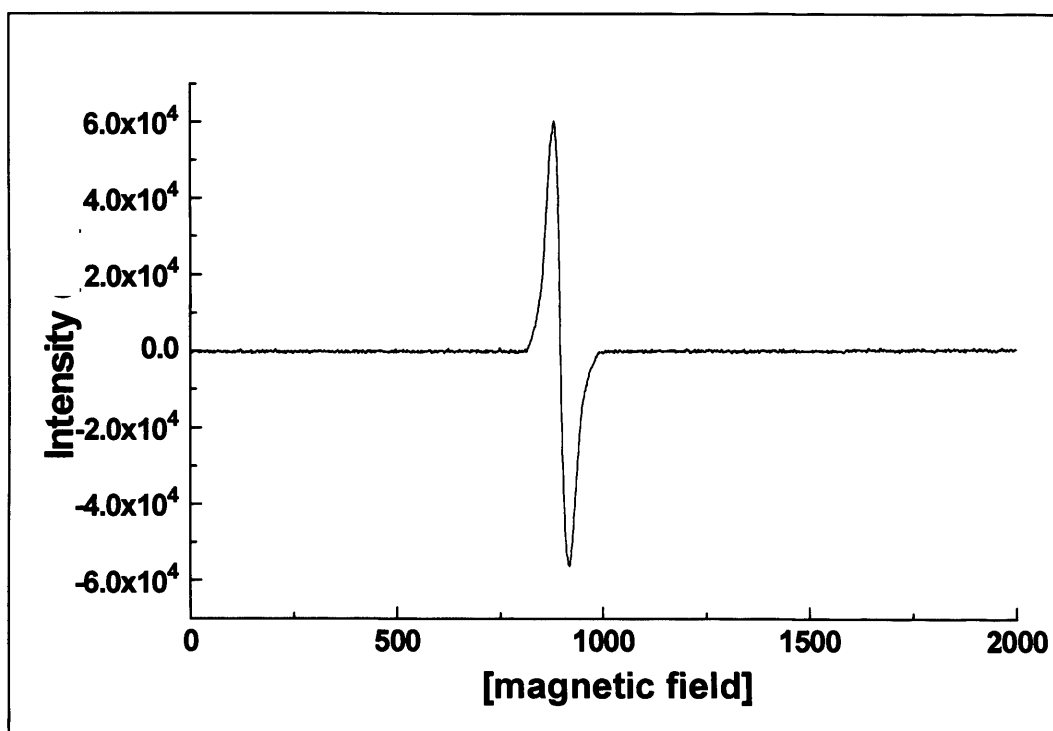


**Figure 4.21** The EPR spectrum of the semiquinone form of YkuP (0.1 mM). The spectrum was collected at 60 Kelvin, 9.658 GHz,  $4.0 \times 10^{-2}$  mW with a 33.5 second sweep time. The corrected g-value was 2.007.

#### 4.9 FMN cofactor binding

Flavodoxins are known to bind their FMN cofactor very tightly. The apoprotein has a non-covalent interaction with the FMN, the  $K_d$  values being in the region of 1 nM in many cases e.g. the  $K_d$  for FMN binding to *D. vulgaris* apoflavodoxin is reported to be 2.4 nM [Murray and Swenson, 2003]. Some flavodoxins (all the long chain and certain short chain flds such as that from *D. vulgaris*) are known to be able to bind riboflavin, i.e. have no specificity for the phosphate group [Pueyo *et al.*, 1996, Walsh *et al.*, 1998]. The dissociation constants for FMN were determined for both YkuN and YkuP apoflavodoxins by fluorescence quenching, and their ability to bind riboflavin was also assessed.

Both apoflavodoxins were generated by treatment of the holoflavodoxins with trichloroacetic acid and subsequent dialysis in KPi (50 mM, 1 mM EDTA, pH 7.0) to allow refolding to occur [Wassink and Mayhew, 1975]. The CD profiles of the apoflavodoxins were measured to check for refolding and their ability to bind FMN was verified by UV-visible spectroscopy, where bound FMN exhibits a shoulder at a longer wavelength *c.f.* free FMN. The binding constants for the cofactors were determined by the addition of 0.5  $\mu$ l aliquots of the apoflavodoxin (0.1  $\mu$ M) to FMN (100 nM solution in 50 mM KPi, pH 7.0) at 25°C [Wassink and Mayhew, 1975]. As the FMN fluorescence is quenched upon its binding to the apoprotein, the binding constant can be determined. The same approach was taken to ascertain whether riboflavin could bind to the apo-form of YkuN or YkuP (Figure 4.22).

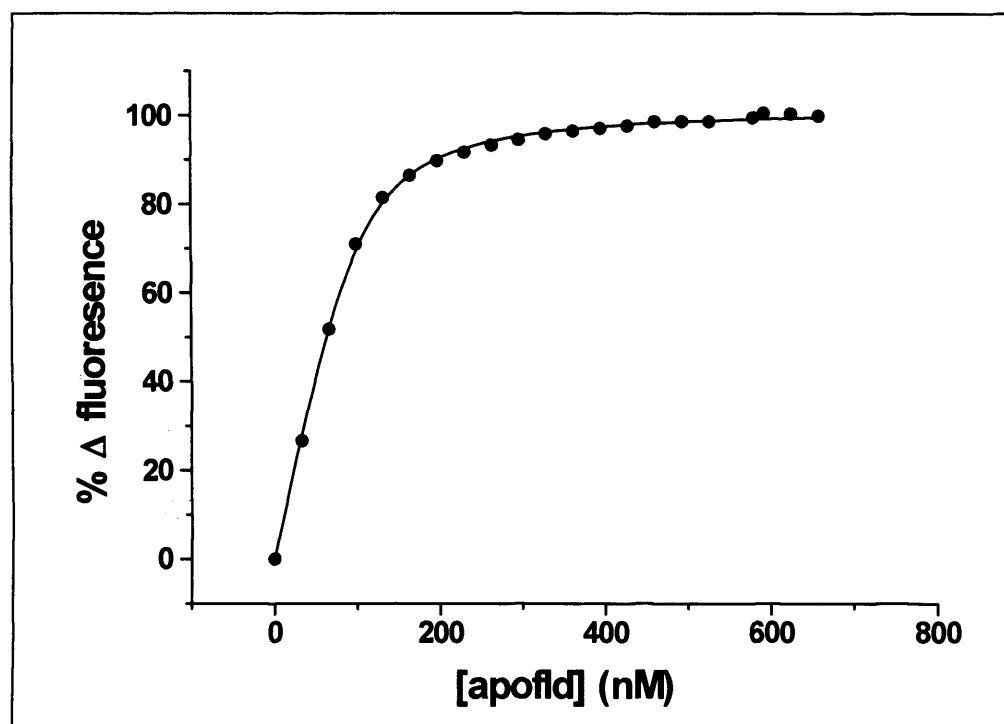


**Figure 4.22** Calculation of the FMN binding constant for YkuN. The binding constant was calculated via measuring the quenching of the FMN (100 nM) upon the addition of the apoprotein (0.5  $\mu$ l aliquots of 66.23 nM protein) using a Cary Eclipse fluorimeter with emission at 529 nm. The titration was carried out in 50 mM KPi, pH 7.0 at 25°C. Excitation was at 450 nm, with the slit widths at 5 nm. The apparent binding constant was found to be  $K_d = 15.6 \pm 1.2$  nM

The binding of FMN by both flavodoxins was weaker than that seen for many other flavodoxin proteins [Mayhew and Ludwig, 1975, Curley *et al.*, 1991], but as anticipated YkuN ( $K_d = 15.6 \pm 1.2$  nM) bound the cofactor more strongly than YkuP (25.2  $\pm$  2.1 nM). These values for the dissociation constants for the cofactor binding are similar to that observed for *C. beijerinckii* apoflavodoxin ( $K_d$  of 18 nM) [Chang and Swenson, 1999] where the FMN is held between a tryptophan and methionine [Ludwig *et al.*, 1997] as opposed to the typical tryptophan/tyrosine pairing such as in the flavodoxins from *H. pylori* and *D. vulgaris* [Freigang *et al.*, 2002, Watenpaugh *et al.*, 1976]. As the concentration of the apoflavodoxin is calculated from the fully quenched FMN value at the end of the titration, it should accurately reflect the content of apoflavodoxin that is capable of binding FMN only. Therefore, the presence of any inactivated (non-flavin binding) apoflavodoxin should be irrelevant as regards the calculation of  $K_d$  values. Phosphate ions from the buffer may be competing with the FMN for the phosphate-binding site, which could impede binding and raise the dissociation constant [Nuallain and Mayhew, 2002]. However, this buffer is commonly used in work with flds from other species when determining dissociation values for their flavin cofactors (for examples see [Walsh *et al.*, 1998, Maldonado *et al.*, 1998]).

Neither of the apoproteins was able to bind riboflavin as no quenching of this compound's fluorescence was observed. This is in agreement with both YkuP and YkuN being typical short-chain flds in requiring the 5'-phosphate group for cofactor binding and/or retention.

#### **4.10 Chemical denaturation of YkuN and YkuP**

The ability of the two flavodoxins to withstand denaturation by the chemical denaturant guanidine hydrochloride (Gdn.HCl) was examined using various spectroscopic techniques. It had been noticed during purification that YkuP had a tendency to lose the FMN cofactor during harsh physical treatments such as concentration via ultrafiltration. Through analysis of the effects of Gdn.HCl treatment on fluorescence from the flavin and the protein's aromatic residues, and on visible spectra of the flavin and CD spectral properties, an integrated view of the stability of secondary

structure, tertiary structure, flavin environment and flavin dissociation can be developed [Munro *et al.*, 1996, Kelly and Price, 1997]. Thus, such studies report upon the flavodoxins' robustness and relationships between protein integrity and flavin binding.

Flds have been used as models to aid the understanding of protein folding as they are archetypal  $\alpha/\beta$  proteins whose fold is shared by nine superfamilies who exhibit little or no sequence similarity (e.g. catalases and chemotactic proteins) [Brenner, 1997]. Gdn.HCl has been used as a denaturant with flds from *D. desulfuricans* and *A. vinelandii*, [Steensma *et al.*, 1998] which both showed evidence of the formation of a stable intermediate in the equilibrium between the folded and unfolded state. By contrast, the urea-mediated unfolding of *Anabaena* fld is observed to unfold directly in a single step [Mierlo and Steensma, 2000].

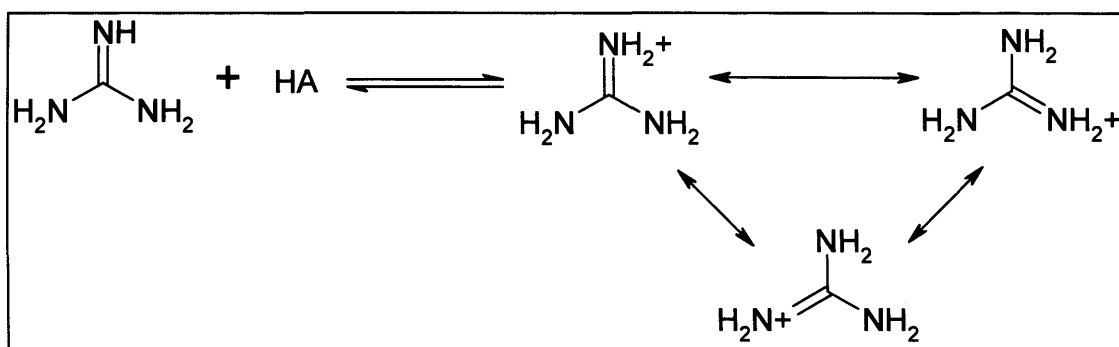


**Figure 4.23** The protonation of guanidine produces the guanidinium ion that, due to its ability to exist in a stabilised resonance state (shown on right), has a high pK<sub>a</sub> of 13. The guanidinium ion acts as a chaotrope, associating with the protein, disrupting side chain and backbone hydrogen bond interactions and reducing hydrophobic interactions, causing it to unfold [Scheraga, 1961].

#### 4.11 The stability of the flavin cofactor

The Gdn.HCl-induced dissociation of FMN from the holoproteins was assessed by UV-visible spectroscopy. Solutions of the flavoprotein (14  $\mu$ M) were prepared in KPi buffer (50 mM, pH 7.0) and the denaturant was added to give various [Gdn.HCl]. After incubation at 25 °C for 15 minutes their spectra were recorded and analysed.



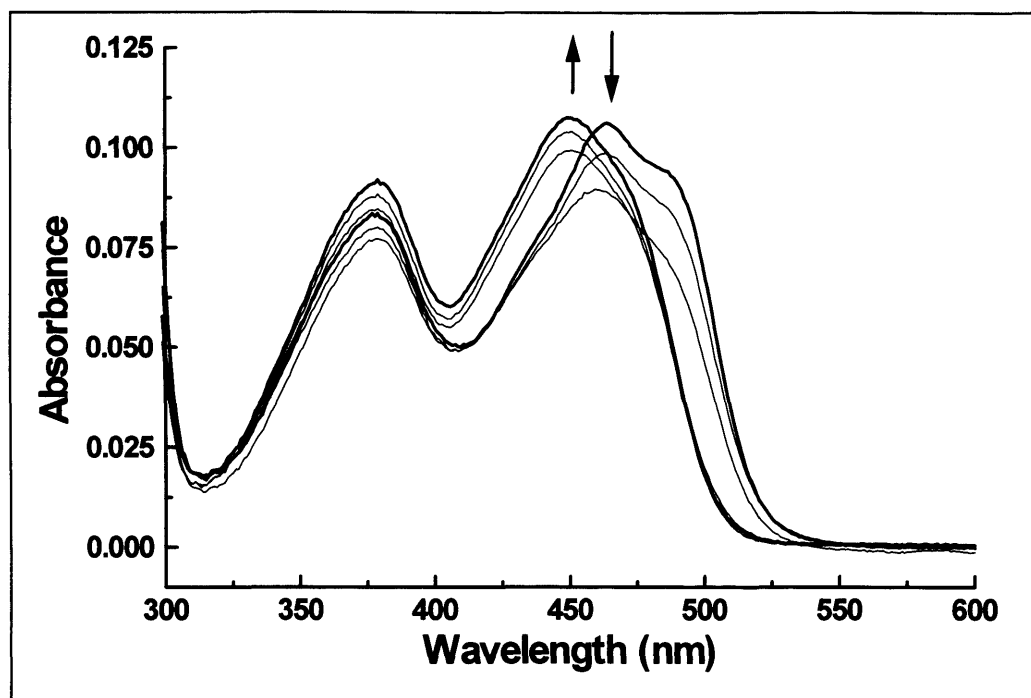


**Figure 4.24** Gdn.HCl denaturation of YkuN (14  $\mu$ M) as monitored by the loss of the FMN cofactor from the protein. The maximum absorbance of the FMN shifts from 463 nm (at 0 M) to 447 nm (5 M). The titration with Gdn.HCl was carried out at 20°C in KPi (50 mM, pH 7.0). 15 minutes equilibration at each [Gdn.HCl] was allowed before spectra were recorded. Spectra shown are for Gdn.HCl at 0, 1, 2, 3 and 5 M Gdn.HCl.

As the FMN cofactor becomes detached from the protein its absorbance shifts to a shorter wavelength due to the chromophore transferring to a more polar environment. Free FMN exhibits UV-visible absorption maxima at both 374 and 446 nm under the same conditions. The final maximum of 447 nm suggests a small degree of association between the FMN and apoprotein at 8.0 M Gdn.HCl, possibly due to the phosphate forming salt bridges with residues such as threonine in the unfolded protein. The plot of this shift in the absorbance maximum against the Gdn.HCl concentration gave a sigmoidal plot indicative of a co-operative unfolding process. By fitting the data points to a sigmoidal function (Equation 7), an estimate for the [Gdn.HCl] at which there is 50 % maximal dissociation of FMN from the protein can be made (Figure 4.25).

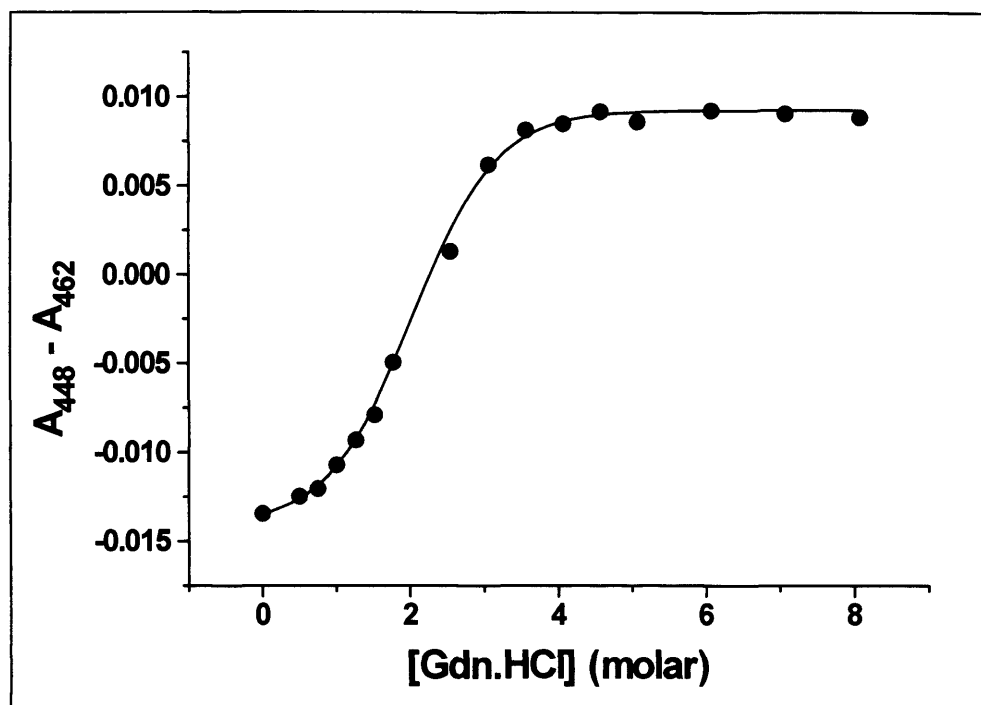


**Figure 4.25** Plot showing the change in the flavin absorption at various [Gdn.HCl] for YkuN. The protein (14  $\mu$ M) was incubated with various [Gdn.HCl] between 0 and 8 M for 15 minutes in KPi buffer (50 mM, pH 7.0) prior to recording a UV-visible spectrum. The relative absorption at wavelengths characteristic for protein bound (462 nm) and free flavin (448 nm) was plotted versus [Gdn.HCl] and the data fitted to Equation 7. The midpoint value is 1.99  $\pm$  0.10 M. Total loss of the FMN (i.e. complete conversion to the species seen at 8 M Gdn.HCl) is observed by 4 M Gdn.HCl.

As anticipated from the loss of the FMN from YkuP during purification and the  $K_d$  values for FMN (see Section 4.9), the midpoint [Gdn.HCl] for the loss of this cofactor was observed at 1.10  $\pm$  0.09 M Gdn.HCl, lower than the midpoint concentration at which YkuN loses its FMN (1.99  $\pm$  0.10 M Gdn.HCl). The reduced stability implies that the cofactor is less tightly held by the apoprotein in YkuP, and/or nearer the surface of the protein, and therefore less shielded and less protected by other residues from chemical attack. Indeed, the starting maximum of 457 nm for the FMN in YkuP implies it is more solvent exposed than that of YkuN, which has a maximum at 462 nm and is therefore likely to be embedded deeper in the protein. However, the flavin binding loops exhibit a high degree of identity between the two *B. subtilis* flavoproteins (see Figure 4.3), the most notable difference being that YkuN contains an additional serine (S94) and tyrosine (Y93), an aromatic that could supply additional hydrogen bonds to the FMN. For

example, FMN binding in *D. vulgaris* flavodoxin is aided by hydrogen bonds between the pyrimidine moiety and residues D95, E99, Y100 and C102, the conserved tyrosine being Y98 [Knauf *et al.*, 1996] and in *D. desulfuricans* hydrogen bonds exist between the isoalloxazine and residues D95, E99, Y101 and C102 [Romero *et al.*, 1996].

#### 4.12 Gdn.HCl-induced loss of tertiary structure

Tertiary structure loss in YkuN and YkuP was monitored by the change in tryptophan fluorescence during treatment with Gdn.HCl. YkuN contains two tryptophan residues and YkuP a single one. It is likely from the sequence data that the conserved tryptophan (W60 in YkuP and W59 in YkuN) is fairly solvent exposed being located in the 60 loop involved in binding the FMN cofactor as seen in the flavodoxins from *D. desulfuricans* [Romero *et al.*, 1996] and *D. vulgaris* [Knauf *et al.*, 1996].

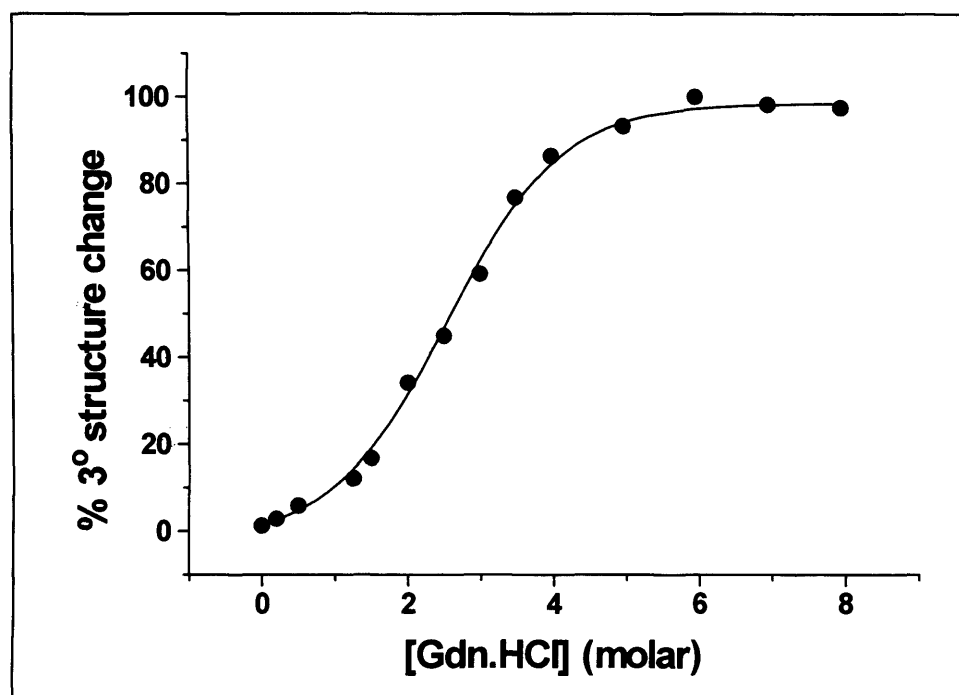


**Figure 4.26** Plot of the change in tertiary structure from tryptophan fluorescence for YkuP against concentration of Gdn.HCl. The % change in tertiary (3°) structure is calculated from the relative proportions of tryptophan emission in the folded and unfolded state ( $E_{360} / E_{348}$ ). YkuP (16  $\mu$ M) was incubated at 25°C in KPi (50 mM, pH 7.0) containing the relevant [Gdn.HCl] for 15 minutes prior to recording fluorescence spectra. Fluorescence excitation was at 290 nm, with emission monitored between 300 and 400

nm. Data were fitted to a sigmoidal (Hill) function. The midpoint value for tertiary structure loss from this fit was  $2.21 \pm 0.30$  M Gdn.HCl.

As the concentration of Gdn.HCl is increased and the protein unfolds, the tryptophan fluorescence was observed to undergo a decrease in intensity at the shorter wavelength maximal for the folded enzyme (348 nm) followed by an increase in intensity at a longer wavelength (360 nm). This shift to a longer wavelength was seen for both flavodoxins. The shift in emission maximum to the longer wavelength with increasing [Gdn.HCl] is in agreement with the residues movement into a more polar media i.e. transferral from the hydrophobic protein environment to being fully solvent exposed. Ultimately, an increase in intensity of the tryptophan fluorescence is also seen due to the reduction of quenching by neighbouring residues and the FMN as the protein structure is disrupted. The initial maximum at 348 nm indicates some degree of solvent exposure *c.f.* the flavodoxin from *A. vinelandii* fld that has an aromatic amino acid emission maximum at 333 nm in the fully folded form [Mierlo and Steensma, 2000].

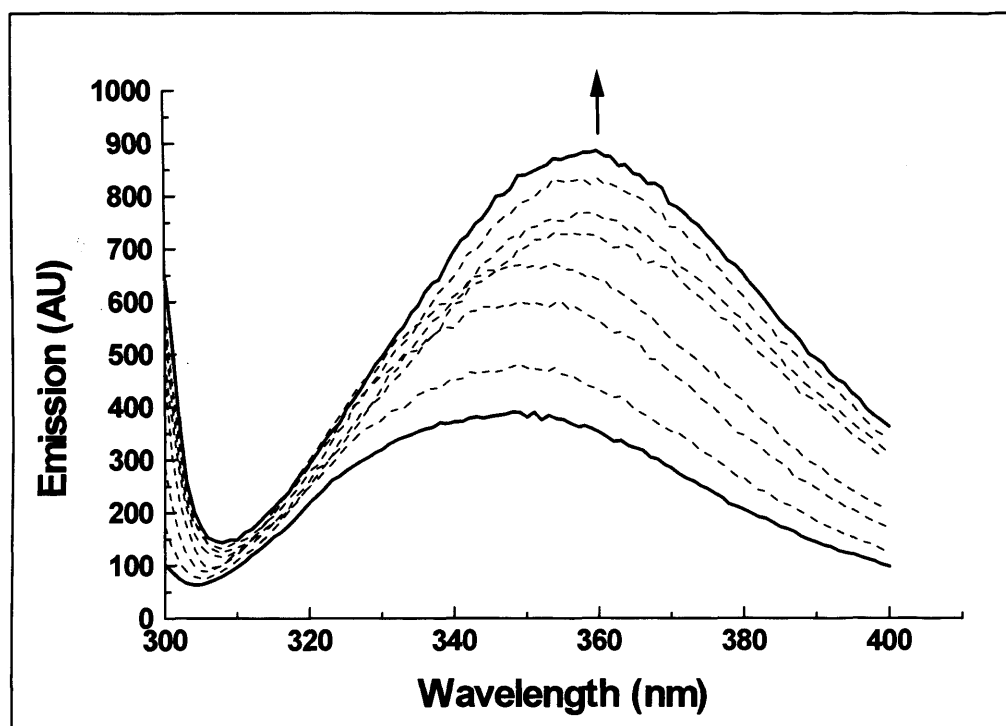


**Figure 4.27** The shift in the fluorescence maximum of YkuN (16  $\mu$ M) after incubating in various [Gdn.HCl] at 25°C in KPi (50 mM, pH 7.0) for 15 minutes is shown. The maximum shifts from 348 nm at 0 M Gdn.HCl to 360 nm at 8 M Gdn.HCl as the tryptophan residues become more solvent exposed. Fluorescence excitation was at 290 nm, with emission monitored between 300 and 400 nm. Data were fitted to a sigmoidal

(Hill) function. The midpoint value for tertiary structure loss from this fit was  $1.74 \pm 0.21$  M Gdn.HCl. AU indicates arbitrary units for fluorescence emission. The solid lines show spectra recorded at 0 M (lower) and 8M (upper) Gdn.HCl.

YkuP (Figure 4.26) appears to exhibit an essentially simple two-phase transition between folded and unfolded states with a midpoint of  $2.21 \text{ M} \pm 0.30 \text{ M}$  Gdn.HCl. The loss of the FMN cofactor at around 1.0 M Gdn.HCl (see next section) may give rise to a slight increase in the tryptophan's fluorescence even in a partially folded state due to the loss of the flavin's quenching effect. YkuN shows a similar pattern, but has a lower midpoint value of  $1.74 \text{ M} \pm 0.21 \text{ M}$  Gdn.HCl.

As a corollary to the study of the holoproteins, the effect of Gdn.HCl on the tertiary structure of the apoflavodoxins that had been generated by acid precipitation with trichloroacetic acid (both YkuN and YkuP) was investigated. This allowed the assessment of the effects of bound flavin on the folding and stability of the proteins [Maldonado *et al.*, 1998, Nuallain and Mayhew, 2002].

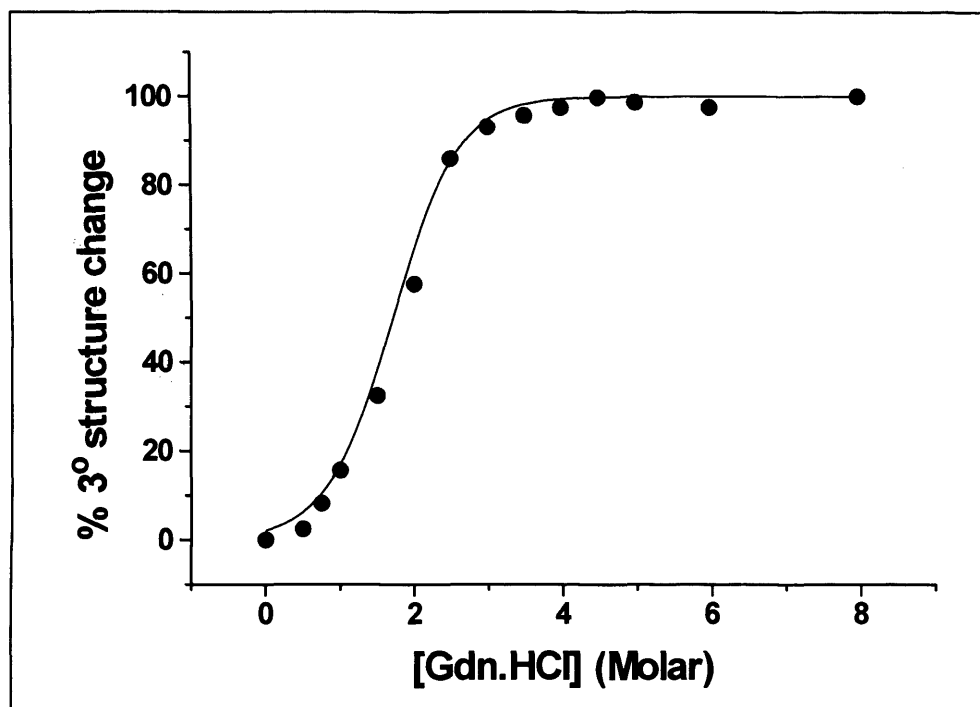


**Figure 4.28** Plot of the change in tertiary structure for YkuN apoprotein against concentration of Gdn.HCl. The % change in tertiary ( $3^\circ$ ) structure is calculated from the relative proportions of tryptophan emission in the folded and unfolded state (Equation 8). YkuN (16  $\mu\text{M}$ ) was treated as previously described. Data were fitted to a sigmoidal

function (Equation 7). The midpoint value for tertiary structure loss from this fit was 1.71  $\pm$  0.10 M Gdn.HCl.

No great difference was observed between the midpoint fluorescence value for the unfolding of YkuN with or without the cofactor present. The initial emission maximum for the tryptophans of YkuN apoprotein was at 350 nm, with a shift to 359 nm upon loss of structure due to incubation with Gdn.HCl. In the holoprotein the initial maximum of 348 nm suggests greater shielding from solvent, which (due to the highly similar CD profiles of the apo- and holoflavodoxin) is probably due to the cofactor providing a more hydrophobic environment for at least one of the tryptophans (W59 in the FMN binding loop). The reverse of this effect is seen with YkuP where the initial maximum for the apoflavodoxin is at 348 nm compared to that of the holoflavodoxin at 352 nm. However, with this flavodoxin the secondary structure was observed to have changed from the comparison of the CD profiles of the apo- and holoproteins and so the treatment of the protein to remove the FMN may have caused a slight refolding or rearrangement of the structure. The shift of the tryptophan emission maximum to 360 nm and 361 nm at 6M Gdn.HCl (YkuN and YkuP respectively) implies the almost full loss of tertiary structure as the emission maximum of free tryptophan in solution is 362 nm [Dawson *et al.*, 1986].

#### 4.13 FMN fluorescence

In flds from species such as *D. vulgaris* and *A. vinelandii*, the FMN binds between two aromatic residues (generally a tryptophan and a tyrosine) and the cofactor's presence has been shown to be capable of stabilising the protein particularly in the oxidised state [Mierlo and Steensma, 2000, Nuallain and Mayhew, 2002]. For instance, with *Anabaena PCC 7119* fld the interaction between the FMN and Y94 stabilises the flavin binding loop [Maldonado *et al.*, 1998]. However, in the unfolding of *D. desulfuricans* fld by Gdn.HCl no cofactor effect was observed upon the stability of either the secondary or tertiary structure [Apiyo *et al.*, 2000]. This fld unfolded via the formation of a 'native type' intermediate that exhibited native topology and no significant disruption of the FMN binding site. It was concluded that only a minor change to the tertiary structure (e.g. helix dissociation from the  $\beta$ -sheet core) occurred upon the formation of the intermediate.



The measurement of FMN fluorescence for YkuN and YkuP (excitation at 450 nm with emission between 500 and 600 nm recorded) was carried out after incubating the relevant holoprotein in denaturant for 15 minutes at 25 °C. As the FMN becomes free from the protein an increase in the emission intensity is seen. The urea-induced unfolding of *D. vulgaris* fld showed full dissociation of the cofactor from the apoflavodoxin despite some tertiary structure being present even at the highest concentrations of urea (indicated by a tryptophan absorbance maximum of 351 nm) [Nuallain and Mayhew, 2002].

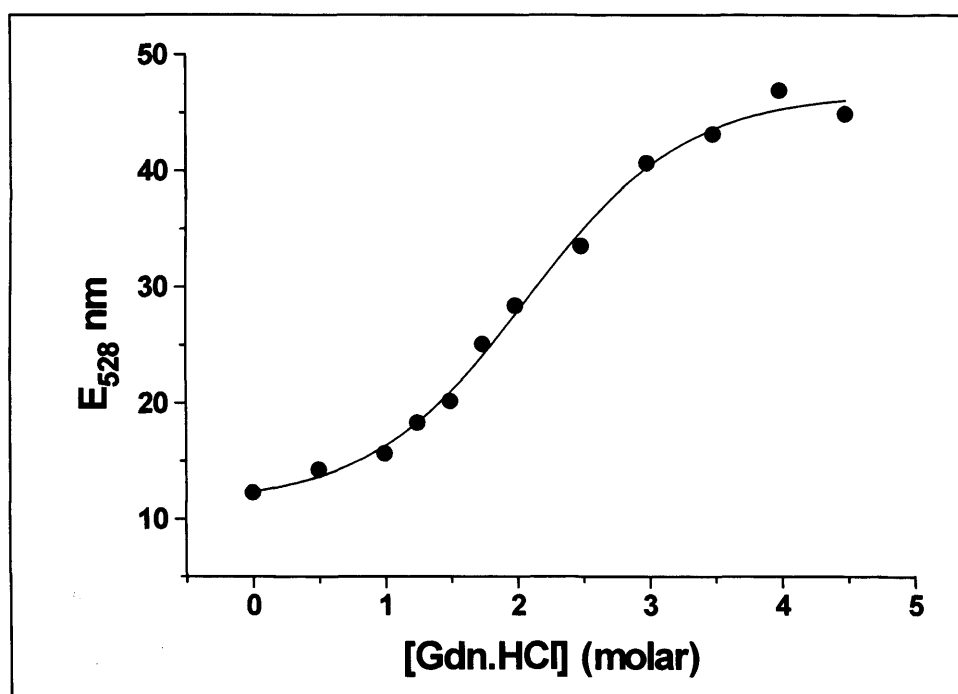


**Figure 4.29** FMN fluorescence of YkuN following treatment of the protein with Gdn.HCl. An overall increase is seen in the FMN chromophore fluorescence as the protein unfolds, reaching a maximum at 4.0 M Gdn.HCl before decreasing due to the quenching effects of Gdn.HCl contaminants. YkuN (16  $\mu$ M) was incubated in KPi (50 mM, pH 7.0, 25°C) containing various [Gdn.HCl] for 15 minutes prior to spectral acquisition. Data were fitted to a sigmoidal (Hill) function indicating a midpoint [Gdn.HCl] for flavin dissociation of 2.09  $\pm$  0.07 M Gdn.HCl. E<sub>528</sub> indicates fluorescence emission at 528 nm (arbitrary units).

With YkuN, UV-visible monitoring of the FMN cofactor's absorption when incubated in the presence of Gdn.HCl had shown that a 50 % structural change occurred at 1.99 M  $\pm$  0.10 M Gdn.HCl (see Section 4.11). As no significant change in the intensity of the absorbance is seen between protein-bound and free FMN, it was difficult

to know whether the FMN had fully dissociated from the protein using this technique. Fully dissociated FMN would be expected to have a much higher fluorescence than that of bound flavin due to the quenching effects of surrounding residues being removed. The Gdn.HCl-induced change in the tertiary structure of the YkuN holoprotein had a midpoint value of 1.74 M  $\pm$  0.21 M Gdn.HCl (Figure 4.29). The final fluorescence maximum of 360 nm for the tryptophan residues implies that the protein is virtually completely unfolded. Therefore any association of the cofactor with the unravelled protein would be surprising. It may be able to remain loosely associated via electrostatic interactions between the FMN's phosphate groups and charged amino acid side-chains. Measurement of the dissociation of FMN from Gdn.HCl-treated YkuN by fluorescence emission showed that a substantial degree of dissociation occurred, as the emission intensity increased by approximately 4-fold over that of the holoprotein.

This change in fluorescence emission is nearly of the same magnitude as that seen when FMN was bound to the apoprotein of YkuN to ascertain its dissociation constant. It is therefore likely that at concentrations of denaturant higher than 4 M Gdn.HCl the cofactor is nearly fully dissociated from the apoprotein. The midpoint value of 2.09  $\pm$  0.07 M Gdn.HCl is similar to that obtained by monitoring the spectral shift of the flavin's absorption maximum (1.99  $\pm$  0.10 M Gdn.HCl).

The loss of the flavin from Gdn.HCl-denatured YkuP was also measured by FMN fluorescence. With YkuP there is also an overall 2-fold increase in the FMN chromophore fluorescence as the protein unfolds, reaching a maximum at 1.75 M Gdn.HCl before decreasing (due to the quenching effects of Gdn.HCl contaminants). 50 % of the FMN cofactor is apparently fully solvent exposed at 0.99  $\pm$  0.43 M Gdn.HCl. The increase in FMN fluorescence intensity observed was less than expected compared to the 4-fold increase seen with YkuN. However, this may be explained through YkuP having increased exposure of the cofactor to solvent in the initial conformation (so the unfolding does little to its environment with respect to the polarity) or that the adjacent aromatic residues (that quench the flavin emission) are distanced further/shielded from the FMN. Alternatively the lack of a shift in the maximum and only moderate increase in the intensity may imply that some or all of the cofactor remains associated to the unfolded protein.

From the results tabulated below it can be seen that the structures of the two flavodoxins differ in terms of their ability to retain their cofactor (FMN) during unfolding. Whilst YkuN appears to unfold at a lower concentration of guanidine from the tryptophan measurements, it is apparently able to retain its FMN at higher Gdn.HCl concentrations. This implies that its tryptophan residues are either more solvent exposed in the starting conformation (although there is little difference in the initial intensity), or that they are nearer the outer surface of the protein. Alternatively YkuN may have more electrostatic/hydrogen bond interactions between the protein and cofactor (e.g. between lysines and the phosphates of the FMN ribityl chain). Clearly there are significant differences in structural stability between the flavodoxins, suggesting that there will be marked differences in their overall structures. It appears that flavin binding has negligible effect on the stability of the tertiary structure for YkuN, but that the presence of FMN destabilises the YkuP holoprotein somewhat. This may imply that the YkuP apoflavodoxin adopts an alternate fold in the absence of FMN as suggested also by CD studies (see Section 4.4).

Protein	50 % FMN loss (M)	Error +/-	50% 3° loss (M)	Error +/-
YkuN Holoprotein	2.09	0.07	1.74	0.21
YkuP Holoprotein	0.99	0.43	2.21	0.30
YkuN Apoprotein	N/D	N/D	1.71	0.09
YkuP Apoprotein	N/D	N/D	3.13	0.24

**Table 4.8** Midpoint values for the [Gdn.HCl] at which either the flavin cofactor dissociates or the tertiary structure (3°) unfolds as reported by flavin or tryptophan fluorescence, respectively. The values were calculated from fitting the change in the fluorescence emission maximum against [Gdn.HCl] to a sigmoidal function (Equation 7) (Origin, Microcal). Data for flavin loss was not determined (N/D) for the apoproteins.

#### 4.14 Secondary structure denaturation

The stability of the two fld's secondary structure to unfolding by the chemical denaturant Gdn.HCl was examined by far UV CD. Samples of the protein (0.25 mg/ml) were incubated in a Gdn.HCl solution of the appropriate molarity for fifteen minutes prior to measurement. The initial spectrum of the flds at 0 M Gdn.HCl shows a minimum

at 222 nm, indicative of a large  $\alpha$ -helical content [Steensma *et al.*, 1998], and the disappearance of this minimum at 8.0 M Gdn.HCl correlates to loss of virtually all secondary structure (Figures 4.30 and 4.32).

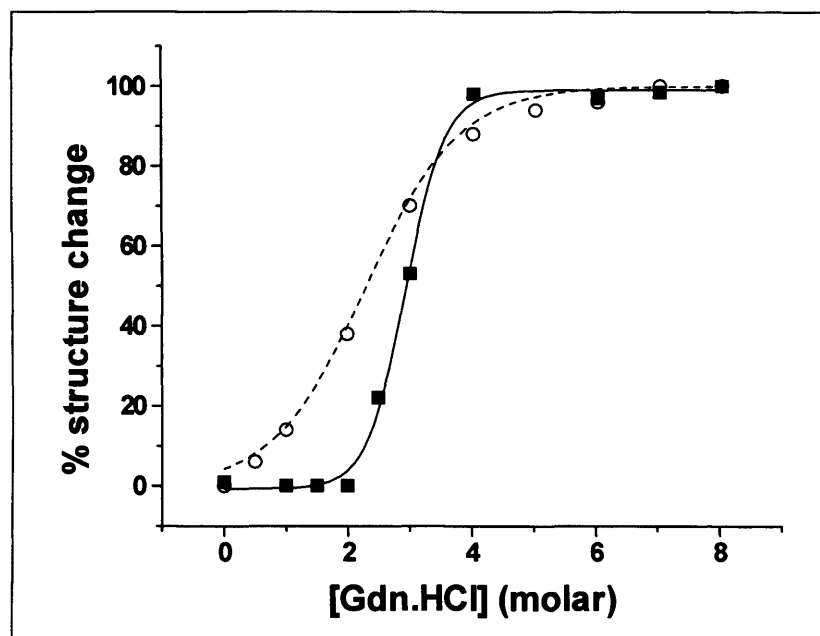


**Figure 4.30** Loss of secondary structure of YkuN (squares) and YkuP (hollow circles) upon incubation with varying [Gdn.HCl]. The % structure change shown is the ratio of the difference between the CD intensity observed at 222 nm at the relevant [Gdn.HCl] and at 8 M Gdn.HCl, divided by the same ratio for the protein at 0 M and 8 M Gdn.HCl (Equation 8). YkuN shows 50 % secondary structure lost at  $2.9 \pm 0.1$  M and YkuP at  $2.3 \pm 0.2$  M Gdn.HCl. A less steep gradient is seen with YkuP compared to YkuN that may reflect the differences in the amount of  $\alpha/\beta$  structure present as seen from the native CD profiles, or a rather less defined point of collapse at a critical [Gdn.HCl]. The fit to a sigmoidal function suggests that the secondary structure of the holoprotein exhibits a two-state unfolding pattern (Native  $\leftrightarrow$  Unfolded).

As can be seen from the sigmoidal trends shown above, YkuN holoprotein undergoes a dramatic loss of structure at  $> 2$  M Gdn.HCl whilst YkuP undergoes a more gradual loss.

The denaturation of the apoproteins with Gdn.HCl was also examined. Work with the apoflavodoxin from *A. vinelandii* [Mierlano and Steensma, 2000] has shown that the cofactor has little if any effect on the stability of the protein towards urea-induced unfolding. The FMN may be expected to have little contribution to the secondary structure due to its positioning between two loops on the extremity of the protein.

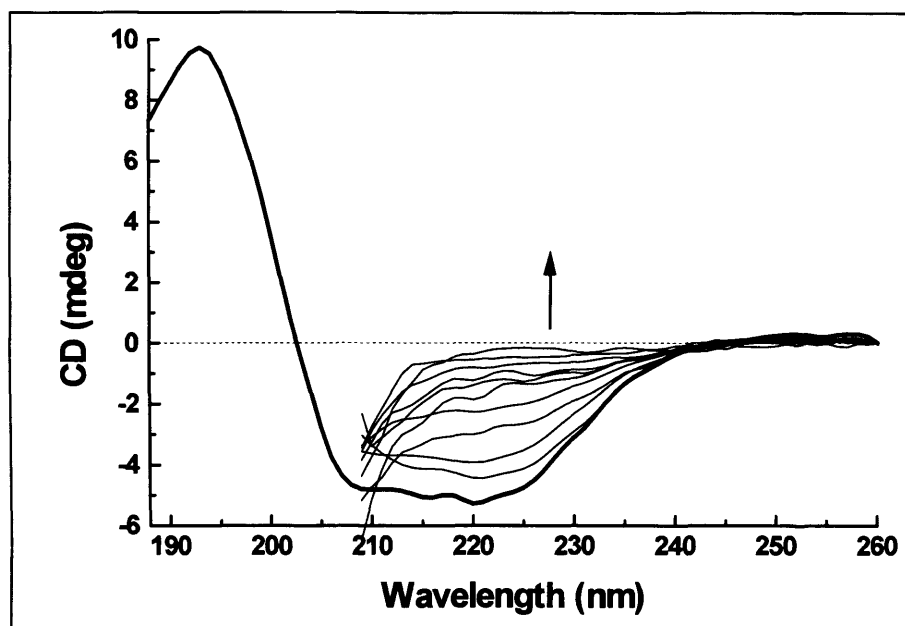


**Figure 4.31** CD spectra showing the loss of the secondary structure of YkuP through the reduction of ellipticity at 222 nm as the concentration of Gdn.HCl is increased from 0 M to 8.0 M. The arrow shows the direction of change. The ellipticity of the protein at 0, 0.5, 1.0, 1.5, 2.0, 3.0, 4.0, 5.0, 6.0, 7.0, and 8.0 M Gdn.HCl are shown. The experiments were carried out at 25 °C in KPi (50 mM, pH 7.0) with 0.25 mg/ml YkuP and a 0.1 cm path-length.

With both *B. subtilis* flds there is little difference between the concentrations of Gdn.HCl that cause the loss of 50 % of the secondary structure for the apoproteins and holoproteins. In the case of YkuP the difference is negligible despite the CD and fluorescence properties for apo- and holoforms being quite distinct. YkuN shows a greater difference, the [Gdn.HCl] at which it loses 50 % of its secondary structure being 2.92  $\pm$  0.04 M for the holoprotein and 2.18  $\pm$  0.11 M for the apoprotein. This difference probably may reflect a small stabilising effect from the binding of the FMN. With YkuN the FMN is tightly held (see Section 4.9) and therefore the harsh chemical treatment to remove the cofactor and/or the impact of the loss of its association (through electrostatic and hydrogen bonds) may have a slight weakening effect on the structure. Alternatively its tighter association may be as a result of it having a greater contribution to the holoflavodoxin's structure than that of YkuP's cofactor.

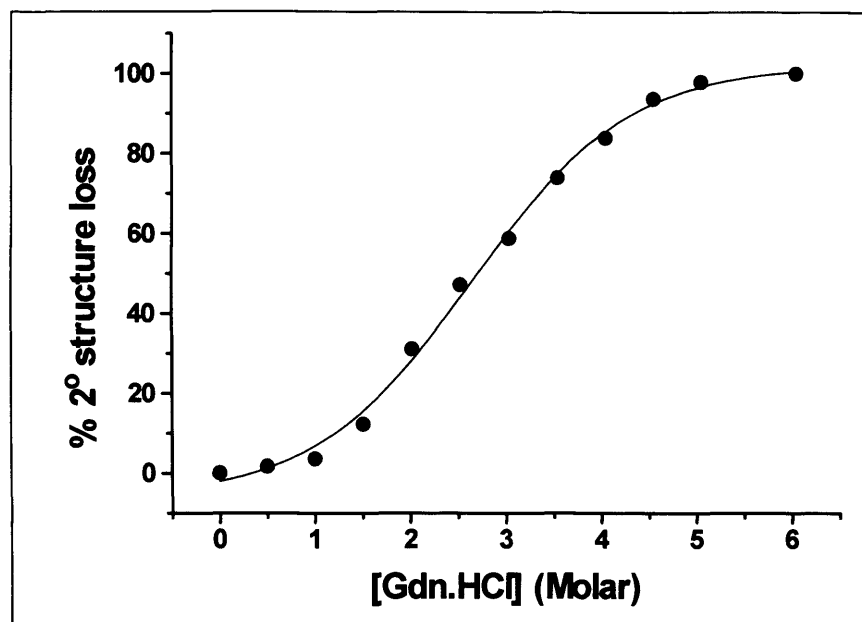


**Figure 4.32** Gdn.HCl-mediated unfolding of YkuP apoflavodoxin. The % structure change shown is the ratio between the difference in CD intensity observed at 222 nm at the relevant [Gdn.HCl], divided by the same ratio for the protein at 0 M and 8 M Gdn.HCl (Equation 8). Data were fitted to a sigmoidal function reflecting a simple two state transition; the midpoint is at  $2.50 \pm 0.16$  M Gdn. Experiments were carried out at 25 °C in KPi (50 mM, pH 7.0) with 0.25 mg/ml YkuP.

Protein	[Gdn.HCl] (M) 50% secondary structure loss	[Gdn.HCl] (M) Onset of structure loss
YkuN holoflavodoxin	$2.92 \pm 0.04$	2.24
YkuP holoflavodoxin	$2.30 \pm 0.19$	0.48
YkuN apoflavodoxin	$2.18 \pm 0.11$	0.61
YkuP apoflavodoxin	$2.50 \pm 0.16$	1.13

**Table 4.9** Values for the loss of secondary structure when YkuN and YkuP (both 0.25 mg/ml) were incubated for 15 minutes in the presence of various [Gdn.HCl] at 25 °C. The % structure change shown is the ratio between the difference in CD intensity observed at 222 nm at the relevant [Gdn.HCl], divided by the same ratio for the protein at 0 M and 8 M Gdn (Equation 8). This was plotted against [Gdn.HCl] and fitted to a sigmoidal function (Equation 7) using Origin (Microcal) software. Onset of secondary structure loss is defined as the value when 10 % change is observed.

It can be seen from the Gdn.HCl-induced unfolding of the two holoflavoproteins that there is a lack of consistency between the midpoint values for the loss of secondary and tertiary structure, particularly in the case of YkuN. For this flavoprotein the loss of 50 % of the tertiary structure (as measured by tryptophan fluorescence) occurs at 1.74 M



Gdn.HCl and that of the secondary structure (measured by far-UV CD) occurs at 2.92 M. This implies that a three-state unfolding model may exist with the formation of an intermediate [Turoverov *et al.*, 1999]. This has been observed in work with the long chain flavodoxin *A. vinelandii* [Mierlo and Steensma, 2000]. Here the formation of a molten globule transition state is seen with around 37 % of the total protein occupying this form at 2.2 M Gdn.HCl. Shown below is the Gdn.HCl denaturation of YkuN holoflavodoxin and the difference in the amount of tertiary and secondary structure lost at different [Gdn.HCl] is clearly evident.

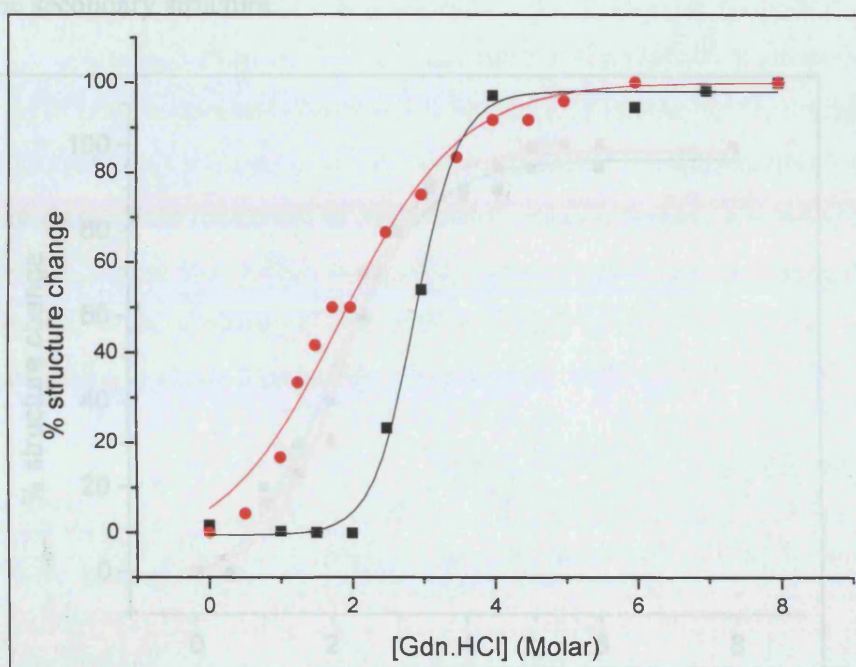


**Figure 4.33** Denaturation of YkuN holoprotein at various [Gdn.HCl]. CD data ( $\Delta$  CD 222 nm) in black squares representing the loss of secondary structure and the fluorescence data in red circles (shift of the emission maximum) representing the loss of tertiary structure. The loss of tertiary structure (interactions between residues and elements of secondary structure) precedes the loss of secondary structure (the actual unfolding of the helices and sheets). All measurements were carried out at 25 °C in KPi buffer (50 mM, pH 7.0).

With the YkuN apoprotein there is less of a difference between the unfolding patterns. This may indicate that the FMN cofactor has an effect upon the mode of unfolding and the formation of a hypothetical intermediate. An intermediate with a being consistent with the loss of the secondary structure. From the [Gdn.HCl] midpoint



degree of secondary structure and little tertiary structure could be expected to exist between 0.1 and 3.5 M Gdn.HCl.

If the midpoint values for the Gdn.HCl-induced denaturation of YkuN are studied in isolation it appears that there is little difference between the stability of the apo- and holo-protein, i.e. that the FMN cofactor doesn't contribute to the stability of the protein. The trend for the holoprotein is as expected, with the tertiary structure becoming disrupted first followed by the loss of the cofactor and finally a loss of secondary structure. The apoprotein shows the loss of tertiary structure in parallel with the loss of the secondary structure.

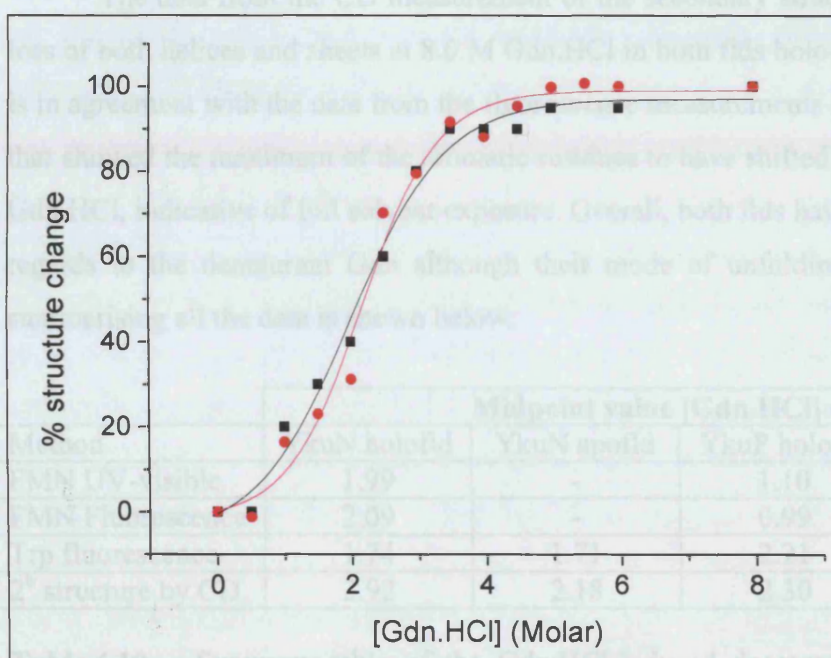


**Figure 4.34** The loss of secondary structure of YkuN apoflavodoxin (red circles) as monitored by the change in the CD profile (loss of minimum at 222 nm) is very similar to the loss of tertiary structure (black squares) of YkuN apoflavodoxin as reported by the change in fluorescence emission maximum for aromatic amino acids. The structure of the apoprotein is dissimilar to that of the holoflavodoxin from CD analysis (see Section 4.15). All measurements were carried out at 25 °C in KPi buffer (50 mM, pH 7.0).

YkuP holoflavodoxin showed less of a discrepancy between the unfolding patterns whether secondary or tertiary structure is followed. This implies that an intermediate form is not part of the unfolding mechanism, the loss of the tertiary structure being concomitant with the loss of the secondary structure. From the [Gdn.HCl] midpoint

values it can be seen that YkuP holoprotein loses its FMN first (50 % lost at around 1.05 M Gdn.HCl) followed by the loss of both secondary and tertiary structure (50 % lost at around 2.25 M Gdn.HCl).

YkuP apoflavodoxin shows a greater difference between the unfolding profiles of the secondary and tertiary structure. This reflects the greater difference observed between the midpoints for the denaturation of the apoprotein (50 % secondary lost at 2.5 M Gdn.HCl, 50 % tertiary lost at 3.1 M Gdn.HCl) compared to the holoprotein. An intermediate that exhibits a degree of secondary structure may be present in a small proportion between 0 and 6 M Gdn.HCl.

The data from the CD measurement of the secondary structure shows clearly the loss of both helices and sheets at 8.0 M Gdn.HCl in both flds holo- and apoproteins. This is in agreement with the data from the fluorescence measurements of the tertiary structure that showed the maximum of the aromatic residues to have shifted to *ca* 360 nm at 8.0 M Gdn.HCl, indicative of full solvent exposure. Overall, both flds have similar stability with regards to the denaturant Gdn although their mode of unfolding may differ. A table summarising all the data is shown below:

Method	Midpoint value [Gdn.HCl] (M)			
	YkuN holo fld	YkuN apo fld	YkuP holo fld	YkuP apo fld
FMN UV-visible	1.99	-	1.10	-
FMN Fluorescence	2.09	-	0.99	-
Trp fluorescence	1.74	1.71	2.21	3.13
2° structure by CD	2.92	2.18	2.30	2.50

**Table 4.10** Summary table of the Gdn.HCl-induced denaturation experiments. The values at which 50 % of the structure (either tertiary or secondary) or the FMN cofactor is lost from the flds are listed (for details and errors see the relevant sections 4.12 to 4.14).

#### 4.15 ANS Fluorescence

Evidence for a molten globule type intermediate, from the binding of ANS (8-anilino-1-naphthalene sulphonate) to the flavodoxins during unfolding, was sought to clarify the differences noted above. ANS is a polarity-sensitive fluorescent probe that undergoes an increase in fluorescence (at *ca* 500 nm) upon binding to hydrophobic surfaces [Ali *et al.*, 1999, John *et al.*, 2001]. ANS free in solution had a maximum at 528 nm when excited at 395 nm in the buffer used (KPi, 50 mM, pH 7.0) at 25 °C. Through the Gdn.HCl-mediated unfolding of the flavodoxins, a shift in the fluorescence maximum from the initial value at 528 nm to a shorter wavelength was seen, moving as far as 486 nm for certain concentrations of the denaturant. Maximal differences in fluorescence intensity of ANS between folded and unfolded proteins were observed at 500 nm, and this wavelength of emission was followed to assess its binding.

A maximum in the ANS emission is seen with the YkuN apoprotein at 0.5 M Gdn.HCl. With YkuN holoflavodoxin the ANS maximum is at 2.0 M Gdn.HCl. This difference between the values for the apo- and holoflavodoxin suggests the cofactor has some impact upon the route of unfolding and that a greater amount of hydrophobic surface is exposed at a higher Gdn.HCl concentration when the FMN is present. The value of 2.0 M for YkuN holoflavodoxin is in good agreement with a molten globule type of intermediate being formed, as implied by the comparison of secondary and tertiary structure loss (see Figure 4.33).

With YkuP apoflavodoxin the maximum was seen at 0.3 M Gdn.HCl and that of the holoflavodoxin at 1.0 M (Figure 4.35). As the values for the apo- and holoflavodoxin differ, it is probable that the cofactor has some impact upon the mode of unfolding, i.e. a greater proportion of the surface is hydrophobic at a higher Gdn.HCl concentration in the holoflavodoxin. Under similar conditions we know that 50 % of the FMN cofactor is lost at 1.0 M Gdn.HCl (YkuP) and 2.0 M Gdn.HCl (YkuN), the same concentration as the maximal ANS emission (Section 4.13). It is therefore likely that the loss of the cofactor from the holoflavodoxin is in some way coupled to the ANS emission, the flavin-binding loops, where the majority of the few aromatic hydrophobic residues are positioned, being the probable main area of interaction with the fluorescent probe [Apiyo *et al.*, 2000].



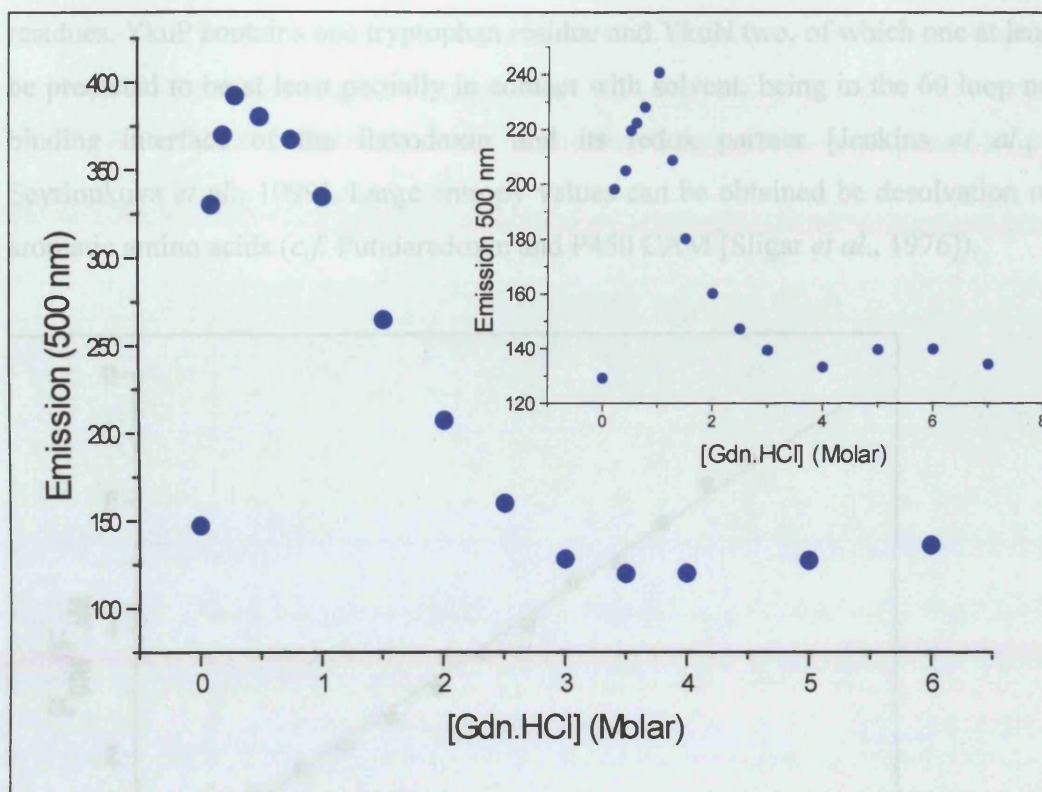


**Figure 4.35** Emission of ANS at 500 nm in the presence of YkuP apoflavodoxin (0.1 μM) incubated at various concentrations of Gdn.HCl. The inset shows the ANS fluorescent emission during Gdn.HCl denaturation of holoflavodoxin (0.1 μM). The emission maximum for the FMN-containing protein was at 1.0 M Gdn.HCl. Both were measured at 25 °C in KPi buffer (50 mM, pH 7.0), excitation was at 395 nm, with a 1 cm pathlength cell and the emission (arbitrary fluorescence units) collected between 450 and 600 nm.

#### 4.16 Stern-Volmer constants

Quenching of the fluorescence of tryptophan and tyrosine residues (and also the FMN cofactor) by a quenching agent such as succinimide (that works via colliding and making contact with the fluorophore) can be used to determine their location and hence amount of solvent exposure [Eftink and Ghiron, 1976]. It is observed experimentally that the manner in which the quencher reduces the fluorescence intensity is proportional to the concentration of the quencher. This is described by the Stern-Volmer equation (Equation 10) that is explained in Section 2.8.

The Stern-Volmer constant was determined for both YkuN and YkuP to provide information upon the degree of solvent exposure of the FMN cofactor and the tryptophan

residues. YkuP contains one tryptophan residue and YkuN two, of which one at least may be predicted to be at least partially in contact with solvent, being in the 60 loop near the binding interface of the flavodoxin and its redox partner [Jenkins *et al.*, 1997, Sevrioukova *et al.*, 1999]. Large entropy values can be obtained by desolvation of such aromatic amino acids (*c.f.* Putidaredoxin and P450 CAM [Sligar *et al.*, 1976]).

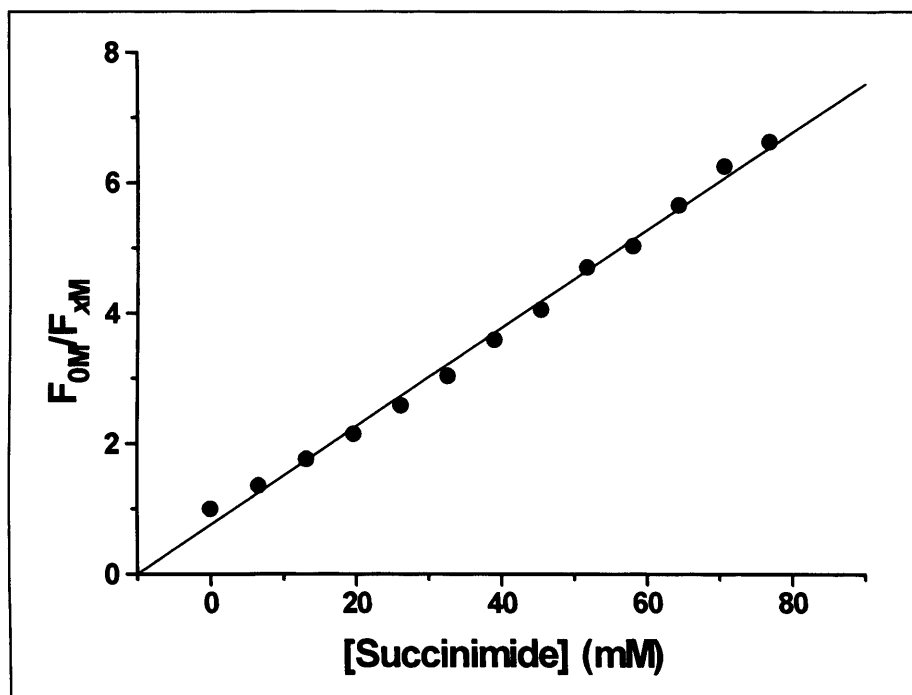


**Figure 4.36** A plot showing the relationship between the change in fluorescence of aromatic residues (fluorescence at 0 M / fluorescence at x M succinimide [ $F_{0M}/F_{XM}$ ]) in YkuN (4  $\mu$ M) and the concentration of the quenching agent succinimide. Data were fitted to a linear function to determine the Stern-Volmer constant (0.075). Data were collected at 25 °C in KPi buffer (50 mM, pH 7.0). Slit widths on the Cary Eclipse fluorimeter were 5 nm, the excitation wavelength was 290 nm, a 1 cm pathlength cell was used, and the emission was measured between 300 and 400 nm.

The Stern-Volmer constant was measured by the addition of aliquots of succinimide (10  $\mu$ l aliquots of a 2 M stock), which causes a reduction in the tryptophan fluorescence (measured by excitation at 290 nm, emission between 300 and 400 nm recorded). Succinimide (2,5-pyrrolidinedione), being an uncharged hydrophilic molecule, quenches fluorescence via a collision process, masking the tryptophans from solvent. Hence, the Stern-Volmer value obtained represents the degree of solvent exposure and hence likelihood of collision each tryptophan residue has with the quenching agent. The



values for fluorescence quenching from the FMN cofactor show the effect that quenching the tryptophan residues has on the flavin emission, hence their negative values represent the increase in flavin emission as the quenching effect of the tryptophans is lessened [Centeno and Gutierrez-Merino, 1992].

Protein	Stern-Volmer constant ( $K_{SV}$ )			
	Tryptophan	Tryptophan (rpt)	FMN	FMN (rpt)
YkuN holofld	0.0750	0.0810	-0.0019	-0.0019
YkuP holofld	0.0600	0.0590	-0.0017	-0.0019
YkuN apofld	0.0065	0.0060	n/a	n/a
YkuP apofld	0.0058	0.0056	n/a	n/a
<i>E. coli</i> FLD	0.0006		-0.0011	

**Table 4.11** Stern-Volmer constants for the fluorophores of YkuN and YkuP indicating degree of solvent exposure. The *B. subtilis* flavodoxins are expected to have a more solvent exposed cofactor compared to the *E. coli* protein, which despite containing four tryptophans, had a lower Stern-Volmer constant. The *E. coli* fld was used in its holoprotein form. N/a means non-applicable as no flavin present in the apoprotein.

The Stern-Volmer constant for YkuN is higher than that of YkuP, which could be due to the fact that YkuN contains double the number of tryptophans, yet it is surprising as it implies that YkuN's tryptophans are more solvent exposed in the native conformation. This is contrary to the tryptophan emission maximum in the native state of YkuN that was at 348 nm compared to that of YkuP at 352 nm.

The Stern-Volmer constants for the apoproteins are around 10-fold lower than those of their corresponding holoproteins. Removal of the FMN cofactor causes a reduction in the degree of solvent exposure of the tryptophans. This may be due to the 60 loop tryptophan packing tightly against the *si*-face residue in the 90 loop upon the removal of FMN, and thereby shielding itself from the quenching agent. A similar phenomenon has been observed in the generation of the *Anabaena* PCC 7119 apoflavodoxin where the flavin-binding loops rearranged to form a more compact structure [Genzor *et al.*, 1996]. The difference in the Stern-Volmer values for the two-forms of YkuP is similar to that of YkuN's two forms despite the CD profile of the holo- and apoprotein being so different (see Figure 4.9). This is possibly due to the extra tryptophan residue in YkuN being positioned more internally to the protein so that the

differences in the secondary structure have no effect upon solvent exposure. The Stern-Volmer values in relation to the increasing FMN emission are virtually identical, which is not surprising as the FMN fluorescence would be most affected by the 60 loop tryptophan, a residue and region that are highly conserved.

#### **4.17 Flavodoxin binding to P450 BioI**

The quenching of FMN fluorescence upon the binding of the flavodoxin to P450 BioI was measured and used to determine an apparent dissociation constant for the interaction between the two proteins. It is expected that the FMN will be held on the surface of the flavodoxin [Watt *et al.*, 1991] and upon binding to the P450 will become partially if not totally buried [Sevrioukova *et al.*, 1999]. Therefore the amount of solvent exposure of the flavin is inversely related to the amount of flavodoxin:P450 complex [Centeno and Gutierrez-Merino, 1992]. Both flavodoxins exhibited a co-operative binding curve. Initial addition of the flavodoxin to a solution of P450 BioI caused a quenching of the FMN fluorescence when the control spectra (no P450 BioI present) were subtracted. No account of light scattering by the presence of a second protein is made.

Total quenching of the FMN in the presence of P450 BioI (2.10 nmol) was found at approx. 1 molar equivalent (YkuP) and almost 2 molar equivalents (YkuN) with the 50 % values being 1.19 nmoles for YkuP and 2.03 nmol for YkuN. As FMN fluorescence is used as a marker of binding, the oxidised form of the flavodoxin was assessed (as the reduced forms of the flavodoxins had decreased fluorescence, and since oxidation of the FMN concomitant with P450 BioI reduction would occur). Although there is little structural change expected upon reduction to the semiquinone or hydroquinone form, any alterations that occur are likely to be in the conformation of the FMN binding loops – the region involved in redox partner docking. For example, reduction of the oxidised flavodoxin from *C. beijerinckii* to its semiquinone results in a peptide flip of the peptide bond between Gly57 and Asp58 as the carbonyl of Gly57 moves to form a hydrogen bond with the isoalloxazine N(5)H [Ludwig *et al.*, 1997, Kasim and Swenson, 2000]. A similar phenomenon is seen when the flavodoxin from *D. desulfuricans* is reduced to its

semiquinone. The carbonyl group of Gly61 points away from the flavin in the oxidised form. Upon reduction, the peptide bond between Gly61 and Met62 flips to allow the Gly61 carbonyl to hydrogen bond to the protonated N(5) of the semiquinone [Romero *et al.*, 1996].

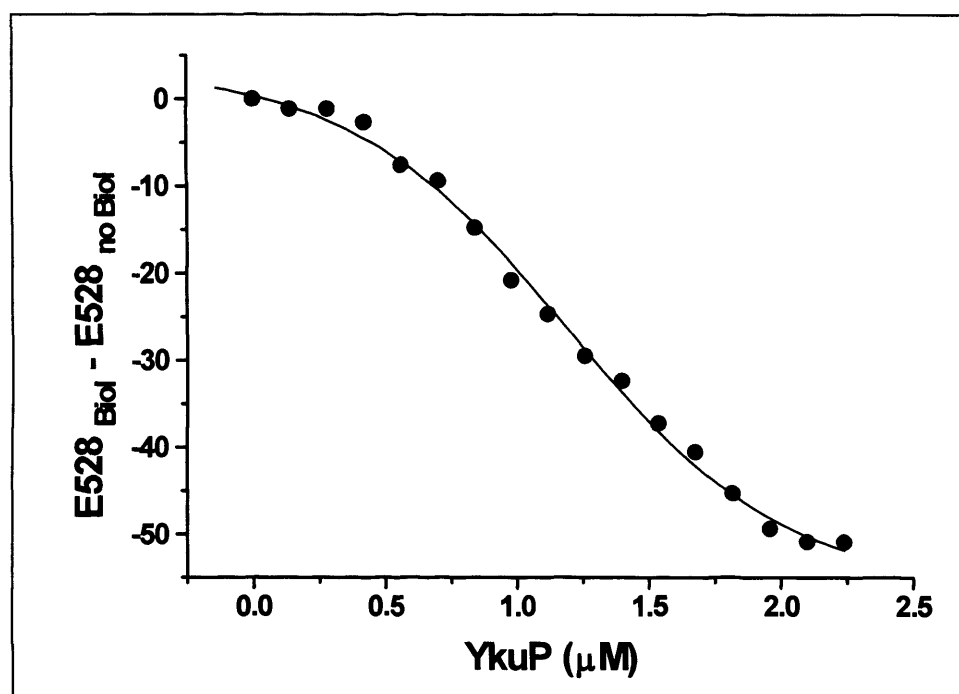


**Figure 4.37** The quenching of FMN fluorescence (emission at 528 nm) when flavodoxin is added to a constant amount of P450 BioI. The midpoint value (1.19 nmoles) is almost half the amount of P450 BioI (2.10 nmoles) in the solution implying a tight binding equilibrium of 1:1. Data were collected at 25 °C in KPi buffer (50 mM, pH 7.0). Slit widths on a Cary Eclipse fluorimeter were 5 nm, the excitation wavelength was 450 nm, a 1 cm pathlength cell was used, and the emission (in arbitrary fluorescence units) was measured between 500 and 600 nm.

The quenching of the FMN fluorescence upon addition of P450 BioI is sigmoidal in nature i.e. indicative of a co-operative process. This could imply that the flavodoxin exists in solution as a dimer. Indeed, adrenodoxin the iron-sulphur electron transfer protein is believed to be a functional dimer in solution [Pikuleva *et al.*, 2000] (see Section 1.3) and the flavodoxin from *A. vinelandii* exists as a dimer, a disulphide bond being present between the monomers [Steensma *et al.*, 1996]. There are many proteins with flavodoxin-like domains that are known to be multimers [Eschenbrenner *et al.*, 1995]; for example, WrbA (a tryptophan repressor binding protein) exhibits multimerization

associated directly with the flavodoxin-like domain itself [Grandori *et al.*, 1998] as does its yeast homologue: Ycp4 [Toda *et al.*, 1991].

#### 4.18 Kinetics of electron transfer from YkuN/P to P450 BioI

Stopped-flow measurements were made to determine the rate constants for the single electron transfer to P450 BioI. These were measured by following the formation of the ferrous-carbon monoxide complex of the P450 (in CO-saturated buffer) that has a strong absorbance at 448 nm ( $\epsilon = 91 \text{ mM}^{-1}\text{cm}^{-1}$  [Omura and Sato, 1964]). The experiment was carried out anaerobically to prevent auto-oxidation of the flavodoxin or the P450. The P450 (4  $\mu\text{M}$ ) was bound to either palmitoleic acid (to give the high-spin complex) or the steroid testosterone (to give a low spin complex). As reduction of the high-spin complex is thermodynamically favoured, this rate is expected to be faster than that for the low-spin complex. The flavodoxin was reduced by sodium dithionite to give predominantly hydroquinone flavin. Excess dithionite was removed (by gel filtration), the reduced flavodoxin was mixed with the P450 and the resulting spectral changes (300 nm – 700 nm) were measured using a photodiode array device connected to the stopped-flow spectrophotometer. The electron transfer is known to occur via a ping-pong mechanism with the flavodoxin shuttling electrons from a reductase to the P450 *in vivo* (see Section 1.3) [Jenkins and Waterman, 1994]. The flavodoxin probably shuttles between hydroquinone and semiquinone forms as it delivers electrons between redox partners.

The formation of the P450-CO adduct was measured and the increase in the absorbance at 449 nm plotted against time. The experiment was repeated with several concentrations of redox partner to identify a maximum rate ( $k_{\text{red}}$ ) and the apparent  $K_d$  for the redox partner – P450 interaction. The PDA data were fitted to a simple model ( $A + B \rightarrow C + D$  where species A (HQ Fld) and B (OX P450) go to form species C (SQ Fld) and D (CO-P450)) to obtain the rates at each concentration of redox partner.

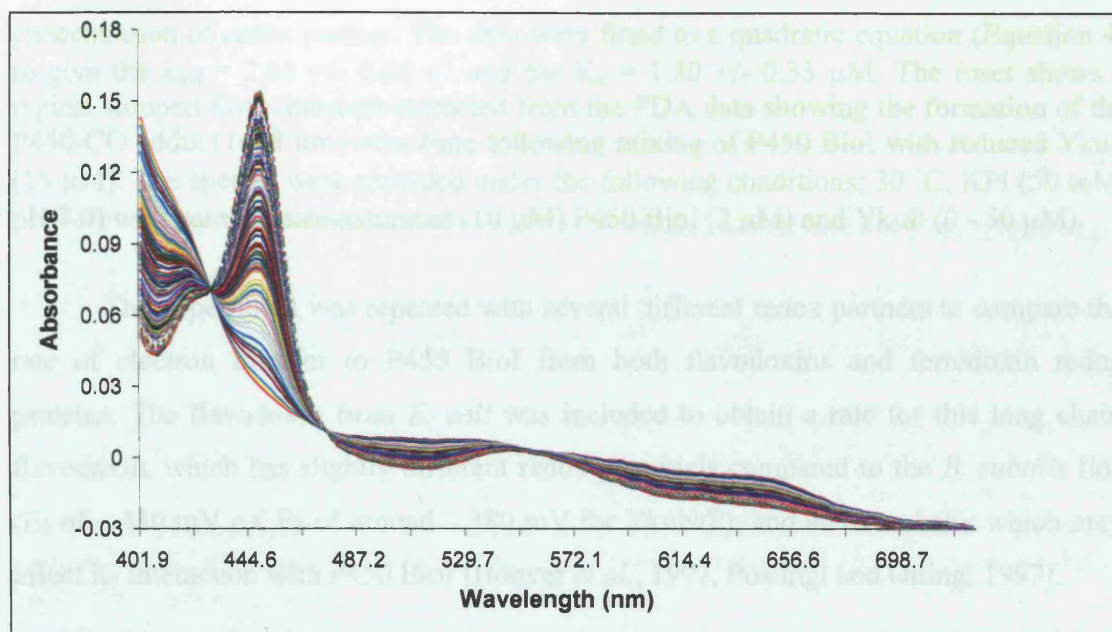


**Figure 4.38** Spectra collected over 8 seconds by stopped-flow diode array spectroscopy following the reduction of P450 BioI by the *B. subtilis* flavodoxin YkuN. The ferrous form of the P450 is trapped by CO ligation and its formation can be seen at 448 nm. The increasing peak at  $\sim 550$  nm is due to the merging of the P450's  $\alpha$  and  $\beta$  bands and the increase at  $\sim 600$  nm is due to the formation of the fld SQ. Conditions were  $30^\circ\text{C}$ , KPi (50 mM, pH 7.0) with P450 BioI (2  $\mu\text{M}$ ) and YkuN (15  $\mu\text{M}$ ).

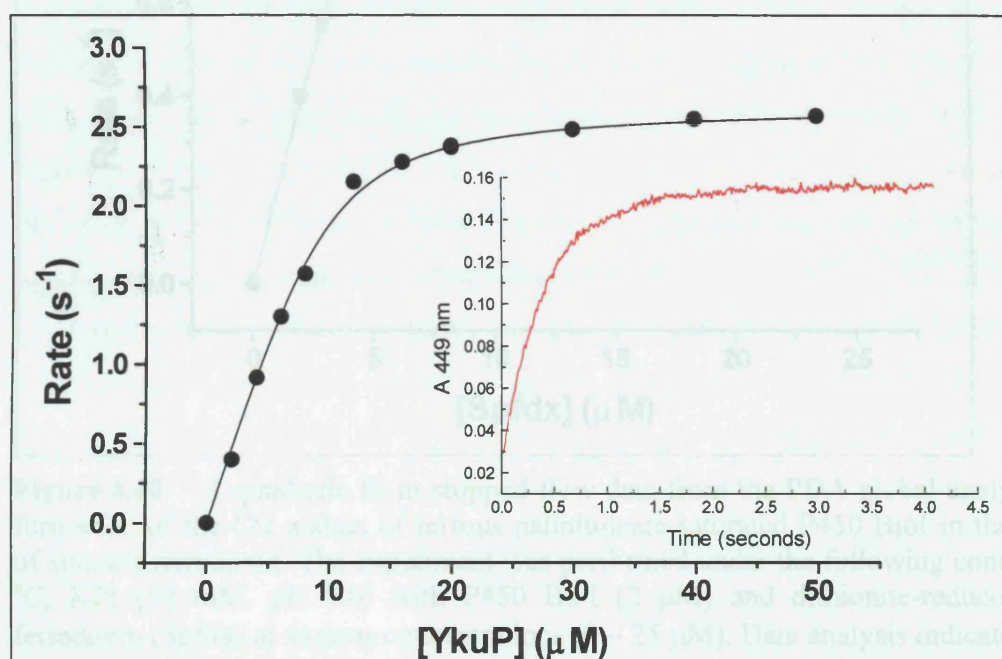


**Figure 4.39** The limiting rate of the 1-electron transfer from pre-reduced YkuP to P450 BioI is found by plotting the apparent rate of formation of the P450 adduct against the

concentration of redox partner. The data were fitted to a quadratic equation (Equation 4) to give the  $k_{red} = 2.64 \pm 0.05 \text{ s}^{-1}$  and the  $K_d = 1.30 \pm 0.33 \text{ }\mu\text{M}$ . The inset shows a typical stopped-flow transient extracted from the PDA data showing the formation of the P450-CO adduct (448 nm) over time following mixing of P450 BioI with reduced YkuP (15  $\mu\text{M}$ ). The spectra were recorded under the following conditions; 30 °C, KPi (50 mM, pH 7.0) with palmitoleate-saturated (10  $\mu\text{M}$ ) P450 BioI (2  $\mu\text{M}$ ) and YkuP (0 - 50  $\mu\text{M}$ ).

The experiment was repeated with several different redox partners to compare the rate of electron transfer to P450 BioI from both flavodoxins and ferredoxin redox proteins. The flavodoxin from *E. coli* was included to obtain a rate for this long chain flavodoxin, which has slightly different redox potentials compared to the *B. subtilis* flds ( $E_2$  of -410 mV *c.f.*  $E_2$  of around -380 mV for YkuN/P), and an extra helix which may affect its interaction with P450 BioI [Hoover *et al.*, 1997, Postingl and Otting, 1997].

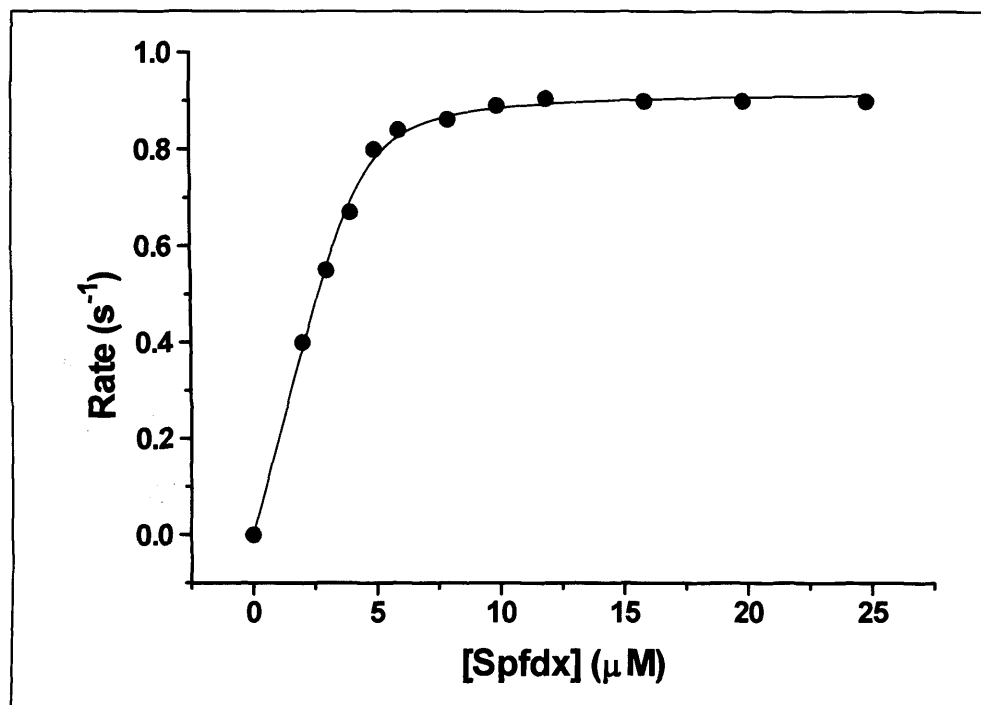


**Figure 4.40** A quadratic fit to stopped-flow data from the PDA global analysis of the formation of the CO adduct of ferrous palmitoleate-saturated P450 BioI in the presence of spinach ferredoxin. The experiment was performed under the following conditions; 30 °C, KPi (50 mM, pH 7.0) with P450 BioI (2  $\mu\text{M}$ ) and dithionite-reduced spinach ferredoxin (Spfdx) at various concentrations (0 - 25  $\mu\text{M}$ ). Data analysis indicates a  $k_{red}$  of  $0.92 \pm 0.01 \text{ s}^{-1}$  and an apparent  $K_d$  of  $0.24 \pm 0.08 \text{ }\mu\text{M}$ .



Redox Partner	Ligand	$k_{\text{red}}$ ( $\text{s}^{-1}$ )	Error (+/-)	$K_d$ ( $\mu\text{M}$ )	Error (+/-)
YkuN	Palmitoleic acid	2.33	0.05	0.36	0.08
YkuP	Palmitoleic acid	2.64	0.05	1.30	0.33
Spinach ferredoxin	Palmitoleic acid	0.92	0.01	0.24	0.08
<i>E. coli</i> FldA	Palmitoleic acid	0.20	0.01	4.54	0.68
YkuN	Testosterone	0.18	0.01	0.52	0.19
YkuP	Testosterone	0.30	0.02	1.23	0.36

**Table 4.12** Kinetic parameters from the stopped-flow analysis of the single electron transfer from a variety of dithionite-reduced redox partners to P450 BioI. Stopped-flow data from the PDA analysis of the rate of formation of the CO adduct of ferrous P450 BioI were plotted against the concentration of redox partner, and fitted to a quadratic equation.  $k_{\text{red}}$  is the maximal rate of electron transfer between redox partner and P450 under the conditions used.

A large difference is seen between the rates depending upon whether the P450 is in high- or low-spin form due to the thermodynamic properties of the heme. The high-spin form favours electron transfer down the electro-potential gradient. The slower rate observed for the steroid-bound form may be affected in part by the CO molecule having to compete with the steroid for the sixth axial ligand position of the heme iron. In addition, coordination of the heme iron by the carbonyl group of the steroid may affect the addition of an electron to the iron atom. By donating electrons to the iron, the carbonyl oxygen may distort the typical electronic arrangement of the iron atom. However, we do not know whether the steroid remains bound to the heme upon the latter's reduction. Whilst redox titrations have shown no sign of hysteresis, it is not clear whether the steroid merely re-ligates upon the oxidation of the heme by ferricyanide, the large excess of the steroid in solution and its small  $K_d$  value ( $< 15 \mu\text{M}$ ) enabling rapid ligation. Indeed, we know that the carbonyl oxygen is a weak ligand, its visible maximum being at 418 nm compared to the stronger nitrogen ligation of the azoles with a maximum at 424 nm. All the rates are relatively slow, *c.f.* electron transfer from putidaredoxin to P450 CAM at  $10 - 15 \text{ s}^{-1}$  [Hintz *et al.*, 1982]. The rate when the *E. coli* fld is used as oppose to P450 BioI's native flds is also substantially slower (about 16 times slower). The rate of the one electron transfer to P450 BioI from its native ferredoxin is reported to

be slow,  $0.03 \text{ s}^{-1}$  in the presence of saturating myristic acid [Green *et al.*, 2001]. Thus YkuN and YkuP are faster reductants of BioI than the host ferredoxin, Fer.

PDA stopped-flow measurements were carried out to find the rate of formation of the P450-CO adduct when *E. coli* flavodoxin reductase (FldR) supplied electrons via the oxidation of NADPH. This involved the rapid mixing of a solution of NADPH ( $40 \text{ }\mu\text{M}$ ) with a mixture of the three proteins (FldR, YkuN or YkuP and P450 BioI [fatty acid-bound]). The rate of the formation of the CO adduct would therefore be an approximate measure of the rate of the transfer of the first electron from its source, NADPH, through the redox partner chain to the terminal electron acceptor, the P450 heme iron. The rate would therefore reflect the interactions of all the proteins with their redox partners and give an indication of the electron transfer rate that would be seen in a catalytic scenario.

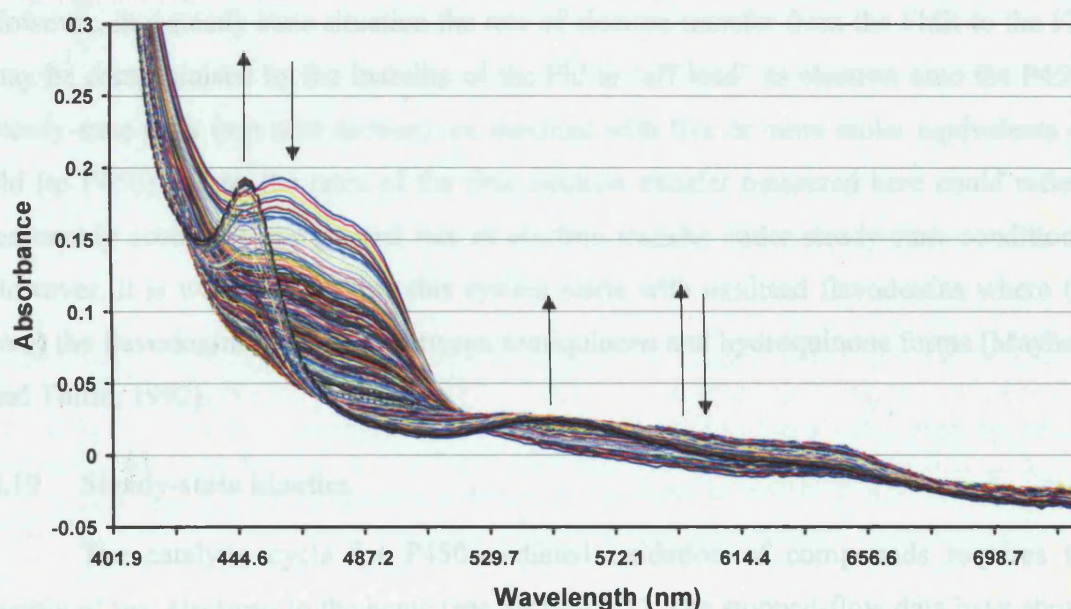


**Figure 4.41** Spectral changes that occur when NADPH ( $40 \text{ }\mu\text{M}$ ) is rapidly mixed with a solution of *E. coli* FldR ( $20 \text{ }\mu\text{M}$ ), YkuN ( $20 \text{ }\mu\text{M}$ ) and P450 BioI ( $4 \text{ }\mu\text{M}$ ). The arrows show the direction of the absorbance change due to the formation of the CO adduct ( $448 \text{ nm}$ ), decay of the oxidised flavins ( $460 \text{ nm}$ ), merging of the heme's  $\alpha$ - and  $\beta$ -bands ( $560 \text{ nm}$ ) and the rise and fall of the semiquinone absorbance (*ca*  $600 \text{ nm}$ ). Spectra were collected over a 200 second timescale in KPi buffer ( $50 \text{ mM}$ , pH 7.0).

The PDA data were fitted using Global Analysis software to find the rate of the electron transfer. Due to the oxidised flavin peak and the formation of the P450-CO peak

overlapping, the software had difficulty fitting a model. To aid fitting, the data were divided into two separate time-scales; the first reflected the reduction of the flavins and was fitted to a simple model ( $A \rightarrow B$ ,  $B \rightarrow C$ ). The second section was fitted to the model ( $A \rightarrow B$ ). The rates for the reaction conditions evaluated with YkuN as the Fld were, for the first sector, ( $A \rightarrow B$ )  $k_1 = 14.0 \text{ s}^{-1}$  and ( $B \rightarrow C$ )  $k_2 = 3.7 \text{ s}^{-1}$ . For the second sector the rate ( $A \rightarrow B$ )  $k_3$  was  $0.55 \text{ s}^{-1}$ . With YkuP (20  $\mu\text{M}$ ) the rates were  $k_1 = 14.3 \text{ s}^{-1}$ ,  $k_2 = 2.4 \text{ s}^{-1}$ , and  $k_3 = 0.8 \text{ s}^{-1}$ . These rates are postulated to reflect the following transitions;  $k_1$  = FAD reduction (bleaching of oxidised peak, *ca* 560 nm),  $k_2$  = FMN reduction (semiquinone formation, *ca* 600 nm) and  $k_3$  = P450 reduction (formation of the 448 nm CO adduct) respectively. As the P450 is trapped in its CO-bound form to allow measurement, these rates can therefore only reflect the transfer of one electron, and from these data it seems that the transfer of an electron from the Fld to the P450 is the slowest step in the process. However, in a steady-state situation the rate of electron transfer from the FldR to the Fld may be compromised by the inability of the Fld to 'off load' its electron onto the P450. Steady-state rates (see next section) are maximal with five or more molar equivalents of Fld (to P450) and so the rates of the first electron transfer measured here could reflect reasonably accurately the general rate of electron transfer under steady-state conditions. However, it is worth noting that this system starts with oxidised flavodoxins where (*in vivo*) the flavodoxins may cycle between semiquinone and hydroquinone forms [Mayhew and Tollin, 1992].

#### 4.19 Steady-state kinetics

The catalytic cycle for P450-mediated oxidation of compounds requires the supply of two electrons to the heme (see Section 1.1). The stopped-flow data have shown the ability of the various redox partners to shuttle a single electron to the P450 reducing it from its 5-coordinate (fatty acid saturated) or 6-coordinate (steroid saturated) ferric state to the 6-coordinate ferrous state (with CO bound). The ability of the various electron transfer proteins to supply a second electron, i.e. reduce the 6-coordinate superoxo-bound ferric heme, therefore needed to be assessed to see if any of the redox partners were able to support P450 BioI's catalytic function. To do this the consumption of NADPH, as observed by a decrease in the absorbance at 340 nm, was used to measure the rate of

turnover of a variety of compounds with various redox partners for P450 BioI. *E. coli* flavodoxin reductase was used to mediate the electron transfer from NADPH to the flavo- or ferredoxin. The experiments were performed with the *B. subtilis* flavodoxins, YkuN and YkuP, the *B. subtilis* [4Fe-4S] ferredoxin, Fer, and the *E. coli* flavodoxin, the rates all being compared.

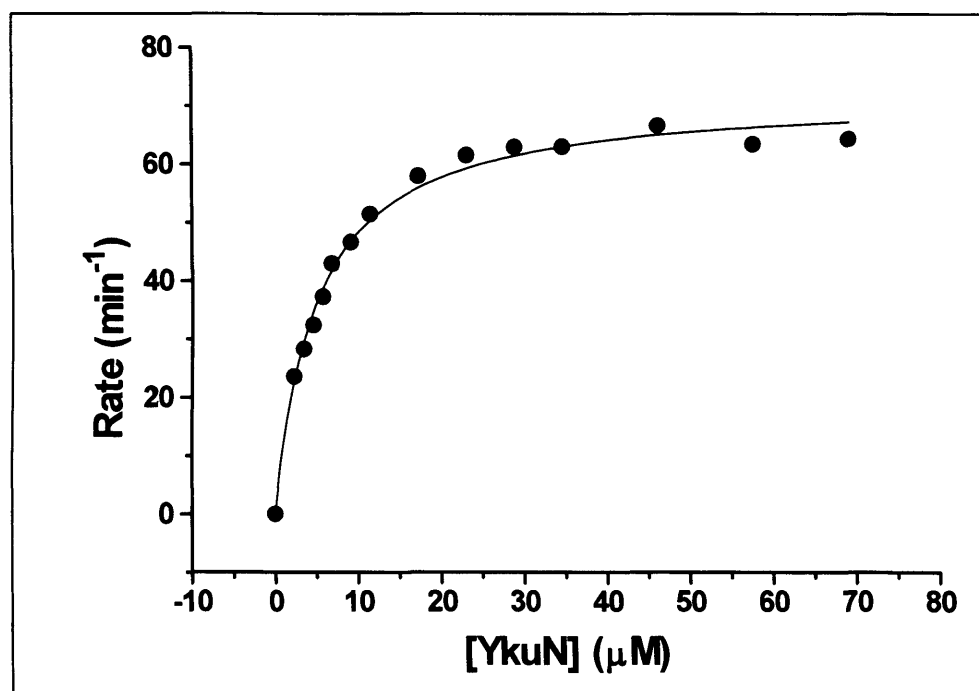


**Figure 4.42** The turnover of palmitic acid by P450 BioI (2.3 μM) with the *B. subtilis* flavodoxin YkuN as redox partner for P450 BioI. Data from the initial rate of oxidation of NADPH versus the concentration of redox partner are fitted to a rectangular hyperbola (Equation 6). Here the  $k_{\text{cat}}$  is  $71.97 \pm 1.14 \text{ min}^{-1}$  and the  $K_d$   $4.95 \pm 0.31 \text{ μM}$ . The experiment was performed under the following conditions; 30 °C, in aerated KPi buffer (50 mM, pH 7.0), the consumption of NADPH being measured by the decrease in absorbance at 340 nm over 3 minutes.

To allow comparison of the ability of the various redox partners to support the catalytic function of P450 BioI, the rates of the turnover of palmitoleic acid (a C16 unsaturated straight-chain fatty acid) was measured with all redox partners at 30 °C. Palmitoleic acid, being one of the tightest binding substrates with a  $K_d$  of  $0.87 \text{ μM} \pm 0.06 \text{ μM}$ , was a good representative of a substrate molecule giving near-full conversion of the heme to high-spin upon saturation, elevating the heme's potential by around 130 mV (see Section 3.8).

Redox partner	$k_{\text{cat}}$ ( $\text{min}^{-1}$ )	Error (+/-)	$K_m$ ( $\mu\text{M}$ )	Error (+/-)
YkuN	25.74	1.48	11.46	1.51
YkuP	23.87	1.04	14.65	1.44
Ferredoxin	61.24	6.27	7.58	1.57
<i>E. coli</i> FLD	No turnover	-	-	-

**Table 4.13** Comparison of the steady-state turnover of palmitoleic acid by P450 BioI (2.3  $\mu\text{M}$ ) when partnered by different redox proteins. Data from the initial rate of oxidation of NADPH (decrease in  $A_{340}$ ) versus the concentration of redox partner are plotted and fitted to a rectangular hyperbola (Equation 6) to calculate the kinetic parameters. The experiments were all performed at 30 °C, in aerated KPi buffer (50 mM, pH 7.0).

The fastest rate was observed with the ferredoxin from *B. subtilis* ( $k_{\text{cat}} = 61.2 \pm 6.3 \text{ min}^{-1}$ ) possibly pointing towards P450 BioI being a typical class I P450 utilising a ferredoxin as a redox partner. However, the [4Fe-4S] cluster in this ferredoxin is distinct from that used in other class I P450s. Indeed, earlier CO-trapping work using spinach ferredoxin had shown relatively fast rates. However, a surprising result was that no steady-state turnover was observed with the *E. coli* fld, even though this protein has been seen to pass electrons to P450 BioI by the formation of the ferrous-carbon monooxy adduct, albeit slowly. BioI and *E. coli* fld were used in a further experiment to examine turnover of myristic acid, but again no turnover was seen even when the fld was at 30-fold molar excess. Little difference was seen between the two *B. subtilis* flds with this substrate. The faster rate observed with the ferredoxin ( $61.24 \pm 6.27 \text{ min}^{-1}$ ) may suggest that a ferredoxin could be the native partner of P450 BioI. In previous studies, tight binding of P450 BioI to the *B. subtilis* ferredoxin, Fer, had been observed ( $K_d = 0.87 \mu\text{M}$ , [Green *et al.*, 2003]). These data may be in agreement with flavodoxins replacing ferredoxins under conditions of iron stress [Ullmann *et al.*, 2000]. As the *ykuNOP* operon is part of the *fur* regulon, their transcription is regulated in response to iron starvation [Baichoo *et al.*, 2002].

Steady-state kinetic studies for a variety of fatty acids and a steroid substrate using YkuN and YkuP as the redox partner were then carried out to see how alternate substrates affected the turnover rate. These experiments gave the following values (Table 4.14), where the concentration of the fld was varied and the concentration of ligand kept constant (near-saturating at *ca* 25 fold molar excess over the P450);

Redox Partner	Substrate	$k_{\text{cat}}$ ( $\text{min}^{-1}$ )	Error (+/-)	$K_m$ ( $\mu\text{M}$ )	Error (+/-)
YkuN	Lauric acid	81.46	2.92	6.00	0.87
YkuN	Myristic acid	75.34	2.59	6.67	0.87
YkuN	Palmitic acid	71.97	1.14	4.95	0.31
YkuN	Testosterone	24.04	0.72	4.44	0.56
YkuP	Lauric acid	103.91	5.24	15.81	2.24
YkuP	Myristic acid	82.87	3.47	20.77	2.15
YkuP	Palmitic acid	88.76	4.70	18.01	2.43
YkuP	Testosterone	28.45	1.35	6.07	0.97

**Table 4.14** Steady-state turnover with a variety of substrates by P450 BioI (2.3  $\mu\text{M}$ ) utilising the *B. subtilis* flavodoxins (various concentrations) as redox partners. Data from the initial rate of oxidation of NADPH (decrease in  $A_{340\text{ nm}}$ ) versus the concentration of redox partner are plotted and fitted to a rectangular hyperbola (Equation 6) to calculate the kinetic parameters. The experiments were all performed at 30 °C, in aerated KPi buffer (50 mM, pH 7.0).

There was little difference observed in the  $k_{\text{cat}}$  values for the three fatty acid substrates analysed, although laurate gave the highest  $k_{\text{cat}}$  value in both cases. This is probably due to the three fatty acids having similar structures and similar binding affinity for P450 BioI. However, rate limiting electron transfer and/or redox partner docking cannot be ruled out at this stage. All three of these substrates give near-full conversion of the heme to high-spin upon binding, thus favouring the reduction of the iron by near-complete removal of the aqua ligand. The much slower rate observed when P450 BioI was bound to the steroid testosterone reflects the diminished ability of the flavodoxins to reduce the heme as seen in the stopped-flow work. This probably mainly arises from the binding of testosterone causing the heme iron to remain in a low-spin configuration, making it thermodynamically harder to reduce. Whether the postulated actual ligation of the heme by the steroid's carbonyl group and the fact that the smaller radius of the low-spin iron causes it to lie in the plane of the porphyrin ring may also play a role in the slower rate of reduction is unclear. However, surprisingly, there is some stimulation of NADPH oxidation in the presence of testosterone.

From the steady-state rates tabulated above, it can be seen that the turnover of fatty acids proceeds at around 90 per minute, i.e. 1.5 per second. This steady-state rate applies to the transfer of two electrons (as it is equal to the loss of the hydride ion) so it



can be seen that, when compared to the earlier data for the single electron transfer to P450 BioI from the flds at *ca.* 3 per second, the rates are reasonably similar. This means that it is likely that it is the electron transfer, as opposed to substrate binding or product release, that is the major rate-limiting step. This is perhaps indicative that the flds are the natural redox partners to P450 BioI, since electron transfer is also known to be rate limiting in the catalytic cycle of P450 CAM [Hintz *et al.*, 1982]. Also of note is that the stopped-flow rate of single electron transfer from the *E. coli* reductase to the flds was again *ca.* 3 per second. However, the rate of electron transfer from this reductase to its endogenous fld has been shown to accelerate significantly when the system is coupled with a terminal electron acceptor such as the heme domain of P450 BM3, perhaps forming a ternary complex [McIver *et al.*, 1998].

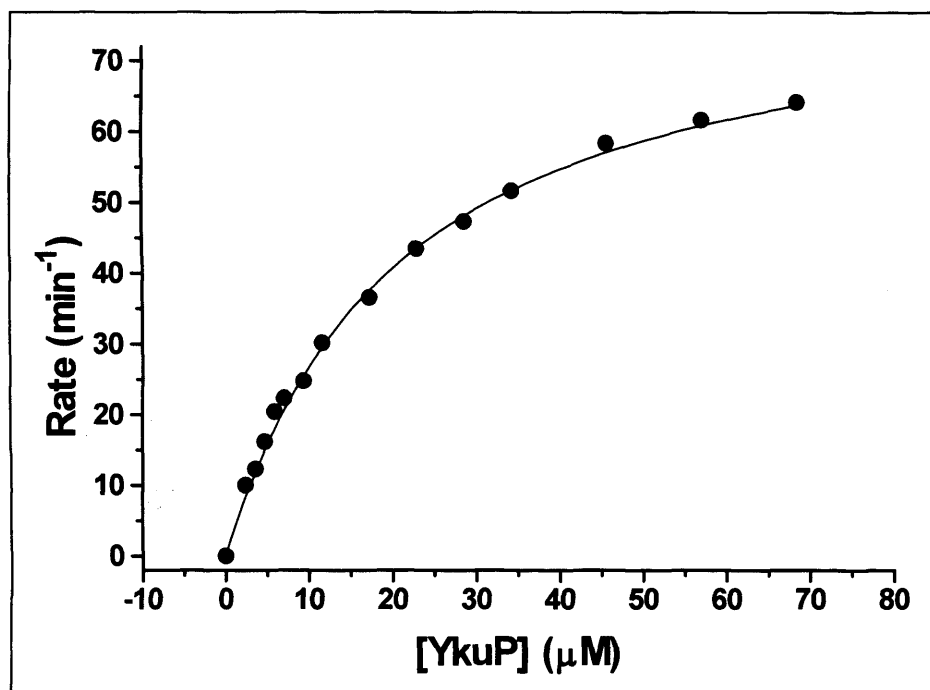


**Figure 4.43** The relationship between the rate of steady-state turnover of myristic acid and the concentration of YkuP. Data from the initial rate of oxidation of NADPH versus the concentration of redox partner are fitted to a hyperbolic function (Equation 6). Here the  $k_{cat}$  is  $82.9 \pm 3.5 \text{ min}^{-1}$  and the  $K_m$  is  $20.8 \pm 2.2 \mu\text{M}$ . The experiment was performed under the following conditions; 30 °C, in KPi buffer (50 mM, pH 7.0), P450 BioI (2.3  $\mu\text{M}$ ), myristic acid (50  $\mu\text{M}$ ) and FldR (0.1 mM). The consumption of NADPH was measured by the decrease in absorbance at 340 nm over 3 minutes.

The steady-state reaction of the P450 BioI system with myristic acid (the tightest binding saturated straight chain fatty acid with a  $K_d$  of *ca* 3 - 5  $\mu\text{M}$ ) was analysed again to determine the  $k_{\text{cat}}$  and  $K_m$  for this substrate. The amount of redox partners remained constant with both the reductase and fld being in five fold excess of P450 BioI (1.0  $\mu\text{M}$ ), and NADPH (2 mM) was in excess to allow multiple turnovers to occur. The concentration of the fatty acid was varied. A stock solution of myristate (25 mM) was prepared in ethanol and this was added to the aqueous solution of proteins to give the desired concentration (0 – 16  $\mu\text{M}$ ). Additional ethanol was then added, if required, so that the concentration of the alcohol remained constant at 0.5 % v/v. At this level the alcohol had negligible effect upon the interaction of P450 BioI with myristate (see Section 3.4).

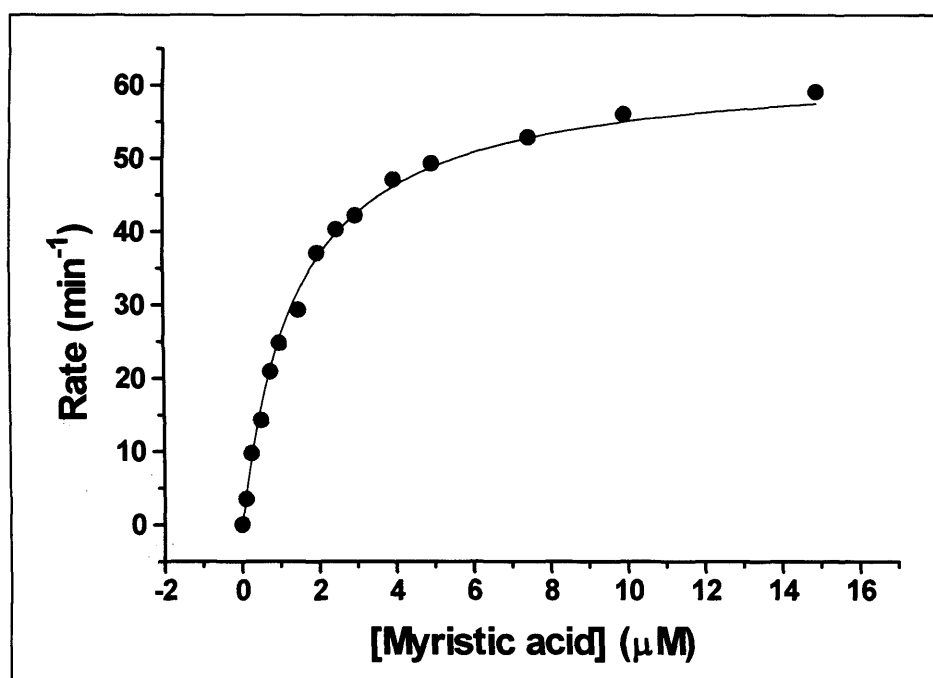


**Figure 4.44** Steady-state turnover of myristic acid with YkuN as the redox partner. NADPH was at 2 mM and myristate was varied between 0 and 16  $\mu\text{M}$ . The initial rate ( $\Delta A_{340}$  nm in the first few seconds) was plotted against the relevant [myristate] and the data fitted to a rectangular hyperbola (Equation 6) to compute the relevant kinetic parameters ( $k_{\text{cat}} = 63.1 \pm 2.0 \text{ min}^{-1}$  and  $K_m = 1.5 \pm 0.2 \mu\text{M}$ ). Reactions were performed at 30 °C in KPi (50 mM, pH 7.0) with P450 BioI (1.0  $\mu\text{M}$ ), YkuN (5.0  $\mu\text{M}$ ) and FldR (5.0  $\mu\text{M}$ ).

The rates measured at the different concentrations of substrate were plotted versus the concentration of fatty acid and fitted to a rectangular hyperbola to find the kinetic parameters. As can be seen from the data tabulated below, there is a large difference

between the  $k_{\text{cat}}$  and  $K_{\text{m}}$  value for myristic acid depending upon which redox partner is used.

Flavodoxin	$k_{\text{cat}}$ ( $\text{min}^{-1}$ )	Error (+/-)	$K_{\text{m}}$ ( $\mu\text{M}$ )	Error (+/-)
YkuN	63.09	1.99	1.47	0.15
YkuP	23.56	1.10	0.45	0.12

**Table 4.15** *B. subtilis* flavodoxins (5.0  $\mu\text{M}$ ) were used as redox partners in the steady state kinetic analysis of myristate oxidation by P450 BioI (2.3  $\mu\text{M}$ ). Data from the initial rate of oxidation of NADPH (decrease in  $A_{340}$ ) versus the redox partner concentration were plotted and fitted to a rectangular hyperbola (Equation 6) to find the kinetic parameters. The experiments were all performed at 30 °C, in aerated KPi buffer (50 mM, pH 7.0).

The ability of both the *B. subtilis* flds to function as catalytically viable redox partners to P450 BioI means that they could substitute for Fer (the sole *B. subtilis* ferredoxin [Green *et al.*, 2003]) in cases of iron limitation, or that they are in fact the actual biological partner to P450 BioI in the biotin biosynthetic pathway. The redox system analysed in the kinetic work described here was used to turn over a variety of substrate-type compounds as described in Chapter 5.

#### 4.20 Crystallisation trials of YkuN and YkuP

To determine the structures of YkuN and YkuP, crystal trials were set-up. Solutions of either fld (10 and 20 mg/ml) were screened against a variety of precipitant conditions using the Molecular Dimensions Ltd Clear Strategy Screen kits I and II, an in house salt screen (prepared by Dr D. Leys, University of Leicester) that consisted of 160 different conditions and various ammonium sulphate and PEG screens. These were repeated with different concentrations of fld stock solution (10 to 40 mg/ml), at different pH values (5.0 to 9.0) and at different temperatures (4 to 20 °C). To date none of the screens has yielded crystals. This was surprising as flavodoxins from other species have been relatively easy to crystallise, many having been crystallised under similar conditions involving ammonium sulphate (1.5 – 2.5 M), e.g. the flavodoxins from *D. desulfuricans* [Romero *et al.*, 1996], *C. beijerinckii* [Ludwig *et al.*, 1997] and *A. nidulans* [Hoover *et al.*, 1999].

#### 4.21 Conclusion

The two genes *ykuN* and *ykuP* were successfully cloned and over-expressed in *E. coli*. Both genes were found to encode short-chain flavodoxins. This was contrary to what was predicted from the published gene sequence in the case of YkuP. The cloned *ykuP* genes had an adenosine nucleotide deletion that brought the termination code forward resulting in a protein of smaller mass. This was in keeping with that of short-chain flavodoxins (around 16 – 18 kDa in size). Subsequent amino acid sequence alignments showed the clone to be a typical short-chain flavodoxin. Further evidence that the original sequence is likely to be wrong is that the predicted extra residues are at the C-terminal and not in the middle of the protein, as would be expected for a bonefide long chain fld.

The protein products were typical of other members of their family. Expressed in their semiquinone form they oxidised to yellow upon purification. Both of the flavodoxins bound FMN tightly ( $K_d$  ca. 20 nM) and were unable to bind riboflavin. The two proteins had a relatively stable neutral semiquinone with negative reduction potentials (e.g.  $E_{SQ/HQ}$  of –381 mV for YkuN). Both flavodoxins were reduced by *E. coli* NADPH-oxidoreductase ( $k_{red} \sim 3 \text{ sec}^{-1}$ ) and, in turn, were capable of reducing P450 BioI to achieve steady-state rates in the region of  $90 \text{ min}^{-1}$  with a range of fatty acids. It is likely that these flavodoxins interact with P450 BioI *in vivo* particularly in cases of iron stress when the native ferredoxin Fer is down-regulated [Baichoo *et al.*, 2002]. The interaction of these two flavodoxins with their native *B. subtilis* reductases is described in the following chapter.

## ***Chapter 5***

### ***B. subtilis NADPH oxidoreductases***

To complete the redox chain and allow constitution of an active catalytic system native to *B. subtilis* P450 systems, suitable candidates to carry out the initial oxidation of NADPH were sought. From BLAST searches of the *B. subtilis* genome using known reductases as a basis for the searches, proteins containing both an NAD(P)H and flavin binding motif were hard to find. However, two thioredoxin reductase-like genes were identified (*ycgT* and *yumC*) as plausible components. These proteins had already been recognised as having a putative role in the final BioB-catalysed step of biotin synthesis (DSM, internal report 1998).

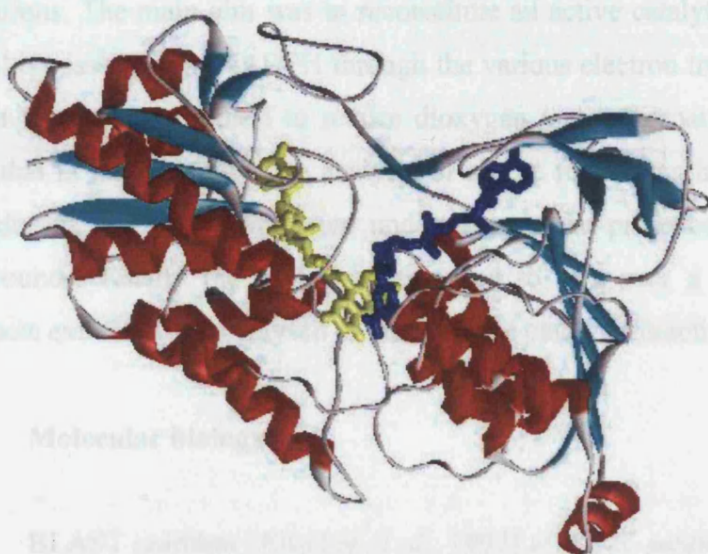


**Figure 5.1** The structure of Adrenodoxin reductase as resolved by x-ray crystallography, showing the FAD cofactor typical of these reductases (yellow) and a bound molecule of NADP<sup>+</sup> (navy) [Ziegler and Schulz, 2000]. The protein is composed of regions of  $\alpha$ -helices (red) and  $\beta$ -sheets (cyan), and unusually for this type of reductase, the NADP<sup>+</sup> is bound in an extended conformation, a conformation more commonly observed in glutathione reductases [Mittl and Schulz, 1994].

The two protein products from the *ycgT* and *yumC* genes were over expressed and purified so that they could be examined for their ability to interact with the flavodoxins YkuN and YkuP. In addition to studying the "traditional" three protein class I system (see Figure 1.6), the diflavin reductase domains of the two class II type P450s native to *B. subtilis* (CYP102A2 and CYP102A3) were cloned with the idea of creating a novel, and possibly more efficient, two-component redox system. It is clearly feasible that the



CYP102A2 and CYP102A3 reductases could support catalytic function of P450s in *B. subtilis* other than those to which they are fused, due to the flexible nature of the peptide linker that joins their reductase domain to their heme domain [Nahri and Fulco, 1987].

After isolation of the various purified reductases basic spectral characterization and N-terminal sequencing was undertaken to confirm the proteins identity and gain information on their overall fold and structure. The various reductase candidates were then studied in terms of their redox properties. Reduction potentials of all of the proteins were measured. The ease in which the proteins were reduced by NADPH and NADH was quantified by kinetic studies involving various electron acceptors under anaerobic conditions. The main aim was to reconstitute an active catalytic system where electrons would be passed from NADPH through the various electron transfer agents to P450 BioI where they would be used to reduce dioxygen and oxygenate a carbon compound. So with this in mind steady-state analysis of all the reductases in a mixture containing the flavodoxins and P450 BioI were undertaken in the presence of various substrate-like compounds. Finally the proteins were used to turn-over a range of fatty acids, the products extracted and analysed to see what the catalytic function of P450 BioI was.

## 5.1 Molecular biology

BLAST searches [Altschul *et al.*, 1997] of the *B. subtilis* genome identifies many genes that encode proteins containing characteristic nucleotide binding motifs such as the N-terminal GXGXXG, a sequence common in nicotinamide binding proteins [Schulz, 1992]. However, when searched against known oxidoreductases such as flavodoxin reductase from *E. coli*, bovine adrenodoxin reductase (Figure 5.1) and FprA from *Mycobacterium tuberculosis*, no significant matches were obtained in *B. subtilis*. A BLAST search of the *B. subtilis* genome with the *E. coli* thioredoxin reductase (EC 1.6.4.5) as the source sequence pulled out many reductase type genes. Unsurprisingly *B. subtilis*' own thioredoxin reductase *trxB* had highest homology, followed by an alkylhydroperoxide reductase NADH dehydrogenase *ahpF* and then the two genes *ycgT* and *yumC* that are also termed thioredoxin reductases. These two genes (*yumC* and *ycgT*) bear a high degree of similarity to one another. Amino acid sequence alignments with

FPRA	----MRPYIIAIVGSGPSAFFFAAASLLKAADTTEDLDMAVDMLEMLPTPWGLVRSQVAPD	56
ADRENODOXIN	-STQEQTQICVVGSGPAGFYTAQHLLKHSR-----AHVDIYEKQLVPFGLVRFQVAPD	54
YumC	MREDTKVYDITIIIGGGPVGGLFTAFYGGMRQAS-----VKIIESLPQLGGQLSALYP--	51
YcgT	MAENQEVYDVTTIIGGGPIGLFTAFYCGMRELK-----TKVIEFLPKLGGKVSLEFFP--	51
TrxB	--GTTKHSKLLILGSGPAGYTAAYVAARANLQ-----PVLITGMKEGGQLTTTTE--	48
FldR	-----MADWVTGKVTQVQNWTDALFSLTVHAP-----VLPFTAG-----	34
	: *	
FPRA	HPKIKSISKQFEKTAEDPRFRFFGNVVGGEHVQPGELSERDYDAVIYAVGAQSDRMLNIPG	116
ADRENODOXIN	HPEVKNVINTFTQTARSDRCAPYGNVEVGRDVTQELQDAYHAVVLSYGAEDHQALDIPG	114
YumC	-----EKYIYDVAGFPKIRAEELINNLKEQMAKFDQTICLEQAVES	92
YcgT	-----EKIIRDIGGIPG TAGQLIEQLKEQATFPDPVNLQRVVTG	92
TrxB	-----VENWGDGPNDLTGPLLMERMHEHATKFEETIIFDHINKV	87
FldR	-----QFTKLGLDGERVQRAYSYVNSPDNPDLFEFYLVTVP	71
	: :	
FPRA	EDLPGSIAAVDFVGVWYNAHPHFQVSPDLSGARAVVIGNGNVALDVARIILLTDPDVLART	176
ADRENODOXIN	EELPGVFSARAFVGVWYNGLPENRELAPDLSCDTAVILGQGNVALDVARIILLTPPDHLEKT	174
YumC	-----VEKQADGVFKLVQMKPPTTLKRSCITAG-NGAFKPRKLELENAEQYEGK	140
YcgT	-----FERLDDGTIVLTGSEGKKHYTRTVILACMGTLLEVNEFDSEDAARYAGK	141
TrxB	-----DLQNRPFRLNGDNGEYTCDALIATG---ASARYLGLPSEAFKGR	130
FldR	-----DGKLSPLAALKPGDEVQVSEAGFFVLDEVPHC	106
	: :	
FPRA	DIADHALESILRP-RGIQEVVIVGRRGPLQAAFTTLELRELADLDGVDVVIDPAELDGITD	235
ADRENODOXIN	DITEAALGALRQ-SRVKTVWIVGRRGPLQVAFTIKELREMIQLPGTRPMLDPADFLGLQD	233
YumC	NLHYFVDDLQKF-AGRRAVAILGGGDSAVDWALMLEPIAKEVSIHRRDKFR-----	190
YcgT	NLHYGVKELDAF-KGKRVVISGGGDTAVDWANELEPIAASVTVVHRRREEFG-----	191
TrxB	GVSACATCDGFFYRNQKQVAVIGGGNTAVEEALYLSNIASEVHLIHRDGRF-----AEKI	185
FldR	ETLWMLATGTAGPYLSILRLGKDLDRFKNLVLVHAARYAADLSYLP-----	153
	: :	
FPRA	EDAAAVGKVKQNIKVLRGYADREP-----RPGHRRMVFRFLTSPIEIK---GKRKV	284
ADRENODOXIN	RIKEAA-RPRKRLMELLRLTATEKPGVEEAARRASASRAWGLRFFRSPQQLVPSPDGRR	292
YumC	AHEHSVENLHASKVNVLTPTFV-----	211
YcgT	GMESSVTMKQSSVRVLTPTPR-----	212
TrxB	LIKRLMDKVENGNIILHTNRT-----	206
FldR	-LMQELEKRYEGKLRIQTVVS-----	173
	: :	
FPRA	ERIVLGRNELVSDGSGRVAAKD-TGEREELPAQLVVRVSVGYRGVPT-PGLPFDDQSGTIP	342
ADRENODOXIN	AGIRLAVTRLEGIG-EATRAVP-TGDVEDLPCGLVLSSIGYKSRPIDPSVPFDPKLGVP	350
YumC	--PAELIG-EDKIEQLVLEEVK-GDRKEILEIDDLIVNYG-----FVSSLGPIK	256
YcgT	--LEQLNGDEEGIKSVTVCHTE-SGQRKDIEIDELIINH-----FKIDLGPMM	258
TrxB	--LEEVTDGDMGVTGVRLRDTQNSDNIESLDVAGLFVAIG-----HSPNTAIFEGQL	256
FldR	-----RETAAGSLTGRIP-----ALIESGELESTIG-----	199
	: *	
FPRA	NVGGRRINGSPPNEYVVGWIKRGPTGVIGTNKKDAQDVTDTLKNLGNAGEGAECKSFPEDH	402
ADRENODOXIN	NMEGRVVDVPGLYCSGWVKRGPTGVITTTMTDSFLTGOILLQDL---KAGHLPSGPRPG	406
YumC	NWGLDIEKN-SIVVKSTMETNIEGFFAAGDICTYEGKVNLIASG-----FGEAPTAV	307
YcgT	EWGLEIEEG-RVKADRHMRNTNLPGVFVAGDAAFYESKLRLIAGG-----FTEGPTAV	309
TrxB	ELENGYIKVQSGIHGNATQTSIPGVFAAGDVMHDHRYQAITSAG-----TGCMAA	306
FldR	-----LPMNKETSHVMLCGNPQMVRDQQLKET-----RQMTKHL	235
	: :	
FPRA	ADQVADWLAAARQPKLVTSAHWQVIDAFERAAGEPHGRPRVKLASLAELLRIGLG-	456
ADRENODOXIN	SAFIKALLDSRGVWPVSFSDWEKLDAAEVSRGQASGKPREKLLDPQEMRLRL-LGH	460
YumC	NNAKAYMDPKARVQPLHSTS--LFENK-----	332
YcgT	NSAKAYLDPKAENMAMYSTHHKKLVHK-----	336
TrxB	LDAERYLDGL-----	316
FldR	RRRPGHMTAEHYW-----	248

**Figure 5.2** CLUSTAL W 1.82 alignment [Thompson *et al.*, 1994] of the two *B. subtilis* reductases YumC and YcgT with the thioredoxin reductase from *E. coli* (TrxB), the well characterised FprA from *M. tuberculosis*, flavodoxin reductase (FldR) from *E. coli* and bovine adrenodoxin reductase (Adrenodoxin). Only the nucleotide binding motif

GXGXXG (highlighted in red) is reasonably well conserved in these proteins, it being partially absent in FprA. The reductase from *E. coli* (FldR), sharing greater similarities with the FNR family from plants, has greater sequence differences. From structural data it is known that the FAD cofactor in FldR is bound in an unusual bent conformation. Amino acids that are conserved are marked with an asterisk (\*), that show high similarity are marked with a colon (:), and that are similar with a dot (.). Residues that are conserved between YcgT and YumC are shown in blue.

well characterised oxidoreductases (CLUSTAL W [Thompson *et al.*, 1994]) highlights the uniformity of the NADPH binding region, but there is little other conservation apart from a few residues known to be involved in binding the FAD cofactor (e.g. Asp285 [YumC] and Asp287 [YcgT] are homologous to Asp286 that binds to the FAD(O3') in *E. coli* thioredoxin reductase) [Lennon *et al.*, 1999]. Despite being classed as thioredoxin reductases there is little in terms of amino acid sequence that indicates that this is the true function of either *yumC* or *ycgT*. Alignment with the well characterised thioredoxin reductase from *E. coli* shows that the disulphide pair vital to the thioredoxin reductases function (Cys135 and Cys138) are absent in the two *B. subtilis* genes as are other important residues such as the pair of phenylalanines involved in docking with thioredoxin (Phe141 and Phe142) and the arginine (Arg293) involved in the FAD switching to its reduced active conformation [Lennon *et al.*, 2000]. Therefore the two genes *yumC* and *ycgT* were pursued as potential NADPH oxidoreductases with the capacity to interact with the flavodoxins and reconstitute our class II system. Clones of *yumC* (332 amino acids) and *ycgT* (336 amino acids) in the expression vectors pBluescript II KS<sup>-</sup> (FNRA01) and pUC18 (FNRB02), respectively, were a gift from Dr. J. Perkins (DSM).

The two class II cytochrome P450s of *B. subtilis* are less well characterised than their well studied homologue CYP102A1 from *B. megaterium*, but the high degree of sequence similarity allows direct comparisons to be drawn. CYP102A1 is a single 119 kDa polypeptide that consists of an N-terminal heme-domain fused to a central FMN binding region, that exhibits good homology to bacterial flavodoxins, and a C-terminal FAD binding domain homologous to ferredoxin reductases [Nahri and Fulco, 1986, Miles *et al.*, 1992]. From aligning the amino acid sequences of all three proteins (see Figure 5.3) the region where the heme-domain is connected by a short peptide linker to the

reductase domain was identified in accordance with previous published work [Govindaraj and Poulos 1997]. This produced the following reductase domains: residues E473 - I1048 for CYP102A2 (*yetO*) and residues K476 - M1054 for CYP102A3 (*yrhJ*).

The genes encoding the reductase domain plus the linker region were amplified from BS168 chromosomal DNA by PCR (1.76 kb *yetO* and 1.74 kb *yrhJ*) using the primers shown in Table 5.1 (for full cloning methodology see 2.4). An *NheI* site was engineered in to give the reductase domains a new N-terminal sequence of M-E-K-T (CYP102A2) and M-A-S-M-K-E-T (CYP102A3). It was not anticipated that the change to the N-terminal sequence would have a significant biophysical effect, as it is at the end of the flexible loop region, whose sole role is possibly to correctly orientate the reductase domain to the heme domain that in this case has been removed. Indeed, expression of several clones of CYP102A1 di-flavin reductase domain have been produced [e.g. Miles *et al.*, 1992, Govindaraj and Poulos, 1997] and have been shown to be catalytically active in electron transfer assays (e.g. cytochrome *c* reduction). However, it has been found that cleavage of the peptide chain that links the two domains of CYP102A1 results in a much less efficient hydroxylase system, the isolated reductase domain having reduced ability to interact with the isolated heme domain [Munro *et al.*, 1994].



[illegible]

**Figure 5.3** Amino acid alignment of the fused P450-oxidoreductases CYP102A2 and CYP102A3 from *B. subtilis* and CYP102A1 from *B. megaterium*. The numbering refers to the full sequence although only the C-terminus of the heme domain is shown (in red). The putative linker region (residues 456 to 472) in CYP102A1 is shown in italics and underlined. The new N-terminals for the reductase domains in A2 and A3 are underlined. Alignment was performed using CLUSTAL W 1.82 alignment [Thompson *et al.*, 1994]. Amino acids that are conserved are marked with an asterisk (\*), ones that show high similarity are marked with a colon (:), and those that are similar with a dot (.). As can be seen from the alignment there is a high degree of identity between the three proteins.

Primer Name	Sequence (5' - 3')	Restriction site engineered
YetO N-term	<u>ACG</u> <u>TGC TAG CAT</u> <u>GGA</u> GAA AAC GGA AGC AAA GGG	<i>NheI</i> at 5' end
YetO C-term	<u>ACG</u> <u>TGG ATC CTA</u> TCT ATA TCC CTG CCC AGA CAT CCT TAG C	<i>BamHI</i> at 3' end
YrhJ N-term	<u>ACG</u> <u>TGC TAG CAT</u> <u>GAA</u> AGA AAC CAA ACC TAA ACA C	<i>NheI</i> at 5' end
YrhJ C-term	<u>ACG</u> <u>TGG ATC CAT</u> TTT ACA TTC CTG TCC AAA CGT CTT TCA C	<i>BamHI</i> at 3' end

**Table 5.1** Primers designed for the amplification of the two diflavin reductase domains of CYP102A2 and A3 (*yetO* and *yrhJ* respectively). The engineered restriction sites are shown in red with any nucleotide changes compared to the published sequence underlined. N-term and C-term refer to the respective ends of the protein-encoding genes amplified by the respective primers.

Initially the purified gene fragments were 'A-tailed' (Qiagen kit) and ligated into a TOPO 2.1 vector (Invitrogen), and these constructs were transformed into *E. coli* XL-10 GOLD (Stratagene) to allow selection of positive colonies ( $\beta$ -galactosidase blue/white screening). Positive colonies were checked for the insert via PCR amplification of the gene using both the M13 forward and reverse primers specific to the TOPO vector, and also the original cloning primers. Confirmation of the presence of the insert preceded preparation of a large stock of plasmid and sequencing of several of the TOPO clones. Clones devoid of mutations were used to isolate and purify plasmids for double digestion with *NheI* and *BamHI* (NEB) to generate the fragment for ligating into the expression vector pET21a (Novagen). Positive colonies (Amp<sup>r</sup>) were selected and streaked onto fresh plates, the original colonies being checked for the correct plasmid by PCR amplification using T7 polymerase promoter forward and reverse primers (producing a 1.9 kb fragment in both cases). Full sequencing (Microsynth CH) of the two clones (pbioRLR1 [*yetO* reductase domain] and pbioRLR3 [*yrhJ* reductase domain]) was undertaken and no mutations were found.

## 5.2 Over-expression and purification

The two putative reductases *yumC* and *ycgT* were both over-expressed in *E. coli* TG1 cells (Stratagene). Even with expression at a high level they were observed to be



non-toxic to the host cells, giving growth rates similar to non-transformed TG1 cells and a good recovery of cell mass. Both reductases were predominantly expressed in their oxidised form, giving the host cells a yellow colouration indicative of their high expression.

On extraction of the protein from the cell debris an increase in the oxidised content of the reductases was observed (both exhibiting a small degree of semiquinone formation in the cell) as signified by an increase in the intensity of their yellow colour. A combination of hydrophobic affinity and anion exchange chromatography, and ammonium sulphate precipitation was used to generate pure protein samples (methods described in Section 2.6).

Purification stage	Total protein (mg)	Total reductase (mg)	Reductase/total protein	Stepwise purity fold	Overall purity fold
Cell lysate	6409	692	0.11	1	1
DEAE	1109	477	0.43	3.9	3.9
Ammonium sulphate	365	201	0.55	1.3	5
Phenyl Spharose	179	140	0.78	1.4	7.1
Q-sepharose	128	118	0.92	1.2	8.4

Purification stage	Stepwise yield	Overall yield
Cell lysate	100	100
DEAE	68.9	68.9
Ammonium sulphate	42.1	29.0
Phenyl Sepharose	69.7	20.2
Q-sepharose	84.1	17.1

**Table 5.2** Purification data for YumC (36.7 kDa) over-expressed in *E. coli* TG1 cells (6 l growth). Total protein concentration was determined spectrophotometrically by  $A_{280} \text{ nm} = 1 = 1 \text{ mgml}^{-1}$ , reductase content was determined spectrophotometrically by  $\epsilon_{459} = 12.954 \text{ mM}^{-1} \text{ cm}^{-1}$  (for calculation of coefficient see Section 2.8). Ammonium sulphate refers to the amount of protein left in solution after a 35 % cut. Figures relate to a typical protein purification from a culture volume of 6 l.

Purification stage	Total protein (mg)	Total reductase (mg)	Reductase/total protein	Stepwise purity fold	Overall purity fold
Cell lysate	4998	510	0.10	1	1
DEAE	2066	372	0.18	1.8	1.8
Ammonium sulphate	482	164	0.34	1.9	3.4
Phenyl Sepharose	211	139	0.66	1.9	6.6
Hydroxyapatite	109	97	0.89	1.3	8.9

Purification stage	Stepwise yield	Overall yield
Cell lysate	100	100
DEAE	72.9	72.9
Ammonium sulphate	44.1	32.2
Phenyl Sepharose	84.8	27.3
Hydroxyapatite	69.8	19.0

**Table 5.3** Purification data for YcgT (36.8 kDa) over-expressed in *E. coli* TG1 cells (6 growth). Total protein concentration was determined spectrophotometrically by  $A_{280} \text{ nm} = 1 = 1 \text{ mgml}^{-1}$ , reductase content was estimated spectrophotometrically by  $\epsilon_{459} = 11.698 \text{ mM}^{-1} \text{ cm}^{-1}$  (for calculation of extinction coefficient see Section 2.8). Ammonium sulphate refers to the amount of protein left in solution after a 45 % cut. Figures relate to a typical protein purification from a culture volume of 6 l.

Following purification using the regimes shown in Tables 5.2 and 5.3, both YcgT and YumC were pure as judged by SDS PAGE. Thus, the values suggested from the columns Reductase/Total Protein (0.92 and 0.89) respectively) are likely underestimates due to the errors inherent in the assumption that  $A_{280} = 1$  is equivalent to  $1 \text{ mgml}^{-1}$  of protein. Samples of the purified reductases were blotted onto a PVDF membrane and submitted to the in-house N-terminal sequencing facility (PNACL) to confirm their identity (for blotting method see Section 2.7). The first six residues of each reductase were sequenced. In the case of YumC the N-terminal methionine is retained, it being next to the relatively bulky residue: arginine, whilst that of YcgT is lost, it being next to the smaller residue alanine. The residue adjacent to the terminal methionine affects the efficiency of its removal by methionyl aminopeptidase, primarily due to steric factors [Hirel *et al.*, 1989; Lathrop *et al.*, 1992].

Cycle No.	YumC		YcgT	
	Residue	Amount (pmol)	Residue	Amount (pmol)
1	Met	119.68	Ala	49.00
2	Arg	442.76	Glu	63.50
3	Glu	197.41	Asn	35.71
4	Asp	298.21	Gln	33.59
5	Thr	119.96	Glu	37.90
6	Lys	106.49	Val	30.67

**Table 5.4** N-terminal sequencing of the two *B. subtilis* reductases. Samples (approx. 10 ng) were blotted onto a PVDF membrane and submitted to the in-house sequencing facility (PNACL).

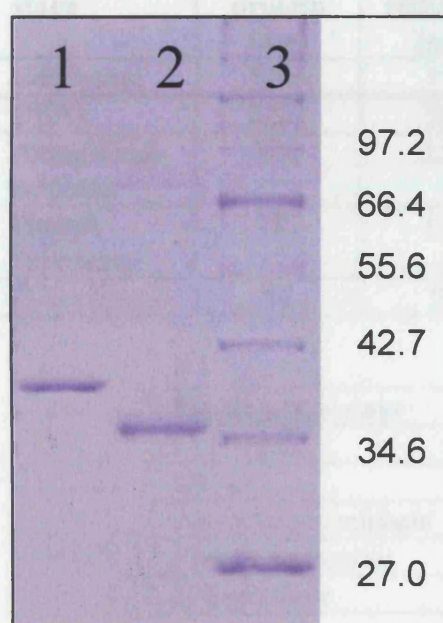


**Figure 5.4** SDS PAGE of purified protein samples. Shown is YumC (predicted mass 36.7 kDa, lane 1), YcgT (predicted mass 36.8 kDa, lane 2) and the pre-stained broad-range protein marker (NEB, lane 3, molecular weights shown to right). Samples were loaded at 50 ng/lane on a 10 % Tris-glycine gel. Despite having similar predicted masses, YumC runs a little heavier (*ca.* 39 kDa) than YcgT.

Over-expression trials of the two diflavin reductase domains of the two class II P450s in *E. coli* host cells BL21 CodonPlus DE3 RP (Stratagene) were carried out. This strain of *E. coli* was chosen to optimise expression of the rare codons such as CCC (proline) and AGG (arginine), both of which are common to the relatively GC-rich

genome of *B. subtilis* [Kunst *et al.*, 1997]. Indeed, these proteins contain between four and five such codons. Over-expression of the CYP102A3 diflavin reductase domain (64.6 kDa) was observed under the induction of IPTG, however, no over-expression of the CYP102A2 counterpart was seen. As full sequencing of the clone had shown no mutations to be present, it is possible that the new N-terminal sequence may cause a destabilisation of the domain causing it to be susceptible to proteolytic digestion within the host cell, or the RNA structure may be incompatible with efficient transcription/translation. As re-cloning would be required to remedy this it was decided to discontinue with this construct and examine the CYP102A3 diflavin construct only.

Purification stage	Total protein (mg)	Total reductase (mg)	Reductase/protein	Stepwise purity fold	Overall purity fold
Cell lysate	5206	312	0.06	1	1
DEAE	2221	244	0.11	1.8	1.8
Ammonium sulphate	806	224	0.28	2.5	4.7
Phenyl Sepharose	231	139	0.60	2.1	10.0
Q-Sepharose	74	70	0.95	1.6	15.8

Purification stage	Stepwise yield	Overall yield
Cell lysate	100	100
DEAE	78.2	78.2
Ammonium sulphate	91.8	71.8
Phenyl Sepharose	62.1	44.6
Q-Sepharose	50.4	22.4

**Table 5.5** Purification data for CYP102A3 reductase domain (64.6 kDa) over-expressed in *E. coli* TG1 cells (6 l preparation). Total protein concentration was estimated spectrophotometrically by  $A_{280 \text{ nm}} = 1 = 1 \text{ mgml}^{-1}$ , reductase content was determined spectrophotometrically by  $\epsilon_{460} = 20.5 \text{ mM}^{-1} \text{ cm}^{-1}$  [Roitel *et al.*, 2003]. Ammonium sulphate refers to the amount of protein left in solution after a 30 % cut.

The diflavin reductase domain of CYP102A3 was over-expressed on a large scale (6 l cultures) and its expression was indicated by the dark yellow colouration of the cell mass. Lysis of the cells yielded a yellow solution indicative of the presence of flavin and the reductase was purified by hydrophobic affinity and anion exchange chromatography

as described in Chapter 2. The purity of the protein at each stage in the purification is shown above in Table 5.5. The purified protein was frozen at -80 °C in 1.0 ml aliquots (50 % v/v glycerol). A sample of the purified reductase was submitted to the in-house N-terminal sequencing facility (PNACL) to confirm identity (method described in Section 2.7). The first six residues of the reductase were sequenced. It was found that the N-terminal methionine is lost, it being next to the small residue alanine [Hirel *et al.*, 1989; Lathrop *et al.*, 1992].

Cycle No.	Residue	Amount (pmole)
1	Ala	52.08
2	Ser	9.09
3	Met	26.93
4	Lys	20.97
5	Glu	34.33
6	Thr	25.21

**Table 5.6** N-terminal sequencing of the diflavin reductase from *B. subtilis* CYP102A3. Samples (approx. 10 ng) were blotted onto a PVDF membrane and submitted to the in-house sequencing facility (PNACL).

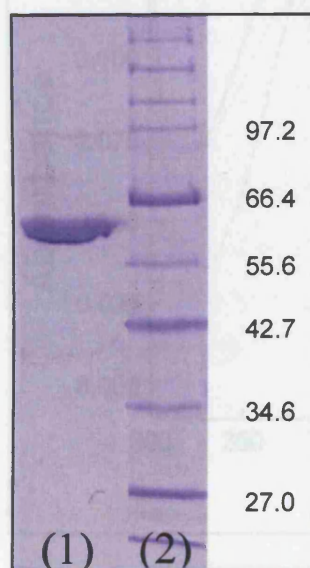


**Figure 5.5** SDS PAGE of purified CYP102A3 diflavin reductase domain (100 ng, lane 1, predicted mass = 64.6 kDa, apparent = 62 kDa) run adjacent to a pre-stained broad-range protein marker (NEB, lane 2, molecular weights (kDa) shown on the right).

### 5.3 UV-visible absorbance, Fluorescence and Circular Dichroism (CD) profiles

Each reductase containing a flavin cofactor is easily examined by UV-visible spectroscopy [Ghisla *et al.*, 1974]. Standard scans of each protein in its oxidised and reduced forms were made. Solutions of each reductase were prepared (5 - 10  $\mu$ M) in KPi buffer (50 mM, pH 7.0) and the spectrum recorded at 25 °C in a 1 cm pathlength cell. Both YumC and YcgT contain a single flavin cofactor, the maximum of its absorbance being at 459 nm and 381 nm in the case of YumC, and 459 nm and 379 nm for YcgT. For comparison, the FAD in *E. coli* thioredoxin reductase exhibits a maximum at 456 nm, being photo-reduced to show a neutral blue semiquinone with a maximum at 610 nm [Lennon *et al.*, 1996].

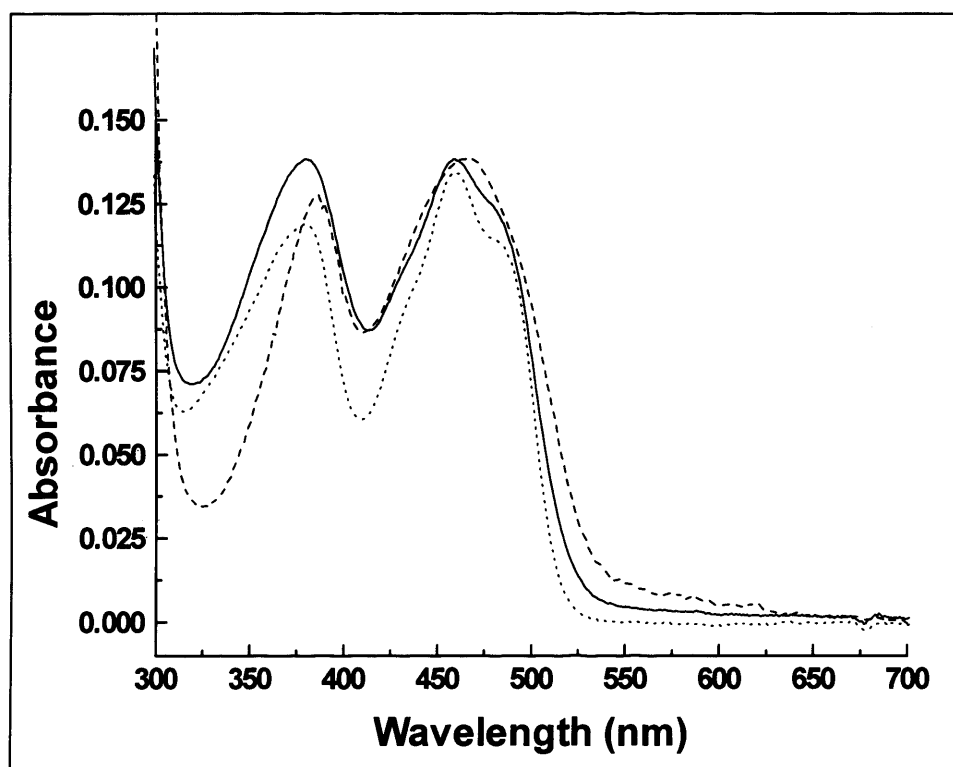


**Figure 5.6** UV-visible absorption spectra for the three oxidised *B. subtilis* reductases. YumC (10  $\mu$ M, dotted line, peaks at 459 and 381 nm), YcgT (10  $\mu$ M, solid line, peaks at 459 and 379 nm) and CYP102A3 (5  $\mu$ M, dashed line, peaks at 466 and 385 nm). All spectra recorded on a Varian CARY 50 spectrophotometer at 25°C in KPi buffer (pH 7.0, 50 mM) using a 1 cm pathlength cell.



On progressive reduction under anaerobic conditions with dithionite both of these reductases accumulate a small amount of neutral blue semiquinone (maximum at 600 nm for YumC and 595 nm for YcgT), before completely bleaching as they are reduced to their two electron reduced hydroquinone form [Muller *et al.*, 1972]. On incubation with NADPH both of these reductases are reduced to their hydroquinone and no semiquinone is seen. Liberation of the free cofactor by denaturation of the protein with a reagent such as SDS (final concentration of 0.4 % v/v) shifts the flavin's maxima to 375 and 449 nm (YumC) and 376 and 450 nm (YcgT). This indicates that, in agreement with previous work [Seo *et al.*, 2004], YumC and YcgT both contain a molecule of FAD (the maximum of the standard under the same conditions being 374 and 446 nm for FMN and 376 and 450 nm for FAD). YumC is a considerably more stable protein than YcgT, complete removal of its cofactor necessitating boiling of the sample for 5 minutes in the presence of SDS (0.4 % v/v).

The diflavin reductase CYP102A3R has an altered UV-visible absorbance spectrum compared to the mono-flavin enzymes due primarily to it containing two flavin cofactors. The oxidised flavin absorbance at 466 nm is a single smooth bell-shaped absorbance with the absence of the shoulder seen in most single flavin containing proteins on the longer wavelength band. Its other maximum is at 385 nm. The absorbance spectrum is similar to that of the reductase domain of its homologue P450 BM3 (CYP102A1) that has maxima at 456 and 385 nm [Roitel *et al.*, 2003]. The reductase of CYP102A3 shows development of a small amount of blue neutral semiquinone on its FAD cofactor (maximum at 605 nm) upon dithionite reduction under anaerobic conditions, the semiquinone bleaching at higher levels of dithionite. The formation of this FAD neutral semiquinone is similar to the other two reductases being examined (see above) and to that observed upon reduction of the reductase domain of P450 BM3 (maximum at 600 nm [Peterson and Boddupali, 1992, Roitel *et al.*, 2003]). Although slower to reduce with nicotinamide reducing agents compared to YumC, incubation with NADPH under anaerobic conditions results in formation of the FAD neutral semiquinone (presumably as a result of inter-flavin electron transfer to give the diradical form  $[FADH^{\bullet}/FMNH^{\bullet}]$  as seen in P450 BM3 [Murataliev *et al.*, 1997]). After prolonged incubation with NADPH CYP102A3 reductase is reduced to a mixture of its 3- and 4-

electron reduced forms, the 3-electron reduced state is thought to inactivate P450 BM3 due to accumulation of FMN hydroquinone [Murataliev *et al.*, 1997].

The fluorescence emission spectrum of the three *B. subtilis* reductases' flavin cofactors and aromatic residues was measured to allow comparison of their tertiary structure and flavin-binding environment (Figure 5.7). Flavin emission was measured by excitation of the proteins at 450 nm and recording the emission between 500 and 600 nm. Exciting at 290 nm and following the emission from 300 to 400 nm measured the emission of the aromatic residues, predominantly tryptophans.

Reductase	Flavin maximum (nm)	Intensity (EU/ $\mu$ M)	Tryptophan maximum (nm)	Intensity (EU/ $\mu$ M)
YumC	529	0.36	346	59.20
YcgT	529	40.85	342	87.69
CYP102A3	528	4.33	340	429.73

**Table 5.7** Results from fluorescence spectroscopy of the three *B. subtilis* reductases. For flavin emission the excitation was at 450 nm and the emission between 500 and 600 nm recorded, for aromatic residues, the excitation was at 290 nm and the emission from 300 to 400 nm was measured. All experiments were done at 25 °C in KPi buffer (50 mM, pH 7.0) on a CARY 50 fluorimeter in a 1 cm path-length cell. Intensity refers to the arbitrary units of fluorescence emitted under identical conditions (EU) divided by the concentration of total protein ( $\mu$ M), typically 3  $\mu$ M.

From the emission intensity of the flavin cofactors it can be seen that the FAD cofactor of YumC is much more quenched than that of YcgT. The flavin cofactors of CYP102A3 reductase are also quenched in comparison to YcgT. The stronger emission of YcgT's cofactor implies it is more solvent exposed [Ottada *et al.*, 1997], possibly indicating a more open and accessible active site. The shift in the maximum of the tryptophans' emission indicates that in CYP102A3R they are comparatively buried, having their maximum at 340 nm, whilst at the other end of the scale those of YumC are the most solvent exposed, their maximum being at 346 nm. Despite a high degree of sequence similarity between YumC and YcgT, particularly in the regions of sequence that contain their only two tryptophan residues, there is a 4 nm difference in their tryptophan fluorescence maximum. The intensity of the tryptophans emission reflects in part the number of such residues present, there being two in both YcgT and YumC in

conserved positions (see Figure 5.2). CYP102A3, being a larger protein comprised of an evolutionary fusion of ferredoxin reductase and flavodoxin components [Porter, 1991], contains a total of seven tryptophan residues and therefore it is of little surprise that the intensity of its emission is several-fold greater.

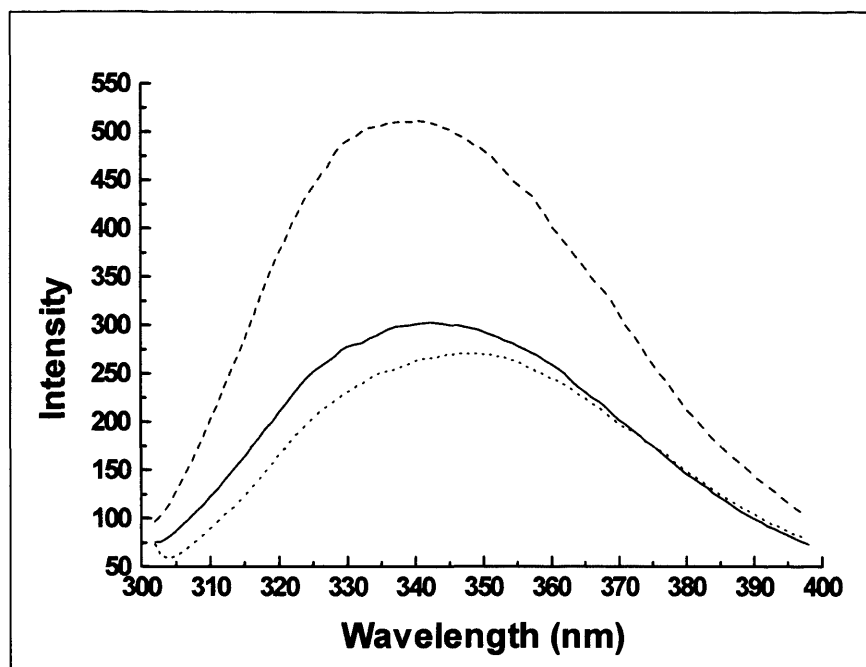


**Figure 5.7** Emission spectra for the three reductases aromatic residues. CYP102A3R (dashed line) has a maximum at 340 nm, YcgT (solid line) has a maximum at 342 nm and YumC (dotted line) has its maximum at 346 nm. Excitation was at 290 nm, emission between 300 and 400 nm. Slit widths were at 10 nm on a Varian Eclipse fluorimeter and proteins (3  $\mu$ M) were in KPi buffer (conditions as described in Table 5.7).

To examine the secondary structure of the reductase candidates, far UV CD was used. NADPH-oxidoreductases are typically comprised of a mixture of  $\alpha$ -helices with  $\beta$ -sheets to aid stabilisation of the flavin- and nicotinamide-cofactor binding domains (see Figure 5.1) [Ziegler and Schulz 2000, Ingleman *et al.*, 1997, Serre *et al.*, 1996]. The diflavin reductase domain of CYP102A3, being a fusion of a ferredoxin reductase and a flavodoxin [Porter, 1991], would be expected to have a similar structure to that of rat cytochrome P450 NADPH reductase, that consists of 4 regions of  $\beta$ -sheet and approximately 16  $\alpha$ -helices [Wang *et al.*, 1997]. Spectra of the reductases were recorded on a Jasco CD spectropolarimeter at 2  $\mu$ M in KPi buffer (50 mM, pH 7.0) at 25  $^{\circ}$ C in a 1 mm pathlength cell (Figure 5.8). All three reductases show a similar profile characterised

by their helical content. This is not surprising for YumC and YcgT as they have a relatively high degree of sequence similarity (see Figure 5.2) and probably have a similar fold and function. Their far UV CD spectra are similar, all sharing a common minimum of 209 nm, similar to that reported for FprA from *M. tuberculosis* [McLean *et al.*, 2003] whose structure is known to conform to the general topology of NAD(P)<sup>+</sup>-oxidoreductases [Bossi *et al.*, 2002]. The far UV CD of CYP102A3 crosses the x-axis at *ca.* 203 nm, compared to YcgT and YumC (200 nm) and displays a very similar profile to the reductase domain of its *B. megaterium* homologue, P450 BM3 [Munro *et al.*, 1994].

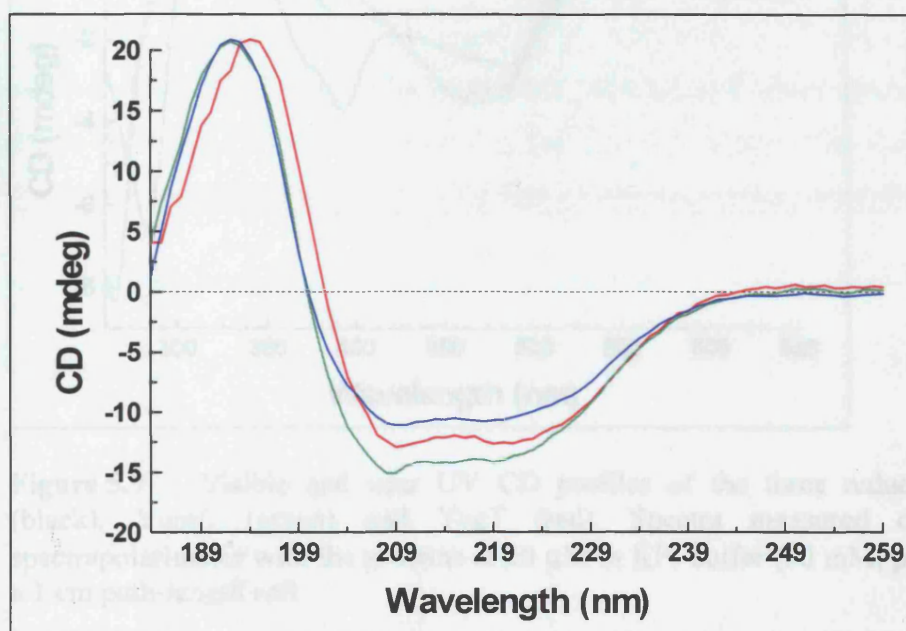


**Figure 5.8** Far UV CD profiles of the three *B. subtilis* reductases; CYP102A3 (red), YumC (blue) and YcgT (green). Spectra measured on a Jasco CD spectropolarimeter with the proteins at 2  $\mu$ M in KPi buffer (50 mM, pH 7.0) at 25 °C in a 1 mm path-length cell.

Visible-near UV CD spectra were recorded for each reductase to examine and compare the environment of the flavin cofactor and of the aromatic amino acids in the proteins. A solution of each reductase was prepared at 20  $\mu$ M in KPi buffer (50 mM, pH 7.0) and the spectrum recorded at 25 °C in a 1 cm path-length cell. All three reductases give visible CD spectra that are predominantly negative in sign across the range 300 to 650 nm, with some positive ellipticity at around 300 nm in all cases. In the near UV spectra all three proteins show a strong negative peak between 260 and 300 nm. The

profiles of YumC and YcgT are highly similar with both proteins having a minimum centered at 460 nm. As observed with the far UV CD, the near UV-visible CD profiles of these two reductases bear an overall similarity to that of FprA. The visible CD spectrum of FprA has a minimum at 451 nm [McLean *et al.*, 2003], similar to that of adrenodoxin reductase with a minimum at 452 nm [Sakamoto *et al.*, 1981].

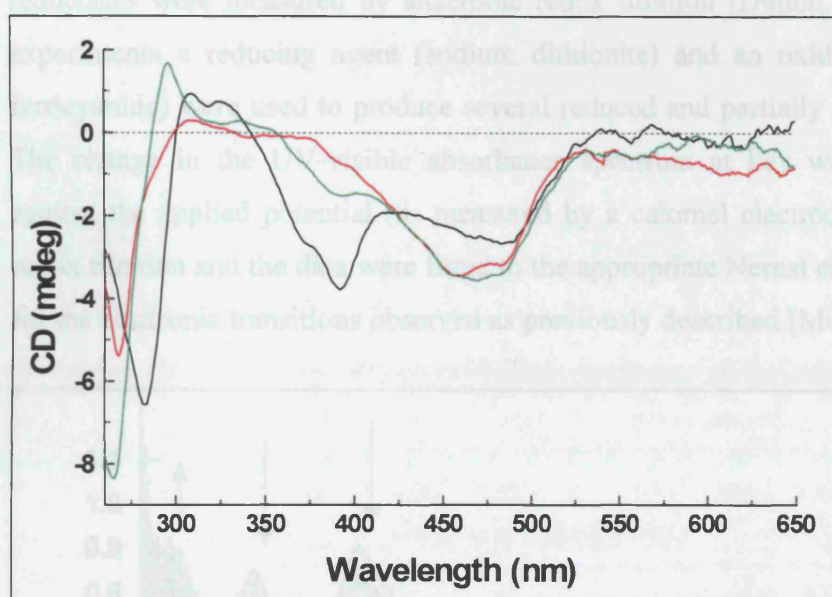


**Figure 5.9** Visible and near UV CD profiles of the three reductases CYP102A3 (black), YumC (green) and YcgT (red). Spectra measured on a Jasco CD spectropolarimeter with the proteins at 20  $\mu$ M in KPi buffer (50 mM, pH 7.0) at 25  $^{\circ}$ C in a 1 cm path-length cell.

The spectrum of the CYP102A3 reductase domain is rather different, due to the protein containing two flavin cofactors in distinct environments. In the case of YumC and YcgT there are distinctive minima only in the region of the longer wavelength absorption band seen in the UV-visible absorption spectrum. For the CYP102A3 reductase there are minima in the regions of both the bands seen in the electronic absorbance spectrum at around 480 nm and 390 nm. There is strong similarity between the visible CD spectrum of the CYP102A3 reductase domain and that of the reductase domain of its homologue P450 BM3 [Munro *et al.*, 1996] that has negative minima at *ca.* 393 and 469 nm.



#### 5.4 Redox potentials

To establish the thermodynamic feasibility of these systems to transfer electrons from NAD(P)H to potential redox partners in *B. subtilis* such as flavodoxins and ferredoxins, the midpoint reduction potentials of the flavins in each of the three reductases were measured by anaerobic redox titration [Dutton, 1978]. As in previous experiments a reducing agent (sodium dithionite) and an oxidising agent (potassium ferricyanide) were used to produce several reduced and partially reduced enzyme forms. The change in the UV-visible absorbance spectrum at key wavelengths was plotted against the applied potential (as measured by a calomel electrode) at each point in the redox titration and the data were fitted to the appropriate Nernst equation to obtain values for the electronic transitions observed as previously described [Munro *et al.*, 2001].

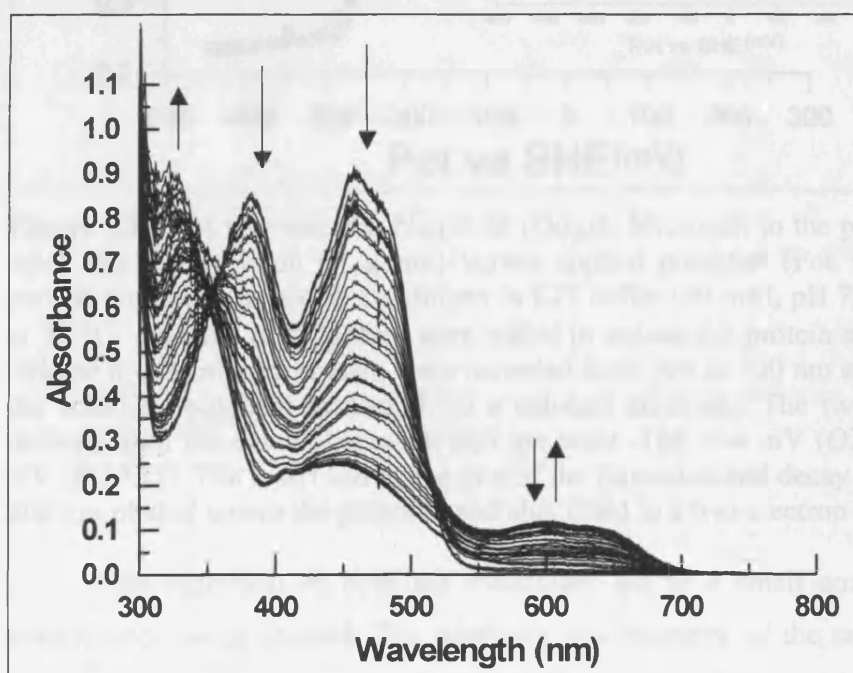


**Figure 5.10** Flavin absorbance spectra of YumC (0.085 mM) collected during the redox titration used to determine its midpoint reduction potentials. The titration was performed under anaerobic conditions in KPi buffer (50 mM, pH 7.0, 10 % v/v glycerol) at 25 °C. Adding small aliquots of dithionite to the solution reduced the protein. After each addition the absorbance spectrum was recorded and the potential of the solution measured by a calomel electrode. Following complete reduction this was repeated with the protein being reoxidised by the addition of small aliquots of ferricyanide. As the oxidised maximum at 460 nm decreases a small semiquinone signal can be observed to



form with a maximum at 600 nm. The isosbestic points for the oxidised to semiquinone transition are at 348 and 521 nm. As the protein is reduced further, the absorption decreases to give the virtually colourless hydroquinone two-electron reduced form. The arrows show the direction of absorbance change at the various wavelengths.

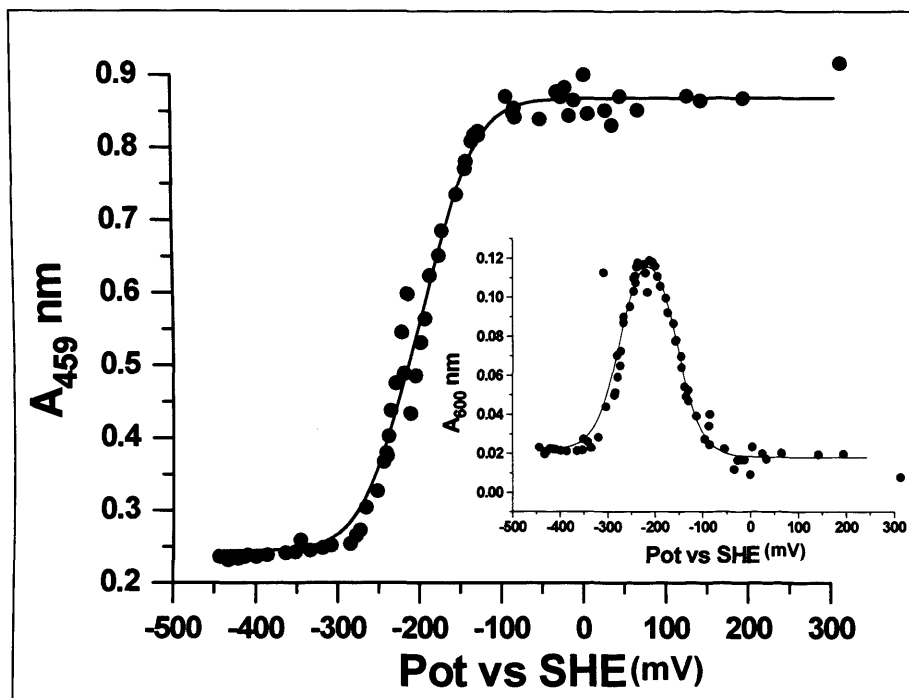


**Figure 5.11** A two-electron Nernst fit (Origin, Microcal) to the plot of YumC's (0.085 mM) flavin absorption ( $A_{459\text{ nm}}$ ) versus applied potential (Pot vs SHE). Experiment carried out under anaerobic conditions in KPi buffer (50 mM, pH 7.0, 10 % v/v glycerol) at 25 °C. Aliquots of dithionite were added to reduce the protein and ferricyanide to re-oxidise it. Absorbance spectra were recorded from 300 to 750 nm after each addition and the solutions potential measured via a calomel electrode. The two midpoint potentials derived from the data collected at 600 nm were  $-184 \pm 4$  mV (OX/SQ) and  $-258 \pm 5$  mV (SQ/HQ). The insert shows the plot of the formation and decay of the semiquinone at 600 nm plotted versus the potential and also fitted to a two-electron Nernst equation.

The reduction of both the reductases led to a small amount of blue neutral semiquinone being formed. The relatively low intensity of the semiquinone of YumC suggests that the redox couples for the addition of the first electron ( $E_1$ ) and the second electron ( $E_2$ ) to the flavin are closely spaced, with the semiquinone form being comparatively less stable than that of the flavodoxins, for example. The development of a semiquinone aided the fitting of the data as the midpoint for the formation and decay of this one-electron reduced species (maximum around 600 nm) could be directly plotted and fitted to a 2-electron Nernst equation (Figure 5.11). These data analyses gave the

values for the two flavin transitions; oxidised to semiquinone (Ox/SQ [ $E_1$ ]) and semiquinone to hydroquinone (SQ/HQ [ $E_2$ ]). The values for the midpoint reduction potential of the reductases are shown in Table 5.8.

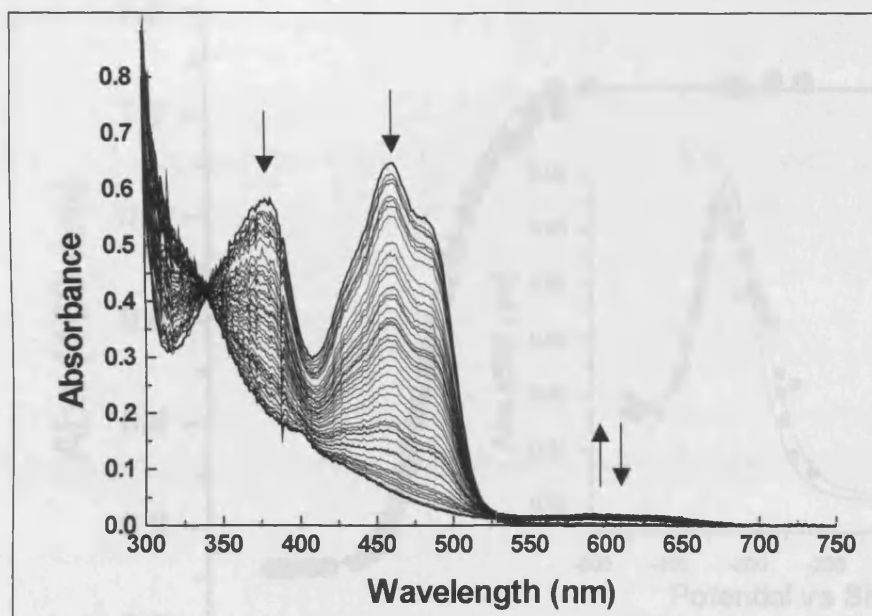


**Figure 5.12** Absorbance spectra from the redox titration of YcgT (0.061 mM). Performed under anaerobic conditions in KPi buffer (50 mM, pH 7.0, 10 % v/v glycerol) at 25 °C. As for data shown in Figure 5.6, the protein was reduced (by addition of dithionite) and after each addition the absorbance spectrum and the potential of the solution was measured (calomel electrode). Upon complete reduction of the protein, this was repeated with the protein being reoxidised (ferricyanide addition). The arrows show the direction of absorbance change as the protein is reduced. A small amount of semiquinone can be observed to form with a maximum at 595 nm. An isosbestic point for the oxidised/semiquinone transition can be seen at 528 nm.

The reduction of YcgT showed a very small amount of blue neutral semiquinone to form at 595 nm. Its very low intensity indicates that the redox couples are inverted as seen in previous studies with proteins such as dihydroorotate dehydrogenase B (both the FMN and FAD cofactor have inverted potentials [Mohsen *et al.*, 2004]) and the FMN of P450 BM3 reductase domain [Sevrioukova *et al.*, 1996]. This is as a result of the semiquinone form being less stable than that of the oxidised and hydroquinone forms. This is in agreement with the reductase cycling between a 0 and 2<sup>-</sup> electron reduced state. The presence of the semiquinone although small, aided the fitting of the data to give the values for the two flavin transitions; oxidised to semiquinone (Ox/SQ) and semiquinone to

hydroquinone (SQ/HQ) as the formation and decay of the semiquinone could be plotted and fitted to a two-electron Nernst equation.

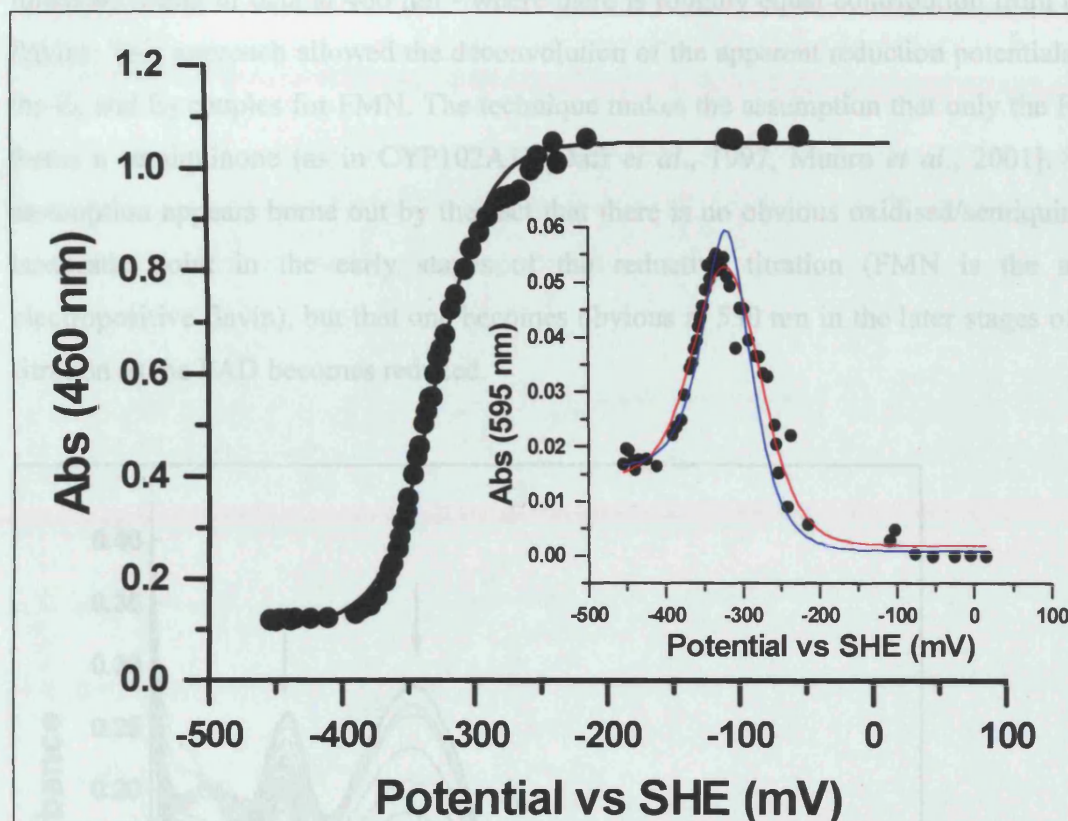


**Figure 5.13** Data fit of a two-electron Nernst equation (Origin) to a plot of absorbance change at 460 nm versus the potential of the protein solution (standardized against the hydrogen electrode [Pot vs SHE] in mV) to determine the midpoint potentials for YcgT. This plot gave the  $E_{\text{OX/HQ}}$  as  $-329 \pm 3$  mV the two separate transitions being hard to distinguish from one another. The formation and decay of the semiquinone (at 595 nm) is shown (inset) from which the two midpoint potentials are calculated. The red fit shows the two-electron function without fixing the absorbance coefficients (indicating that  $E_{\text{OX/SQ}}$  is more positive than  $E_{\text{SQ/HQ}}$ ) and the blue is with the coefficients fixed (indicating that  $E_{\text{SQ/HQ}}$  is more positive than  $E_{\text{OX/SQ}}$ ). The standard red fit gives the coefficient for the SQ as *ca* 0.08. This is too low as a typical blue SQ would have a coefficient (relative to the 460 nm flavin absorption of 1.1) of 0.3 to 0.4 (at full population). By constraining the SQ coefficient between 0.28 and 0.4 the blue fit is obtained. This is in agreement with the small amount of SQ populated in the titration indicating that  $E_{\text{SQ/HQ}}$  is more positive than  $E_{\text{OX/SQ}}$ , but that the potentials are sufficiently close that some SQ is seen. This fit gave  $E_{\text{OX/SQ}} = -341 \pm 4$  mV and  $E_{\text{SQ/HQ}} = -292 \pm 5$  mV.

The redox titration of the reductase domain of CYP102A3 also exhibited the formation of a blue neutral semiquinone. The maximum of this species (608 nm) was

plotted versus the applied potential to obtain values for the two transitions of the FAD cofactor. These values were then used to enable the more complex (4-electron Nernst function) fitting of data at 466 nm - where there is roughly equal contribution from both flavins. This approach allowed the deconvolution of the apparent reduction potentials for the  $E_1$  and  $E_2$  couples for FMN. The technique makes the assumption that only the FAD forms a semiquinone (as in CYP102A1) [Daff *et al.*, 1997, Munro *et al.*, 2001]. This assumption appears borne out by the fact that there is no obvious oxidised/semiquinone isosbestic point in the early stages of the reductive titration (FMN is the more electropositive flavin), but that one becomes obvious at 530 nm in the later stages of the titration as the FAD becomes reduced.

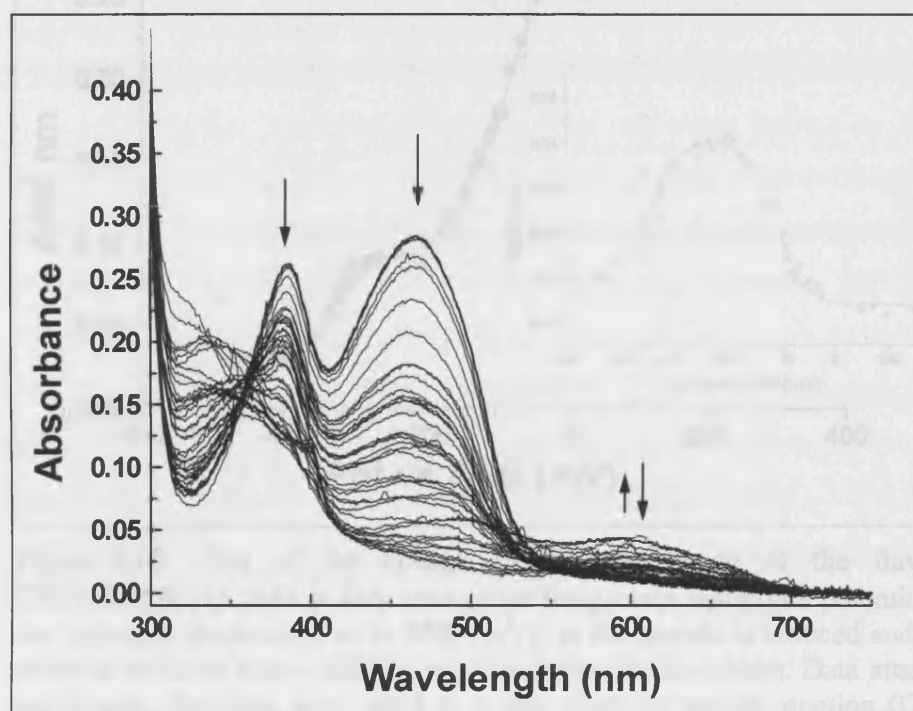


**Figure 5.14** Absorbance spectra accompanying the reduction and oxidation of CYP102A3R (0.015 mM) under anaerobic conditions, as described previously. Arrows show the direction of change in absorbance during the reductive phase of the titration. The decay in the absorbance of the oxidised flavins at 466 nm can be seen and the formation and subsequent decay of a small amount of semiquinone at 608 nm is also observed. Like the two other reductases, the flavin cofactor in CYP102A3R undergoes full bleaching to give its hydroquinone form in the presence of excess dithionite.

From studies on the reductase domain of P450 BM3 it is thought that the FMN semiquinone is destabilized relative to its hydroquinone contrary to the scenario observed in flavodoxins where the semiquinone form of FMN is stabilized. This results in an inversion of the midpoint potentials for the FMN OX/SQ and SQ/HQ [Daff *et al.*, 1997, Sevrioukova *et al.*, 1996]. Two lysine residues (K572 and K580) and a histidine (H539) are believed to contribute to the partial stabilisation and neutralization of the anionic FMN hydroquinone in CYP102A1 [Sevrioukova *et al.*, 1999]. CYP102A3 contains two basic arginine residues that could perform a similar role.

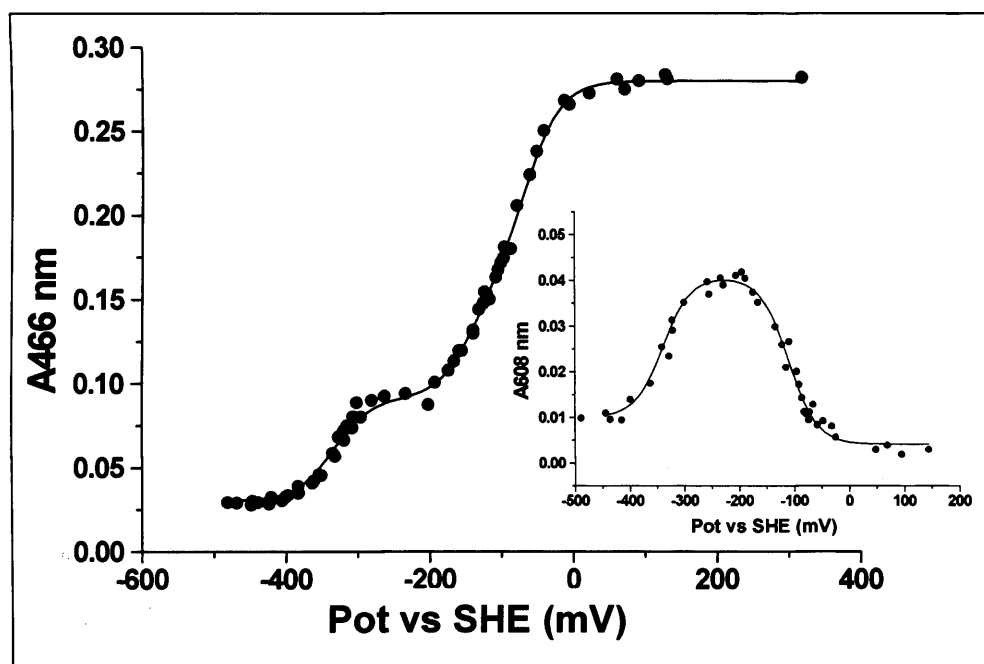


**Figure 5.15** Plot of the change in the absorbance of the flavin cofactors of CYP102A3R (15  $\mu$ M) at 466 nm against the protein solution's potential standardized to the hydrogen electrode (Pot vs SHE [mV]) as the protein is reduced and reoxidised by an artificial electron donor (dithionite) or acceptor (ferricyanide). Data attained as described previously. The data were fitted to a four electron Nernst equation (Origin, Microcal). The inset shows the formation and decay of the FAD semiquinone (A608 nm) fitted to a 2-electron Nernst equation. Values derived from the A608 data were fixed in the analysis of the A466 data to facilitate determination of the FMN redox couples.



Reductase	E <sub>1</sub> (mV) Ox/SQ	E <sub>2</sub> (mV) SQ/HQ	E <sub>12</sub> (mV) Ox/HQ
YumC	-184 +/- 4	-258 +/- 3	-201 +/- 5
YcgT	-341 +/- 4	-292 +/- 5	-329 +/- 3
CYP102A3R	-109 (FAD) +/- 5 -145 (FMN) +/- 8	-339 (FAD) +/- 7 -57 (FMN) +/- 5	

**Table 5.8** Redox midpoint potentials for the *B. subtilis* reductase enzymes. Data were collected under anaerobic conditions as described previously. Changes in absorbance spectra of the reductases were plotted against the applied potential and the data fitted to an appropriate 2- or 4-electron Nernst equation to obtain estimated values for the single electron transitions. E<sub>1</sub> refers to the one-electron transition from oxidised to semiquinone form (Ox/SQ) and E<sub>2</sub> to the second one-electron transition from semi- to hydroquinone form (SQ/HQ). E<sub>12</sub> refers to the apparent midpoint potential for the two-electron transition determined by fitting data at the oxidised flavin maximum versus potential to a two-electron Nernst function.

Reductases accepting electrons from pyridine nucleotide coenzymes cycle between their hydroquinone and oxidised state accepting two electrons at a time from the hydride ion donated by NAD(P)H. The potential for the two-electron oxidation of NADPH has been recorded as -317 mV [Jenkins and Waterman, 1998]. It is therefore of little surprise that the three reductases all have midpoint values for their acceptor flavin that are compatible with electron transfer from NAD(P)H. Comparison of the recorded values to those of published values of related enzymes such as the of *E. coli* FldR, that has an E<sub>2</sub> of -268 mV and an E<sub>1</sub> of -308 mV [McIver *et al.*, 1998], shows the redox couples for YcgT to be a little more negative in value, and those for YumC to be more positive. This subtle change in midpoint potential may reflect differences in the flavin cofactors' environment. Indeed, fluorescence emission spectra of the two reductases suggests that the flavin of YumC is more highly quenched and therefore in a less solvent exposed situation than that of YcgT (Section 5.3) which may contribute to its more positive potential.

The potentials of P450 BM3 reductase domain, whose values are recorded as -292 mV (FAD E<sub>1</sub>), -372 mV (FAD E<sub>2</sub>), -213 mV (FMN E<sub>1</sub>) and -193 mV (FMN E<sub>2</sub>) [Daff *et al.*, 1997], are more negative than those found for CYP102A3 reductase domain, e.g. the value for the FAD Ox/SQ transition (E<sub>1</sub> = -109 +/- 5 mV) is 183 mV more negative in



BM3. Studies with the reductase domain of BM3 have shown that this reductase is purified in an oxidised state being converted to its two electron reduced form on reduction by NADPH [Murataliev *et al.*, 1997]. The reductase domain of CYP102A3 is also isolated in its oxidised state. This, together with the similar FAD HQ/SQ transition ( $E_2 = 339 \pm 7$  mV), may imply that the reductase domain of CYP102A3 also cycles between a zero- and two-electron reduced form as opposed to cycling between the one- and three-electron reduced forms, as seen in microsomal CPR where the semiquinone form of the FMN cofactor is stabilized [Vermillion *et al.*, 1981] (Section 1.3.3).

## 5.5 NADPH and NADH reduction kinetics

Reduction of the reductases by the transfer of a hydride ion from a nicotinamide cofactor is the initial step in our multi-component catalytic cycle. Therefore this rate has the capacity to be highly influential on the rate of oxygenation of substrates ultimately carried out by P450 BioI. Both YumC and YcgT are clearly flavin-binding, pyridine nucleotide-dependent dehydrogenases. To determine their relative specificities for NADH and NADPH, kinetic studies were performed in both stopped-flow and steady-state modes. The rate of electron transfer from both NADPH and NADH to the flavin cofactor of each of the reductases was measured using stopped-flow equipment. The absorbance change at *ca* 460 nm was recorded over time, following the reduction of the flavin from its oxidised yellow form to the two electron reduced colourless hydroquinone form. A solution of reductase (10  $\mu$ M) was prepared in anaerobic KPi buffer (50 mM, pH 7.0) and mixed rapidly with solutions of NADPH (0 to 4.0 mM) or NADH (0 to 40 mM) prepared in the same buffer. The experiment was carried out at 30 °C. The rate of flavin bleaching was fitted accurately to a double exponential function (a single exponential giving a poor fit) and the resulting rate plotted against the concentration of the nicotinamide cofactor. These data were analysed by fitting to a rectangular hyperbola to find the apparent  $K_d$  and  $k_{red}$  values.

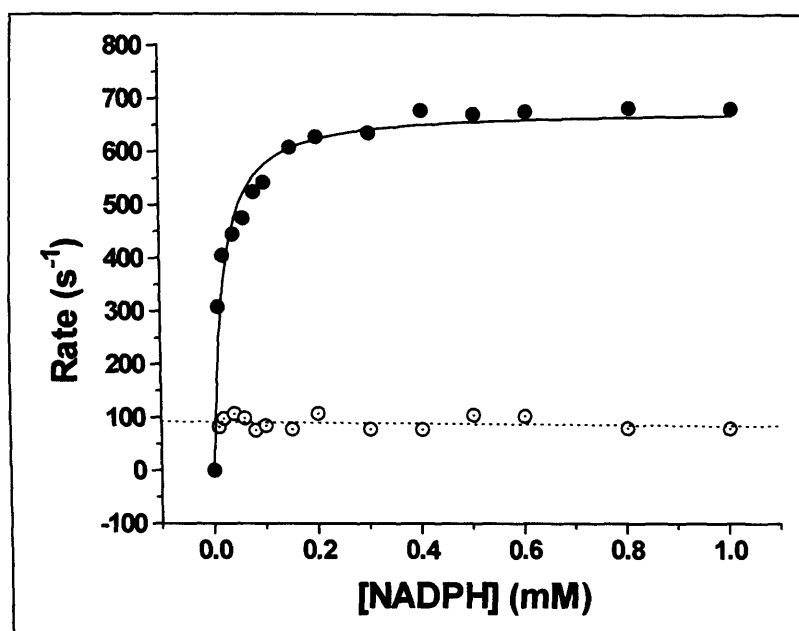


**Figure 5.16** Data for the apparent rate of flavin reduction of YumC (10  $\mu$ M) by various concentrations of NADPH. Experiment was carried out on a stopped-flow instrument maintained in an anaerobic glove box at 30 °C. The change in absorbance ( $A_{460}$ ) versus the concentration of NADPH was fitted to a double exponential function to obtain the rate constants. The first rapid phase (filled spheres) is fitted to a rectangular hyperbola. The second slower phase (hollow spheres) appears independent of NADPH concentration with a  $k_{\text{red}} = 88.2 \pm 6.8 \text{ s}^{-1}$ . The fit for the first phase produces an apparent value of  $k_{\text{red}} = 681.1 \pm 17.8 \text{ s}^{-1}$  and a  $K_d = 18.3 \pm 0.3 \mu\text{M}$ .

Reductase	NADPH			
	$k_{\text{red}} (\text{s}^{-1})$	Error +/-	$K_d (\mu\text{M})$	Error +/-
<b>YumC</b>	681	18	18.3	0.3
<b>YcgT</b>	25.6	1.3	86.0	1.1
<b>CYP102A3</b>	16.8	1.6	1293	264

**Table 5.9** Kinetic values for the reduction of the reductases' flavin cofactor by NADPH. Data were measured using stopped-flow equipment under anaerobic conditions. The reductase (10  $\mu$ M) in degassed KPi buffer (50 mM, pH 7.0) was mixed with NADPH (0 to 4.0 mM) prepared in the same buffer at 30 °C. The decrease in the absorbance of the oxidised flavin (*ca* 460 nm) was followed over time and data fitted to a double exponential function. Data for the first phase of the biphasic transients were fitted to a rectangular hyperbola to obtain the parameters shown. The second phase showed no apparent dependence on NADPH concentration, yielding rates of  $88.2 \pm 6.8 \text{ s}^{-1}$  (YumC) and  $1.3 \pm 0.2 \text{ s}^{-1}$  (CYP102A3). In the case of YcgT, the second phase was linearly dependent on NADPH concentration ( $\text{rate} (\text{s}^{-1}) = 2.10 + ([\text{NADPH} (\text{mM})] \times 0.45)$ ).

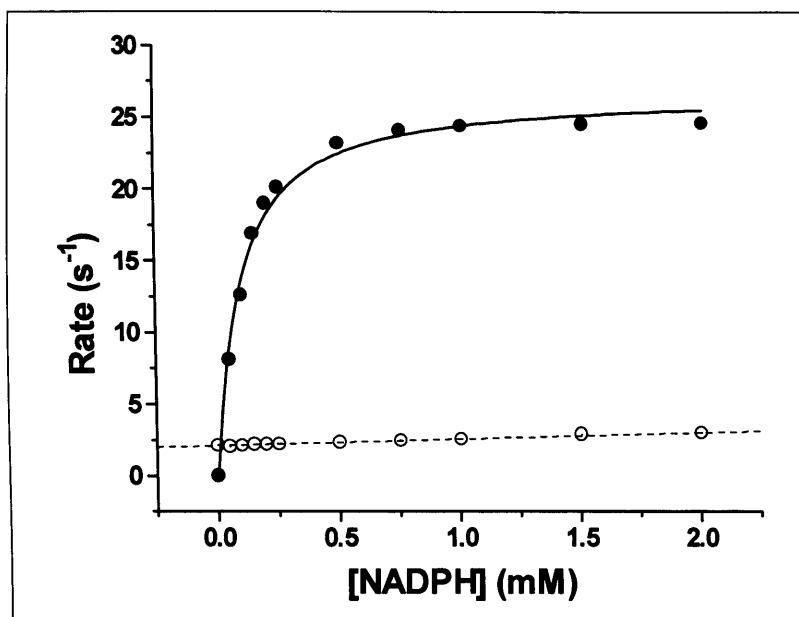


**Figure 5.17** Data for the apparent rate of flavin reduction of YcgT (5  $\mu$ M) by various concentrations of NADPH. Experiment was carried as described above. The change in absorbance ( $A_{460}$ ) versus the concentration of NADPH was fitted to a double exponential function to obtain the rate constants. The first faster phase (filled spheres) is fitted to a rectangular hyperbola producing an apparent value of  $k_{\text{red}} = 25.6 \pm 1.3 \text{ s}^{-1}$  and a  $K_d = 86.0 \pm 1.1 \mu\text{M}$ . The second slower phase (hollow spheres) is also dependent on NADPH concentration with a gradient affected by the concentration of NADPH (rate ( $\text{s}^{-1}$ ) =  $2.10 + ([\text{NADPH}] \times 0.45)$ ).

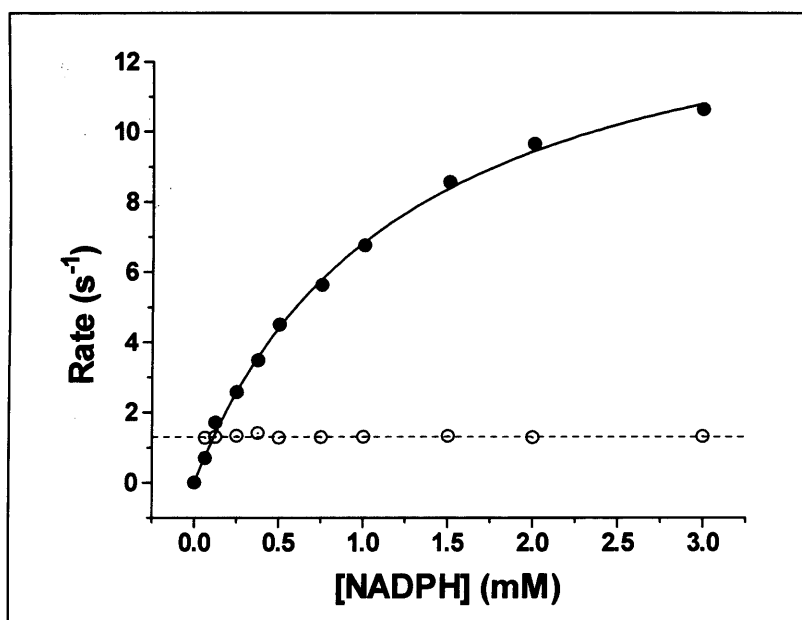


**Figure 5.18** Data for the apparent rate of flavin reduction of CYP102A3R (10  $\mu$ M) by various concentrations of NADPH. Experiment was carried out as described above. The

change in absorbance ( $A_{460}$ ) versus the concentration of NADPH was fitted to a double exponential function to obtain the rate constants. The first rapid phase (filled spheres) is fitted to a rectangular hyperbola. The second slower phase (hollow spheres) is independent of NADPH concentration ( $k_{red} = 1.3 \pm 0.2 \text{ s}^{-1}$ ). The fit for the first phase produces an apparent value of  $k_{red} = 16.8 \pm 1.6 \text{ s}^{-1}$  and a  $K_d = 1293 \pm 264 \mu\text{M}$ .

Reductase	NADH			
	$k_{red} (\text{s}^{-1})$	Error +/-	$K_d (\text{mM})$	Error +/-
YumC	12.51	0.39	0.064	0.009
YcgT	1.06	0.06	0.961	0.121
CYP102A3	0.81	0.08	0.89	0.09

**Table 5.10** Kinetic values for the reduction of the reductases' flavin cofactor by NADH (first fast phase). Data were collected as described above, with the proteins mixed with NADH (0 to 40 mM) at 30 °C. The decrease in the absorbance of the oxidised flavin (*ca* 460 nm) was followed over time and fitted to a double exponential function. The rate of reduction of CYP102A3 reductase by NADH is an estimate from an anaerobic spectroscopy experiment on a standard spectrophotometer, since the reaction was too slow to be measured accurately on the stopped-flow instrument. The second phase showed no apparent dependence on NADH concentration, yielding rates of  $2.35 \pm 0.21 \text{ s}^{-1}$  (YumC),  $0.06 \pm 0.02 \text{ s}^{-1}$  (CYP102A3) and  $0.17 \pm 0.02 \text{ s}^{-1}$  (YcgT).

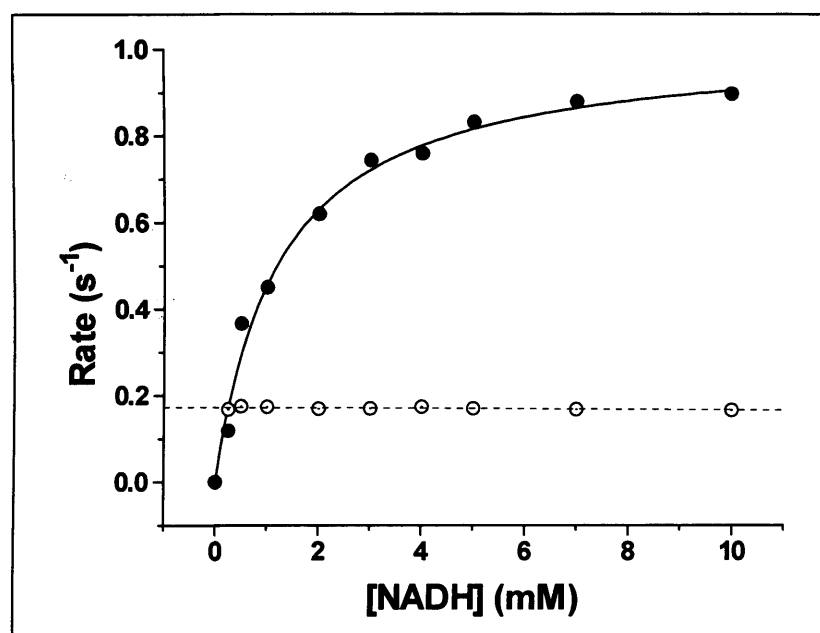


**Figure 5.19** Data for the apparent rate of flavin reduction of YcgT (10  $\mu\text{M}$ ) by various concentrations of NADH. Experiment was carried out on a stopped-flow instrument maintained in an anaerobic glove box at 30 °C. The change in absorbance ( $A_{460}$ ) versus the concentration of NADH was fitted to a double exponential function to obtain the rate constants. The first rapid phase (filled spheres) is fitted to a rectangular hyperbola. The

second slower phase (hollow spheres) appears independent of NADH concentration with a  $k_{\text{red}} = 0.17 \pm 0.02 \text{ s}^{-1}$ . The fit for the first phase produces an apparent value of  $k_{\text{red}} = 1.06 \pm 0.06 \text{ s}^{-1}$  and a  $K_d = 0.96 \pm 0.12 \mu\text{M}$ .

From the values in Tables 5.9 and 5.10 it can be seen that YumC favors the NADPH cofactor over NADH, the kinetics for the electron transfer being almost sixty times faster, and the interaction with NADPH is tighter giving an apparent  $K_d$  of 18.3  $\mu\text{M}$ . Flavin reduction kinetics with both reductants were biphasic, the second slower phase of which was independent of reductant concentration (2<sup>nd</sup> phase rate =  $88.2 \pm 6.8 \text{ s}^{-1}$  (NADPH),  $2.35 \pm 0.21 \text{ s}^{-1}$  (NADH)). YcgT was much slower to reduce than its homologue, although it also seemed to favour interacting with NADPH as opposed to NADH. With NADPH as the reductant the second slower phase of the reduction of YcgT showed an apparent linear dependence on [NADPH]. The gradient was affected by the concentration of NADPH (rate ( $\text{s}^{-1}$ ) =  $2.10 + ([\text{NADPH}] \times 0.45)$ ). In the case of NADH, the second phase (rate =  $0.17 \pm 0.2 \text{ s}^{-1}$ ) was independent of coenzyme concentration. The faster rate of reduction of YumC *c.f.* YcgT is in agreement with the redox potential data that indicates that reduction of its flavin should be substantially more thermodynamically favorable. Data published for the interaction of the *E. coli* flavodoxin reductase with NADPH gives a rate ( $k_{\text{red}}$ ) of  $15 \text{ s}^{-1}$  as measured using stopped-flow techniques, and a  $K_d$  of 3.85  $\mu\text{M}$  from steady-state experiments [McIver *et al.*, 1998]. This rate is more comparable with that of YcgT, although the reported steady-state data implies a tighter interaction between the *E. coli* reductase and the NADPH substrate. The limiting rate of reduction of *E. coli* thioredoxin reductase by NADPH at 25 °C is published as  $590 \text{ s}^{-1}$  [Lennon *et al.*, 1996] a rate similar to that measured here for YumC, albeit at a slightly different temperature. There is clearly a much greater driving force for electron transfer to the YumC flavin, but other reasons for the differences in electron transfer rates may require structural resolution of the proteins.

The diflavin reductase from CYP102A3 was very slow to reduce, contrary to expectations. Rates of reduction of the CYP102A1 reductase domain by NADPH have been recorded as being  $238 \text{ s}^{-1}$  at 5 °C [Roitel *et al.*, 2003]. When NADPH was used to reduce the reductase from CYP102A3, a rate of only  $16.8 \text{ s}^{-1}$  was measured for the first fast phase; the second phase (independent of NADPH concentration) had a rate =  $1.30 \pm$

0.20 s<sup>-1</sup>. With NADH the reduction was so slow that it could not be measured accurately on a stopped-flow instrument. However, in a separate experiment under anaerobic conditions it was found that incubation of the protein with a 10-fold molar excess of NADH did eventually cause near full reduction of the flavins. A separate experiment was then undertaken to get an estimate of the  $k_{\text{red}}$  and apparent  $K_d$  by manually mixing the protein with various concentrations of NADH on a standard spectrophotometer housed in an anaerobic glove box. The change in flavin absorbance was scanned over time. This gave a  $k_{\text{red}} = 0.81 \text{ s}^{-1}$  for the first phase and a rate of  $0.06 \pm 0.02 \text{ s}^{-1}$  for the second [NADH] independent phase. Therefore it is concluded that the favoured reagent for the diflavin reductase domain is also NADPH. This was not a surprise as the rate of reduction of the reductase domain of CYP102A1 with NADH is also much slower than the equivalent rate when NADPH is used [Munro *et al.*, 1996]. The reasons for the very slow rates observed with NADPH were unclear, but steady-state analysis of the cleaved domain was pursued with NADPH and NADH as the hydride source.

Analysis of the stopped-flow data for all three reductases interacting with either reductant showed a biphasic relationship between the decrease in nicotinamide cofactor absorbance and time (seconds). This data fit is in agreement with at least two separate processes occurring simultaneously during coenzyme-dependant reduction that affect flavin absorption. In the case of the diflavin reductase, CYP102A3R, this is likely to be due to the initial reduction of the FAD cofactor followed by inter-flavin electron transfer as the electrons are distributed between the FAD and FMN of the reductase. With YumC and YcgT where there is only one flavin cofactor, it is possible that the first phase equates to the reduction of the flavin by the nicotinamide reductant and the second, much slower phase to the dissociation of the oxidised product and/or a conformational rearrangement. By comparison with the steady-state rates (see following sections) it is unlikely that the second slower step reports on the actual flavin reduction as, in the case of YumC, this would give a rate several times slower than that seen in the steady-state scenario.



### 5.6 Steady-state rates of electron transfer from *B. subtilis* reductases to P450 BioI, cytochrome *c* and ferricyanide

To further analyse preference towards NADPH or NADH and to characterise electron transfer from the three reductases, the rate of reduction of two artificial electron acceptors; the small molecule ferricyanide and the large protein cytochrome *c* (horse heart, Sigma), by the various reductases was measured. Reactions were set up at 25 °C in KPi buffer (50 mM, pH 7.0) with *ca* 1.0  $\mu\text{M}$  of reductase present. The electron acceptor ferricyanide (0 to 12 mM) or cytochrome *c* (0 to 0.1 mM) was added and the rate of reduction of these acceptors measured by the increase in absorbance at 550 nm (cytochrome *c*  $\epsilon_{550} = 22640 \text{ M}^{-1} \text{ cm}^{-1}$ ) or decrease in absorbance at 420 nm (ferricyanide  $\epsilon_{420} = 1010 \text{ M}^{-1} \text{ cm}^{-1}$ ). The ferricyanide assay was carried out using a dual beam spectrophotometer to discount any direct reduction of ferricyanide by NAD(P)H.

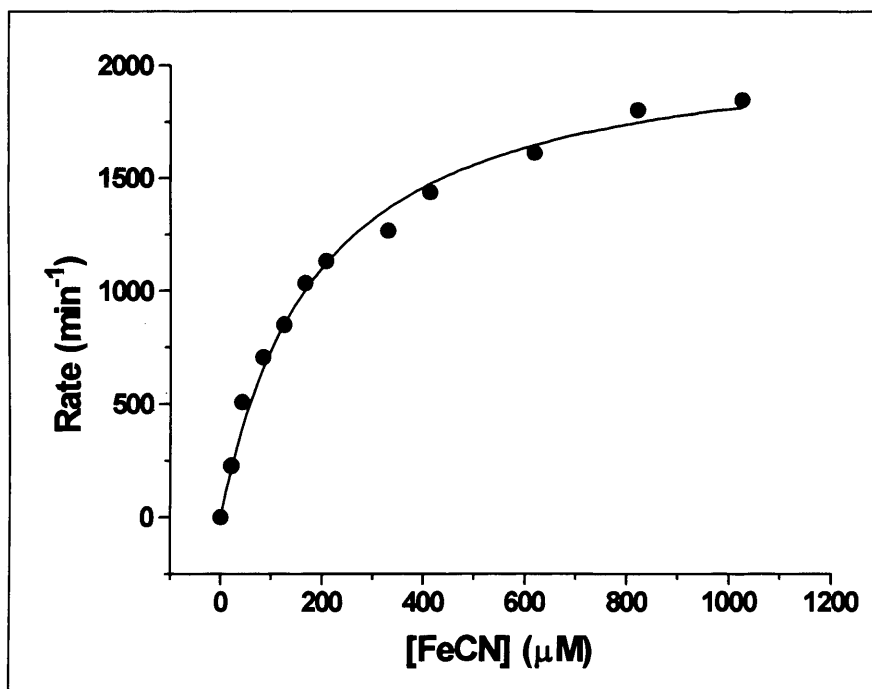


**Figure 5.20** Hyperbolic fit to a plot of the rate of ferricyanide reduction by YcgT. Rates are plotted versus the concentration of ferricyanide (FeCN). Conditions were YcgT (1.12  $\mu\text{M}$ ), ferricyanide (0 - 1000  $\mu\text{M}$ ), NADPH (2.0 mM). Rates were measured at 30 °C in KPi (50 mM, pH 7.0).

Assay	YumC		YcgT		A3R	
	$k_{cat}$ (min <sup>-1</sup> )	$K_m$ ( $\mu$ M)	$k_{cat}$ (min <sup>-1</sup> )	$K_m$ ( $\mu$ M)	$k_{cat}$ (min <sup>-1</sup> )	$K_m$ ( $\mu$ M)
$\Delta$ Ferricyanide	35300	29	2130	188	1840	401
Error (+/-)	133	1.9	107	22.0	103	52.4
$\Delta$ NADPH (FeCN)	25200	4.5	1530	105	1620	96.0
Error (+/-)	609	0.3	110	9.2	106	8.4
$\Delta$ Cytochrome c	642	40.6	91.2	37.1	437	47.9
Error (+/-)	34.7	4.7	3.9	3.5	34.6	7.3
$\Delta$ NADPH (Cyt c)	548	2	71.0	17.2	408	42
Error (+/-)	11.8	0.3	7.6	1.2	21.3	5.1

**Table 5.11** Steady-state kinetic parameters for the reduction of artificial electron acceptors by the various *B. subtilis* reductases (*ca* 1.0  $\mu$ M) when incubated with NADPH at 30 °C in KPi buffer (50 mM, pH 7.0). Assay refers to which factor was being varied, either the [NADPH] or [electron acceptor] and the  $K_m$  refers to the binding constant for that component varied. Error rows (shaded) refer to the figures in the row above them.

Comparison with the published data for the *E. coli* flavodoxin reductase (whose rates were  $k_{cat} = 1610 \text{ min}^{-1}$ ,  $K_m = 23.6 \mu\text{M}$  (FeCN) and  $k_{cat} = 141 \text{ min}^{-1}$  and a  $K_m = 17.6 \mu\text{M}$  (cytochrome *c*) [McIver *et al.*, 1998]) shows that YcgT behaves in a similar manner to the *E. coli* reductase whilst YumC appears to be a faster reductase in accordance with its fast reduction by NADPH in the absence of electron acceptors (see Section 5.4). When either YumC or YcgT were used as the reductase in the ferricyanide assay it was found that the steady-state rates were slower than the stopped-flow rates for NADPH reduction. This indicated that a step other than the reduction of the flavin is rate limiting, e.g. NADP<sup>+</sup> release.

Rates of ferricyanide and cytochrome *c* reduction by the full-length form of CYP102A3 are reported to be 37050 min<sup>-1</sup> and 3520 min<sup>-1</sup> respectively at 30 °C in MOPS buffer (20 mM, pH 7.4, 100 mM KCl) [Gustafsson *et al.*, 2004]. The rates measured here with the cleaved domain are many times slower indicating that the reductase domain is kinetically compromised by dissociation from its P450, or that the buffers phosphate ions are impeding the docking of the reductant. The slower steady-state rates observed here are in accordance with the slow reduction rates found with the stopped-flow reduction of

the reductase domain by NADPH in Section 5.4 suggesting that in this case the reduction of the flavin by NADPH is rate limiting.

The steady-state assays were then repeated under the same conditions with NADH as the hydride source. It was anticipated from the earlier stopped-flow data that these rates would be slower than those recorded when NADPH is used. This was found to be the case, with YumC showing the most dramatic decrease. For example, the rate of reduction of ferricyanide fell by around 200-fold when NADH was used as the hydride source. As seen with the stopped-flow data, the binding and electron transfer from NADPH is much more favorable for this protein. The steady-state reactions also give apparent  $K_m$  values that show NADPH binds much more tightly (around 3.2  $\mu\text{M}$ ) than NADH (around 322  $\mu\text{M}$ ). With YcgT and CYP102A3 the rates with NADPH were slower than those of YumC, and the stopped-flow experiments also showed this to be the favoured nicotinamide coenzyme for these proteins. When NADH was used in these steady-state assays, YcgT showed rates around 75-fold (FeCN) and 30-fold (cytochrome *c*) slower than those when NADPH was used. CYP102A3 reductase also showed slower rates in the presence of NADH (over 100-fold with cytochrome *c* and around 20-fold with FeCN), although the apparent  $K_m$  values for NADH (83.2  $\pm$  8.1  $\mu\text{M}$  with cytochrome *c* and 131.7  $\pm$  13.4  $\mu\text{M}$  with FeCN) were similar to those of NADPH (41.8  $\pm$  5.1  $\mu\text{M}$  with cytochrome *c* and 96.0  $\pm$  8.4  $\mu\text{M}$  with FeCN).

Assay	YumC		YcgT		A3R	
	$k_{cat}$ ( $\text{min}^{-1}$ )	$K_m$ ( $\mu\text{M}$ )	$k_{cat}$ ( $\text{min}^{-1}$ )	$K_m$ ( $\mu\text{M}$ )	$k_{cat}$ ( $\text{min}^{-1}$ )	$K_m$ ( $\mu\text{M}$ )
<b><math>\Delta</math> Ferricyanide</b>	85.9	28.7	26.7	120.6	64.4	118
<b>Error (+/-)</b>	1.9	2.6	0.5	9.3	1.5	10.6
<b><math>\Delta</math>NADH (FeCN)</b>	167	562	38.6	381	79.6	131
<b>Error (+/-)</b>	11.5	76.7	1.1	31.7	2.5	13.4
<b><math>\Delta</math> Cytochrome <i>c</i></b>	137	115	3.3	10.5	3.3	65.0
<b>Error (+/-)</b>	5.8	8.5	0.1	0.5	0.1	5.7
<b><math>\Delta</math>NADH (Cyt <i>c</i>)</b>	82.7	82.5	4.0	90.4	3.5	83.2
<b>Error (+/-)</b>	5.0	10.1	0.2	9.5	0.2	8.1

**Table 5.12** Steady-state kinetic parameters for the reduction of artificial electron acceptors by the *B. subtilis* reductases (1.0  $\mu\text{M}$ ) when incubated with NADH at 25 °C in

KPi buffer (50 mM, pH 7.0). Assay refers to which factor was being varied, either the [NADH] or [electron acceptor] and the  $K_m$  refers to the binding constant of that component varied. Error rows (shaded) refer to the figures in the row above them.

Steady-state rates of the *B. subtilis* reductase-supported P450 BioI redox systems were also measured. The oxidation of NADPH ( $\epsilon_{340} = 6.21 \text{ mM}^{-1} \text{ cm}^{-1}$ ) was monitored over time to assess efficiency of electron transfer to the P450. The catalytic system was set up using  $1.8 \text{ }\mu\text{M}$  of P450 BioI, an excess of NADPH (0.2 mM), and an excess of substrate (myristic acid at  $25 \text{ }\mu\text{M}$ ). The *B. subtilis* flavodoxins (YkuN and YkuP) were used to shuttle electrons between the reductases and P450 BioI. All the reactions were carried out at  $30 \text{ }^\circ\text{C}$  in KPi buffer (50 mM, pH 7.0) and either i) the amount of reductase was varied with the flavodoxins at a 10-fold excess over P450 ( $18 \text{ }\mu\text{M}$ ), or ii) the concentration of the flavodoxin was varied with the reductase being at 10-fold excess ( $18 \text{ }\mu\text{M}$ ). When the concentration of reductase was varied and plotted against the observed rates, a hyperbolic dependence was observed. Data were fitted to a rectangular hyperbola to yield  $k_{cat}$  for the reaction and apparent  $K_d$  values for the varied component (Figure 5.21). However, when the concentration of flavodoxins was varied with YumC as the reductase, a linear, second order fit was observed where in the case of YkuN;  $\text{Rate (min}^{-1}) = 32.57 + (3.73 \times [\text{YkuN (}\mu\text{M)}])$ , and with YkuP;  $\text{Rate (min}^{-1}) = 30.42 + (3.94 \times [\text{YkuP (}\mu\text{M)}])$  (see Figure 5.22).

With YcgT as the reductase hyperbolic fits of rate versus flavodoxin concentration again prevailed when YkuN and YkuP concentrations were varied. This could indicate that in the case of the faster reductase YumC, the middle flavodoxin-catalysed steps limit the steady-state rates, as they shuttles back and forth from reductase to P450. With the slower reductase YcgT, one of the first steps, probably the reduction of the flavodoxin, is rate-limiting. The rates recorded for YumC above are similar to those previously observed when the reductase from *E. coli* was used to reconstitute the reductase system (see Chapter 4) and myristate was used as a substrate. This again predicts the rate-limiting step to be that involving the shuttle proteins YkuN and YkuP interacting with the P450. With YcgT as the reductase, the slower rates probably report upon the less efficient interaction of the reductase with the flavodoxins.

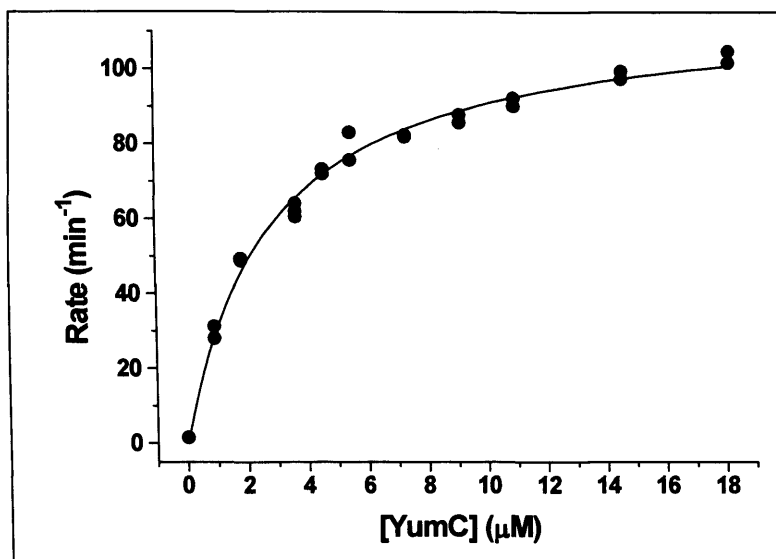


**Figure 5.21** Hyperbolic plot of the rate of NADPH consumption ( $\epsilon_{340} = 6.21 \text{ mM}^{-1} \text{ cm}^{-1}$ ) versus concentration of reductase YumC (0 - 18  $\mu\text{M}$ ) in turn-over reaction with P450 BioI. Conditions were P450 BioI (1.72  $\mu\text{M}$ ), YkuN (17.2  $\mu\text{M}$ ), NADPH (0.02 mM), and myristate (25  $\mu\text{M}$ ). Reactions were all performed at 30 °C in KPi (50 mM, pH 7.0). This fit produced a  $k_{cat}$  of  $119 \pm 4.4 \text{ min}^{-1}$  and an apparent  $K_d$  of  $2.8 \pm 0.3 \mu\text{M}$  for the interaction of YumC with YkuN.

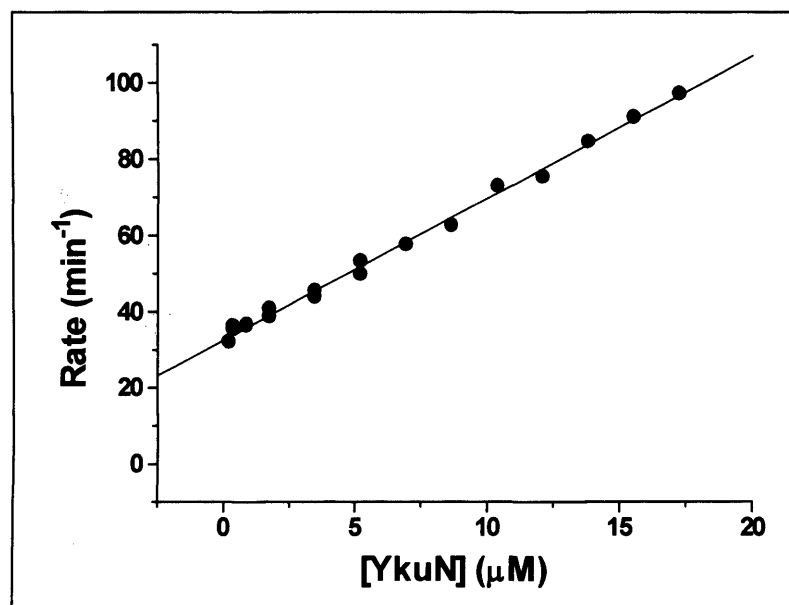


**Figure 5.22** Linear plot of the rate of NADPH consumption ( $\epsilon_{340} = 6.21 \text{ mM}^{-1} \text{ cm}^{-1}$ ) versus concentration of flavodoxin YkuN (0 - 18  $\mu\text{M}$ ) in turn-over reaction with P450 BioI. Conditions were P450 BioI (1.72  $\mu\text{M}$ ), YumC (17.2  $\mu\text{M}$ ), NADPH (0.02 mM), saturating level of myristate (25  $\mu\text{M}$ ). Reactions were all performed at 30 °C in KPi (50 mM, pH 7.0). This fit produced a  $\text{Rate (min}^{-1}\text{)} = 32.57 + (3.73 \times [\text{YkuN (}\mu\text{M)}])$ .

Reductase	YumC				YcgT			
Flavodoxin	$k_{cat}$ (min <sup>-1</sup> )	Error +/-	$K_d$ ( $\mu$ M)	Error +/-	$k_{cat}$ (min <sup>-1</sup> )	Error +/-	$K_d$ ( $\mu$ M)	Error +/-
$\Delta$ [YkuN]	Second order (see text)				19.7	0.3	0.3	0.1
$\Delta$ [YkuP]	Second order (see text)				18.6	0.3	0.1	0.02
YkuN $\Delta$ [reductase]	119	5	2.8	0.3	32.4	1.9	8.2	1.1
YkuP $\Delta$ [reductase]	86.3	3.2	2.0	0.3	22.3	1.5	7.3	0.9

**Table 5.13** Steady-state parameters for the reconstituted P450 BioI redox system. The oxidation of NADPH ( $\epsilon_{340} = 6.21 \text{ mM}^{-1} \text{ cm}^{-1}$ ) was measured over time and the rate calculated from these data. Reactions were performed at 30 °C in KPi buffer (50 mM, pH 7.0) with 1.8  $\mu$ M P450 BioI, NADPH (20  $\mu$ M), substrate (myristic acid, 25  $\mu$ M) and the amount of reductase or flavodoxin varied, the other redox partner maintained at a ten-fold excess (18  $\mu$ M). Rates at different concentrations of reductase or flavodoxin were measured and plotted versus protein concentration. Fitting of these data to hyperbolic functions allowed calculation of  $k_{cat}$  and  $K_d$  values.

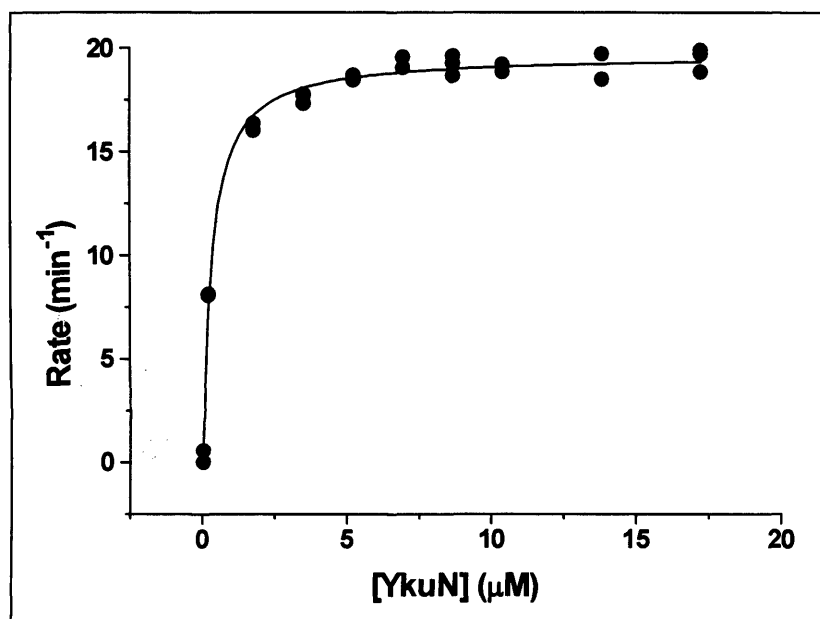


**Figure 5.23** Hyperbolic fit to a plot of the concentration of YkuN versus the rate of oxidation of NADPH as measured in a steady-state assay with P450 BioI as the terminal electron acceptor. The oxidation of NADPH ( $\epsilon_{340} = 6.21 \text{ mM}^{-1} \text{ cm}^{-1}$ ) was measured over a minute and the rate calculated. Performed at 30 °C in KPi buffer (50 mM, pH 7.0) with 1.8  $\mu$ M P450 BioI, NADPH (20  $\mu$ M), substrate (myristic acid, 25  $\mu$ M), YcgT was at a ten-fold excess (18  $\mu$ M) over the P450 and the amount of YkuN was varied. Rates at different concentrations of flavodoxin were measured and plotted versus protein concentration. These data were fitted to a rectangular hyperbola to give the  $k_{cat}$  as 19.7 min<sup>-1</sup> and the apparent  $K_d$  as 0.3  $\mu$ M.



The attempt to replace the traditional class I P450 redox system with the CYP102A3 diflavin reductase was not as successful as when YumC or YcgT coupled to a flavodoxin were used, as the rate fell around 10-fold to give an apparent  $k_{cat} = 9.0 \pm 0.8 \text{ min}^{-1}$  and a  $K_d$  of  $9.2 \pm 0.9 \text{ }\mu\text{M}$ . Whether this is due to poor interaction with the P450 or due to the relatively slow NADPH reduction step and slow reductase to P450 electron transfer is unclear. Further stopped-flow experiments were carried out to determine rates for selected individual steps within the reaction sequence, in order to develop a clearer understanding of the reaction mechanisms.

### **5.7 Electron transfer to the flavodoxins and to P450 BioI**

The rate of the single electron transfer to the flavodoxins from the pre-reduced reductases (reduced via NADPH incubation) was measured using stopped-flow instrumentation, with the spectrum between 300 and 800 nm recorded by photodiode array equipment and analysed by global analysis software (Applied Photophysics). The pre-reduced reductases (0 to 100  $\mu\text{M}$ ) were mixed rapidly with the oxidised flavodoxins YkuN and YkuP (15  $\mu\text{M}$ ). The reduction of the oxidised flavodoxins was observed by a decrease in the absorbance at around 455 to 465 nm and the formation of their semiquinone form at approximately 600 nm. This experiment was carried out under anaerobic conditions in KPi buffer (50 mM, pH 7.0) at 30 °C and data were corrected for the reductive photo bleaching that the flavodoxins undergo on prolonged exposure to the intense light source.

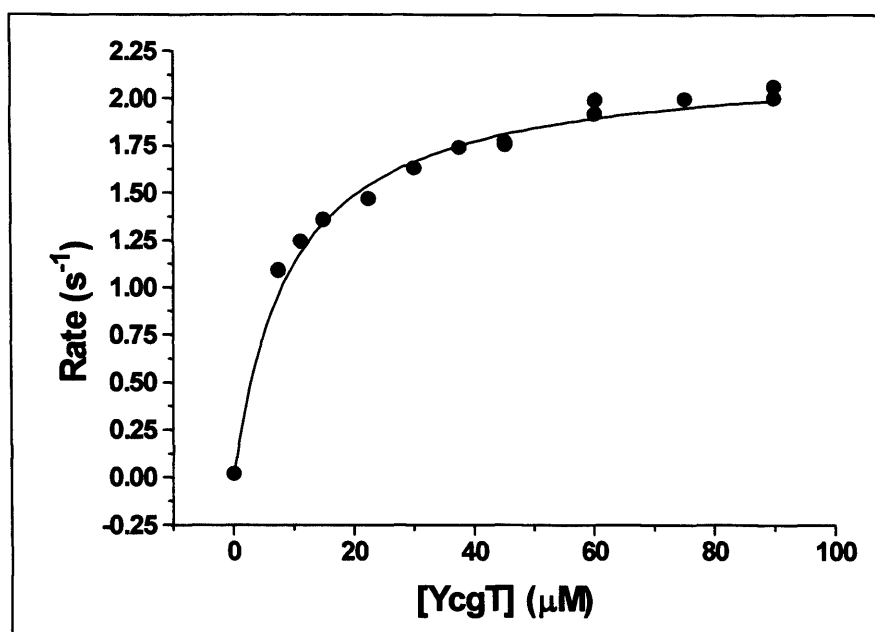


**Figure 5.24** Rate of reduction of YkuN (15  $\mu\text{M}$ ) by various concentrations (0 - 100  $\mu\text{M}$ ) of pre-reduced YcgT, as measured by photo-diode array stopped-flow. Experiment was carried out under anaerobic conditions in KPi buffer (50 mM, pH 7.0) at 30 °C. The absorbance spectra were collected between 300 and 800 nm and analysed by global analysis software (Applied Photophysics). The rate for each concentration of reductase was determined and a plot of rate versus reductase concentration is shown above fitted to a rectangular hyperbola (Origin, Microcal). This gave apparent values of  $k_{red}$  of  $2.2 \pm 0.2 \text{ s}^{-1}$  and a  $K_d$  of  $9.7 \pm 0.8 \mu\text{M}$ .

In both reactions with YkuN and YkuP, the reductase YumC gave the faster rates and tighter interaction. By comparing these rates to those measured in the steady-state assays above, it can be predicted that the rate-limiting step is the flavodoxin interacting with the P450 in the system where YumC is the reductase. In the case of YcgT similar rates are observed to that of the *E. coli* reductase (approx.  $3.0 \text{ s}^{-1}$  see Chapter 4) with YkuN, implying that it is the interaction of the reductase with NADPH and electron transfer from NADPH that may be at least partially limiting in steady-state catalysis. YcgT reduces YkuP rather faster than it does YkuN, but the reason is not clear. The single electron transfer from the flavodoxins (pre-reduced with dithionite) to P450 BioI has already been described (see Chapter 4) and gave rates of around  $3 \text{ s}^{-1}$  in both cases.

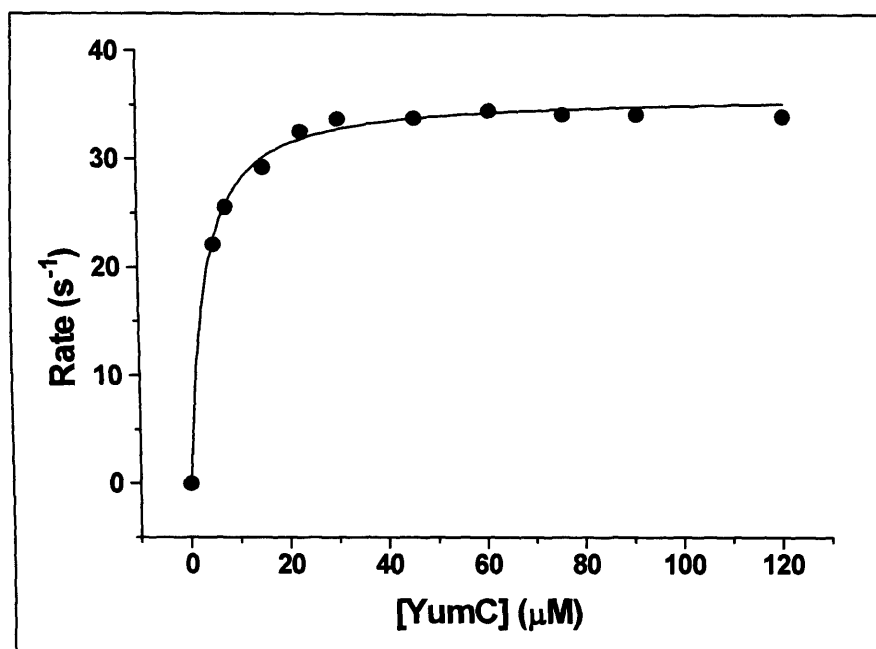


**Figure 5.25** The rate of reduction of YkuP (15  $\mu\text{M}$ ) by various concentrations (0 - 25  $\mu\text{M}$ ) of pre-reduced YumC, as measured by photodiode array stopped-flow absorption spectroscopy. Experiment was carried out under anaerobic conditions as previously described. Absorbance spectra were collected between 300 and 800 nm and analysed by global analysis software (Applied Photophysics). The rate for each concentration of reductase was determined and a plot of rate versus reductase concentration is shown above fitted to a rectangular hyperbola (Origin, Microcal). This gave a  $k_{\text{red}}$  of  $36.0 \pm 0.6 \text{ s}^{-1}$  and a  $K_d$  of  $2.9 \pm 0.3 \mu\text{M}$ .

Protein	YkuN				YkuP			
	$k_{\text{red}}$ ( $\text{s}^{-1}$ )	Error (+/-)	$K_d$ ( $\mu\text{M}$ )	Error (+/-)	$k_{\text{red}}$ ( $\text{s}^{-1}$ )	Error (+/-)	$K_d$ ( $\mu\text{M}$ )	Error (+/-)
YumC	26.9	0.2	1.1	0.1	36.0	0.6	2.9	0.3
YcgT	2.2	0.2	9.7	0.8	11.1	1.1	19.8	3.1

**Table 5.14** Stopped-flow measurements of the rate of electron transfer from the pre-reduced reductases (0 to 100  $\mu\text{M}$ ) to the oxidised flavodoxins YkuN and YkuP (15  $\mu\text{M}$ ). Reactions were carried out as previously described.

The transfer of a single electron from pre-reduced CYP102A3 reductase domain to the oxidised fatty acid-bound form of P450 BioI was measured on the stopped-flow by monitoring the formation of the ferrous-carbon monooxy adduct (448 nm) over time. A solution of P450 BioI (8.0  $\mu\text{M}$ ) near-saturated with myristate (0.025 mM) in KPi buffer (50 mM, pH 7.0) was mixed with a solution of CYP102A3 reductase (0 - 40  $\mu\text{M}$ ) also in

the same buffer at 30 °C. The absorbance spectrum was measured from 300 to 750 nm and analysed by a global analysis programme (Applied Photophysics) to determine a rate for each concentration of reductase. These rates were then plotted versus reductase concentration and fitted to a rectangular hyperbolic function to determine a  $k_{red}$  of 0.26  $\pm$  0.02 s<sup>-1</sup> and an apparent  $K_d$  of 17.7  $\pm$  1.5  $\mu$ M. This rate is slower than that observed for the interaction of the pre-reduced flds with P450 BioI, ( $k_{red}$  was *ca* 3.0 s<sup>-1</sup>) but this was not surprising as, in an interaction governed mainly by electrostatics [Roitberg *et al.*, 1998], the diflavin reductase domain has relatively little dipole compared to the flavodoxins, it being normally fused to its redox partner by a short peptide linker [Nahri and Fulco 1987]. This rate is slower than that measured for the reduction of the reductase domain by NADPH (16.8 s<sup>-1</sup>) and indicates that it is probably the electron transfer interaction between the reductase and P450 that limits the steady-state reaction rates.

Stopped-flow PDA analysis of the electron transfer from NADPH to myristate-saturated P450 BioI via either YumC or YcgT reductase plus either YkuN or YkuP fld was carried out to get an estimate of the rate of transfer of the first electron from the initial hydride donor right through the redox system to the ferric heme. As the PDA allows monitoring of all wavelengths, the initial decrease in NADPH absorbance and oxidised flavin absorbance, followed by the formation of the ferrous-CO peak at 448 nm can be seen. In the case of the three protein component systems, the reductase was kept at 5 molar equivalents over the P450 BioI (e.g. 20  $\mu$ M : 4  $\mu$ M) and the amount of flavodoxin changed from 1 to 5 molar equivalents over the P450 (e.g. 4 : 20  $\mu$ M). This gave the following  $k_{red}$  and  $K_d$  parameters (based on the assumption that the interaction between the reduced flavodoxin and oxidised P450 are rate limiting) shown below.

Reductase system	$k_{red}$ (s <sup>-1</sup> )	Error (+/-)	$K_d$ ( $\mu$ M)	Error (+/-)
YumC + $\Delta$ [YkuN]	9.10	1.21	14.1	3.7
YumC + $\Delta$ [YkuP]	3.42	1.22	12.5	1.5
YcgT + $\Delta$ [YkuN]	1.87	0.14	1.61	0.76
YcgT + $\Delta$ [YkuP]	2.52	0.11	1.54	0.41

**Table 5.15** Kinetic parameters for the PDA stopped-flow analysis of the transfer of the first electron from NADPH to P450 BioI (4  $\mu$ M) via the reductase systems shown in the column above. Reductases YumC and YcgT were kept constant at 20  $\mu$ M and the

concentration of flavodoxin varied from 4 to 20  $\mu\text{M}$ . The experiment was carried out under anaerobic conditions as described previously. The  $K_d$  parameter here is complex and probably represents interactions of the flavodoxin with both the reductase and the P450.

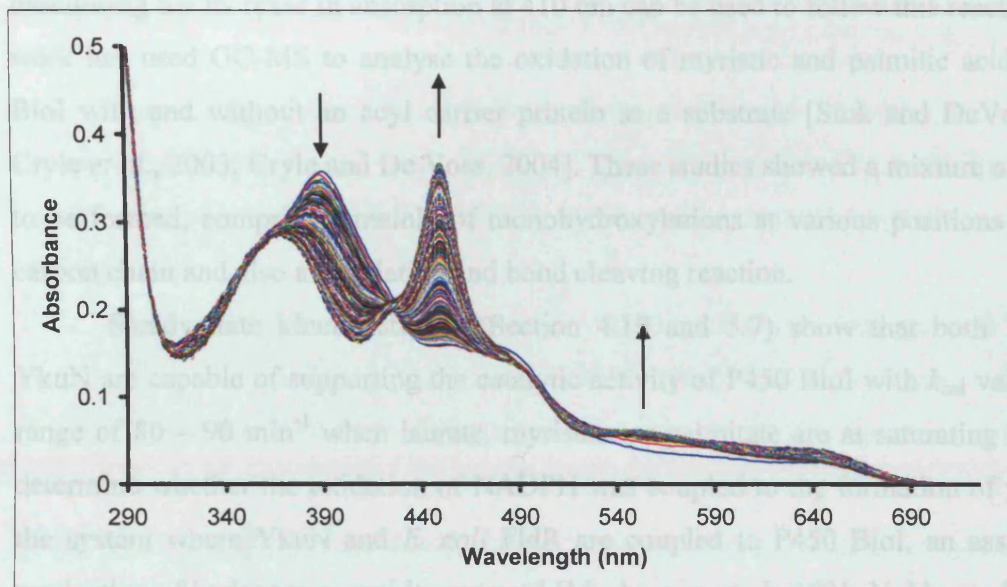


**Figure 5.26** UV-visible spectra recorded from the photodiode array stopped-flow experiment to measure the rate of electron transfer from NADPH (0.05 mM) to P450 BioI (4.0  $\mu\text{M}$ ) saturated with myristate (0.025 mM) via the reductase YumC (8.0  $\mu\text{M}$ ) and flavodoxin YkuN (8.0  $\mu\text{M}$ ). The spectrum shown above is with a limiting amount of NADPH (maximum at 364 nm) allowing the shift of the heme Soret maximum (from 394 to 448 nm) to be clearly seen.

### 5.8 Reconstitution of the active catalytic P450 BioI system

The ability of P450 BioI to productively oxidise a straight chain, saturated fatty acid (myristic acid) when coupled to its various redox partners was examined. Previous work had used a soluble form of human CPR to pass electrons to P450 BioI in an attempt to oxidise myristic acid [Green 2000].  $^1\text{H}$  NMR had been used to follow the reaction, but the low solubility of the fatty acid in  $\text{D}_2\text{O}$  and the high solubility of NADPH had made the spectra difficult to interpret and no conclusive signs of product formation were seen. The ability of P450 BioI to oxidise the reagent *p*-nitrophenoxydodecanoic acid (12-pNCA) was examined and this led the investigators to conclude that P450 BioI functioned as an  $\omega$ -hydroxylase. Hydroxylation of this compound by P450s leads to the

conversion of *p*-nitrophenoxycarboxylic acids (pNCA) into unstable hemiacetal intermediates that dissociates into the corresponding  $\omega$ -oxycarboxylic acid and the yellow chromophore *p*-nitrophenolate [Schwaneberg *et al.*, 1999]. As a result, monitoring the increase in absorption at 410 nm can be used to follow this reaction. Other work has used GC-MS to analyse the oxidation of myristic and palmitic acid by P450 BioI with and without an acyl carrier protein as a substrate [Stok and DeVoss, 2000, Cryle *et al.*, 2003, Cryle and De Voss, 2004]. These studies showed a mixture of products to be formed, comprising mainly of monohydroxylations at various positions along the carbon chain and also an acylation and bond cleaving reaction.

Steady-state kinetic studies (Section 4.19 and 5.7) show that both YkuP and YkuN are capable of supporting the catalytic activity of P450 BioI with  $k_{\text{cat}}$  values in the range of 80 – 90 min<sup>-1</sup> when laurate, myristate or palmitate are at saturating levels. To determine whether the oxidation of NADPH was coupled to the formation of product in the system where YkuN and *E. coli* FldR are coupled to P450 BioI, an assay for the production of hydrogen peroxide was used [Macheroux *et al.*, 1991, Noble *et al.*, 1999].

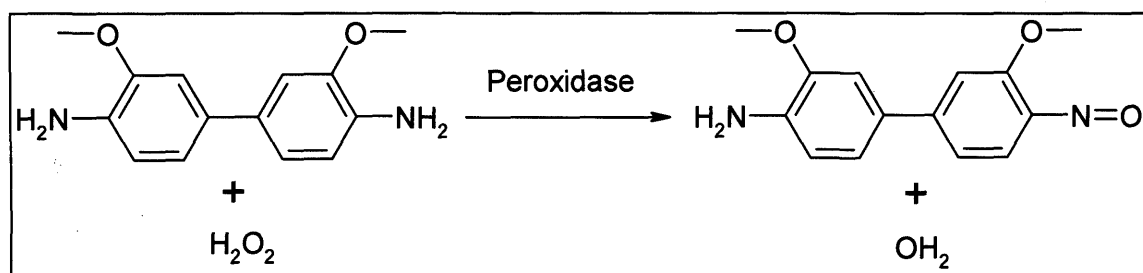


**Figure 5.27** Determination of the amount of H<sub>2</sub>O<sub>2</sub> produced by the oxidation of *o*-dianisidine by peroxidase follows the mechanism above. The orange colour generated has a maximum absorbance at 440 nm corresponding to an extinction coefficient of 11600 M<sup>-1</sup>cm<sup>-1</sup> [Macheroux *et al.*, 1991].

Following the measurement of steady-state rates, reaction mixtures were allowed to oxidise until no traces of NADPH remained (30 minutes). To the reaction mixture *o*-dianisidine (0.40  $\mu$ moles) was added and the absorbance at 440 nm measured. Horseradish peroxidase was added (2  $\mu$ l of 50 mg/ml stock) and after standing for 3 minutes the increase in absorbance at 440 nm due to the oxidation of the dye was measured (see Method 2.8). Uncoupling of NADPH oxidation from substrate oxygenation did not seem to occur to any significant extent, as the assay for H<sub>2</sub>O<sub>2</sub>



production showed that no more than 3.07 nmol of H<sub>2</sub>O<sub>2</sub> was produced per 1.00 µmol of substrate oxidised, i.e. < 0.31 % uncoupling towards peroxide production.

To look for the formation of any product, electrospray mass-spectrometry was used (Micromass Quattro electrospray ionisation mass-spectrometer). Successful oxidation of a compound is seen by the increase in *m/z* corresponding to the addition of one or more atoms of oxygen. From the binding constant data obtained previously (see Section 3.6), myristic acid was chosen as the initial substrate to look for oxidative activity, having a low *K<sub>d</sub>* of < 5 µM and a reasonable solubility in the aqueous buffer (0.02 mg/ml).

Preliminary reactions used the flavodoxin reductase from *E. coli* (2.0 µM) coupled with the *B. subtilis* flavodoxin YkuN (6.0 µM) to pass electrons from NADPH (8.8 µmol) to P450 BioI (3.0 µM). The reaction mixture was set up in the buffer (3 ml) often used in turnover studies with P450 BM3; 20 mM MOPS, 100 mM KCl at pH 7.4 [Noble *et al.*, 1999]. The substrate, myristic acid (4.4 µmol, *m/z* 227), was added to the buffer and stirred vigorously to produce a fine suspension. The three proteins were then added and the mixture allowed to equilibrate for 5 minutes prior to the addition of NADPH. Owing to the maximum rate of reduction of BioI by YkuN in the presence of myristic acid being 2.7 s<sup>-1</sup> (see Section 4.9) the reaction was left to proceed at room temperature (23 °C) overnight (16 hours). The fatty acids were recovered by acidification of the aqueous phase (1M HCl) and extraction into chloroform (2 vol) (see Section 2.8). Analysis of the organic phase by electrospray mass spectrometry (ionisation 70 eV, 20 µl injection loop) showed a small amount of putative mono-hydroxylated product (*m/z* 243, ES<sup>-</sup> spectrum) and a large amount of starting material (*m/z* 227) with no other impurities visible. The conversion of starting material to product was poor though, < 3 % being oxidised.

To maximise the yield of hydroxylated myristic acid, the effect of the various reaction parameters upon the oxidative activity of P450 BioI was investigated. To do this efficiently a fractional factorial experiment was set up using DX5 software (Stat-Ease, USA). In this case a two level fractional (1/16) factorial was used, which allowed the assessment of seven variables in ten experiments. The parameters investigated are outlined below:

Variable	Units	Low limit	High limit
pH	none	6.0	8.0
temperature	°C	23	37
P450	nmol	20	80
Volume	ml	2	12
Flavodoxin	eq <sup>1</sup>	0.5	10
Flavodoxin reductase	eq <sup>1</sup>	0.5	5
NADPH	eq <sup>2</sup>	0.5	3.5

<sup>1</sup> equivalents to P450 BioI (in moles)

<sup>2</sup> equivalents to Myristic acid (in moles)

The constants were the starting material (myristic acid, 8.0 µmol), buffer (20 mM MOPS, 100 mM KCl), time (16 hours) and continuous stirring. The variables are set to a relatively broad range to allow full evaluation of each effect, with the aim to maximise yield. The design plan that was used is shown below in Table 5.16. Reactions were terminated by acidification (pH 1.0, 1M HCl). The fatty acids were extracted into chloroform (2 vol) and analysed by electrospray mass-spectrometry (as described above). The yield of hydroxylated product (m/z 243) was calculated from the mass spectra and analysed by the software package. A further unknown impurity (m/z 208) was also seen and this was included in the data analysis.

Std	Run	Block 1	pH	Temperature Celsius	P450 nmoles	Volume ml	Fld eq (1)	Fldr eq (1)	NADPH eq (2)
9	1	Block 1	7	30	50	7	5.25	5.25	2
5	2	Block 1	6	23	80	12	0.5	0.5	3.5
8	3	Block 1	8	37	80	12	10	10	3.5
6	4	Block 1	8	23	80	2	10	0.5	0.5
3	5	Block 1	6	37	20	2	10	0.5	3.5
10	6	Block 1	7	30	50	7	5.25	5.25	2
7	7	Block 1	6	37	80	2	0.5	10	0.5
2	8	Block 1	8	23	20	2	0.5	10	3.5
1	9	Block 1	6	23	20	12	10	10	0.5
4	10	Block 1	8	37	20	12	0.5	0.5	0.5

**Table 5.16** Design plan for the two-level fractional factorial generated from the DX5 software (Stat Ease USA) to study the effect of the various factors on the oxidative activity of P450 BioI. The parameters are entered in a high/low value pattern to generate the 1/16 factorial (std 1 – 8) and the two centre points are added (std 9 and 10). The software then randomises the experiments to give the Run order. Fld refers to flavodoxin and Fldr to reductase, the equivalents (eq (1) and (2)) are explained above.

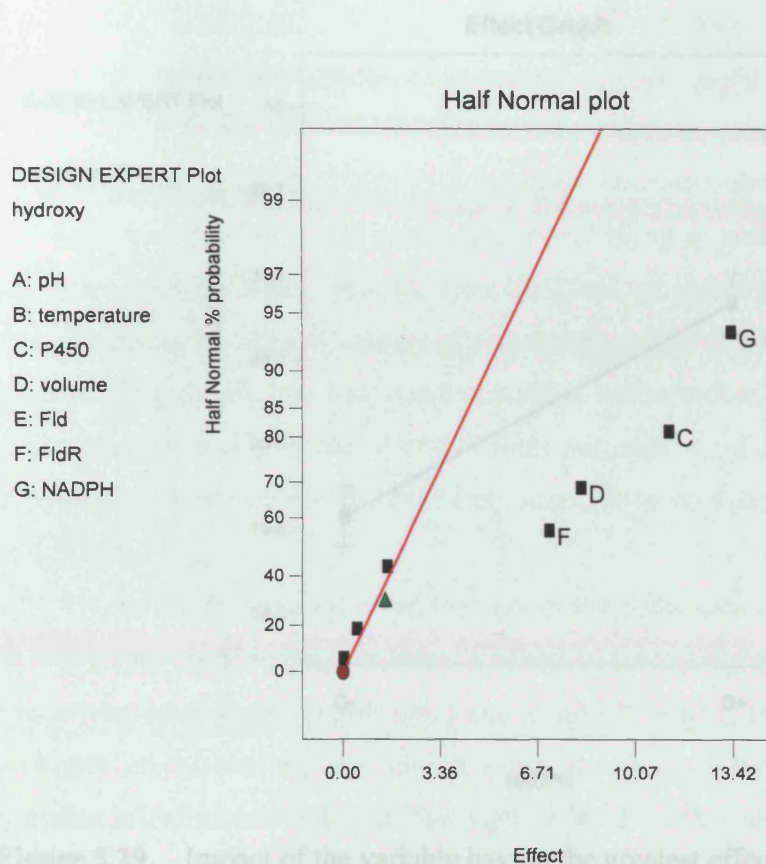


**Figure 5.28** An effect plot for the amount of hydroxylated myristic acid produced in the P450 BioI-catalysed oxidation of myristic acid. Each factor is plotted against the effect it has upon the % yield of mono-hydroxylated myristic acid. The four factors having the greatest effect are annotated (amount of NADPH (G), amount of P450 (C), the reaction volume (D) and the amount of FldR (F)). The remaining, unlabelled factors had negligible effect. The triangle symbol shows the degree of reproducibility of the experiments and the impact of experimental error on the yield of product.

As can be seen from the effect plot shown above the consistency between the centre points (triangle symbol) is good, i.e. the reactions are reproducible. The factors that have the greatest effect upon the yield of mono-hydroxylated myristic acid were the following; (G) amount of NADPH (molar equivalents to substrate), (C) amount of P450 (nmoles), (D) volume of reaction (ml) and (F) amount of flavodoxin reductase (molar equivalents to P450 BioI).

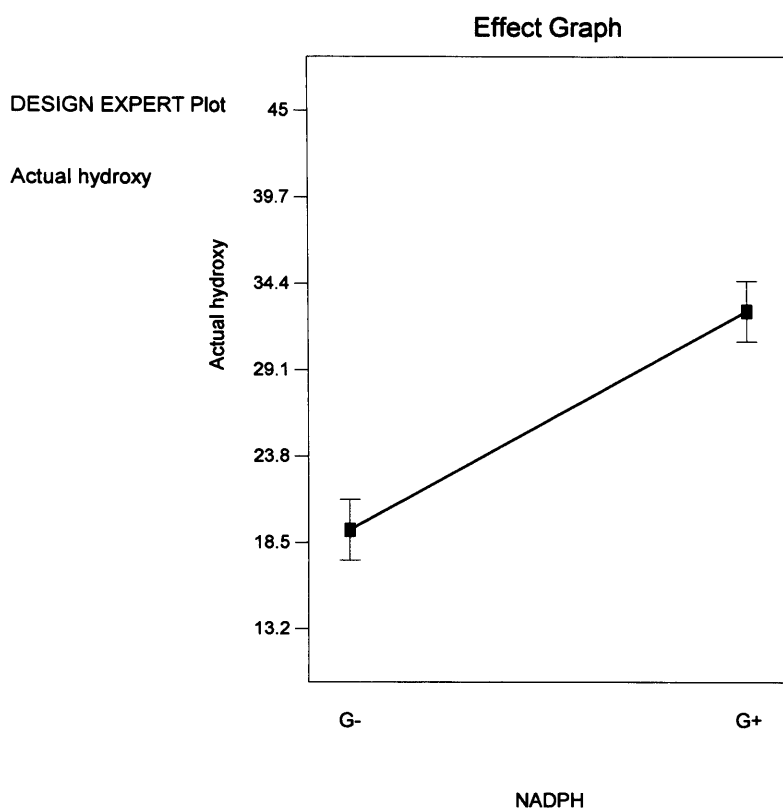


**Figure 5.29** Impact of the variable having the greatest effect, amount of NADPH, upon the amount of hydroxylated product formed (actual hydroxy) in the P450 BioI catalysed oxidation of myristic acid. It can be seen that the highest level of NADPH (3.5 molar equivalents) gives the highest yield within the range of NADPH concentrations studied (0.5 (G-) to 3.5 (G+) molar equivalents of NADPH).

Factors such as the pH, amount of flavodoxin and temperature had negligible effect upon the yield. Whilst the pH is known to affect the binding of substrate by P450 BioI (see Section 3.2), there is little effect within the range studied here (6.0 – 8.0). A lower pH value was not investigated as the protein is known to denature upon prolonged incubation in more acidic conditions, and a higher value causes a notable reduction in the ability of the P450 to bind myristic acid. The temperature range (23 to 37 °C) was chosen with the knowledge that *B. subtilis*, being a soil bacterium, grows under relatively mild conditions, temperatures less than 18 °C resulting in a cold shock response [Kaan *et al.*, 2002].

The results of the fractional factorial experiment were analysed by fitting to a linear model. This gave a high  $R^2$  value (0.983) and showed no significant curvature

(Probability >F of 0.0021) and a general good fit (the lack of fit having Probability >F 0.8980). From the effect graphs it can be seen that increasing the amount of NADPH and P450 BioI increases the yield of hydroxylated myristic acid (see Figure 5.28). This is despite the fact that NADPH is in 3.5 fold excess over substrate at the maximum level and despite only ~ 80 % of the starting material being consumed to produce a mixture of the mono-hydroxylated compound (m/z 243) and the unknown impurity (m/z 208). This result suggests that a large amount of uncoupling and/or degradation of the substrate may be occurring, despite the low results obtained in the *o*-dianisidine assay for H<sub>2</sub>O<sub>2</sub>. The difference may reflect consumption of some peroxide in oxidative damage of proteins in the solution. Alternatively, the P450 may uncouple to produce water or superoxide [Loida and Sligar, 1993].

Overall the model showed that, under the conditions studied, the greatest yield of hydroxylated myristic acid could be obtained by having the greatest amounts of NADPH (3.5 molar equivalents to substrate) and P450 (80 nmol), the largest volume (12.0 ml, probably on account of the limited solubility of the substrate) and concentration of flavodoxin reductase (although the highest level in this study was still less than 5.0 equivalents of P450). Having now identified the factors that have the greatest effect upon the oxidation of myristic acid by P450 BioI, the conditions were optimised to give the maximum yield to allow characterisation of the turnover products when different redox partners are used to drive the catalysis.

Confirmation reactions and optimisation of the conditions to maximise the yield of mono-oxygenated product were undertaken. The electrospray mass spectrum of a P450 BioI-catalysed myristic acid oxidation is shown in Figure 5.30. In this reaction 72.4% of the starting material (m/z 227) has been converted to the mono-hydroxylated product (m/z 243), the unknown impurity being 3.0 % (m/z 208). The peak at m/z 259 is related to the residual palmitic acid bound to the isolated and purified P450 BioI used in the assay (Section 3.3). The reaction conditions were 0.6 mg of myristic acid suspended in buffer (5 ml, 20 mM MOPS, 100 mM KCl, pH 7.0) at room temperature. The proteins P450 BioI (50 nmol), YkuN (30 nmol) and *E. coli* FldR (10 nmol) were added to the suspension. After equilibrating for five minutes, NADPH (6.0  $\mu$ mol) was added. The reaction mixture was stirred overnight (16 hours) at room temperature (23 °C). Extraction

of the fatty acids for analysis was as described previously. The reaction was performed in triplicate and the yield of the mono-hydroxylated product varied from 70.2 % to 72.4 %. A reaction in which P450 BioI is absent was also set up as a control. Extraction and analysis of this mixture revealed no decomposition of the starting material had occurred. The 27-fold increase in yield obtained in this experiment over the conditions initially used was deemed good enough to allow evaluation of alternate redox partners.

A reaction where the optimal conditions were used (see previous paragraph) was prepared and an NADPH regenerating system was added. This consisted of glucose-6-phosphatase dehydrogenase (50.0 units) and its substrate, glucose-6-phosphate (5.0 mg). Analysis of the reaction showed no real change in yield, the amount of mono-hydroxylated myristic acid being 73.7 %. It was decided not to continue with this regeneration system, the current excess of NADPH seeming adequate.

To check that the oxidation of NADPH was coupled to product formation in all of the various redox systems under evaluation, reaction mixtures were prepared and the P450 BioI-catalysed oxygenation of myristate was carried out. Solutions of P450 BioI (80 nmol), and either YkuN or YkuP (20 nmol) plus either YcgT or YumC (20 nmol) were prepared in MOPS buffer (12 ml, 20 mM, pH 7.0, 100 mM KCl) that had 1.0 mg of myristate suspended in it. NADPH (16 mg) was added and the suspension incubated with mild agitation for 16 hours at 30 °C. Extraction of any product and remaining substrate with chloroform was carried out (see Method 2.8) and the resulting organic phase analysed by electrospray mass-spectrometry (as previously described). In all cases, varying proportions of myristic acid had been mono-oxygenated, showing that an active catalytic system had been configured. The most active system from this experiment appeared to be that of YumC combined with YkuN, an observation in agreement with YumC being the more active reductase. It was also found that when the standard class I system was replaced by the diflavin reductase domain of CYP102A3, a substantial amount of product was formed (35 %), suggesting that although this system may be slower, it is fully functional. Control reactions (reductase plus flavodoxin with no P450 present) were also set-up under the same conditions, as were two reactions containing the reductase and P450 BioI but no flavodoxin. When analysed, these controls were found to contain only starting material with no sign of oxidative or degradative activity.



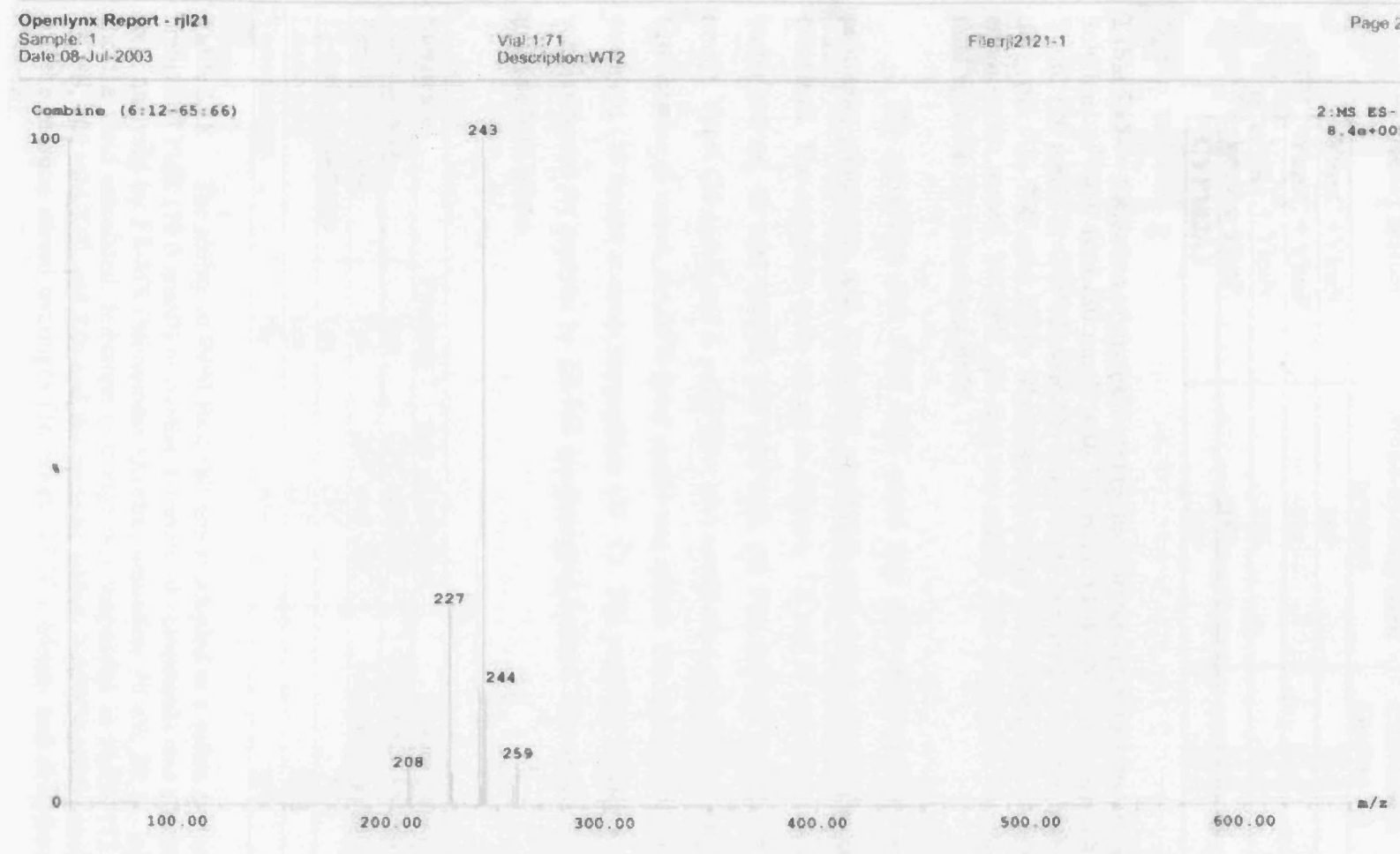


**Figure 5.30** Mass spectrum of the chloroform extract from the P450 BioI-catalysed myristic acid oxidation. Electrospray ionisation was used (70 eV) with a quadrupole detector (Micromass Quattro). Peaks are an unknown impurity (m/z 208), starting material (m/z 227), monohydroxylated product (m/z 243) and palmitate derived impurity (m/z 259). Myristic acid (0.6 mg) was suspended in buffer (5 ml, 20 M MOPS, 100 mM KCl, pH 7.0) and BioI (50 nmol), YkuN (30 nmol) and FldR (9.5 nmol) were added. NADPH (6.0  $\mu$ mol) was added and the reaction stirred overnight (16 hours at 23  $^{\circ}$ C) prior to analysis.

Redox system	Mono-hydroxylated product	Conversion (molar %)
YumC + YkuN	yes	75.0
YumC + YkuP	yes	43.6
YcgT + YkuN	yes	25.0
YcgT + YkuP	yes	15.4
CYP102A3	yes	35.4

**Table 5.17** Oxidation of myristic acid by the various combinations of redox systems. Solutions of P450 BioI (80 nmol) with YkuN or YkuP (20 nmol) plus either YcgT or YumC (20 nmol) or CYP102A3R (20 nmol) were prepared in MOPS buffer (12 ml, 20 mM, pH 7.0, 100 mM KCl). Myristate (1.0 mg) was added and, following a brief equilibration period, NADPH (16 mg) was added. The suspension was incubated with mild agitation for 16 hours at 30 °C.

The possibility that P450 BioI could turn over different fatty acids (laurate, palmitate, palmitoleic and 13-methyl myristate) and also a steroid (testosterone) was examined. The reactions were set up as follows; 1.0 mg of substrate was suspended in buffer (12 ml, 20 mM MOPS, 100 mM KCl, pH 7.0) and the proteins P450 BioI (80 nmol), YkuN (20 nmol) and *E. coli* FldR (10.0 nmol) were added to the suspension. After equilibration (5 mins), NADPH (16.0 µmol) was added. The reaction mixture was stirred overnight (16 hours) at room temperature (23 °C). The potential substrates and products were extracted for analysis by ES-MS (as described before). The results are summarised in Table 5.18 below:

Substrate	Product ?	m/z of product	Conversion (%)
Palmitic acid	Yes	271 <sup>-</sup> and 287 <sup>-</sup>	5.6 and 2.2 respectively
Palmitoleic acid	Yes	269 <sup>-</sup> and 285 <sup>-</sup>	3.0 and 4.0 respectively
13-methyl myristate	Yes	257 <sup>-</sup>	3.0
Lauric acid	Yes	215 <sup>-</sup>	55.0
Testosterone	No	n/a	n/a

**Table 5.18** The ability of P450 BioI (80 nmol) coupled to a redox system (YkuN (20 nmol) and FldR (10.0 nmol)) to oxidise a variety of compounds was assessed. Products were analysed by ES-MS (Micromass Quattro, ionisation 70 eV, 20 µL injection loop) and the yield calculated. Substrate (1.0 mg) was suspended in buffer (12 ml, 20 mM MOPS, 100 mM KCl, pH 7.0) and the proteins added. NADPH (16.0 µmol) was added and the reaction stirred overnight (16 hours, 23 °C). Mono- and di-hydroxylation was observed.

All four of the fatty acids were oxidised by P450 BioI to their mono-hydroxy (and in the case of palmitic and palmitoleic acid, di-hydroxy) derivatives. In the case of palmitic acid the lower solubility of the substrate (0.007 mg/ml in water at 25 °C) probably has a detrimental effect upon yield. Indeed the palmitic acid that is bound to samples of purified P450 BioI is never seen to be oxidised in turnover reactions with other substrates such as myristate. This may also explain why di-hydroxylation of both the C16 fatty acids is seen, as mono-hydroxylation could possibly increase their solubility to be in the same range as myristate (0.020 mg/ml), the C14 fatty acid for which conditions have been optimised. Lauric acid, despite having a lower  $K_d$  than palmitic acid (measured  $K_d$  being 11.0  $\mu$ M for laurate and 7.2  $\mu$ M for palmitate), has a higher solubility (0.055 mg/ml at 25 °C) and a higher amount of oxidation is observed to give 55 % conversion to a unique mono-hydroxylated product. The turnover of 13-methyl myristate is of note, as this compound gave a reverse type I shift at high concentrations (> 30  $\mu$ M) in binding titrations (although a shift to high-spin at lower concentrations was observed) and the presence of the methyl group means that one of the possible hydroxylation positions is blocked. The steroid did not give a unique product, some decomposition was observed.

Whilst analysis by electrospray mass-spectrometry shows that P450 BioI is able to mono-hydroxylate both lauric and myristic acid in reasonable yield, it is unable to show whether one unique mono-hydroxylated product is formed or whether a mixture of regio- and stereoisomers is produced. More detailed analysis by NMR and other chromatographic techniques is therefore required to fully characterise the structure of the products. Identification of P450 BioI's function *in vivo* is still unclear. It is unlikely to be a simple  $\omega$ -1 to  $\omega$ -3 fatty acid hydroxylase, despite the results shown here, as *B. subtilis* contains two BM3 homologs (CYP102A2 and CYP102A3) that are both able to hydroxylate saturated straight-chain fatty acids of 12 to 16 carbons in length at a considerably greater rate than P450 BioI [Gustafsson *et al.*, 2004]. CYP102A3 is in an operon whose transcription is regulated by the protein FatR, whose binding to the operator sequence is thought to be repressed by oleic and palmitic acid, which were found to induce the expression of this operon to a considerable extent [Lentz *et al.*, 2004, Gustafsson *et al.*, 2004, Lee *et al.*, 2001]. The oxidation of a fatty-acid bound to an acyl-

carrier protein (ACP) as previously observed to produce pimelic acid [Stok and DeVoss, 2000] could be as a result of the ACP causing some structural perturbation of the P450. In this work no ACP was observed to co-purify with the P450 and so was not included in the oxidation studies. This work shows that YkuN and YkuP, in addition to the *B. subtilis* ferredoxin, can act as functional redox partners to P450 BioI, resulting in the mono-oxidation of fatty acids.

## **5.9 Conclusions**

Three different reductase systems were evaluated. Of the two typical class I systems the two reductases YumC and YcgT were found to be able to interact with the two flavodoxins YkuN and YkuP in such a way as to support the mono-oxygenation of myristic acid by P450 BioI. These two reductases were found to have quite different kinetic and thermodynamic properties from one another, although they are both able to carry out the same role *in vitro* with respect to P450 reduction. YumC was found to have much faster rates of reduction by NADH and NADPH than YcgT, and this was reflected in faster steady-state rates with a variety of electron acceptors. Their redox potentials, fluorescence and absorbance profiles suggest differences in the immediate environment of their different flavin cofactor and it is this that may explain the large differences in their activity, despite their reasonably high sequence similarity.

Cloning the reductase domains of the two class II P450s native to *B. subtilis*, CYP102A2 and CYP102A3, generated two diflavin reductases. Of these only that of CYP102A3 was found to express to a high level and this protein was isolated and characterised. The main aim of cloning these diflavin proteins was to produce a more efficient catalytic system to drive P450 BioI, as two replaced three proteins. However, the separation of the reductase domain from its heme partner appeared to disrupt its ability to either bind and/or be reduced by NADH and NADPH, despite no notable difference in the far UV or visible CD spectrum *c.f.* that reported for the reductase domain of P450 BM3 [Munro *et al.*, 1996]. The loss in reactivity of this initial step resulted in comparably slow rates in steady-state reactions *c.f.* the intact flavocytochrome. However, despite the reductive interaction of the pre-reduced diflavin reductase domain with P450 BioI also

being comparatively slow ( $0.26\text{ s}^{-1}$ ), this system was shown to be catalytically competent converting 35 % of myristate to its mono-hydroxylated form. As has been observed in the factorial work, a slower rate can be coupled to a more efficient reaction, with less harmful side products such as superoxide species being formed. Thus, the use of this reductase system *in vivo* is still plausible where, in any case, the rates of other steps in the biotin pathway are slower still (e.g. conversion of KAPA to DAPA by BioA is  $0.013\text{ s}^{-1}$  [Eliot *et al.*, 2002]). Work at a molecular level, where the N-terminal of these domains seems to be unexpectedly important to their folding and function, may yet produce a reductase domain with reduction rates that rival those of YumC, the advantage of which being that the electron transfer from FAD to FMN will be several-fold more efficient and this may be translated to more effective P450 reduction. The ability of P450 BioI to interact with a wide variety of redox partners (ferredoxins, flavodoxins, and larger di-flavin containing proteins) implies a general non-specific binding site for the docking of electron-transfer proteins to the P450. This would allow P450 BioI to utilize various proteins intracellularly, literally pulling electrons off whatever reduced protein it interacts with. This would mean that P450 BioI could theoretically compete with the heme domain of intact CYP102A3 for electrons, although the linked nature of CYP102A3 means that its own heme domain would have a natural advantage.

## *Chapter 6*

### *Conclusions*



## 6.1 Cytochrome P450 BioI

P450 BioI is a protein encoded by the gene *bioI*, a member of an operon of genes involved in the biosynthesis of biotin [Bower *et al.*, 1996], their transcription being regulated by the intercellular concentration of the vitamin [Xu *et al.*, 1996]. The protein product of the cloned gene had previously been over-expressed and characterised as a cytochrome P450 [Green *et al.*, 2001] and its function found to be a mixture of acyl-bond cleavage reactions [Stok and DeVoss, 2001] and oxidations close to the  $\omega$ -terminal of fatty acids [Cryle *et al.*, 2003, Green *et al.*, 2001]. The work described here extends the characterisation of the protein. Spectroscopic techniques aided characterisation of the protein as a typical bacterial P450. CD profiles show P450 BioI to be predominantly  $\alpha$ -helical in nature with the far UV CD signature resembling those of other bacterial P450s. The spectrum of the near UV-visible region showed the presence of a mixed-spin heme with two minima (348 and 404 nm) in the negatively signed Soret CD signature. The mixed-spin nature of the heme was also shown in EPR and resonance Raman spectra. EPR spectra of P450 BioI in both its mixed-spin and low-spin states were recorded. The spectrum of the low-spin form differed slightly depending upon whether the heme was low-spin due to pH or steroid binding. The subtle differences in the g-values between the two forms are probably due to the co-ordination of the steroids carbonyl oxygen to the heme and the bulk of the steroid causing slight distortion of the porphyrin ring. Changes in the pH can cause alteration of hydrogen bonding pathways in the active site.

In this project P450 BioI was over-expressed in an *E. coli* expression host (Origami DE3 [Novagen]) and it was observed that, when purified, it was in a mixed-spin form. This was found to be due to the presence of palmitic acid bound in the active site of a large proportion of isolated P450 BioI. Palmitate is present in *E. coli* in great abundance. It is believed that in the absence of any redox partners capable of fuelling oxidative catalysis (*E. coli*'s native flavodoxin being unable to supply the second electron required for P450 catalysis, as established in work presented in this thesis) the binding constant for palmitic acid is tight enough ( $K_d$  5 – 8  $\mu$ M) to cause its retention in the binding cavity of P450 BioI throughout its isolation and subsequent purification.

From binding experiments it became clear that not only does this P450 have the ability to bind a variety of saturated straight chain fatty acids typical of bacterial P450s, but also branched chain and unsaturated derivatives such as may be found in its host organism (*B. subtilis*) under various growth conditions [Klein *et al.*, 1999]. From amino acid alignments it was clear that P450 BioI had a high similarity to the P450 eryF, a P450 involved in erythromycin biosynthesis [Cupp-Vickery *et al.*, 1991]. The similarity may stretch from the primary structure to the overall fold of these P450s, as it was found that P450 BioI also had the capability to bind polycyclic compounds such as arenes and steroids. However, whilst able to accommodate such molecules within the active site, P450 BioI is not believed to catalyse oxidations on this type of compound *in vivo*. Efficient binding of steroids was only achieved when a carbonyl group was present (e.g. testosterone and progesterone) that allowed formation of a tightly bound low-spin form of the P450. Cyclic hydrocarbons that lacked this group were not able to bind strongly and did not always cause full conversion of the heme to its high-spin form at saturation. The lack of a truly high-spin form means that the monooxygenation of these compounds is less thermodynamically favoured compared to that with fatty acids. Whilst the P450 may bind a variety of compounds, its oxidase activity is more selective. Indeed analysis of a catalytic mixture of testosterone bound-P450 BioI showed that no oxidation had taken place, although NADPH oxidation was stimulated by testosterone binding.

The redox potential of the heme in P450 BioI was measured in both its high-spin substrate-bound state and low-spin steroid-bound form, in addition to the unbound low-spin state. This produced thermodynamic values for the reduction of the heme and showed that, as in the case of the well documented P450 CAM [Sligar and Gunsalus, 1976] and BM3 [Daff *et al.*, 1997], the binding of a substrate type molecule acts as a thermodynamic switch causing the redox potential of the heme to elevate by 131 mV. This elevation in potential increases the energetic drive to transfer an electron from the reduced redox partner to the oxidised P450. It was also shown that by desolvation of the binding cavity in the presence of a bulky steroid molecule, the redox potential of the heme also became more positive, albeit by a lesser amount (74 mV). This measurement showed that the redox potential of the heme is affected not only by the spin state of the iron, but also by the hydrophilicity of its environment.

In the absence of a structure of the P450, a model was built to give some insights into the structure of P450 BioI. The model, based on the structures of P450s with the highest homology to P450 BioI, was found to indicate the presence of a disulphide bond within the P450 between Cys250 and Cys275. Further experiments with Ellman's reagent, and the fact that the P450 is over-expressed better in strains of *E. coli* containing the *gor522::Tn* and *trxB::kan* mutations, indicate that this P450 does contain a disulphide bond, a novel bond in a cytochrome P450. Docking of the two ligands myristic acid and testosterone into the active site of P450 BioI allowed us to speculate that the steroid does indeed bind by co-ordination of the heme with its carbonyl group, the C17-hydroxyl forming a hydrogen bond with Glu65 near the entrance to the active site. Myristic acid could be docked most favourably when its carboxylate group acted as a hydrogen acceptor from Ser67 and Tyr179. The long alkyl chain then lay down the binding cavity held between the lipophilic phenylalanine residues (Phe83 and Phe384). The docking of this substrate agreed with the observed hydroxylation of fatty acids near the  $\omega$ -end [Cryle *et al.*, 2003] as the  $\omega$ -terminus carbons lay directly above the heme surface.

Studies on the stability of P450 BioI were also undertaken. It was found that breakage of the putative disulphide bond by treatment with dithiothreitol had no effect on either the  $T_M$  of the protein (69 °C) or the midpoint values when Gdn.HCl was used as a chemical denaturant. A small effect was observed by the binding of various compounds to P450 BioI, the binding of a fatty acid (palmitoleate) lowering the  $T_M$  (63.5 °C) and the binding ofazole containing compounds raising the amount of Gdn.HCl required to denature the protein. These subtle alterations in the protein's stability probably reflect small conformational changes that occur upon ligand binding. P450 BioI might be expected to have quite a flexible binding cavity due to the diverse range of substances it is able to bind.

## **6.2 The flavodoxins; YkuN and YkuP**

The sole ferredoxin in the *B. subtilis* genome had previously been cloned and characterised [Green *et al.*, 2003]. It was found to be capable of interacting with P450 BioI, but electron transfer was observed to proceed at a slow rate. Whilst, given the low

cellular requirement for biotin, this ferredoxin may be the natural partner to P450 BioI *in vivo*, the development of a more productive strain of *B. subtilis* would allow alternate electron providers to be used. Other possible candidates for redox partners to P450 BioI were sought and two putative flavodoxins were identified in the genome, encoded by *ykuN* and *ykuP*. Flavodoxins are well documented as being able to replace ferredoxins under conditions of iron limitation [Rogers, 1987]. These genes were cloned into pET16b expression vectors and their protein products expressed in *E. coli* and purified. It was found that both genes encoded short-chain flavodoxins of 17.8 kDa (YkuN) and 16.8 kDa (YkuP), contrary to the published sequence for the hypothetical YkuP long-chain flavodoxin (> 20 kDa) [Subtilist web server, Pasteur Institute]. The protein sequence for the short-chain form of YkuP (resulting from the deletion of a single erroneous adenosine nucleotide from the database sequence resulting in an earlier stop codon) aligned well with the sequences for other short-chain flavodoxins, lacking the insert region seen in all long-chain flavodoxins characterised to date.

The two flavodoxins were found to have very similar biophysical properties to each other as implied by the great similarity of their amino acid sequences. Both formed a very stable neutral blue semiquinone with a large separation (> 250 mV) between the values for the one- and two-electron reduction. Both of the flavodoxins were found to have a high affinity for P450 BioI. By monitoring the quenching of their co-factors' fluorescence, both YkuN and YkuP were found to form tight complexes with P450 BioI. Measurement of the redox potentials of these complexes showed that, whilst there was little change in the midpoint potentials of the flavodoxins, the potential of the fatty acid-bound heme became more negative. This was a surprise as docking of a ferredoxin to P450 CAM has been shown to shift the potential of the heme in a positive direction, encouraging electron transfer to the heme via its desolvation [Sligar and Gunsalus, 1976]. It is possible that the heme in P450 BioI is more buried *c.f.* P450 CAM and therefore the change in solvation upon the binding of the flavodoxin is small.

Both flavodoxins exhibited similar binding constants for their FMN cofactors (*ca.* 16 - 25 nM), although these were less tight than those previously documented for *D. vulgaris* flavodoxin (< 1.0 nM [Mayhew, 1971]). Neither YkuN nor YkuP were able to bind riboflavin, even in the presence of phosphate ions. This is in agreement with them

both being short-chain flavodoxins, as although long-chain flavodoxins can readily bind riboflavin, only one short-chain flavodoxin has been shown capable of binding riboflavin to date [Pueyo *et al.*, 1996]. Chemical denaturation of the two flavodoxins with Gdn.HCl showed that YkuN bound the FMN cofactor more tightly than YkuP. This property was observed during purification of the proteins when a higher proportion of FMN was seen to dissociate from YkuP. It was found that the removal of the cofactor from YkuP caused a reorganisation of the apo-protein, the apo-form having differing CD and fluorescence profiles compared to the holo-form. The denaturation of the holo-forms of both flavodoxins is believed to occur via the loss of the cofactor resulting in a collapse of the flavin binding loops. This step is then followed by a reorganisation of the apo-protein in the case of YkuP, before both apo-proteins unfold further until virtually no secondary structure remains.

Artificially reduced forms of YkuN and YkuP were used to reduce P450 BioI in an anaerobic environment. The rate of electron transfer from the flavodoxins to the P450 was *ca.*  $3.0\text{ s}^{-1}$  when the P450 was saturated with palmitoleate. Unlike the long-chain flavodoxin from *E. coli*, both the short-chain flavodoxins from *B. subtilis* can pass two successive electrons to P450 BioI to produce a catalytically competent system. This was shown by the use of the NADPH-oxidoreductase from *E. coli* and YkuN/P coupled to P450 BioI to oxidise myristate to a mono-hydroxylated product. With this catalytic system limiting steady-state rates of around  $90\text{ min}^{-1}$  were recorded when the amount of the flavodoxins was saturating. With testosterone-bound BioI, the steady-state rate fell to around  $25\text{ min}^{-1}$ , indicative of the reduction of the low-spin heme being less thermodynamically favoured.

### 6.3 NAD(P)H oxidoreductases

To complete the redox chain, two typical *B. subtilis* NAD(P)H-oxidoreductases and one diflavin reductase were over-expressed and studied. The two NAD(P)H-dependent oxidoreductases (YumC and YcgT) had previously been cloned and were gifts from Dr. J. Perkins (DSM). The diflavin enzyme was the reductase domain of the *B. subtilis* CYP102A3 P450 flavocytochrome, and was studied with the idea of increasing

the rate of electron transfer from NADPH to P450 BioI. The diflavin reductase domains from both CYP102A2 and CYP102A3 were cloned into pET21a expression vectors. However, only that from CYP102A3 was expressed in *E. coli* to any significant level and so this was the sole diflavin candidate used.

Both CYP102A3 diflavin reductase and the native NADPH-oxidoreductases were found to over-express well in *E. coli* and were easily purified by column chromatography. Purification under aerobic conditions resulted in all three reductases being prepared in their yellow oxidised forms. YcgT and YumC were reduced by dithionite under anaerobic conditions to their blue neutral semiquinone form; further reduction yielded the colourless hydroquinone. Reduction of the diflavin reductase domain of CYP102A3 by dithionite also gave a colourless hydroquinone, and an intermediate neutral blue semiquinone on the FAD cofactor. All three reductases had similar far UV CD profiles being typified by a large negative signal with a minimum at 209 nm and, being similar in shape and character to that published for the reductase domain of P450 BM3 [Munro *et al.*, 1994]. The near UV-visible CD reflected the differing cofactors of the reductases with YumC and YcgT sharing a similar profile with a single minimum at around 460 nm. CYP102A3R, which binds two flavins, has two minima at 480 and 390 nm. All of the reductases were fully folded and functional proteins.

All three of the reductases assessed (YumC, YcgT, CYP102A3R) were found to favour NADPH as a reducing agent over NADH. This preference for the 5'-ribityl phosphate group of NAD(P)H is not uncommon in bacterial reductases. The  $k_{red}$  for YumC with either NADPH (680 s<sup>-1</sup>) or NADH (12.5 s<sup>-1</sup>) was found to be several fold faster than that of its counterpart YcgT (25.6 and 1.1 s<sup>-1</sup> respectively), the reason for the difference in reactivity may be explained in part by the difference in the redox potentials of the two proteins. YumC was found to have a more positive reduction potential than YcgT ( $E_{OX/HQ}$  for YumC = -201 mV compared to that of -329 mV for YcgT). It was observed that both the mono-flavin reductases had much less stable semiquinones *c.f.* the two flavodoxins, with the two separate reduction transitions (OX/SQ and SQ/HQ) being of similar values, presumably due to the reductases cycling from their oxidised to 2-electron reduced form upon reduction by NAD(P)H. The semiquinone form of YcgT had



a reduced intensity compared to that of YumC, indicating that only a relatively small amount of YcgT ever exists in the one-electron reduced state upon reduction. This implies a destabilisation of the semiquinone form, and subsequent fitting of the two-electron Nernst equation showed the two midpoint potentials to be inverted.

The cleavage of the diflavin reductase domain from the heme domain of CYP102A3 seemed to have reduced the ability of the reductase domain to interact with or accept hydride ions from NADPH,  $k_{red}$ , the limiting flavin reduction rate, ( $16.8 \text{ s}^{-1}$ ) being several fold slower than that measured for the full-length form [Gustafsson *et al.*, 2004]. This initial step, although slow, was found not to limit the turnover of P450 BioI, subsequent electron transfer assays showed the electron transfer from the reductase to the P450 ( $0.3 \text{ s}^{-1}$ ) most likely to be rate-limiting.

All of the reductases were used to re-constitute a functional catalytic system able to drive the reduction of P450 BioI. Both YumC and YcgT were able to reduce the two *B. subtilis* short-chain flavodoxins YkuN and YkuP, their electron transfer rate ( $k_{red}$  of *ca.*  $3 \text{ sec}^{-1}$ ) being similar to that observed with *E. coli*'s FldR. In steady-state assays with myristate-bound BioI, the rates with YumC as the reductase were limited by the amount of flavodoxin present. When YkuN/P were in excess, rates of around  $100 \text{ min}^{-1}$  were observed. Steady-state rates with YcgT as the reductase were not limited by the amount of flavodoxin and had maximal rates of around  $23 \text{ min}^{-1}$ . Analysis of catalytic mixtures involving either of these reductases coupled to fatty acid-bound P450 BioI and a flavodoxin showed that mono-oxygenation of the fatty acid had occurred. The diflavin reductase was also found to be capable of passing a second successive electron to P450 BioI ( $k_{cat}$  of *ca.*  $9 \text{ min}^{-1}$ ) with mono-oxygenated myristate being observed to form.

From these studies it seems apparent that P450 BioI is able to interact with a variety of different redox partners. As a class I P450 with a comparatively low rate of transcription [Bower *et al.*, 1996] and turnover ( $k_{cat}$  *ca.*  $90 \text{ min}^{-1}$ ), involved in a slow biosynthetic process (e.g. BioA  $k_{cat}$  of  $0.78 \text{ min}^{-1}$  [Eliot *et al.*, 2002] and BioD  $k_{cat}$  of  $3.73 \text{ min}^{-1}$  [Yang *et al.*, 1997]) it is probably able to rely upon random collisions with reduced flavo- or ferredoxins within the cell in order to perform its catalytic role. Driven by electrostatic and hydrophobic forces, these chance interactions power its catalytic function. As a result, increased output of the natural product of P450 BioI, known to be necessary for

biotin synthesis, will depend upon the increased expression of both the P450 and its various redox partners to improve the chances of a constructive collision occurring.

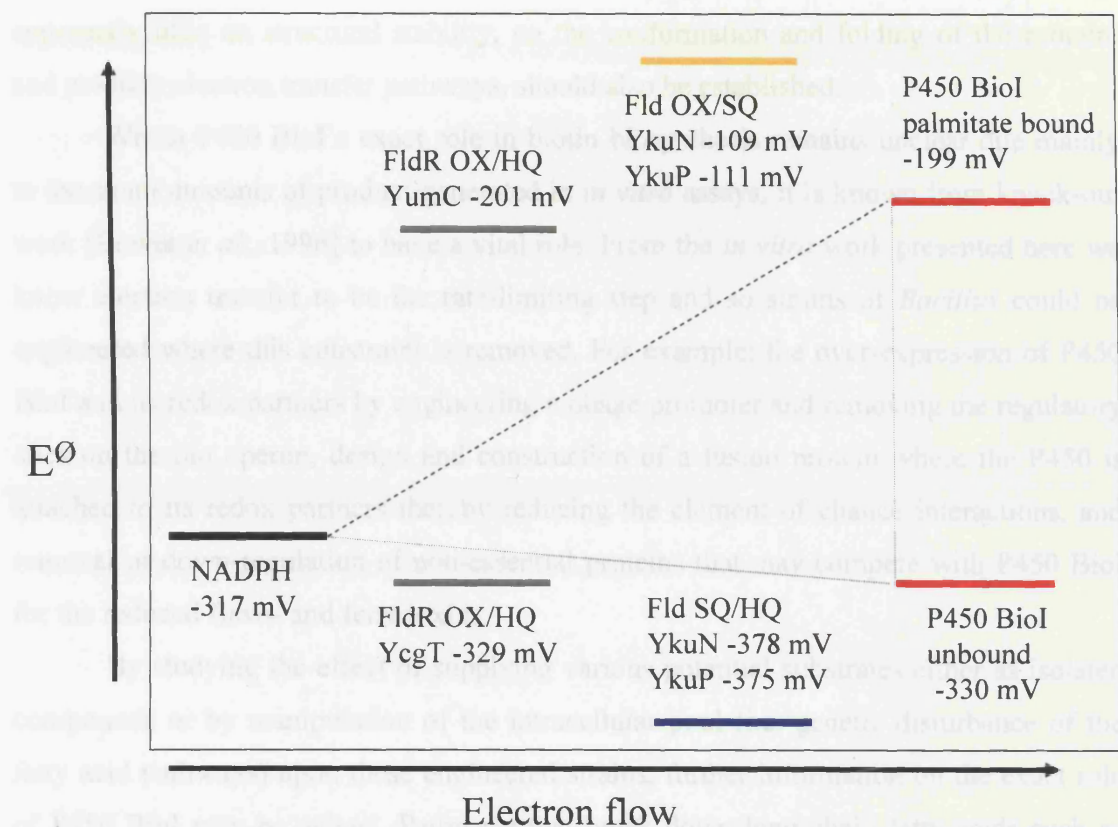


**Figure 6.1** A scheme showing the relative energetics of electron transfer from NADPH to P450 BioI. The various protein's potentials are shown above or below coloured bands symbolising the proteins position relative to one another. The diagram is not to scale. The dashed line shows the overall flow of electrons from NADPH to the substrate-bound form of P450 BioI, it's positive gradient showing a favourable process. Note the reduction of both fld's appears energetically unfavourable if they are in their SQ form but the net energy gain on reduction of the palmitate-bound P450 may help 'pull' the electrons through the pathway.

#### 6.4 Future work

Further characterisation of the various proteins of the P450 BioI redox system principally requires their structures to be resolved, something that has so far remained elusive. Alternative approaches to crystallising P450 BioI have already been outlined in Section 3.16. Mutagenic studies could then be undertaken to establish the roles of

residues in catalysis, not only in substrate binding and the various mechanistic steps but also with respect to the interactions between the proteins themselves. The presence of a disulphide bond in P450 BioI could be established by mutagenesis and its impact, whilst apparently little on structural stability, on the conformation and folding of the protein, and possibly electron transfer pathways, should also be established.

Whilst P450 BioI's exact role in biotin biosynthesis remains unclear due mainly to the small amounts of product generated in *in vitro* assays, it is known from knock-out work [Bower *et al.*, 1996] to have a vital role. From the *in vitro* work presented here we know electron transfer to be the rate-limiting step and so strains of *Bacillus* could be engineered where this constraint is removed. For example: the over-expression of P450 BioI and its redox partners by engineering a phage promoter and removing the regulatory sites on the bio operon, design and construction of a fusion protein where the P450 is attached to its redox partners thereby reducing the element of chance interactions, and removal or down-regulation of non-essential proteins that may compete with P450 BioI for the reduced flavo- and ferredoxins.

By studying the effect of supplying various potential substrates either as isolated compounds or by manipulation of the intracellular pool (i.e. genetic disturbance of the fatty acid pathways) upon these engineered strains, further information on the exact role of P450 BioI may be gained. Pathways that break down long chain fatty acids such as palmitate could be knocked out or down-regulated to see if an increase in the amount of pimelate results (i.e. removal of competitors may aid identification of P450 BioI's favoured substrate). Metabolic analyses of engineered strains of *B. subtilis* where genes are knocked-out, such as P450 BioI itself (i.e. increased substrate level compared to wild-type strain), or subsequent users of pimelate are deleted (i.e. reduced flux of pimelate so less demand on P450 BioI to oxidise other substances to produce pimelate) would be useful. The removal of these genes may allow potential candidates for the P450's substrate *in vivo* to be identified. A library of potential compounds could then be screened against P450 BioI, initially for binding and subsequently for oxidation. One of the fatty acid synthesis pathways in *B. subtilis* is relatively well understood. This could allow genes such as *fabI* and *fabL* to be over-expressed. These two genes encode enoyl-acyl carrier protein reductases that are essential in the synthesis of long chain fatty acids

[Heath *et al.*, 2000, Kobayashi *et al.*, 2003]. Combining their over-expression with an increased feed of compounds such as butyrate may result in an increase in P450 BioI type substrates in the cell. This would avoid the problems associated with feeding-in large amounts of long chain fatty acids such as myristate that have poor water solubility and create emulsions. Increasing the expression of *acpA*, the gene that encodes the acyl-carrier protein [Morbidoni *et al.*, 1996] that may interact with P450 BioI [Stok and DeVoss, 2001] could also be studied, using biotin production as a response.

Overall, whilst this work has sought to characterise P450 BioI and identify potential redox partners to the P450, further work on the exact catalytic function of the P450 and its relevant cellular substrate(s) is required in order to enable the enzyme(s) producing these molecules to be identified and so aid elucidation of catalysts involved in the early stages of biotin biosynthesis in *B. subtilis*. With the identification and isolation of the proteins that enable P450 BioI to function at a considerable rate (reported here), the possibility of resolving these questions is enhanced.

## *Chapter 7*

### *References*

Akhtar M., Calder M.R., Corina D.L., Wright J.N., (1982). Mechanistic studies on C-19 demethylation in estrogen biosynthesis. *Biochemical Journal* **201**, 569 - 580.

Alexeev D., Alexeeva M., Baxter R.L., Campopiano D.J., Webster S.P., Sawyer L., (1998). The crystal structure of 8-amino-7-oxononanoate synthase: A bacterial PLP-dependent Acyl-CoA-condensing enzyme. *Journal of Molecular Biology* **284**, 401 - 419.

Alexeev D., Baxter R.L., Campopiano D.J., McApine R.S., McIver L., Sawyer L., (1998). Rational design of an inhibitor of dethiobiotin synthase; interaction of 6-hydroxypyrimidin-4(3H)-one with the adenine base binding site. *Tetrahedron* **54**, 15891 - 15898.

Alexeev D., Sawyer L., Baxter R.L., Alexeeva M.V., Campopiano D., (2000). Crystal Structure of Adenosylmethionine-8-Amino-7-Oxonanoate Aminotransferase with Pyridoxal Phosphate Cofactor. Protein Data Bank (PDB 1DTY).

Ali V., Prakash K., Kulkarni S., Ahmad A., Madhusudan K.P., Bhakuni V., (1999). 8-anilino-1-naphthalene sulfonic acid (ANS) induces folding of acid unfolded cytochrome *c* to molten globule state as a result of electrostatic interactions. *Biochemistry* **38**, 13635 - 13642.

Aliverti A., Piubelli L., Zanetti G., Lubberstedt T., Herrmann R.G., Curti B., (1993). The role of cysteine residues of spinach ferredoxin-NADP<sup>+</sup> reductase as assessed by site-directed mutagenesis. *Biochemistry* **32**, 6374 - 6380.

Aliverti A., Zanetti G., (1997). A three-domain iron-sulfur flavoprotein obtained through gene fusion of ferredoxin and ferredoxin-NADP<sup>+</sup> reductase from spinach leaves. *Biochemistry* **36**, 14771 - 14777.

Aliverti A., Deng Z., Ravasi D., Piubelli L., Karplus A., Zanetti G., (1998). Probing the function of the invariant glutamyl residue 312 in spinach ferredoxin-NADP<sup>+</sup> reductase. *Journal of Biological Chemistry* **273**, 34008 - 34015.

Altschul, S.F., Madden, T.L., Schaffer, A.A., Zhang, J., Zhang, Z., Miller, W. and Lipman, D.J., (1997). Gapped BLAST and PSI-BLAST: a new generation of protein database search programs. *Nucleic Acids Research*. **25**, 3389 - 3402.

Anderson R.F., (1983). Energetics of the one-electron reduction steps of riboflavin, FMN and FAD to their fully reduced forms. *Biochimica et Biophysica Acta* **722**, 158 - 162.

Anderson J.F., Tatsuka K., Gunji H., Ishiyama T., Hutchinson C.R., (1993). Substrate specificity of 6-deoxyerythronolide B hydroxylase, a bacterial cytochrome P450 of erythromycin A biosynthesis. *Biochemistry* **32**, 1905 - 1913.

Aoki M., Ishimori K., Morishima I., (1998). Roles of the negatively charged surface residues of putidaredoxin in interactions with redox partners in P450 CAM monooxygenase system. *Biochimica et Biophysica Acta* **1386**, 157 - 167.

Apiyo D., Guidry J., Wittung-Stafshede P., (2000). No cofactor effect on equilibrium unfolding of *Desulfovibrio desulfuricans* flavodoxin. *Biochimica et Biophysica Acta* **1479**, 214 - 224.

Appel D., Lutz-Wahl S., Fischer P., Schwaneberg U., Schmid R.D., (2001). A P450 BM-3 mutant hydroxylates alkanes, cycloalkanes, arenes and heterogametes. *Journal of Biotechnology* **88**, 167



- 171.

Arakaki A., Orellano E.G., Calcaterra N.B., Ottado J., Ceccarelli E.A., (2001). Involvement of the flavin *si*-face tyrosine on the structure and function of Ferredoxin-NADP<sup>+</sup> Reductases. *Journal of Biological Chemistry* **276**, 44419 - 44426.

Arakawa T., Timasheff S.N., (1984). Protein stabilisation and destabilisation by guanidinium salts. *Biochemistry* **23**, 5924 - 5929.

Arnold F.H., (1998). When blind is better: Protein design by evolution. *Nature Biotechnology*, **16**, 617-618.

Aslanidis C., de Jong P.J., (1990). Ligation-independent cloning of PCR products (LIC-PCR). *Nucleic Acids Research* **18**, 6069 - 6074.

Atkins W.M., Sligar S.G., (1988). The roles of active site hydrogen bonding in Cytochrome-P450CAM as revealed by site-directed mutagenesis. *Journal of Biological Chemistry* **263**, 18842 - 18849.

Atkinson J.K., Ingold K.U., (1993). Cytochrome-P450 hydroxylation of hydrocarbons - variation in the rate of oxygen rebound using cyclopropyl radical clocks including 2 new ultrafast probes. *Biochemistry* **32**, 9209 - 9214.

Auclair K., Hu Z., Little D.M., Ortiz de Montellano P.R., Groves J.T., (2002). Revisiting the mechanism of P450 enzymes with the radical clocks norcarane and spiro[2,5]octane. *Journal of the American Chemical Society* **124**, 6020 - 6027.

Baalmann E., Scheibe R., Cerff R., Martin W., (1996). Functional studies of chloroplast glyceraldehyde-3-phosphate dehydrogenase subunits A and B expressed in *Escherichia coli*: Formation of highly active A(4) and B-4 homotetramers and evidence that aggregation of the B-4 complex is mediated by the B subunit carboxy terminus. *Plant Molecular Biology* **32**, 505 - 513.

Baichoo N., Wang T., Ye R., Helmann J.D., (2002). Global analysis of the *Bacillus subtilis* Fur regulon and the iron starvation stimulation. *Molecular Microbiology* **45**, 1613 - 1629.

Bailey D.G., Spence J.D., Munoz C., Arnold J.M.O., (1991). Interaction of citrus juices with felodipine and nifedipine. *Lancet* **337**, 268 - 269.

Baldwin J.E., Morris G.M., Richards W.G., (1991). Electron-transport in cytochromes P-450 by covalent switching. *Proceedings of the Royal Society of London Series B-Biological Sciences* **245**, 43 - 51.

Bangcharoenpaurpong O., Champion P.M., Jollie D., Sligar S.G., (1986). Resonance Raman detection of bound dioxygen in cytochrome P450 CAM. *Journal of Biological Chemistry* **261**, 8089 - 8092.

Bartroli J., Turmo E., Alguero M., Boncompte E., Vericat M.L., Conte L., Ramis J., Merlos M., Garcia-Rafanell J., Forn J., (1998). New azole antifungals. 2. Synthesis and antifungal activity of heterocyclecarboxamide derivatives of 3-amino-2-aryl-1-azoyl-2-butanol. *Journal of Medicinal Chemistry* **41**, 1855 - 1868.

- Baum M., Amin S., Guengerich F.P., Hecht S.S., Kohl W., Eisenbrand G., (2001). Metabolic activation of benzo[c]phenanthrene by cytochrome P450 enzymes in human liver and lung. *Chemical Research in Toxicology* **14**, 686 - 693.
- Beckert V., Dettmer R., Bernhardt R., (1994). Mutations of tyrosine 82 in bovine adrenodoxin that affect binding to cytochrome P450 11A1 and P450 11B1 but not electron transfer. *Journal of Biological Chemistry* **269**, 2568 - 2573.
- Bell S.G., Chen X., Sowden R.J., Xu F., Williams J.N., Wong L-L., Rao Z., (2003). Molecular recognition in (+)- $\alpha$ -pinene oxidation by cytochrome P450 CAM. *Journal of the American Chemical Society* **125**, 705 - 714.
- Bell S.G., Chen X., Xu F., Rao Z., Wong L-L., (2003). Engineering substrate recognition in catalysis by cytochrome P450 CAM. *Biochemical Society Transactions* **31**, 558 - 562.
- Bell S.G., Orton E., Boyd H., Stevenson J.A., Riddle A., Campbell S., Wong L.L., (2003). Engineering cytochrome P450 CAM into an alkane hydroxylase. *Dalton Transactions* **11**, 2133 - 2140.
- Bellamine A., Mangla A.T., Nes W.D., Waterman M.R., (1999). Characterisation and catalytic properties of the sterol 14 $\alpha$ -demethylase from *Mycobacterium tuberculosis*. *Proceedings of the National Academy of Sciences USA* **96**, 8937 - 8942.
- Berman, H.M., Westbrook, J., Feng, Z., Gilliland, G., Bhat, T.N., Weissig, H., Shindyalov, I.N. and Bourne, P. E., (2000). The protein data bank. *Nucleic Acids Research* **28**, 235 - 242.
- Bernhardt R., (1996). Cytochromes P450: Structure, function and generation of reactive oxygen species. *Review of Physiology, Biochemistry and Pharmacology* **127**, 137 - 221.
- Bessette P.H., Aslund F., Beckwith J., Georgiou G., (1999). Efficient folding of proteins with multiple disulphide bonds in the *Escherichia coli* cytoplasm. *Proceedings of the National Academy of Science USA* **96**, 13703 - 13708.
- Bhakta M.N., Wimalasena K., (2002). Microsomal P450 catalysed N-dealkylation of N,N-dialkylanilines: Evidence for a C $\alpha$ -H abstraction mechanism. *Journal of the American Chemical Society Communications* **124**, 1844 - 1845.
- Binda C., Coda A., Aliverti A., Zanetti G., Mattevi A., (1998). Structure of the mutant E92K of [2Fe-2S] ferredoxin I from *Spinacia oleracea* at 1.7 Å resolution. *Acta Crystallographica D Biological Crystallography* **54**, 1353.
- Binieda A., Fuhrmann M., Lehner B., Rey-Berthod C., Frutiger-Hughes S., Hughes G., Shaw N.M., (1999). Purification, characterisation, DNA sequence and cloning of a pimeloyl-CoA synthase from *Pseudomonas mendocina* 35. *Biochemistry Journal* **340**, 793 - 801.
- Birch O., Brass J., Fuhrmann M., Shaw N., (Lonza AG, CH) (1994). *International Patent Application* WO9408023.
- Birch O.M., Hewitson K.S., Fuhrmann M., Burgdorf K., Baldwin J.E., Roach P.L., Shaw N.M., (2000). MioC is an FMN-binding protein that is essential for *Escherichia coli* biotin synthase activity *in vitro*. *Journal of Biological Chemistry* **275**, 32277 - 32280.

- Blanchard C.Z., Lee Y.M., Frantom P.A., Waldrop G.L., (1999). Mutations at four active site residues of biotin carboxylase abolish substrate-induced synergism by biotin. *Biochemistry* **38**, 3393 - 3400.
- Boddupalli S.S., Estabrook R.W., Peterson J.A., (1990). Fatty acid monooxygenation by cytochrome P-450BM3. *Journal of Biological Chemistry* **265**, 4233 - 4239.
- Boddupalli S.S., Hasemann Ca, Ravichandran Kg, Lu Jy, Goldsmith Ej, Deisenhofer J, Peterson J.A., (1992). Crystallization and preliminary-x-ray diffraction analysis of P450 terp and the hemoprotein domain of P450 BM-3, enzymes belonging to 2 distinct classes of the cytochrome P450 superfamily. *Proceedings Of The National Academy of Sciences USA* **89**, 5567 - 5571.
- Boddupalli S.S., Oster T., Estabrook R.W., Peterson J.A., (1992). Reconstitution of the fatty acid hydroxylation function of cytochrome P-450BM3 utilizing its individual recombinant hemo- and flavoprotein domains. *Journal of Biological Chemistry* **267**, 10375 - 10380.
- Boddupalli S.S., Pramanik B.C., Slaughter C.A., Estabrook R.W., Peterson J.A., (1992). Fatty acid monooxygenation by P450BM3: Product identification and proposed mechanisms for the sequential hydroxylation reactions. *Archives of Biochemistry and Biophysics* **292**, 20 - 28.
- Bondon A., Macdonald T.L., Harris T.M., Guengerich F.P., (1989). Oxidation of cycloalkylamines by cytochrome P-450. *Journal of Biological Chemistry* **264**, 1988 - 1997.
- Bossi R.T., Aliverti A., Raimondi D., Fischer F., Zanetti G., Ferrari D., Tahallah N., Maier C.S., Heck A.J.R., Rizzi M., Mattevi A., (2002). A covalent modification of NADP<sup>+</sup> revealed by the atomic resolution structure of FprA, a *Mycobacterium tuberculosis* oxidoreductase. *Biochemistry* **41**, 8807 - 8818.
- Bovill A.J., McConnell A.A., Rospendowski B.N., Smith W.E., (1992). Overtone and combination band raman-spectra of alpha-copper phthalocyanine. *Journal of The Chemical Society-Faraday Transactions* **88**, 455 - 459.
- Bower S., Perkins J., Yocum R., Serror P., Sorokin A., Rahaim P., Howitt C.L., Prasad N., Ehrlich, S.D., Pero, J., (1995). Cloning and characterization of the *Bacillus subtilis* *birA* gene encoding a repressor of the biotin operon. *Journal of Bacteriology* **177**, 2572 - 2575.
- Bower S., Perkins J., Yocum R.R., Howitt C.L., Rahaim P., Prasad N., Pero J., (1995). The biotin biosynthetic genes of *Bacillus subtilis*. *FASEB Journal* **9**, A1274 - A1274.
- Bower, S.G., Perkins, J.B., Pero, J.G., Yocum, R.R., (1995). Hoffmann-La Roche AG Switz, *European Patent Application*. EP 94-108998.
- Bower S., Perkins, J.B., Yocum, R.R., Howitt, C.L., Rahaim, P., Pero, J., (1996). Cloning, sequencing, and characterization of the *Bacillus subtilis* biotin biosynthetic operon. *Journal of Bacteriology* **178**, 4122 - 4130.
- Brandt M.E., Vickery L.E., (1993). Charge pair interactions stabilizing ferredoxin-ferredoxin reductase complexes. Identification by complementary site-specific mutations. *Journal of Biological Chemistry* **268**, 17126 - 17130.

- Brenner S.E., (1997). Population statistics of protein structures: lessons from structural characterizations. *Current Opinion in Structural Biology* **7**, 369 - 376.
- Brewer C.B., Peterson J.A., (1986). Single turnover kinetics of the reaction between oxyctochrome P450 CAM and reduced putidaredoxin. *Journal of Biological Chemistry* **263**, 791 - 798.
- Brodie A.M.H., (1994). Aromatase inhibitors in the treatment of breast cancer. *Journal of Steroid Biochemistry* **49**, 281 - 287.
- Bruns C. M., Karplus P. A., (1995). Refined crystal structure of spinach ferredoxin reductase at 1.7 Å resolution: oxidized, reduced and 2'-phospho-5'-AMP bound states. *Journal of Molecular Biology* **247**, 125 - 136.
- Buchanan J.F., Fulco A.J., (1978). Formation of 9, 10-epoxy palmitic acid 9, 10-dihydroxypalmitate from palmitoleic acid. *Biochemical and Biophysical Research Communications* **85**, 1254 - 1260.
- Bui B.T.S., Florentin D., Fournier F., Ploux O., Mejean A., Marquet A., (1998). Biotin synthase mechanism: on the origin of sulphur. *FEBS Letters* **440**, 226 - 230.
- Bulaj G., Korternme T., Goldenberg D.P., (1998). Ionisation-reactivity relationships for cysteine thiols in polypeptides. *Biochemistry* **37**, 8965 - 8972.
- Bumpus J.A., Tien M., Wright D., Aust S.D., (1985). Oxidation of persistent environmental pollutants by a white rot fungus. *Science* **228**, 1434 - 1436.
- Burlat V., Oudin A., Courtois M., Rideau M., St-Pierre B., (2004). Co-expression of three MEP pathway genes and geraniol 10-hydroxylase in internal phloem parenchyma of *Catharanthus roseus* implicates multicellular translocation of intermediates during the biosynthesis of monoterpene indole alkaloids and isoprenoid-derived primary metabolites. *Plant Journal* **38**, 131-141.
- Burnett R.M., Darling G.D., Kendall D.S., Le Quesne M.E., Mayhew S.G., Smith W.W., Ludwig M.L., (1974). The structure of the oxidized form of *Clostridial* flavodoxin at 1.9-Å resolution. Description of the flavin mononucleotide binding site. *Journal of Biological Chemistry* **249**, 4385 - 4392.
- Caldeira J., Palma P.N., Regalla M., Lampreia J., Calvete J., Schafer W., Legall J., Moura I., Moura J.J.G., (1994). Primary sequence, oxidation-reduction potentials and tertiary-structure prediction of *Desulfovibrio-desulfuricans* ATCC 27774 flavodoxin. *European Journal of Biochemistry* **220**, 987 - 995.
- Campbell R.L., Swaine R.R., Dekker E.E., (1978). Purification, separation, and characterization of two molecular forms of D-1-amino-2-propanol:NAD<sup>+</sup> oxidoreductase activity from extracts of *Escherichia coli* K-12. *Journal of Biological Chemistry* **253**, 7282 - 7288.
- Cao P., Bernhardt R., (1999). Modulation of aldosterone biosynthesis by adrenodoxin mutants with different electron transport efficiencies. *European Journal of Biochemistry* **265**, 152 - 159.
- Casas J.L., Navarro J.A., Hervas M., Losato A., De la Rosa M.A., Gomez-Moreno C., Sancho J.,

Medina M., (2002). *Anabaena* sp. PCC 7119 Flavodoxin as electron carrier from photosystem I to ferredoxin-NADP<sup>+</sup> reductase. *Journal of Biological Chemistry* **277**, 22338 - 22344.

Ceccarelli C, Grodsky NB, Ariyaratne N, Colman RF, Bahnson BJ., (2002). Crystal structure of porcine mitochondrial NADP<sup>+</sup>-dependent isocitrate dehydrogenase complexed with Mn<sup>2+</sup> and isocitrate - Insights into the enzyme mechanism. *Journal of Biological Chemistry* **277**, 43454 - 43462.

Centeno F., Gutierrez-Merino C., (1992). Location of functionalised centers in the microsomal P450 system. *Biochemistry* **31**, 37 - 45.

Champion P.M., Gunsalus I.C., Wagner G.C., (1978). Resonance Raman investigations of cytochrome P450 CAM from *Pseudomonas putida*. *Journal of the American Chemical Society* **100**, 3743 - 3751.

Chang F.C., Swenson R.P., (1999). The midpoint potentials for the oxidized-semiquinone couple for Gly57 mutants of the *Clostridium beijerinckii* flavodoxin correlate with changes in the hydrogen-bonding interaction with the proton on N(5) of the reduced flavin mononucleotide cofactor as measured by NMR chemical shift temperature dependencies. *Biochemistry* **38**, 7168 - 7176.

Chang, F., Bradley L.H., Swenson R.P., (2001). Evaluation of the hydrogen bonding interactions and their effects on the oxidation-reduction potentials for the riboflavin complex of the *Desulfovibrio vulgaris* flavodoxin. *Biochimica et Biophysica Acta* **1504**, 319 - 328.

Chapman-Smith A., Cronan J.E., (1999). The enzymatic biotinylation of proteins: a post-translational modification of exceptional specificity. *Trends In Biochemical Science* **24**, 359 - 363.

Chauhan J., Dakshinamurti K., (1991). Transcriptional regulation of the glycosidase gene by biotin in starved rats. *Journal of Biological Chemistry* **266**, 10035 - 10038.

Chen H., Hubbard B.K., O'Connor S.E., Walsh C.T., (2002). Formation of beta-hydroxy histidine in the biosynthesis of nikkomycin antibiotics. *Chemical Biology* **9**, 103 - 112.

Choi K-H., Heath R.J., Rock C.O., (2000).  $\beta$ -ketoacyl-acyl carrier protein synthase III (FabH) is a determining factor in branched chain fatty acid biosynthesis. *Journal of Bacteriology* **182**, 365 - 370.

Coco W.M., Levinson W.E., Crist M.J., Hektor H.I., Darzins A., Pienkos P.T., Squires C.H., Monticello D.J., (2001). DNA shuffling methods for generating highly recombined genes and evolved enzymes. *Nature Biotechnology* **19**, 354 - 359.

Cole P.A., Robinson C.H., (1988). A peroxide model reaction for placental aromatase. *Journal of the American Chemical Society* **110**, 1284 - 1285.

Collu G., Unver N., Peltenburg-Looman A.M.G., van der Heijden R., Verpoorte R., Memelink J., (2001). Geraniol 10-hydroxylase, a cytochrome P450 enzyme involved in terpenoid indole alkaloid biosynthesis. *FEBS Letters* **508**, 215 - 220.

Coon M.J., Vaz A.D.N., McGinnity D.F., Peng H.M., (1998). Multiple activated oxygen species

in P450 catalysis - Contributions to specificity in drug metabolism. *Drug Metabolism And Disposition* **26**, 1190 - 1193.

Cosper M.M., Jameson G.N.L., Davydov R., Eidsness M.K., Hoffman B.M., Huynh B.H., Johnson M.K., (2002). The  $[4\text{Fe-4S}]2^+$  cluster in reconstituted biotin synthase binds S-adenosyl-L-methionine. *Journal of the American Chemical Society* **124**, 14006 - 14007.

Cotton F.A., Wilkinson G., Murillo C.A., Bochmann M., (1999). The hydroxides and oxides of iron. *Advanced Inorganic Chemistry 6<sup>th</sup> edition*, 777 - 807. John Wiley and Sons Inc N.Y.

Cryle M.J., Matovic N.J., De Voss J.J., (2003). Products of cytochrome P450Biol (CYP107H1)-catalysed oxidation of fatty acids. *Organic Letters* **5**, 3341 - 3344.

Cryle M.J., De Voss J.J., (2004). Carbon-carbon bond cleavage by cytochrome P450Biol (CYP107H1). *Chemical Communications*, 86 - 87.

Cupp-Vickery J.R., Poulos T.L., (1995). Structure of cytochrome P450 eryF involved in erythromycin biosynthesis. *Nature Structural Biology* **2**, 144 - 153.

Cupp-Vickery J.R., Han O., Hutchinson C.R., Poulos T.L., (1996). Substrate assisted catalysis in cytochrome P450 eryF. *Nature Structural Biology* **3**, 632 - 637.

Cupp-Vickery J.R., Poulos T.L., (1997). Structure of cytochrome P450 eryF: Substrate, inhibitors, and model compounds bound in the active site. *Steroids* **62**, 112 - 116.

Cupp-Vickery J.R., Anderson R., Hatziris Z., (2000). Crystal structure of ligand complexes of P450 eryF exhibiting homotropic cooperativity. *Proceedings of the National Academy of Sciences USA* **97**, 3050 - 3055.

Cupp-Vickery J.R., Garcia C., Hofacre A., McGee-Estrada K., (2001). Ketoconazole induced conformational changes in the active site of cytochrome P450 eryF. *Journal of Molecular Biology* **311**, 101 - 110.

Curley G.P., Carr M.C., Mayhew S.G., Voordouw G., (1991). Redox and flavin-binding properties of recombinant flavodoxin from *Desulfovibrio vulgaris* (Hildenborough). *European Journal of Biochemistry* **202**, 1091 - 1100.

Daff S.N., Chapman S.K., Turner K.L., Holt R.A., Govindaraj S., Poulos T.L., Munro A.W., (1997). Redox control of the catalytic cycle of flavocytochrome P-450 BM3. *Biochemistry* **36**, 13816 - 13823.

Daley C.J.A., Holm R.H., (2001). Reactivity of  $[\text{Fe}_4\text{S}_4(\text{SR})_4]2-,3-$  clusters with sulfonium cations: Analogue reaction systems for the initial step in biotin synthase catalysis. *Inorganic Chemistry* **40**, 2785 - 2793.

D'Anna Jr., J.A., Tollin G., (1972). Studies of flavin-protein interaction in flavoproteins using protein fluorescence and circular dichroism. *Biochemistry* **11**, 1073 - 1080.

Davies M.D., Qin L., Beck J.L., Suslick K.S., Koga H., Horiuchi T., Sligar S.G., (1990). Putidaredoxin reduction of cytochrome P-450cam - Dependence of electron-transfer on the identity of putidaredoxins C-terminal amino-acid. *Journal of the American Chemical Society* **112**,



7396 - 7398.

Davies M.D., Sligar S.G., (1992). Genetic variants in the putidaredoxin-cytochrome P-450CAM electron transfer complex: Identification of the residue responsible for redox-dependent conformers. *Biochemistry* **31**, 11383 - 11389.

Dawson J.H., Anderson L.A., Sono M., (1982). Spectroscopic investigations of ferric cytochrome P-450 CAM ligand complexes - identification of the ligand trans to cysteinate in the native enzyme. *Journal of Biological Chemistry* **257**, 3606 - 3617.

Dawson R.M.C., Elliot D.C., Elliot W.H., Jones K.M., (1986). *Data for Biochemical Research*, 3<sup>rd</sup> Ed. Clarendon Press, Oxford, U.K., 124 - 126.

Dawson J.H., (1988). Probing structure-function relationships in heme-containing oxygenases and peroxidases. *Science* **240**, 433 - 439.

Demain A.L., (2000). Small bugs, big business: The economic power of the microbe. *Biotechnology Advances* **18**, 499 - 514.

Dolphin D., Traylor T.G., Xie L.Y., (1997). Polyhaloporphyrins: Unusual ligands for metals and metal catalysed oxidations. *Accounts of Chemical Research* **30**, 251 - 259.

Druhan L.J., Swenson R.P., (1998). Role of methionine 56 in the control of the oxidation-reduction potentials of the *Clostridium beijerinckii* flavodoxin: Effects of substitutions by aliphatic amino acids and evidence for a role of sulfur-flavin interactions. *Biochemistry* **37**, 9668 - 9678.

Duee E., Olivier-Deyris L., Fanchon E., Corbier C., Branlant G., Dideberg O., (1996). Comparison of the structures of wild-type and a N313T mutant of *Escherichia coli* glyceraldehyde 3-phosphate dehydrogenases: Implication for NAD binding and cooperativity. *Journal of Molecular Biology* **257**, 814 - 838.

Dunn A.R., Hays A-M.A., Goodin D.B., Stout C.D., Chiu R., Winkler J.R., Gray H.B., (2002). Fluorescent probes for cytochrome P450 structural characterization and inhibitor screening. *Journal of the American Chemical Society* **124**, 10254 - 10255

Dutton P.L., (1978). Redox Potentiometry: Determination of midpoint potentials of oxidation-reduction components of biological electron-transfer systems. *Methods in Enzymology* **54**, 411 - 435.

Edmondson D.E., Tollin G., (1971). Flavoprotein chemistry I. Circular Dichroism studies of the flavin chromophore and the relation between redox properties and flavin environment in oxidases and dehydrogenases. *Biochemistry* **10**, 113 - 124.

Eftink M.R., Ghiron C.A., (1976). Exposure of tryptophanyl residues in proteins. Quantitative determination by fluorescence quenching studies. *Biochemistry* **15**, 672 - 680.

Eftink M.R., Ghiron C.A., (1984). Indole fluorescence quenching studies on proteins and model systems - use of the inefficient quencher succinimide. *Biochemistry* **23**, 3891 - 3899.

Eidsness M.K., Burden A.E., Richie K.A., Kurtz D.M., Scott R.A., Smith E.T., Ichiye T., Beard

- B., Min T.P., Kang C.H., (1999). Modulation of the redox potential of the [Fe(SCys)(4)] site in rubredoxin by the orientation of a peptide dipole. *Biochemistry* **38**, 14803 - 14809.
- Eisenberg M.A., Star C., (1968). Synthesis of 7-oxo-8-aminopelargonic acid, a biotin vitamer, in cell free extracts of *Escherichia coli* biotin auxotrophs. *Journal of Bacteriology* **96**, 1291 - 1297.
- Eisenstein E., Beckett D., (1999). Dimerization of the *Escherichia coli* biotin repressor: Corepressor function in protein assembly. *Biochemistry* **38**, 13077 - 13084.
- Elliot A.C., Sandmark J., Schneider G., Kirsch J.F., (2002). The dual-specific active site of 7,8-diaminopelargonic acid synthase and the effect of the R391A mutation. *Biochemistry* **41**, 12582 - 12589.
- Ellman G.L., (1959). Tissue sulfhydryl groups. *Archives of Biochemistry and Biophysics* **82**, 70 - 77.
- England P.A., Harford-Cross C.F., Stevenson J.A., Rouch D.A., Wong L-L., (1998). The oxidation of naphthalene and pyrene by cytochrome P450 CAM. *FEBS Letters* **424**, 271 - 274.
- Eriksson A.E., Baase W.A., Wozniak J.A., Matthews B.W., (1992). A cavity-containing mutant of T4-lysozyme is stabilised by buried benzene. *Nature* **355**, 371 - 373.
- Eschenbrenner, M., Coves, J., and Fontecave, M., (1995). NADPH-sulfite reductase flavoprotein from *Escherichia coli*: contribution to the flavin content and subunit interaction. *FEBS Letters* **374**, 82 - 84
- Estabrook R.W., Shet M.S., Fisher C.W., Fisher C.W., Jenkins C.M., Waterman M.R., (1996). The interaction of NADPH-P450 reductase with P450: An electrochemical study of the role of the flavin mononucleotide-binding domain. *Archives of Biochemistry and Biophysics* **333**, 308 - 315.
- Evrard A., Zeghouf M., Fontecave M., Roby C., Coves J., (1999). <sup>31</sup>P nuclear magnetic resonance study of the flavoprotein component of the *Escherichia coli* sulfite reductase. *European Journal of Biochemistry* **261**, 430 - 437.
- Falck J.R., Reddy Y.K., Haines D.C., Reddy K.M., Krishna U.M., Graham S., Murry B., Peterson J.A., (2001). Practical, enantiospecific syntheses of 14, 15-EET and leukotoxin B (vernolic acid). *Tetrahedron Letters* **42**, 4131 - 4133.
- Farinas E.T., Schwaneberg U., Glieder A., Arnold F.H., (2001). Directed evolution of a cytochrome P450 monooxygenase for alkane oxidation. *Advanced Synthesis Catalogue* **343**, 601 - 606.
- Faro M., Hurley J.K., Medina M., Tollin G., Gomez-Moreno C., (2002). Flavin photochemistry in the analysis of electron transfer reactions: Role of charged and hydrophobic residues at the carboxyl terminus of ferredoxin-NADP<sup>+</sup> reductase in the interaction with its substrates. *Bioelectrochemistry* **56**, 19 - 21.
- Faro M., Gomez-Moreno C., Stankovich M., Medina M., (2002). Role of critical charged residues in reduction potential modulation of ferredoxin-NADP<sup>+</sup> reductase. *European Journal of Biochemistry* **269**, 2656 - 2661.

- Faulkner K.M., Shet M.S., Fisher C.W., Estabrook R.W., (1995). Electrocatalytically driven  $\omega$ -hydroxylation of fatty acids using cytochrome P450 4A1. *Proceedings of the National Academy of Science USA* **92**, 7705 - 7709.
- Fersht A., Enzyme Structure and Mechanism, 2<sup>nd</sup> ed., (1985), 248 - 251, W.H. Freeman and Co., NY
- Fisher M.T., Sligar S.G., (1987). Temperature jump relaxation kinetics of the P-450 CAM spin equilibrium. *Biochemistry* **26**, 4797 - 4803.
- Fischer R.T., Trzaskos J.M., Magolda R.L., Ko S.S., Brosz C.S., Larsen B., (1991). Lanosterol 14 $\alpha$ -methyl demethylase: Isolation and characterisation of the third metabolically generated oxidative demethylation intermediate. *Journal of Biological Chemistry* **266**, 6124 - 6132.
- Freigang J., Diederichs K., Schafer K., Welte W., Paul R., (2002). Crystal structure of oxidised flavodoxin, an essential protein in *Helicobacter pylori*. *Protein Science* **11**, 253 - 261.
- Garfinkel D., (1958). Studies on pig liver microsomes. *Archives of Biochemistry and Biophysics* **77**, 493 - 509.
- Gassner G.T., Ludwig M.L., Gatti D.L., Correll C.C., Ballou D.P., (1995). Flavoprotein structure and mechanism 7. Structure and mechanism of the iron-sulfur flavoprotein phthalate dioxygenase reductase. *FASEB Journal*, **9**, 1411 - 1418.
- Genzor C.G., Perales-Alcon A., Sancho J., Romero A., (1996). Closure of a tyrosine/tryptophan aromatic gate leads to a compact fold in apoflavodoxin. *Nature Structural Biology* **3**, 329 - 332.
- Gerber N.C., Sligar S.G., (1992). Catalytic mechanism of cytochrome-P-450 - evidence for a distal charge relay. *Journal of the American Chemical Society* **114**, 8742 - 8743.
- Ghisla S., Massey V., Lhoste J-M., Mayhew S.G., (1974). Fluorescence and optical characteristics of reduced flavins and flavoproteins. *Biochemistry* **13**, 589 - 597.
- Gibson J.F., Poole R.K., Hughes M.N., Rees J.F., (1984). Filamentous growth of *Escherichia coli* K12 elicited by dimeric, mixed valence complexes of ruthenium. *Archives of Microbiology* **139**, 265 - 271.
- Gibson K.J., Lorimer G.H., Rendina A.R., Taylor W.S., Cohen G., Gatenby A.A., Payne W.G., Roe D.C., Lockett B.A., Nudelman A., Marcovi D., Nachum A., Wexler B.A., Marsilii E.L., Turner I.M., Howe L.D., Kalbach C.E., Chi H., (1995). Dethiobiotin synthase: The carbonylation of 7,8-diaminononanoic acid proceeds regiospecifically via the N7-carbamate. *Biochemistry* **34**, 10976 - 10984.
- Gilardi G., Meharena Y.T., Isosou G.E., Sadeghi S.J., Fair head M., Giannini S., (2002). Molecular Lego: design of molecular assemblies of P450 enzymes for nanobiotechnology. *Biosensors and Bioelectronics* **17**, 133 - 145.
- Gloeckler R., Ohsawa I., Speck D., Ledoux C., Bernard S., Zinsius M., Villeval D., Kisou T., Kamogawa K., Lemoine R., (1990). Cloning and characterization of the *Bacillus sphaericus* genes controlling the bioconversion of pimelate into dethiobiotin. *Gene* **87**, 63 - 70.

Goldberg, M.W., Sternbach, L.H., (1974). Hoffmann-La Roche N.J., U.S.A., *US Patent Applications*, US2489235 and US2489236.

Govindaraj S., Poulos T.L., (1997). The domain architecture of cytochrome P450 BM-3. *Journal of Biological Chemistry* **272**, 7915 - 7921.

Grandori R., Khalifah P., Boice J.A., Fairman R., Giovanielli K., Carey J., (1998). Biochemical characterization of WrbA, founding member of a new family of multimeric flavodoxin-like proteins. *Journal of Biological Chemistry* **273**, 20960 - 20966.

Grau R., de Mendoza D., (1993). Regulation of the synthesis of unsaturated fatty acids by growth temperature in *Bacillus subtilis*. *Molecular Microbiology* **8**, 535 - 542.

Green A.J., (2000). Biol: The P450 implicated in biotin biosynthesis. PhD Thesis, University of Edinburgh, UK.

Green A.J., Rivers S.L., Cheesman M., Reid G.A., Quaroni L.G., Macdonald I.D.G., Chapman S.K., Munro A.W., (2001). Expression, purification and characterization of cytochrome P450Biol: A novel P450 involved in biotin synthesis in *Bacillus subtilis*. *Journal of Biological Inorganic Chemistry* **6**, 523 - 533.

Green A.J., Munro A.W., Cheesman M.R., Reid G.A., von Wachenfeldt C., Chapman S.K., (2003). Expression, purification and characterisation of a *Bacillus subtilis* ferredoxin: A potential electron transfer donor to a cytochrome P450 Biol. *Journal of Inorganic Biochemistry* **93**, 92 - 99.

Greener A., Callahan M., Jerpseth B., (1997). An efficient random mutagenesis technique using an *E-coli* mutator strain. *Molecular Biotechnology* **7**, 189-195.

Griffith O.W., Stuehr D.J., (1995). Nitric Oxides Synthases – Properties and catalytic mechanism. *Annual Review of Physiology* **57**, 707 - 736.

Grinberg A.V., Hannemann F., Schiffler B., Muller J., Heinemann U., Bernhardt R., (2000). Adrenodoxin: Structure, stability, and electron transfer properties. *Proteins: Structure, Function, and Genetics* **40**, 590 - 612.

Grodberg J., Dunn J.J., (1988). *ompT* encodes the *Escherichia coli* outer-membrane protease that cleaves T7-RNA polymerase during purification. *Journal of Bacteriology* **170**, 1245 - 1253.

Groves J.T., McClusky G.A., White R.E., Coon M.J., (1978). *Biochemical and Biophysical Research Communications* **81**, 154 - 160.

Groves J.T., Han Y-Z., (1995). in *Cytochrome P450: Structure, Mechanism, and Biochemistry* 2<sup>nd</sup> ed., Chapter 1, 3 - 48. Ed., Ortiz de Montellano P.R., Plenum Press NY.

Guengerich F.P., (1991). Reactions and significance of cytochrome P-450 enzymes. *Journal of Biological Chemistry* **266**, 10019 - 10022.

Guengerich F.P., (1995). In *Cytochrome P450: Structure, Mechanism and Biochemistry*, Chapter 5, 473 - 535. Ed., Ortiz de Montellano, Plenum Press NY.

Guengerich F.P., (2002). Cytochrome P450 enzymes in the generation of commercial products. *Nature Drug Discovery* **1**, 359 - 366.

Gustafsson M.C.U., Roitel O., Marshall K.R., Noble M.A., Chapman S.K., Pessegueiro A., Fulco A.J., Cheesman M.R., von Wachenfeldt C., Munro A.W., (2004). Expression, purification, and characterization of *Bacillus subtilis* cytochromes P450 CYP102A2 and CYP102A3: Flavocytochrome homologues of P450 BM3 from *Bacillus megaterium*. *Biochemistry* **43**, 5474 - 5487.

Gutierrez A., Dohr O., Paine M., Wolf C.R., Scrutton N.S., Roberts G.C.K., (2000). Trp-676 facilitates nicotinamide coenzyme exchange in the reductive half-reaction of human cytochrome P450 reductase: Properties of the soluble W676H and W676A mutant reductases. *Biochemistry* **39**, 15990 - 15999.

Gutierrez A., Paine M., Wolf C.R., Scrutton N.S., Roberts G.C.K., (2002). Relaxation kinetics of cytochrome P450 reductase: Internal electron transfer is limited by conformational change and regulated by coenzyme binding. *Biochemistry* **41**, 4626 - 4637.

Hall D.A., Vander Kooi C.W., Stasik C.N., Stevens S.Y., Zuiderweg E.R.P., Matthews R.G., (2001). Mapping the interactions between flavodoxin and its physiological partners flavodoxin reductase and cobalamin-dependent methionine synthase. *Proceedings of the National Academy of Sciences USA* **98**, 9521 - 9526.

Halliwell B., (1987). Oxygen Radicals in Tissue Injury. Upjohn Press Inc, USA, 2 - 20.

Halliwell B., (1991). Switches in Enzymes. *Nature* **354**, 191 - 192.

Halpert J.R., Domanski T.L., Adali O., Biagini C.P., Cosme J., Dierks E.A., Johnston E.F., Jones J.P., Ortiz de Montellano P., Philpot R.M., Sibbesen O., Wyatt W.K., Zheng Z., (1998). Structure-function of cytochromes P450 and flavin-containing monooxygenases: Implications for drug metabolism. *Drug Metabolism and Disposition* **26**, 1223 - 1231.

Hamamoto I., Ichikawa Y., (1984). Modification of a lysine residue of adrenodoxin reductase, essential for complex-formation with adrenodoxin. *Biochimica et Biophysica Acta*, **786**, 32 - 41.

Hamilton G.A., (1974). In Molecular Mechanisms of Oxygen Activation. Ed., Hayaishi O., Chapter 10, 405 - 451, Academic Press, NY.

Hanna I.H., Krausers J.A., Cai H., Kim M-S., Guengerich F.P., (2001). Diversity in mechanisms of substrate oxidation by cytochrome P450 2D6. *Journal of Biological Chemistry* **276**, 39553 - 39561.

Hara T., Kimura T., (1989). Purification and catalytic properties of a cross-linked complex between adrenodoxin reductase and adrenodoxin. *Journal of Biochemistry* **105**, 594 - 600.

Harris D.L., (2002). Oxidation and electronic state dependence of proton transfer in the enzymatic cycle of cytochrome P450eryF. *Journal of Inorganic Biochemistry* **91**, 568 - 585.

Harris J.I., Waters M., (1976). In The Enzymes. Ed., Boyer P.D., 1 - 49. Academic Press NY.

Hasemann, C.A., Ravichandran, K.G., Peterson, J.A., and Deisenhofer, J. (1994). Crystal

structure and refinement of cytochrome P450terp at 2.3 Å resolution. *Journal of Molecular Biology* **236**, 1169 - 1185.

Hawkes D.B., Adams G.W., Burlingames A.L., Ortiz de Montellano P.R., De Voss J.J., (2002). Cytochrome P450 CIN (CYP176A), isolation, expression, and characterisation. *Journal of Biological Chemistry* **277**, 27725 - 27732.

Hayaishi O., (1974). In *Molecular Mechanisms of Oxygen Activation*. Ed., Hayaishi O., Chapter 1, 1 - 28, Academic Press, NY.

Hazzard J.T., Govindaraj S., Poulos T.L., Tollin G., (1997). Electron transfer between the FMN and heme domains of cytochrome P450BM-3. *Journal of Biological Chemistry* **272**, 7922 - 7926.

Heath R.J., Su N., Murphy C.K., Rock C.O., (2000). The enoyl-[acyl-carrier-protein] reductases FabI and FabL from *Bacillus subtilis*. *Journal of Biological Chemistry* **275**, 40128 - 40133.

Hedegaard J., Gunsalus I.C., (1965). Mixed function oxidation IV. An induced methylene hydroxylase in camphor oxidation. *Journal of Biological Chemistry* **240**, 4038 - 4043.

Helms V., Depez E., Gill E., Barret C., Hui Bon Hoa G., Wade R.C., (1996). Improved binding of cytochrome P450CAM substrate analogues designed to fill extra space in the substrate binding pocket. *Biochemistry* **35**, 1485 - 1499.

Hickel A., Radke C.J., Blanch H.W., (1999). Hydroxynitrile lyase at the diisopropyl ether/water interface: Evidence for interfacial enzyme activity. *Biotechnology and Bioengineering* **65**, 425 - 436.

Hintz M.J., Mock D.M., Peterson L.L., Tuttle K., Peterson J.A., (1982). Equilibrium and kinetic studies of the interaction of cytochrome-P-450CAM and putidaredoxin. *Journal of Biological Chemistry* **257**, 4324 - 4332.

Hiratsuka M., Agatsuma Y., Omori F., Narahara K., Inoue T., Kishikawa Y., Mizugaki M., (2000). High throughput detection of drug-metabolizing enzyme polymorphisms by allele-specific fluorogenic 5' nuclease chain reaction assay. *Biological and Pharmaceutical Bulletin* **23**, 1131 - 1135.

Hirel P.H., Schmitter J.M., Dessen P., Fayat G., Blanquet S., (1989). Extent of n-terminal methionine excision from escherichia-coli proteins is governed by the side-chain length of the penultimate amino-acid. *Proceedings of the National Academy of Sciences USA* **86**, 8247 - 8251.

Hishiki T., Shimada H., Nagano S., Egawa T., Kanamori Y., Makino R., Park S.Y., Adachi S., Shiro Y., Ishimura Y., (2000). X-ray crystal structure and catalytic properties of Thr252Ile mutant of cytochrome P450CAM: Roles of Thr252 and water in the active centre. *Journal of Biochemistry* **128**, 965 - 974.

Ho R.C., Cordain L., (2000). The potential role of biotin insufficiency on essential fatty acid metabolism and cardiovascular disease risk. *Nutrition Research* **20**, 1201 - 1212.

Hoeltzli S.D., Frieden C., (1995). Stopped-flow NMR spectroscopy real-time unfolding studies of 6-F-19-tryptophan labeled *Escherichia coli* dihydrofolate reductase. *Proceedings of the National Academy of Science USA* **92**, 9318 - 9322.



- Holden H.M., Jacobson B.L., Hurley J.K., Tollin G., Oh B-H., Skjeldal L., Chae J.K., Cheng H., Xia B., Markley J.L., (1994). Structure-function studies of [2Fe-2S] ferredoxins. *Journal of Bioengineering and Biomembranes* **26**, 67 - 88.
- Hoover D.M., Ludwig M.L., (1997). A flavodoxin that is required for enzyme activation: The structure of oxidized flavodoxin from *Escherichia coli* at 1.8 angstrom resolution. *Protein Science* **6**, 2525 - 2537.
- Hoover D.M., Jarrett J.T., Sands R.H., Dunham W.R., Ludwig M.L., Matthews R.G., (1997). Interaction of *Escherichia coli* colbamin-dependent methionine synthase and its physiological partner flavodoxin: Binding of flavodoxin leads to axial ligand dissociation from the colbamin cofactor. *Biochemistry* **36**, 127 - 138.
- Hoover D.M., Drennan C.L., Metzger A.L., Osborne C., Weber C.H., Pattridge K.A., Ludwig M.L., (1999). Comparisons of wild-type and mutant flavodoxins from *Anacystis nidulans*. Structural determinants of the redox potentials. *Journal of Molecular Biology* **294**, 725 - 743.
- Hori H., Yonetani T., (1985). Powder and single crystal electron paramagnetic resonance studies of yeast cytochrome *c* peroxides and its peroxide compound, compound ES. *Journal of Biological Chemistry* **260**, 349 - 355.
- Huang J.J., Kimura T., (1973). Studies on adrenal steroid hydroxylases. Oxidation-reduction properties of adrenal iron-sulphur proteins. *Biochemistry* **12**, 406 - 409.
- Hubbard P.A., Shen A.L., Paschke R., Kasper C.B., Kim J-J.P., (2001). NADPH-cytochrome P450 oxidoreductase. Structural basis for hydride and electron transfer. *Journal of Biological Chemistry* **276**, 29163 - 29170.
- Hurley J.K., Salamon Z., Meyer T.E., (1993). Amino acid residues in *Anabaena* ferredoxin crucial to the interaction with ferredoxin-NADP reductase: Site-directed mutagenesis and laser flash photolysis. *Biochemistry* **32**, 9346 - 9354.
- Hymes J., Wolf B., (1996). Biotinidase and its roles in biotin metabolism. *Clinical Chimica Acta* **255**, 1 - 11.
- Ifuku O., Miyaoka H., Koga N., Kishimoto J., Haze S., Wachi Y., Kajiwara M., (1994). Origin of carbon atoms of biotin. <sup>13</sup>C-NMR studies on biotin biosynthesis in *Escherichia coli*. *European Journal of Biochemistry* **220**, 585 - 591.
- Imai Y., Nakamura M., (1989). Point mutations at threonine-301 modify substrate-specificity of rabbit liver microsomal cytochromes-P-450 (laurate (omega-1)-hydroxylase and testosterone 16-alpha-hydroxylase). *Biochemical and Biophysical Research Communications* **158**, 717 - 722.
- Ingelman M., Bianchi V., Eklund H., (1997). The three-dimensional structure of flavodoxin reductase from *Escherichia coli* at 1.7 Å resolution. *Journal of Molecular Biology* **268**, 147 - 157.
- Ingelman M., Ramaswamy S., Niviere V., Fontecave M., Eklund H., (1999). Crystal structure of NAD(P)H:Flavin oxidoreductase from *Escherichia coli*. *Biochemistry* **38**, 7040 - 7049.
- Ingraham L.L., Meyer D.L., (1985). *Biochemistry of Dioxygen*, Plenum Press NY.

- Inouye M., Arnheim N., Sternglanz R., (1973). Bacteriophage T7 Lysozyme Is an N-Acetylmuramyl-L-alanine Amidase. *Journal of Biological Chemistry* **248**, 7247 - 7252.
- Iwasaki I., Juvonen R., Lindenberg R., Negishi M., (1991). Alteration of high and low-spin equilibrium by a single mutation of amino acid-209 in mouse cytochromes-P450. *Journal of Biological Chemistry* **266**, 3380 - 3382.
- Izumi Y., Kano Y., Inagaki K., Kawase N., Tani Y., Yamada H., (1981). Characterization of biotin biosynthetic-enzymes of *Bacillus sphaericus* – A dethiobiotin producing bacterium. *Agricultural and Biological Chemistry, Kyoto University*, **49**, 1983 - 1989.
- Jenkins C.M., Waterman M.R., (1994). Flavodoxin and NADPH-flavodoxin reductase from *Escherichia coli* support bovine cytochrome P450c17 hydroxylase activities. *Journal of Biological Chemistry* **269**, 27401 - 27408.
- Jenkins C.M., Gonzor C.G., Fillat M.F., Waterman M.R., Gomez-Moreno C., (1997). Negatively charged *Anabaena* Flavodoxin residues (Asp144 and Glu145) are important for reconstitution of cytochrome P450 17 $\alpha$ -hydroxylase activity. *Journal of Biological Chemistry* **272**, 22509 - 22513.
- Jenkins C.M., Waterman M.R., (1998). NADPH-Flavodoxin reductase and flavodoxin from *Escherichia coli*: Characteristics as a soluble microtonal P450 reductase. *Biochemistry* **37**, 6106 - 6113.
- Jennewein S., Rithner C.D., Williams R.M., Croteau R.B., (2001). Taxol biosynthesis: Taxane 13 $\alpha$ -hydroxylase is a cytochrome P450-dependent monooxygenase. *Proceedings of the National Academy of Science USA* **98**, 13595 - 13600.
- Jerina D.M., Daly J.W., Wiktop B., Zaltzman-Nirenberg P., Udenfriend S., (1968). The role of arene oxide-oxepin systems in the metabolism of aromatic substrates. III. Formation of 1,2-naphthalene oxide from naphthalene by liver microsomes. *Journal of the American Chemical Society* **90**, 6525.
- Jerpseth, J., Callahan M., and Greener A., (1992). XL1-Blue MRF' *E. coli* cells: McrA-, McrCB-, McrF-, Mrr-, HsdR- derivative of XL1-Blue cells. *Strategies* **6**, 81.
- Jerpseth B., Callahan M., and Greener A., (1998). New Competent Cells for Highest Transformation Efficiencies. *Strategies* **10**, 37 - 38.
- Jerpseth M., Jerspeth B., Briester L., Greener A., (1998). High-efficiency derivatives of the BL21 series for protein expression. *Strategies* **11**, 3 - 4.
- Ji H., Zhang W., Zhou Y., Zhang M., Zhu J., Song Y., Lu J., Zhu J., (2000). A three dimensional model of lanosterol 14 $\alpha$ -demethylase of *Candida albicans* and its interaction with azole antifungals. *Journal of Medicinal Chemistry* **43**, 2493 - 2505.
- John B., D'Silva P.R., Lala A.K., (2001). Analysis of protein folding using polarity sensitive fluorescent probes. *Current Science Research Communications* **80**, 287 - 290.
- Jones, B.C., Tyman, C.A. and Smith, D.A. (1997). Identification of the cytochrome P450 isoforms involved in the O-demethylation of 4-nitroanisole in human liver microsomes.

*Xenobiotica* **27**, 1025 - 1037.

Jose J., Bernhardt R., Hannemann F., (2002). Cellular surface display of dimeric Adx and whole cell P450-mediated steroid synthesis on *E. coli*. *Journal of Biotechnology* **95**, 257 - 268.

Joo H., Lin Z.L., Arnold F.H., (1999). Laboratory evolution of peroxide-mediated cytochrome P450 hydroxylation. *Nature* **399**, 670 - 673.

Jung C., Bec N., Lange R., (2002). Substrates modulate the rate-determining step for CO binding in cytochrome P450 CAM (CYP101) - a high pressure stopped-flow study. *European Journal of Biochemistry* **269**, 2989 - 2996.

Kaan T., Homuth G., Mader U., Bandow J., Schweder T., (2002). Genome-wide transcriptional profiling of the *Bacillus subtilis* cold-shock response. *Microbiology* **148**, 3441 - 3455.

Kabsch, W. and Sander, C. (1983). Dictionary of protein secondary structure: pattern recognition of hydrogen-bonded and geometrical features. *Biopolymers* **22**, 2577 - 2637.

Kack H., Sandmark J., Gibson K.J., Schneider G., Lindqvist Y., (1998). Crystal structure of two quaternary complexes of dethiobiotin synthase, enzyme-MgADP-AlF<sub>3</sub>-diaminoperlarginic acid and enzyme-MgADP-dethiobiotin-phosphate; implications for catalysis. *Protein Science* **7**, 2560 - 2566.

Kack H., Sandmark J., Gibson K.J., Schneider G., Lindqvist Y., (1999). Crystal structure of diaminoperlarginic acid synthase: Evolutionary relationship between paradoxical-5'-phosphate-dependant enzymes. *Journal of Molecular Biology* **291**, 857 - 876.

Kadkhodayan S., Coulter E.D., Maryniak D.M., Bryson T.A., Dawson J.H., (1995). Uncoupling oxygen-transfer and electron-transfer in the oxygenation of camphor analogs by cytochrome P450-CAM - direct observation of an intermolecular isotope effect for substrate C-H activation. *Journal of Biological Chemistry* **270**, 28042 - 28048.

Kasim M., Swenson R.P., (2000). Conformational energies of a reverse turn in the *Clostridium beijerinckii* flavodoxin are directly coupled to the modulation of its oxidation-reduction potentials. *Biochemistry* **39**, 15322 - 15332.

Kasim M., Swenson R.P., (2001). Alanine-scanning of the 50's loop in the *Clostridium beijerinckii* flavodoxin: Evaluation of the additivity and the importance of interactions provided by the main chain in the modulation of the oxidation-reduction potentials. *Biochemistry* **40**, 13548 - 13555.

Kelley, L.A., Gardner, S.P. and Sutcliffe, M.J. (1996). An automated approach for clustering an ensemble of NMR-derived protein structures into conformationally related subfamilies. *Protein Engineering* **9**, 1063-1065.

Kelly S.M., Price N.C., (1997). Application of circular dichroism to studies of protein folding and unfolding. *Biochimica et Biophysica Acta* **1338**, 161 - 185.

Kelly W.L., Townsend C.A., (2002). Role of cytochrome P450 NocL in nocardicin A biosynthesis. *Journal of the American Chemical Society Communications* **124**, 8186 - 8187.

Khan J.A., Vulfson E.N., (2002). Microencapsulation of enzymes and cells for non-aqueous biotransformations. *Institute of Food Research, UK*.

Klein W., Weber M.H.W., Marahiel M.A., (1999). Cold shock response of *Bacillus subtilis*: Isoleucine-dependent switch in the fatty acid branching pattern for membrane adaptation to low temperatures. *Journal of Bacteriology* **181**, 5341 - 5349.

Klingenberg M., (1958). Pigments of rat liver microsomes. *Archives of Biochemistry and Biophysics* **75**, 376 - 386.

Knauf M.A., Lohr F., Blumel M., Mayhew S.G., Ruterjans H., (1996). NMR investigation of the solution conformation of oxidized flavodoxin from *Desulfovibrio vulgaris*. *European Journal of Biochemistry* **238**, 423 - 434.

Kobayashi K., Ehrlich S.D., Albertini A., Amati G., Andersen K.K., *et al.*, (2003). Essential *Bacillus subtilis* genes. *Proceedings of the National Academy of Science USA* **100**, 4678 - 4683.

Koga H., Yamaguchi E., Matsunaga K., Aramaki H., Horiuchi T., (1989). Cloning and nucleotide-sequences of nadh-putidaredoxin reductase gene (CAMA) and putidaredoxin gene (CAMB) involved in cytochrome-P-450 CAM hydroxylase of *Pseudomonas putida*. *Journal of Biochemistry* **106**, 831 - 836.

Koga H., Sagara Y., Yaoi T., Tsujimura M., Nakamura K., Sekimizu K., Makino R., Shimada H., Ishimura Y., Yura K., Go M., Ikeguchi M., Horiuchi T., (1993). Essential role of the Arg112 residue of cytochrome P450 CAM for electron transfer from reduced putidaredoxin. *FEBS Letters* **331**, 109 - 113.

Komives E. A., Ortiz de Montellano P.R., (1987). Mechanisms of oxidation of  $\pi$  bonds by cytochrome P450. Electronic requirements of the transition state in the turnover of phenyl acetylenes. *Journal of Biological Chemistry* **262**, 9793 - 9802.

Korzekwa K.R., Swinney D.C., Trager W.F., (1989). Isotopically labeled chlorobenzenes as probes for the mechanism of cytochrome P-450 catalysed aromatic hydroxylation. *Biochemistry* **28**, 9019 - 9027.

Kostic M., Popchapsky S.S., Obenauer J., Mo H., Pagani G.M., Pejchal R., Popchapsky T.C., (2002). Comparison of functional domains in vertebrate-type ferredoxins. *Biochemistry* **41**, 5978 - 5989.

Krebs B., Strater N., (1994). X-ray structure-analysis of methane monooxygenase - an important step toward understanding the oxidation of methane in biological-systems. *Angewandte Chemie-International Edition* **33**, 841 - 843.

Kunst K., Ogasawara N., Moszer I., Albertini A.M., Azevedo V., *et al.*, (1997). The complete genome sequence of the Gram-positive bacterium *Bacillus subtilis*. *Nature* **390**, 249 - 256.

Lamb D.C., Fowler K., Kieser T., Manning N., Podust L.M., Waterman M.R., Kelly D.E., Kelly S.L., (2002). Sterol 14 $\alpha$ -demethylase activity in *Streptomyces coelicolor* A3 (2) is associated with an unusual member of the CYP51 gene family. *Biochemical Journal* **364**, 555 - 562.

Lambeth J.D., Kamin H., (1979). Adrenodoxin reductase-adrenodoxin complex: Flavin to iron-

sulphur electron transfer as the rate-limiting step in the NADPH-cytochrome *c* reductase reaction. *Journal of Biological Chemistry* **254**, 2766 - 2774.

Lambeth J.D., Kriensiri S., (1985). Cytochrome P450 scc-adrenodoxin interactions: Ionic effects on binding, and regulation of cytochrome reduction by bound steroid substrates. *Journal of Biological Chemistry* **260**, 8810 - 8816.

Lathrop B.K., Burack W.R., Biltonen R.L., Rule G.S., (1992). Expression of a group-II phospholipase-a(2) from the venom of agkistrodon-piscivorus-piscivorus in *Escherichia coli* - recovery and renaturation from bacterial inclusion-bodies. *Protein Expression and Purification* **3**, 512 - 517.

Leadbeater C., McIver L., Campopiano D.J., Webster S.P., Baxter R.L., Kelly S.M., Price N.C., Lysek D.A., Noble M.A., Chapman S.K., Munro A.W., (2000). Probing the NADPH-binding site of *Escherichia coli* flavodoxin oxidoreductase. *Biochemical Journal* **352**, 257 - 266.

Lee D-S., Yamada A., Matsunaga I., Ichihara K., Adachi S., Park S-Y., Shiro Y., (2003). Crystallisation and preliminary X-ray diffraction analysis of fatty-acid hydroxylase cytochrome P450 Bsβ from *Bacillus subtilis*. *Acta Crystallographica (D)* **58**, 687 - 689.

Lee D-S., Yamada A., Sugimoto H., Matsunaga I., Ogura H., Ichihara K., Adachi S., Park S-Y., Shiro Y., (2003). Substrate recognition and molecular mechanism of fatty acid hydroxylation by cytochrome P450 from *Bacillus subtilis*. *Journal of Biological Chemistry* **278**, 9761 - 9767.

Lee J-M., Zhang S., Saha S., Anna S.S., Jiang C., Perkins J., (2001). RNA expression analysis using an antisense *Bacillus subtilis* genome array. *Journal of Bacteriology* **183**, 7371 - 7380.

Lee T.R., Hsu H.P., Shaw G.C., (2001). Transcriptional regulation of the *Bacillus subtilis* bscR-CYP102A3 operon by the BscR repressor and differential induction of cytochrome CYP102A3 expression by oleic acid and palmitate. *Journal of Biochemistry* **130**, 569 - 574.

Leeder J.S., Lu X.L., Timsit Y., Gaedigk A., (1998). Non-monoxygenase cytochromes P450 as potential human autoantigens in anticonvulsant hypersensitivity reactions. *Pharmacogenetics* **8**, 211 - 225.

Lehrer S.S., (1971). Solute perturbation of protein fluorescence. The quenching of the tryptophyl fluorescence of model compounds and of lysozyme by iodide ion. *Biochemistry* **10**, 3254 - 3263.

Lennon B.W., Williams C.H.Jr., (1996). Enzyme monitored turnover of *Escherichia coli* thioredoxin reductase: Insights for catalysis. *Biochemistry* **35**, 4704 - 4712.

Lennon B.W. Williams C.H.Jr., (1999). Crystal structure of reduced thioredoxin reductase from *Escherichia coli*: Structural flexibility in the isoalloxazine ring of the flavin adenine dinucleotide cofactor. *Protein Science* **8**, 2366 - 2379.

Lennon B.W., Williams C.H.Jr., Ludwig M.L., (2000). Twists in catalysis: Alternating conformations of *Escherichia coli* thioredoxin reductase. *Science* **289**, 1190 - 1199.

Lentz O., Urlacher V., Schmid R.D., (2004). Substrate specificity of native and mutated cytochrome P450 (CYP102A3) from *Bacillus subtilis*. *Journal of Biotechnology* **108**, 41 - 49.

Lewis D.F.V., Hlavica P., (2000). Interactions between redox partners in various cytochrome P450 systems: Functional and structural aspects. *Biochimica et Biophysica Acta* **1460**, 353 - 374.

Li H.Y., Darwish K., Poulos T.L., (1991). Characterization of recombinant *Bacillus-megaterium* cytochrome-P450 BM3 and its 2 functional domains. *Journal of Biological Chemistry* **266**, 11909 - 11914.

Li H.Y., Poulos T.L., (1997). The structure of cytochrome P450 BM3 heme domain complexed with the fatty acid substrate, palmitoleic acid. *Nature Structural Biology* **4**, 140 - 146.

Li Q.S., Schwaneberg U., Fischer P., Schmid R.D., (2000). Directed evolution of the fatty-acid hydroxylase P450 BM-3 into an indole-hydroxylating catalyst. *Chemistry-A European Journal*, **6**, 1531 - 1536.

Lindenmayer A., Smith L., (1964). Cytochromes and other pigments of Bakers yeast grown aerobically and anaerobically. *Biochimica et Biophysica Acta* **93**, 445 - 461.

Lippard S.J., (1993). Methane monooxygenase, models and mechanism. *Abstracts of Papers of The American Chemical Society Inorganic Part 1* **205**, 551 - 553.

Lipscomb J.D., Sligar S.G., Namtvedt M.J., Gunsalus I.C., (1976). Autooxidation and hydroxylation reactions of oxygenated cytochrome P-450cam. *Journal of Biological Chemistry* **251**, 1116 - 1124.

Livaniou E., Costopoulou D., Vassiliadou I., Leondiadis L., Nyalala J.O., Ithakissios D.S., Evangelatos G.P., (2000). Analytical techniques for detecting biotin. *Journal of Chromatography A* **881**, 331 - 343.

Loew G.H., Kert C.J., Hjelmeland L.M., Kirchner R.F., (1977). Active site models of horseradish peroxidase compound I and a cytochrome P-450 analog: electronic structure and electric field gradients. *Journal of the American Chemical Society* **99**, 3534 - 3536.

Loida P.J., Sligar S.G., (1993). Molecular recognition in cytochrome P-450: Mechanism for the control of uncoupling reactions. *Biochemistry* **32**, 11530 - 11538.

Losato A., Gomez-Moreno C., Mayhew S.G., Sancho J., (1997). Differential stabilisation of the three FMN redox forms by tyrosine 94 and tryptophan 57 in flavodoxin from *Anabaena* and its influence on the redox potentials. *Biochemistry* **36**, 14334 - 14334.

Ludwig M.L., Luschinsky C.L., (1992). Structure and redox properties of Clostridial flavodoxin. *Chemistry and Biochemistry of Flavoenzymes*, Ed., Muller F., **3**, 427 - 466, CRC Press, Boca Raton, FL.

Ludwig M.L., Patridge K.A., Metzger A.L., Dixon M.M., (1997). Control of oxidation-reduction potentials in flavodoxin from *Clostridium beijerinckii*: The role of conformational changes. *Biochemistry* **36**, 1259 - 1280.

Luschinsky C.L., Dunham W.R., Osborne K.A., Patridge K.A., Ludwig M.L., (1992). Flavins and Flavoproteins, 409 - 414. Ed., Curti B., Ronchi S., Zanetti G., de Gruyter Press, Berlin.

Macdonald I.D.G., Smith W.E., Munro A.W., (1996). Inhibitor/fatty acid interactions with



cytochrome P-450 BM3. *FEBS Letters* **396**, 196 - 200.

Macheroux P., Massey V., Thiele D.J., (1991). Expression of spinach glycolate oxidase in *Saccharomyces cerevisiae*: Purification and characterisation. *Biochemistry* **30**, 4612 - 4619.

Macheroux P., (1999). UV-visible spectroscopy as a tool to study flavoproteins. *Methods in Molecular Biology*, **131**. Flavoprotein protocols 1 - 7. Humana Press Inc., N.J. Editors S.K. Chapman, G.A. Reid.

Maldonado S., Losato A., Irun M.P., Fernandez-Recio J., Genzor C.G., Gonzalez E.B., Rubio J.A., Luquita A., Daoudi F., Sancho J., (1998). Apoflavodoxin: Structure, stability, and FMN binding. *Biochimie* **80**, 813 - 820.

Maldonado S., Jimenez M.A., Langdon G.M., Sancho J., (1998). Cooperative stabilization of a molten globule apoflavodoxin fragment. *Biochemistry* **37**, 10589 - 10596.

Marquet A., Bui B.T.S., Florentin D., (2001). Biosynthesis of biotin and lipid acid. *Vitamins and Hormones – Advances in Research and Applications*, Academic Press Inc., San Diego. 1<sup>st</sup> edition, **61**, 51 - 101.

Martinis S.A., Ropp J.D., Sligar S.G., Gunsalus I.C., (1991). Molecular recognition by cytochrome P450 CAM: Substrate specificity, catalysis and electron transfer. In *Microbial and Plant Cytochromes P450: Biochemical Characteristics, Genetic Engineering and Practical Implications. Frontiers in Biotransformation*. **4**, 54 - 86. Ed., Ruckpaul K., Rein H., Taylor and Francis, London.

Martinis S.A., Blanke S.R., Hager L.P., Sligar S.G., Hoa G.H.B., Rux J.J., Dawson J.H., (1996). Probing the heme iron coordination structure of pressure-induced cytochrome P420 CAM. *Biochemistry*, **35**, 14530-14536.

Mason H.S., North J.C., Vanneste M., (1965). Microsomal mixed-function oxidations: The metabolism of xenobiotics. *Federation Proceedings: Federation of American Societies for Experimental Biology*, **24**, 1172 - 1180.

Maugard T., Enaud E, Choisy P, Legoy M.D., (2001). Identification of an indigo precursor from leaves of *Isatis tinctoria* (Woad). *Phytochemistry* **58**, 897 - 904.

Mayhew S.G., Ludwig M.L., (1975). Flavodoxins and electron-transferring flavoproteins. In *The Enzymes* 3<sup>rd</sup> Ed., **12B**, 57 - 109. Ed., Boyer P.D., Academic Press NY.

Mayhew S.G., Tollin G., (1992). General properties of flavodoxins, in *Chemistry and Biochemistry of Flavoenzymes*. Ed. Muller F., **3**, 389 - 426, CRC Press, Boca Raton, FL.

Mayhew S.G., O'Connell D.P., O'Farrell P.A., Yalloway G.N., Geoghegan S.M., (1996). Regulation of the redox potentials of flavodoxins: Modification of the flavin binding site. *Biochemical Society Transactions* **24**, 122 - 127.

Mayoral T., Medina M., Sanz-Aparicio J., Gomez-Moreno C., Hermoso J.A., (2000). Structural basis of the catalytic role of Glu301 in *Anabaena* PCC 7119 Ferredoxin-NADP<sup>+</sup> reductase revealed by X-ray crystallography. *Proteins: Structure, Function, and Genetics* **38**, 60 - 69.

- Mazzola J.L., Sirover M.A., (2001). Reduction of glyceraldehyde-3-phosphate dehydrogenase activity in Alzheimer's disease and in Huntington's disease fibroblasts. *Journal of Neurochemistry* **76**, 442 - 449.
- McCarthy A.A., Walsh M.A., Verna C.S., O'Connell D.P., Reinhold M., Yalloway G.N., d'Arcy D., Higgins T.M., Voordouw G., Mayhew S.G., (2002). Crystallographic investigation of the role of aspartate 95 in the modulation of the redox potentials of *Desulfovibrio vulgaris* flavodoxin. *Biochemistry* **41**, 10950 - 10962.
- McIver L., Leadbeater C., Campopiano D.J., Baxter R.L., Daff S.N., Chapman S.K., Munro A.W., (1998). Characterisation of flavodoxin NADP<sup>+</sup> oxidoreductase and flavodoxin; key components of electron transfer in *Escherichia coli*. *European Journal of Biochemistry* **257**, 577 - 585.
- McLean K.J., Cheesman M.R., Rivers S.L., Richmond A., Leys D., Chapman S.K., Reid G.A., Price N.C., Kelly S.M., Clarkson J., Smith W.E., Munro A.W., (2002). Expression, purification and spectroscopic characterization of the cytochrome P450CYP121 from *Mycobacterium tuberculosis*. *Journal of Inorganic Biochemistry* **91**, 527 - 541.
- McLean K.J., Scrutton N.S., Munro A.W., (2003). Kinetic, spectroscopic and thermodynamic characterization of the *Mycobacterium tuberculosis* adrenodoxin reductase homologue FprA. *Biochemical Journal* **372**, 317 - 327.
- Medina M., Peleato M.L., Mendez E., Gomezmoreno C., (1992). Identification of specific carboxyl groups on *Anabaena* PCC-7119 flavodoxin which are involved in the interaction with ferredoxin-NADP<sup>+</sup> reductase. *European Journal of Biochemistry* **203**, 373 - 379.
- Mierlo C.P.M., Steensma E., (2000). Protein folding and stability investigated by fluorescence, circular dichroism (CD), and nuclear magnetic resonance (NMR) spectroscopy: the flavodoxin story. *Journal of Biotechnology* **79**, 281 - 298.
- Miles C.S., Ost T.W.B., Noble M.A., Munro A.W., Chapman S.K., (2000). Protein engineering of cytochromes P450. *Biochimica et Biophysica Acta* **1543**, 383 - 407.
- Miles J.S., Munro A.W., Rospendowski B.N., Smith W.E., McKnight J., Thomson A.J., (1992). Domains of the catalytically self-sufficient cytochrome P-450 BM-3: Genetic construction, overexpression, purification and spectroscopic characterization. *Biochemistry Journal* **288**, 503 - 509.
- Miller G.P., Hanna I.H., Nishimura Y., Guengerich F.P., (2001). Oxidation of phenethylamine derivatives by cytochrome P450 2D6: The issue of substrate protonation in binding and catalysis. *Biochemistry* **40**, 14215 - 14223.
- Mitchell S.C., Waring R.H., (1986). the early history of xenobiotic sulfoxidation. *Drug Metabolism Review* **16**, 255 - 284.
- Mittl P.R.E., Schulz G.E., (1994). Structure of glutathione-reductase from *Escherichia coli* at 1.86 Angstrom resolution - comparison with the enzyme from human erythrocytes. *Protein Science* **3**, 799 - 809.
- Miura Y., Fulco A.J., (1975).  $\omega$ -1,  $\omega$ -2 and  $\omega$ -3 hydroxylation of long-chain fatty acids, amides

and alcohols by a soluble enzyme system from *Bacillus megaterium*. *Biochimica et Biophysica Acta* **388**, 305 - 317.

Miura S., Ichikawa Y., (1991). Conformational change of adrenodoxin induced by reduction of iron-sulphur cluster. *Journal of Biological Chemistry* **266**, 6252 - 6258.

Mo H., Popchapsky S.S., Popchapsky T.C., (1999). A model for the solution structure of oxidised terpredoxin, a Fe<sub>2</sub>S<sub>2</sub> ferredoxin from *Pseudomonas*. *Biochemistry* **38**, 5666 - 5675.

Modi S., Paine M.J., Sutcliffe M.J., Lian L-Y., Primrose W.U., Wolf C.R., Roberts G.C.K., (1996). A model for human cytochrome P450 2D6 based on homology modelling and NMR studies of substrate binding. *Biochemistry* **35**, 4540 - 4550.

Modi S., Gillham D.E., Sutcliffe M.J., Lian L-Y., Primrose W.U., Wolf C.R., Roberts G.C.K., (1997). 1-methyl-4-phenyl-1,2,3,6-tetrahydropyridine as a substrate of cytochrome P450 2D6: Allosteric effects of NADPH-cytochrome P450 reductase. *Biochemistry* **36**, 4461 - 4470.

Mohsen A.W.A., Rigby S.E.J., Jensen K.F., Munro A.W., Scrutton N.S., (2004). Thermodynamic basis of electron transfer in dihydroorotate dehydrogenase B from *Lactococcus lactis*: Analysis by potentiometry, EPR spectroscopy, and ENDOR spectroscopy. *Biochemistry* **43**, 6498 - 6510.

Moonen C., Vervoort J., Muller F., (1984). Reinvestigation of the structure of oxidized and reduced flavin - C-13 and N-15 nuclear magnetic-resonance study. *Biochemistry* **23**, 4859 - 4867.

Moonen C., Vervoort J., Muller F., (1984). Some new ideas about the possible regulation of redox potentials in flavoproteins with special reference to flavodoxins. In *Flavins and Flavoproteins* 493 - 496. Ed., Bray R.C., Engel P.C., Mayhew S.G., de Gruyter Press, Berlin.

Moore J.D., Hawkins A.R., Charles I.G., Deka R., Coggins J.R., Cooper A., Kelly S.M., Price N.C., (1993). Characterisation of the type-I dehydroquinase from *Salmonella typhi*. *Biochemical Journal* **295**, 277 - 285.

Morales R., Chron M.H., Hudry-Clergeon G., Petillot Y., Norager S., Medina M., Frey M., (1999). Refined X-ray structures of the oxidized, at 1.3 Angstrom, and reduced, at 1.17 angstrom, [2Fe-2S] ferredoxin from the cyanobacterium *Anabaena* PCC7119 show redox-linked conformational changes. *Biochemistry* **38**, 15764 - 15773.

Morales R., Charon M.H., Kachalova G., Serre L., Medina M., Gomez-Moreno C., Frey M., (2000). A redox dependent interaction between two electron transfer partners involved in photosynthesis. *EMBO Reports* **1**, 271 - 276.

Morant M., Bak S., Moller B.L., Werck-Reichhart D., (2003). Plant cytochromes P450: Tools for pharmacology, plant protection and phytoremediation. *Current Opinion in Biotechnology* **14**, 151 - 162.

Morbidoni H.R., de Mendoza D., Cronan J.E.Jr., (1996). *Bacillus subtilis* acyl carrier protein is encoded in a cluster of lipid biosynthetic genes. *Journal of Bacteriology* **178**, 4794 - 4800.

Mougin A., Corbier C., Soukri A., Wonacott A., Branlant C., Branlant G., (1998). Use of site-directed mutagenesis to probe the role of Cys149 in the formation of charge-transfer transition in glyceraldehyde-3-phosphate dehydrogenase. *Protein Engineering, Design and Selection* **2**, 45 -

53.

- Mueller E.J., Loida P.J., Sligar S.G., (1995). Twenty five years of P450 CAM research. In *Cytochrome P450: Structure, Mechanism and Biochemistry*, Chapter 3, 83 - 124. Ed., Ortiz de Montellano, Plenum Press NY.
- Muller A., Muller J.J., Muller Y.A., Uhlmann H., Bernhardt R., Heinemann U., (1998). New aspects of electron transfer revealed by the crystal structure of a truncated bovine adrenodoxin, Adx(4-108). *Structure* **6**, 269 - 280.
- Muller E-C., Lapko A., Otto A., Muller J.J., Ruckpaul K., Heinemann U., (2001). Covalently cross linked complexes of bovine adrenodoxin with adrenodoxin reductase and cytochrome P450<sub>scc</sub>. *European Journal of Biochemistry* **268**, 1837 - 1843.
- Muller F., Hemmerich P., Ehrenberg A., Palmer G., Massey V., (1970). The chemical and electronic structure of the neutral flavin radical as revealed by electron spin resonance spectroscopy of chemically and isotopically substituted derivatives. *European Journal of Biochemistry* **14**, 185 - 196.
- Muller F., Brustlein M., Hemmerich P., Massey V., Walker W.H., (1972). Light-absorption studies on neutral flavin radicals. *European Journal of Biochemistry* **25**, 573 - 580.
- Muller J.J., Muller A., Rottmann M., Bernherdt R., Heinemann U., (1999). Vertebrate-type and plant-type ferredoxins: Crystal structure comparison and electron transfer pathway modelling. *Journal of Molecular Biology* **294**, 501 - 513.
- Munro A.W., Lindsay J.G., Coggins J.R., Kelly S.M., Price N.C., (1994). Structural and enzymological analysis of the interaction of isolated domains of cytochrome P450 BM3. *FEBS Letters* **343**, 70 - 74.
- Munro A.W., Malarkey K., McKnight J., Thomson A.J., Kelly S.M., Price N.C., Lindsay J.G., Coggins J.R., Miles J.S., (1994). The role of tryptophan 97 of cytochrome P450 BM3 from *Bacillus megaterium* in catalytic function. *Biochemical Journal* **303**, 423 - 428.
- Munro A.W., Lindsay J.G., (1996). Bacterial cytochromes P-450. *Molecular Microbiology* **20**, 1115 - 1125.
- Munro A.W., Lindsay J.G., Coggins J.R., Kelly S.M., Price N.C., (1996). Analysis of the structural stability of the multinomial enzyme flavocytochrome P-450 BM3. *Biochimica et Biophysica Acta* **1296**, 127 - 137.
- Munro A.W., Kelly S.M., Price N.C., (1999). Circular Dichroism of flavoproteins. *Methods in Molecular Biology*, **131**. Flavoprotein protocols 111 - 123. Humana Press Inc., N.J. Ed. S.K. Chapman, G.A. Reid.
- Munro A.W., Noble M.A., Robledo L., Daff S.N., Chapman S.K., (2001). Determination of the redox properties of human NADPH-cytochrome P450 reductase. *Biochemistry* **40**, 1956 - 1963.
- Murataliev M.B., Klein M., Fulco A., Feyereisen R., (1997). Functional interactions in cytochrome P450 BM3: Flavin semiquinone intermediates, role of NAD(P)H, and mechanism of electron transfer by the flavoprotein domain. *Biochemistry* **36**, 8401 - 8412.

Murataliev M.B., Feyereisen R., (2000). Interaction of NADP(H) with oxidised and reduced P450 reductase during catalysis. Studies with nucleotide analogues. *Biochemistry* **39**, 5066 - 5074.

Murataliev M.B., Feyereisen R., (2000). Functional intermediates in cytochrome P450 BM3. Evidence that NADP(H) binding controls redox potentials of the flavin cofactor. *Biochemistry* **39**, 12699 - 12707.

Murray T.A., Swenson R.P., (2003). Mechanism of flavin mononucleotide cofactor binding to the *Desulfovibrio vulgaris* flavodoxin. 1. Kinetic evidence for cooperative effects associated with the binding of inorganic phosphate and the 5'-phosphate moiety of the cofactors. *Biochemistry* **42**, 2307 - 2316.

Murugan R, Mazumdar S., (2004). Role of substrate on the conformational stability of the heme active site of cytochrome P450 CAM: Effect of temperature and low concentrations of denaturants. *Journal of Biological Inorganic Chemistry* **9**, 477 - 488.

Nagy I., Schloofs G., Compennolle F., Proost P., Vanderleyn J., De Mot R., (1995). Degradation of the thiocarbamate herbicide EPTC (S-ethyl dipropylcarbamothioate) and biosafening by *Rhodococcus* sp. Strain NI86/21 involve an inducible cytochrome P450 system and aldehyde dehydrogenase. *Journal of Bacteriology* **177**, 676 - 687.

Nahri L.O., Fulco A.J., (1986). Characterisation of a catalytically self-sufficient 119,000-Dalton cytochrome P-450 monooxygenase induced by barbiturates in *Bacillus megaterium*. *Journal of Biological Chemistry* **261**, 7160 - 7169.

Nahri L.O., Fulco A.J., (1987). Identification and characterisation of two functional domains in cytochrome P-450 BM-3, a catalytically self-sufficient monooxygenase induced by barbiturates in *Bacillus megaterium*. *Journal of Biological Chemistry* **262**, 6683 - 6690.

Nakamura K., Horiuchi T., Yasukochi T., Sekimizu K., Hara T., Sagara Y., (1994). Significant contribution of arginine 112 and its positive charge of *Pseudomonas putida* P450 CAM in the electron transport from putidaredoxin. *Biochimica et Biophysica Acta* **1207**, 40 - 48.

Nelson D.R., Kamataki T., Waxman D.J., Guengerich F.P., Estabrook R.W., Feyereisen R., Gonzalez F.J., Coon M.J., Gunsalus I.C., Gotoh O., Okuda K., Nebert D.W., (1993). The P450 superfamily: Update on new sequences, gene mapping, accession numbers, early trivial names of enzymes, and nomenclature. *DNA Cellular Biology* **12**, 1 - 51.

Nelson D.R., Koymans L., Kamataki T., Stegeman J.J., Feyereisen R., Waxman D.J., Waterman M.R., Gotoh O., Coon M.J., Estabrook R.W., Gunsalus I.C., Nebert D.W., (1996). P450 superfamily: Update on new sequences, gene mapping, accession numbers and nomenclature. *Pharmacogenetics* **6**, 1 - 42.

Nelson D.R., (1999). Cytochrome P450 and the individuality of species. *Archives of Biochemistry and Biophysics* **369**, 1 - 10.

Newcomb M., Le-Tadic-Biadatti M-H., Chestney D.L., Roberts E.S., Hollenberg P.F., (1995). A nonsynchronous concerted mechanism for cytochrome-P-450 catalyzed hydroxylation. *Journal of the American Chemical Society* **117**, 12085 - 12091.

Newcomb M., Aebischer D., Shen R., Chandrasena R.E.P., Hollenberg P.F., Coon M.J., (2003). Kinetic isotope effects implicate two electrophilic oxidants in cytochrome P450-catalysed hydroxylations. *Journal of the American Chemical Society* **125**, 6064 - 6065.

Nisimoto Y., Edmondson D.E., (1992). Effect of KCl on the interactions between NADPH - cytochrome-P-450 reductase and either cytochrome-c, cytochrome-b5 or cytochrome-P-450 in octyl glucoside micelles. *European Journal of Biochemistry*, **204**, 1075 - 1082.

Niviere V., Fieschi F., Decout J-L., Fontecave M., (1996). Is the NAD(P)H:Flavin oxidoreductase from *Escherichia coli* a member of the ferredoxin-NADP<sup>+</sup> reductase family? *Journal of Biological Chemistry* **271**, 16656 - 16661.

Noble M.A., Quaroni L., Chumanov G.D., Turner K.L., Chapman S.K., Hanzlik R.P., Munro A.W., (1998). Imidazolyl carboxylic acids as mechanistic probes of flavocytochrome P-450 BM3. *Biochemistry* **37**, 15799 - 15807.

Noble M.A., Miles C.S., Chapman S.K., Lysek D.A., Mackay A.C., Reid G.A., Hanzlik R.P., Munro A.W., (1999). Roles of key active-site residues in flavocytochrome P450 BM3. *Biochemical Journal* **339**, 371 - 379.

Nogues I., Martinez-Julvez M., Navarro J.A., Hervas M., Armenteros L., Angel de la Rosa M., Brodie T.B., Hurley J.K., Tollin G., Gomez-Moreno C., Medina M., (2003). Role of hydrophobic interactions in the flavodoxin mediated electron transfer from photosystem I to ferredoxin-NADP<sup>+</sup> reductase in *Anabaena* PCC 7119. *Biochemistry* **42**, 2036 - 2045.

Nohl H., Stolze K., (1993). Chemiluminescence from activated heme compounds detected in the reaction of various xenobiotics with oxyhemoglobin - comparison with several heme hydrogen-peroxide systems. *Free Radical Biology and Medicine* **15**, 257 - 263.

Nuallain B.O., Mayhew S.G., (2002). A comparison of the urea-induced unfolding of apoflavodoxin and flavodoxin from *Desulfovibrio vulgaris*. *European Journal of Biochemistry* **269**, 212 - 223.

O'Farrell P.A., Walsh M.A., McCarthy A.A., Higgins T.M., Voordouw G., Mayhew S.G., (1998). Modulation of the redox potentials of FMN in *Desulfovibrio vulgaris* flavodoxin: Thermodynamic properties and crystal structures of glycine-61 mutants. *Biochemistry* **37**, 8405 - 8416.

O'Keefe D.P., Gibson K.J., Emptage M.H., Lenstra R., Romesser J.A., Little P.J., Omer C.A., (1991). Ferredoxins from two sulphonylurea herbicide monooxygenase systems in *Streptomyces griseolus*. *Biochemistry* **30**, 447 - 455.

Oku H., Kaneda T., (1988). Biosynthesis of branched-chain fatty acids in *Bacillus subtilis*. A decarboxylase is essential for branched-chain fatty acid synthetase. *Journal of Biological Chemistry* **263**, 18386 - 18396.

Oliver C.F., Modi S., Primrose W.U., Lian L-Y., Roberts G.C.K., (1997). Engineering the specificity of *Bacillus megaterium* P450 BM3: hydroxylation of alkyl triammonium compounds. *Biochemical Journal* **327**, 537 - 544.

Oliver CF, Modi S, Sutcliffe MJ, Primrose WU, Lian LY, Roberts GCK., (1997). A single



mutation in cytochrome P450 BM3 changes substrate orientation in a catalytic intermediate and the regiospecificity of hydroxylation. *Biochemistry* **36**, 1567 - 1572.

Ollagnier-de-Choudens S., Sanakis Y., Hewitson K.S., Roach P., Baldwin J.E., Munck E., Fontecave M., (2000). Iron-sulfur centre of biotin synthase and lipoate synthase. *Biochemistry* **39**, 4165 - 4173.

Ollagnier-de-Choudens S., Mulliez E., Hewitson K.S., Fontecave M., (2002). Biotin synthase is a pyroxidal phosphate-dependent cysteine desulfurase. *Biochemistry* **41**, 9145 - 9152.

Omura T., Sato R., (1964). The Carbon Monoxide-binding Pigment of Liver Microsomes. II. Solubilization, purification, and properties. *Journal of Biological Chemistry* **239**, 2379 - 2385.

Oprian D.D., Coon M.J., (1982). Oxidation-reduction states of FMN and FAD in NADPH-cytochrome P-450 reductase during reduction by NADPH. *Journal of Biological Chemistry* **257**, 8935 - 8944.

Ortiz de Montellano P.R., Mico B.A., (1980). Destruction of cytochrome P-450 by ethylene and other olefins. *Molecular Pharmacology* **18**, 128 - 135.

Ortiz de Montellano P.R., Mangold B.L.K., Wheeler C., Kunze K., Reich N.O., (1983). Stereochemistry of cytochrome P-450 catalysed epoxidation and prosthetic heme alkylation. *Journal of Biological Chemistry* **258**, 4208 - 4213.

Ortiz de Montellano P.R., Stearns R.A., (1987). Timing of the radical recombination step in cytochrome-P-450 catalysis with ring-strained probes. *Journal of the American Chemical Society* **109**, 3415 - 3420.

Ortiz De Montellano P.R., Fruetel J.A., Collins J.R., Camper D.L., Loew G.H., (1991). theoretical and experimental-analysis of the absolute stereochemistry of cis-beta-methylstyrene epoxidation by cytochrome-P450 CAM. *Journal of The American Chemical Society*, **113**, 3195 - 3196.

Ortiz de Montellano P.R., (1995). Cytochrome P450: Structure, Mechanism and Biochemistry, Chapter 1, 1 - 48. Ed., Ortiz de Montellano, Plenum Press NY.

Osborne C., Chen L-M., Matthews R.G., (1991). Isolation, cloning, mapping, and nucleotide sequencing of the gene encoding flavodoxin in *Escherichia coli*. *Journal of Bacteriology* **173**, 1729 - 1737.

Ost T.W.B., Miles C.S., Murdoch J., Cheung Y-F., Reid G.A., Chapman S.K., Munro A.W., (2000). Rational re-design of the substrate binding site of flavocytochrome P450 BM3. *FEBS Letters* **486**, 173 - 177.

Ost T.W.B., Munro A.W., Mowat C.G., Taylor P.R., Pesseguiro A., Fulco A.J., Cho A.K., Cheesman M.A., Walkinshaw M.D., Chapman S.K., (2001). Structural and spectroscopic analysis of the F393H mutant of flavocytochrome P450 BM3. *Biochemistry* **40**, 13430 - 13438.

Ost T.W.B., Miles C.S., Munro A.W., Murdoch J., Reid G.A., Chapman S.K., (2001). Phenylalanine 393 exerts thermodynamic control over the heme of flavocytochrome P450 BM3. *Biochemistry* **40**, 13421 - 13429.

Otsuka A.J., Buoncristiani M.R., Howard P.K., Flamm J., Johnson C., Yamamoto R., Uchida K., Cook C., Ruppert J., Matsuzaki J., (1988). The *Escherichia-coli* biotin biosynthetic enzyme sequences predicted from the nucleotide-sequence of the *bio* operon. *Journal of Biological Chemistry*, **263**, 19577 - 19585.

Ottada J., Calcaterra N.B., Arakaki A.K., Orellano E.G., Carrillo N., Ceccarelli E.A., (1997). On the role of aromatic amino acids interacting with FAD in plant-type ferredoxin-NADP<sup>+</sup> reductases, in *Flavins and Flavoproteins 1997*, Eds Stevenson K.J., Massey V., Williams C.H. Jr. P., University of Calgary Press Canada, 501 - 508.

Pacheco-Alvarez D., Solorzano-Vargas R.S., Del Rio A.L., (2002). Biotin in metabolism and its relationship to human disease. *Archives of Medical Research* **33**, 439 - 447.

Paine M.J.I., Ayivor S., Munro A.W., Tsan P., Lian L-Y., Roberts G.C.K., Wolf C.R., (2001). Role of the conserved phenylalanine 181 of NADPH-cytochrome P450 oxidoreductase in FMN binding and catalytic activity. *Biochemistry* **40**, 13439 - 13447.

Panke S., Wubbolts M.G., (2002). Enzyme technology and bioprocess engineering. *Current Opinion in Biotechnology* **13**, 111 - 116.

Park S.M., Shimizu H., Adachi S., Nakagawa A., Tanaka I., Nakahara K., Shoun H., Obayashi E., Nakamura H., Iizuka T., Shiro Y., (1997). Crystal structure of nitric oxide reductase from denitrifying fungus *Fusarium oxysporum*. *Nature Structural Biology* **4**, 827 - 832.

Pereira H.M., Cleasby A., Pena S.D.J., Franco G.R., Garratt R.C., (2003). Cloning, expression and preliminary crystallographic studies of the potential drug target purine nucleoside phosphorylase from *Schistosoma mansoni*. *Acta Crystallographica Section D-Biological Crystallography* **59**, 1096 - 1099.

Perkins J.B., Bower S., Howitt C.L., Yocum R.R., Pero J., (1996). Identification and characterization of transcripts from the biotin biosynthetic operon of *Bacillus subtilis*. *Journal of Bacteriology* **178**, 6361 - 6365.

Peterson J.A., Boddupalli S.S., (1992). P450 BM3: reduction by NADPH and sodium dithionite. *Archives of Biochemistry and Biophysics* **294**, 654 - 661.

Peterson J.A., Lu J-Y., Geisselsoder J., Graham-Lorence S., Carmona C., Witney F., Lorence M.C., (1992). Cytochrome P-450terp. Isolation and purification of the protein and cloning and sequencing of its operon. *Journal of Biological Chemistry* **267**, 14193 - 14203.

Peterson J.A., Graham S.E., (1998). A close family resemblance: the importance of structure in understanding cytochromes P450. *Structure* **6**, 1079 - 1085.

Pikuleva I.A., Mackman R.L., Kagawa N., Waterman M.R., Demontellano P.R.O., (1995). Active-site topology of bovine cholesterol side-chain cleavage cytochrome-P450 (P450SCC) and evidence for interaction of tyrosine-94 with the side-chain of cholesterol. *Archives of Biochemistry And Biophysics* **322**, 189 - 197.

Pikuleva I.A., Tesh K., Waterman M.R., Kim Y., (2000). The tertiary structure of full-length bovine adrenodoxin suggests functional dimers. *Archives of Biochemistry and Biophysics* **373**, 44

- 55.

Ploux O., Marquet A., (1992). The 8-amino-7-oxopelargonate synthase from *Bacillus sphaericus* – purification and preliminary characterization of the cloned enzyme over-produced in *Escherichia coli*. *Biochemical Journal* **283**, 327 - 331.

Ploux O., Marquet A., (1996). Mechanistic studies on the 8-amino-7-oxopelargonate synthase, a pyridoxial-5'-phosphate-dependent enzyme involved in biotin biosynthesis. *European Journal of Biochemistry* **236**, 301 - 308.

Ploux O., Breyne O., Carillon S., Marquet A., (1999). Slow-binding and competitive inhibition of 8-amino-7-oxopelargonate synthase, a pyridoxal-5'-phosphate dependant enzyme involved in biotin biosynthesis, by substrate and intermediate analogues. *European Journal of Biochemistry* **259**, 63 - 70.

Ponstingl H., Otting G., (1997). NMR assignments, secondary structure and hydration of oxidised *Escherichia coli* flavodoxin. *European Journal of Biochemistry* **244**, 384 - 399.

Pochapsky T.C., Ye X.M., Ratnaswamy G., Lyons T.A., (1994). An NMR derived model for the solution structure of oxidised putidaredoxin, a 2-Fe, 2-S ferredoxin from *Pseudomonas*. *Biochemistry* **33**, 6424 - 6432.

Pochapsky T.C., Ratnaswamy G., Patera A., (1994). Redox-dependent <sup>1</sup>H NMR spectral features and tertiary structural constraints on the C-terminal region of putidaredoxin. *Biochemistry* **33**, 6433 - 6441.

Pochapsky TC, Jain NU, Kuti M, Lyons TA, Heymont J., (1999). A refined model for the solution structure of oxidized putidaredoxin. *Biochemistry* **38**, 4681 - 4690.

Pochapsky T.C., Kostic M., Jain N., Pejchal R., (2001). Redox-dependant conformational selection in a Cys<sub>4</sub>Fe<sub>2</sub>S<sub>2</sub> ferredoxin. *Biochemistry* **40**, 5602 - 5614.

Porter T.D., (1991). An unusual yet strongly conserved flavoprotein reductase in bacteria and mammals. *Trends in Biochemical Sciences* **16**, 154 - 158.

Porter T.D., Coon M.J., (1991). Cytochrome-P-450 - multiplicity of isoforms, substrates, and catalytic and regulatory mechanisms. *Journal of Biological Chemistry* **266**, 13469 - 13472.

Ponstingl H., Otting G., (1997). NMR assignments, secondary structure and hydration of oxidized *Escherichia coli* flavodoxin. *European Journal of Biochemistry*, **244**, 384 - 399.

Poupin P., Ducrocq V., Hallier-Soulier S., Truffaut N., (1999). Cloning and characterisation of the genes encoding a cytochrome P450 (PipA) involved in piperidine and pyrrolidine utilization and its regulatory protein (PipR) in *Mycobacterium smegmatis* mc2155. *Journal of Bacteriology* **181**, 3419 - 3426.

Poulos, T.L., Finzel, B.C. and Howard, A.J. (1986). Crystal structure of substrate-free *Pseudomonas putida* cytochrome P-450 cam. *Biochemistry* **25**, 5314 - 5322.

Poulos T.L., Finzel B.C., Howard A.J., (1987). High-resolution crystal-structure of cytochrome P450 CAM. *Journal of Molecular Biology* **195**, 687 - 700.

- Primo C.D., Hui Bon Hoa G., Douzou P., Sligar S., (1990). Mutagenesis of a single hydrogen bond in cytochrome P-450 alters cation binding and heme solvation. *Journal of Biological Chemistry Communication* **265**, 5361 - 5363.
- Proud V.K., Rizzo W.B., Patterson J.W., Heard G.S., Wolf B., (1990). Fatty-acid alterations and carboxylase deficiencies in the skin of biotin-deficient rats. *American Journal of Clinical Nutrition*, **51**, 853 - 858.
- Pueyo J.J., Gomez-Moreno C., Mayhew S.G., (1991). Oxidation-reduction potentials of ferredoxin-NADP reductase and flavodoxin from *Anabaena* PCC 7119 and their electrostatic and covalent complexes. *European Journal of Biochemistry* **202**, 1065 - 1071.
- Pueyo J.J., Curley P., Mayhew S.G., (1996). Kinetics and thermodynamics of the binding of riboflavin, riboflavin 5'-phosphate and riboflavin 3',5'-phosphate by apoflavodoxins. *Biochemical Journal* **313**, 855 - 861.
- Que L., Jr., (1993). In Bioinorganic Catalysis, *Reddijk Journal.*, 347 - 393. Ed., Dekker M., NY.
- Raadt A., Griengl H., (2002). The use of substrate engineering in biohydroxylation. *Current Opinion in Biotechnology* **13**, 537 - 542.
- Raag R., Poulos T.L., (1991). Crystal structures of cytochrome P-450 CAM complexed with camphene, thiocamphor, and adamantane: Factors controlling P-450 substrate hydroxylation. *Biochemistry* **30**, 2674 - 2684.
- Raag R., Li H., Jones B.C., Poulos T.L., (1993). Inhibitor-induced conformational change in cytochrome P-450 CAM. *Biochemistry* **32**, 4571 - 4578.
- Radford S.E., Dobson C.M., Evans P.A., (1992). The folding of hen lysozyme involves partially structured intermediates and multiple pathways. *Nature* **358**, 302 - 307.
- Ramarao M., Kemper B., (1995). Substitution at residue-473 confers progesterone 21-hydroxylase activity to cytochrome-P450-2C2. *Molecular Pharmacology*, **48**, 417 - 424.
- Ramm P.J., Caspi E., (1969). The stereochemistry of tritium at carbon atoms 1, 7, and 15 in cholesterol derived from (3R,2R)-(2-3H)-mevalonic acid. *Journal of Biological Chemistry* **244**, 6064 - 6073.
- Ravichandran K.G., Boddupalli S.S., Hasemann C.A., Peterson J.A., Deisenhofer J., (1993). Crystal structure of hemprotein domain of P450 BM-3, a prototype for microsomal P450's. *Science* **261**, 731 - 736.
- Reipa V., Mayhew M.P., Vilker V.L., (1997). A direct electrode-driven P450 cycle for biocatalysis. *Proceedings of the National Academy of Science USA* **94**, 13554 - 13558.
- Reipa V., Holden M.J., Mayhew M.P., Vilker V.L., (2000). Temperature dependence of the formal reduction potential of putidaredoxin. *Biochimica et Biophysica Acta* **1459**, 1 - 9.
- Ritz D., Lim J., Reynolds C.M., Poole L.B., Beckwith J., (2001). Conversion of a peroxiredoxin into a disulphide reductase by a triplet repeat expansion. *Science* **294**, 158 - 160.

- Rizzo C.J., (2001). Further computational studies on the conformation of 1,5-dihydrolumiflavin. *Antioxidants and Redox Signaling* **3**, 737 - 746.
- Roberts G.A., Grogan G., Greter A., Flitsch S.L., Turner N.J., (2002). Identification of a new class of cytochrome P450 from a *Rhodococcus* sp. *Journal of Bacteriology* **184**, 3898 - 3908.
- Roberts G.C.K., (1999). NMR spectroscopy in structure-based drug design. *Current Opinion in Biotechnology* **10**, 42 - 47.
- Rogers L.J., (1987). Ferredoxins, flavodoxins and related proteins: Structure, function and evolution. The Cyanobacteria, Ed. Fay P., Van Baalen C., Amsterdam, NL, 35 - 67.
- Rogers L.J., Smith A.J., Turner A.J., (1995). Involvement of the oxidized-semiquinone couple in photoreduction of algal flavodoxins. *Phytochemistry* **39**, 1287 - 1292.
- Roitberg A.E., Holden M.J., Mayhew M.P., Kurnikov I.V., Beratan D.N., Vilker V.L., (1998). Binding and electron transfer between putidaredoxin and cytochrome P450 CAM. Theory and experiments. *Journal of the American Chemical Society* **120**, 8927 - 8932.
- Roitel O., Scrutton N.S., Munro A.W., (2003). Electron transfer in flavocytochrome P450 BM3: Kinetics of flavin reduction and oxidation, the role of cysteine 999, and relationships with mammalian cytochrome P450 reductase. *Biochemistry* **42**, 10809 - 10821.
- Romero A., Caldeira J., Legall J., Moura I., Moura J.J.G., Romao M.J., (1996). Crystal structure of flavodoxin from *Desulfovibrio desulfuricans* ATCC 27774 in two oxidation states. *European Journal of Biochemistry* **239**, 190 - 196.
- Rosenburg A.H., Lade B.N., Chui D.S., Lin S.W., Dunn J.J., Studier F.W., (1987). Vectors for selective expression of cloned DNAs by T7 RNA-polymerase. *Gene* **56**, 125 - 135.
- Ruterjans H., Fleischmann G., Knauf M., Lohr F., Blumel M., Lederer F., Mayhew S.G., Muller F., (1996). NMR studies of flavoprotein. *Biochemical Society Transactions* **24**, 116 - 121.
- Rypniewski W.R., Breiter D.R., Benning M.M., Wesenberg G., Oh. B.H., Markley J.L., Rayment I., Holden H.M., (1991). Crystallization and structure determination to 2.5-Å resolution of the oxidized [Fe<sub>2</sub>-S<sub>2</sub>] ferredoxin isolated from *Anabaena-7120*. *Biochemistry* **30**, 4126 - 4131.
- Sanders-Loehr J., (1989). In Iron Carriers and Iron Proteins. Ed., Loehr V.C.H., N.Y., **5**, 373 - 466.
- Sanyal I., Gibson K.J., Flint D.H., (1996). *Escherichia coli* biotin synthase: An investigation into the factors required for its activity and its sulfur donor. *Archives of Biochemistry and Biophysics*, **326**, 48 - 56.
- Sakamoto H., Ichikawa Y., Yamano T., Takagi T., (1981). Circular dichroic studies on the interaction between reduced nicotinamide adenine dinucleotide phosphate-adrenodoxin reductase and adrenodoxin. *Journal of Biochemistry* **90**, 1445 - 1452.
- Sali, A., and Blundell, T.L. (1993). Comparative protein modelling by satisfaction of spatial restraints. *Journal of Molecular Biology* **234**, 779 - 815.

- Sambrook, J., Fritsch, E.F. and Maniatis, T. (1989) in "Molecular Cloning, a laboratory manual", 2nd Edition, Cold Spring Harbor Laboratory Press.
- Sandalova T., Schneider G., Kack H., Lindqvist Y., (1999). Structure of dethiobiotin synthetase at 0.97 angstrom resolution. *Acta Crystallography section D* **55**, 610 - 624.
- Scheraga H., (1961). In "Protein Structure, Molecular Biology Volume I", Ed. Kaplan, N. O., Scheraga, H. A., Academic Press, New York.
- Schiffler B., Kiefer M., Wilken A., Hannemann F., Adolph H.W., Bernhardt R., (2001). The interaction of bovine adrenodoxin with CYP11A1 (cytochrome P450 SCC) and CYP11B1 (cytochrome P45011 $\beta$ ). *Journal of Biological Chemistry* **276**, 36225 - 36232.
- Schlichting I., Jung C., Schulze H., (1997). Crystal structure of cytochrome P450 CAM complexed with the (1S)-camphor enantiomer. *FEBS Letters* **415**, 253 - 257.
- Schlichting I., Berendzen J., Chu K., Stock A. M., Maves S.A., Benson D.E., Sweet R.M., Ringe D., Petsko G.A., Sligar S.G., (2000). The Catalytic Pathway of Cytochrome P450 CAM at Atomic Resolution. *Science* **287**, 1615.
- Schneider G., Lindqvist Y., (1997). Structure of ATP-dependent carboxylase, dethiobiotin synthase Vitamins and coenzymes, Part I. *Methods In Enzymology*, **279**, 376 - 385.
- Schneider G., Lindqvist Y., (2001). Structural enzymology of biotin biosynthesis. *FEBS Letters*, **495**, 7 - 11.
- Schulz G.E., (1992). Binding of nucleotides by proteins. *Current Opinion in Structural Biology* **2**, 61 - 67.
- Schulze H., Schuler A., Stuber D., Dobeli H., Langen H., Huber G., (1993). Rat-brain glyceraldehyde-3-phosphate dehydrogenase interacts with the recombinant cytoplasmic domain of Alzheimers beta-amyloid precursor protein. *Journal of Neurochemistry* **60**, 1915 - 1922.
- Schwaneberg U., Schmidt-Dannert C., Schmitt J., Schmid R.D., (1999). A continuous spectrophotometric assay for P450 BM-3, a fatty acid hydroxylating enzyme, and its mutant F87A. *Analytical Biochemistry* **269**, 359 - 366.
- Schwanenberg U., Appel D., Schmitt J., Schmid R.D., (2000). P450 in biotechnology: Zinc driven  $\omega$ -hydroxylation of *p*-nitrophenoxystyrene using P450 BM-3 F87A as a catalyst. *Journal of Biotechnology* **84**, 249 - 257.
- Senda T., Yamada T., Sakuri N., Kubota M., Nishizaki T., Masai E., Fukuda M., Mitsui Y., (2000). Crystal Structure of NADH-dependent ferredoxin reductase component in biphenyl dioxygenase. *Journal of Molecular Biology* **304**, 397 - 410.
- Seo D., Kamino K., Inoue K., Sakurai H., (2004). Purification and characterization of ferredoxin-NAD(P)<sup>+</sup> reductase from *Bacillus subtilis*. *Plant Cell Physiology* **45**, S140 - S140.
- Serizawa N., Matsuoka T., (1993). The role of cytochrome P450 SCA in *Streptomyces* -



interaction of azole compounds with cytochrome-P450 SCA. *Bioscience, Biotechnology and Biochemistry* **57**, 1777 - 1778.

Serre L., Vellieux F.M.D., Medina M., Gomez-Moreno C., Fontecilla-Camps J.C., Frey M., (1996). X-ray structure of the ferredoxin:NADP<sup>+</sup> reductase from the cyan bacterium *Anabaena* PCC 7119 at 1.8 Å resolution, and crystallographic studies of NADP<sup>+</sup> binding at 2.25 Å resolution. *Journal of Molecular Biology* **263**, 20 - 39.

Sevrioukova I.F., Shaffer C., Ballou D.P., Peterson J.A., (1996). Equilibrium and Transient State Spectrophotometric Studies of the Mechanism of Reduction of the Flavoprotein Domain of P450 BM3. *Biochemistry* **35**, 7058 - 7068.

Sevrioukova I.F., Li H., Zhang H., Peterson J.A., Poulos T.L., (1999). Structure of a cytochrome P450-redox partner electron transfer complex. *Proceedings of the National Academy of Science USA* **96**, 1863 - 1868.

Shafiee A., Hutchinson C.R., (1988). Purification and reconstitution of the electron transport components for 6-deoxyerythronolide B hydroxylase, a cytochrome P450 enzyme of macrolide antibiotic (erythromycin) biosynthesis. *Journal of Bacteriology* **170**, 1548 - 1553.

Shaw G.C., Fulco A.J., (1993). Inhibition by barbiturates of the binding of Bm3R1 repressor to its operator site on the barbiturate inducible cytochrome P450 BM3 gene of *Bacillus megaterium*. *Journal of Biological Chemistry* **268**, 2997 - 3004.

Shen B., Hutchinson C.R., (1993). Tetracenomycin F1 monooxygenase: oxidation of a naphthacenone to a naphthacenequinone in the biosynthesis of tetracenomycin C in *Streptomyces glaucescens*. *Biochemistry* **32**, 6656 - 6663.

Shen A.L., Kasper C.B., (1996). Role of Ser457 of NADPH-cytochrome P450 oxidoreductase in catalysis and control of FAD oxidation-reduction potential. *Biochemistry* **35**, 9451 - 9459.

Shen A.L., Sem D.S., Kasper C.B., (1999). Mechanistic studies on the reductive half-reaction of NADPH-cytochrome P450 oxidoreductase. *Journal of Biological Chemistry* **274**, 5391 - 5398.

Shimada H., Nagano S., Ariga Y., Unno M., Egawa T., Hishiki T., Ishimura Y., Masuya F., Obata T., Hori H., (1999). Putidaredoxin-cytochrome P450 CAM interaction. Spin state of the heme iron modulates putidaredoxin structure. *Journal of Biological Chemistry* **274**, 9363 - 9369.

Shou M., Grogan J., Mancewicz J.A., Krausz K.W., Gonzalez F.J., Gelboin H.V., Korzekwa K.R., (1994). Activation of CYP3A4: Evidence for the simultaneous binding of two substrates in a cytochrome P450 active site. *Biochemistry* **33**, 6450 - 6455.

Shyadehi A.Z., Lamb D.C., Kelly S.L., Kelly D.E., Schunck W-H., Wright J.N., Corina D., Akhtar M., (1996). The mechanism of the acyl-carbon bond cleavage reaction catalysed by recombinant sterol 14 $\alpha$ -demethylase of *Candida albicans* (other names are: Lanosterol 14 $\alpha$ -demethylase, P-45014DM and CYP51). *Journal of Biological Chemistry* **271**, 12445 - 12450.

Sieber V., Martinez C.A., Arnold F.H., (2001). Libraries of hybrid proteins from distantly related sequences. *Nature Biotechnology* **19**, 456 - 460.

Silver J., (1993). In "The Chemistry of Iron", Blackie Academic Press, London, 264 - 266.

Silverman R.B., (1992). The Organic Chemistry of Drug Design and Drug Action. Academic Press, NY, USA.

Sligar S.G., Debrunner P.G., Lipscomb J.D., Namtvedt M.J., Gunsalus I.C., (1974). A role for putidaredoxin COOH-terminus in P450 CAM (cytochrome m) hydroxylations. *Proceedings of the National Academy of Science USA* **71**, 10.

Sligar S.G., (1976). Coupling of spin, substrate and redox equilibria in cytochrome P450. *Biochemistry* **15**, 5399 - 5406.

Sligar S.G., Gunsalus I.C., (1976). A thermodynamic model of regulation: Modulation of redox equilibria in camphor monooxygenase. *Proceedings of the National Academy of Science* **73**, 1078 - 1082.

Sligar S.G., Gunsalus I.C., (1979). Proton coupling in the cytochrome P-450 spin and redox equilibria. *Biochemistry* **18**, 2290 - 2295.

Sligar S.G., Filipovic D., Stayton P.S., (1991). Mutagenesis of cytochrome P450 CAM binding surface as defined by site-directed mutagenesis and electrostatic modelling. *Biochemistry* **29**, 7381 - 7386.

Smith W.W., Burnett R.M., Darling G.D., Ludwig M.L., (1977). Structure of semiquinone form of flavodoxin from *Clostridium-MP* - extension of 1.8 Å resolution and some comparisons with oxidized state. *Journal of Molecular Biology* **117**, 195 - 225.

Sono M., Roach M.P., Coulter E.D., Dawson J.H., (1996). Heme-containing oxygenases. *Chemical Reviews* **96**, 2841 - 2887.

Stayton P.S., Poulos T.L., Sligar S.G., (1989). Putidaredoxin competitively inhibits cytochrome *b<sub>5</sub>*-cytochrome P450 CAM electron transfer complex. *Biochemistry* **28**, 7381 - 7386.

Stayton P.S., Sligar S.G., (1990). The cytochrome P-450 CAM binding surface as defined by site-directed mutagenesis and electrostatic modelling. *Biochemistry* **29**, 7381 - 7386.

Steensma E., Heering H.A., Hagen W.R., Van Mierlo C.P.M., (1996). Redox properties of wild-type, Cys69Ala, and Cys69Ser *A. vinelandii* flavodoxin II as measured by cyclic voltammetry and EPR spectroscopy. *European Journal of Biochemistry* **235**, 167 - 172.

Steensma E., Nijman M.J.M., Bollen Y.J.M., (1998). Apparent local stability of the secondary structure of *Azotobacter vinelandii* holoflavodoxin II as probed by hydrogen exchange: implications for redox potential regulation and flavodoxin folding. *Protein Science* **7**, 306 - 317.

Stevenson J.A., Westlake A.C.G., Whittock C., Wong L.L., (1996). The catalytic oxidation of linear and branched alkanes by cytochrome P450 CAM. *Journal of the American Chemical Society* **118**, 12846 - 12847.

Stevenson J.A., Jones J.P., Wong L.L., (2000). Mutations of phenylalanine 193 in the putative substrate access channel alter the substrate specificity of cytochrome P450 CAM. *Israel Journal of Chemistry* **40**, 55 - 62.

- Stok J.E., De Voss J.J., (2000). Expression, purification and characterization of Biol: A carbon-carbon bond cleaving cytochrome P450 involved in biotin biosynthesis in *Bacillus subtilis*. *Archives of Biochemistry and Biophysics* **384**, 351 - 360.
- Streaker E.D., Beckett D., (1998). Coupling of site-specific DNA binding to protein dimerisation in assembly of the biotin repressor-biotin operator complex. *Biochemistry* **37**, 3210 - 3219.
- Streaker E.D., Beckett D., (1999). Ligand-linked structural changes in the *Escherichia coli* biotin repressor. The significance of surface loops for binding and allostery. *Journal of Molecular Biology* **292**, 619 - 632.
- Stryer L., (1999). Biochemistry, W.H.Freeman and Company, N.Y., 4<sup>th</sup> ed.
- Studier F.W., Moffat B.A., (1986). Use of bacteriophage-T7 RNA-polymerase to direct selective high-level expression of cloned genes. *Journal of Molecular Biology* **189**, 113 - 130.
- Studier F.W., (1991). Use of bacteriophage-T7 lysozyme to improve an inducible T7 expression system. *Journal of Molecular Biology* **219**, 37 - 44.
- Sullivan D.T., MacIntyre R., Fuda N., Fiori J., Barrilla J., Ramizel L., (2003). Analysis of glycolytic enzyme co-localization in *Drosophila* flight muscle. *Journal of Experimental Biology* **206**, 2031 - 2038.
- Sutherland J.B., (1986). Demethylation of veratrole by cytochrome-P-450 in *Streptomyces setonii*. *Applied Environmental Microbiology* **154**, 260 - 266.
- Swenson R.P., Krey G.D., (1994). Site-directed mutagenesis of tyrosine-98 in the flavodoxin from *Desulfovibrio-vulgaris* (Hildenborough) - regulation of oxidation-reduction properties of the bound FMN cofactor by aromatic, solvent, and electrostatic interactions. *Biochemistry* **33**, 8505 - 8514.
- Szklarz G.D., Halpert J.R., (1998). Molecular basis of P450 inhibition and activation. Implications for drug development and drug therapy. *Drug Metabolism and Disposition* **26**, 1179 - 1184.
- Tafi A., Anastassopoulou J., Theophanides T., Botta M., Corelli F., Massa S., Artico M., Costi R., Di Santo R., Ragno R., (1996). Molecular modelling of azole antifungal agents active against *Candida albicans* 1. A comparative molecular field analysis study. *Journal of Medicinal Chemistry* **39**, 1227 - 1235.
- Thompson, J.D., Higgins, D.G. and Gibson, T.J. (1994). CLUSTAL W: improving the sensitivity of progressive multiple sequence alignment through sequence weighting, position-specific gap penalties and weight matrix choice. *Nucleic Acids Research* **22**, 4673 - 80.
- Tippelt A., Jahnke L., Poralla K., (1998). Squalene-hopene cyclase from *Methylococcus capsulatus* (Bath): a bacterium producing hopanoids and steroids. *Biochimica et Biophysica Acta - Lipids And Lipid Metabolism* **1391**, 223 - 232.
- Toda T., Shimanuki M., Saka Y., Yamano H., Adachi Y., Shirakawa M., Kyogoku Y., Yanagida M., (1992). Fission yeast pap1-dependent transcription is negatively regulated by an essential nuclear protein, crm1. *Molecular and Cellular Biology*, **12**, 5474 - 5484.

- Tomoczyk N.H., Nettleship J.E., Baxter R.L., Crichton H.J., Webster S.P., Campopiano D.J., (2002). Purification and characterisation of the BioH protein from the biotin biosynthetic pathway. *FEBS Letters* **513**, 299 - 304.
- Tosha T., Yoshioka S., Hori H., Takahashi S., Ishimori K., Morishima I., (2002). Molecular mechanism of the electron transfer reaction in cytochrome P450 CAM-putidaredoxin: Roles of glutamine 360 at the heme proximal site. *Biochemistry* **41**, 13883 - 13893.
- Townsley J.D., Brodie H.J., (1968). Mechanism of estrogen biosynthesis. III. Stereochemistry of aromatization of C19 and C18 steroids. *Biochemistry* **7**, 33 - 40.
- Trower M.K., Emptage M.H., Sariaslani F.S., (1990). Purification and characterization of a 7Fe ferredoxin from *Streptomyces-griseus*. *Biochimica et Biophysica Acta* **1037**, 281 - 289.
- Truan G., Komandla M.R., Falck J.R., Peterson J.A., (1999). P450 BM-3: Absolute configuration of the primary metabolites of palmitic acid. *Archives of Biochemistry and Biophysics* **366**, 192 - 198.
- Tuck S.F., Graham-Lorence S., Peterson J.A., Ortiz de Montellano P.R., (1993). Active-sites of the cytochrome P450CAM (CYP101) F87W and F87A mutants - evidence for significant structural reorganisation without alteration of catalytic regiospecificity. *Journal of Biological Chemistry* **268**, 269 - 275.
- Turoverov K.K., Biktashev A.G., Khaitina S.Y., Kuznetsova I.M., (1999). The structure and dynamics of partially folded actin. *Biochemistry* **38**, 6261 - 6269.
- Ueng Y-F., Kuwaba T., Chun Y-J., Guengerich F.P., (1997). Cooperativity in oxidations catalysed by cytochrome P450 3A4. *Biochemistry* **36**, 370 - 381.
- Ugulava N.B., Gibney B.R., Jarrett J.T., (2000). Iron-sulfur cluster interconversions in biotin synthase: Dissociation and reassociation of iron during conversion of [2Fe-2S] to [4Fe-4S] clusters. *Biochemistry* **39**, 5206 - 5214.
- Ugulava N.B., Surerus K.K., Jarrett J.T., (2002). Evidence from Mossbauer spectroscopy for distinct [2Fe-2S](2<sup>+</sup>) and [4Fe-4S](2<sup>+</sup>) cluster binding sites in biotin synthase from *Escherichia coli*. *Journal of the American Chemical Society* **124**, 9050 - 9051
- Ugulava N.B., Frederick K.K., Jarrett J.T., (2003). Control of adenosylmethionine-dependent radical generation in biotin synthase: A kinetic and thermodynamic analysis of substrate binding to active and inactive forms of BioB. *Biochemistry* **42**, 2708 - 2719.
- Uhlmann H., Iametti S., Vecchio G., Bonomi G., Bernhardt R., (1997). Pro108 is important for folding and stabilisation of adrenal ferredoxin, but does not influence the functional properties of the protein. *European Journal of Biochemistry* **248**, 897 - 902.
- Ullmann G.M., Hauswald M., Jensen A., Knapp E-W., (2000). Structural alignment of ferredoxin and flavodoxin based on their electrostatic potentials: Implications for their interactions with photosystem I and ferredoxin-NADP<sup>+</sup> reductase. *Proteins: Structure, Function and Genetics* **38**, 301 - 309.

Ullrich V., (1979). Cytochrome P450 and biological hydroxylation reactions. *Topics in Current Chemistry* **83**, 67 - 104.

Unno M., Shimada H., Toba Y., Makino R., Ishimura Y., (1996). Role of Arg112 of cytochrome P450 CAM in the electron transfer from reduced putidaredoxin – analysis with site-directed mutants. *Journal of Biological Chemistry* **271**, 17869 - 17874.

Unno M., Christian J.F., Benson D.E., Gerber N.C., Sligar S.G., Champion P.M., (1997). Resonance Raman investigations of cytochrome P450 CAM complexed with putidaredoxin. *Journal of the American Chemical Society* **119**, 6614 – 6620.

Urlacher V., Schmid R.D., (2002). Biotransformations using prokaryotic P450 monooxygenases. *Current Opinion in Biotechnology* **13**, 557 - 564.

Usanov S.A., Graham S.E., Lepesheva G.I., Azeva T.N., Strushkevich N.V., Gilep A.A., Estabrook R.W., Peterson J.A., (2002). Probing the interaction of bovine cytochrome P450<sub>scc</sub> (CYP11A1) with adrenodoxin: Evaluating site-directed mutations by molecular modelling. *Biochemistry* **41**, 8310 - 8320.

Uversky V.N., Fink A.L., (2002). The chicken-egg scenario of protein folding revisited. *FEBS Letters* **515**, 79 - 83.

Vanden Bossche H., Koymans L., Moereels H., (1991). P450 inhibitors of use in medical treatment: focus on mechanisms of action. *Pharmacology and Therapeutics* **67**, 79 - 100.

Vaz A.D.N., Roberts E.S., Coon M.J., (1991). Olefin formation in the oxidative deformylation of aldehydes by cytochrome-P-450 - mechanistic implications for catalysis by oxygen-derived peroxide. *Journal of the American Chemical Society* **113**, 5886 - 5887.

Vaz A.D.N., Coon M.J., (1994). On the mechanism of action of cytochrome P450: Evaluation of hydrogen abstraction in oxygen dependent alcohol oxidation. *Biochemistry* **33**, 6442 - 6449.

Vaz A.D.N., McGinnity D.F., Coon M.J., (1998). Epoxidation of olefins by cytochrome P450: Evidence from site-specific mutagenesis for hydroperoxo-iron as an electrophilic oxidant. *Proceedings of The National Academy of Sciences USA* **95**, 3555 - 3560.

Vermillion J.L., Coon M.J., (1974). Highly purified detergent solubilised NADPH-cytochrome P450 reductase from Phenobarbital-induced rat liver microsomes. *Biochemical and Biophysical Research Communications* **60**, 849 - 851.

Vermilion J., Ballou D.P., Massey V., Coon M.J., (1981). Separate roles for FMN and FAD in catalysis by liver microsomal NADPH-cytochrome P-450 reductase. *Journal of Biological Chemistry* **256**, 266 - 277.

Vervoort J., van Berkel W.J.H., Mayhew S.G., Muller F., Bacher A., Nielsen P.J.L., (1986). Properties of the complexes of riboflavin 3',5'-bisphosphate and the apoflavodoxins from *Megaphaera elsdenii* and *Desulfovibrio vulgaris* (Hildenborough). *European Journal of Biochemistry* **161**, 749 – 756.

Vervoort J., Muller F., Mayhew S.G., van der Berg W.A.M., Moonen C.T.W., Bacher A., (1986). A comparative C-13, N-15, and P-31 nuclear-magnetic-resonance study on the flavodoxins from

*Clostridium-MP, Megasphaera elsdenii, and Azotobacter vinelandii. Biochemistry* **25**, 6789 – 6799.

Vidakovic M., Sligar S.G., Li H.Y., Poulos T.L., (1998). Understanding the role of the essential Asp251 in cytochrome P450CAM using site-directed mutagenesis, crystallography and kinetic solvent isotope effect. *Biochemistry* **37**, 9211 - 9219.

Wada A., Waterman M.R., (1992). Identification by site-directed mutagenesis of 2 lysine residues in cholesterol side-chain cleavage cytochrome-P450 that are essential for adrenodoxin binding. *Journal of Biological Chemistry* **267**, 22877 - 22882.

Walsh M.A., McCarthy A., O'Farrell P.A., McArdle P., Cunningham P.D., Mayhew S.G., Higgins T.M., (1998). X-ray crystal structure of the *Desulfovibrio vulgaris* (Hildenborough) apoflavodoxin-riboflavin complex. *European Journal of Biochemistry* **258**, 362 - 371.

Wan J.T., Jarrett J.T., (2002). Characterization of a complex between biotin synthase and flavodoxin. *Biochemistry* **41**, 128 - 135.

Wang M., Roberts D.L., Paschke R., Shea T.M., Masters B.S.S., Kim J-J.P., (1997). Three-dimensional structure of NADPH-cytochrome P450 reductase: Prototype for FMN- and FAD-containing enzymes. *Proceedings of the National Academy of Science USA* **94**, 8411 - 8416.

Wang S.L., Lai M.D., Huang J.D., (1999). G169R mutation diminishes the metabolic activity of CYP2D6 in Chinese. *Drug Metabolism and Disposition* **27**, 385 – 388.

Wassink J.M., Mayhew S.G., (1975). Fluorescence titration with apoflavodoxin: a sensitive assay for riboflavin 5'-phosphate and flavin adenine dinucleotide in mixtures. *Analytical Biochemistry* **68**, 609 – 616.

Watenpaugh, K. D., Sieker, L. C., Jensen, L. H., (1976). A crystallographic structural study of the oxidation states of *Desulfovibrio Vulgaris* flavodoxin. in "*Flavins and Flavoproteins*", 405.

Watt W., Tulinsky A., Swenson R.P., Watenpaugh K.D., (1991). Comparison of the crystal structures of a flavodoxin in its three oxidation states at cryogenic temperatures. *Journal of Molecular Biology* **218**, 195 – 208.

Webster S.P., Alexeev D., Campopiano D.J., Watt R.M., Alexeeva M., Sawyer L., Baxter R.L., (2000). Mechanism of 8-amino-7-oxononanoate synthase: Spectroscopic, kinetic and crystallographic studies. *Biochemistry* **39**, 516 - 528.

Wen L-P., Fulco A.J., (1987). Cloning of the gene encoding a catalytically self-sufficient cytochrome P-450 fatty acid monooxygenase induced by barbiturates in *Bacillus megaterium* and its functional expression and regulation in heterologous (*Escherichia coli*) and homologous (*Bacillus megaterium*) hosts. *Journal of Biological Chemistry* **262**, 6676 - 6682.

White R.E., Coon M.J., (1980). Oxygen activation by cytochrome P-450 *Annual Review of Biochemistry* **49**, 315 – 356.

White R.E., (1991). The involvement of free-radicals in the mechanisms of monooxygenases. *Pharmacology and Therapeutics* **49**, 21 - 42.



- Wirtz M., Klucik J., Rivera M., (2000). Ferredoxin-mediated electro catalytic dehalogenation of haloalkanes by cytochrome P450 CAM. *Journal of the American Chemical Society* **122**, 1047 - 1056.
- Xia B., Volkman B.F., Markley J.L., (1998). Evidence for oxidation-state-dependent conformational changes in human ferredoxin from multinuclear, multidimensional NMR spectroscopy. *Biochemistry* **37**, 3965 - 3973.
- Xiang H., Tschirret-Guth R.A., Ortiz de Montellano P.R., (2000). An A245T mutation conveys on cytochrome P450eryF the ability to oxidise alternate substrates. *Journal of Biological Chemistry* **275**, 35999 - 36006.
- Xu W.Y., Bak S., Decker A., Paquette S.M., Feyereisen R., Galbraith D.W., (2001). Microarray based analysis of gene expression in very large gene families: The cytochrome P450 gene superfamily of *Arabidopsis thaliana*. *Gene* **272**, 61 - 74.
- Xu Y., Beckett D., (1995). Temperature-dependence of the biotin repressor-allosteric effector interaction. *FASEB Journal* **9**, A1284 - A1284.
- Xu Y., Johnson C.R., Beckett D., (1996). Thermodynamic analysis of small ligand binding to the *Escherichia coli* repressor of biotin biosynthesis. *Biochemistry* **35**, 5509 - 5517.
- Yalloway G.N., Mayhew S.G., Malthouse J.P.G., Gallagher M.E., Curley G.P., (1999). pH-dependent spectroscopic changes associated with the hydroquinone of FMN in flavodoxins. *Biochemistry* **38**, 3753 - 3762.
- Yamamoto H., Uchiyama S., Nugroho F.A., Sekiguchi J., (1997). A 23.4 kb segment at the 69 degrees-70 degrees region of the *Bacillus subtilis* genome. *Microbiology* **143**, 1317 - 1320.
- Yang G., Sandalova T., Lohman K., Lindqvist Y., Rendina A.R., (1997). Active site mutants of *Escherichia coli* dethiobiotin synthase: Effects of mutations on enzyme catalytic and structural properties. *Biochemistry* **36**, 4751 - 4760.
- Yanisch-Perron, C., Viera, J., and Messing, J., (1985). Improved M13 phage cloning vectors and host strains: nucleotide sequences of the m13mp18 and pUC19 vectors, *Gene* **33**, 103 - 199.
- Yoshioka S., Takahashi S., Ishimori K., Morishima I., (2000). Roles of the axial push effect in cytochrome P450 CAM studied with the site-directed mutagenesis at the heme proximal site. *Journal of Inorganic Biochemistry* **81**, 141 - 151.
- Yoshioka S., Tosha T., Takahashi S., Ishimori K., Hori H., Morishima I., (2002). Roles of the proximal hydrogen bonding network in cytochrome P450 CAM catalysed oxygenation. *Journal of the American Chemical Society* **124**, 14571 - 14579.
- Yun C-H., Miller G.P., Guengerich F.P., (2001). Oxidations of *p*-alkoxyacylanilides catalysed by human cytochrome P450 1A2: Structure-activity relationships and simulation of rate constants of individual steps in catalysis. *Biochemistry* **40**, 4521 - 4530.
- Yun M., Park C-G., Kim J-Y., Park H-W., (2000). Structural analysis of glyceraldehydes 3-phosphate dehydrogenase from *Escherichia coli*: Direct evidence of substrate binding and cofactor induced conformational changes. *Biochemistry* **39**, 10702 - 10710.

- Zeghouf M., Defaye G., Fontecave M., Coves J., (1998). The flavoprotein component of the *Escherichia coli* sulfite reductase can act as a cytochrome P450c17 reductase. *Biochemical and Biophysical Research Communications* **246**, 602 - 605.
- Zerbe K., Pylypenko O., Vitali F., Zhang W., Rousett S., Heck M., Vrijbloed J.W., Bischoff D., Bister B., Sussmuth R.D., Pelzer S., Wohlleben W., Robinson J.A., Schlichting I., (2002). Crystal structure of OxyB, a cytochrome P450 implicated in an oxidative phenol coupling reaction during vancomycin biosynthesis. *Journal of Biological Chemistry* **277**, 47476 - 47485.
- Zhao H., Chockalingam K., Chen Z., (2002). Directed evolution of enzymes and pathways for industrial biocatalysis. *Current Opinion in Biotechnology* **13**, 104 - 110.
- Zheng Y-J., Ornstein R.L., (1996). A theoretical study of the structures of flavin in different oxidation and protonation states. *Journal of the American Chemical Society* **118**, 9402 - 9408.
- Zhou Z., Swenson R.P., (1995). Electrostatic effects of surface acidic amino-acid-residues on the oxidation-reduction potentials of the flavodoxin from *Desulfovibrio-vulgaris* (Hildenborough). *Biochemistry* **34**, 3183 - 3192.
- Zhou Z., Swenson R.P., (1996). The cumulative electrostatic effect of aromatic stacking interactions and the negative electrostatic environment of the flavin mononucleotide binding site is a major determinant of the reduction potential for the flavodoxin from *Desulfovibrio vulgaris* (Hildenborough). *Biochemistry* **35**, 15980 - 15988.
- Ziegler G.A., Vonnrhein C., Hanukoglu I., Schulz G.E., (1999). The structure of adrenodoxin reductase of mitochondrial P450 systems: Electron transfer for steroid biosynthesis. *Journal of Molecular Biology* **289**, 981 - 990.
- Ziegler G.A., Schulz G.E., (2000). Crystal structures of adrenodoxin reductase in complex with NADP<sup>+</sup> and NADPH suggesting a mechanism for the electron transfer of an enzyme family. *Biochemistry* **39**, 10986 - 10995.
- Zollner A., Hannemann F., Lisurek M., Bernhardt R., (2002). Deletions in the loop surrounding the iron-sulfur cluster of adrenodoxin severely affect the interactions with its native redox partners adrenodoxin reductase and cytochrome P450 SCC (CYP11A1). *Journal of Inorganic Biochemistry* **91**, 644 - 654.